VOYAGER
DESIGN STUDIES

Volume Three: Systems Analysis

Prepared Under Contract Number NASw 697 ■ Research and Advanced Development Division ■ Avco Corporation ■ Wilmington, Massachusetts ■ National Aeronautics and Space Administration ■ Avco/RAD ■ TR-63-34 ■ 15 October 1963

VOYAGER DESIGN STUDIES

Volume III: Systems Analysis

Avco RAD-TR-63-34

15 October 1963

FOREWORD

The Voyager Design Study final report is divided into six volumes, for convenience in handling. A brief description of the contents of each volume is listed below.

Volume I -- Summary

A completely self-contained synopsis of the entire study.

Volume II -- Scientific Mission Analysis

Mission analysis, evolution of the Voyager program, and science payload.

Volume III -- Systems Analysis

Mission and system tradeoff studies; trajectory analysis; orbit and landing site selection; reliability; sterilization

Volume IV -- Orbiter-Bus System Design

Engineering and design details of the orbiter-bus

Volume V -- Lander System Design

Engineering and design details of the lander.

Volume VI -- Development Plan

Proposed development plan, schedules, costs, problem areas.

ACKNOWLEDGMENT

TABLE OF CONTENTS

TABLE OF CONTENTS (Concl'd)

LIST OF TABLES

LIST OF TABLES (Cont'd)

LIST OF TABLES (Concl'd)

LIST OF TABLES (Cont'd)

LIST OF FIGURES

LIST OF FIGURES (Cont'd)

LIST OF FIGURES (Concl'd)

SUMMARY

This report presents the results of a 6-month conceptual design study conducted by Avco Research and Advanced Development Division for the National Aeronautics and Space Administration. The objectives of the study were the synthesis of a conceptual design of an unmanned spacecraft to perform scientific orbiter-lander missions to Mars and Venus during planetary opportunities from 1969 to 1975, and the formulation of a plan delineating the development program leading to first launch during the Mars 1969 opportunity.

The basic approach makes use of a 6000- to 7000-pound orbiter-lander; tradeoff studies were conducted to determine the payload and mission capabilities with smaller and larger spacecraft. The orbiter-lander was selected as yielding the maximum in scientific value short of manned exploration. The lander separates from the orbiter-bus and descends to the planet surface by parachute, where it makes atmospheric and surface measurements and conducts a variety of scientific experiments. The information obtained is relayed to Earth via the orbiter-bus which meanwhile is placed in a planetocentric orbit. The orbiter-bus collects scientific data in transit and maps the planet while in orbit. The lifetime of both orbiter-bus and lander is 6 months for the Mars missions. For Venus, the orbiter life is also 6 months, but the lander life is only 10 to 20 hours because of the hostile environment. A small capsule was designed for Venus, in addition to the lander, to conduct atmospheric measurements after entering from orbit; the capsule does not survive landing. Landers and capsules would be sterilized to avoid contamination of the planets, but the orbiter-bus would be placed on a trajectory which would ensure that it would remain above the sensible atmosphere for at least 50 years; thus, no sterilization would be required. The development plan shows that to obtain the scientific value desired, two spacecraft should be scheduled for each launch opportunity and hardware development should begin in 1964 to meet the 1969 launch date for Mars.

1. INTRODUCTION

The system analysis volume presents the results of interdisciplinary analyses and tradeoff studies which influence the Voyager spacecraft design. A mission profile is presented which outlines the sequential operations throughout the spacecraft mission and develops, in some detail, the anticipated environment for each segment of the operational spacecraft life. Representative results of system analysis studies presented in this volume were used in the development of the orbiter and lander vehicles and the scientific mission discussed in volumes 2, 4 and 5.

Because of the voluminous nature of the system analysis results for the Voyager program, in some cases only representative results are presented. In general, they are presented in tabular rather than graphical form. Several specialized related studies are presented in appendixes A through F.

2. VOYAGER MISSION PROFILE

The sequence of events and environmental conditions of the Voyager mission are tabulated in subsequent sections. The sequential operations of the Voyager spacecraft are shown in tables 1 through 4. The Voyager mission can be divided into phases as follows:

2.1 Factory to Launch

The spacecraft is disassembled, packaged, and shipped to the launch site. At the launch site, the vehicle is reassembled, checked out, and placed onto the booster. Further checks are made on the launch pad.

2.2 Orbiter-Bus Mission from Launch to Lander Separation

The orbiter-bus is injected by the three-stage Saturn booster into an interplanetary transfer orbit. The vehicle remains in unpowered flight, except for brief periods on the interplanetary trajectory. The attitude of the spacecraft is stabilized by reference to the sun and star, Canopus. During any period in which thrust is applied to the vehicle, the antennas and instruments mounted on booms must be stowed because of the deleterious effects of the acceleration forces and also to prevent a shift in the center of gravity which would alter the direction of the applied velocity increment. Three midcourse corrections are planned; in the case of the Mars mission, the third correction at 10,000,000 km from planet encounter will also adjust the time of arrival to control the longitude of the landing site. The 35-watt OS-1 transmitter is used for in-transit communication of low bit-rate engineering and scientific data to the DSIF. Scientific measurements of energetic particles, radiation, magnetic fields, electron density, and micrometeoroids are all made in transit.

A tabulation of these measurements is given in figure 1. Lander-orbiter separation takes between 1,000,000 and 300,000 km from the planet.

2.3 Lander Mission

After separation, a velocity increment normal to the flight path is imparted to the lander to alter its course from a fly-by to an impact trajectory at a specified atmospheric entry angle which determines the landing site. After atmospheric entry, the drogue chute is opened at a preset Mach number to slow down the lander. The main chute is opened between 10,000 and 20,000 feet upon actuation by a radar altimeter.

Lander scientific data collection begins at entry into the planetary atmosphere. Television pictures are taken after main chute opening. The LS-1 transmitter relays real-time data to the orbiter from lander/orbiter separation to opening of the lander main chute. The LV-1 system transmits recorded descent data, TV pictures, and some real-time data to the orbiter relay during a 10-minute period centered about planet impact. Descent data includes pressure, density, and temperature measurements and also atmospheric sampling.

The lander vehicle impacts the planet and reerects itself to an upright position. The 5-foot-diameter, direct-link lander antenna and the scientific instruments are erected, deployed, and a programed sequence of scientific measurements is performed as indicated in figure 2. Atmospheric measurements are continued. In addition, biological and soil studies are performed. Instrumentation power requirements are given in figure 3. Scientific data collected on the planet surface are transmitted at regular intervals by the LV-1 on orbiter relay command and by the LS-3 transmitter on DSIF command. The LS-2, which transmits at very low bit rate (2bps) directly to the DSIF, is used for emergency backup. In the Venus mission, there is no transmission directly to the DSIF. All data are transmitted via orbiter relay. Martian surface measurements will continue for 6 months; however, most of the significant data will be obtained within 48 hours.

2.4 Orbiter Mission

After lander/orbiter separation, retrothrust is applied to the orbiter so that it will lag behind the lander at planet encounter. This is required to position the orbiter to relay to Earth the entry and impact data transmitted by the lander. A planet tracker is used for terminal guidance as the orbiter approaches the planet. The orbiter vehicle is retrothrusted to establish a 1700 by 10,000 km elliptical orbit about Mars. The planetary surface is mapped by TV cameras. After orbit injection, there is a switchover to the 120-watt OS-2 transmitter for transmission of the TV mapping data and relay of surface scientific measurements made by the lander vehicle. Data relay continues for 6 months.

2.5 Environmental Conditions

The environmental conditions anticipated for each segment of the spacecraft flight are summarized in tables 5, as supplemented by tables 6 and 7 and figures 4, 5, and 6.

	Event	Function	Comments -- Method of Command	Time
32.	Receive and store information for : a)time and direction of lander launch and ΔV magnitude. b) Direction and magnitude of orbiter retrothrust			
33.	Null rate integrating gyros	For attitude memory		
34.	Orient vehicle for lander launch			
35.	Separate lander			S
36.	Renull gyros			
37.	Orient orbiter to retrothrust attitude			
38.	Null axial accelerometer			
39.	Stow antennas and sensors on booms			
40.	Retrothrust orbiter	To obtain ΔV so that orbiter lags lander		
41.	Command thrustoff			
42.	Deploy antennas and sensors			
43.	Reorient orbiter to resume cruise			
44.	Turn on planet tracker	For terminal guidance		
45.	Aim planet tracker along expected LOS by orienting vehicle.			
46.	Acquire lock-on to planet			
47.	Take a navigational fix on planet	To refine computed position		
48.	Reorient vehicle for thrust			
49.	Stow antennas and sensors			

	Event	Function	Comments-Method of Command	Time
17.	Turn on digital control unit (DCU)	For first midcourse correction	DSIF command	M - 2 hr.
18.	Turn on rate integrating gyros	For attitude memory	Events 18 to 28 programed by DCU	M - 2 hr.
19.	Receive and store reorientation commands and (ΔV) command			M - 1 hr.
20.	Null rate integrating gyros	For attitude memory		M - 0.6 hr.
21.	Perform reorientation for thrust	$\Delta\psi$, then $\Delta\theta$		M - 0.5 hr.
22.	Null axial accelerometer output	To measure ΔV		M - 0.1 hr.
23.	Stow antennas and sensors mounted on booms			
24.	Command thruston	To acquire ΔV for trajectory correction		M
25.	Command thrustoff based on ΔV	To acquire ΔV for trajectory correction		
26.	Reorient vehicle to reference attitude (Sun-Canopus axes)	To resume cruise mode		M + 0.5 hr.
27.	Acquisition mode -- reacquire Sun, Canopus, Earth			M + 0.6 hr.
28.	Turn off DCU			M + 1 hr.
29.	Resume cruise mode. Repeat steps 17 to 28 for additional midcourse corrections.		Corrections will be made at 1 week and 2 weeks after launch (T) and at 10,000,000 km before encounter. Last correction adjusts time of arrival.	
30.	Turn on DCU	For lander orbiter separation operations	DSIF command	S - 2 hr.
31.	Turn on gyros	For attitude memory	Events 30 to 70 programed by DCU with DSIF command as backup	

Event	Function	Comments-Method of Command
1. S-1 engine ignite	Main booster engine	
2. Liftoff		Booster time periods are typical for 1969 launch
3. S-1 engine cutoff		
4. Staging	Separation	
5. S-4B engine ignite	Second stage engine	
6. Eject nose fairing	Jettison payload shroud	
7. S-4B engine cutoff		Begin parking orbit
8. Staging	Separation	
9. Coast in orbit		
10. S-6 engine start	Injection into transfer orbit	
11. S-6 engine cutoff		
12. Jettison S-6 engine Activate Voyager G&C		Discrete signal from Saturn G&C
13. Acquisition mode	For P + Y control	DCU command
a. Acquire Sun w/Sun sensor, and orient roll axis along the sun line		
b. Acquire Canopus with tracker and orient in roll by Canopus	For roll control	
c. Acquire Earth	For antenna orientation	By ground command
14. Turn on OS-1 transmitter	For tracking and verification of commands and transmitting scientific measurements	DSIF command. OS-1 transmitter is turned on and off regularly in transit. See figure 1 for in-transit and orbital scientific measurement sequence.
15. Turn off OS-1 transmitter		DSIF command
16. Maintain Attitude control with SS&C tracker inputs and reaction jets	For vehicle orientation during cruise mode	

Time			Function	Comments -- Method of Command	Time
			To correct interplanetary orbit		
- 0		sors			
+ 2. 55 min.		r			
		and nder			
+ 2. 59 min.		:scent			
+ 3. 37 min.		o- c			
+ 10. 4 min.		·s			
+ 56. 4 min.		; in	To obtain desired planetary orbit		
+ 61. 8 min.		ors			
+ 5 min.		·e			
		·S			
+ 15 min.			To obtain local vertical		
+ 25 min.		cal			
			To relay scientific data	OS-1 transmitter is backup	
M - 2 hr.		:e			

-6-

TABLE 2

MARS VOYAGER MISSION PROFILE--LANDER (After Separation)

	Event	Function	Comments--Method of Command	Time
1.	Mechanical separation of lander and orbiter		Orbiter DCU	S
2.	Start communication and instrumentation programmer, operations sequencer and navigation computer clock.		Discrete signal from orbiter G&C Note: All commands are from operations sequencer unless otherwise noted.	S+25 msec
3.	Turn on LS-1 transmitter low bit rate	For transmitting engineering status data to orbiter and survival information to DSIF	Transmitter will be turned on and off at regular intervals.	S+50 msec
4.	Electrical disconnect		Orbiter DCU	S+100 msec
5.	Eject lander		Spring mechanism	S+100 msec
6.	Initiate spin rockets. Jettison sterilization can by cutting with shaped charge.	Stabilization to reduce launch angle error		S+100 msec
7.	Ignite main lander rockets	To reorient lander trajectory to achieve impact		S+5 sec.
8.	Terminate thrust after obtaining required ΔV		Accelerometer switch	

TABLE 2 (Cont'd)

	Event	Function	Comments--Method of Command	Time
9.	Power sensors for accelera-tion, pressure and altitude measurements during entry. Start programmed sequence of scientific and engineering measurements during entry and descent			D - 1/2 hr.
10.	Turn on high bit rate output of LS-1 transmitter	Transmit engineering status data, entry measurements, and survival data in real time	Accelerometer switch	D - 1/2 hr.
11.	Record scientific and en-gineering data during initial entry and blackout period			
12.	Fire drogue chute at preset Mach number (2.5)	Reduce velocity	Base pressure and accelerometer measurements used to determine Mach number	D-5 min. to D-10 sec. (Depends on atmosphere properties and trajectory
13.	Ignite shaped charge which jettisons front and rear heat shields, drogue chute and at same time pulls out main chute.		Radar altimeter to open main chute at 10,000 to 20,000 feet	D

TABLE 2 (Cont'd)

Event	Function	Comments--Method of Command	Time
14. Turn off LS-1 transmitter			D
15. Turn on LV-1 transmitter	Transmit descent and impact data		
16. Turn on LS-2	Transmit survival data to DSIF		
17. Record descent data and TV pictures			
18. Playback recorded data and real time data to orbiter relay via LV-1 transmitter			L-5 min.
19. Impact planet surface			L
20. Release parachute			
21. Actuate mechanism to erect vehicle			
22. Stop playback of recorded data			L+5 min.
23. Turn off LV-1 transmitter			L+5 min.
24. Turn off LS-2 transmitter			
25. Activate attitude sensing system	For antenna orientation		

TABLE 2 (Cont'd)

Event	Function	Comments--Method of Command	Time
26. Erect parabolic antenna for DSIF communication			
27. Activate navigation computer to determine direction of Earth. Orient antenna.		System consists of sun sensor, pendulum to determine local vertical and clock	
28. Start programmed scientific instrumentation sequences for surface measurements and record data.		See figures 2 and 3 for details of instrumentation sequences.	
29. Turn on LS-3 transmitter and playback recorded scientific data		DSIF command	After L+40 hrs. (transmit 4 hrs. every day)
30. Turn on LV-1 transmitter on command from orbiter relay and playback recorded data.		Orbiter relay command - altimeter on orbiter produces coded pulses in orbiter transmitter output which turns on LV-1 transmitter	After L+40 hrs. (transmit 15 min. every 1 to 3 days)
31. Turn on LS-2 transmitter		DSIF or orbiter relay command. Backup system only 2 BPS data rate	

TABLE 2 (Concl'd)

Terminology

T - time of liftoff

S - spacecraft separation time

I - time of injection into transfer orbit

E - planetary encounter

V - change in spacecraft velocity

λ - Canopus angle

ψ - heliocentric angle

M - time of midcourse correction

D - time of planet descent (opening of main chute)

L - time of planet landing

DCU - digital control unit

Transmitters

Orbiter OS-1 - S band, 4-foot parabola, 35 w.

OS-2 - S band, 8-foot parabola, 120 w.

Lander LS-1 - S band, omni, 35 w.

LS-2 - S band, slot, 120 w.

LS-3 - S band, 5-foot, parabola, 120 w.

LV-1 - VHF, slot, 120 w.

TABLE 3

VENUS VOYAGER MISSION PROFILE -- ORBITAL MISSION

The Venus mission profile differs from the Mars mission for the following events:

Event	Function	Comments -- Method of Command	Time
13c. Acquire Earth	For antenna orientation	By ground command with Earth sensor as optional backup.	I + 25 min.
29. Resume cruise mode. Repeat steps 17 to 28 for additional corrections.		Corrections will be made 1 week and 2 weeks after launch (T) and at 10,000,000 km before encounter. The last correction only corrects trajectory and not time of arrival	
66. Turn on radar	For mapping planet surface	Dense cloud cover precludes use of TV.	

In an alternate design for the Venus lander, separation and launch take place after orbit about the planet is established in order to slow down the vehicle before entering the dense atmosphere. In this design, only atmospheric measurements are made and the vehicle does not survive impact. Launch from orbit necessitates changes in the sequence of events. Events 30 through 43 are taken out of sequence and replace events 56 through 62.

TABLE 4

VENUS VOYAGER MISSION PROFILE -- LANDER
(After Separation)

Event	Function	Comments -- Method of Command	Time
2. Start communication and instrumentation programmer and operations sequencer.		Discrete signal from orbiter G&C	S + 25 msec
12. Eliminate step			
16. Eliminate step			
21. Eliminate step			
24. to 27. Eliminate steps			
29. Eliminate step			
31. Eliminate step			

In the alternate design, only atmospheric measurements are made. The mission profile ends at step 19.

TABLE 5

ENVIRONMENTAL CRITERIA FOR VOYAGER

Environment	Phase 1	Phase 2	Phase 3	Phase 4	Phase 5	Phase 6	Phase 7
	Transportation from factory to launching site	Handling and checkout at launch site, assembly onto booster, checkout on launching pad	Powered flight, injection into interplanetary orbit	Cruise	Atmospheric entry of lander vehicle	Lander vehicle on surface of planet	Orbiter vehicle in orbit about planet
Configuration and Duration	The spacecraft will be disassembled and packaged for shipment in containers providing vibration isolation. All shipments will receive special handling and will be shipped by air transportation. Shipping time will not exceed 12 hours. Possible time standing in containers is 2 weeks.	The spacecraft will be assembled and checked out in a controlled atmosphere. It will then be assembled into the fairing along with the third stage engine and placed atop the booster checkout time is about 2 weeks. Total time on launching pad is assumed not to exceed 2 weeks.	The spacecraft will be injected into interplanetary transfer orbit by three-stage Saturn booster. Time from launch to injection is about 1 hour.	The spacecraft is in unpowered flight on the interplanetary trajectory. Engine is turned on several times for midcourse corrections and separation maneuvers. The lander is separated from the orbiter approximately 10^6 Km from the planet. The flight time to Mars is up to 300 days and about 120 days for Venus.	The lander vehicle is subjected to the high heat loads and acceleration loads associated with atmospheric entry. There are additional mechanical loads on opening of drogue and main chutes. Total entry and descent time is from 10 to 20 min., depending on atmospheric model.	The lander vehicle lands on the planet. A programmed sequence of scientific measurements are made. Data are transmitted to DSIF, both directly and via orbiter relay. Measurements will continue for 6 months; however most of significant data will be obtained within 48 hours.	The orbiter vehicle establishes a 1500 km by 10,000 km about Mars and a 1000 km circular orbit in the case of Venus. The planetary surface is mapped and scientific data from the lander are relayed to DSIF for period of 6 months.
Temperature	-50 to 150 °F (25 °F temperature rise caused by solar radiation on shipping container)	60 to 80 °F in assembly checkout facility; 32 to 150 °F on launch pad; up to 300 °F for sterilization.	Temperature of spacecraft components is result of atmospheric heating and solar radiation. Temperature of equipment ranges from 0 to 150 °F operating, 0 to 300 °F nonoperating. Temperature of solar panels and sensors may be as high as 220°F.	Same comment as for Phase 3	Same comment as for Phase 3	Mars: -100 to 85 °F Venus: 800 °F on surface; 200 °F at bottom of cloud layer, about 70 km altitude, -30 to -60 °F at top, 100 km altitude	Same comment as for Phase 3
Pressure	760 mm Hg to 86 mm Hg at 50,000 feet	Normal sea level ambient	Sea level to 10^{-12} mm Hg	10^{-12} mm Hg	Mars: 10^{-12} mm Hg to 85 mb (recent estimate of 20 mb) Venus: 10^{-12} mm Hg. to 10 atm	Mars: 85 mb (recent estimate of 20 mb) Venus: 10 atm	10^{-12} mm Hg
Humidity	0 to 100 percent R.H.	0 to 100 percent R.H.	Not applicable	Not applicable	Not applicable	Not applicable	Not applicable
Sand and Dust	Dust particles up to 0.001 mm in diameter with a concentration of 1000 particles/cm³ in a still atmosphere	Same as Phase 1	Not applicable	Not applicable	Not applicable	To be determined	Not applicable
Fungus	The fungus environment will be considered to be that simulated by the test specified in paragraph 4.8.1 of MIL-E-5272	Same as Phase 1	Not applicable	Not applicable	Not applicable	Not applicable	Not applicable
Precipitation	Rain -- max. rate of 4 in/hr blown by a 60 mph wind; Snow -- precipitation rate up to 4 in/hr; Hail -- 0.5 to 15 mm dia meter, max. rate of 4 in/hr; Ice -- exterior coating of 0.5 inch at 0 °F	Same as Phase 1	Not applicable	Not applicable	Not applicable	Not applicable	Not applicable

TABLE 5 (Concl'd)

	Phase 1	Phase 2	Phase 3	Phase 4	Phase 5	Phase 6	Phase 7
Atomic Radiation From Natural Sources	Negligible except for cosmic rays	Same as Phase 1	See Table 1	See table 1. Intensity of Solar Flare varies with distance from sun similar to solar radiation in figure 1.	Radiation environment of Mars and Venus is not known. Atmosphere should provide some shielding against solar flares and cosmic range.	Comments for Phase 5 apply.	Solar flare and cosmic ray data of table 1 are applicable with adjustment for distance from sun.
Solar Radiation	0.113 w/cm², 0.054 to 0.086 w/cm² in the wave length range above 7800 A. See table 2. Atmosphere absorbs all ultraviolet radiation below about 2900A and attenuates up to 3500A.	Same as Phase 1	At Earth's mean distance (1 AU), the total solar electromagnetic flux is 0.140 w/cm². Table 2 gives the energy distribution. Figure 1 gives the variation of intensity with distance from the sun.	See table 2 and figure 1	See table 2 and figure 1. Atmosphere will attenuate radiation.	Comments for Phase 5 apply.	See table 2 and figure 1. There should be very little attenuation of radiation at orbital altitudes.
Meteoroids (meteorites, meteors, dust)	Not applicable	Not applicable	Meteoroid flux is given in figure 2. Meteoroid velocities range as high as 72 km/sec. relative to Earth, with the average from 3 to 10 km/sec. Frequency of perforation is given in figure 3.	Comments for Phase 3 apply. In interplanetary space, the dust concentration increases toward the Sun as about the -3/2 power of solar distance. Out of the ecliptic plane, the concentration is believed to decrease by a factor of 2 within 15 degrees, with little dust beyond 20 degrees.	Atmosphere should provide shield against meteoroids.	Same as Phase 5	Same as Phase 4
Vibration	The maximum vibration that the packaged spacecraft will experience will be considered to be. Freq. Range cps / Vibration d.a. or peak / g 2 to 26 — ± 1.3g 26 to 52 — ± 0.036 in. 52 to 300 — ± 5g	The max. vibration that the unpackaged spacecraft will receive during handling and transportation can be represented by Freq. Range cps / Vibration g rms 2 to 50 — ± 3.5 50 to 300 — ± 1.5	The maximum vibration level should be below 0.01 g²/cps from 5 to 200 cps and 0.003 g²/cps from 200 to 3000 cps.	Negligible	Negligible	Negligible	Negligible
Shock	The shock conditions for shipping and storage will be considered to be as per MIL-P-7936.	100 g half-sine pulse for a duration of 11 m sec. applied along 3 principal axes in both directions	Negligible	Negligible	See Acceleration Load	See Acceleration Load	Negligible
Acoustic Noise	Not applicable	Not applicable	Up to 155 db.	Not applicable	Not applicable	Not applicable	Not applicable
Acceleration Load	Not applicable	Not applicable	Axial load: 5 g Lateral load: 1g	Negligible	Mars: 130 g max on entry for $M/C_D A = 0.9$ and Schilling atmospheric model; 13 g as result of drogue chute opening Venus: 340 g max for direct entry, $M/C_D A = .6$, Kaplan atmospheric model; 185 g max for entry from orbit.	Impact load will not exceed that due to entry	Negligible

TABLE 6

RADIATION DOSAGES IN SPACE PRODUCED BY ATOMIC PARTICLES

		Energy (ev)	Ionization, erg/gm-yr[1]		
			Extreme Surface	Through 1 mg/cm^2	Through 1 gm/cm^2 [2]
Inner Radiation Belt 400/1200 km to 10,000 km	protons	10^3 to 7×10^8	10^{12}	10^{11}	10^7
	electrons	$< 2 \times 10^4$ to 10^6	10^{14}	10^{14}	0
	photons[3]	$< 2 \times 10^4$ to 10^6	10^7	10^7	10^7 to 10^8
	total		10^{14}	10^{14}	10^7 to 10^8
Outer Radiation Belt 10,000 km to 60,000/85,000 km	electrons	2×10^4 to 5×10^6	10^{13} to 10^{15}	10^{13} to 10^{15}	10^5
	photons	2×10^4 to 5×10^6	10^7 to 10^9	10^7 to 10^9	10^6 to 10^8
	total		10^{13} to 10^{15}	10^{13} to 10^{15}	10^6 to 10^8
Solar Flares	Protons	2×10^7 to 10^9	10^5 to 10^6	10^5 to 10^6	10^4 to 10^5
	electrons	$\sim 5 \times 10^4$	10^7 to 10^9	10^7 to 10^9	0
	photons	$\sim 5 \times 10^4$	10^2 to 10^4	10^2 to 10^4	10^2 to 10^4
	total		10^7 to 10^9	10^7 to 10^9	10^4 to 10^5
Cosmic Rays	protons	10^8 to 10^{17}	10^2 to 10^3	10^2 to 10^3	10^2 to 10^3

Notes: (1) 1 roentgen = 93 erg/gm
        1 rad = 100 erg/gm
    (2) Earth's atmosphere places about 1000 g/cm^2 between the surface and space.
    (3) Bremstrahlung photons

TABLE 7

ENERGY DISTRIBUTION OF SOLAR ELECTROMAGNETIC RADIATIONS

Type	Wavelength Interval (angstroms)	Approximate Percentage of Radiant Energy
X-ray	1 to 2000	0.2
ultraviolet	2000 to 3800	7.8
visible	3800 to 7000	41
infrared	7000 to 10,000	22
infrared	10,000 to 20,000	23
infrared	20,000 to 100,000	6

Notes: 1. At Earth's mean distance from the sun (1 AU) the total solar radiant flux is 0.140 w/cm^2. The value of this factor in various systems of units is as follows:

1.40×10^6 erg/cm^2 - sec
2.0 cal/cm^2 - min
440 Btu/ft^2 - hr

At the orbit of Venus, the intensity of solar radiation will be 1.9 times that at Earth's orbit, and at the orbit of Mars, 0.43 times.

    2. Albedo factor (reflectance)
        Earth: 0.40
        Venus: 0.65
        Mars: 0.14
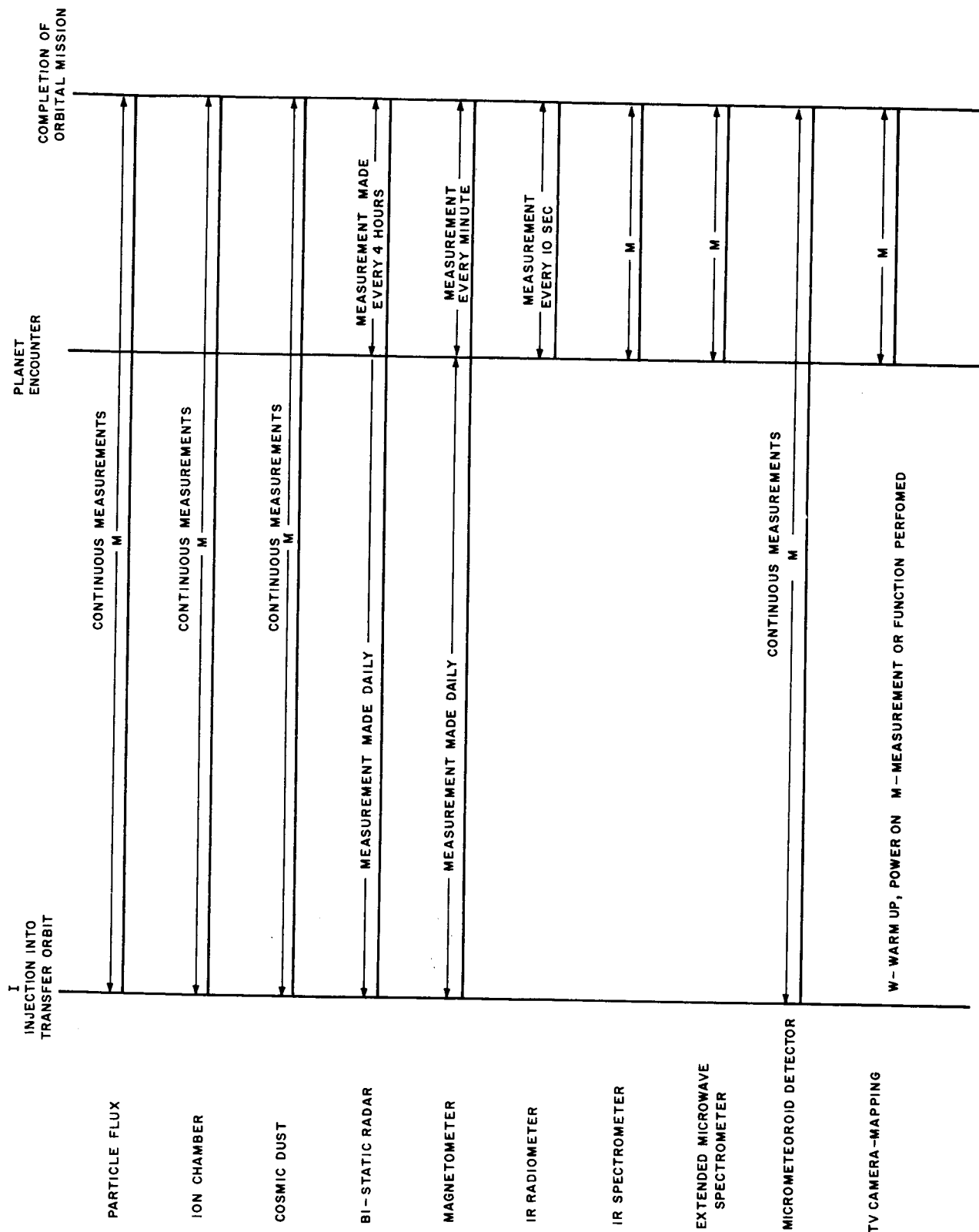
FIGURE 1 IN-TRANSIT AND ORBITAL SCIENTIFIC MEASUREMENTS

63-8902

-17-

63-8903

Figure 2 PLANETARY SCIENTIFIC MEASUREMENTS

63-8904

63-8906

ADVANCED MASS SPECTROMETER — MEASUREMENT HOUR FOR 12 HR — L+13 HRS — MEASUREMENT ONCE EVERY 12 HRS — MEASUREMENT ONCE EVERY 2 DAYS

PETRO MICROSCOPE — 1/2 HR PER MEASUREMENT — 12 MEASUREMENTS OVER 6 MONTH PERIOD — L+1HR L+2HR L+3HR L+4 L+4.5HR

X-RAY SPECTROMETER — L+1HR — MEASUREMENT EVERY 10 MIN FOR 24 HOURS — MEASUREMENT EVERY 12 HRS — MEASUREMENT ONCE EVERY 2 DAYS

TURBIDITY AND PH GROWTH — L+4HRS — 2 MEASUREMENTS PER HOUR FOR 21 DAYS

CORE DRILL AND MILL — L+1HR L+2HR L+3HR L+4HR 1HR 1HR 1HR 1HR 1HR — SAMPLE EVERY INCH OF DEPTH FOR 12 INCH TOTAL DEPTH OVER 6 MONTH PERIOD

THREE AXIS SEISMOGRAPH

LANDING-VEHICLE ERECTION L | L+24 HRS | L+1 WEEK | L+3 WEEKS | L+5 3/4 MONTHS | L+6 MONTHS

63-8905

X-RAY DIFFRACTOMETER — ONE MEASUREMENT EVERY 6 HRS — MEASUREMENT EVERY 12 HRS — MEASUREMENT EVERY 2 DAYS

GAS CHROMATOGRAPH

CELL GROWTH

LANDING VEHICLE ERECTION L | L+4 HRS | L+12 HRS | L+24 HRS | L+1 WEEK | L+5 3/4 MONTHS | L+6 MONTHS

63-9286

Figure 3 POWER PROFILE

TIME FROM LANDING, hours

LANDING

POWER, watts

SPIKES
1 SEC
990W

Figure 4 SOLAR RADIATION VERSUS DISTANCE
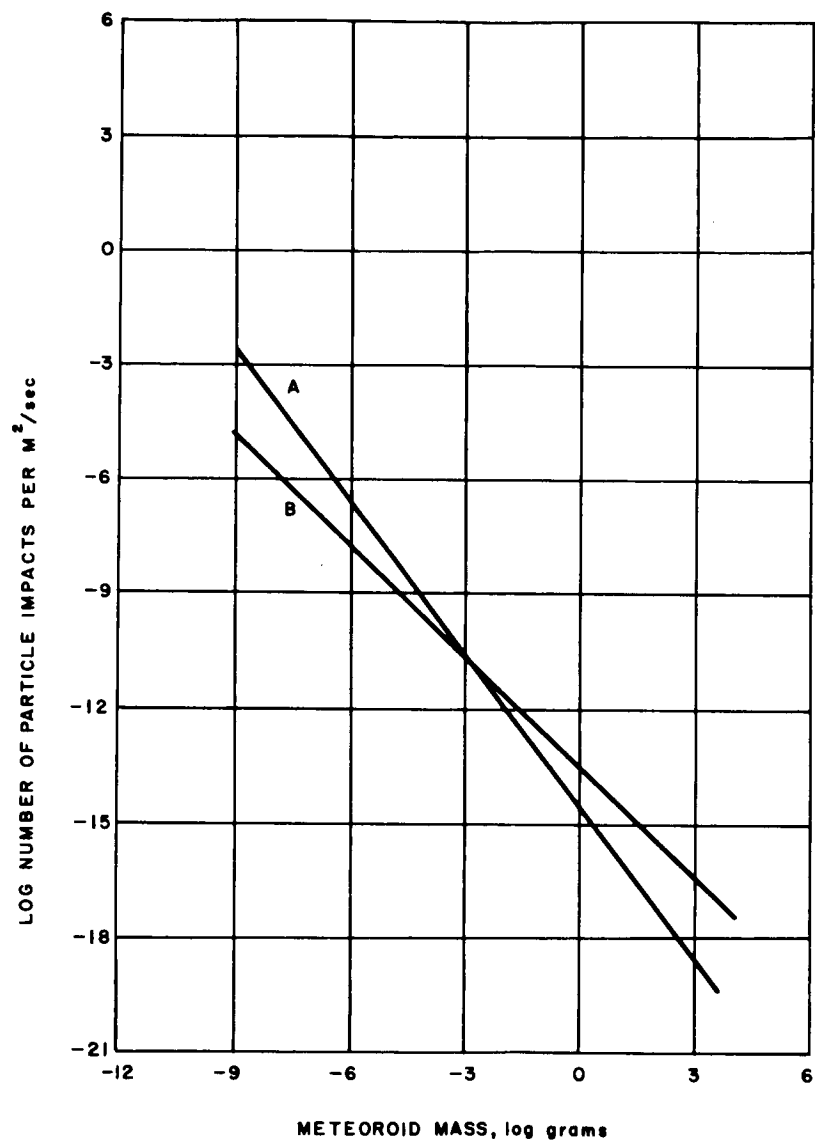
63-8898

63— 8899

Figure 5 CUMULATIVE METEOROID IMPACT RATE NEAR EARTH

-22-
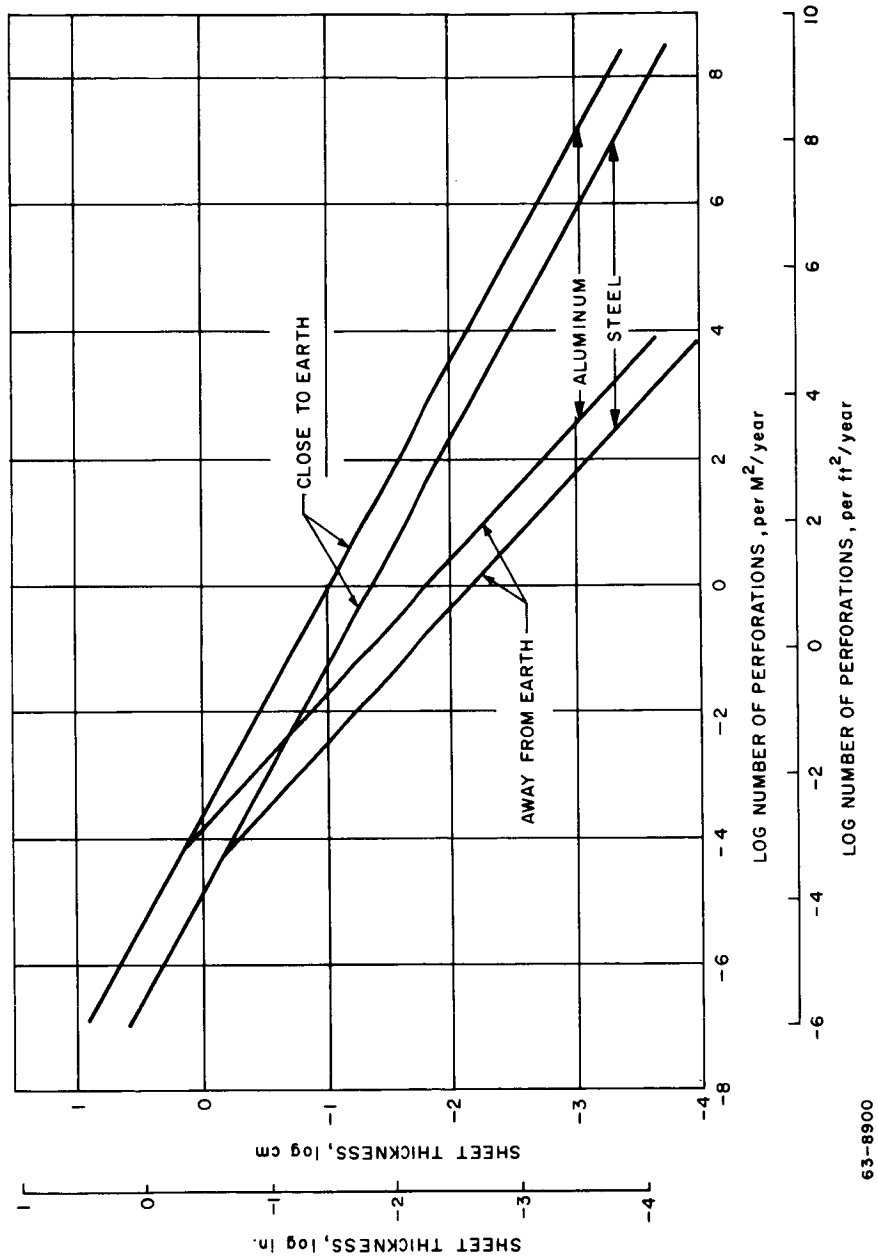
Figure 6 FREQUENCY OF METEORIC PERFORATION IN VICINITY
OF EARTH'S ORBIT

63-8900

3. MISSION TRADEOFFS

3.1 Introduction

In the process of the Voyager Spacecraft Study, certain mission tradeoffs were investigated. The results of these tradeoffs were strongly influenced by the Voyager scientific objectives, weight limitations, and launch window constraints which were furnished to the study. As the study progressed, major mission tradeoffs were made which, in turn, influenced the final spacecraft configuration:

1. The decision was made to split the mission of the spacecraft into an orbiting vehicle and landing vehicle on a single launch vehicle rather than to design a spacecraft that would be used as an orbiter or lander alone. This decision was the single most important result of the tradeoff studies.

2. The decision to design a split payload led to the selection of a booster with a 7000-pound payload capability. Studies showed that the split-payload spacecraft weight, necessary to meet program objectives with a high probability of mission success, was less than 7000 pounds but greatly in excess of 4000 pounds. The results excluded the use of a booster with only a 4000-pound payload capacity.

3. The decision was made to use a hard lander, a vehicle capable of completing its mission regardless of its attitude immediately following impact, rather than a soft lander, a vehicle always capable of maintaining its attitude prior to and immediately following impact. The hard lander was designed with a low-gain antenna system so that communications would not depend on its attitude. It was found that a high information transmission rate to Earth could be achieved if the orbiter, designed to perform scientific measurements, were also used as a communications relay.

4. The decision was made to incorporate design features into the spacecraft so that it could be adapted for exploration of both Mars and Venus, could carry more than one lander, and could also be utilized with a 60,000-pound spacecraft. In general, it was found that this adaptability could only achieved with some moderate degree of spacecraft modification.

3.2 Split Payload

The advantages of the split payload are manifest in the many possible design relaxations and subsequent design improvements that are permitted in the

overall Voyager spacecraft. The most important of all spacecraft design relaxations that can be achieved with the split payload mission concept lies in the lander antenna system. A low-gain antenna system which is independent of lander attitude can be used for Mars and Venus rather than a high-gain antenna system which is dependent on lander attitude. Scientific mission studies have indicated that a high bit rate for transmission of information is necessary if the Voyager mission objectives are to be achieved. Direct communication from the planet to Earth requires a high-gain antenna to obtain a high data rate; whereas a high data rate can be achieved from a low gain lander antenna if an orbiter is used as a communications relay. During the early missions, when the surface characteristics and low-altitude atmospheric environment of the planets will not be known, studies have shown that it will be relatively difficult to design a lander that will have a high assurance of landing in a designed orientation. The proper orientation of the lander is paramount to the use of a high-gain antenna for direct transmission of information at a high data rate. Studies of Martian landers have indicated that information can be transmitted at 1500 bps through a 5-foot antenna. If the lander attitude cannot be assured so that a low-gain antenna direct link system must be used, studies have indicated that the anticipated bit rate will be less than 5 bps. Mission objectives will not be met at this bit rate. By using a low-gain antenna system for transmission of information through the orbiter, information can be transmitted at the rate of 10,000 bps. The orbiter is designed to transmit about 4500 bps from Mars to Earth through its communication system which incorporates a high-gain antenna. The resultant bit rate achievable by the use of a low-gain antenna system in the lander with an orbiter as relay would be 4500 bps. This approach relaxes the problem of lander attitude, but introduces an additional communication link. It seemed judicious to choose a system which was independent of lander attitude and defendent upon the calculable reliability of an orbiter link, rather than a system which was dependent on the lander attitude designed for landing on an unpredictable surface.

The concept of coordinating the orbiter and lander to complement each other's scientific investigations is most attractive. For instance, during the passage of the wave of darkening over the Martian surface, dual measurements from an orbiter and lander would be more significant than from either one alone.

Another advantage accruing from the split payload using the orbiter as a relay is the relaxation in landing site. Although current scientific mission analyses have indicated that the landing site would be visible to Earth after landing so that direct communication can be used as a backup to relay communication, the use of an orbiter as a relay would permit landing in latitudes that would not be visible to Earth for months.

The split payload of an orbiter and lander is also consistent with the desire to achieve a single Voyager spacecraft design that could be used for the duration of the program. If an orbiter(s) is sent on a single booster, then a bus mode of operation must be provided for the interplanetary cruise. This mode

must include guidance, attitude control, midcourse propulsion, monitoring of external influences, such as meteoroid and high-energy-particle disturbances, and internal monitoring of operating conditions. This information must be communicated back to Earth if the spacecraft performance is to be evaluated. For an orbiting mission, a vehicle will have to be provided with all of these functions; the approach has been to design the orbiter to fulfill its orbital mission objectives and also to use its systems for the bus mode. Since the orbiter is also a bus, there is very little penalty for adding a lander. In contrast, if a lander(s) is sent on a single booster, then a bus mode must be provided. It is for these reasons that the orbiter is referred to as an orbiter/bus. The major difference between the orbiter and bus requirements is the propulsion system. The propulsion system required for the bus mode of operation must provide an incremental velocity capability of about 0.2 km/sec, whereas the propulsion system for the orbiter mode of operation must be capable of 2 to 4 km/sec. It is possible to design a propulsion system that can accommodate both propellant loadings. The main penalty resulting from this dual-purpose propulsion design is that about 400 pounds of unnecessary dry propulsion system must be carried for the bus mode of operation, if a redesign of propulsion tankage is to be avoided.

3.3 Selection of 7000-Pound Spacecraft

Design studies have indicated that the characteristic weight of the split payload Voyager spacecraft that is consistent with the scientific mission objectives with a high probability of success is compatible with the 7000-pound class of vehicle. Studies have also shown that the spacecraft for Mars would be divided into 4000 pounds for the orbiter and 1700 pounds for the lander; for Venus, the spacecraft weight with the atmospheric capsules would be 5500 pounds for the orbiter and a total of 570 pounds for the capsules. These weights are less than the 7000-pound characteristic weight, but considerably greater than 4000 pounds. Therefore, the split-payload spacecraft that has been designed to fulfill the Voyager mission objectives, and achieve a high probability of success over the lifetime of the program, is compatible with the 7000-pound spacecraft. It is possible to design a 4000-pound, split-payload spacecraft, but either the mission objectives would have to be lowered, or the probability of success be reduced.

3.4 Hard-Lander Decision

Many types of landing systems have been investigated, and they may be categorized into two basic classes: those systems that always remain erect, that is, in an upright position during and after impact, and those that are toppled during the impact phase. The class that topples can be further divided into two

categories: those systems that allow for reerection of the lander after impact, and those systems that permit operation in any attitude. The designation of hard lander implies a high-impact velocity and soft lander implies a low-impact velocity. A soft-landing system, which can use a retrorocket system to effect touchdown, will generally be a system that would also be designed to stay erect. A hard-landing system can fall into both categories, that is, both erect and re-erect. Figure 7 shows examples of the various classes of landing systems considered.

The main limitation in the soft lander lies in the accuracy of the sensors required during the controllable descent and not in the control system itself. If touchdown velocities are to be controlled within 10 ft/sec or less, it was found that the lander must be controlled to within a few feet of the surface. Almost no free fall is permissible if the 10 ft/sec impact velocity is not to be exceeded. If free fall is not allowed, then the only error in the vehicle's terminal velocity will be limited to the accuracy to which the velocity can be determined. The problem of sensing velocity below about a 20-foot altitude where velocimeters are no longer accurate can be circumvented by the introduction of integrating accelerometers. Horizontal velocity can be sensed by means of three symmetrically placed doppler radar antennas. An error analysis has shown that 3 ft/sec (3σ) random error due to each beam results in a horizontal velocity error of about 10 ft/sec (3σ). Perturbations due to gust loads on the lander have not been factored into the study. Even if the lander achieves a soft touchdown, it is questionable whether it would necessarily remain in an upright position, due to uncertainties in the planet's topological features.

If the ability to remain in an upright position after soft landing is questionable, then it is doubtful that the soft lander is a sound approach. Current design calls for a hard lander with a reerection system to allow performance of the programed mission. However, partial mission success is assured even if it remains in a toppled state.

The design of a hard lander that reerects can be predicated on fewer assumptions about the topology of the planet than that of a soft lander. The use of a hard lander with orbiter relay relaxes the requirements placed upon the lander which must be designed for operation on an unknown surface. A hard lander can be designed to accommodate a wider spectrum of surface conditions for the same allowable weight. The orbiter relay can be designed for a narrower range of operating conditions since the upper atmospheric environment is known more accurately than the planetary surface. Thus the split payload mission and hard lander with a low gain prime communication link through the orbiter represents a sound engineering design. If the payload limitations will allow inclusion of the high-gain direct communications link within the lander design, an additional increase in system capability, reliability, and potential can be achieved.
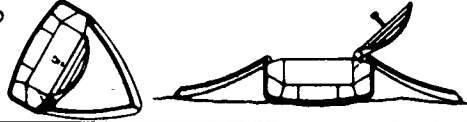
E R E C T	SOFT LANDER	1
	AIR BAG	2
	OUTRIGGER	3
RE- ERECT	CLAM SHELL	4
	SPHERE IN SPHERE	5
	TULIP BUD	6
STAY TOPPLED	TURTLE SHELL	7
	TETRAHEDRON	8
	POTTED SPHERE	9

Figure 7 LANDING SYSTEMS

3.5 Adaptability

It was found that the major modifications in the spacecraft designed for both Mars and for Venus occurred in the lander. For the lander, the thermo-structural shield for the two planets would be significantly different, representing two distinct design efforts. For the Venus lander, the payload would be immersed in a liquid-ammonia boiloff bath for limited-duration thermal protection. This would not be necessary for a Mars lander where passive thermal control can be achieved. The modifications required in the orbiter include the removal of the television cameras from the mapping gimbal on the Mars orbiter and replacement with microwave and radar antennas for the Venus orbiter. In addition, for the Venus spacecraft the number of solar cells could be reduced, and the surface coatings of the orbiter and lander changed to adjust to the significant difference in solar-radiation flux.

It was also found that the positions of the communication antennas and scientific instrument gimbal on the orbiter/bus would have to be altered to account for the varying look angle excursions for trips to two different planets. The decision to utilize a fixed-solar-cell panel will allow any clock angle position for an antenna or scientific instrument gimbal for both the single and twin lander orbiter configurations. The rather different propulsion requirements for missions to the two planets, and even between successive missions to the same planet, can be accommodated by a single propulsion system weighing 3860 pounds, 460 pounds of which is dry propulsion weight. With this propulsion system, the dual-planet mission objectives could be met. In general, if was found that for missions to Mars the propellant tanks would not have to be filled to capacity, and for Venus the tank size is too small to permit the spacecraft to achieve its maximum allowable injected weight, resulting in some weight penalty in each case.

The spacecraft could be designed to accommodate more than one lander for missions to both Mars and Venus, providing that the sum of the lander diameters did not exceed the nominal diameter of the spacecraft. A structural modification must also be made in the orbiter/bus if the landers are to be released at different times. To satisfy this design condition, a center support must be provided for the landers. The resulting loads from this support are carried through the orbiter/bus, but fortunately, along existing load paths, so that the resulting weight increase is less than 40 pounds.

Application of the orbiter designed for the 7000-pound split payload to a 60,000-pound spacecraft was also investigated. The 60,000-pound spacecraft has a characteristic diameter of 240 inches, the same as the 7000-pound spacecraft. Examples of adaptation of an orbiter/bus designed for a 7000-pound spacecraft and utilized with a 60,000-pound spacecraft are shown in figures 8 and 9. The orbiter/bus configurations that are shown represent early design concepts.

However, the design refinements that were finally incorporated into the reference design of the orbiter/bus would not alter the adaptation approach presented. In concept, the orbiter/bus for the 7000-pound spacecraft would serve as a bus for the 60,000-pound system. Figures 8 and 9 show the orbiter/bus with a Mars entry capsule that has been scaled up to take advantage of the larger weight and dimension limits. To arrive at some criterion for establishing the spacecraft configuration, a lander concept was selected. With this large available weight, a roving vehicle would be a desirable payload for the Voyager. A sterilization can is also shown, although by the time such a large payload could be launched, sterilization requirements may have been reduced. In figure 8 the orbiter/bus is mounted so that its inertial loads during launch are carried by the lander, and in figure 9 the orbiter/bus and lander loads are transmitted independently to the spacecraft adapter. In both cases, the load paths were chosen to require no modification of the spacecraft structure. It is to be noted that both figures cite that the gross spacecraft weight is 50,000 pounds. Based on an allowable impact velocity, a corresponding M/C_DA can be evaluated. The M/C_DA and allowable lander diameter furnished by the booster shroud constraint led to an entry vehicle weight of 46,000 pounds. The orbiter/bus with propellant weighs about 4000 pounds, for a total spacecraft weight of 50,000 pounds. The impact velocity limitation is arbitrary, however. If the spacecraft weighs 60,000 pounds, the greater impact velocity resulting from the increased M/C_DA could be offset by the introduction of a retropropulsion system to achieve the lower impact velocity.

A brief study showed that the propulsion system sized for midcourse corrections of the orbiter/bus and injection of the orbiter/bus into an orbit was compatible with the propulsion system that would be required for midcourse corrections of the much larger spacecraft. The 460-pound propulsion system for the nominal orbiter/bus design can contain about 3400 pounds of propellants. Only 2800 pounds of propellant are required for the midcourse velocity corrections of a 60,000-pound spacecraft. The major incompatibility was the size of the attitude control system. For the 7000-pound spacecraft, 22 pounds of cold gas are required for the mission life. The gross weight of the reaction control system is about 50 pounds. For the 60,000-pound spacecraft, 100 pounds of cold gas are required, and the total system weight is about 250 pounds. If a hypergolic system which draws reaction mass from the main propulsion system is used, then only about 24 pounds of gas are required. The total weight of this system would be about 60 pounds, if the required tankage to contain this propellant is charged to the main propulsion system. Another problem that would possibly arise, but which has not been fully explored, is the look-angle interference of this much larger spacecraft.
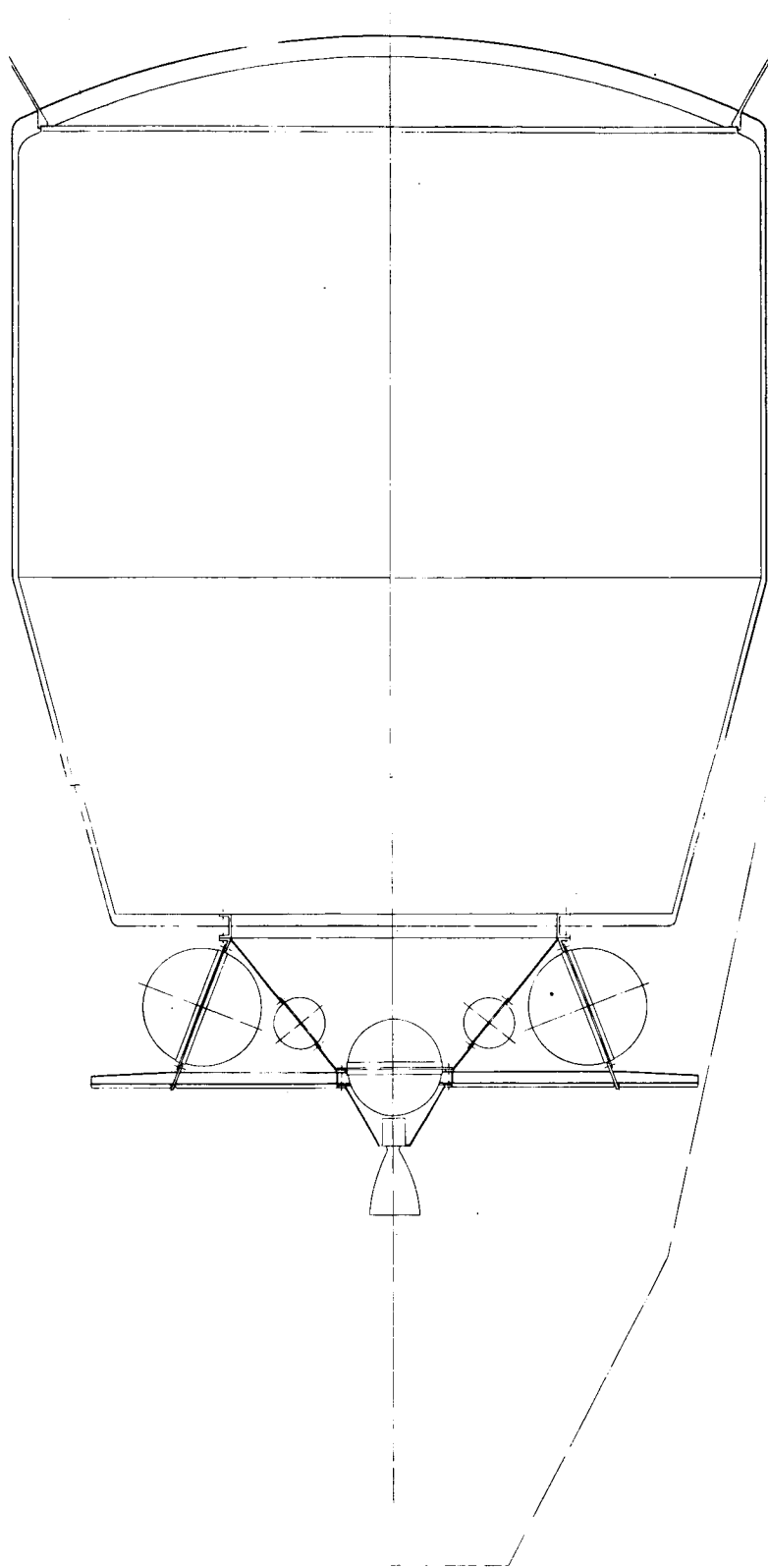
Figure 8 ORBITER-BUS WITH 46,000-POUND ENTRY VEHICLE -- CONCEPT I

-31-
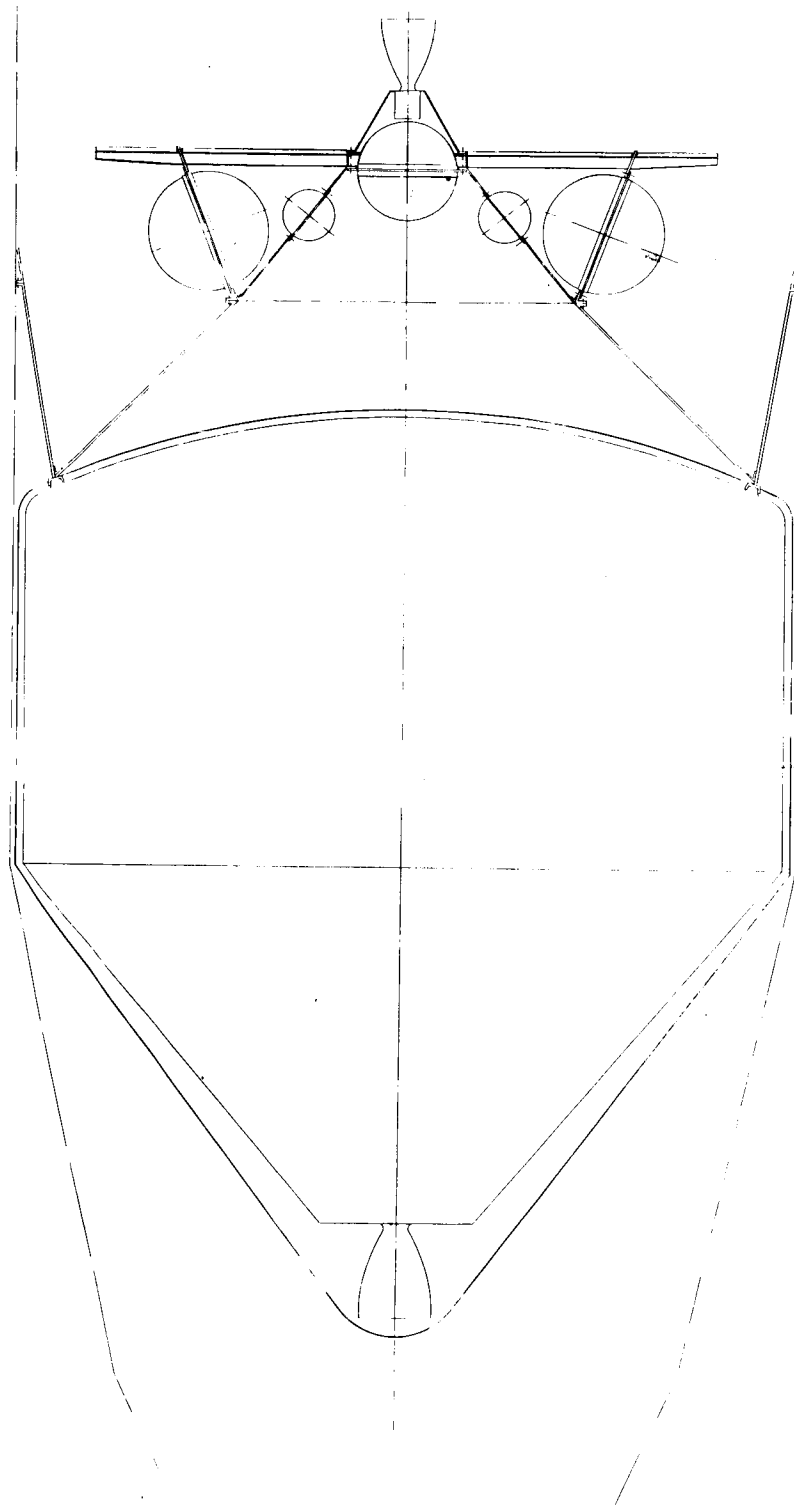
Figure 9 ORBITER-BUS WITH 46,000-POUND ENTRY VEHICLE -- CONCEPT II

3.6 Summary

In conclusion, the major system tradeoff result has been the selection of a split-payload spacecraft. It was found that not less than a 7000-pound spacecraft is compatible with a split payload that can achieve mission objectives with a high probability of success. The design of a hard lander to increase the probability of a successful landing is compatible with the split payload spacecraft in that relay through the orbiter from a low gain antenna system will still allow for a high bit rate of information transmitted to Earth. A common orbiter/bus can be designed with one or two landers and adapted for missions to both Mars and Venus. Finally, the 7000-pound spacecraft can be adapted to a 60,000-pound spacecraft with major alteration only to the attitude control system.

4. PAYLOAD STUDIES

4.1 Introduction

An integral part of a preliminary design study for an interplanetary mission entails analysis of the various trajectory characteristics associated with each launch opportunity. In theory, there are an unlimited number of possible interplanetary trajectories for a given target planet as there are at least four trajectory paths per given departure energy per day. This vast wealth of information can be reduced to a tolerable limit by the employment of realistic engineering constraints. An evaluation of the characteristics of present and proposed boost vehicles in conjunction with desirable mission payloads places an upper bound on the injection energy requirements. Additional engineering constraints which must also be considered are:

1.   Maximum communication distance at encounter and at termination of the scientific mission

2.   Vehicle-sun distance for thermal considerations

3.   Approach geometry that yields favorable lighting condition at encounter for lander vehicles and proper orbital orientation for the mapping and scientific functions of the orbiter vehicle

4.   Time of flight for reliability considerations (even though the heliocentric transfer angle is constrained to be less than 360 degrees, times of flight to Mars can exceed 400 days)

5.   Launch azimuth constraint which eliminates from consideration those trajectories where the declination of the geocentric asymptote exceeds the maximum orbital inclination achievable with an AMR launch. (This constraint may be relaxed or removed entirely by the employment of a dog-leg maneuver.)

With these and additional engineering constraints, the range of acceptable departure trajectories approaches manageable proportions for each launch opportunity.

Since the cost per pound of scientific payload is extremely high for a Voyager type interplanetary program, it is obvious that either scientific payload or the desired planetocentric orbit must be maximized for each launch opportunity. There is a marked payload variation associated with the various launch opportunities due to the changing energy requirements associated with the fact that the planetary orbits are neither circular nor coplanar with the ecliptic plane. The payload occurring at the extremity of the best 15-, 30-, or 45-day window associated with the minimum payload launch opportunity can be selected for the purpose

of mission commonality as the reference design. The achievable payload increase within this and the other launch opportunities can be utilized for additional scientific equipment, additional landers (if a split-capsule mission is envisioned), or redundant systems to improve mission reliability. An alternate approach to varying the mission payload is to select a reference payload and nominal orbit, and optimize (increase negatively) the orbital energy while maintaining a fixed payload and periapsis altitude.

The final optimizing approach selected is a function of the scientific mission, mapping techniques (optical or radar), and communication requirements.

4.2 Discussion

1. __Analytic solution.__ There is a variety of possible mission payload optimizing techniques, varying in complexity, depending upon the desired accuracy. An exact analytic solution is extremely difficult to formulate due to the number of variables. The weight injected into the heliocentric orbit is a function of the propulsion characteristics, staging, and trajectory profile of the boost trajectory. The hyperbolic excess departure velocity is a function of the launch and arrival dates while the hyperbolic excess approach velocity is a function of the transfer orbit characteristics and the components of the planet's orbital velocity at encounter (sphere of influence). Even if it is assumed that the maximum weight injected into the transfer orbit is known as a function of departure velocity, an analytic expression relating the departure and arrival velocities is required. The weight injected into the transfer orbit is a function of the departure velocity and the weight injected into the planetocentric orbit is a function of the arrival velocity. Therefore, if for a given launch date these velocities could be simultaneously minimized, the maximum weight would be injected into the heliocentric transfer orbit and subsequently into the planetocentric orbit. Since upon examination of the departure and arrival velocities it was found that the relationship between the velocities changed drastically from day to day within a given launch opportunity, this approach was not pursued further.

2. __Numerical techniques.__

a. __N-body trajectory program.__ After the configuration has been completely determined for each launch opportunity, i. e., all orbiter, orbiter-direct lander, fly-by lander, etc., the mission payload can be optimized by simulating the total mission, including thrusting periods for orbital trim requirements, with an N-body trajectory program. This method can be used to obtain the variation in payload as a function of time of flight for a single launch date and an iteration performed to determine the daily maximum payload as well as the variation in the daily maximums for the complete launch opportunity. While yielding accurate payload weights, this method is extremely time-consuming due to the general complexity associated with such a program.

b. Two-body trajectory program. The same iteration process, previously mentioned, can also be achieved with a two-body program with less accurate results due to the approximate nature of the departure and arrival velocities. This procedure is essentially the one performed with velocity information obtained from ref. (1).

4.3 Employment of Minimum Departure Velocity

With the summary trajectory information supplied by JPL to be employed in the Voyager Program payload analysis, the trajectory parameters associated with the daily minimum departure velocities are most accurately obtained at the vertical asymptotes at the extremes of a given energy contour. Since the daily minimum departure velocity maximizes the weight injected into the heliocentric transfer orbit, this velocity was utilized in determining initial values for optimum launch periods in a given launch opportunity and the associated mission payloads.

The configurations investigated in this analysis include all lander, all orbiter, and the combination orbiter/lander where the lander portion of this split capsule is separated from the orbiter before reaching the target planet. Within each launch opportunity there are two types of trajectories (Type I with heliocentric transfer angles less than 180 degrees, and Type II with heliocentric transfer angles greater than 180 degrees) and within each type the minimum energy trajectory is the separation point between class I and class II trajectories. Class I trajectories have shorter times of flight and smaller transfer angles than the corresponding class II trajectories. The existence of six paths, as noted in ref. (2), is a rare occurrence and is possible only for short intervals (several days) within selected launch opportunities. Favorable launch opportunities for Venus occur every 19.2 months. It has been noted in ref. (2) that there is a cyclic recurrence of the same absolute space-fixed geometry of the earth and Venus. These cycles, known as metonic cycles, are related to the synodic period and, for Venus, this cycle is approximately 8 years or 5 synodic periods. For Venus missions, launch opportunities between 1964 and 1970 were analyzed for both Type I and Type II trajectories. Thus from the metonic cycle the Venus launch opportunity trajectory characteristics for 1972 are approximately the same as for 1964, and 1973 is the same as 1965 and 1975 is the same as 1967.

For Mars missions, favorable launch opportunities occur every 25.6 months and the metonic cycle is approximately 15 years or 7 synodic periods. Payload studies for the above mentioned missions were conducted for Mars Type I trajectories between 1969 and 1975 and for Type II trajectories in 1969, 1971, and 1975. The weight injected into the heliocentric transfer orbit, as a function of the hyperbolic excess velocity at departure, was obtained from NASA Headquarters and is the reference booster capability for the Voyager Program. This information, as a function of the square of the hyperbolic excess velocity (C_3), is

presented in figure 10. In this analysis it was assumed that the combined mid-course, approach, and terminal ΔV corrections totaling 0.3 km/sec were applied impulsively, and in the split-capsule mission, that the lander was not separated from the orbiter-bus until after the final terminal correction.

A representative value for the specific impulse was selected as 310 seconds. The dry weight of the propulsion system can be expressed as a function of the propellant weight. In this analysis a recommended value for the propellant mass fraction, defined by

$$\frac{\text{Propellant } (W_p)}{\text{Propellant } + \text{ Dry Propulsion System } (W_{ps})}$$

was 0.865. Then the dry weight of the propulsion system can be expressed by

$$W_{ps} = 0.156 \, W_p \quad .$$

The weight of all the lander mission vehicle including propulsion system, structures, and heat shield can be computed by

$$W_{lander} = W_i e^{-\frac{\Delta V}{c}}$$

where

c = effective exhaust velocity, $g_0 I_{sp}$

W_i = weight injected into heliocentric transfer orbit

$\Delta V = 0.3$ km/sec.

For this mission, the lander weight is maximized when we employ the minimum departure velocity since this, in turn, maximizes the weight injected into the heliocentric transfer orbit. Venus Type I and II trajectories in 1967, Mars Type I in 1971, and Mars Type II in 1969 represent the most favorable launch opportunities for maximizing the weight of the all-lander mission. However, for Venus, the launch opportunities yielding the absolute maximum payloads are not necessarily the same opportunities that yield the maximum payloads at the extremities of the best 30-day launch period due to the variation in the slope of the curves for different launch opportunities. For all launch opportunities, the dry weight of the propulsion system for the all-lander is approximately 100 pounds.

For the all-orbiter mission, the same midcourse, approach, and terminal correction ΔV capability was employed. Therefore, the burnout weight in the desired planetocentric orbit for the mission can be computed by
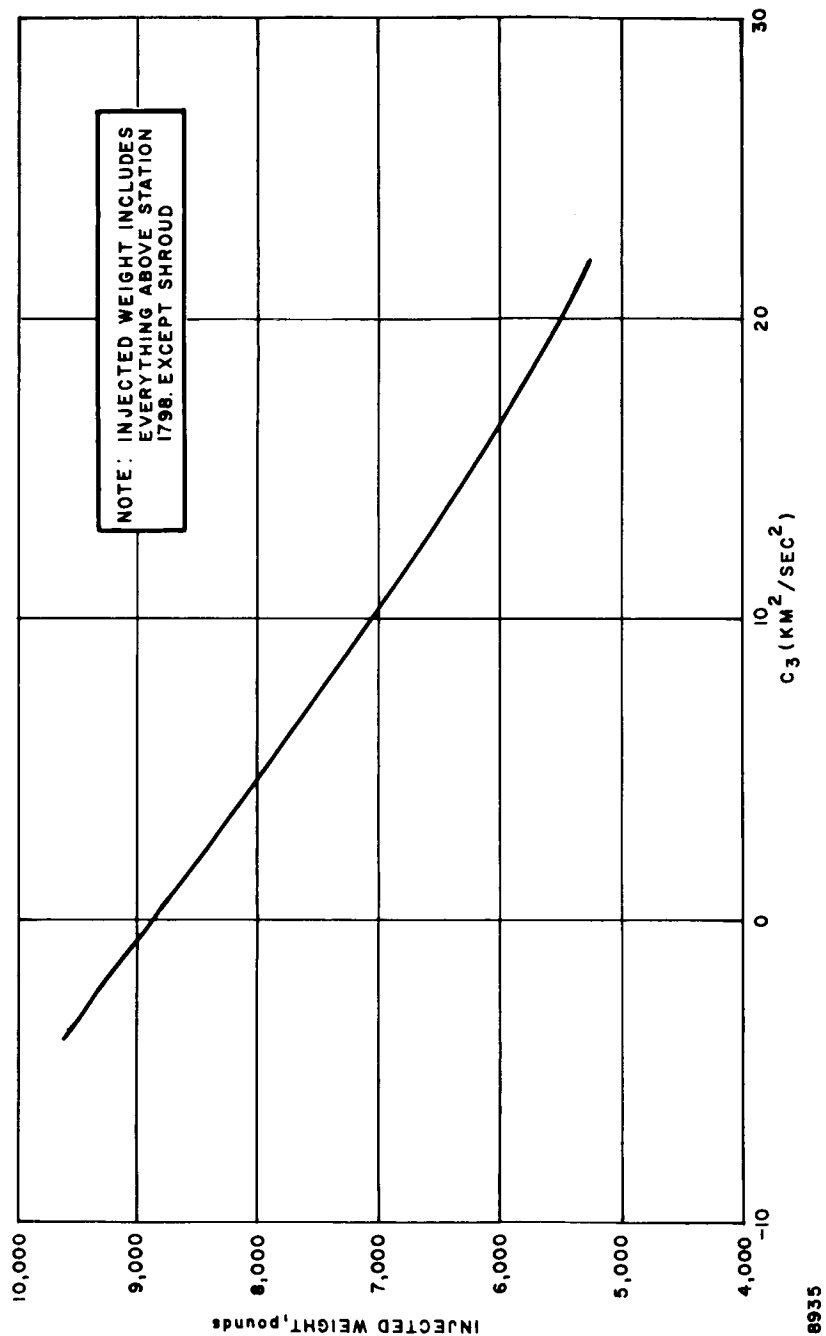
Figure 10 VOYAGER DESIGN STUDIES

63-8935

-38-

$$W_{orbiter} = W_{lander} \, e^{-\frac{\Delta V}{c}}$$

where

ΔV = the difference between the hyperbolic velocity at periapsis and the velocity in the capture orbit at that point.

In establishing an elliptic orbit about the planet, the velocity decrement was applied impulsively and it was assumed that periapsis of the approach hyperbola and periapsis of the ellipse were coincident.

Therefore, the velocity to be removed can be expressed by

$$\Delta V = \sqrt{V_\infty^2 + \frac{2\mu}{r_p}} - \sqrt{\frac{r_a}{r_p} \cdot \frac{2\mu}{r_a + r_p}}$$

where

V_∞ = planetary approach velocity

μ = gravitational parameter

r_p = periapsis radius

r_a = apoapsis radius.

The planetary approach velocity is a function of the transfer orbit characteristics and target planet velocity components, and for the various launch opportunities in question, was obtained from ref. (1). For Venus, the reference planetocentric orbit was a circular orbit with a 1000-km altitude, and for Mars both a circular orbit with an 1800-km altitude and an elliptic orbit with periapsis and apoapsis altitudes of 1500 and 10,000 km, respectively, were analyzed.

As the hyperbolic approach velocity is a function of several variables, in general, the approach velocity associated with the absolute minimum departure velocity is not a minimum. Since the orbiter payload is a function of both the departure and arrival velocities, the orbiter payload mission peaks at a different date in each launch opportunity than does the corresponding lander mission. For the all-orbiter mission, the maximum payload occurs for Venus 1967 and Mars 1971 launch opportunities for both Type I and II trajectories.

For Venus, the minimum payload (payload at the extremity of the best 30-day launch period), exclusive of the dry propulsion system weight, varies between a low of 465 pounds in 1964 (1972) to a high of 1100 pounds in 1967 (1975) for

Type I trajectories. Similar payloads for Type II trajectories are 200 pounds and 1240 pounds, respectively. Prior to the 1969 launch period, Type II trajectories result in slightly larger payloads than the corresponding Type I trajectories due to the lower energy requirements; this reduced payload in 1964 (1972) results from the fact that the optimum portion of this curve is not usable due to range safety constraints (to be discussed in detail later). In general, the dry weight of the propulsion system for these Venus missions is approximately 900 pounds. For Mars missions in 1971, the minimum payloads, exclusive of the dry propulsion system weight, for the optimum 30-day launch window are 3400 and 2800 pounds for Type I and II trajectories, respectively, for the elliptic orbit. The penalty associated with the attainment of a circular rather than elliptic orbit is approximately 800 pounds for this launch opportunity. Due to the different orbits considered affecting ΔV requirements, the dry propulsion system weights vary from 450 to 850 pounds for Martian orbits. For the split-payload orbiter/lander mission, the terminal ΔV requirements are identical with those associated with the all-orbiter mission. The spacecraft weight at periapsis of the approach hyperbola is reduced since the lander is separated from the orbiter to injection into a planetocentric orbit. Therefore, the propellant weight, and consequently the dry weight of the propulsion system is reduced for this mission in comparison with the all-orbiter mission. The burnout weight of the orbiter portion of the split capsule mission is computed by

$$W_{orbiter/lander} = (W_{all-lander} - W_{lander/orbiter})\, e^{-\frac{\Delta V}{c}}$$

where

ΔV = velocity to be removed to establish desired orbit

$W_{all-lander}$ = weight injected into the heliocentric transfer orbit minus the propellant for the midcourse, approach and terminal corrections

$W_{lander/orbiter}$ = weight of the capsule ejected from the spacecraft prior to final orbit establishment.

Again due to the varying approach velocities and varying orbiter weights at the point of orbit establishment, the maximum weight for the split-capsule mission does not necessarily occur at the same launch date for which the payload weights for the other missions are also maximum. Similar to the all-orbiter mission, the maximum payload for split-capsule Venus configuration occurs in 1967 and for Mars in 1971.

For an optimum 30-day launch window in each opportunity, the minimum payloads vary between 250 and 700 pounds for Venus Type I trajectories. Ignoring for the moment range safety constraints, approximately 100 additional pounds of payload can be obtained with Type II trajectories prior to the 1968

launch opportunity. For Martian missions, the minimum payloads vary between 1050 and 2300 pounds for the elliptic orbit. A decrease of approximately 600 pounds is associated with the establishment of the circular orbit. For Mars, Type II trajectories yield larger payloads prior to the 1971 opportunity than the corresponding Type I trajectories. While the orbital payloads associated with the split-capsule mission are less than those associated with the all-orbiter mission, the combined lander and orbiter scientific payload may be substantially increased. In these analyses, Mars Type I trajectories in 1969 and 1975 were computed for completeness, even though the launch azimuth constraint negates the entire 30-day window.

For the optimum 30-day window for each opportunity, the burnout payloads, along with the propulsion system weights, are summarized in table 8 in addition to the vehicle weight injected into the heliocentric transfer orbit. The weights are presented in this fashion so that the payload weight can be computed if the propellant mass fraction varies. The dry weight of the propulsion system is based upon the maximum amount of fuel required for the particular mission during that particular launch opportunity. In general, this weight of propellant for each mission is maximum on the date corresponding to the absolute minimum injection velocity. In addition to payload information, this tabulation also indicates those launch opportunities where either a portion or the total opportunity is unacceptable due to launch azimuth constraints.

For each launch opportunity, the burnout weights for each mission (lander, orbiter, and orbiter/lander) are presented in graphical form for a minimum of a 60-day period in figures 11 through 28. These 60-day windows were analyzed to determine the above optimum 30-day windows.

In the preceding mission payload analysis, the split-capsule lander weight was 2000 pounds. Since the orbiter weights associated with this lander are unacceptable during certain launch opportunities and are only marginally acceptable during others, a brief analysis was undertaken to determine the increase in the orbiter payload associated with a decrease in the lander weight. In the limit, as the lander weight approaches zero, the split-capsule orbiter weight approaches the all-orbiter weight. For the day in each launch opportunity where the split capsule orbiter weight was maximized, an influence coefficient was computed to determine the increase in the orbiter payload as a function of the decrease in the lander weight. These results are based on lander weights of 2000, 1500, and 1000 pounds and are presented in table 9.

In addition to these influence coefficients, the variation in orbiter payload over a complete launch opportunity was analyzed for Mars Type II trajectories in 1969 and Venus Type I trajectories in 1964 (1972). This information indicates that whereas the above mentioned influence coefficients are not applicable over the entire launch opportunity, they do afford a reasonably simple method for analyzing the associated tradeoffs. These data are presented in figures 29 and 30.

-41-

TABLE 8

COMPARISON OF MISSION BURNOUT WEIGHTS FOR OPTIMUM 30 DAY PERIOD

Planet	Orbit (km)	Type	Injected Weight Date of Maximum Weight+	Injected Maximum Weight (pounds)	Injected Minimum Weight (pounds)	Lander Date of Maximum Weight+	Lander Maximum Weight (pounds)	Lander Minimum Weight (pounds)	Lander Propulsion System Weight (pounds)	Orbiter Date of Maximum Weight+	Orbiter Maximum Weight (pounds)	Orbiter Minimum Weight (pounds)	Orbiter Propulsion System Weight (pounds)	Orbiter/2000-lb Lander Date of Maximum Weight+	Orbiter/2000-lb Lander Maximum Weight (pounds)	Orbiter/2000-lb Lander Minimum Weight (pounds)	Orbiter/2000-lb Lander Propulsion System Weight (pounds)
Venus	1000/1000	I	3/30/64 (72)	6680	6370	3/30/64	6070	5770	98	4/11/64	1400	1300	835	4/06/64	900	840	588
Venus	1000/1000	I	11/13/65 (73)	6550	6200	11/13/65	5940	5650	93	12/01/65	1890	1610	762	11/28/65	1200	1100	538
Venus	1000/1000	I	6/10/67 (75)	7750	6970	6/10/67	7020	6310	110	6/13/67	2260	1960	860	6/12/67	1640	1350	647
Venus	1000/1000	I	1/12/69	7490	7270	1/12/69	6790	6590	106	1/13/69	1920	1880	866	1/13/69	1350	1310	642
Venus	1000/1000	I	8/18/70	7350	7140	8/18/70	6660	6470	104	8/20/70	1640	1590	890	8/19/70	1150	1110	655
Venus	1000/1000	II	4/ 8/64 (72)	7430	7260	4/11/64	6730	6000*	105	4/11/64	1670*	1100*	894	4/11/64	1180*	750*	660
Venus	1000/1000	II	11/11/65 (73)	7570	7350	11/12/65	6890	6690	98	11/12/65	2030	1950	866	11/15/65	1450	1370	646
Venus	1000/1000	II	6/0 3/67 (75)	7820	7480	6/13/67	7080	6780	111	6/03/67	2350	2090	857	6/03/67	1670	1480	647
Venus	1000/1000	II	2/14/69	6700	6590	12/09/68	6070	5100*	95	12/09/68	1910*	1600*	753	12/09/68	1260	1000*	537
Venus	1000/1000	II	9/15/70	6990	6700	9/27/70	6290*	5500*	100	9/27/70	1240*	750*	885	9/27/70	840	600*	637
Mars	1500/10,000	I	3/03/69	7300*	7000*	3/03/69	6610*	6340*	107	3/26/69	3030*	2690*	790	3/25/69	2040*	1810*	581
Mars	1500/10,000	I	5/24/71	7470	7270	5/24/71	6770	6590	106	5/24/71	4150	3900	527	5/24/71	2920	2720	402
Mars	1500/10,000	I	7/29/73	6310	6000	7/29/73	5720	5440	90	8/08/73	3440	3170	465	8/06/73	2200	1990	360
Mars	1500/10,000	I	9/15/75	5700	5200	9/15/75	5160*	4710*	81	9/24/75	2750*	2450*	503	9/22/75	1650*	1390*	334*
Mars	1800/1800	I	3/03/69	7300*	7000*	3/03/69	6610*	6340*	107	3/26/69	2510*	2210*	854	3/25/69	1650*	1500*	625
Mars	1800/1800	I	5/24/71	7470	7270	5/24/71	6770	6590	106	5/22/71	3390	3170	640	5/24/71	2390	2200	482
Mars	1800/1800	I	7/29/73	6310	6000	7/29/73	5720	5440	90	8/7/73	2830	2630	585	8/06/73	1820	1650	410
Mars	1800/1800	I	9/15/75	5700	5200	9/15/75	5160*	4710*	81	9/24/75	2250*	1990*	568	9/22/75	1350*	1130*	374
Mars	1500/10,000	II	4/01/69	7460	7400	4/01/69	6760	6700	106	1/25/69	3040	2900	793	1/30/69	2050	2000	588
Mars	1500/10,000	II	5/10/71	7160	6520	5/10/71	6490	5910	101	5/10/71	3820	3300	513	5/10/71	2640	2170	390
Mars	1500/10,000	II	8/27/73	6090	6010	8/27/73	5520	5450	86								
Mars	1500/10,000	II	9/17/75	6540	6370	9/17/75	5930	5770	93								
Mars	1800/1800	II	4/01/69	7460	7400	4/01/69	6760	6700	106	1/25/69	2470	2320	860	1/30/69	1670	1600	635
Mars	1800/1800	II	5/10/71	7160	6520	5/10/71	6490	5910	101	5/10/71	3120	2660	627	5/10/71	2175	1800	465
Mars	1800/1800	II	8/27/73	6090	6010	8/27/73	5520	5450	86								
Mars	1800/1800	II	9/17/75	6540	6370	9/17/75	5930	5770	93								

+ Trajectory analysis for 1964-1970 (Venus) period pertinent to 1972-1978 period with at most a 5-day shift in the window.

* Declination of geocentric asymptote exceeds acceptable limits over portion of launch opportunity.
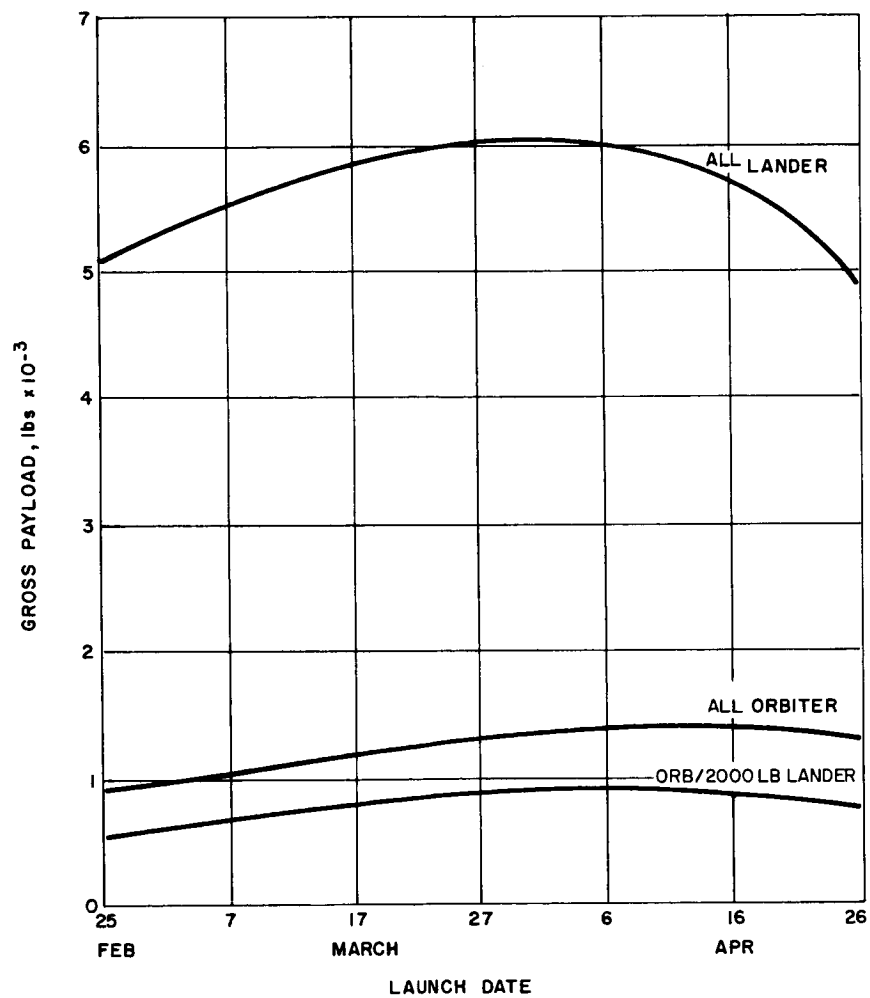
63-8732

Figure 11 MISSION GROSS PAYLOADS VERSUS LAUNCH DATE,
VENUS 1964, TYPE I
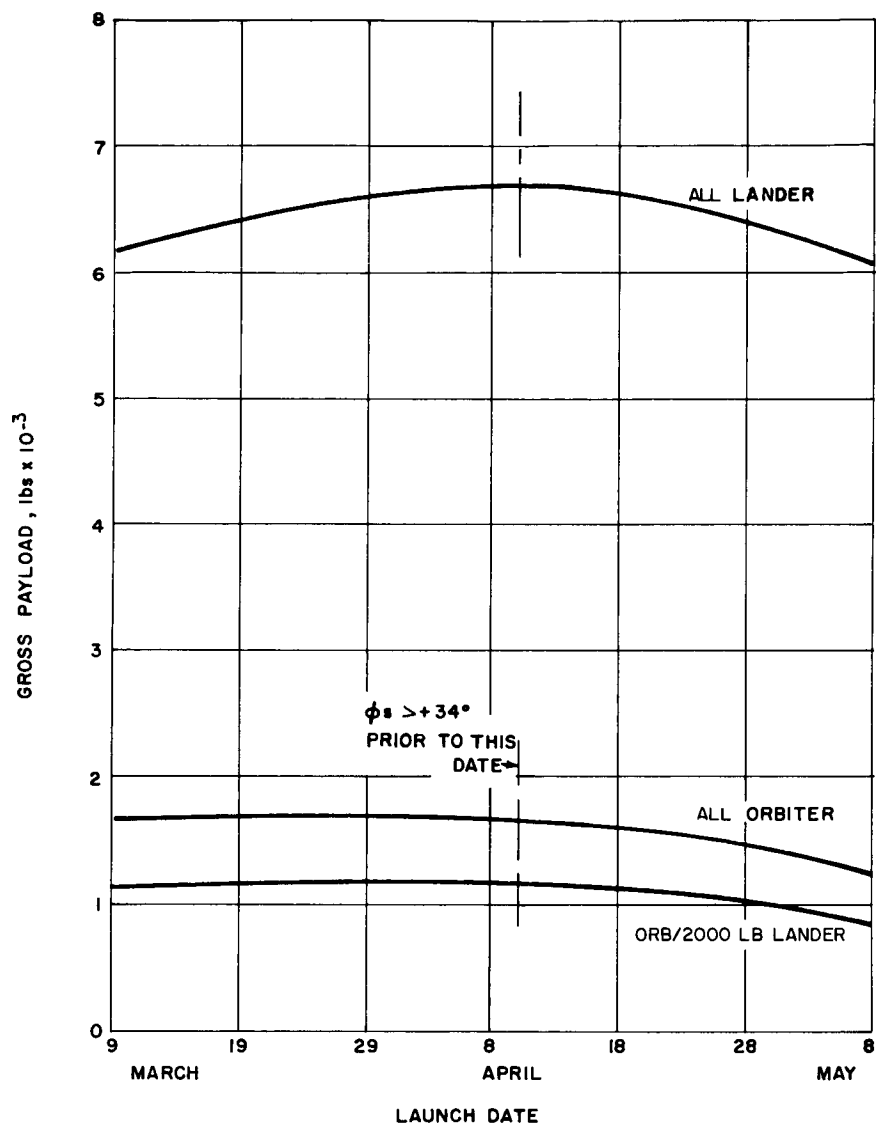
63-8733

Figure 12 MISSION GROSS PAYLOADS VERSUS LAUNCH DATE,
VENUS 1964, TYPE II
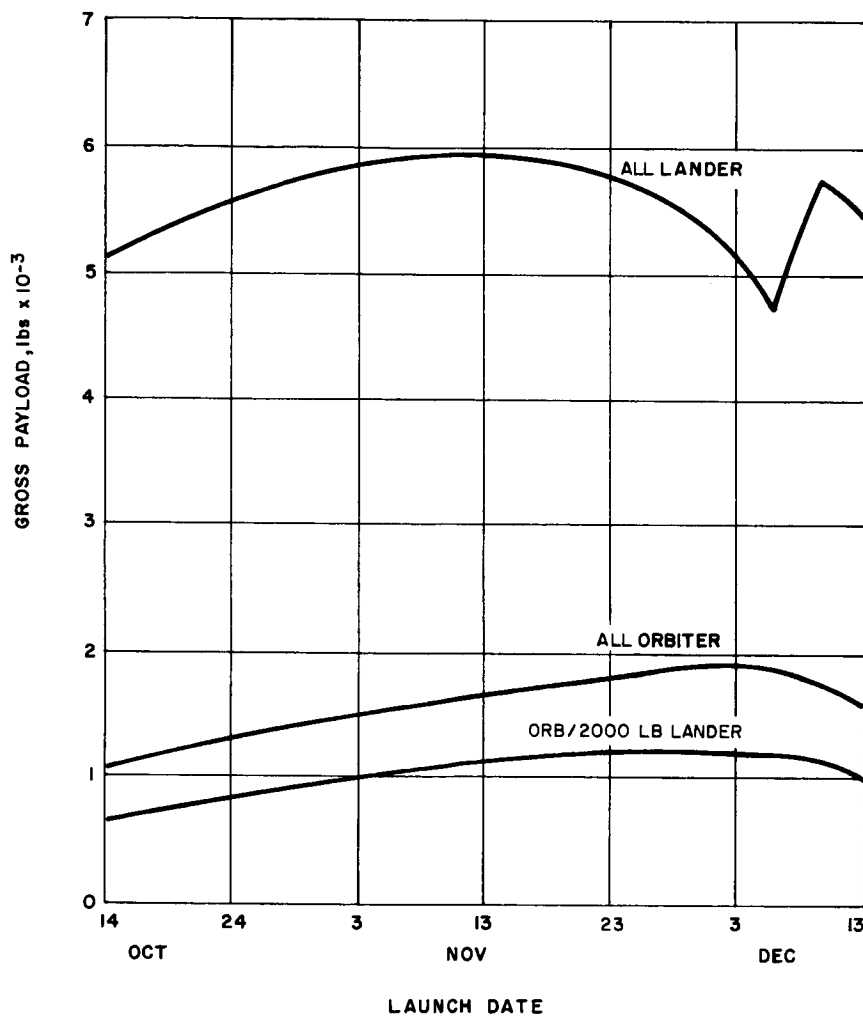
-44-

Figure 13 MISSION GROSS PAYLOADS VERSUS LAUNCH DATE,
VENUS 1965, TYPE I

63-8734

-45-
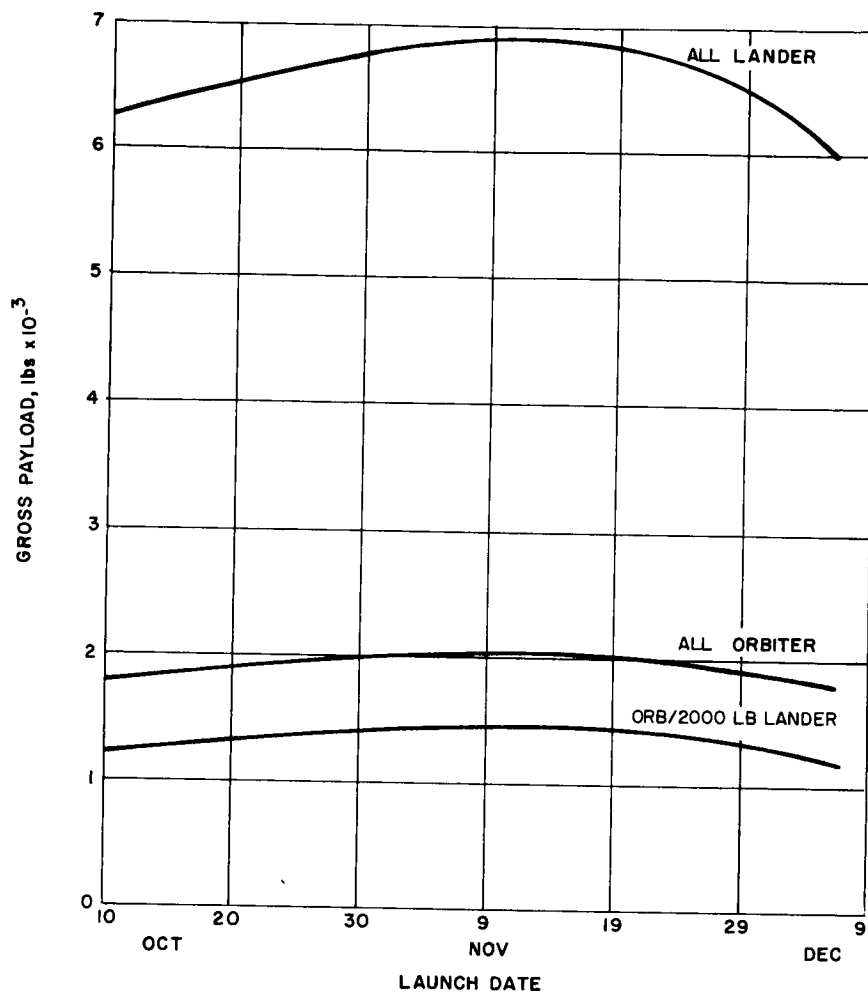
63-8735

Figure 14 MISSION GROSS PAYLOADS VERSUS LAUNCH DATE,
VENUS 1965, TYPE II
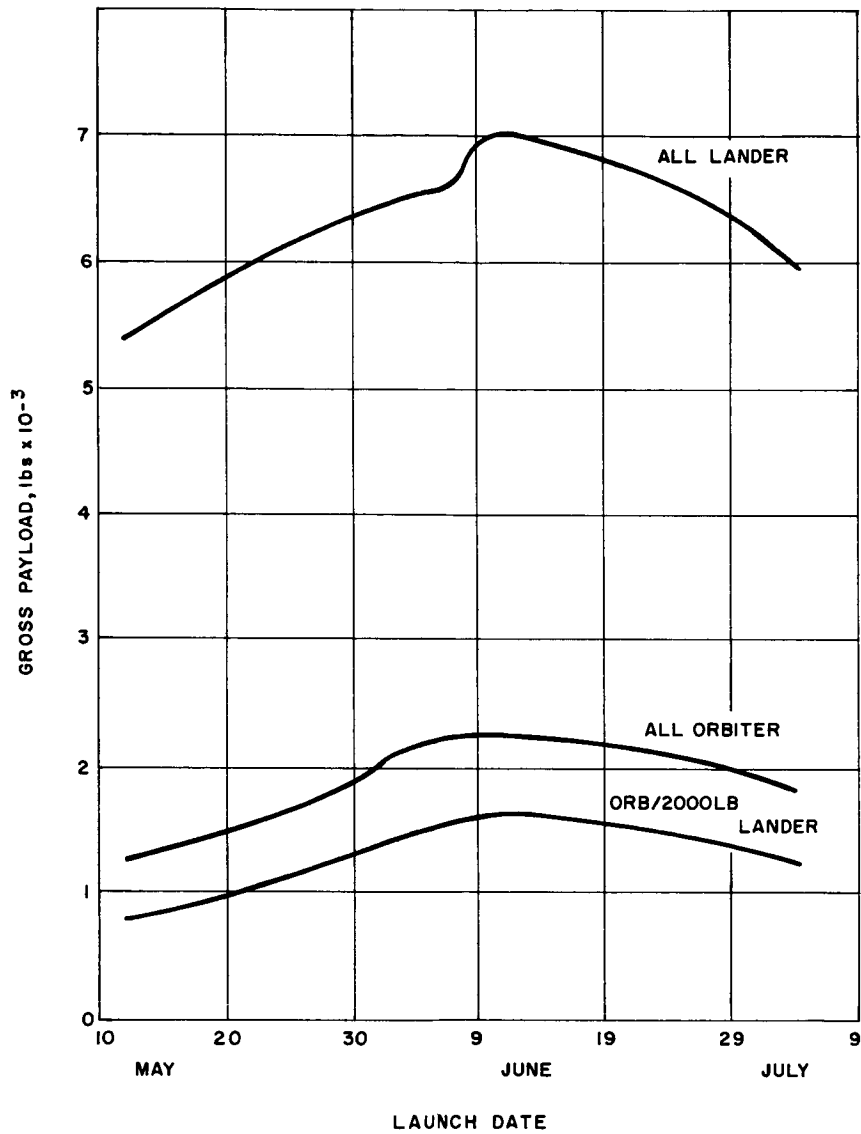
Figure 15 MISSION GROSS PAYLOADS VERSUS LAUNCH DATE, VENUS 1967, TYPE I

63-8736

-47-
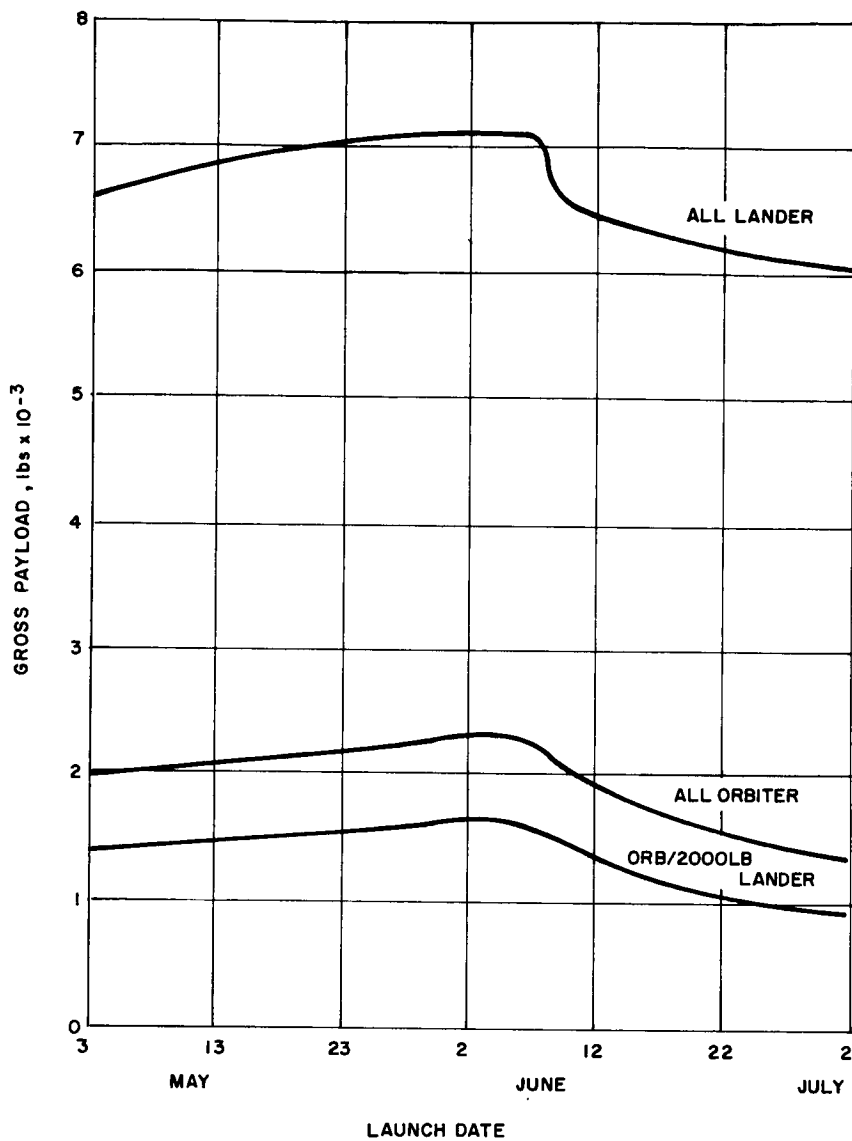
63-8737

Figure 16 MISSION GROSS PAYLOADS VERSUS LAUNCH DATE,
VENUS 1967, TYPE II

GROSS PAYLOAD, lbs x 10^{-3}

ALL LANDER

ALL ORBITER

ORB/2000 LB LANDER

13   23   2   12   22   I   II

DEC   JAN   FEB
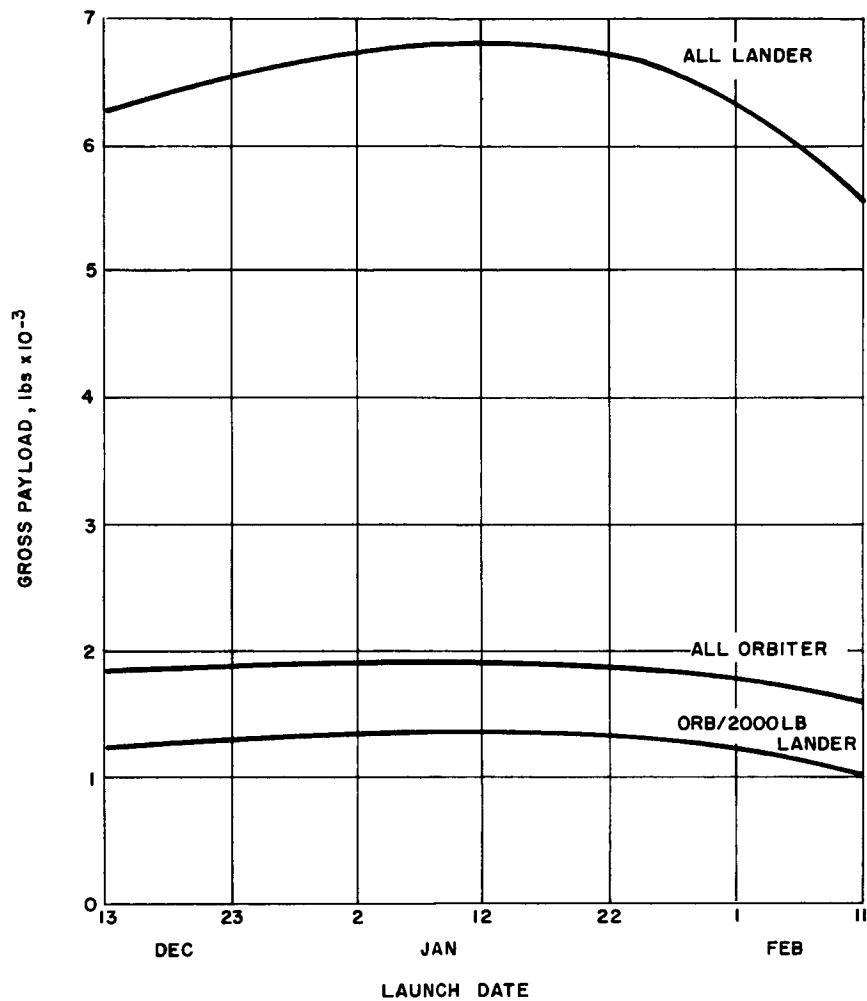
LAUNCH DATE

63-8783

Figure 17 MISSION GROSS PAYLOADS VERSUS LAUNCH DATE, VENUS 1969, TYPE I
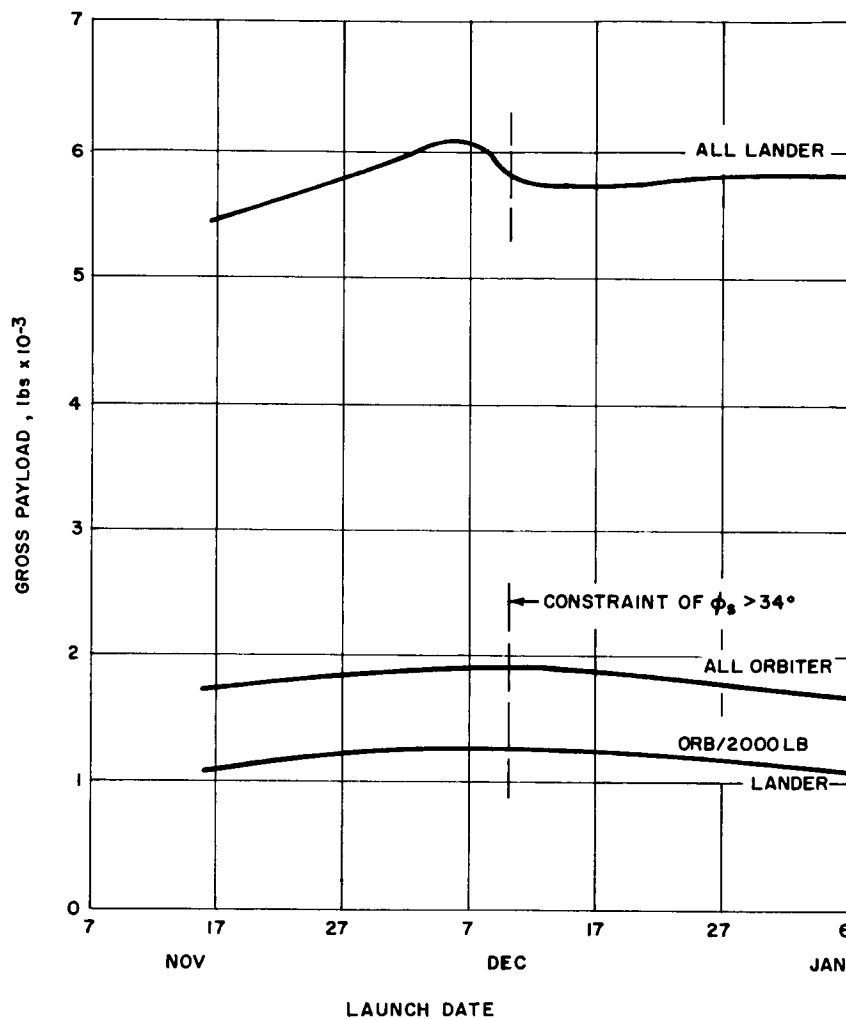
63-8739

Figure 18 MISSION GROSS PAYLOADS VERSUS LAUNCH DATE,
VENUS 1969, TYPE II

-50-
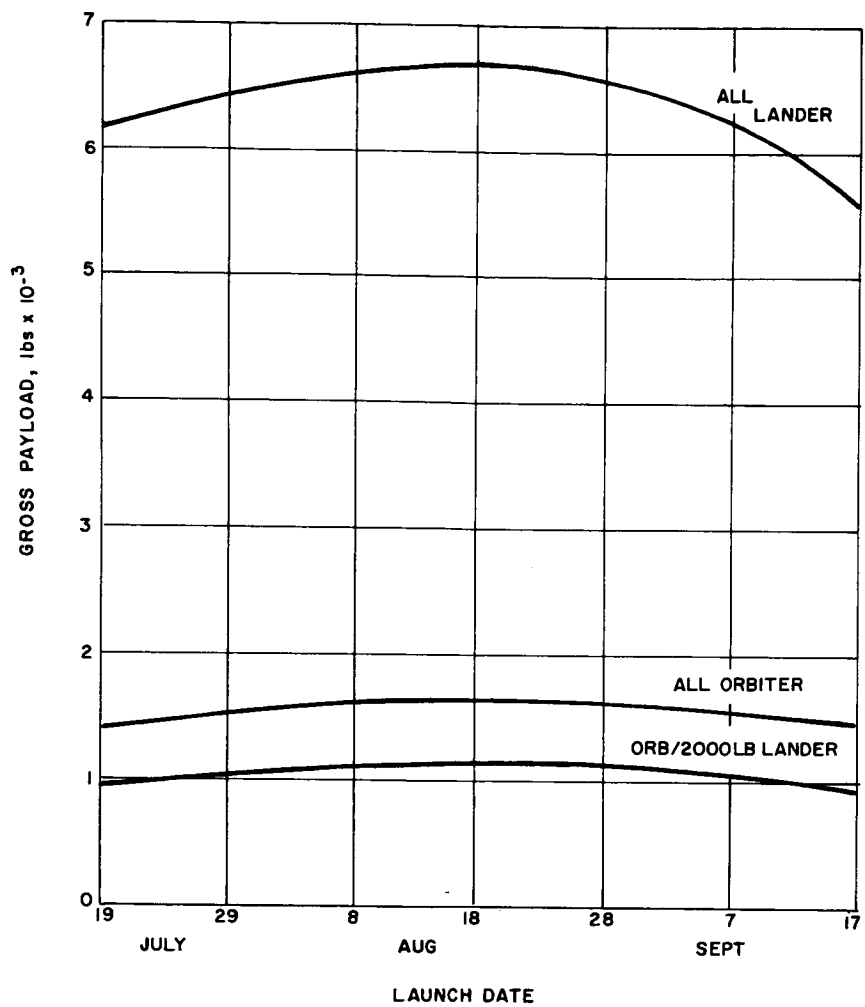
63-8740

Figure 19 MISSION GROSS PAYLOADS VERSUS LAUNCH DATE,
VENUS 1970, TYPE I

-51-

GROSS PAYLOAD, lbs x 10^{-3}

7

6 — ALL LANDER

5

4

3

2 — PRIOR TO THIS DATE
CONSTRAINT OF $\phi_s < -34°$ →

ALL ORBITER

1 — ORB/2000 LB
LANDER

0

16   26   5   15   25   5   15
AUG   SEPT   OCT
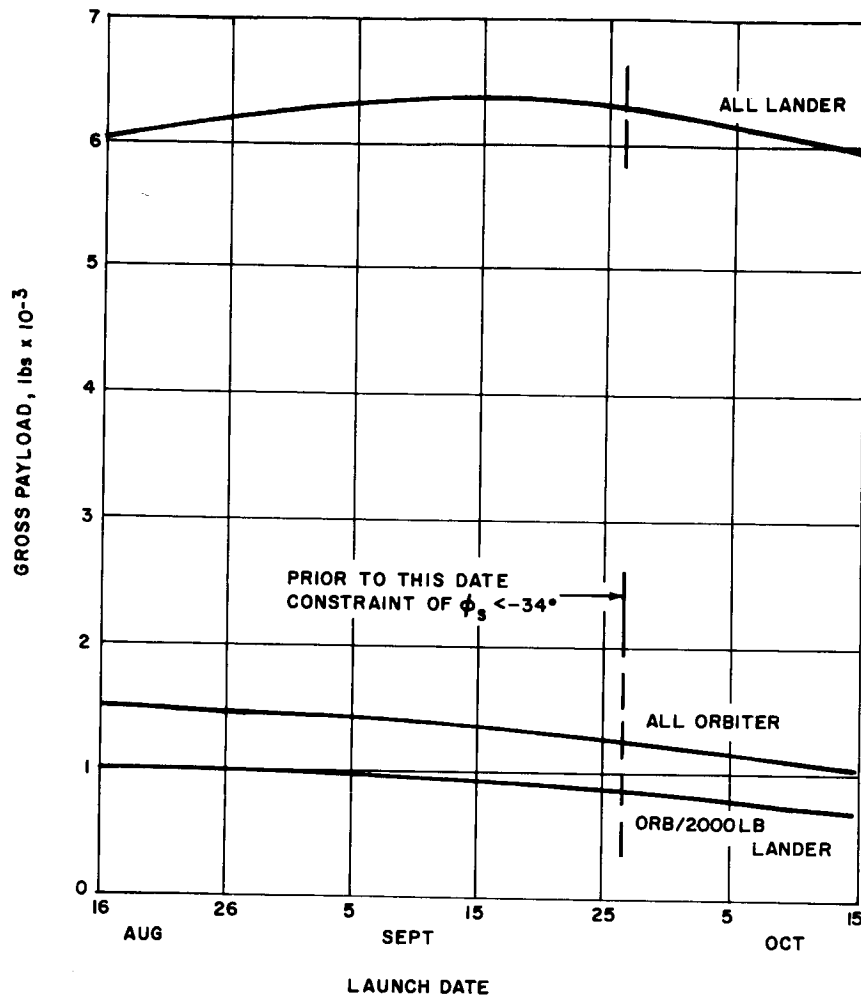
LAUNCH DATE

63-8741

Figure 20 MISSION GROSS PAYLOADS VERSUS LAUNCH DATE,
VENUS 1970, TYPE II

-52-

GROSS PAYLOAD, lbs x10⁻³

7

ALL LANDER

6

5

NOTE: DECLINATION OF GEOCENTRIC ASYMPTOTE
EXCEEDS 34° FOR ENTIRE LAUNCH OPPOTUNITY

4

ALL ORBITER

3

ORB/2000LB LANDER

2

1

0
10   20   2   12   22   1   11
FEB   MARCH   APR
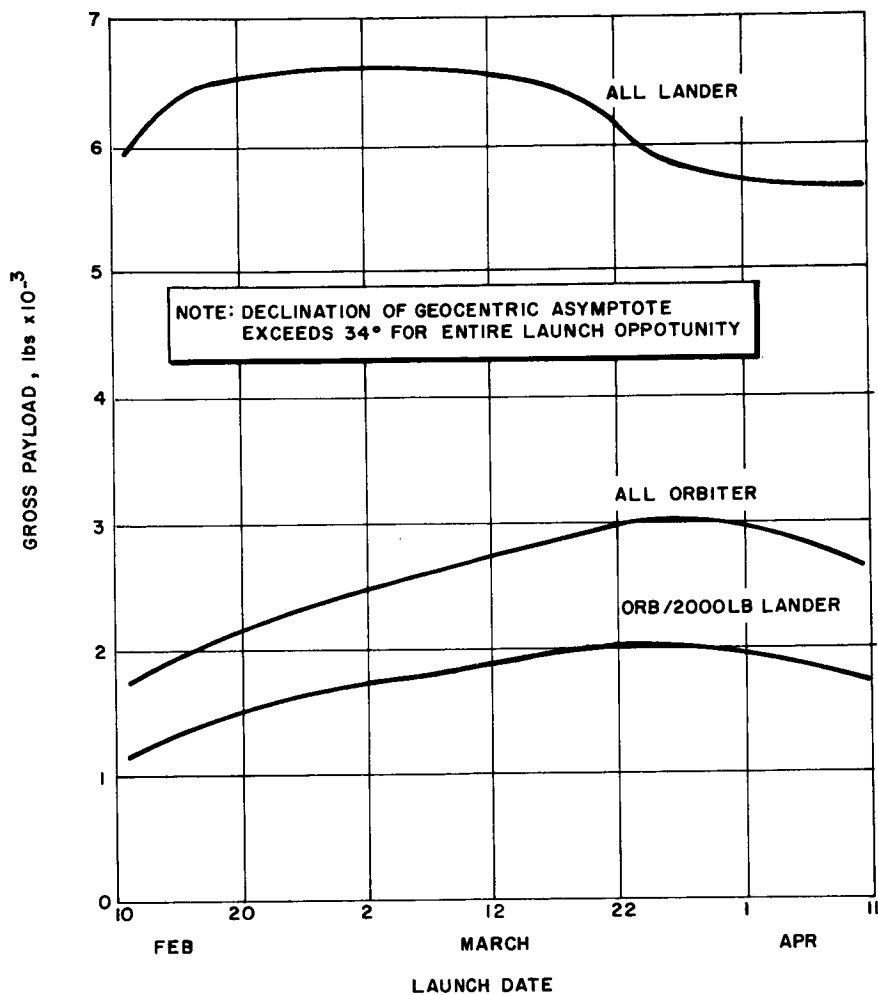
LAUNCH DATE

63-8742

Figure 21 MISSION GROSS PAYLOADS VERSUS LAUNCH DATE,
MARS 1969, TYPE I
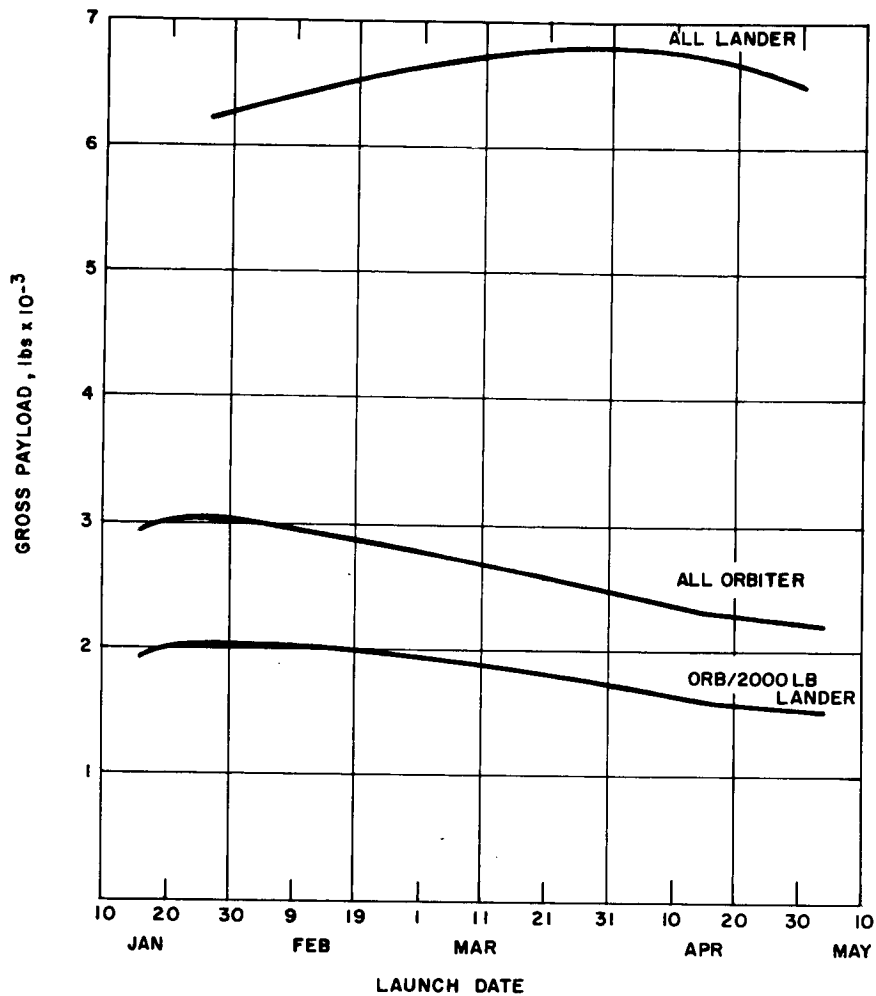
Figure 22 MISSION GROSS PAYLOADS VERSUS LAUNCH DATE, MARS 1969, TYPE II

63-8743

-54-

GROSS PAYLOAD, lbs x 10^{-3}

ALL LANDER

ALL ORBITER

ORB/2000 LB LANDER

PRIOR TO THIS DATE
CONSTRAINT OF $\phi_s < -34°$

24 APR.

4 MAY

14

24

3 JUNE

13

23

63-8855
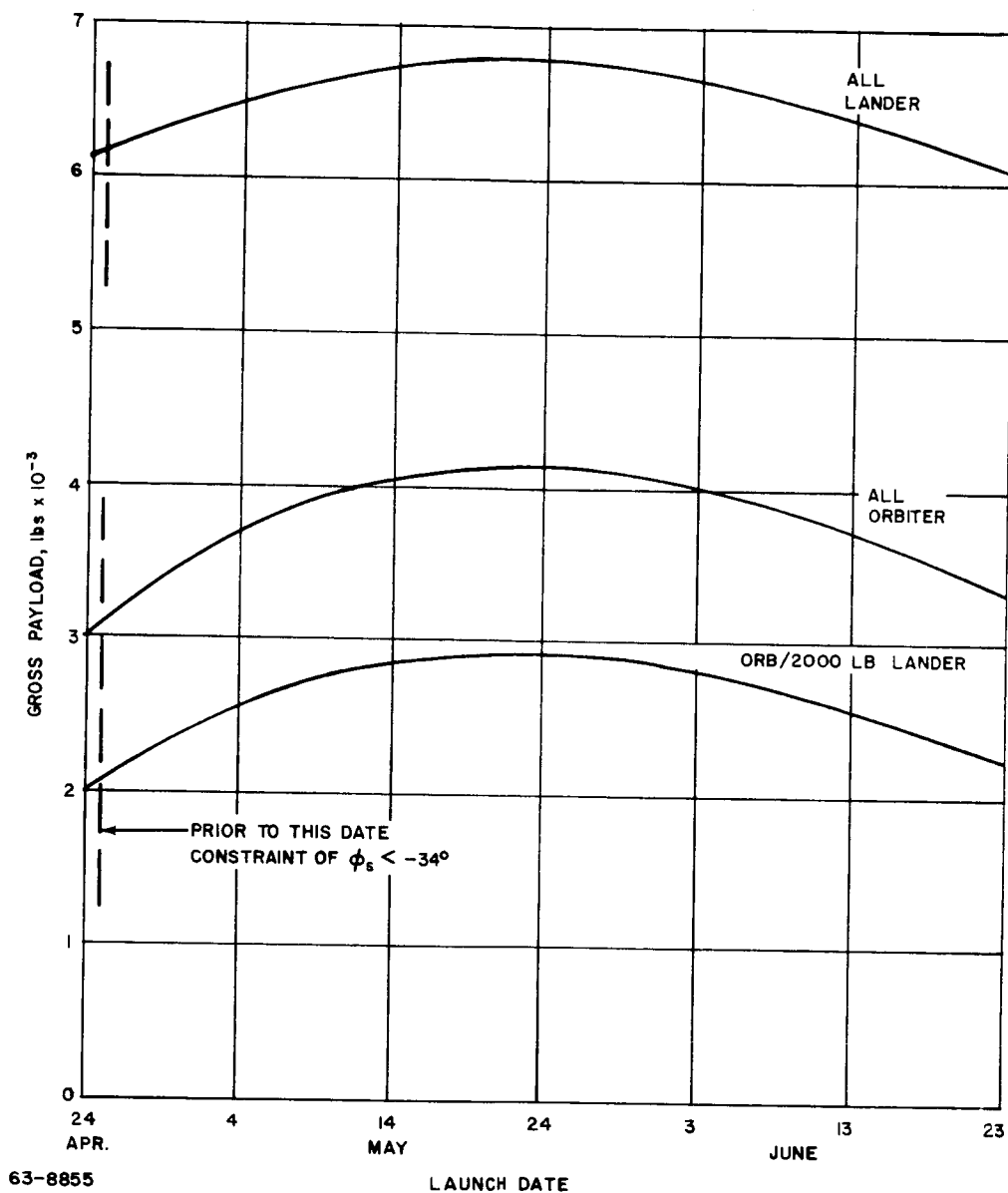
LAUNCH DATE

Figure 23 MISSION GROSS PAYLOADS VERSUS LAUNCH DATE,
MARS 1971, TYPE I
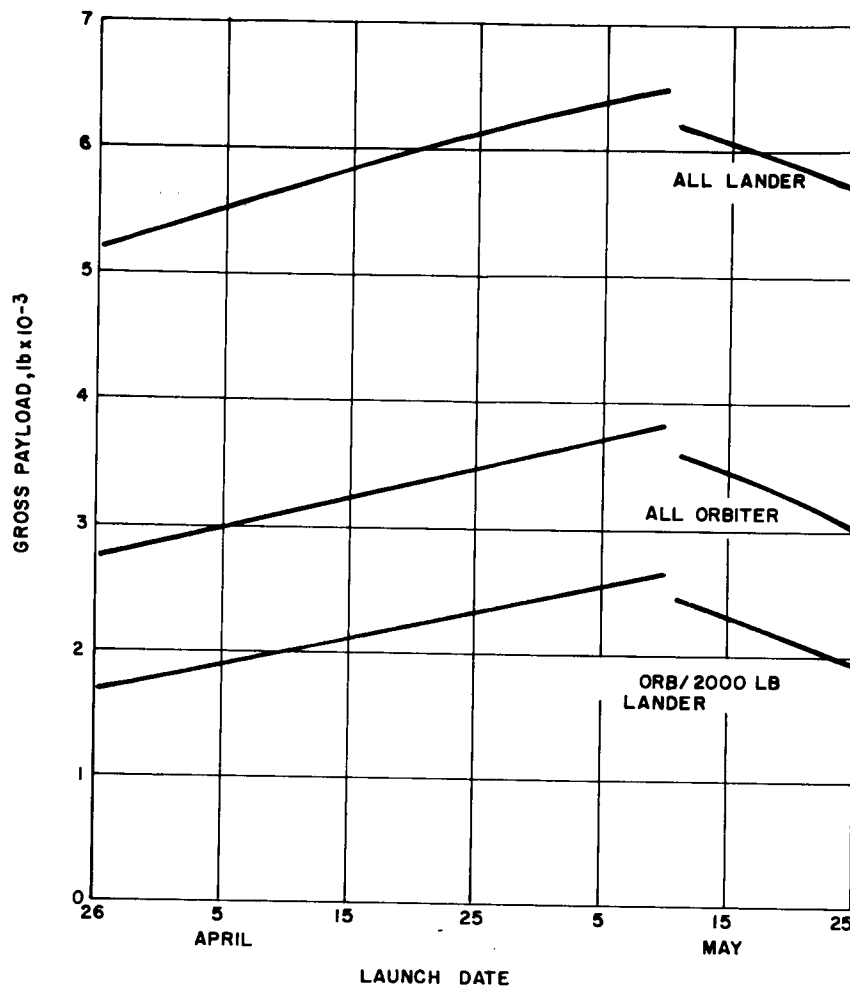
63-8745

Figure 24 MISSION GROSS PAYLOADS VERSUS LAUNCH DATE,
MARS 1971, TYPE II

GROSS PAYLOAD, lbs x 10^{-3}

ALL LANDER

ALL ORBITER

ORB/2000LB
LANDER

30 10 20 30 9 19 29
JUNE   JULY   AUG.
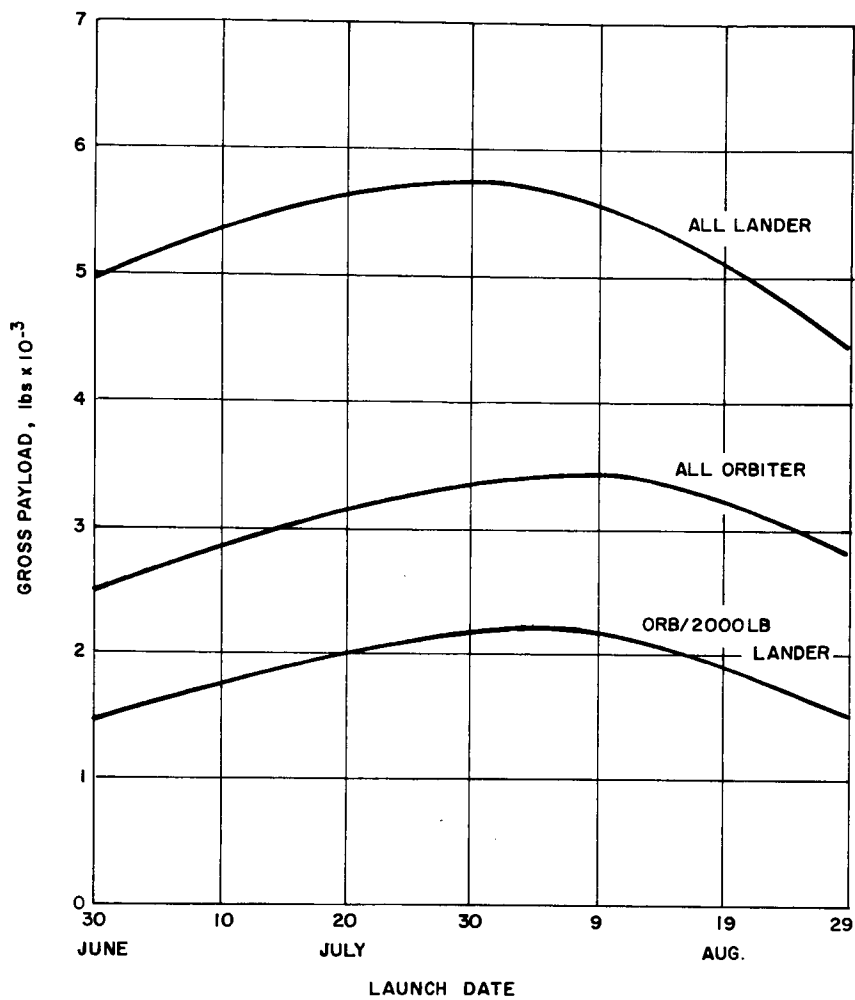
LAUNCH DATE

63-8745

Figure 25 MISSION GROSS PAYLOADS VERSUS LAUNCH DATE,
MARS 1973, TYPE I
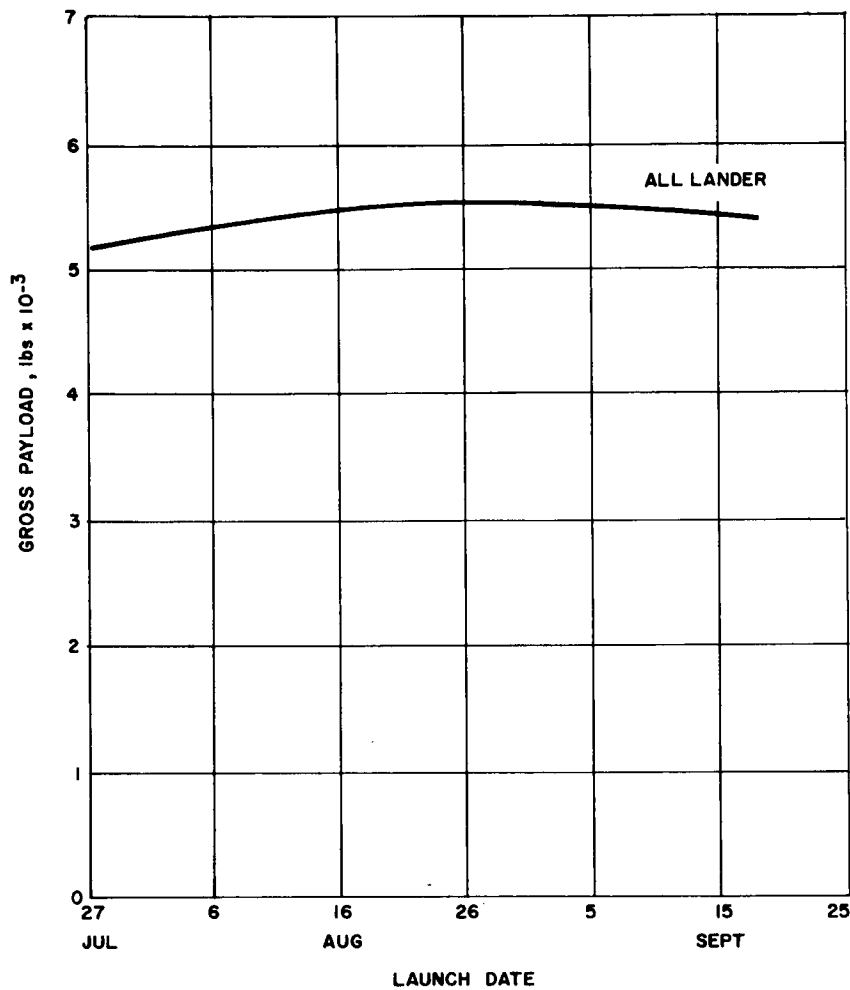
63-8747

Figure 26 MISSION GROSS PAYLOADS VERSUS LAUNCH DATE,
MARS 1973, TYPE II

-58-

NOTE: DECLINATION OF GEOCENTRIC ASYMPTOTE EXCEEDS 34° FOR ENTIRE LAUNCH OPPORTUNITY

ALL LANDER

ALL ORBITER

ORB/2000LB LANDER

GROSS PAYLOAD, lbs x 10⁻³
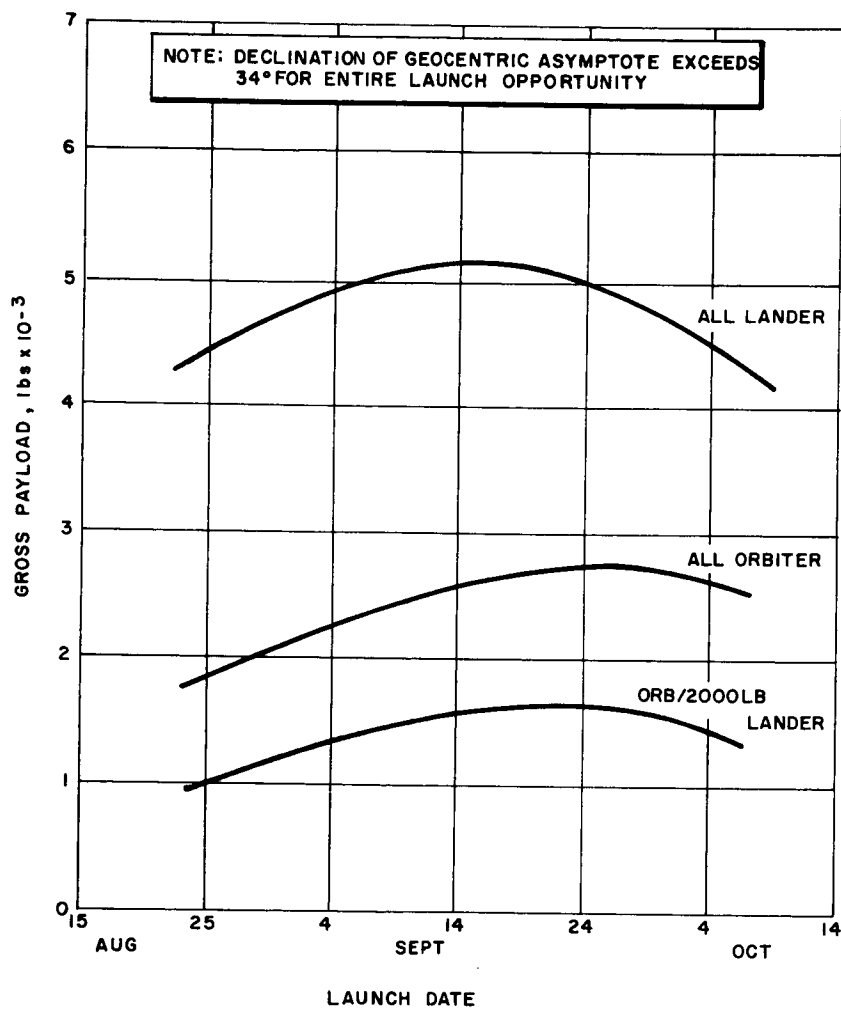
LAUNCH DATE

63-8748

Figure 27 MISSION GROSS PAYLOADS VERSUS LAUNCH DATE, MARS 1975, TYPE I
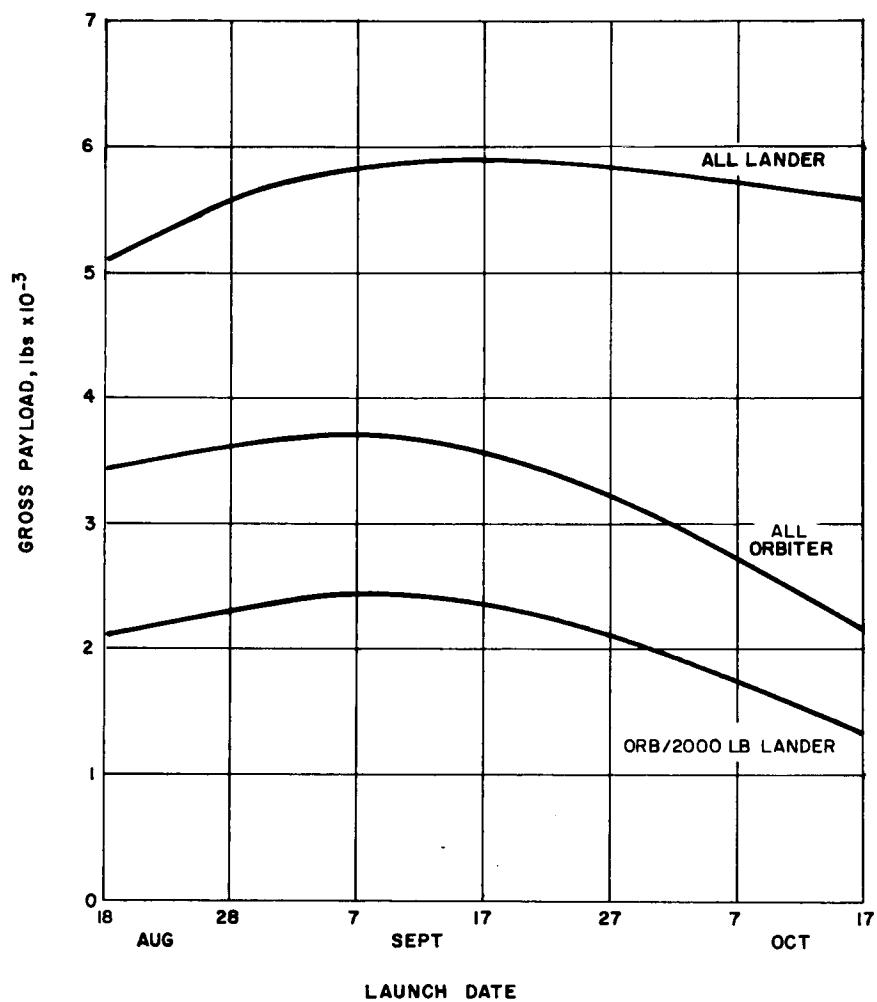
63-8749

Figure 28 MISSION GROSS PAYLOADS VERSUS LAUNCH DATE,
MARS 1975, TYPE II
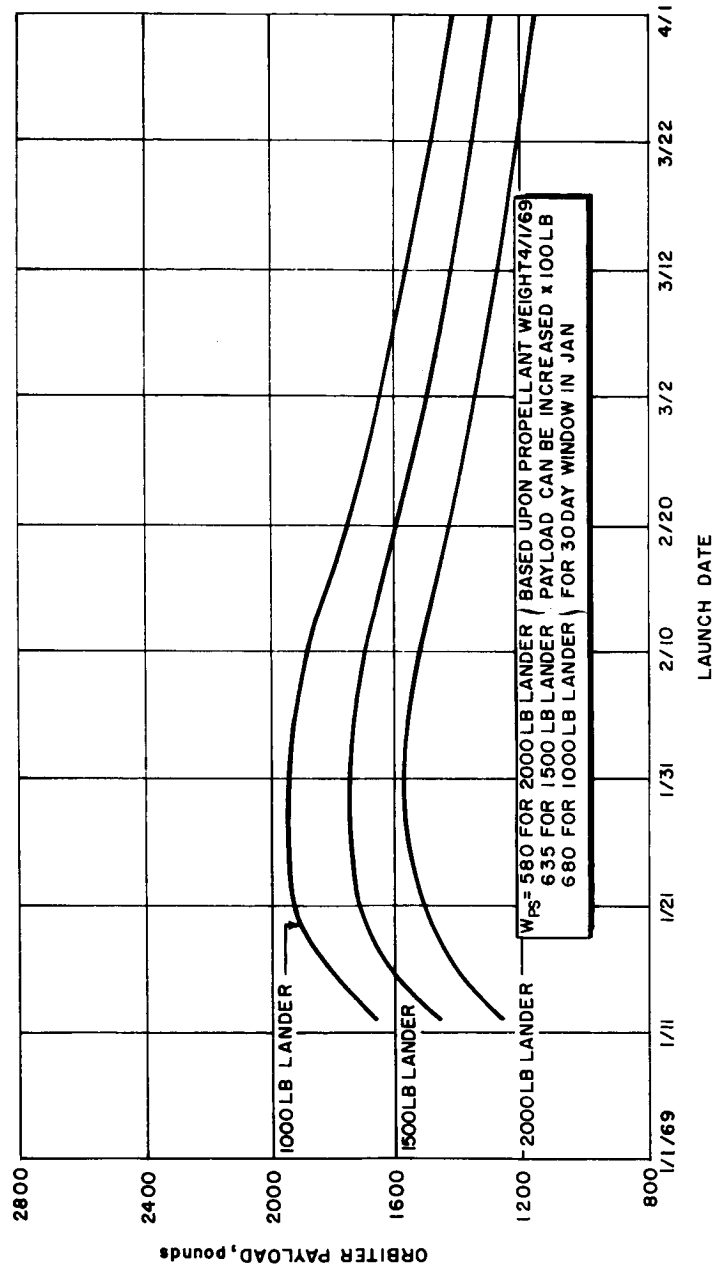
Figure 29 ORBITER PAYLOAD VERSUS LAUNCH DATE, MARS, 1969, TYPE II

63-10197

-61-
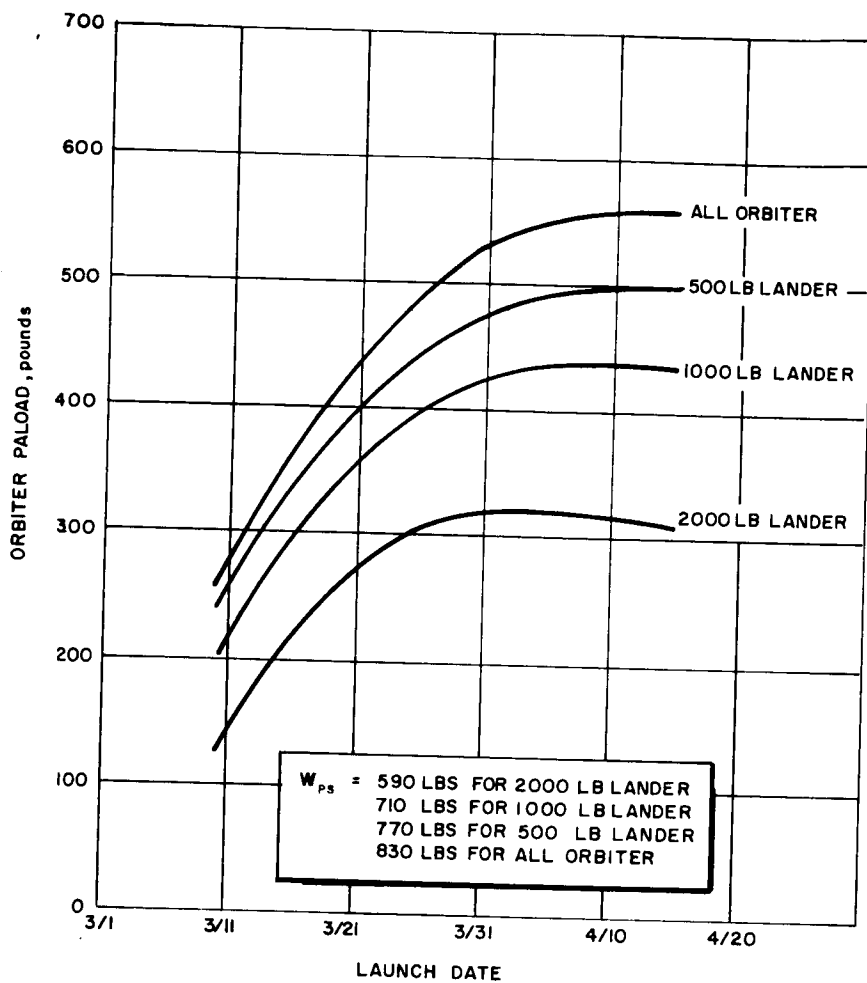
Figure 30 ORBITER PAYLOAD VERSUS LAUNCH DATE, VENUS, 1964, TYPE I

63-10198

-62-

TABLE 9

VARIATION IN SPLIT-CAPSULE ORBITER WEIGHT WITH LANDER WEIGHT VARIATION

Planet	Orbit	Type I		Type II	
		Date	$\partial W_{O/L}/\partial W_{L/O}$	Date	$\partial W_{O/L}/\partial W_{L/O}$
Venus	1000/1000 km	4-15-64	0.13	2-28-64	0.16
		11-30-65	0.24	11-10-65	0.19
		6-11-67	0.21	6- 3-67	0.22
		1-13-69	0.17	12-11-68	0.23
		8-19-70	0.13	8-11-70	0.14
Mars	1500/10000 km	3-25-69	0.44		
		5-24-71	0.55		
		8-10-73	0.56		
		9-24-75	0.48		
Mars	1800/1800 km	3-25-69	0.33		
		5-24-71	0.42		
		7-30-73	0.40		
		9-24-75	0.36		

An additional area that may be analyzed to obtain increased payloads is the tradeoff between orbiter payload and specific impulse. As previously mentioned, the nominal value of specific impulse used in this analysis is 310 seconds. For the Mars Type II trajectories in the 1969 launch opportunity payload weights can be increased 1.0 percent for every 1.0 percent increase in the specific impulse. However, without further investigations for other launch opportunities, it is impossible to state how this influence coefficient varies as a function of the mission and launch opportunity.

For Venus Type I and Type II trajectories for launch opportunities between 1964 and 1970, Mars Type I trajectories between 1969 and 1975, and Mars Type II trajectories for 1969, 1971, and 1975, the pertinent trajectory parameters, mission payloads, and approach parameters are tabulated for at least a 60-day period in tables 10 and 11, respectively. For Venus the mission payload weights are based upon a circular orbital altitude of 1000 km. For Mars, both the information pertaining to the circular orbit with an altitude of 1800 km and the elliptic orbit with periapsis and apoapsis altitudes of 1500 and 10,000 km, respectively, are presented.

The elements in the tables are defined as follows:

TABLE 10

TRAJECTORY DATA -- VENUS 1964-1970

$1^{[1]}$ Launch Dates	2 Type	2 Class	3 Flight Time T_f (days)	4 Earth Departure Velocity $V_{\infty E}$ (km/sec)	5 Injected Weight W_i (lb)	6 Planet Approach Velocity $V_{\infty P}$ (km/sec)	7 Final Orbit Altitude Min/Max (km/km)	8 Velocity at Closest Passing Point V_P (km/sec)	9 Terminal Orbit Injection ΔV (km/sec)	10 Burnout Weight$^{[2]}$ Lander (lb)	11 All Orbiter (lb)	12 Orbiter with 2000-lb Lander (lb)	13 Declination of Geocentric Asymptote ϕ_s (degrees)	14 Communication Distance at Arrival R_p (10^6 km)	15 Planet Orbit γ_p (degrees)	16 Sunline ζ_p (degrees)
2/26/64	I		135	4.36	5660	7.19	1000/1000	11.9	5.2	5145	926	566	-2	52	30	34
3/3/64			132	4.12	5940	7.00		11.8	5.1	5399	999	629	-4	53	29	33
3/10/64			127	3.87	6240	6.75		11.64	4.94	5672	1106	716	-5	55	28	33
3/21/64			119	3.61	6520	6.38		11.42	4.72	5927	1239	821	-7	57	27	32
3/30/64 (1972)			112	3.51	6680	6.00		11.24	4.54	6072	1354	908	-7.5	60	26	32
4/7/64			106	3.61	6520	5.79		11.13	4.43	5927	1363	903	-4	63	23	31
4/15/64			101	3.87	6240	5.45		10.95	4.25	5672	1390	900	-2	65	20	32
4/19/64			97	4.12	5940	5.24		10.83	4.13	5399	1377	867	-0.5	66	19	34
4/23/64			96	4.36	5660	5.13		10.79	4.09	5145	1327	811	-0.5	68	19	37
4/26/64			94	4.58	5380	4.94		10.70	4.0	4890	1301	769	1	69	19	40
4/29/64			93	4.80	5130	4.63		10.57	3.87	4663	1292	738	1.2	71	20	43
2/2/64	II		201	4.36	5660	4.11	1000/1000	10.35	3.65	5145	1538	940	48	96	-34	118
2/11/64			197	4.12	5940	4.32		10.39	3.69	5399	1593	1003	47	102	-36	120
2/19/64			194	3.87	6240	4.46		10.49	3.79	5672	1622	1050	46.5	107	-37.5	124
2/28/64 (1972)			189	3.61	6520	4.72		10.61	3.91	5927	1630	1080	46	112	-38	125
4/9/64			169	2.85	7400	5.40		10.92	4.22	6727	1668	1172	32	136	-30	140
5/13/64			165.5	3.61	6520	7.06		11.83	5.13	5927	1085	719	3	167	-9	165
5/21/64			165.8	3.87	6240	7.71		12.24	5.54	5672	913	591	-2	176	-6	170
5/30/64			166	4.12	5940	8.35		12.65	5.95	5399	756	496	-9	185	-3	174
10/14/65	I		125	4.36	5660	6.34	1000/1000	11.42	4.72	5145	1075	657	16	48	-25	30
10/20/65			121	4.12	5940	5.96		11.22	4.52	5399	1209	761	17	51	-24	30
10/27/65 (1973)			117	3.87	6240	5.55		11.00	4.30	5672	1367	885	18	54	-21	30
11/12/65			108	3.61	6550	4.72		10.60	3.89	5954	1661	1103	12	60	-16	33
11/25/65			105	3.87	6240	3.58		10.15	3.45	5672	1815	1175	8	71	-11	47
11/30/65			113	4.12	5940	2.91		9.90	3.20	5399	1879	1183	6	84	-9	84
10/2/65	II		182	3.61	6520	4.54	1000/1000	10.53	3.83	5927	1659	1099	-30	97	43	117
10/10/65			177	3.32	6920	4.45		10.49	3.79	6290	1793	1223	-27	100	42	118
11/10/65 (1973)			156	2.70	7570	4.24		10.41	3.71	6881	2016	1430	-20	112	36	125
12/2/65			137	3.32	6920	4.22		10.40	3.70	6290	1849	1261	-12	116	26	130
12/7/65			132	3.61	6520	4.11		10.35	3.65	5927	1778	1178	13	149	1	160

(1) Trajectory analysis for 1964 - 1970 period pertinent to 1972 - 1978 period with at most a 5-day shift in the window.

(2) Burnout weights include the effects of 0.3 km/sec ΔV for midcourse, approach, and terminal corrections.

TABLE 10 (Cont'd)

Launch Dates	Trajectory Type	Trajectory Class	Flight Time T_f (days)	Earth Departure Velocity $V_{\infty E}$ (km/sec)	Injected Weight W_i (lb)	Planet Approach Velocity $V_{\infty P}$ (km/sec)	Final Orbit Altitude Min/Max (km/km)	Velocity at Closest Passing Point V_P (km/sec)	Terminal Orbit Injection ΔV (km/sec)	Burnout Weight[2] Lander (lb)	Burnout Weight[2] All Orbiter (lb)	Burnout Weight[2] Orbiter with 2000-lb Lander (lb)	Declination of Geocentric Asymptote ϕ_s (degrees)	Communication Distance at Arrival R_p (10^6 km)	Angle between planet Approach Asymptote and: Planet Orbit γ_p (degrees)	Angle between planet Approach Asymptote and: Sunline γ_p (degrees)
5/12/67	I	Min Ener.	135	4.12	5940	5.75	1000/1000	11.09	4.38	5399	1277	804	-27	54	17	27
5/17/67			133	3.87	6250	5.40		10.91	4.20	5681	1424	923	-27	55	15	28
5/22/67			132	3.61	6570	4.90		10.68	3.96	5972	1620	1077	-26	59	13	31
5/29/67			131	3.32	6920	4.25		10.39	3.68	6290	1777	1276	-25	65	10	39
6/7/67 (1975)			138	3.00	7270	3.10		9.98	3.27	6608	2253	1571	-25	80	0	76
6/11/67			142	2.51	7740	3.75		10.20	3.49	7036	2232	1597	15	94	-42	97
6/16/67			138	2.65	7620	3.60		10.15	3.43	6927	2236	1590	13	93	-40	96
6/25/67			130	3.00	7270	3.75		10.20	3.49	6608	2096	1462	16	92	-41	99
6/30/67			126	3.32	6920	3.90		10.26	3.54	6290	1959	1336	18	94	-42	102
7/4/67			122	3.61	6570	4.05		10.31	3.60	5972	1824	1213	20	95	-42	104
5/2/67	II		180	3.00	7260	4.0	1000/1000	10.30	3.59	6599	2013	1403	12	88	-45	102
5/19/67			166	2.60	7655	3.8		10.23	3.52	6958	2171	1547	7	92	-42	101
5/29/67			156	2.50	7750	3.6		10.15	3.44	7045	2258	1617	6	93	-40	100
6/3/67 (1975)			152	2.41	7840	3.4		10.08	3.37	7127	2345	1687	7	93.5	-38	99
6/9/67			153	3.03	7200	3.3		10.05	3.34	6545	2166	1504	-24	100	2	119
6/14/67			161	3.23	6980	4.25		10.40	3.69	6345	1872	1282	-25	120	6	137
6/24/67			168	3.46	6720	5.25		10.85	4.14	6102	1545	1039	-30	130	7	155
7/4/67			169	3.61	6570	6.12		11.30	4.59	5972	1314	873	-31	147	11	159

(1) Trajectory analysis for 1964 - 1970 period pertinent to 1972 - 1978 period with at most a 5-day shift in the window.

(2) Burnout weights include the effects of 0.3 km/sec ΔV for midcourse, approach, and terminal corrections.

TABLE 10 (Cont'd)

1	2		3	4	5	6	7	8	9	10	11	12	13	14	15	16
	Trajectory									Burnout Weight[2]					Angle between Planet Approach Asymptote and:	
Launch Dates	Type	Class	Flight Time T_f (days)	Earth Departure Velocity $V_{\infty E}$ (km/sec)	Injected Weight W_i (lb)	Planet Approach Velocity $V_{\infty P}$ (km/sec)	Final Orbit Altitude Min/Max (km/km)	Velocity at Closest Passing Point V_p (km/sec)	Terminal Orbit Injection ΔV (lb)	Lander (lb)	All Orbiter (lb)	Orbiter with 2000-lb Lander (lb)	Declination of Geocentric Asymptote ϕ_a (degrees)	Communication Distance at Arrival R_p (10^6 km)	Planet Orbit γ_p (degrees)	Sunline ζ (degrees)
12/14/68	I	Min. Ener.	152	3.32	6920	4.30	1000/1000	10.42	3.71	6290	1849	1261	9	66	33	54.5
12/19/68			147	3.18	7030	4.32		10.44	3.73	6390	1860	1277	8	66.5	34	54
12/31/68			137	2.92	7370	4.55		10.53	3.82	6699	1889	1325	4	67	36	52
1/13/69			126	2.78	7470	4.55		10.53	3.82	6790	1915	1351	2	71	37	52.5
1/29/69			112	3.13	7100	4.50		10.51	3.80	6454	1840	1269	-5	72	36	54
2/13/69			100	4.12	5940	4.30		10.42	3.71	5399	1587	999	-9	74	36	61
11/16/68	II	Min. Ener.	183	4.10	5960	3.60	1000/1000	10.15	3.44	5418	1734	1094	9	66	33	78
11/23/68			175.5	3.87	6250	3.60		10.15	3.44	5681	1818	1178	12.5	68	31.5	71
12/6/68			175	3.52	6700	3.95		10.28	3.57	6090	1870	1256	13	66	31	57
12/11/68			175.5	3.74	6400	3.20		10.01	3.30	5790	1955	1280	37	88	-3	88
12/21/68			176	3.77	6370	3.10		9.95	3.24	5762	1960	1280	43	100	-14	114
1/6/69			176.5	3.73	6440	4.30		10.40	3.69	5854	1740	1140	.47	118	-19	131
7/12/70	I	Min. Ener.	146.5	3.61	6560	5.81	1000/1000	11.13	4.41	5963	1396	928	-7	51	-34	44
7/23/70			138	3.32	6920	5.74		11.10	4.39	6290	1472	1004	-4	53	-34.5	44
8/19/70			116	2.92	7350	5.47		10.95	4.24	6681	1644	1152	-0.5	59	-33	43
9/6/70			102	3.32	6920	5.31		10.89	4.18	6290	1579	1077	0.5	60	-32.5	49
9/10/70			98	3.61	6560	5.12		10.80	4.09	5963	1544	1026	0.7	62	-32	46.7
9/15/70			94	3.87	6250	5.10		10.77	4.06	5681	1488	964	1	64	-32.5	49
9/18/70			93	4.12	5940	4.90		10.69	3.98	5399	1452	914	1.5	66	-32.5	53
8/11/70	II	Min. Ener.	181	3.61	6560	5.22	1000/1000	10.84	4.13	5963	1532	1018	-52	119	28	140
9/2/70			172	3.32	6920	5.99		11.21	4.50	6290	1422	970	-46	135	27	146
9/16/70			166	3.26	7000	6.35		11.42	4.71	6363	1336	916	-41	145	25.5	149
9/27/70			163	3.32	6920	6.74		11.65	4.94	6290	1227	837	-32	153	22.5	154
10/13/70			161	3.61	6560	7.42		12.05	5.24	5963	1055	701	-22	167	16.5	160

(1) Trajectory analysis for 1964 - 1970 period pertinent to 1972 - 1978 period with at most a 5-day shift in the window.

(2) Burnout weights include the effects of 0.3 km/sec ΔV for midcourse, approach, and terminal corrections.

-66-

TABLE 11

TRAJECTORY DATA -- MARS 1969-1975

1 Launch Date	2 Type	2 Class	3 Flight Time T_f (Days)	4 Earth Departure Velocity $v_{\infty E}$ (km/sec)	5 Injected Weight W_I	6 Planet Approach Velocity $v_{\infty P}$ (km/sec)	7 Final Orbital Altitude Min/Max (km/km)	8 Velocity at Closest Passing Point v_P (km/sec)	9 Terminal Orbit Injection ΔV (km/sec)	10 Lander (lb)	11 Burnout Weight* All-Orbiter (lb)	12 Burnout Weight* Orbiter with 2000-pound Lander (lb)	13 Declination of Geocentric Asymptote ϕ_s (deg)	14 Communication Distance at Arrival R_p (10^6 km)	15 Planet Orbit γ_p (degrees)	16 Sunline ζ_p (degrees)
2/3/69	I	Min. Energy	185	3.87	6240	6.5	1500/10,000	7.724	4.154	5653	1441	931	-56	99	15.5	147
2/11/69			184	3.46	6540	6.0		7.308	3.738	5925	1732	1148	-57	105	14.5	145
2/19/69			182	2.97	7190	5.6		6.984	3.414	6514	2119	1468	-56	110	13.5	143
3/3/69			178	2.97	7300	5.02		6.528	2.958	6614	2499	1744	-50	118	12.5	138
3/15/69			176	3.16	7190	4.5		6.137	2.567	6514	2800	1940	-44	126	11.5	130
3/25/69			192	3.46	6750	3.7		5.577	2.007	6112	3158	2125	-43	152	14	104
4/10/69			220	3.87	6240	4.0		5.780	2.211	5653	2685	1765	-49	194	13	61
2/3/69			185	3.87	6240	6.5	1800/1800	7.659	4.795	5653	1167	754	-56	99	15.5	147
2/11/69			184	3.46	6540	6.0		7.239	4.375	5925	1405	931	-57	105	14.5	145
2/19/69			182	2.97	7190	5.6		6.912	4.048	6514	1720	1192	-56	110	13.5	143
3/3/69			178	2.97	7300	5.02		6.451	3.587	6614	2032	1417	-50	118	12.5	138
3/15/69			176	3.16	7190	4.5		6.055	3.191	6514	2280	1580	-44	126	11.5	130
3/25/69			192	3.46	6750	3.7		5.486	2.622	5925	2501	1657	-43	152	14	104
4/10/69			220	3.87	6240	4.0		5.693	2.829	5653	2229	1440	-49	194	13	61
2/11/69	II	Min. Energy	283	3.13	7130	4.23	1500/10,000	5.95	2.38	6447	2940	2030	5	194	-18	58
3/10/69			292	2.9	7370	4.8		6.37	2.80	6700	2668	1870	0	232	-17	44
3/17/69			293	2.85	7420	4.9		6.44	2.88	6750	2618	1840	-2	240	-16	41
4/1/69			299	2.81	7450	5.17		6.44	3.07	6770	2478	1742	-7	260	-14	37
4/16/69			301	2.86	7400	5.36		6.78	3.22	6725	2320	1630	-18	280	-10	33
5/4/69			306	3.16	7100	5.44		6.79	3.23	6454	2230	1540	-30	300	-4	28
2/11/69			283	3.13	7130	4.23	1800/1800	5.88	3.02	6447	2382	1642	5	194	-18	58
3/10/69			292	2.9	7370	4.8		6.30	3.44	6700	2150	1510	0	232	-17	44
3/17/69			293	2.85	7420	4.9		6.36	3.50	6750	2140	1508	-2	240	-16	41
4/1/69			299	2.81	7450	5.17		6.57	3.71	6770	1997	1408	-7	260	-14	37
4/16/69			301	2.86	7400	5.35		6.72	3.86	6725	1882	1324	-18	280	-10	33
5/4/69			306	3.16	7100	5.44		6.78	3.92	6454	1772	1225	-30	300	-4	28
4/8/71	I	Min. Energy	181	4.24	5800	4.60	1500/10,000	6.21	2.65	5272	2198	1364	-38	81	12	137
4/15/71			185	3.87	6250	4.15		5.90	2.34	5681	2619	1959	-37	92	10	132
4/24/71			188	3.46	6750	3.55		5.48	1.92	6136	3252	2192	-34	103	7	124
5/3/71			193	3.16	7100	3.21		5.28	1.72	6454	3659	2525	-32	118	3.5	115
5/8/71			195	3.00	7270	3.03		5.17	1.61	6608	3886	2710	-30	126	2	107
5/19/71			206	2.83	7440	2.84		5.08	1.52	6763	4098	2882	-23	150	-6	87
5/24/71			210	2.81	7470	2.87		5.06	1.50	6790	4142	2922	-18	163	-9	82
5/28/71			214	2.83	7440	2.90		5.09	1.53	6763	4065	2863	-15	175	-12	76
6/7/71			220	3.00	7270	3.02		5.16	1.60	6608	3899	2719	-8	196	-16.5	67
6/14/71			221	3.16	7100	3.17		5.23	1.67	6454	3737	2579	-4	206	-18	62
6/22/71			227	3.46	6750	3.35		5.26	1.80	6136	3387	2283	-1	225	-19.5	58
6/30/71			233	3.87	6250	3.60		5.52	1.96	5681	2983	1706	2	246	-20	54
4/8/71			181	4.24	5800	4.60	1800/1800	6.15	3.29	5272	1777	1103	-38	81	12	137
4/15/71			185	3.87	6250	4.15		5.82	2.96	5681	2142	1388	-37	92	10	132
4/24/71			188	3.46	6750	3.55		5.42	2.56	6136	2638	1778	-34	103	7	124
5/3/71			193	3.16	7100	3.21		5.21	2.35	6454	2969	2049	-32	118	3.5	115
5/8/71			195	3.00	7270	3.03		5.09	2.23	6608	3180	2220	-30	126	2	107
5/19/71			206	2.83	7440	2.84		4.96	2.10	6763	3382	2382	-23	150	-6	87
5/24/71			210	2.81	7470	2.87		4.98	2.12	6790	3380	2387	-18	163	-9	82
5/28/71			214	2.83	7440	2.90		5.00	2.14	6763	3334	2348	-15	175	-12	76
6/7/71			220	3.00	7270	3.02		5.09	2.23	6608	3180	2220	-8	196	-16.5	67
6/14/71			221	3.16	7100	3.17		5.16	2.30	6454	3027	2089	-4	206	-18	62
6/22/71			227	3.46	6750	3.35		5.28	2.42	6136	2765	1865	-1	225	-19.5	58
6/30/71			233	3.87	6250	3.60		5.45	2.59	5681	2420	1568	2	246	-20	54

*Burnout weights include the effects of 0.3 km/sec ΔV for midcourse, approach, and terminal corrections.

Columns 15 and 16 are grouped under the heading "Angle Between Planet Approach Asymptote and:".

TABLE 11 (Concl'd)

| | Trajectory | | | | | | | | Burnout Weight* | | | | | Angle Between Planet Approach Asymptote and: | |
Launch Date	Type	Class	Flight Time T_f (Days)	Earth Departure Velocity $V_{\infty E}$ (km/sec)	Injected Weight W_i (lb)	Planet Approach Velocity $V_{\infty P}$ (km/sec)	Final Orbital Altitude Min/Max (km/km)	Velocity at Closest Passing Point V_p (km/sec)	Terminal Orbit Injection ΔV (km/sec)	Lander (lb)	All-Orbiter (lb)	Orbiter with 2000-pound Lander (lb)	Declination of Geocentric Asymptote ϕ_s (deg)	Communication Distance at Arrival R_p (10^6 km)	Planet Orbit γ_p (degrees)	Sunline ζ_p (degrees)
3/26/71	II	Min. Energy	250	4.243	5700	3.58	1500/10,000	5.498	1.928	5181	2748	1687	2	139	-23	80
4/10/71			250	3.873	6250	3.47		5.427	1.857	5681	3084	1998	3.5	158	-22	77.2
4/25/71			250	3.464	6750	3.33		5.338	1.768	6136	3430	2312	2	177	-19.5	66.8
5/10/71			244	3.114	7150	3.07		5.180	1.610	6500	3827	2650	-13	190	-7.5	63.7
5/13/71			256	3.464	6750	3.20		5.258	1.688	6136	3521	2374	-27	209	4.5	56.2
5/25/71			286	3.873	6250	3.62		5.524	1.954	6136	2987	1936	-27	264	9.5	43
6/22/71			338	4.243	5700	4.08		5.836	2.266	5181	2458	1509	-20.5	352	13	32
3/26/71	II	Min. Energy	250	4.243	5700	3.58	1800/1800	5.406	2.542	5181	2245	1378	2	139	-23	80
4/10/71			250	3.873	6250	3.47		5.244	2.470	5681	2521	1633	3.5	158	-22	77.2
4/25/71			250	3.464	6750	3.33		5.244	2.380	5681	2804	1890	2	177	-19.5	66.8
5/10/71			244	3.114	7150	3.07		5.083	2.219	6500	3132	2169	-13	190	-7.5	63.7
5/13/71			256	3.464	6750	3.20		5.162	2.298	6136	2881	1942	-27	209	4.5	56.2
5/25/71			286	3.873	6250	3.62		5.433	2.569	5681	2440	1581	-27	264	9.5	43
6/22/71			338	4.243	5700	4.08		5.749	2.885	5181	2006	1234	-20.5	352	13	32
6/30/73	I	Min. Energy	198	4.58	5380	3.65	1500/10,000	5.56	2.0	4890	2523	1491	32.5	143	-23	134
7/9/73			197	4.24	5800	3.46		5.43	1.87	5263	2853	1770	33	153	-24.5	133
7/17/73			196	4.0	6080	3.24		5.31	1.75	5526	3100	1978	32.5	164	-25	132
7/30/73			195	3.82	6300	3.02		5.18	1.62	5726	3350	2180	31	186	-22	131
8/10/73			199	4.0	6080	2.75		5.02	1.46	5526	3426	2187	25	198	-22.5	122
8/16/73			201	4.24	5800	2.65		4.98	1.42	5263	3300	2046	24	208	-23	116
8/31/73			231	5.2	4750	2.55		4.91	1.35	4317	2767	1486	27	276	-25	83
6/30/73	I	Min. Energy	198	4.58	5380	3.65	1800/1800	5.48	2.62	4890	2054	1214	32.5	143	-23	134
7/9/73			197	4.24	5800	3.46		5.33	2.47	5263	2338	1450	33	153	-24.5	133
7/17/73			196	4.0	6080	3.24		5.23	2.37	5526	2537	1619	32.5	164	-25	132
7/30/73			195	3.82	6300	3.02		5.08	2.22	5726	2749	1789	31	186	-22	131
8/10/73			199	4.0	6080	2.75		4.92	2.06	5526	2802	1788	25	198	-22.5	122
8/16/73			201	4.24	5800	2.65		4.86	2.00	5263	2716	1684	24	208	-23	116
8/31/73			231	5.2	4750	2.55		4.80	1.94	4317	2275	1221	27	276	-25	83
8/23/75	I	Min. Energy	200	5.20	4720	4.8	1500/10,000	6.36	2.70	4290	1755	937	52.5	183	-19	150
8/27/75			204	4.90	5010	4.53		6.17	2.61	4554	1922	1078	52.4	192	-18	149.5
8/31/75			205	4.69	5250	4.4		6.07	2.51	4772	2081	1209	52.4	200	-17	149
9/6/75			206	4.47	5510	4.2		5.94	2.38	5009	2284	1371	52	209	-16.5	148.5
9/15/75			206	4.30	5700	3.8		5.65	2.09	5181	2596	1594	47.5	222	-15.3	147
9/24/75			206	4.47	5510	3.35		5.37	1.81	5009	2750	1652	42.5	233	-14	144
9/29/75			209	4.69	5250	3.2		5.28	1.72	4772	2710	1574	40	242	-13.5	142
10/3/75			212	4.90	5010	3.1		5.22	1.66	4554	2637	1479	38.5	253	-13	138
10/7/75			214	5.20	4720	3.0		5.16	1.60	4290	2531	1351	37	262	-12.5	123
8/23/75	I	Min. Energy	200	5.20	4720	4.8	1800/1800	6.28	3.24	4290	1360	726	52.5	183	-19	150
8/27/75			204	4.90	5010	4.53		6.10	3.14	4554	1562	876	52.4	192	-18	149.5
8/31/75			205	4.69	5250	4.4		6.00	2.99	4772	1694	984	52.4	200	-17	149
9/6/75			206	4.47	5510	4.2		5.85	2.72	5009	1868	1122	52	209	-16.5	148.5
9/15/75			206	4.30	5700	3.8		5.58	2.42	5181	2114	1298	47.5	222	-15.3	147
9/24/75			206	4.47	5510	3.35		5.28	2.33	5009	2254	1354	42.5	233	-14	144
9/29/75			209	4.69	5250	3.2		5.19	2.27	4772	2214	1286	40	242	-13.5	142
10/3/75			212	4.90	5010	3.1		5.13	2.20	4554	2149	1205	38.5	253	-13	138
10/7/75			214	5.20	4720	3.0		5.06		4290	2076	1108	37	262	-12.5	123
8/9/75	II	Min. Energy	331	4.688	5255	2.381	1500/10,000	4.804	1.234	4761	3172	1839	6.52	330	25.8	78.7
8/25/75			346	4.047	6037	2.480		4.854	1.284	5470	3585	2274	7.09	353	25.2	67.6
9/1/75			353	3.850	6276	2.564		4.897	1.328	5686	3674	2381	8.40	361	23.9	62.5
9/8/75			362	3.719	6435	2.692		4.966	1.396	5831	3684	2420	11.07	369	22.1	57.5
9/15/75			372	3.657	6510	2.868		5.063	1.494	5898	3609	2385	14.62	374	18.5	50.6
9/22/75			386	3.660	6507	3.138		5.221	1.651	5895	3424	2263	19.54	378	15.1	44.5
10/8/75			427	3.803	6334	4.132		5.872	2.302	5739	2690	1753	30.09	371	7.0	30.8

*Burnout weights include the effects of 0.3 km/sec ΔV for midcourse, approach, and terminal corrections.

1. <u>Launch date</u>: Date of departure from Earth.

2. <u>Trajectory type and class</u>: Type I refers to trajectories where the heliocentric transfer angle (angle between sun-Earth line at departure and sun-planet line at encounter) is less than 180 degrees, and Type II trajectories have angles greater than 180 degrees. This entire analysis was conducted with minimum energy departure velocities which represent the singularity separating class I trajectories from class II trajectories within each trajectory type. Class I trajectories have shorter transfer times and smaller transfer angles than the corresponding class II trajectories for a given launch date within each trajectory type.

3. <u>Flight time</u>: Time in days from Earth departure to planetary impact

4. <u>Earth departure velocity</u>: Geocentric asymptotic departure velocity (hyperbolic excess velocity). It is equal to the square root of twice the energy per unit mass.

5. <u>Injected weight</u>: The total weight of the spacecraft injected into the interplanetary orbit.

6. <u>Planetary approach velocity</u>: The planetocentric asymptotic approach velocity.

7. <u>Final orbit altitude (Min/Max)</u>: The minimum and maximum altitudes for the terminal orbit about the destination planet. In the cases where the min/max altitudes are equal, the orbits are circular.

8. <u>Velocity at closest passing point</u> - The periapsis velocity along the approach hyperbola.

9. <u>Terminal orbit injection ΔV</u>: The velocity increment for impulsive injection into the terminal orbit at the periapsis point from the approach trajectory.

10. <u>Burnout weight, lander</u>: The all-lander weight is equal to the weight injected into the heliocentric transfer orbit minus the propellant weight for the 0.3 km/sec midcourse, approach, and terminal corrections.

11. <u>Burnout weight, all-orbiter</u>: The all-orbiter weight is equal to the all-lander weight minus the propellant weight for injection into the desired planetocentric orbit.

12. <u>Burnout weight, orbiter with 2000-pound lander</u>: The split-capsule orbiter weight is equal to the all-lander weight less the 2000-pound lander weight minus the propellant weight required to establish the desired planetocentric orbit.

13. <u>Declination of the geocentric asymptote</u>: The declination of the departure velocity asymptote or hyperbolic excess velocity vector with respect to the Earth's equatorial plane.

14. <u>Communication distance at arrival</u>: The Earth-to-planet distance at encounter.

15. <u>Angle between approach asymptote and the orbital plane of the planet</u>: The angle between asymptotic approach velocity vector and the plane of the planet's orbit about the sun. The angle is positive for the case of an approach from below the planet's orbital plane.

16. <u>Angle between approach asymptote and sunline</u>: The angle between the asymptotic approach velocity vector and the planet sunline is measured from the sunline on the dark side of the planet clockwise for Venus and counterclockwise for Mars.

4.4 Determination of Departure Velocity to Maximize Daily Mission Payloads

For the all-orbiter and split-capsule orbiter/lander missions, the final payload (exclusive of dry propulsion system weights) placed in a given planetocentric orbit is a function of the hyperbolic excess departure velocity (heliocentric injected weight varies approximately linearly with the square of the departure velocity) and the hyperbolic excess velocity at encounter. The dependence of payload on variations in hyperbolic excess approach velocity can be shown through the velocity decrement required to establish the desired planetocentric orbit by

$$\Delta V = \sqrt{V_\infty^2 + \frac{2\mu}{r_p}} - \sqrt{\frac{r_a}{r_p} \frac{2\mu}{r_a + r_p}}$$

and

$$W_{pL} = W_o \left[1 + \frac{1}{PMF} \left(e^{-\frac{\Delta V}{c}} - 1 \right) \right]$$

where

V_∞ =   asymptotic approach velocity

μ =   gravitational parameter

r_a, r_p = apoapsis and periapsis radii

c = effective exhaust velocity

PMF = propellant mass fraction

W_o = weight along approach hyperbola.

If all other variables remain constant, the required velocity decrement decreases as the asymptotic approach velocity decreases and the corresponding orbital payload increases. Therefore, the maximum weight is injected into the heliocentric transfer orbit when the minimum hyperbolic excess departure velocity is employed, and the maximum weight is injected into the desired planetocentric orbit when the hyperbolic excess approach velocity is minimized for a given weight along the approach hyperbola. Since the approach velocity vector is a function of the transfer orbit characteristics, including departure velocity, the distance from the sun at encounter and the components of the planet's orbital velocity, the minimum departure and approach velocities, in general, are not simultaneously achieved. For a given departure date, the time of interplanetary flight between trajectories possessing the characteristics of minimum departure velocity and minimum arrival velocity can vary from 0 to 50 days, depending upon the target planet and launch opportunity.

A second payload analysis, similar to that previously conducted for the minimum departure velocity, was conducted for 5 or 6 different launch dates in each opportunity where, for a given launch date, the time of flight was varied in 2-day intervals between the time corresponding to the minimum departure and arrival velocities. These results indicated that the "all-orbiter" payload mission is maximized daily when the sum of the departure and arrival velocities is minimized. Generally, payload increases between 25 to 100 pounds are achieved over those associated with the minimum departure velocity.

For the split-capsule orbiter/lander mission the maximum daily payload occurs at or within a few days time of flight of the minimum sum. The increased payloads for this mission are reduced slightly, in general, from those of the corresponding all-orbiter mission.

It is interesting to note that, in general, the minimum sum occurs closer to the minimum arrival velocity in time than to the minimum departure velocity. For Mars Type II trajectories in 1969 and 1975, the minimum sum is achieved for a class I transfer, whereas for Type I trajectories in 1971 and 1973, the location of the minimum sum changes from class II to class I near the middle of the launch opportunity. For Venus Type II trajectories in 1972, the minimum sum occurs for a class I transfer, while in 1973 it is for a class II transfer.

For Venus Type I trajectories in 1970, the minimum sum occurs for a class II transfer, while in 1975 there is a switch from class II to class I.

While this analysis was conducted for both Type I and II transfers in each launch opportunity, one transfer (in each opportunity) is more desirable than the other when consideration is made regarding launch azimuth constraints and injection energy requirements. For the above mentioned transfer trajectories, these results are presented in summary tabular form for Venus in table 12 and Mars in table 13. Slight discrepancies may be noted between the minimum departure velocity results associated with the analysis and those previously presented. These discrepancies arise from the fact that the departure and arrival velocities for this present analysis were obtained from JPL trajectory data whereas the original set of velocities was obtained from summary curves in ref. (1).

In addition to the increases in the burnout weight, there is an additional payload increase resulting from the fact that the propulsion system weights associated with the minimum of the sum of the departure and arrival velocities is reduced. Associated with this daily maximization technique, there is also a 1- to 2-day shift in the best 30-day window.

This comparison, in addition to the propulsion system requirements, is presented in table 14. The propulsion system is sized, in general, by the absolute minimum departure velocity for a given launch opportunity, and this minimum is increased when departure velocities associated with the minimum sum are employed.

4.5 Final Mission Payload Analysis

1. <u>Mars.</u> Since it has been shown that the daily payload for the all-orbiter and split-capsule orbiter/lander mission for a fixed set of propulsion system characteristics is essentially maximized when the sum of the departure and arrival velocities is minimized, these velocity components are employed in the daily calculations for the final mission payload analysis. In this analysis, revised propulsion system characteristics are also employed. The specific impulse has been increased to 327 seconds from 310 seconds and the propellant mass fraction increased to 0.88 from 0.865.

For Mars, the optical mapping system and communication systems have been developed for a nominal elliptic orbit with periapsis and apoapsis altitudes of 1500 and 10,000 km, respectively. Therefore, the purpose of the analysis is to determine the maximum orbiter scientific payload that can be placed in the nominal planetocentric orbit with the final lander design weight of 1880 pounds. In 1971, due to the increased payload capability a two-lander mission is envisioned; a single lander mission in 1969 and 1973 is contemplated while a lander-fly-by mission will be employed in 1975. The nominal periapsis altitude has been increased from 1500 to 1700 km because a 3-sigma estimate

TABLE 12

TRAJECTORY PARAMETERS ASSOCIATED WITH DAILY PAYLOAD MAXIMIZATION -- VENUS

Planet	Type	Date	Time of Flight (days)	Departure Velocity (km/sec)	Approach Velocity (km/sec)	Injected Weight (lbs)	Burnout Weight			Propellant Weight (lbs)
							All Lander (lbs)	All Orbiter (lbs)	Orbiter with 2,000 Lander (lbs)	
Venus	I	12/14/68	150	3.3925	4.0449	6826	6184	1888	1278	3548
			152	3.3086	4.2620	6923	6272	1861	1268	3655
		12/30/68	136	2.9512	4.4864	7313	6626	1907	1331	3982
			138	2.9266	4.4966	7342	6652	1909	1335	4007
		1/7/69	130	2.8131	4.5381	7449	6749	1928	1357	4093
			132	2.8110	4.5386	7450	6750	1928	1357	4093
		1/13/69	126	2.7785	4.5279	7490	6786	1941	1369	4121
		1/19/69	120	2.8267	4.5422	7433	6734	1922	1351	4082
			122	2.8301	4.4941	7430	6732	1935	1360	4070
		1/27/69	114	3.0323	4.4782	7230	6551	1887	1311	3919
			116	3.0437	4.4275	7220	6541	1898	1317	3903
		2/12/69	102	4.0294	4.3161	6058	5487	1617	1027	3031
			104	4.0344	4.2731	6052	5483	1625	1032	3020
			106	4.0489	4.2726	6035	5468	1620	1028	3007

TABLE 12 (Cont'd)

Planet	Type	Date	Time of Flight (days)	Departure Velocity (km/sec)	Approach Velocity (km/sec)	Injected Weight (lbs)	Burnout Weight			Propellant Weight (lbs)
							All Lander (lbs)	All Orbiter (lbs)	Orbiter with 2,000 Lander (lbs)	
		8/5/70	128	3.0432	5.5729	7220	6542	1593	1106	4114
			130	3.0806	5.5221	7181	6506	1597	1106	4075
		8/13/70	120	2.9413	5.5739	7324	6636	1615	1128	4196
			124*	2.9826	5.3641	7282	6598	1662	1158	4124
			126	3.0619	5.3559	7201	6524	1646	1141	4060
		8/19/70	116	2.9195	5.4246	7346	6656	1660	1161	4185
			118	2.9353	5.2941	7329	6640	1692	1182	4147
			120*	2.9811	5.2165	7285	6600	1703	1187	4098
			122	3.0631	5.2015	7200	6523	1687	1170	4030
		8/25/70	110	2.9681	5.4297	7298	6612	1648	1150	4149
			112	2.9808	5.2587	7295	6609	1694	1181	4114
			114	2.9958	5.1315	7270	6587	1722	1199	4071
			116*	3.0465	5.5041	7217	6539	1730	1201	4016
			118	3.1274	5.0343	7130	6460	1715	1182	3948
		9/4/70	102	3.2412	5.2451	7003	6345	1629	1116	3887
			104	3.2463	5.0599	6997	6339	1676	1147	3850
			106	3.2665	4.9137	6973	6318	1708	1167	3806
			108	3.3033	4.8100	6930	6279	1724	1175	3755
			110*	3.3588	4.7531	6865	6220	1722	1169	3697
			112	3.4364	4.7483	6773	6137	1700	1146	3627

* Time of flight corresponding to the minimum of the sum of departure and arrival velocites.

-74-

TABLE 12(Cont'd)

Planet	Type	Date	Time of Flight (days)	Departure Velocity (km/sec)	Approach Velocity (km/sec)	Injected Weight (lbs)	Burnout Weight			Propellant Weight (lbs)
							All Lander (lbs)	All Orbiter (lbs)	Orbiter with 2,000 Lander (lbs)	
Venus	II	2/24/72*	184	3.618	4.619	6555	5958	1682	1118	3437
		(2/29/64)	186**	3.574	4.631	6615	6013	1695	1131	3484
			188	3.554	4.676	6640	6036	1690	1130	3510
		3/19/72*	178	3.222	4.882	7020	6381	1733	1190	3830
		(3/15/64)	180**	3.184	4.900	7065	6422	1740	1198	3867
			182	3.171	4.951	7080	6436	1730	1193	3887
		3/24/72*	170	2.991	5.114	7275	6613	1733	1209	4066
		(3/29/64)	172**	2.938	5.115	7330	6663	1747	1222	4108
			174	2.913	5.151	7355	6686	1743	1221	4134
			176	2.913	5.216	7355	6686	1725	1209	4146
		4/8/72*	162	2.957	5.346	7310	6645	1679	1174	4136
		(4/13/64)	164**	2.903	5.353	7365	6695	1690	1185	4180
			166	2.875	5.393	7390	6718	1684	1183	4207
			168	2.867	5.461	7400	6727	1668	1172	4228
		4/25/72*	152	3.370	5.651	6855	6231	1503	1021	3834
		(4/30/64)	154**	3.308	5.667	6925	6295	1508	1029	3896
			156	3.263	5.715	6975	6340	1507	1032	3943
			158	3.232	5.785	7010	6372	1496	1027	3983
			160	3.212	5.872	7035	6395	1480	1017	4018
			162	3.203	5.973	7045	6404	1456	1001	4044

*These values were obtained from a comparison of the 1964-1972 Metonic cycle. The 1972 dates of launch indicate a (-5) day shift when compared to 1964.

**Time of flight corresponding to the minimum of the sum of departure and arrival velocities.

-75-

TABLE 12 (Cont'd)

Planet Type	Date	Time of Flight (days)	Departure Velocity (km/sec)	Approach Velocity (km/sec)	Injected Weight (lbs)	Burnout Weight			Propellant Weight (lbs)
						All Lander (lbs)	All Orbiter (lbs)	Orbiter/ 2,000 Lander (lbs)	
Venus II	10/11/73* (10/16/65)	172 174	3.151 3.151	4.416 4.385	7105 7105	6437 6437	1871 1879	1289 1295	3816 3810
	10/26/73* (10/31/65)	164 166	2.796 2.821	4.276 4.273	7468 7446	6766 6746	2004 1999	1412 1406	4056 4040
	11/3/73* (11/8/65)	158 160	2.706 2.725	4.216 4.201	7550 7533	6840 6825	2043 2042	1445 1444	4105 4089
	11/10/73* (11/15/65)	152 154	2.720 2.729	4.185 4.143	7549 7530	6840 6822	2051 2057	1451 1454	4098 4076
	11/17/73* (11/22/65)	146 148	2.848 2.853	4.158 4.091	7415 7410	6718 6714	2022 2038	1420 1431	3995 3979
	11/23/73* (11/28/65)	142 144	3.068 3.089	4.057 4.040	7194 7172	6518 6498	1987 1986	1378 1375	3816 3797

*These values were obtained from a comparison of the 1965-1973 Metonic cycle. The 1973 dates of launch indicate a (-5) day shift when compared to 1965.

TABLE 12 (Cont'd)

Planet Type	Date	Time of Flight (days)	Departure Velocity (km/sec)	Approach Velocity (km/sec)	Injected Weight (lbs)	Burnout Weight			Propellant Weight (lbs)
						All Lander (lbs)	All Orbiter (lbs)	Orbiter 2,000 Lander (lbs)	
Venus I	5/27/75* 6/1/67	130	3.2337	3.8985	7007	6348	1975	1353	3654
		132	3.2356	3.6958	7005	6347	2024	1386	3619
		133	3.2408	3.6038	7000	6342	2045	1400	3600
		135	3.2617	3.4405	6980	6324	2077	1420	3560
		137	3.3023	3.3091	6930	6279	2093	1426	3504
		138**	3.3319	3.2576	6900	6252	2095	1425	3475
		140	3.4202	3.1931	6800	6161	2079	1404	3296
		141	3.4869	3.1869	6710	6079	2053	1377	3233
	6/1/75* (6/6/67)	134	3.0726	3.1273	7190	6514	2214	1534	3656
		135	3.0735	3.0681	7188	6512	2226	1542	3646
		137	3.0815	2.9698	7180	6505	2246	1555	3625
		138	3.0896	2.9308	7170	6496	2251	1558	3612
		140**	3.1193	2.8756	7140	6469	2253	1557	3583
		141	3.1449	2.8609	7110	6442	2247	1550	3560
		142	3.1840	2.8580	7065	6401	2234	1536	3529
	6/6/75* (6/11/67)	137	2.8255	2.8840	7445	6745	2348	1652	3793
		138	2.7942	2.8876	7480	6777	2358	1662	3818
		140**	2.7063	2.9470	7560	6850	2369	1678	3882
		141	2.6418	3.0298	7627	6910	2371	1685	3942
		142	2.5592	3.2118	7700	6976	2350	1676	4024
		143	2.5128	3.7258	7740	7013	2228	1593	4147
	6/11/75* (6/16/67)	130	2.8671	3.0247	7400	6705	2302	1615	3785
		132	2.8119	3.0282	7460	6759	2320	1633	3827
		133**	2.7805	3.0501	7490	6786	2324	1639	3851
		135	2.7100	3.1534	7555	6845	2319	1642	3913
		137	2.6384	3.4013	7630	6913	2281	1621	4009
		138	2.6227	3.6431	7640	6922	2221	1580	4060

*These values were obtained from a comparison of the 1967-1975 Metonic cycle. The 1975 dates of launch indicate a (-5) day shift when compared to 1967

**Time of flight corresponding to the minimum of the sum of departure and arrival velocities.

Table 12 (Concl'd)

Planet Type	Date	Time of Flight (days)	Departure Velocity (km/sec)	Approach Velocity (km/sec)	Injected Weight (lbs)	Burnout Weight			Propellant Weight (lbs)
						All Lander (lbs)	All Orbiter (lbs)	Orbiter/ 2,000 Lander (lbs)	
Venus I	6/16/75*	126	2.9740	3.1446	7295	6609	2241	1563	3732
	(6/21/67)	128**	2.9219	3.1852	7345	6655	2247	1572	3773
		130	2.8677	3.2888	7405	6709	2241	1573	3832
		132	2.8200	3.4895	7450	6750	2201	1549	3901
		133	2.8073	3.6488	7465	6763	2169	1527	3938
	6/21/75*	120	3.2401	3.2558	7000	6342	2126	1456	3544
	(6/26/67)	122**	3.1942	3.2753	7055	6392	2138	1469	3586
		123	3.1707	3.3023	7080	6415	2139	1472	3608
		125	3.1244	3.3970	7145	6474	2137	1477	3668
		128	3.0704	3.6804	7191	6514	2082	1443	3748
		129	3.0656	3.8326	7196	6520	2045	1418	3778

*These values were obtained from a comparison of the 1967-1975 Metonic cycle. The 1975 dates of launch indicate a (-5) day shift when compared to 1967.

**Time of flight corresponding to the minimum of the sum of departure and arrival velocities.

TABLE 13

TRAJECTORY PARAMETERS ASSOCIATED WITH DAILY PAYLOAD MAXIMIZATION--MARS

Planet	Type	Date	Time of Flight (days)	Departure Velocity (km/sec)	Approach Velocity (km/sec)	Injected Weight (lb)	Burnout Weight			Propellant Weight (lb)
							All Lander (lb)	All Orbiter (lb)	Orbiter with 2000 pound Lander (lb)	
Mars	II	1/15/69	270	3.5986	3.7266	6581	5963	3064	2036	2545
			272*	3.5980	3.7306	6592	5972	3065	2039	2553
			274	3.5839	3.7401	6597	5977	3062	2037	2560
			276	3.5831	3.7548	6599	5979	3053	2032	2567
		1/25/69	268	3.4704	3.8228	6739	6106	3071	2065	2678
			270	3.4435	3.8236	6785	6147	3091	2085	2700
			272	3.4233	3.8306	6788	6150	3088	2085	2704
			274*	3.4092	3.8434	6805	6165	3086	2085	2720
			276	3.4009	3.8615	6815	6175	3080	2082	2733
			278	3.3977	3.8844	6820	6179	3065	2073	2747
		1/31/69	270	3.3826	3.9113	6837	6194	3054	2068	2769
			272	3.3528	3.9174	6872	6226	3066	2081	2791
			274*	3.3307	3.9297	6897	6249	3069	2086	2811
			276	3.3154	3.9476	6916	6266	3065	2086	2830
			278	3.3065	3.9705	6927	6276	3054	2080	2847
			280	3.3033	3.9980	6930	6279	3036	2069	2861
		2/16/69	272	3.2851	4.2317	6960	6306	2918	1993	2967
			274	3.2279	4.2319	7020	6360	2943	2017	3003
			276	3.1831	4.2399	7070	6406	2959	2035	3035
			278	3.1491	4.2545	7110	6442	2965	2044	3066
			280*	3.1247	4.2748	7135	6464	2932	2025	3110
			282	3.1088	4.3001	7150	6478	2920	2019	3131
			284	3.1006	4.3298	7160	6487	2904	2009	3151
			286	3.0993	4.3633	7160	6487	2881	1993	3167
		3/2/69	278	3.1243	4.5516	7134	6464	2744	1897	3237
			280	3.0790	4.5566	7192	6516	2763	1916	3277
			282	3.0274	4.5687	7237	6557	2772	1926	3311
			284	2.9975	4.5867	7268	6585	2771	1930	3338
			286	2.9777	4.6097	7288	6603	2764	1926	3362
			288	2.9670	4.6368	7299	6613	2749	1918	3381
			290	2.9642	4.6675	7302	6616	2717	1905	3397

*Time of flight corresponding to the minimum to the sum of departure and arrival velocities.

TABLE 13 (Cont'd)

Planet	Type	Date	Time of Flight (days)	Departure Velocity (km/sec)	Approach Velocity (km/sec)	Injected Weight (lb)	Burnout Weight			Propellant Weight (lb)
							All Lander (lb)	All Orbiter (lb)	Orbiter with 2000 pound Lander (lb)	
		4/24/71	188	3.4806	3.5868	6721	6721	6089	2165	2556
			190	3.4832	3.5184	6717	6086	3270	2195	2522
			192	3.4893	3.4556	6710	6079	3310	2221	2489
			194	3.4991	3.3984	6698	6069	3344	2242	2456
			196	3.5129	3.3469	6682	6054	3372	2258	2424
			198	3.5313	3.3014	6660	6034	3392	2268	2392
			200	3.5547	3.2620		6010	3405	2272	2361
			202*	3.5839	3.2291	6598	5978	3410	2269	2329
			204	3.6200	3.2030	6555	5939	3406	2259	2296
			206	3.6644	3.1846	6501	5890	3390	2239	2262
			208	3.7190	3.1748	6435	5830	3362	2209	2226
		5/10/71	198	2.9212	2.9163	7343	6653	4034	2821	2522
			200	2.9217	2.8938	7343	6653	4051	2833	2510
			202	2.9231	2.8749	7341	6651	4064	2842	2499
			204	2.9255	2.8594	7339	6649	4075	2849	2490
			206	2.9288	2.8471	7336	6647	4082	2854	2482
			208	2.9329	2.8380	7332	6643	4087	2857	2476
			210*	2.9379	2.8319	7327	6638	4089	2857	2470
			212	2.9437	2.8286	7321	6633	4088	2855	2466
			214	2.9503	2.8279	7314	6627	4085	2852	2462
		5/24/71	204	2.8142	2.8222	7448	6748	4164	2929	2518
			206*	2.8100	2.8235	7502	6797	4193	2959	2543
			208	2.8088	2.8274	7503	6798	4190	2958	2545
			210	2.8083	2.8336	7503	6798	4186	2954	2549
		6/9/71	192	3.1254	2.8836	7133	6463	3942	2722	2411
			194	3.1122	2.8851	7147	6475	3949	2729	2418
			196	3.1015	2.8887	7159	6486	3953	2734	2425
			198	3.0914	2.8943	7169	6495	3955	2737	2432
			200*	3.0818	2.9019	7179	6505	3955	2739	2441
			202	3.0728	2.9114	7189	6513	3953	2739	2450
			204	3.0644	2.9225	7198	6521	3949	2738	2460
			206	3.0568	2.9354	7206	6528	3944	2736	2470

*Time of flight corresponding to the minimum to the sum of departure and arrival velocities.

TABLE 13 (Cont'd)

Planet	Type	Date	Time of Flight (days)	Departure Velocity (km/sec)	Approach Velocity (km/sec)	Injected Weight (lb)	Burnout Weight			Propellant Weight (lb)
							All Lander (lb)	All Orbiter (lb)	Orbiter with 2000 pound Lander (lb)	
Mars	I	6/9/71	208	3.0499	2.9499	7213	6535	3937	2732	2481
			210	3.0439	2.9560	7219	6541	3929	2727	2492
			212	3.0388	2.9837	7225	6546	3918	2721	2504
			214	3.0347	3.0030	7229	6549	3906	2713	2516
			216	3.0313	3.0239	7232	6553	3892	2704	2528
			218	3.0303	3.0463	7233	6553	3876	2693	2540
			220	3.0303	3.0705	7233	6553	3858	2680	2553
		6/25/71	180	3.9714	3.0478	6130	5554	3284	2101	2029
			184	3.9278	3.0516	6182	5601	3309	2128	2055
			188	3.8855	3.0618	6234	5648	3330	2151	2083
			192	3.8447	3.0774	6283	5693	3346	2171	2112
			196	3.8055	3.0979	6330	5735	3358	2187	2143
			200*	3.7682	3.1227	6375	5776	3365	2200	2175
			204	3.7332	3.1514	6418	5815	3369	2210	2208
			206	3.7167	3.1671	6438	5833	3369	2214	2224
			208	3.7008	3.1837	6457	5850	3368	2216	2241
			210	3.6857	3.2011	6475	5867	3365	2218	2257
			214	3.6583	3.2387	6508	5896	3357	2218	2290
			218	3.6351	3.2798	6537	5923	3344	2215	2322
			222	3.6171	3.3247	6559	5943	3325	2206	2353
			226	3.6058	3.3742	6572	5954	3298	2190	2382
			230	3.6030	3.4291	6575	5957	3262	2167	2409

*Time of flight corresponding to the minimum of the sum of departure and arrival velocities.

TABLE 13 (Cont'd)

Planet	Type	Date	Time of Flight (days)	Departure Velocity (km/sec)	Approach Velocity (km/sec)	Injected Weight (lb)	Burnout Weight			Propellant Weight (lb)
							All Lander (lb)	All Orbiter (lb)	Orbiter with 2000 pound Lander (lb)	
Mars	I	7/22/73	194	3.8751	3.1588	6247	5660	3274	2117	2130
			196	3.8757	3.1130	6246	5659	3303	2136	2110
			198	3.8791	3.0715	6241	5655	3328	2151	2090
			200	3.8852	3.0343	6234	5648	3348	2163	2071
			202	3.8944	3.0017	6223	5638	3363	2170	2053
			204	3.9067	2.9739	6208	5625	3373	2174	2034
			208*	3.9421	2.9327	6164	5585	3376	2167	1997
			212	3.9940	2.9131	6102	5529	3354	2141	1961
		8/7/73	192	3.9111	2.8463	6202	5619	3452	2223	1979
			194	3.9114	2.8065	6202	5619	3477	2240	1962
			196	3.9131	2.7700	6200	5617	3499	2253	1947
			198	3.9162	2.7369	6197	5614	3518	2265	1932
			200	3.9206	2.7070	6192	5610	3535	2274	1917
			202	3.9265	2.6804	6185	5604	3548	2282	1904
			204	3.9339	2.6572	6176	5595	3557	2285	1890
			206	3.9430	2.6373	6164	5585	3563	2287	1877
			208	3.9537	2.6208	6151	5573	3566	2286	1865
			210*	3.9663	2.6078	6136	5559	3565	2282	1854
			212	3.9808	2.5981	6119	5544	3561	2276	1842
			214	3.9974	2.5921	6098	5525	3553	2267	1832
			216	4.0163	2.5896	6075	5504	3541	2254	1821
		8/15/73	196	4.1807	2.6328	5868	5317	3394	2118	1751
			198	4.1815	2.6501	5867	5316	3410	2127	1740
			200	4.1832	2.5803	5865	5314	3424	2135	1730
			202	4.1858	2.5583	5862	5311	3435	2142	1721
			204	4.1939	2.5229	5862	5302	3450	2149	1704
			208	4.1995	2.5094	5845	5296	3454	2149	1696
			212*	4.2142	2.4908	5827	5279	3454	2146	1682
			214	4.2235	2.4856	5815	5296	3450	2140	1675
			216	4.2342	2.4833	5801	5256	3443	2133	1668
		8/23/73	206	4.6081	2.4534	5351	4848	3192	1875	1476
			208	4.6080	2.4437	5351	4848	3197	1878	1473
			210	4.6087	2.4364	5350	4847	3200	1880	1470
			212*	4.6100	2.4312	5348	4845	3202	1880	1466
			216	4.6150	2.4275	5341	4839	3200	1877	1464

*Time of flight corresponding to the minimum of the sum of departure and arrival velocities.

TABLE 13 (Cont'd)

Planet	Type	Date	Time of Flight (days)	Departure Velocity (km/sec)	Approach Velocity (km/sec)	Injected Weight (lb)	Burnout Weight			Propellant Weight (lb)
							All Lander (lb)	All Orbiter (lb)	Orbiter with 2000 pound Lander (lb)	
Mars	II	8/25/75	334	4.074	2.451	6004	5440	3583	2265	1739
			336	4.065	2.451	6015	5450	3589	2272	1743
			338	4.058	2.453	6024	5458	3593	2277	1747
			340*	4.053	2.457	6030	5463	3595	2279	1751
			342	4.050	2.463	6034	5467	3593	2279	1755
			344	4.048	2.471	6036	5469	3590	2277	1759
			346	4.047	2.480	6037	5470	3585	2274	1763
		9/1/75	338	3.896	2.510	6221	5636	3676	2371	1850
			340	3.884	2.511	6236	5650	3684	2380	1856
			342	3.875	2.514	6247	5660	3688	2385	1862
			344*	3.867	2.519	6256	5668	3691	2388	1868
			346*	3.860	2.526	6265	5676	3691	2391	1874
			348	3.856	2.535	6270	5680	3689	2390	1880
			350	3.853	2.545	6273	5683	3684	2388	1885
			352	3.851	2.557	6276	5686	3678	2384	1891
			354	3.851	2.571	6276	5686	3669	2379	1897
		9/8/75	342	3.791	2.588	6348	5751	3701	2414	1934
			344	3.776	2.590	6367	5769	3711	2424	1943
			346	3.763	2.594	6382	5782	3717	2431	1951
			348	3.752	2.600	6395	5794	3720	2436	1959
			350*	3.742	2.608	6408	5805	3723	2440	1968
			352	3.735	2.618	6416	5813	3721	2441	1975
			354	3.729	2.630	6423	5819	3717	2440	1983
			356	3.725	2.643	6428	5823	3711	2437	1991
			358	3.722	2.658	6432	5827	3704	2433	1999
			360	3.720	2.675	6435	5830	3694	2427	2008
			362	3.719	2.692	6436	5831	3684	2420	2015

*Time of flight corresponding to the minimum of the sum of departure and arrival velocities.

TABLE 13 (Concl'd)

Planet	Type	Date	Time of Flight (days)	Departure Velocity (km/sec)	Approach Velocity (km/sec)	Injected Weight (lb)	Burnout Weight			Propellant Weight (lb)
							All-Lander (lb)	All-Orbiter (lb)	Orbiter with 2000-pound Lander (lb)	
Mars	II	9/15/75	344	3.788	2.686	6352	5755	3640	2375	1977
			346	3.766	2.686	6378	5779	3655	2390	1988
			350	3.731	2.694	6420	5817	3674	2410	2010
			352	3.716	2.702	6439	5833	3679	2418	2021
			354*	3.704	2.711	6453	5847	3681	2422	2032
			356	3.693	2.723	6466	5858	3681	2424	2042
			358	3.684	2.736	6477	5868	3678	2425	2052
			360	3.677	2.751	6486	5876	3674	2423	2063
			364	3.665	2.785	6500	5889	3659·	2416	2084
			368	3.659	2.824	6508	5896	3637	2403	2105
			370	3.657	2.845	6510	5898	3624	2395	2115
			372	3.657	2.868	6510	5898	3609	2385	2125
			374	3.657	2.891	6510	5898	3593	2375	2135
		9/22/75	348	3.848	2.802	6279	5689	3523	2285	1984
			352	3.801	2.808	6336	5741	3551	2314	2022
			356	3.764	2.825	6381	5781	3565	2332	2049
			358	3.748	2.836	6400	5799	3569	2338	2062
			360*	3.734	2.849	6417	5814	3570	2342	2075
			362	3.722	2.864	6432	5827	3568	2343	2088
			364	3.711	2.880	6445	5839	3564	2343	2101
			368	3.692	2.917	6468	5860	3553	2340	2128
			372	3.679	2.959	6483	5874	3533	2330	2153
			376	3.669	3.006	6495	5885	3508	2315	2180
			380	3.663	3.056	6503	5892	3478	2297	2206
			384	3.660	3.109	6507	5895	3444	2276	2231
			388	3.660	3.166	6507	5895	3405	2250	2256

*Time of flight corresponding to the minimum of the sum of departure and arrival velocities.

TABLE 14

COMPARISON OF BEST 30 DAY LAUNCH PERIOD BURNOUT AND PROPULSION SYSTEM WEIGHTS

Planet	Date[1]	Type	Daily Maximum Orbiter/Lander Burnout Weight				Minimum Departure Velocity Orbiter/Lander Burnout Weight			
			Min Weight (lb)	Max Weight (lb)	30 Day Window	Propulsion System Weight[2] (lb)	Min Weight (lb)	Max Weight (lb)	30 Day Window	Propulsion System Weight[2] (lb)
Venus	1969	I	1320	1370	26 Dec – 25 Jan	645	1315	1370	26 Dec – 25 Jan	645
	1970	I	1130	1200	8 Aug – 7 Sep	645	1110	1160	6 Aug – 5 Sep	655
	1964 (1972)	II	1190	1225	13 Mar – 12 Apr	655	1180	1215	12 Mar – 11 Apr	660
	1965 (1973)	II	1390	1450	27 Oct – 26 Nov	640	1390	1450	27 Oct – 26 Nov	640
	1967 (1975)	I	1380	1680	30 May – 29 Jun	615	1320	1595	31 May – 30 Jun	645
Mars	1969	II	2040	2090	15 Jan – 14 Feb	470	2015	2075	12 Jan – 11 Feb	480
	1971	I	2800	2960	7 May – 6 Jun	400	2750	2955	7 May – 6 Jun	400
	1973	I	2085	2295	20 July – 19 Aug	320	2050	2250	18 July – 17 Aug	335
	1975	II	2295	2445	25 Aug – 24 Sep	325	2245	2420	23 Aug – 22 Sep	350

[1] Trajectory analysis for 1964 - 1970 Venus period pertinent to 1972-1978 period with at most a 5-day shift in the window

[2] Propellant mass fraction ~ 0.88
Specific impulse ~ 310 sec.

of periapsis uncertainty from guidance considerations is approximately 200 km. This uncertainty is essentially an average of the uncertainties that may be expected with and without onboard terminal guidance equipment.

In 1969 and 1975, Type II transfers to Mars are preferable to Type I since a dogleg maneuver with significant payload losses is required to overcome the launch azimuth constraint. In 1971 and 1973, a Type I is desirable due to the increased payload capability and shorter flight time.

The summary of nominal velocity increments employed for this final payload analysis for both Mars and Venus is given in table 15.

TABLE 15

SUMMARY OF NOMINAL VELOCITY INCREMENTS
FOR MARS-VENUS PAYLOAD ANALYSIS

Mars and Venus Direct Entry	Venus Capsule Entry
(1) Midcourse and time of arrival velocity correction ΔV_M= 0.125 km/sec (3σ)	(1) Same
(2) Lander ejection	(2) Not applicable
(3) Orbiter slowdown ΔV_{SD} = 0.052 km/sec	(3) Not applicable
(4) Terminal correction ΔV_T = 0.030 km/sec (3σ)	(4) Same
(5) Orbit establishment ΔV as required	(5) Same

The final payload in the desired planetocentric Martian orbit can be expressed by

$$W_{pL} = W_i - W_p - W_{ps} - W_L$$

where

W_i = weight injected into heliocentric transfer orbit

W_p = propellant weight

W_{ps} = dry propulsion weight

W_L = lander weight.

The propellant requirements exclusive of orbit trim maneuvers can be expressed by

$$W_p = W_i \left[1 - e^{-\frac{(\Delta V_M + \Delta V_{SD} + \Delta V_T + \Delta V)}{c}} \right] - W_L \left[1 - e^{-\frac{(\Delta V_{SD} + \Delta V_T + \Delta V)}{c}} \right]$$

where

W_L = lander weight

ΔV_M = midcourse velocity correction

ΔV_{SD} = orbiter slowdown velocity requirement

ΔV_T = terminal velocity correction

ΔV = orbit establishment velocity requirements,

and the weight of the dry propulsion system can be expressed in terms of the propellant requirements by

$$W_{ps} = W_p \left(\frac{1}{PMF} - 1 \right)$$

where PMF = propellant mass fraction.

During the four launch opportunities under investigation, the burnout weight in the planetocentric orbit at the extremity of the best 30-day period varies from a low of 1980 pounds in 1971 to a high of 2585 pounds in 1975. While the energy requirements are most favorable for interplanetary flight to Mars in 1971, this reduced payload results from the fact that a comparison is being made between a two-lander mission in 1971 and a one-lander mission for the other launch opportunities.

These planetocentric burnout weights also include the dry propulsion weight. This weight varies from a high of 403 pounds in 1969 to a low of 219 pounds in 1971. If, in the interest of engine commonality, the engine size is based upon 1969 launch opportunity propellant requirements, a payload penalty of approximately 140 to 180 pounds exists for the remaining launch opportunities. This penalty may be reduced slightly if smaller propellant tanks are incorporated with the fixed engine size. This, in effect, results in a lower propellant mass fraction than theoretically achievable if a propulsion system was designed for the propellant requirement for each specific launch opportunity.

The pertinent trajectory, payload, and propulsion system characteristics are summarized in table 16 for the Martian launch opportunities between 1969 and

TABLE 16

MARTIAN PAYLOAD FOR FIXED ORBIT

Date	Trajectory Type	Time of Flight (days)	Departure Velocity (km/sec)	Injected Weight (lb)	Approach Velocity (km/sec)	Orbit Established Velocity Decrement (km/sec)	Burnout Weight (lb)	Propellant Weight (lb)	Dry Propulsion System Weight (lb) [1]	Payload 2 (lb)	Payload 3 (lb)
1/15/69	II	272	3.589	6592	3.731	2.021	2314	2398		1911	1911
1/17/69		272	3.551	6637	3.746	2.031	2330	2427		1927	1927
1/25/69		274	3.409	6805	3.843	2.097	2364	2561	403	1961	1961
1/31/69		274	3.331	6897	3.930	2.156	2365	2652		1962	1962
2/16/69		280	3.125	7135	4.275	2.399	2298	2957		1895	1895
4/24/71	I	202	3.584	6598	3.229	1.699	1483	1355		1264	1080
5/10/71		210	2.938	7327	2.832	1.465	2028	1539		1809	1625
5/18/71		208	2.837	7426	2.819	1.458	2092	1574		1873	1689
5/24/71		206	2.810	7502	2.824	1.461	2135	1607	219	1916	1732
6/1/71		202	2.887	7377	2.848	1.474	2052	1565		1833	1649
6/9/71		200	3.082	7179	2.902	1.505	1916	1503		1697	1513
6/25/71		206	3.717	6438	3.167	1.661	1412	1266		1193	1009
7/6/73	I	204	4.356	5658	3.342	1.769	1999	1779		1749	1596
7/22/73		208	3.942	6164	3.933	1.523	2454	1830		2204	2051
7/30/73		208	3.873	6249	2.765	1.428	2578	1791	250	2328	2175
8/7/73		210	3.966	6136	2.608	1.343	2578	1678		2328	2175
8/15/73		212	4.214	5827	2.491	1.282	2434	1513		2184	2031
8/23/73		212	4.610	5348	2.431	1.252	2153	1315		1903	1750
8/9/75	II	330	4.689	5254	2.379	1.226	2111	1263		1852	1708
8/25/75		340	4.053	6030	2.457	1.265	2575	1575		2316	2172
9/1/75		346	3.860	6265	2.526	1.300	2694	1691		2435	2291
9/8/75		350	3.742	6408	2.608	1.343	2746	1782	259	2487	2343
9/15/75		354	3.704	6453	2.711	1.398	2727	1846		2468	2324
9/22/75		360	3.734	6417	2.849	1.475	2641	1896		2382	2238
10/8/75		370	4.103	5965	3.235	1.703	2210	1875		1951	1807

(1) based upon maximum propellant requirement for launch opportunity
(2) based upon maximum dry propulsion system weight for launch opportunity
(3) based upon maximum dry propulsion system weight for the four opportunities

Note: Payload consists of weight in Martian orbit exclusive of dry propulsion system.

1975. The variation in payload weight due to off-loading propellant in the vehicle propulsion system can be assessed from this table. For example, the propulsion system for the 1969 opportunity is sized by the propellant requirement (2957 pounds) for a 16 February launch. The propellant requirement for a 15 January launch is 2398 pounds to achieve the desired nominal planetocentric orbit. Therefore, if the maximum amount of propellant were employed on this date, the planetocentric payload weight would be reduced by 559 pounds.

The burnout weight for these opportunities is also presented in graphical form in figures 31 through 34. Since there is a vertical translation from burnout weight to payload weight depending upon the particular propulsion system selected, these figures were utilized in determining the best 15-, 30-, and 45-day launch periods for each launch opportunity. In 1969, the best 45-day launch period is not presented since trajectory parameters were not available prior to 15 January 1969.

This optimum launch period information is summarized in table 17. Due to the variations in the slopes on either side of the maximum weight, the maximum weight is not necessarily centered in the middle of the best window.

In order to assess the perturbations in planetocentric payload resulting from variations in injected weight, propulsion system characteristics, and lander weight, an error analysis was conducted for the 1969 launch opportunity. These results (summarized in figures 35 and 36) indicate:

      a. A 50-pound variation in orbiter payload for a 100-pound change in lander weight

      b. A 90-pound variation in orbiter payload for a 5 percent change in specific impulse

      c. A 325-pound variation in orbiter payload for a 10 percent variation in the weight injected into the heliocentric transfer orbit

      d. A 9 percent variation in the propulsion system weight for a 1 percent change in the propellant mass fraction.

In designing a common engine for all Martian launch opportunities, a 403-pound engine results in the previous mentioned penalties for the other three opportunities. The penalties in the 1971, 1973, and 1975 launch opportunities can be minimized if an engine size of 260 pounds is selected. This approach results in a sizable payload penalty for only the 1969 opportunity. In an attempt to determine this penalty, the maximum weight placed in the desired planetocentric orbit was computed. Since the maximum amount of onboard propellant is fixed by the propulsion system size, the weight injected into the heliocentric transfer orbit such that the desired planetocentric orbit is achieved is obtained by

TABLE 17

LOCATION OF BEST LAUNCH WINDOW FOR
MARTIAN LAUNCH OPPORTUNITIES

Duration of Window (days)	Launch Opportunity	Trajectory Type	Date	Burnout Weight	
				Minimum (lb)	Maximum (lb)
15	1969	II	21 Jan - 5 Feb	2350	2370
15	1971	I	15 May - 30 May	2070	2135
15	1973	I	26 Jul - 10 Aug	2525	2600
15	1975	II	2 Sep - 17 Sep	2710	2745
30	1969	II	15 Jan - 14 Feb	2310	2370
30	1971	I	7 May - 6 June	1980	2135
30	1973	I	18 Jul - 17 Aug	2370	2600
30	1975	II	26 Aug - 25 Sep	2585	2745
45	1969	II	-----*	----*	2370
45	1971	I	30 April - 14 June	1790	2135
45	1973	I	9 July - 23 Aug	2110	2600
45	1975	II	18 Aug - 20 Oct	2385	2745

* Pertinent trajectory parameters are not available since the center of this window occurs over 60 days from the absolute minimum departure velocity date of 1 April 1963.

TABLE 18

MARTIAN PAYLOAD COMPARISON FOR TWO PROPULSION SYSTEM WEIGHTS

Launch Date	Trajectory Type	Time of Flight (days)	Departure Velocity (km/sec)	Approach Velocity (km/sec)	Orbit Established Velocity Decrement (km/sec)	Dry Propulsion System Weight			
						403 pounds		260 pounds	
						Injected Weight (lb)	Payload (lb)	Injected Weight (lb)	Payload (lb)
1/15/69	II	272	3.589	3.731	2.021	6592	1911	5609	1564
1/17/69		272	3.551	3.746	2.031	6637	1927	5598	1553
1/25/69		274	3.409	3.843	2.097	6805	1961	5526	1481
1/31/69		274	3.331	3.930	2.156	6897	1962	5465	1420
2/16/69		280	3.125	4.275	2.399	7135	1895	5245	1200

Note: Payload consists of weight in Martian orbit exclusive of dry propulsion system.

$$W_i = \frac{W_p + W_L \left[1 - e^{-\frac{(\Delta V_{SD} + \Delta V_T + \Delta V)}{c}}\right]}{\left[1 - e^{-\frac{(\Delta V_M + \Delta V_{SD} + \Delta V_T + \Delta V)}{c}}\right]}$$

and the final payload computed by

$$W_{pL} = W_i - W_p - W_{ps} - W_L \ .$$

However, since the vehicle is light at launch, the departure and arrival velocities associated with the minimum sum are not so efficient as employing the departure velocity corresponding to the minimum approach velocity. The penalty associated with the 260-pound propulsion system for the 1969 opportunity is presented in table 18. This penalty is difficult to assess for the given launch window due to the resulting shift in the window when the vehicle is light at launch; however, it appears to be on the order of 400 pounds.

This present Martian payload analysis has been conducted for a split-capsule orbiter/lander vehicle. Since it is desirous to achieve the same probability of success for two landers and two orbiters, it was found necessary to switch from an orbiter/lander in 1975 to a fly-by bus/two-lander configuration. With this new configuration, the bus weights, propellant, and propulsion system requirements are presented in table 19.

TABLE 19

MARTIAN BUS WEIGHTS FOR TWO-LANDER CONFIGURATION

Launch Date	Trajectory Type	Injected Weight (lb)	Propellant Weight (lb)	Propulsion System Weight (lb)	Bus Payload (lb)
8/9/75	II	5254	222	30	1242
8/22/75		6030	264	36	1970
9/1/75		6265	276	38	2191
9/8/75		6408	284	39	2325
9/15/75		6453	287	39	2367
9/22/75		6417	284	39	2334
10/8/75		5965	260	35	1910

Figure 31 BURNOUT WEIGHT VERSUS LAUNCH DATE, MARS 1969, TYPE II

65-8936

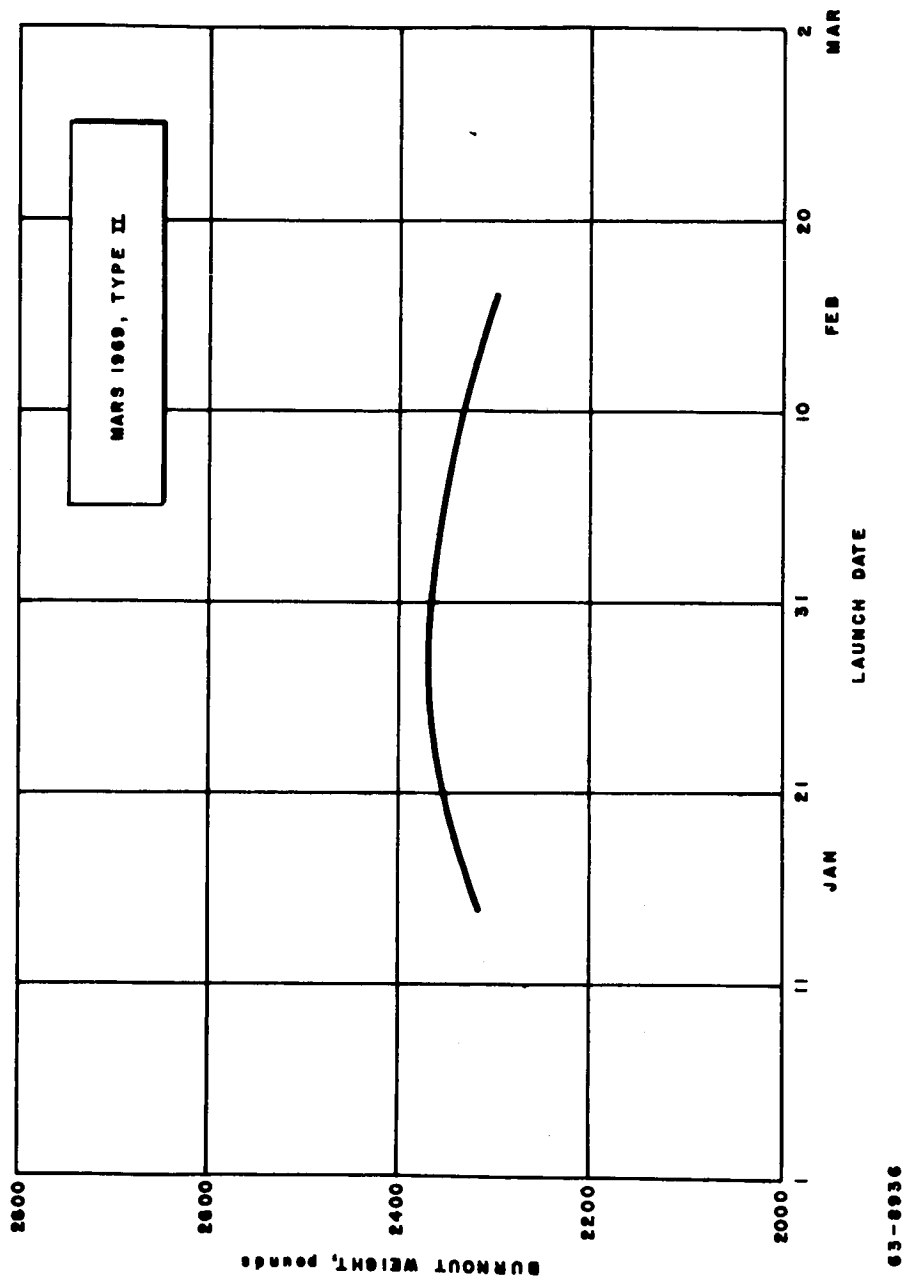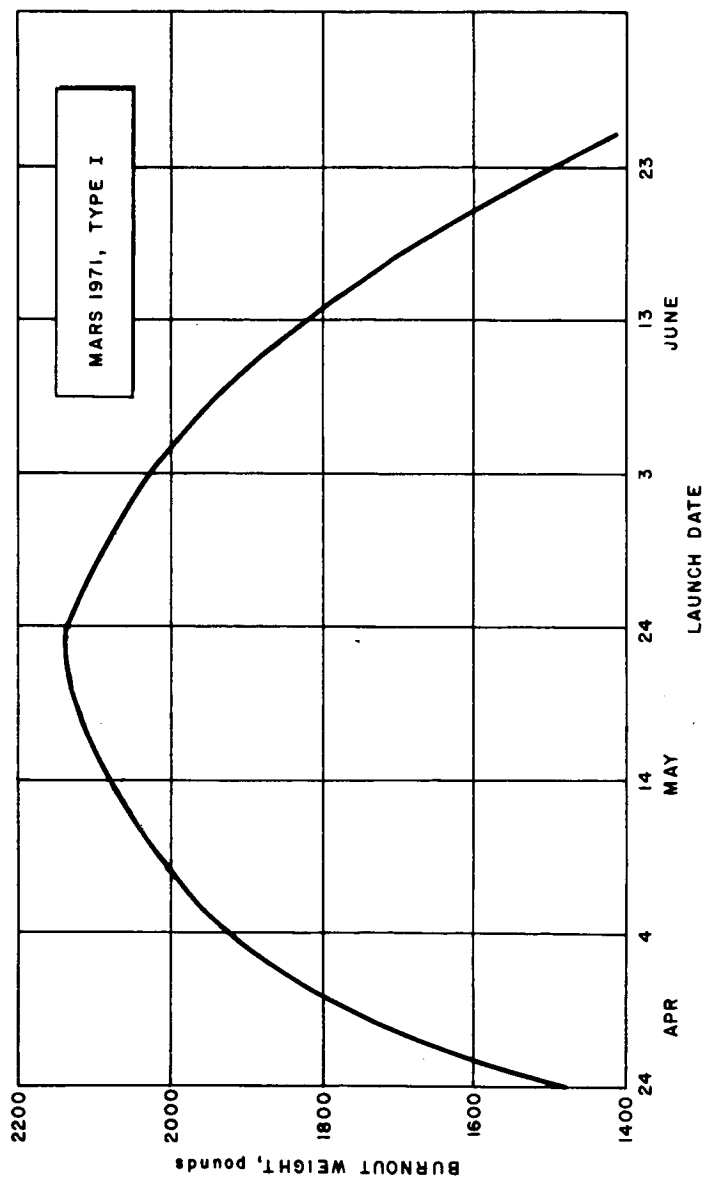Figure 32 BURNOUT WEIGHT VERSUS LAUNCH DATE, MARS 1971, TYPE I
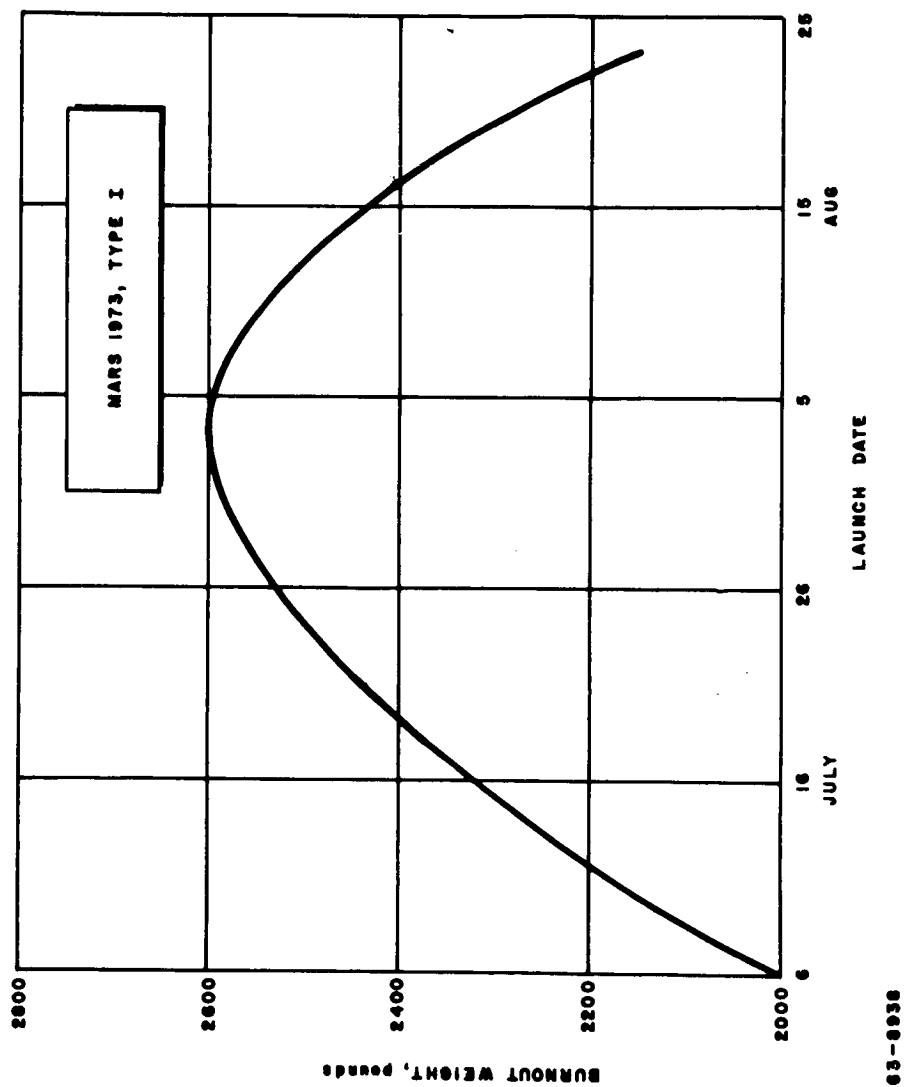
63 - 8937

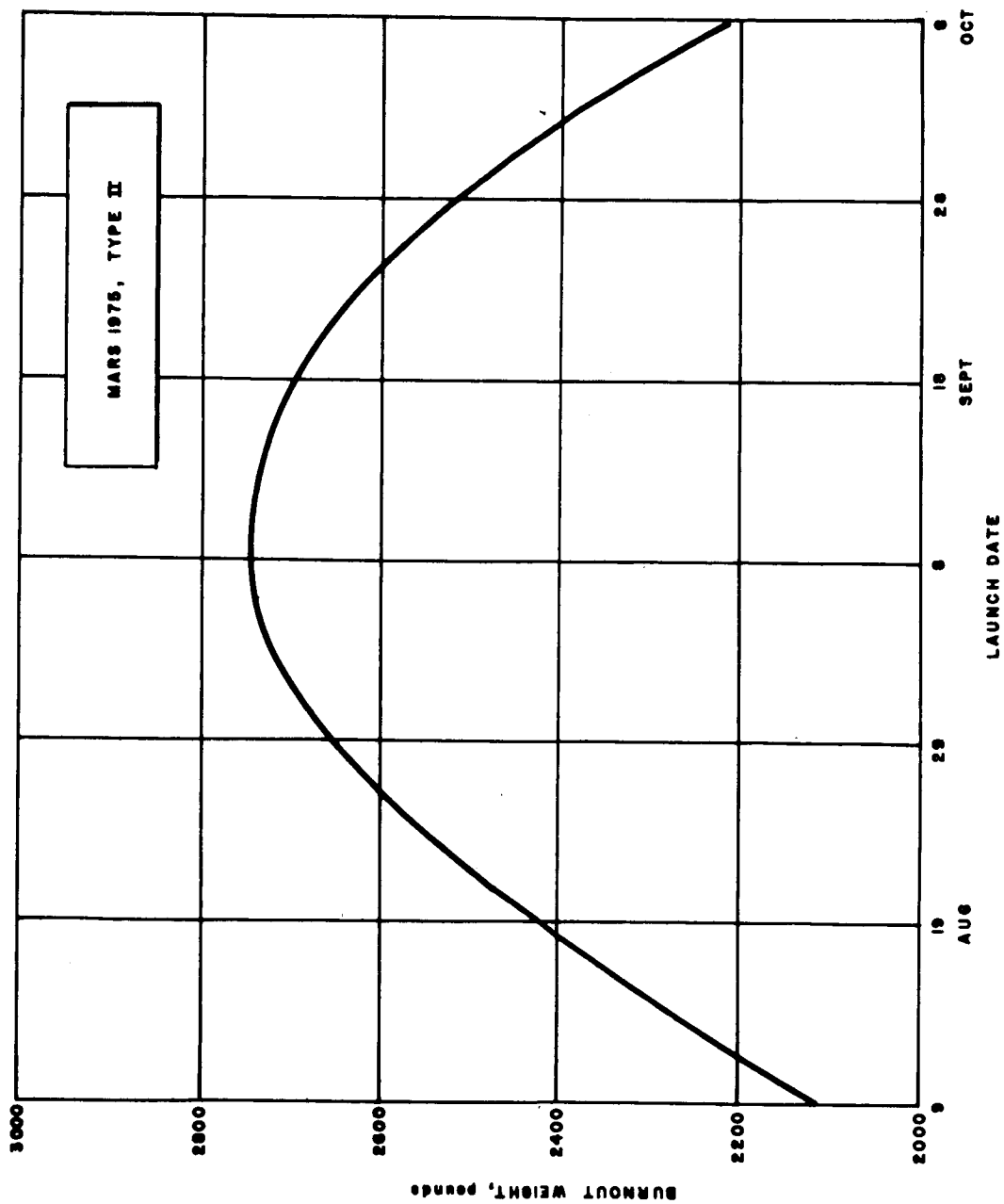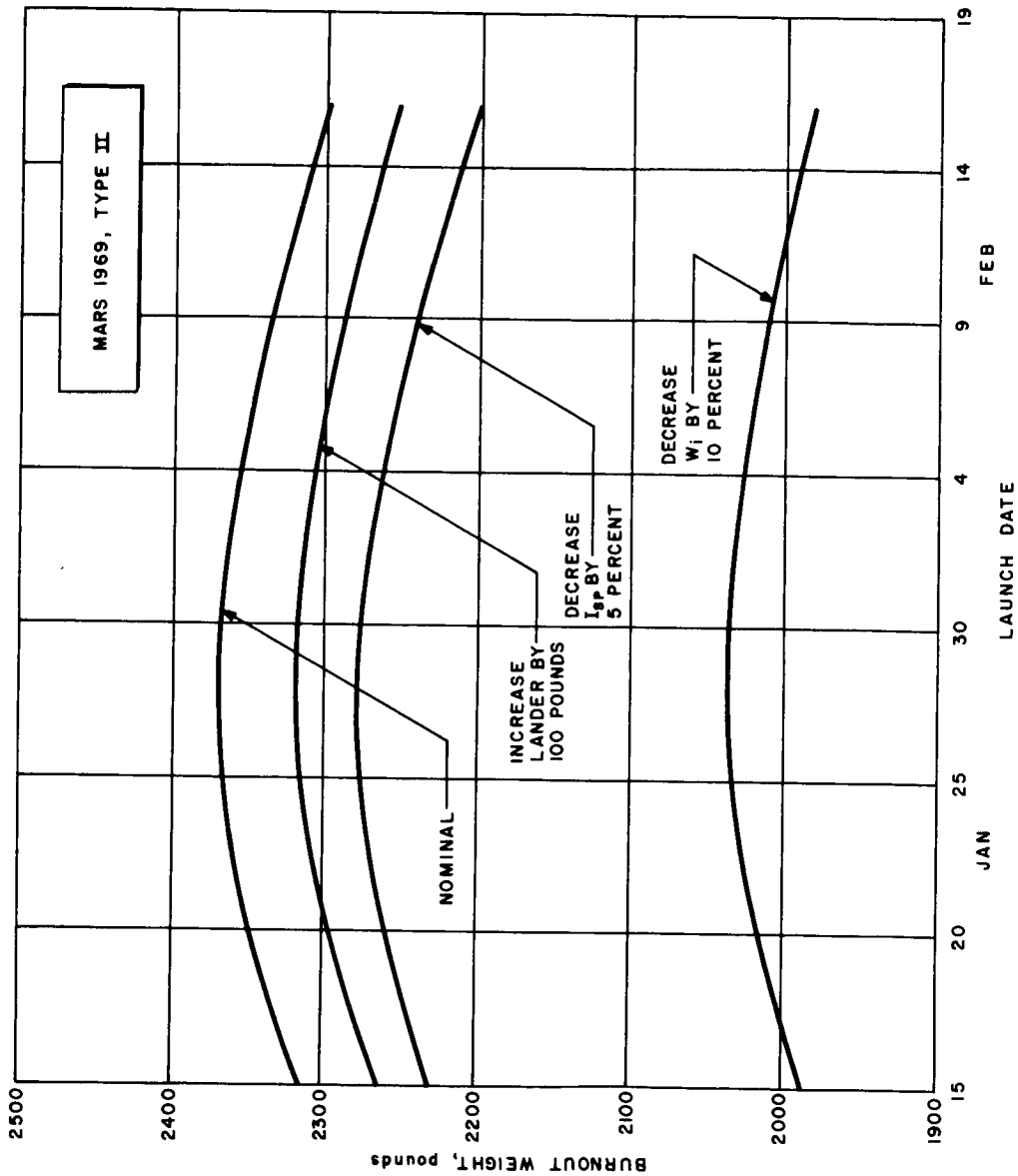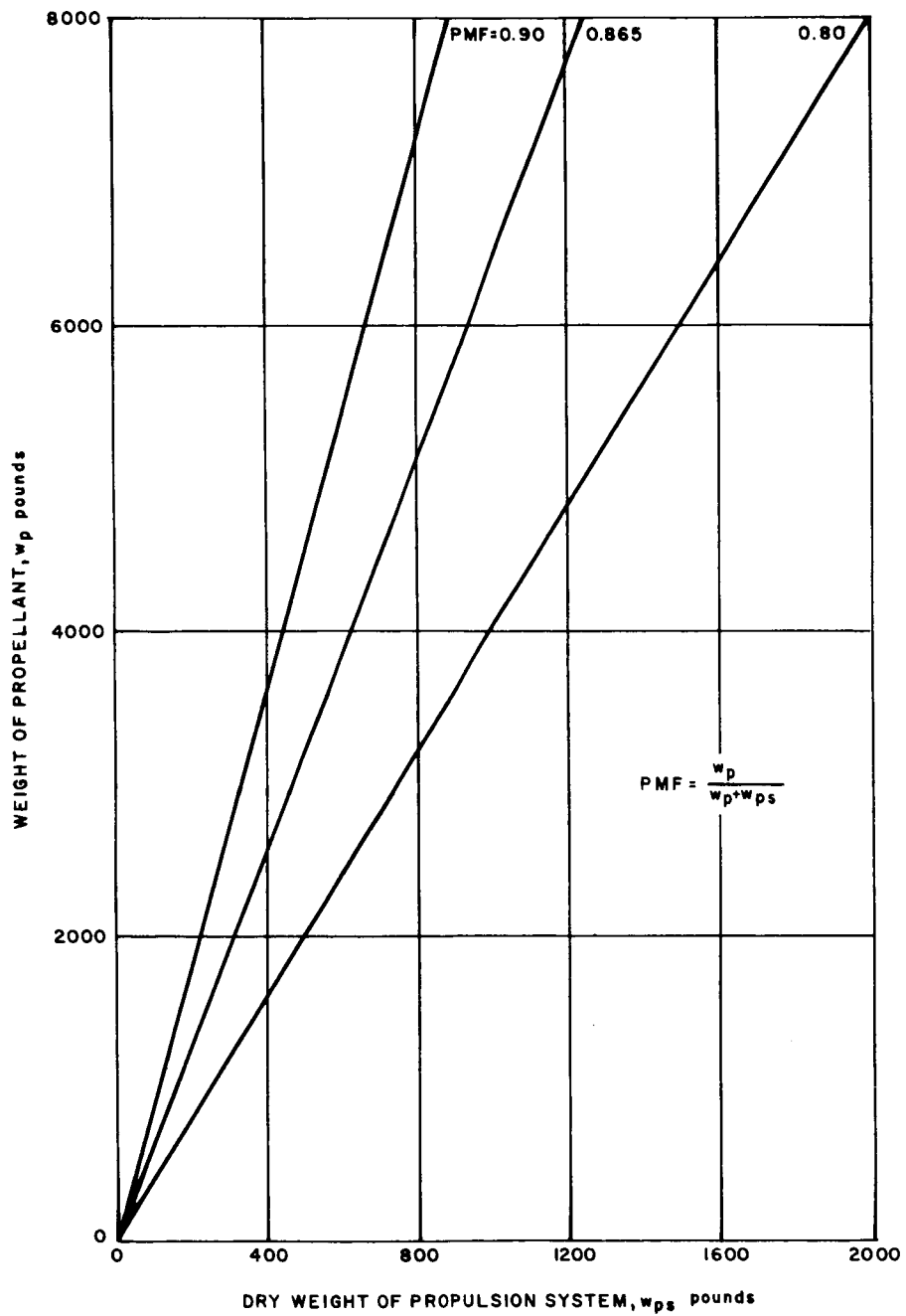Figure 33 BURNOUT WEIGHT VERSUS LAUNCH DATE, MARS 1973, TYPE I

-94-

Figure 34 BURNOUT WEIGHT VERSUS LAUNCH DATE, MARS 1975, TYPE II

63-8938

Figure 35 BURNOUT WEIGHT VERSUS LAUNCH DATE FOR ERROR ANALYSIS,
MARS 1969, TYPE II

63-8940

-96-

Figure 36 DRY WEIGHT OF PROPULSION SYSTEM VERSUS WEIGHT
OF PROPELLANT

63-8941

-97-

At the extremity of the best 30-day launch period (2 September to 2 October), the payload is 2210 pounds and increases to 2370 pounds in the middle of the window. These payloads will be reduced if it is desirous to achieve minimum approach velocities to maximize the fly-by dwell time in the vicinity of the planet. In this analysis, the same midcourse, time of arrival, and bus slowdown velocity requirements previously employed were used.

2. <u>Venus.</u> Since it is presently envisioned that three 200-pound vehicles (85-pound nonsurvivable landers) will be ejected after the establishment of a planetocentric orbit, this mission, in essence, is an all-orbiter mission. The previous daily maximization payload analysis for Venus indicated that the all-orbiter mission varied from a low of approximately 550 pounds in 1964 (1972) to a high of 1150 pounds in 1967 (1975) for a circular orbit with a 1000-km altitude. This low-payload capability dictated the selection of an elliptic orbit to realize substantial payload improvements. Where a prime objective of this program is radar mapping of the planet surface, the periapsis altitude was fixed at 1000 km and a nominal apoapsis altitude of 10,000 km selected. With this nominal orbit, an initial analysis was conducted to determine the payload at the extremity of the best 30-day window within each launch opportunity. The same equations employed in the Martian analysis are applicable with the exception that the lander weight and orbiter slowdown requirements are zero. The weight at the extremity of the best 30-day window in that opportunity yielding minimum payloads (1972) can be utilized in sizing the orbiter vehicle. In selecting the minimum orbiter payload, allowance must be made for the additional 600 pounds of lander weight. Due to launch azimuth constraints and injection energy requirements, it appears that Type I transfers are preferable in 1968-69, 1970, and 1975 with Type II transfers being employed in 1972 and 1973. The results of this fixed orbit analysis indicate that the payload at the extremities of the best 30-day launch period varies from a low of approximately 2000 pounds in 1970 to a high of 2750 in 1975 when a common propulsion system weight of 630 pounds, required in 1972, is employed for all opportunities. Therefore, exclusive of the 600-pound lander weight, the orbital payload varies between 1400 and 2150 pounds. The results of this analysis are presented in table 20. Whereas, for Mars, the requirement was to maximize the weight in a given planetocentric orbit, the requirement for Venus is to obtain the minimum energy (minimum semimajor axis) planetocentric orbit for a fixed payload and propulsion system weight. The weight of the reference orbiter was selected as 1300 pounds yielding a desired burnout weight in orbit of 1900 pounds. To achieve propulsion system commonality, the fixed propulsion system employed in this analysis was sized for the 1972 launch opportunity requirements, i.e., 630-pound dry propulsion system with the capability of carrying 4620 pounds of propellant. Therefore, the maximum weight to be placed in the heliocentric transfer orbit is 7150 pounds. If, due to departure energy requirements, this weight is greater than the largest injection weight possible for the desired departure velocity, propellant is removed. However, if this weight is less than the maximum allowable injected weight the fixed weight of 7150 pounds is employed. While the current departure and arrival velocities employed are those corresponding to the minimum

TABLE 20

MAXIMUM PAYLOAD WEIGHT FOR FIXED VENUSIAN ORBIT

Date*	Trajectory Type	Time of Flight (days)	Departure Velocity (km/sec)	Injected Weight (lb)	Approach Velocity (km/sec)	Orbit Established Velocity Decrement (km/sec)	Burnout Weight (lb)	Propellant Weight (lb)	Dry Propulsion System Weight (lb) [1]	Payload 2 (lb)	Payload 3 (lb)
12/14/68	I	150	3.393	6826	4.045	2.420	3058	3768		2467	2429
12/30/68		138	2.927	7342	4.497	2.605	3104	4238		2513	2475
1/7/69		132	2.811	7450	4.539	2.623	3132	4318		2541	2503
1/13/69		126	2.779	7490	4.528	2.619	3154	4336	591	2563	2525
1/19/69		122	2.830	7430	4.494	2.604	3143	4287		2552	2514
1/27/69		116	3.044	7220	4.428	2.576	3081	4139		2490	2452
2/12/69		104	4.034	6052	4.273	2.512	2635	3417		2044	2006
7/20/70	I	140	3.384	6836	5.740	3.195	2405	4431		1782	1776
8/5/70		130	3.081	7181	5.522	3.084	2615	4566		1992	1986
8/13/70		124	2.983	7282	5.364	3.005	2718	4564	623	2095	2089
8/19/70		120	2.981	7285	5.217	2.933	2781	4504		2158	2152
8/25/70		116	3.047	7217	5.054	2.856	2822	4395		2199	2193
9/4/70		110	3.359	6865	4.753	2.718	2803	4062		2180	2174
9/18/70		100	4.181	5868	4.398	2.564	2514	3354		1891	1885
3/1/64	II	186	3.574	6615	4.631	2.663	2747	3868		2118	2118
3/15/64		180	3.184	7065	4.900	2.784	2825	4240		2196	2196
3/29/64 (1972)		172	2.938	7330	5.115	2.884	2841	4489	629	2212	2212
4/13/64		164	2.903	7365	5.353	2.999	2754	4611		2125	2125
4/30/64		154	3.308	6925	5.667	3.157	2464	4461		1835	1835
10/16/65	II	174	3.151	7105	4.385	2.558	3049	4056		2471	2420
10/31/65		164	2.796	7468	4.276	2.513	3250	4218		2672	2621
11/8/65 (1973)		158	2.706	7550	4.216	2.488	3311	4239	578	2733	2682
11/15/65		154	2.729	7530	4.143	2.459	3333	4197		2755	2704
11/22/65		148	2.853	7410	4.091	2.438	3301	4109		2723	2672
11/28/65		142	3.068	7194	4.057	2.425	3218	3976		2640	2589
5/27/67	I	138	3.537	6655	3.706	2.292	3103	3552		2591	2474
6/1/67		138	3.332	6900	3.258	2.137	3376	3524		2864	2747
6/6/67 (1975)		140	3.119	7140	2.876	2.020	3623	3517	512	3111	2994
6/11/67		140	2.706	7550	2.947	2.041	3807	3743		3295	3178
6/16/67		133	2.781	7490	3.050	2.072	3740	3750		3228	3111
6/21/67		128	2.922	7345	3.185	2.104	3631	3714		3119	3002
6/26/67		122	3.194	7055	3.275	2.143	3445	3610		2933	2816

* Trajectory analysis for 1964 - 1970 period pertinent to 1972 - 1978 period with at most a 5-day shift in the window

(1) based upon maximum propellant requirement for launch opportunity

(2) based upon maximum dry propulsion system weight for launch opportunity

(3) based upon maximum dry propulsion system weight for the five opportunities

Note: Payload consists of weight in Venusian orbit exclusive of dry propulsion system, and includes landers which are ejected after achieving orbit.

sum, additional benefits can be realized when the vehicle is light by increasing the departure velocity up to the point of obtaining minimum arrival velocity.

At each step in the calculation, the propellant and vehicle weight are computed for each velocity correction by

$$W_f = W_o \, e^{-\frac{\Delta V}{c}}$$

and

$$W_p = W_o \left(1 - e^{-\frac{\Delta V}{c}} \right)$$

where

W_o = weight before each velocity correction

W_p = propellant requirement to obtain required velocity correction.

At periapsis of the approach hyperbola, the maximum velocity decrement that can be applied is a function of the remaining propellant as the final burnout weight is fixed. This velocity decrement can be expressed by

$$\Delta V = c \ln \frac{W_{pL} + W_p + W_L + W_{ps}}{W_{pL} + W_L + W_{ps}}$$

The relationship between the applied velocity decrement and planetocentric periapsis velocity is a function of the velocity at periapsis along the approach hyperbola, expressed by

$$\Delta V = V_{P_H} - V_{P_E}$$

where

$$V_{P_H} = \sqrt{V_\infty^2 + \frac{2\mu}{r_p}}$$

Hence, the periapsis velocity

$$V_{P_E} = \sqrt{\frac{r_a}{r_p} \frac{2\mu}{r_a + r_p}}$$

is determined and the corresponding apoapsis altitude is obtained by

$$h_a = \frac{V_{P_E}^2 \, r_P^2}{2\mu - V_{P_E}^2 \, r_P} - r_e$$

where

r_e = planet radius.

Since the reference orbiter design is 1300 pounds, 100 pounds below the minimum payload in the nominal orbit, this guarantees that the apoapsis altitude at the extremity of the best 30-day window will be less than 10,000 km when the 630-pound propulsion system is employed. The results of this varying orbit analysis are presented in table 21. While the optimization has not been performed when the launch vehicle is light, it appears that the apoapsis altitudes vary from a low of 1100 to 3800 km in 1967 (1975) to a high of 6400 to 8000 km in 1970.

Up to this point, propulsion system commonality has been implied for each target planet. While propulsion system commonality appears to yield larger penalties for Mars than Venus due to the different methods employed, an additional analysis was conducted for Venus with a 460-pound propulsion system. This propulsion system is slightly larger than that required for the heaviest Mars mission due to the variation in propulsion system weight with off-nominal propulsion system characteristics. The payload penalty for Mars can be obtained by employing the burnout weights presented in table 16 with this propulsion system.

However, the Venusian penalty is much harder to assess since the heliocentric injected weight is now only 6070 pounds. Except for a few days at the extremes of the launch opportunities the launch weight is less than the maximum possible and there is a sizable shift in the optimum launch period. A comparison of the apoapsis altitudes for the 460-and 630-pound propulsion systems for Venus missions is presented in table 22.

When less than the maximum weight is injected into orbit, the minimum apoapsis altitude moves to the direction of minimum approach velocity for that launch opportunity.

Previously, it has been assumed that three 200-pound vehicles would be ejected after the establishment of the best planetocentric orbit. However, the Venusian mission evolution program indicates it may be desirable to employ a direct lander (1340 pounds) for the last two launch opportunities--1973 Type II and 1975 Type I. To determine the minimum apoapsis altitudes for these missions and the penalties associated with propulsion system commonality, an analysis was performed for both the 460-pound and 630-pound propulsion systems. The sequence of events for these missions is identical with those for the Martian

missions summarized in table 15. With a 1300-pound orbiter payload, the
maximum apoapsis altitude at the extremity of the best 30-day window is ap-
proximately 2000 km for both launch opportunities when the 630-pound propulsion
system is employed. The corresponding apoapsis altitudes in 1973 and 1975
for the 460-pound propulsion system are 3500 and 1550 km, respectively.
Whereas the 460-pound engine yields the lower altitude at the extremity of the
1975 launch window, the 630-pound engine yields the minimum altitude during
the middle of the window. If the injected weight is the same for both vehicles,
as it is for 6 July 1967, the weight along the approach hyperbola is identical,
and therefore a larger orbit establishment velocity decrement can be achieved
with the smaller engine due to the fact that the corresponding burnout weight
is less and hence a lower apoapsis altitude achieved. From this analysis, it
is apparent that there is an optimum engine size between these two extremes.
These results are presented in table 23.

In conclusion, a direct comparison of the final mission parameters (payload
in a fixed orbit for Mars and apoapsis altitude for Venus) is, in a sense, meaning-
less for the launch opportunities under consideration due to the variety of missions
considered in the evolution of the Voyager Program - orbiter/direct lander,
bus/direct lander, orbiter/atmospheric probe. However, for illustrative pur-
poses only, the orbiter/bus payloads for the Martian phase of this study are
presented in table 24 for the launch opportunities between 1969 and 1975, and the
minimum apoapsis altitudes achievable for Venusian missions are presented in
table 25. In both tables, these data are for the extremity of the best 30-day
window in each launch opportunity for the respective missions. The penalties
associated with engine commonality to perform the above mentioned missions
are presented in table 26. For each planet, two engine sizes were examined
to perform the intended mission with commonality between the heavy engine
for Mars and the light engine for Venus. After finalization of the mission evolu-
tion program, a program can be initiated to determine the optimum engine size
with associated propellant weights to maximize the desired mission parameters.
With the propulsion system and reference payload sized, the final desired para-
meters can be optimized and the best 30-day window in each launch opportunity
selected. Further improvement may then be obtained by such techniques as off-
loading propellent techniques, varying departure and arrival velocities, etc.

In the present analysis, the only semi-optimization study conducted was to
determine the departure and arrival velocities to daily maximize the planetocentric
orbital payload when the maximum weight was injected into the heliocentric trans-
fer orbit. These payload weights and apoapsis altitudes may be slightly optimistic
since velocity decrements were applied impulsively.

TABLE 21

MINIMUM APOAPSIS ALTITUDE FOR FIXED VENUSIAN PAYLOAD

630-Pound Propulsion System

	Date	Trajectory Type	Time of Flight (days)	Departure Velocity (km/sec)	Injected Weight (lb)	Arrival Velocity (km/sec)	Orbit Est. Vel. Dec. (km/sec)	Apoapsis Altitude (km)
1968-1969	12/14/68	I	150	3.393	6826	4.045	3.027	4156.
	12/30/68	I	138	2.927	7150	4.497	3.176	4414.
	1/7/69	I	132	2.811	7150	4.539	3.176	4545.
	1/13/69	I	126	2.779	7150	4.528	3.176	4510.
	1/19/69	I	122	2.830	7150	4.494	3.176	4406.
	1/27/69	I	116	3.044	7150	4.428	3.176	4205.
	2/12/69	I	104	4.034	6052	4.273	2.642	8398.
1970	7/20/70	I	140	3.384	6836	5.740	3.032	
	8/5/70	I	130	3.081	7150	5.522	3.176	8834.
	8/13/70	I	124	2.983	7150	5.364	3.176	7940.
	8/19/70	I	120	2.981	7150	5.217	3.176	7191.
	8/25/70	I	116	3.047	7150	5.054	3.176	6448.
	9/4/70	I	110	3.359	6865	4.753	3.046	6378.
	9/18/70	I	100	4.181	5868	4.398	2.543	10,342.
1972	3/1/64	II	186	3.574	6615	4.631	2.927	6990
	3/15/64	II	180	3.184	7065	4.900	3.138	6149
	3/29/64	II	172	2.938	7150	5.115	3.176	6718
	4/13/64	II	164	2.903	7150	5.353	3.176	7892
	4/30/64	II	154	3.308	6925	5.667	3.074	11,176
1973	10/16/65	II	174	3.151	7105	4.385	3.156	4222.
	10/31/65	II	164	2.796	7150	4.276	3.176	3777.
	11/8/65	II	158	2.706	7150	4.216	3.176	3618.
	11/15/65	II	154	2.729	7150	4.143	3.176	3431.
	11/22/65	II	148	2.853	7150	4.091	3.176	3268.
	11/28/65	II	142	3.068	7150	4.097	3.176	3220.

-103-

TABLE 21 (Concl'd)

	Date*	Trajectory Type	Time of Flight (days)	Departure Velocity (km/sec)	Injected Weight (lb)	Arrival Velocity (km/sec)	Orbit Est. Vel. Dec. (km/sec)	Apoapsis Altitude (km)
	5/27/67	I	138	3.537	6655	3.706	2.946	3838.
	6/1/67	I	138	3.332	6900	3.258	3.062	2240.
1975	6/6/67	I	140	3.119	7140	2.876	3.172	1148.
	6/11/67	I	140	2.706	7150	2.947	3.176	1220.
	6/16/67	I	133	2.781	7150	3.050	3.176	1361.
	6/21/67	I	128	2.922	7150	3.185	3.176	1508.
	6/26/67	I	122	3.194	7055	3.275	3.133	1905.

* Trajectory analysis for 1964-1970 period pertinent to 1972-1978 period with at most a 5-day shift in the window.

TABLE 22

MINIMUM-ENERGY VENUSIAN ORBIT WITH FIXED PAYLOAD AND PROPULSION SYSTEM WEIGHTS

Launch Date	Time of Flight (days)	Departure Velocity (km/sec)	Approach Velocity (km/sec)	Dry Propulsion System Weight			
				460 pounds		630 pounds	
				Injected Weight (lb)	Apoapsis Altitude (km)	Injected Weight (lb)	Apoapsis Altitude (km)
12/14/68	150	3.393	4.045	6070	5299	6826	4156
12/30/68	138	2.927	4.497	6070	6936	7150	4414
1/7/69	132	2.811	4.539	6070	7114	7150	4545
1/13/69	126	2.779	4.528	6070	7067	7150	4510
1/19/69	122	2.830	4.494	6070	6926	7150	4406
1/27/69	116	3.044	4.28	6070	6655	7150	4205
2/12/69	104	4.034	4.273	6052	6205	6052	8398
7/20/70	140	3.384	5.740	6070	15365	6836	12417
8/5/70	130	3.081	5.522	6070	13219	7150	8834
8/13/70	124	2.983	5.364	6070	11902	7150	7940
8/19/70	120	2.981	5.217	6070	10816	7150	7191
8/25/70	116	3.047	5.054	6070	9757	7150	6448
9/4/70	110	3.359	4.753	6070	8101	6865	6378
9/18/70	100	4.181	4.398	5868	7611	5868	10342
3/1/64 ⎫	186	3.574	4.631	6070	7522	6615	6990
3/15/64 ⎪	180	3.184	4.900	6070	8865	7065	6149
3/29/64 ⎬ 1972	172	2.938	5.115	6070	10140	7150	6718
4/13/64 ⎪	164	2.903	5.353	6070	11814	7150	7892
4/30/64 ⎭	154	3.308	5.667	6070	14596	6925	11176
10/16/65 ⎫	174	3.151	4.385	6070	6488	7105	4222
10/31/65 ⎪	164	2.796	4.276	6070	6078	7150	3777
11/8/65 ⎨ 1973	158	2.706	4.216	6070	5865	7150	3618
11/15/65 ⎪	154	2.729	4.143	6070	5617	7150	3431
11/22/65 ⎪	148	2.853	4.091	6070	5445	7150	3268
11/28/65 ⎭	142	3.068	4.057	6070	5337	7150	3220
5/27/67 ⎫	138	3.537	3.706	6070	4331	6655	3838
6/1/67 ⎪	138	3.332	3.258	6070	3243	6900	2240
6/6/67 ⎨ 1975	140	3.119	2.876	6070	2622	7140	1148
6/11/67 ⎬	140	2.706	2.947	6070	2740	7150	1220
6/16/67 ⎪	133	2.781	3.050	6070	2918	7150	1361
6/21/67 ⎪	128	2.922	3.185	6070	3107	7150	1508
6/26/67 ⎭	122	3.194	3.275	6070	3346	7055	1905

* Trajectory analysis for 1964-1970 period pertinent to 1972-1978 period with at most a 5-day shift in the window.

NOTE: Payload consists of a 1300-pound orbiter exclusive of dry propulsion system, plus three 200-pound landers carried into orbit.

TABLE 23

MINIMUM VENUSIAN APOAPSIS ALTITUDE
ORBITER/DIRECT LANDER MISSION

Launch Date*	Traj. Type	Time of Flight (days)	Departure Velocity (km/sec)	Approach Velocity (km/sec)		460-Pound Engine			630-Pound Engine	
						Injected Weight (lb)	Apoapsis Altitude (km)		Injected Weight (lb)	Apoapsis Altitude (km)
10/16/65	II	174	3.151	4.385		6470	3844		7105	3316
10/31/65	II	164	2.796	4.276		6470	3552		7468	1965
11/8/65	II	158	2.706	4.216		6470	3398		7550	1634
11/15/65	II	154	2.729	4.143		6470	3219		7530	1546
11/22/65	II	148	2.853	4.091		6470	3095		7410	1751
11/28/65	II	147	3.068	4.057		6470	3017		7194	2280
5/27/67	I	138	3.537	3.706		6470	2282		6655	3315
6/1/67	I	138	3.332	3.258		6470	1523		6900	1689
6/6/67	I	140	3.119	2.876		6470	1004		7140	582
6/11/67	I	140	2.706	2.947		6470	1093		7550	0
6/16/67	I	133	2.781	3.050		6470	1228		7490	39
6/21/67	I	128	2.922	3.185		6470	1416		7345	504
6/26/67	I	122	3.194	3.275		6470	1549		7055	1300
7/1/67	I	117	3.517	3.384		6470	1719		6670	2590
7/6/67	I	112	3.899	3.504		6218	2790		6218	4722

1973 (brace covering 10/16/65–11/28/65)
1975 (brace covering 5/27/67–7/6/67)

* Trajectory analysis for 1964-1970 period pertinent to 1972-1978 period with at most a 5-day shift in the window.

TABLE 24

MARTIAN PAYLOADS AT EXTREMITY OF BEST 30-DAY LAUNCH PERIOD*

Date	Configuration	Trajectory Type	Minimum Injected Weight (pound)	Propellant Weight (pound)	Dry Propulsion Weight (pound)	Minimum Orbiter-Bus Weight (pound)
1969	O/L	II	6600	2652	403	1907
1971	O/2L	I	7270	1530	219	1761
1973	O/L	I	5730	1500	250	2120
1975	B/2L	II	6070	287	39	2210

*1880-lb Direct Entry Lander
1700 km Periapsis Altitude
10,000 km Apoapsis Altitude

TABLE 25

MAXIMUM APOAPSIS ALTITUDE AT EXTREMITY OF 30-DAY LAUNCH PERIOD FOR VENUS*

Date	Configuration	Trajectory Type	Minimum Injected Weight (pound)	Maximum Apoapsis Altitude (km)
1970	O/3L	I	6450	8100
1972	O/3L	II	6700	6900
1973	O/L	II	7250	2150
1975	O/L	I	6850	2000

*1300-lb Orbiter Weight
630-lb Dry Propulsion Weight
3 200-lb Orbital Entry Landers
1340-lb Direct Entry Lander
1000 km Periapsis Altitude

TABLE 26

COMMON PROPULSION SYSTEM
PENALTY -- 30-DAY WINDOW

Planet	Date	Orbiter-Bus Weight (pound)		
		260-pound Engine	460-pound Engine	
Mars	1969	1300	1850	
Mars	1971	1760	1560	
Mars	1973	2190	1990	

Planet	Date		Orbiter Apoapsis Altitude (km)	
			460-pound Engine	630-pound Engine
Venus	1970		8500	8100
Venus	1972		8900	6900
Venus	1973		3300	2150
Venus	1975		1700	2000

5. TRAJECTORY ANALYSES

5.1 Planetary Approach Geometry

The approach geometry parameters, three components of the approach velocity, or a velocity magnitude with two reference directions may place constraints on the heliocentric transfer trajectories. For a fly-by mission with or without a lander, the minimum approach velocity may be desired to maximize the probe dwell time in the vicinity of the planet. For other missions, where lighting conditions at encounter are important, the direction of the approach velocity may limit the number of acceptable interplanetary trajectories. For the present preliminary design study, the approach geometry parameters have not been employed to place constraints on the allowable interplanetary trajectories.

The magnitude of the approach velocity vector, the difference between the vehicle and planet velocity vectors with respect to the sun at the point the vehicle intersects the planet's orbital path, is employed in determining the velocity at periapsis of the approach hyperbola. This in turn allows for the computation of the velocity decrement to achieve a given planetocentric orbit or for a given velocity decrement to determine the minimum apoapsis altitude. The hyperbolic approach velocity vector is related to the velocity at periapsis by

$$V_{H_P} = \sqrt{V_\infty^2 + \frac{2\mu}{r_p}}$$

where

r_p = periapsis radius

μ = gravitational parameter of planet.

For the launch opportunities under consideration, the approach velocity vector for Mars varies between 2.4 and 4.3 km/sec and for Venus between 2.9 and 5.7 km/sec. These approach velocity magnitudes are those associated with the minimum of the sum of the departure and arrival velocities. A comparison of these approach velocities with those associated with the minimum departure velocities is presented in figures 37 through 45. In general, for both Mars and Venus, the minimum approach velocities are associated with Type I class II and Type II class I interplanetary transfer trajectories.

A second important approach parameter, the angle between the approach asymptote and the planet-sun line ζ_p is essentially the sun-vehicle-planet angle several days prior to encounter. Since the heliocentric speed of the vehicle is greater than that of Venus, the vehicle is essentially overtaking the planet and

is therefore approaching from the trailing edge. For Type I trajectories, the vehicle is approaching from the dark side. In general, ζ_p varies between 30 and 90 degrees for Type I trajectories. However, portions of the Venus 1967 launch opportunity contradict this rule with the angle increasing to 100 degrees, which implies the probe is approaching from the sunlit side. This, in turn, implies that the vehicle has passed perihelion in the transfer orbit. The opposite situation arises for Type II trajectories with the vehicle generally approaching Venus from the sunlit side. Here ζ_p varies between 100 and 175 degrees except in 1969 where the angle decreases to 60 degrees, and the vehicle approaches the planet from the dark side.

For Martian approaches the heliocentric speed of the vehicle is less than that of the planet and the vehicle is essentially being overtaken by the planet. Therefore, approaches occur along the leading edge of Mars. For Type I trajectories, ζ_p varies between 60 and 150 degrees with the approach, in general, in the sunlit region. For Type II trajectories ζ_p is less than 90 degrees for the 1969 and 1971 launch opportunities with the vehicle approaching the planet from the dark side.

The third important parameter is the angle between the approach asymptote and the planet's orbit plane γ_p. This angle is zero only if the heliocentric transfer plane and the planet's orbital plane are coplanar. Negative angles indicate the vehicle is approaching above the planet's orbital plane. The importance of this parameter is that it defines the minimum planetocentric orbital inclination with respect to the orbital plane of the planet. In other words, if γ_p is 0 degrees, inclinations between 0 and 180 degrees are achievable; if γ_p is 45 degrees, the resulting inclination may vary between 45 and 135 degrees; and if γ_p is 90 degrees, only orbits normal to the orbital plane of the planet are achievable. If the inclination is less than 90 degrees, the vehicle is travelling in the same direction as the planet rotation.

For Mars, the orientation of the North Pole vector is essentially fixed in inertial space and the minimum orbital inclination with respect to the Martian equator can be obtained by

$$i_{min} = \sin^{-1} [\underline{1}_{NP} \cdot \underline{1}_{V_\infty}] .$$

These angles are presented in table 27 for the four Martian launch opportunities under investigation.

The approach geometry angles presented in figures 46 through 54 apply to the minimum departure velocity case. However, as the minimum of the sum of the departure and arrival velocities occurs generally within ±10 days of the minimum departure velocity, the angles are representative of those to be encountered for the Voyager program. It is to be noted that the angle between the approach asymptote and the planet-sun line moves in the direction normal to the sun-line as the approach velocity is reduced.
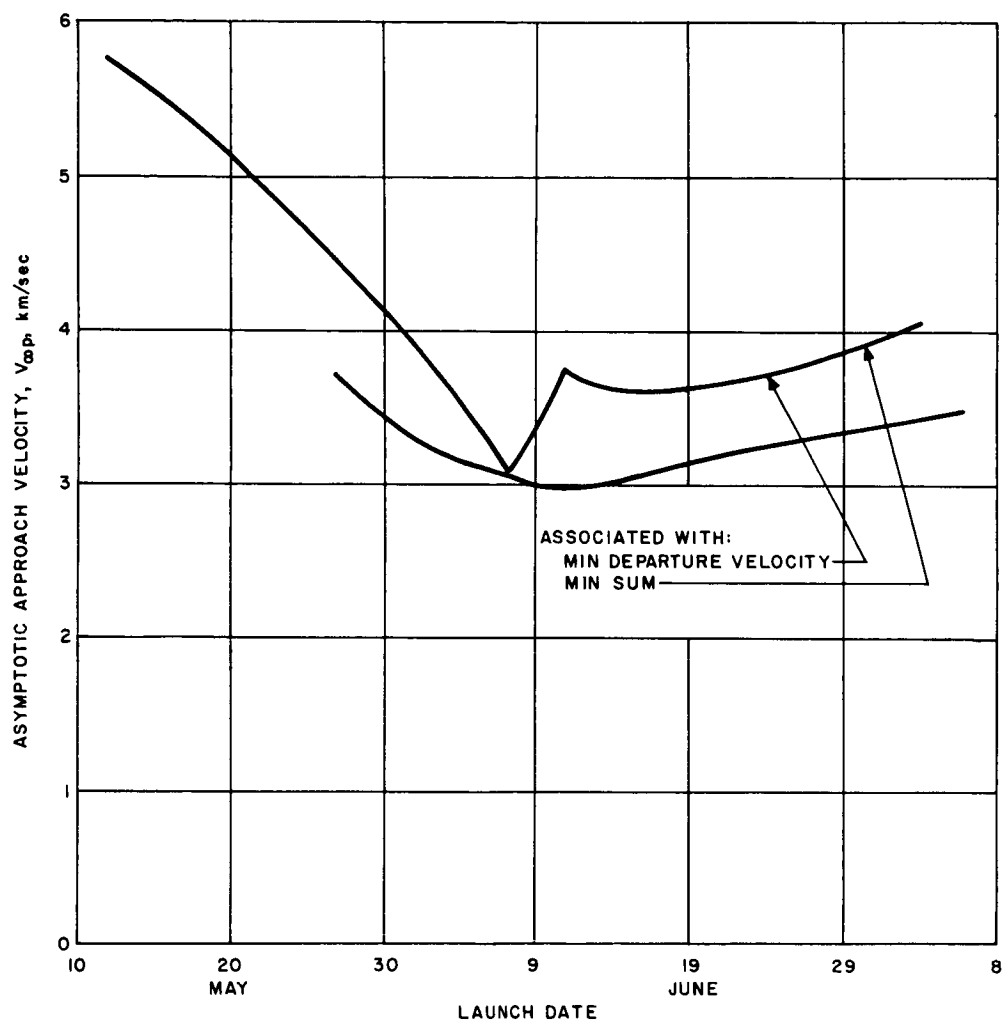
-110-
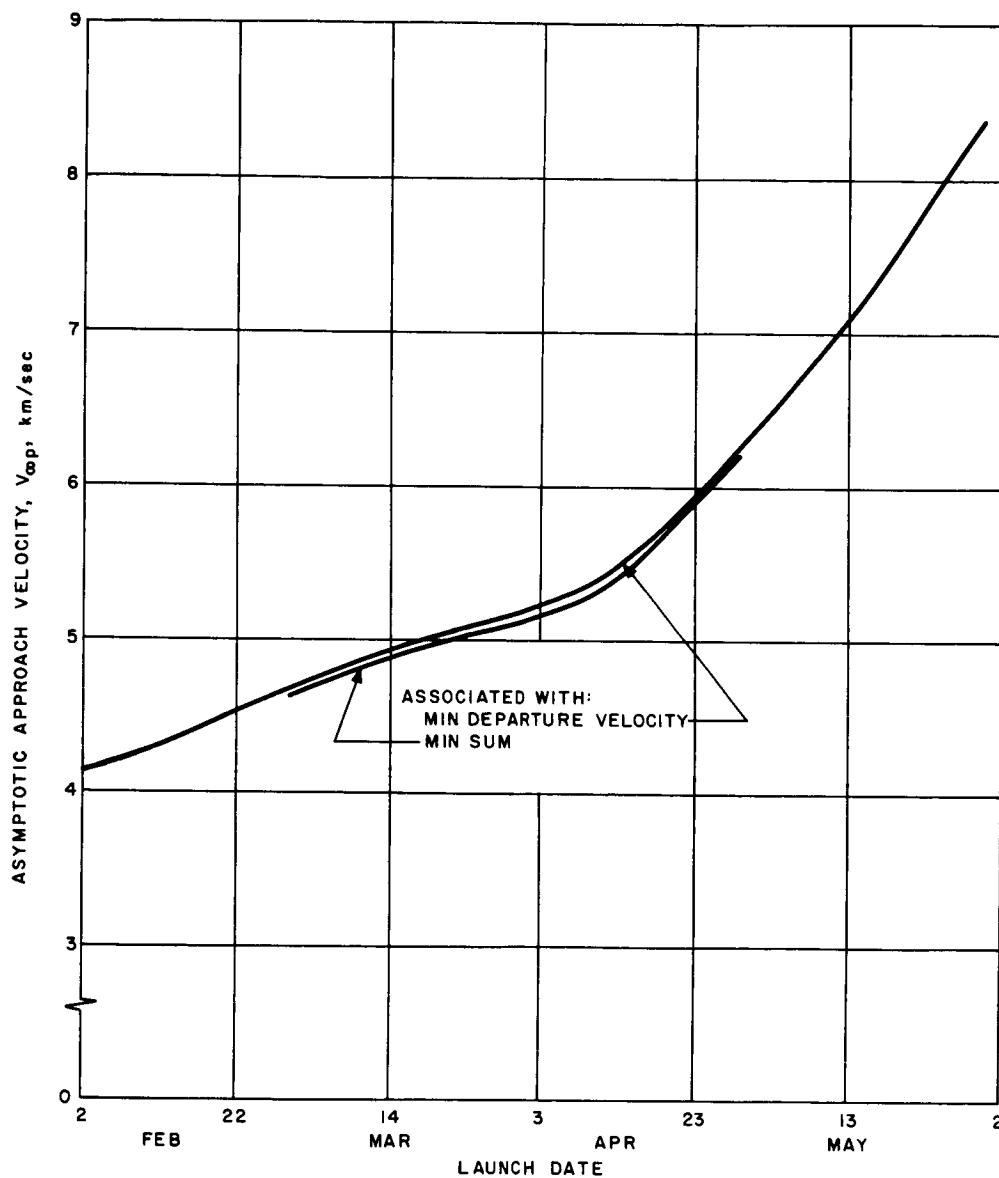
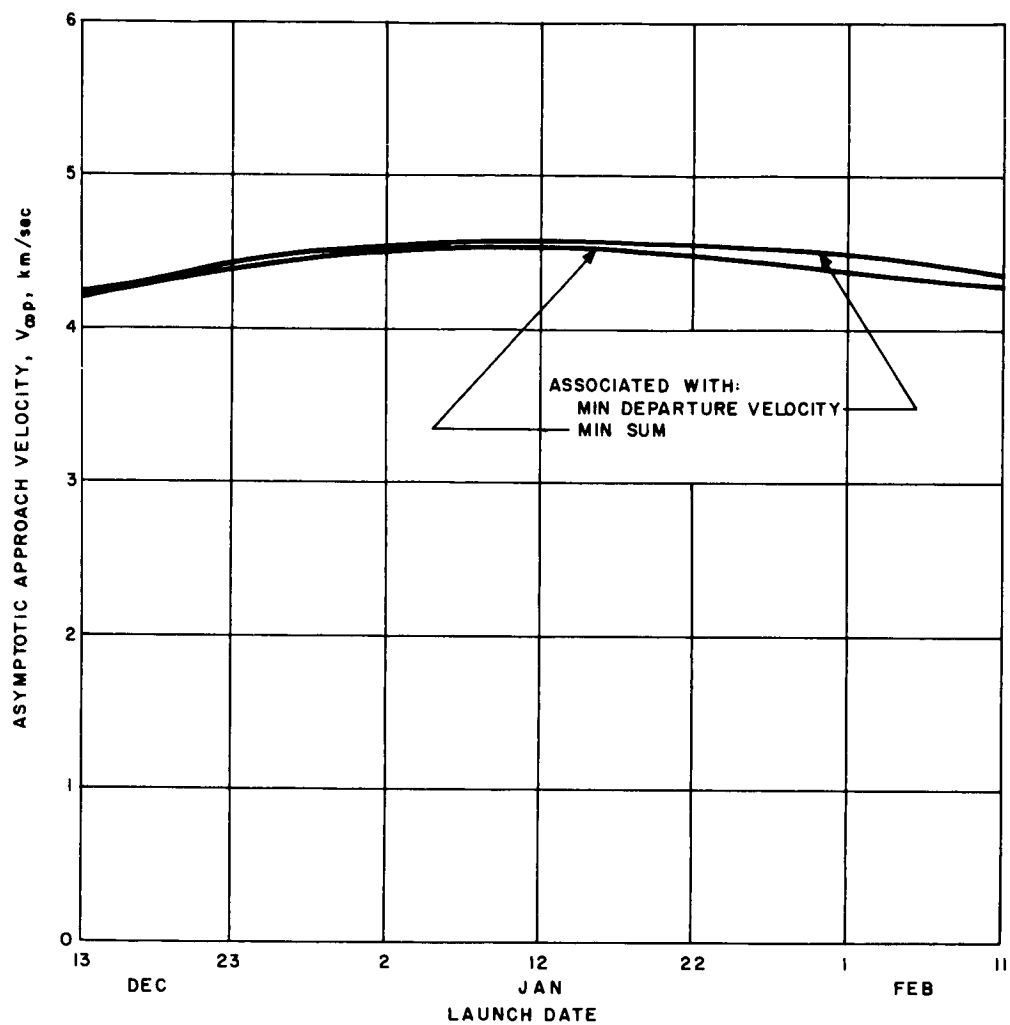Figure 37 ASYMPTOTIC APPROACH VELOCITY VERSUS LAUNCH DATE,
VENUS 1964, TYPE II

63-8914

-111-
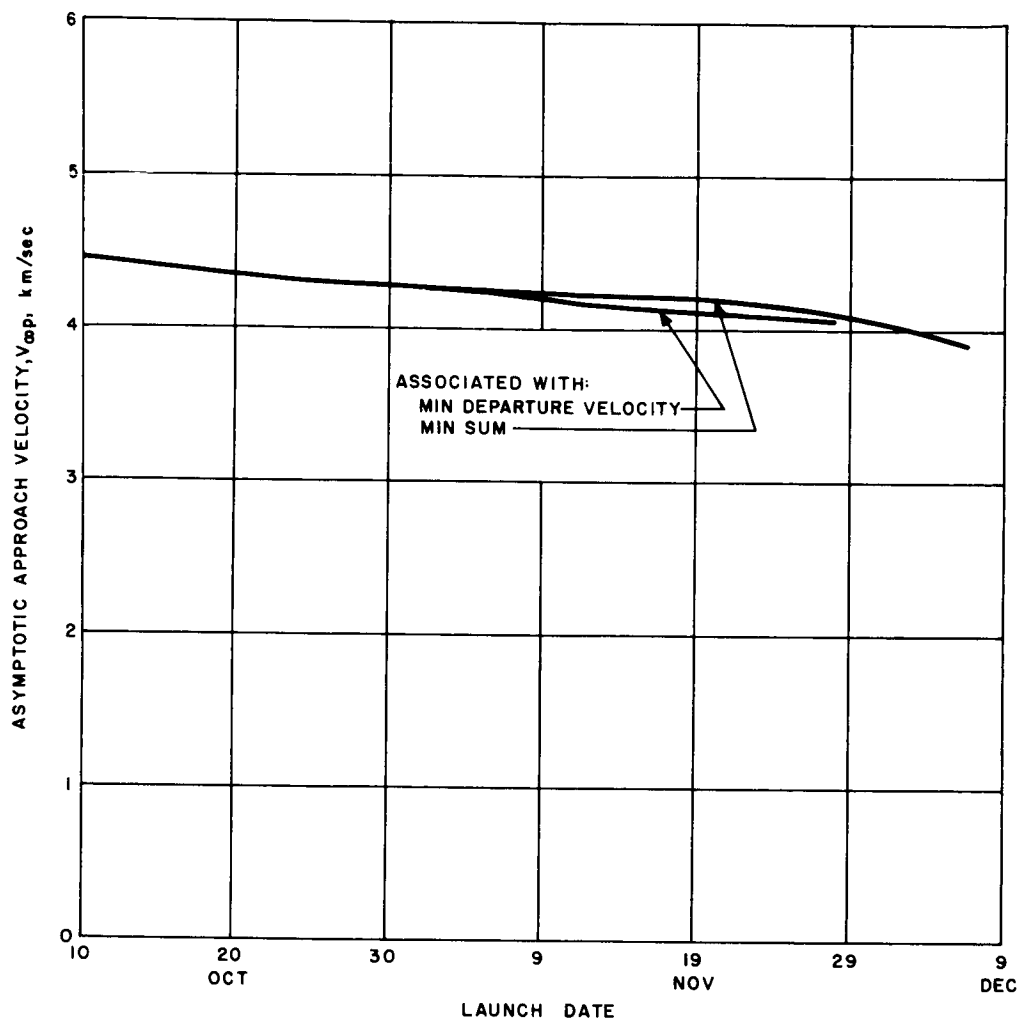
63-8915

Figure 38 ASYMPTOTIC APPROACH VELOCITY VERSUS LAUNCH DATE,
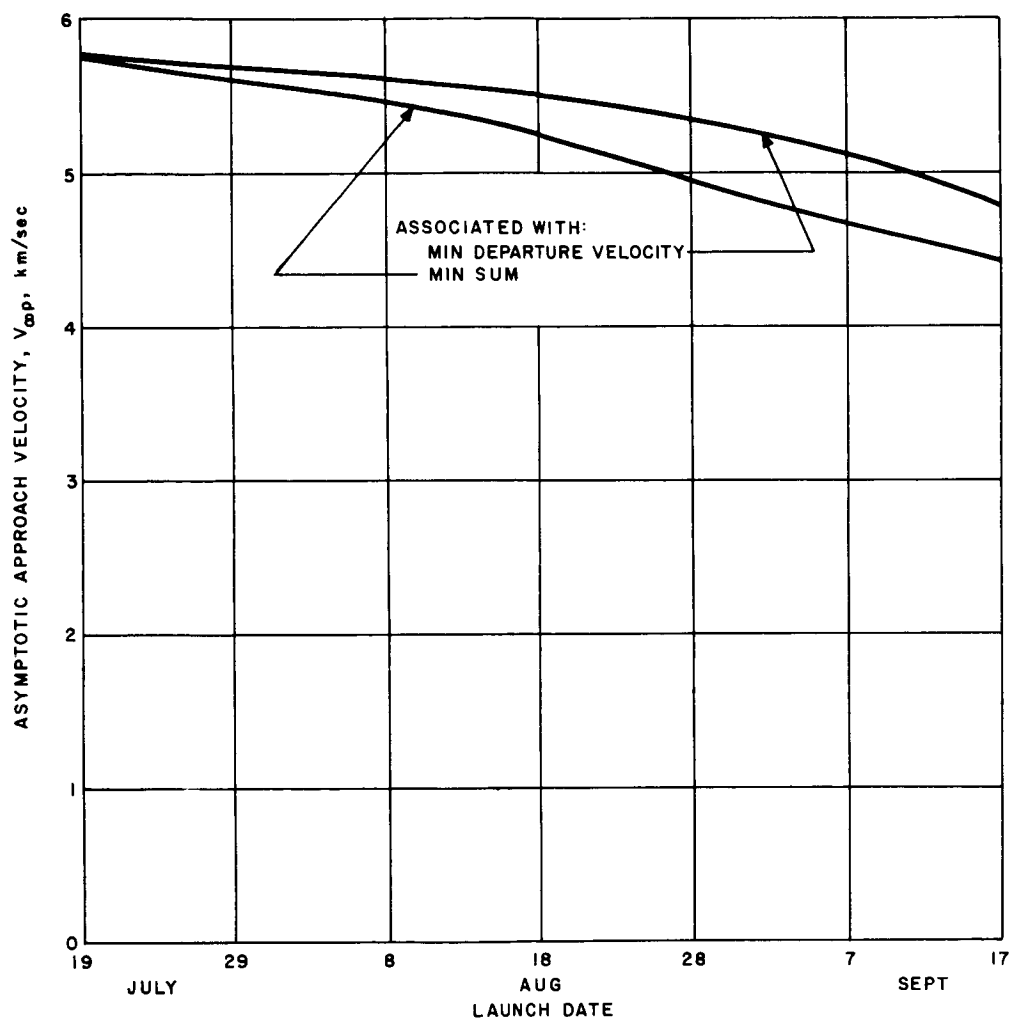VENUS 1965, TYPE II

-112-

63-8907

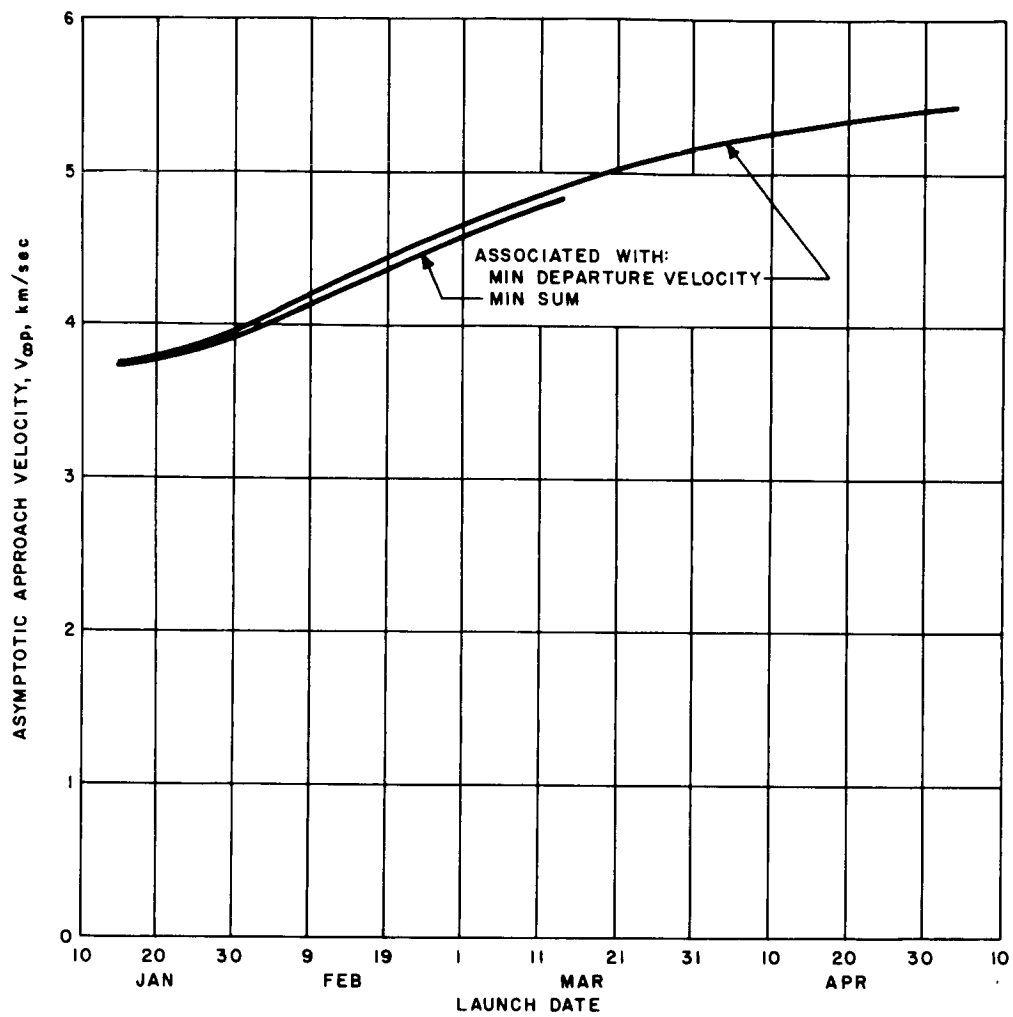Figure 39 ASYMPTOTIC APPROACH VELOCITY VERSUS LAUNCH DATE,
VENUS 1967, TYPE I

-113-

63-8912

Figure 40 ASYMPTOTIC APPROACH VELOCITY VERSUS LAUNCH DATE,
VENUS 1969, TYPE I
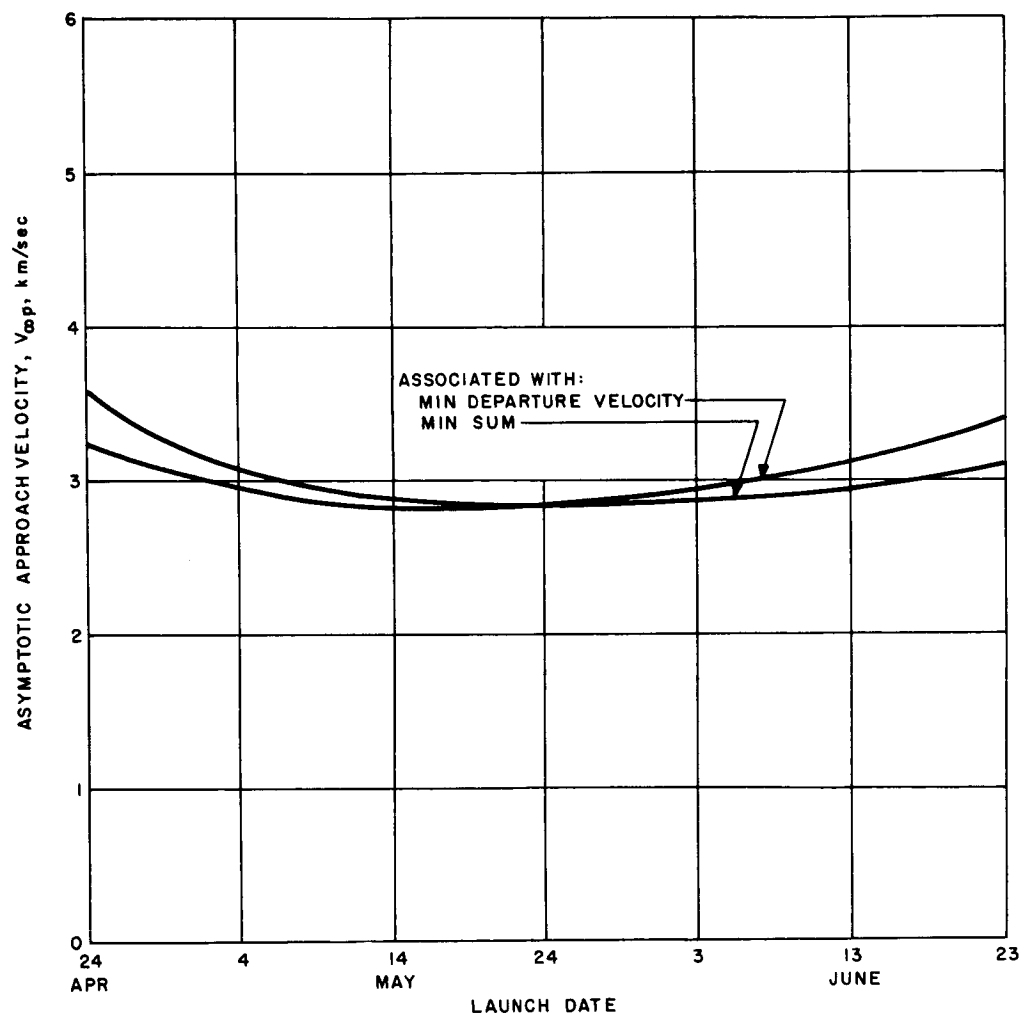
-114-

ASSOCIATED WITH:
MIN DEPARTURE VELOCITY
MIN SUM

63-8913

Figure 41 ASYMPTOTIC APPROACH VELOCITY VERSUS LAUNCH DATE,
VENUS 1970, TYPE I

-115-

Figure 42 ASYMPTOTIC APPROACH VELOCITY VERSUS LAUNCH DATE,
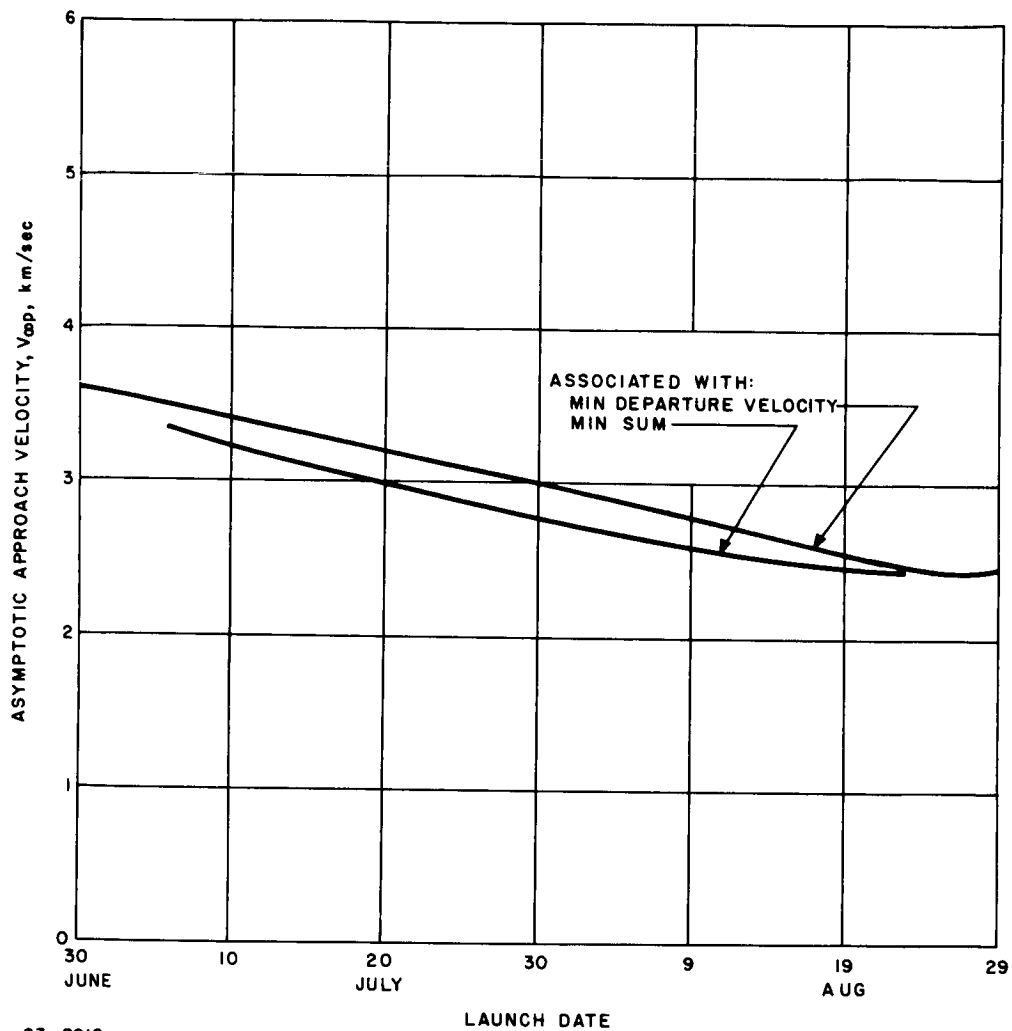MARS 1969, TYPE II

63-8908

-116-

63-8909

Figure 43 ASYMPTOTIC APPROACH VELOCITY VERSUS LAUNCH DATE,
MARS 1971, TYPE I

Figure 44 ASYMPTOTIC APPROACH VELOCITY VERSUS LAUNCH DATE,
MARS 1973, TYPE I

63-8910
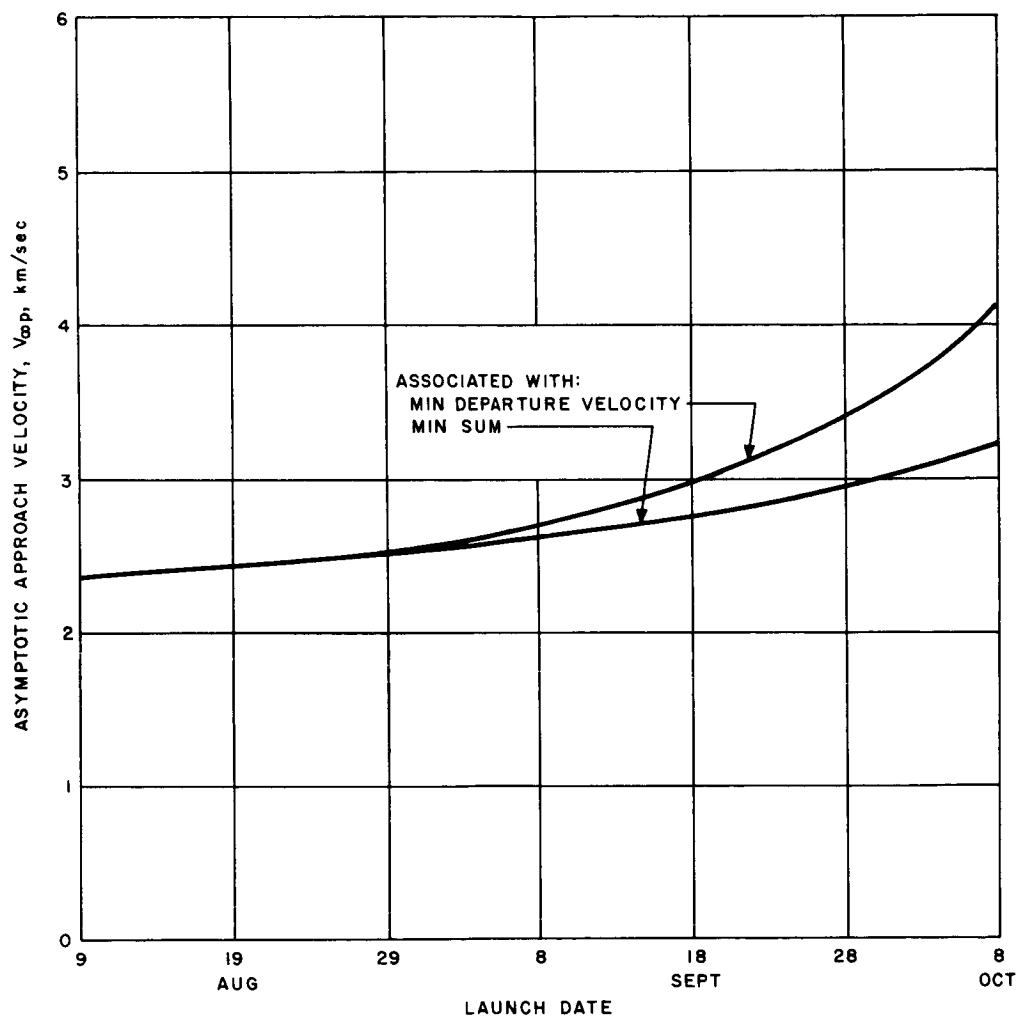
-118-

63-8911

Figure 45 ASYMPTOTIC APPROACH VELOCITY VERSUS LAUNCH DATE,
MARS 1975, TYPE II

Figure 46 PLANETARY APPROACH GEOMETRY, VENUS 1964, TYPE II

63-8723

-120-

Figure 47 PLANETARY APPROACH GEOMETRY, VENUS 1965, TYPE II

63-8724

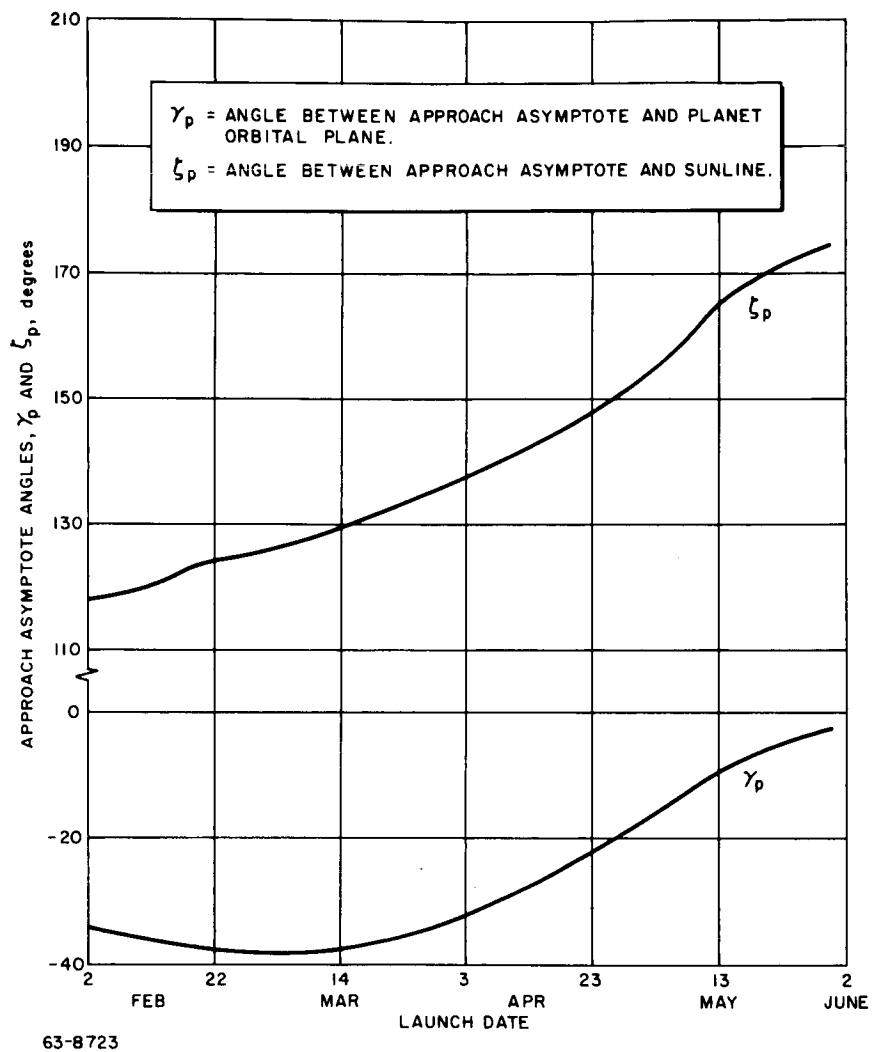Figure 48 PLANETARY APPROACH GEOMETRY, VENUS 1967, TYPE I

63-8859

-122-

Figure 49 PLANETARY APPROACH GEOMETRY, VENUS 1969, TYPE I

63-8858

-123-

Figure 50 PLANETARY APPROACH GEOMETRY, VENUS 1970, TYPE I

63-8727

-124-
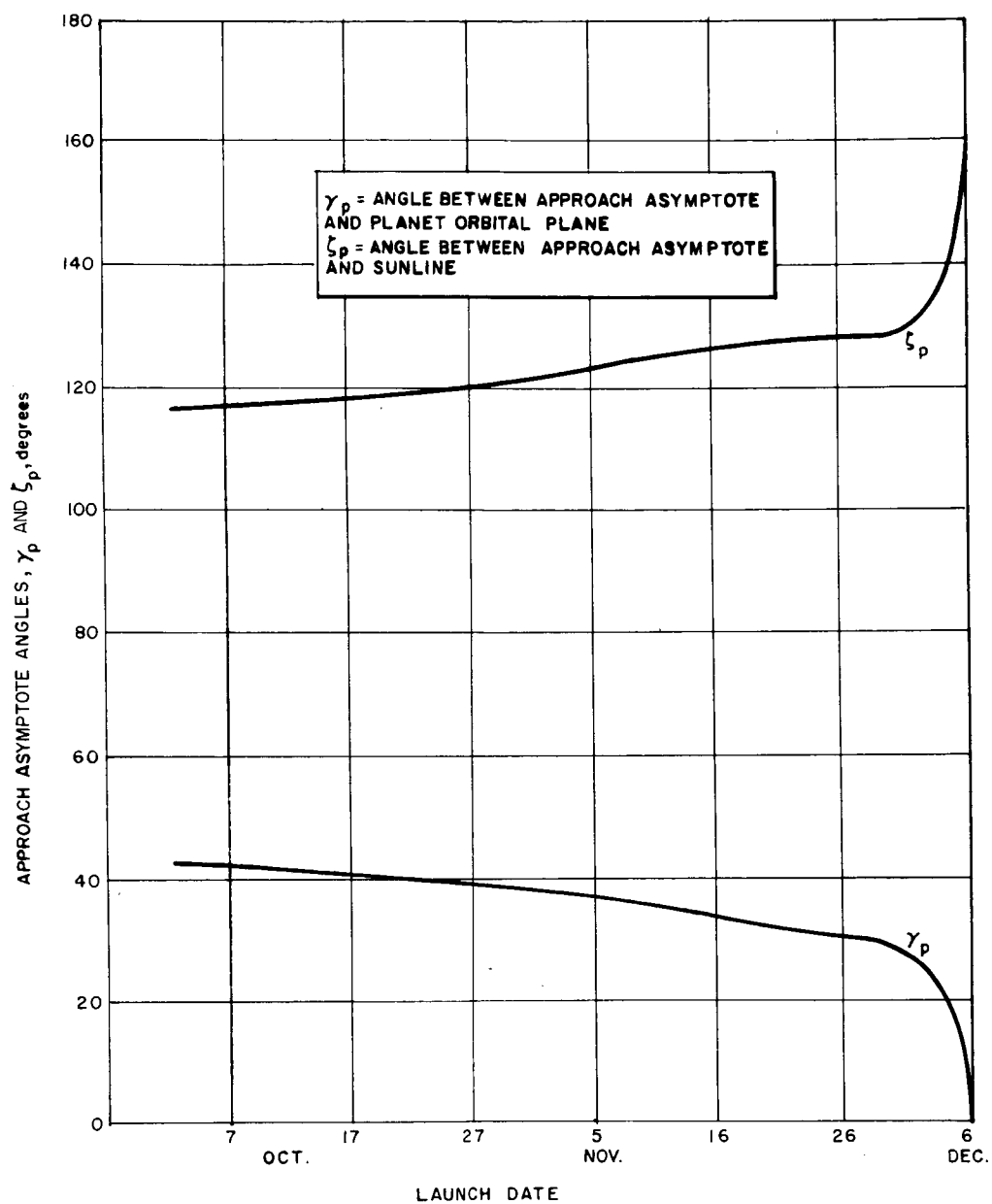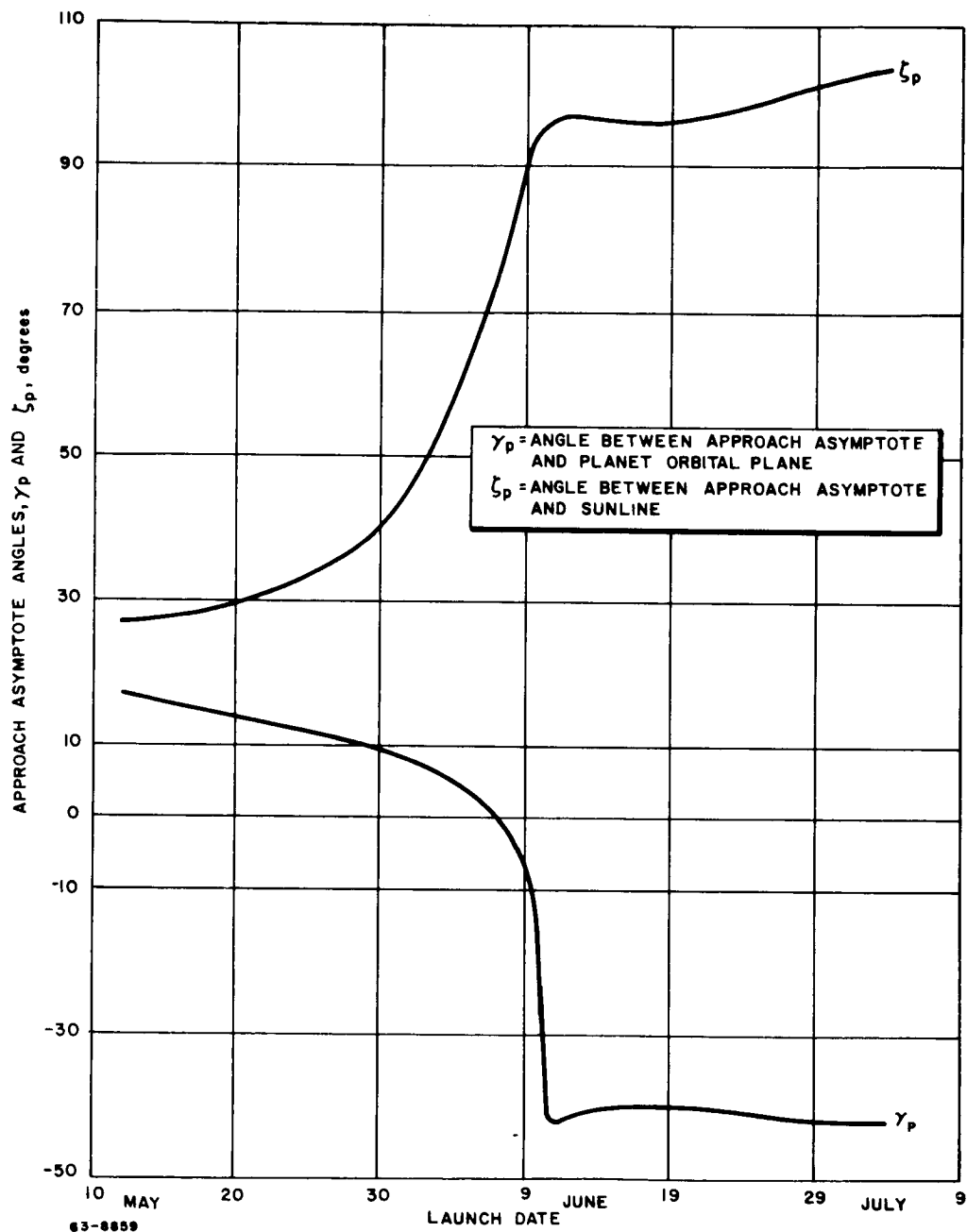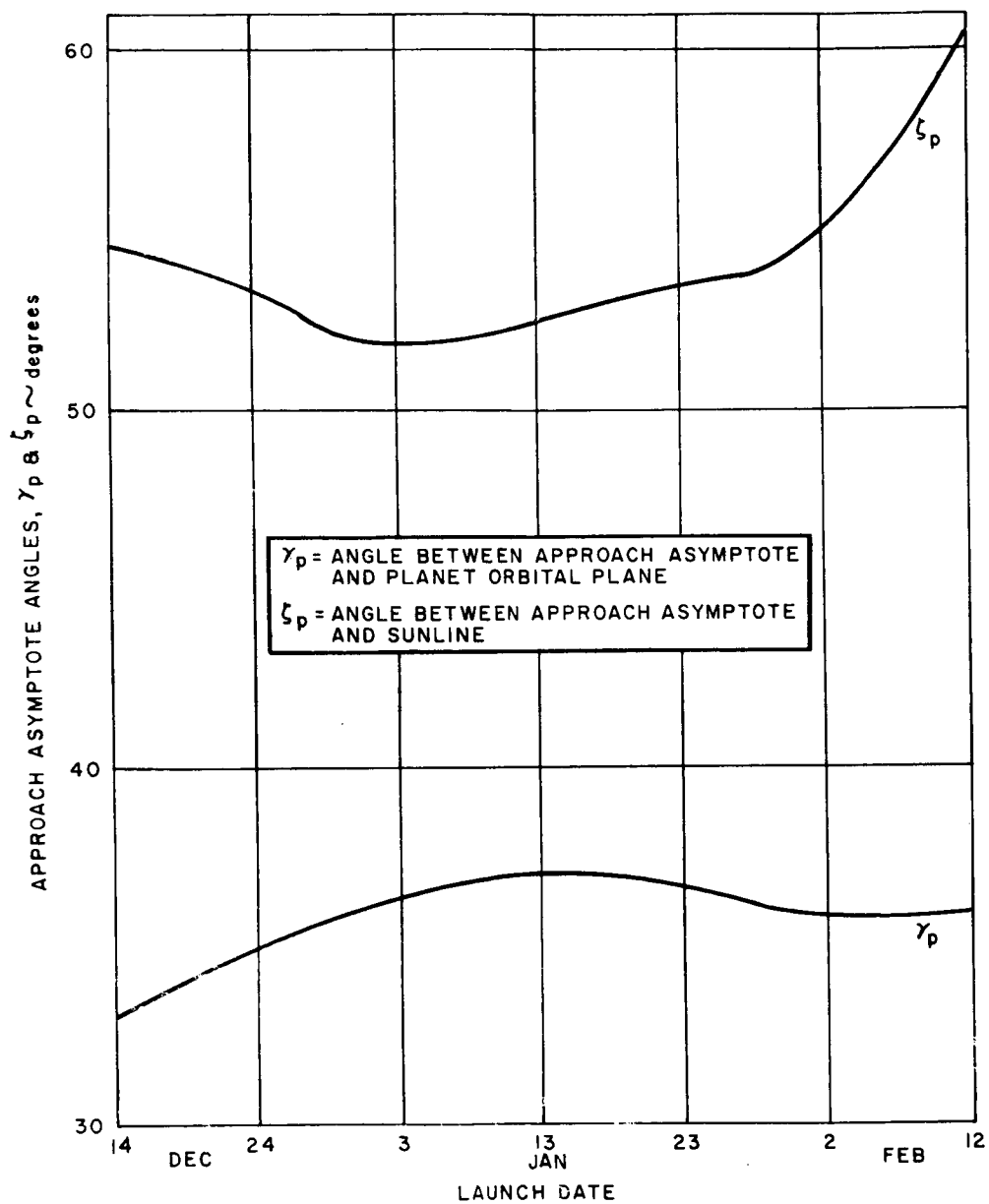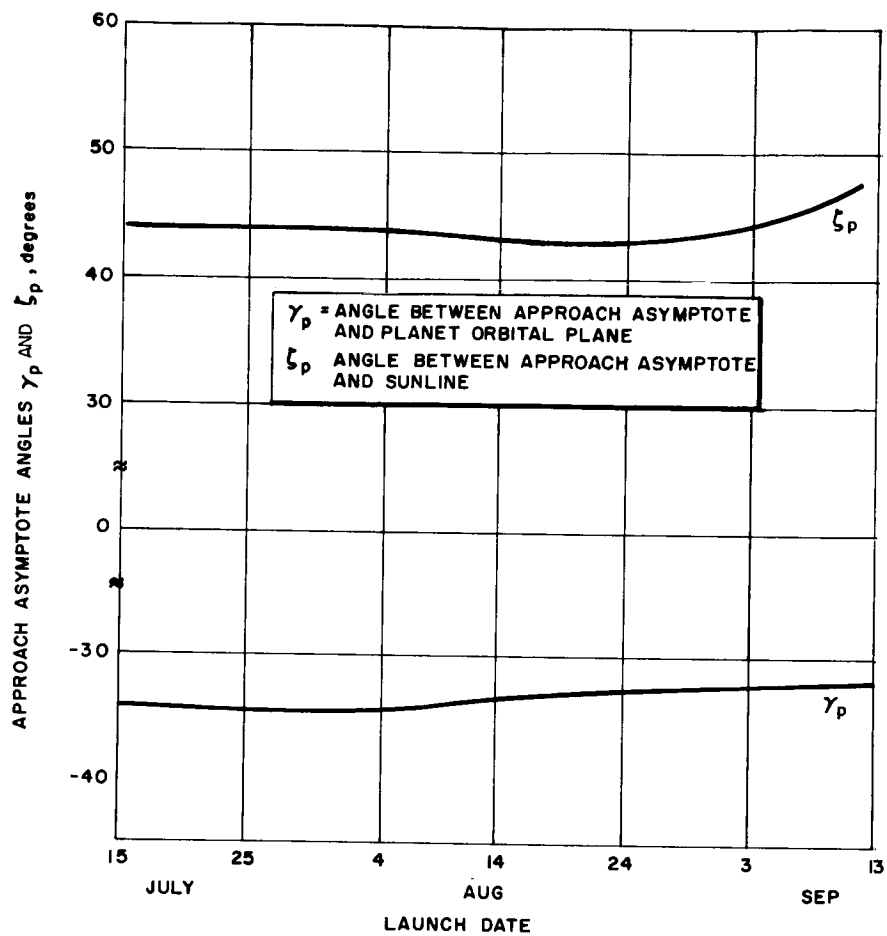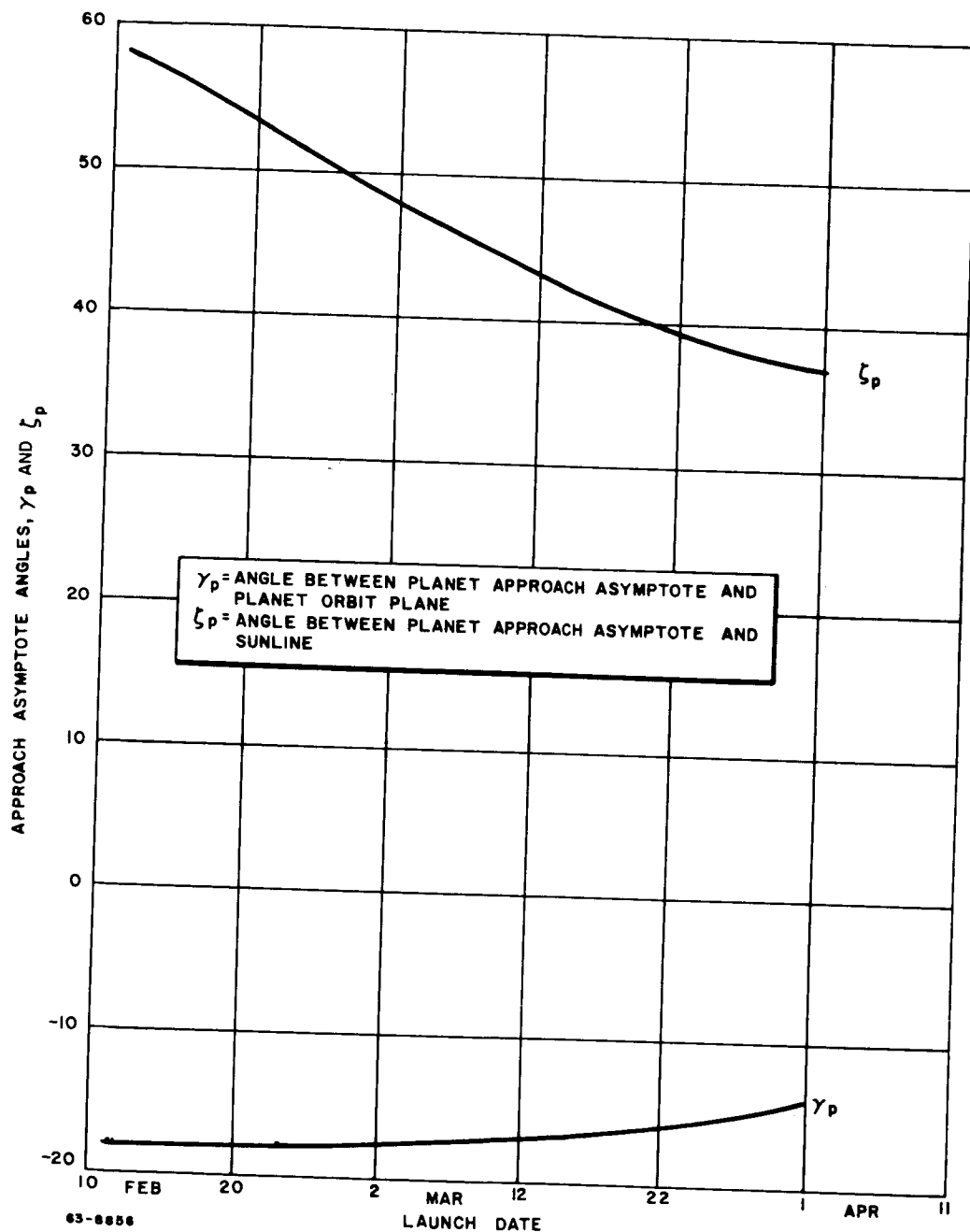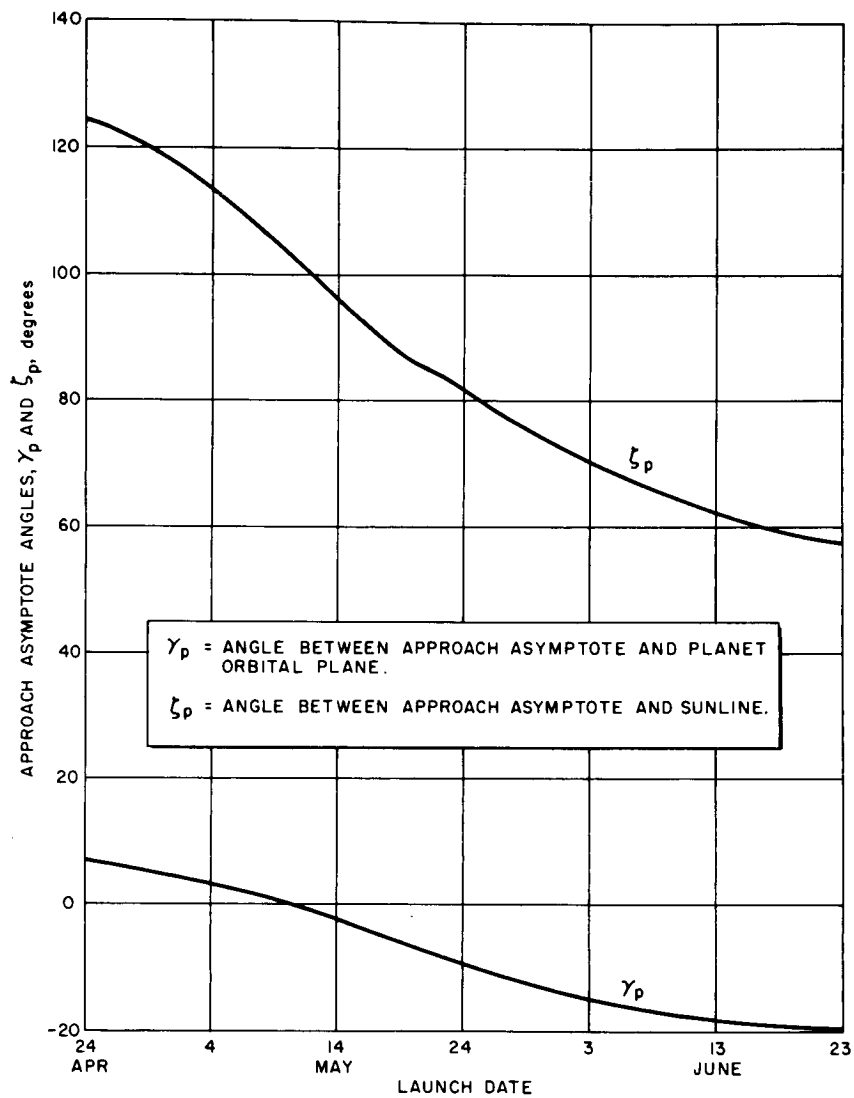
Figure 51 PLANETARY APPROACH GEOMETRY, MARS 1969, TYPE II

63-8729

Figure 52 PLANETARY APPROACH GEOMETRY, MARS 1971, TYPE I

-126-
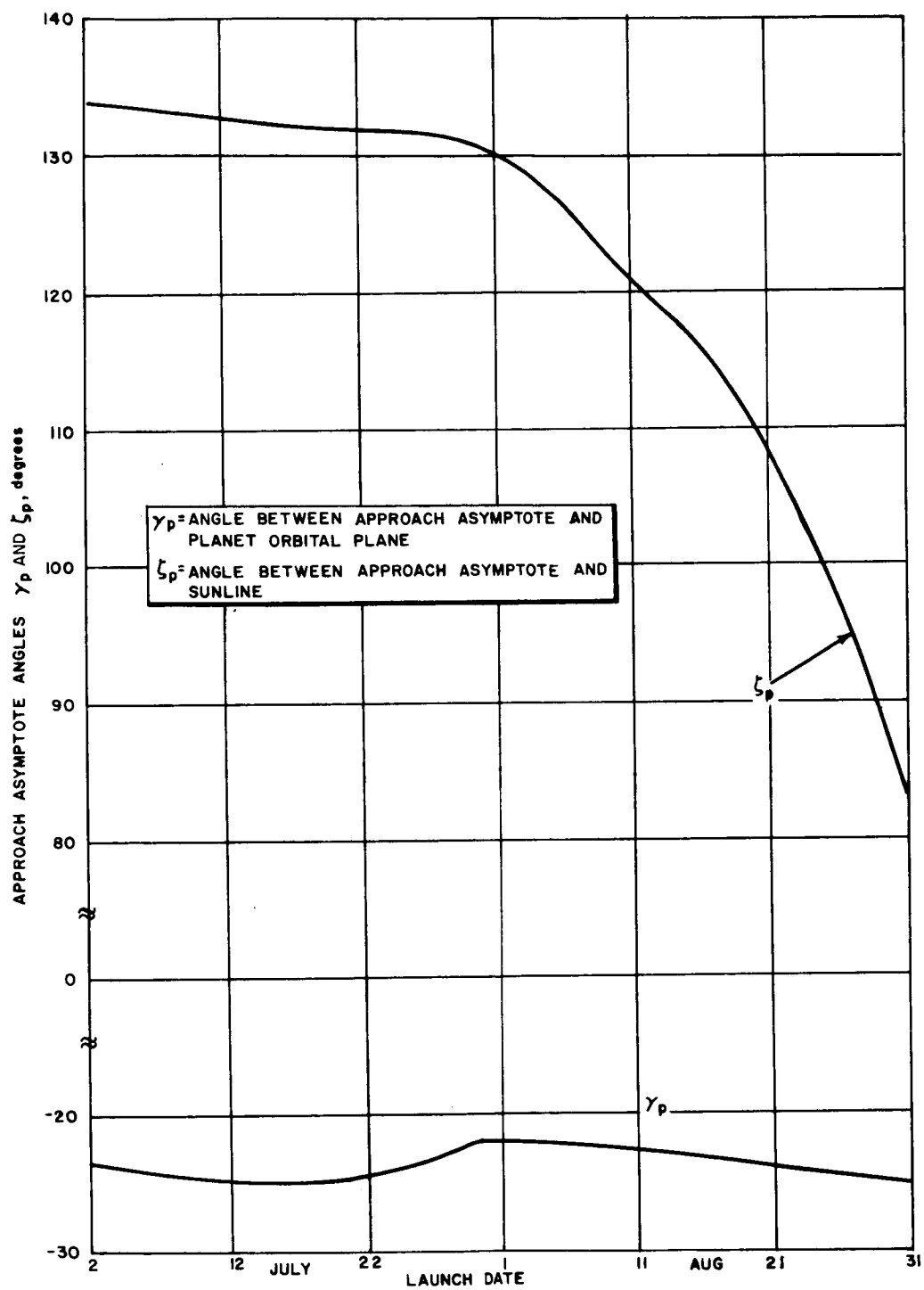
Figure 53 PLANETARY APPROACH GEOMETRY, MARS 1973, TYPE I

63-8857
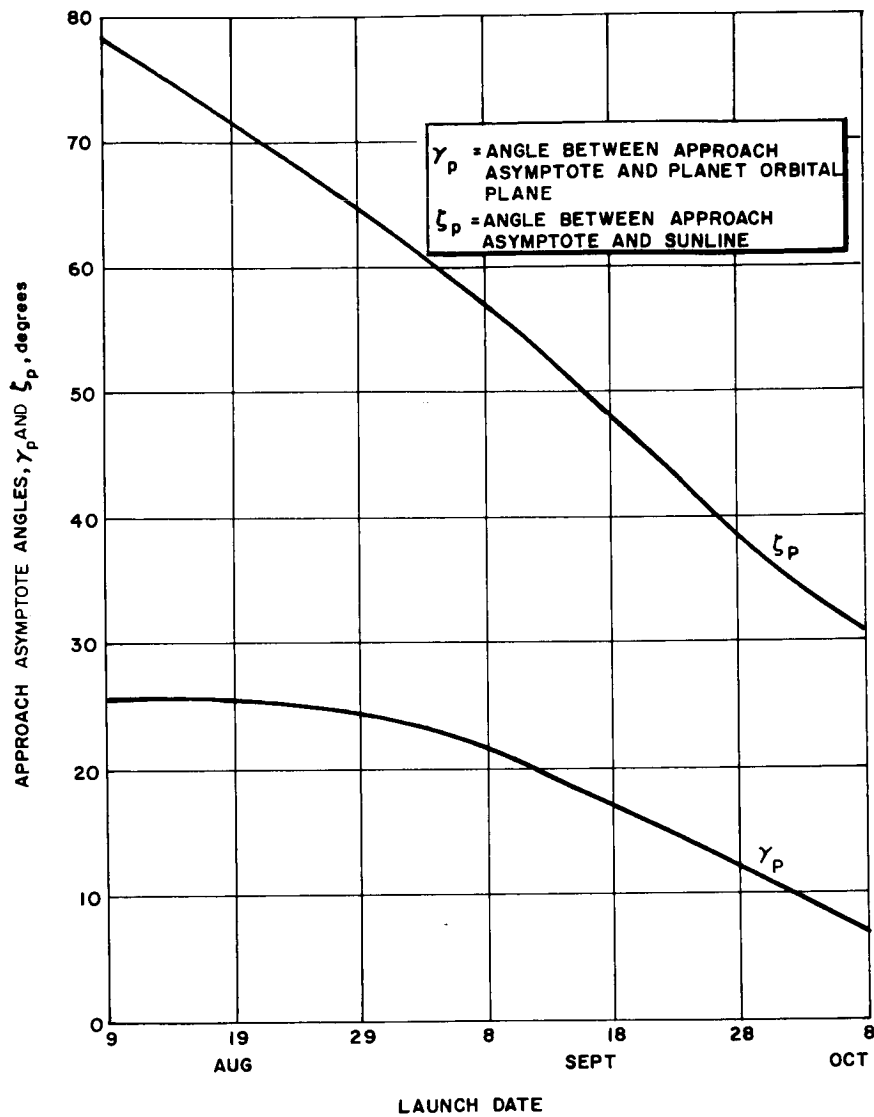
63-8731

Figure 54 PLANETARY APPROACH GEOMETRY, MARS 1975, TYPE II

-128-

TABLE 27

MINIMUM ORBITAL INCLINATION

Planet	Type	Launch Date	Time of Flight	Arrival Date	Minimum Orbital Inclination
Mars	II	8/21/75	358	7/24/76	33 degrees - 24 minutes
		8/31/75	344	8/ 9/76	32 degrees - 24 minutes
		9/10/75	351	8/27/76	25 degrees - 40 minutes
		9/20/75	358	9/13/76	20 degrees - 39 minutes
		9/30/75	365	2/29/76	19 degrees - 25 minutes
Mars	I	7/16/73	203	2/ 4/74	7 degrees - 38 minutes
		7/26/73	204	2/15/74	6 degrees - 40 minutes
		8/ 5/73	206	2/27/74	6 degrees - 49 minutes
		8/15/73	208	3/11/74	5 degrees - 19 minutes
		8/25/73	214	3/27/74	3 degrees - 34 minutes
Mars	I	5/ 4/71	208	11/28/71	19 degrees - 29 minutes
		5/14/71	209	12/ 9/71	11 degrees - 51 minutes
		5/24/71	206	12/16/71	7 degrees - 25 minutes
		6/ 3/71	200	12/20/71	5 degrees - 4 minutes
		6/13/71	202	1/1/72	2 degrees - 18 minutes
Mars	II	1/15/69	272	10/14/69	28 degrees - 39 minutes
		1/30/69	274	10/31/69	31 degrees - 38 minutes
		2/14/69	278	11/19/69	32 degrees - 59 minutes
		2/24/69	281	12/ 2/69	32 degrees - 04 minutes

5.2 Look Angle

A spacecraft designed for interplanetary missions contains many sensors — solar panels, planet and star trackers, communication antennas, etc. — that must remain oriented to the desired target for the duration of the interplanetary flight except for possible short durations during thrusting periods. To determine the optimum location, degrees of freedom and gimballing requirements for each instrument, and to ensure satisfactory operation throughout the mission, it is necessary to determine the look angle requirements for each sensor. In this analysis, it was assumed that the sun, Earth, target planet, and two stars, Canopus and Vega, were the bodies of interest. A vehicle-centered coordinate system is established where one axis e_3 is the vehicle-sun line, the second axis e_2 is normal to the vehicle-sun-Canopus plane, and the third axis e_1 is in the vehicle-sun-Canopus plane normal to the vehicle-sun line. Expressed mathematically,

$$e_3 = \underline{1}_{vs}$$

$$e_2 = e_3 \times \underline{1}_{vc}$$

$$e_1 = e_2 \times e_3 \ .$$

In this vehicle-centered coordinate system (which rotates as a function of time), the direction cosines or cone-clock angles (see figure 55) to the desired target can be obtained as a function of time for a specified launch date. For three separate segments of the mission, interplanetary, hyperbolic approach, and planetocentric, programs were developed to obtain the above mentioned angles.

1. <u>Interplanetary transfer.</u> For this segment of the problem, the basic parameters of the transfer ellipse (with respect to the sun) were obtained from the previously mentioned two-body program where launch date and time of flight from a massless departure planet to a massless approach planet are the required inputs. Knowing the semimajor axis a, eccentricity e, radius r_e, and radial velocity V_r, the true anomaly f, at departure T_d, can be obtained from

$$\cos\left(f(T_D)\right) = \frac{1}{e}\left[\frac{a(1-e^2)}{r_e(T_D)} - 1\right]$$

and

$$\sin\left(f(T_D)\right) = \frac{\sqrt{a(1-e^2)}}{e\sqrt{\mu_s}}V_r$$

-130-

where

μ_s = the gravitational parameter of sun.

The eccentric anomaly E_d, at departure is related to the true anomaly by

$$\tan \frac{E_d}{2} = \sqrt{\frac{1 - e}{1 + e}} \ \tan \frac{f(T_D)}{2}$$

The time of perihelion passage can now be calculated from

$$\tau = T_D + \frac{1}{n} [e \sin E_d - E_d]$$

where n, the mean orbital motion, is defined by

$$n = \sqrt{\frac{\mu_s}{a^3}} \ .$$

The inclination of the transfer orbit with respect to a heliocentric equatorial system can be obtained from

$$i = \cos^{-1} \left[\frac{\underline{i}_R \times \underline{i}_P}{\sin \theta_D} \cdot e_z \right]$$

where

$\underline{i}_R$ = unit vector of Earth at departure

$\underline{i}_P$ = unit vector of target planet at arrival

θ_D = heliocentric transfer angle

e_z = North Pole vector.

A coordinate system with respect to the orbital plane is established where e_n is normal to the orbital plane, e_N in the direction of the ascending node of the transfer orbit with respect to the heliocentric equatorial system, and $e_N{}'$ chosen to form a right-hand system is computed by

$$e_n = \frac{\underline{i}_R \times \underline{i}_P}{\sin \theta_D}$$

$$e_N = \frac{e_z \times e_n}{\sin i}$$

$$e_N{}' = e_n \times e_N \ .$$

SUN-PROBE-TARGET PLANE

TARGET

CONE
ANGLE

SUN

e_3

PROBE

CLOCK-
ANGLE

e_2

SUN-PROBE-CANOPUS
PLANE

e_1

TO
CANOPUS
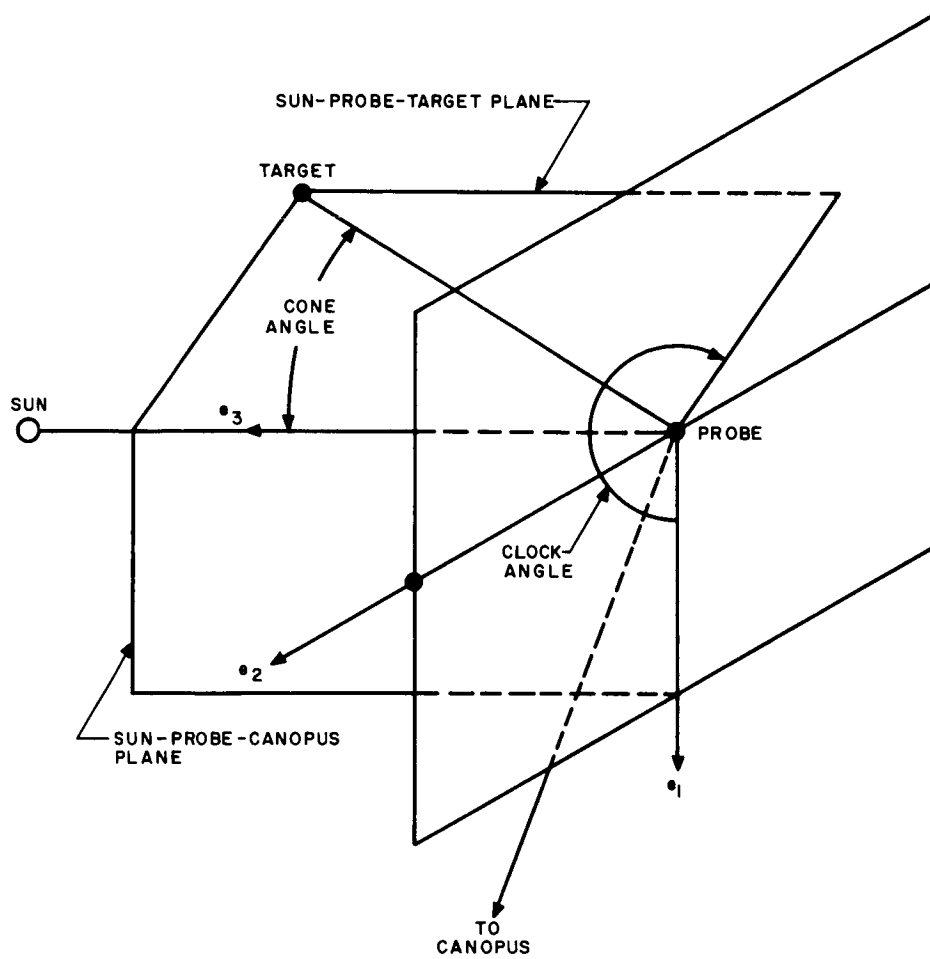
63-8942

Figure 55 VEHICLE CENTERED COORDINATE SYSTEM

The argument of perihelion w, is obtained from

$$\cos [w + f(T_D)] = \underline{i}_R \cdot e_N$$

$$\sin [w + f(T_D)] = (e_N \times \underline{i}_R) \cdot e_n \, .$$

For any value of time after T_D, the eccentric anomaly is computed

$$E - e \sin E = n(t - \tau)$$

by iteration where an initial estimate E_o is calculated from

$$E_o = M + 2 \left[\frac{1}{2} e \left(1 - \frac{1}{8} e^2 \right) + \frac{1}{142} e^4 \right] \sin M + \frac{1}{2} e^2 \left[1 - \frac{1}{3} e^2 \right] \sin 2M + \dots$$

where

$$M = n(t - \tau) \, .$$

The true anomaly is obtained and hence the radius vector can be determined by

$$r(t) = |r_{sv}| = \frac{a(1 - e^2)}{1 + e \cos f} \, .$$

A unit sun vehicle vector is obtained with respect to the orbital plane coordinates system from

$$\underline{i}_{sv} = -\underline{i}_{vs} = e_N \cos [w + f(t)] + e_{N'} \sin [w + f(t)] \, .$$

The direction cosines and cone-clock angle for the desired reference bodies can now be obtained. The direction cosines for the reference body, represented by the unit vector $\underline{e}_{vt}$, are

$$XVVT = e_1 \cdot e_{vt}$$

$$YVVT = e_2 \cdot e_{vt}$$

$$ZVVT = e_3 \cdot e_{vt}$$

and the corresponding cone and clock angles are

$$(\text{Cone Angle})_T = \cos^{-1} (e_3 \cdot e_{vt})$$

$$(\text{Clock Angle})_T = \tan^{-1} \frac{e_2 \cdot e_{vt}}{e_1 \cdot e_{vt}}$$

At the specified time of arrival T_{em}, defined as the intersection of the transfer plane and the planet's orbital path, the vehicle velocity vector is computed by

$$\underline{V}_{sv} = \sqrt{\frac{\mu_s}{a (1 - e^2)}} \; \{ e_N [-e \sin w - \sin (w + f (T_D + T_{em}))]$$

$$+ e_N' [e \cos w + \cos (w + f (T_D + T_{em}))] \} .$$

The planet velocity vector is obtained from ephemeris data and hence the relative velocity of the vehicle with respect to the planet is

$$\underline{V}_{pv} = \underline{V}_{sv} - \underline{V}_{sp} .$$

If e_z' is the unit North Pole vector of the planet in the heliocentric equatorial coordinate system, the minimum orbital inclination with respect to the planetary equator is

$$i_{min} = \sin^{-1} [\underline{1}_{V_{pv}} \cdot e_z'] .$$

This minimum orbital inclination is used to determine the range of feasible inclinations for the approach and planetocentric phases of this problem. Occultation of the Earth by the moon can occur when

$$\frac{r_{vm}}{r_{ve}} < 1$$

and

$$R_{vm} \sin [\cos^{-1} (\underline{1}_{R_{vm}} \cdot \underline{1}_{R_{ve}})] < R_m .$$

In this segment of the program, the vehicle distances with respect to the Earth, target planet, and sun, in addition to the Earth and target planet distances from the sun, are obtained as auxiliary outputs.

-134-

2. <u>Hyperbolic approach phase.</u> In this phase of the program, it is assumed that the vehicle velocity vector with respect to the target planet at time of arrival T_{em} is approximately the same as the relative velocity vector at the planet sphere of influence where the hyperbolic phase is initiated.

A conversion from the heliocentric equatorial coordinate system (e_x, e_y, e_z) to a planetary equatorial coordinate system (e_x', e_y', e_z') is performed,

$$e_x' = \frac{e_z \times e_z'}{|e_z \times e_z'|}$$

$$e_y' = e_z' \times e_x'$$

where

e_z' = North Pole vector (see Figure 56).

The angle $\bar{\Omega}$ between the heliocentric and planetocentric x axes is

$$\cos \bar{\Omega} = e_x \cdot e_x'$$

and

$$\sin \bar{\Omega} = e_z \cdot (e_x \times e_x') \ .$$

The unit vector in the direction of the hyperbolic velocity vector is

$$e_{ap} = \frac{\underline{V}_\infty}{|\underline{V}_\infty|}$$

and, the angle between the North Pole vector and the approach velocity vector β_{ap} is

$$\beta_{ap} = \cos^{-1} [e_z' \cdot e_{ap}] \ .$$

An auxiliary coordinate system is set up which is employed to establish the coordinate system with two axes in the plane of the approach hyperbola

$$e_{ap} = e_{ap}$$

$$\underline{j}_1 = \frac{e_{ap} \times e_z'}{|e_{ap} \times e_z'|}$$

$$\underline{j}_2 = j_1 \times e_{ap}$$

NORTH POLE VECTOR

z

z'

y'

y

x

x'

$\bar{\Omega}$
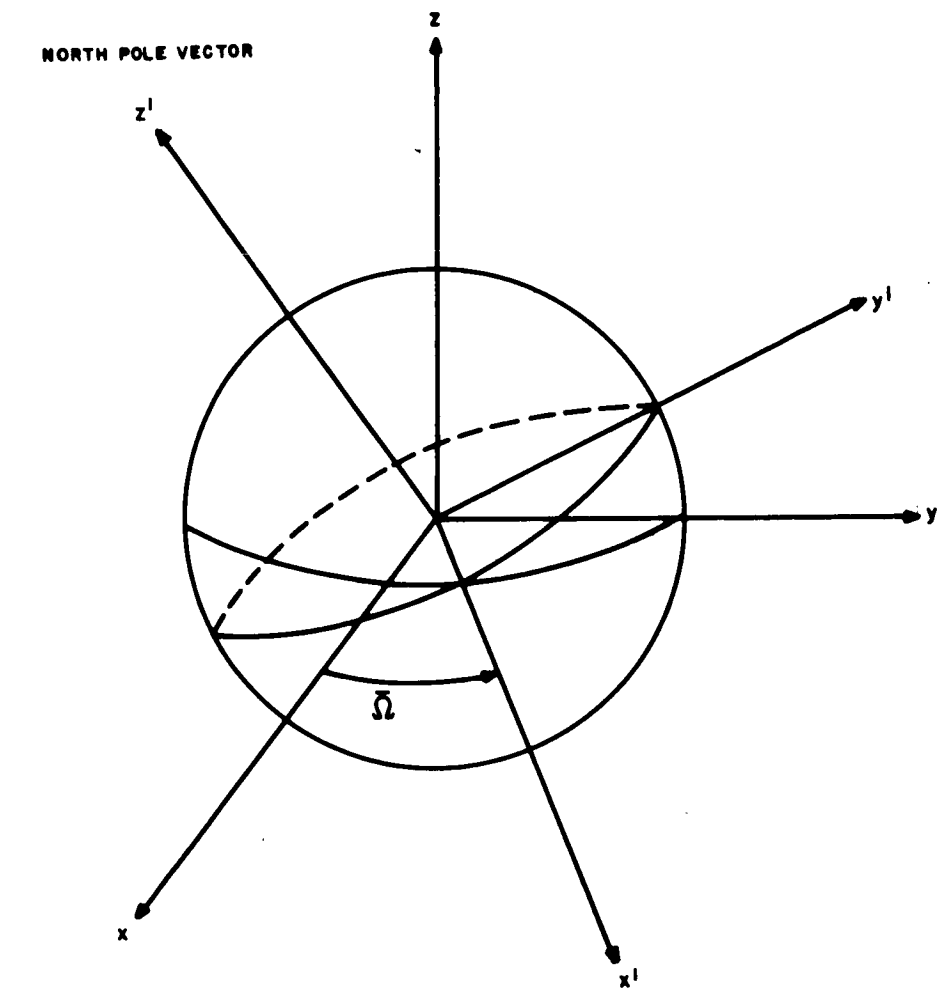
63-8943

Figure 56 RELATIONSHIP BETWEEN HELIOCENTRIC AND PLANETOCENTRIC COORDINATE SYSTEMS

-136-

and

$$\Phi = \cos^{-1} \left[\frac{\cos i}{\sin \beta_{ap}} \right]$$

where $i \geq \beta_{ap} \sim$ desired orbital inclination.

With just the approach velocity vector and desired inclination specified, there are two possible orientations of the hyperbolic plane . (This reduces to one when the minimum inclination is selected.) This can be visualized by assuming a cone with half angle i is generated about the North Pole vector. If the minimum inclination angle is selected, the normal approach to the velocity vector is tangent to the cone. However, if a greater inclination is selected, the normal to the approach velocity vector intersects this cone in two locations. These two normal vectors are computed

$$e_{n_1} = -\underline{j}_1 \sin \Phi + \underline{j}_2 \cos \Phi$$

and

$$e_{n_2} = \underline{j}_1 \sin \Phi + \underline{j}_2 \cos \Phi .$$

The remaining vectors required to establish a coordinate system in each hyperbolic plane are

$$e_N = \frac{e_{z'} \times e_n}{\sin i}$$

and

$$e_{N'} = e_n \times e_N$$

where both e_{n_1} and e_{n_2} are employed.

The angle between the planetocentric x-axis and the ascending node Ω of the approach hyperbola is

$$\cos \Omega = e_N \cdot e_{x'}$$

and

$$\sin \Omega = e_{z'} \cdot (e_{x'} \times e_N) .$$

The angle between the approach velocity vector and the nodal line $\bar{\omega}$ is

$$\cos \bar{\omega} = e_{ap} \cdot e_N$$

and

$$\sin \bar{\omega} = e_n \cdot (e_N \times e_{ap}) .$$

The angle between the approach velocity vector and the periapsis radius vector θ is (see figure 57)

$$\theta = \cos^{-1} \left[\frac{1}{1 + \dfrac{R_p V_\infty^2}{\mu_p}} \right]$$

where

R_p = periapsis radius vector

μ_p = gravitational parameter of planet.

The argument of perigee ω can now be determined by

$$\omega = \bar{\omega} - \theta$$

or

$$\omega = \bar{\omega} + \theta .$$

These two values of ω are obtained since there is the option of passing on either side of the planet and approaching perigee along the ascending or descending segment of the hyperbola.

The orbital parameters of the hyperbola can be computed:

$$a = \frac{\mu_p}{V_\infty^2}$$

$$e = 1 + \frac{R_p}{a}$$

$$p = a(e^2 - 1)$$

$$f_\infty = \cos^{-1} \left[\frac{P - r_\infty}{r_\infty e} \right]$$

$$E_\infty = \sinh^{-1} \left[\frac{\sqrt{e^2 - 1} \ \sin f_\infty}{1 + e \cos f_\infty} \right]$$

$$\tau = T_a + \sqrt{\frac{a^3}{\mu_p}} \ \left| e \sinh E_\infty - E_\infty \right| .$$

where

T_a = time from launch to r_∞ .

The initial value of the vehicle-planet position vector e_{pv} is

$$e_{pv} = -e_{vp} = e_N \cos(\omega + f_\infty) + e_N' \sin(\omega + f_\infty) .$$

The positions of Earth, planet, Canopus, and Vega are obtained from the ephemeris data and the direction cosines and cone-clock angle determined as before at specified increments of time. In this segment of the problem occultation of Earth, sun, Canopus, and Vega by the planet must be determined.

3. Planetocentric phase. At periapsis of the approach hyperbola, there is an instantaneous change to an elliptic orbit with the same inclination, and the apoapsis and periapsis of the desired planetocentric orbit are specified where the orbital elements may be computed as

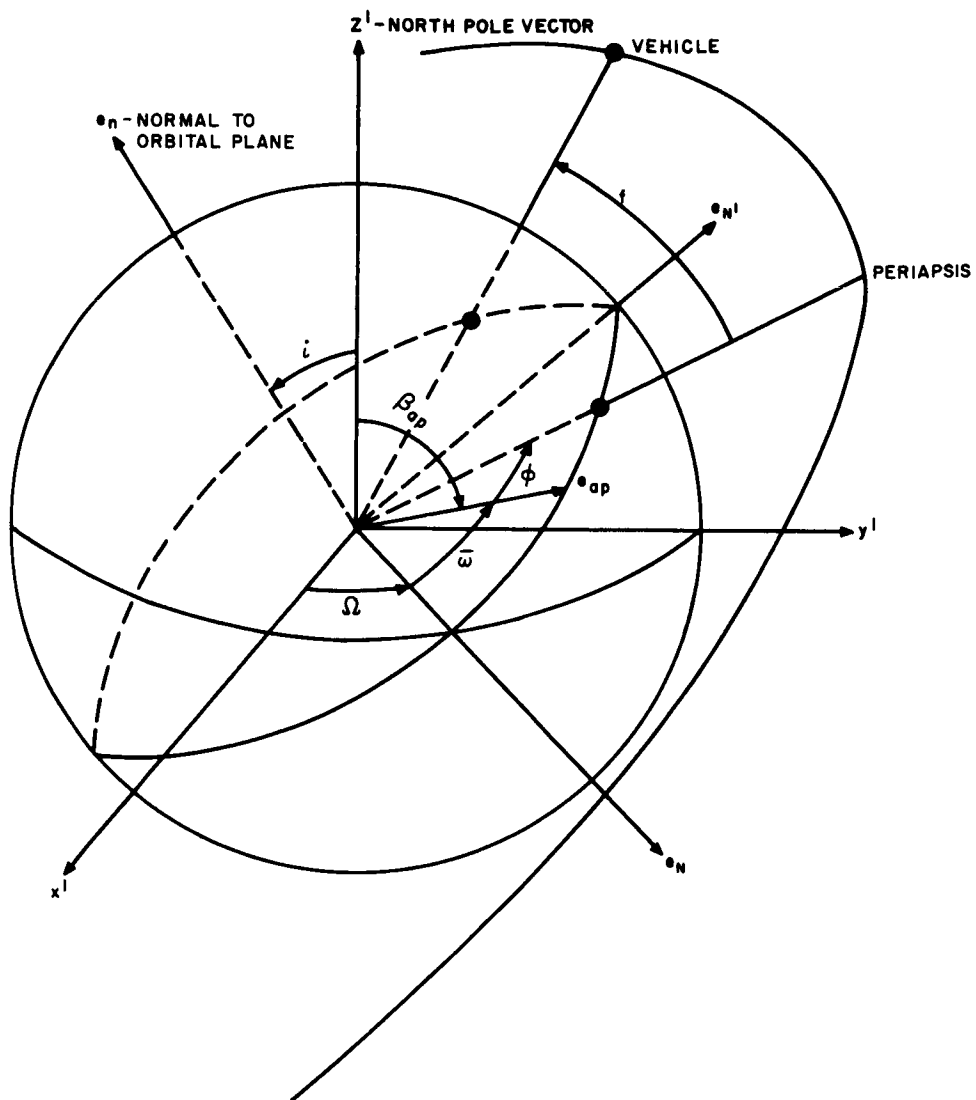$$a = \frac{r_a + r_p}{2}$$

$$e = \frac{r_a - r_p}{r_a + r_p}$$

$$n = \sqrt{\frac{\mu_p}{a^3}}$$

$$p = a(1 - e^2) .$$

The time of perigee passage is specified and the eccentric anomaly, true anomaly, and vehicle-planet radius vector computed. The program now proceeds to compute the desired angles and occultation parameters as a function of time.

-139-

Figure 57   APPROACH GEOMETRY

63-8944

For the Mars 1969 launch opportunity, the direction cosines to Earth, Mars, Canopus, and Vega during the interplanetary portion of the transfer are presented as a function of time in tables 28 through 31 for four representative launch dates. The corresponding vehicle-Earth, vehicle-sun, and vehicle-Mars distances are presented in table 32.

During the approach phase, the cone-clock angle to Earth, Canopus, and Vega are relatively constant for the specified launch window. For a representative departure date (30 January 1969), these angles, in addition to the cone-clock angles for Mars, are presented in table 33. The variation in the vehicle-Mars angles are presented for four representative departure dates in table 34.

During the orbital phase, the vehicle cone-clock angles and periods of occultation of the Earth, sun, Vega, and Canopus by Mars are presented for typical orbits during the 1st and 180th days of the mission in tables 35 and 36, respectively. The variation in the Earth cone-clock angles as a function of time in orbit is illustrated in table 37.

5.3 Planetary Aspects of Communication

1. <u>Communication limitation</u>. In this section, communication limitations are defined as those limitations imposed by the motion of the planets in orbit about the sun. The vehicle-Earth communication distance during the interplanetary transfer is a function of the transfer trajectory. After encounter, the communication distance is purely a function of the planet and Earth positions in the respective orbits about the sun, and is determined by

$$R_{ep} = \sqrt{(R_{x_{se}} - R_{x_{sp}})^2 + (R_{y_{se}} - R_{y_{sp}})^2 + (R_{z_{se}} - R_{z_{sp}})^2}$$

where

R_{ep} = Earth planet distance

R_{se} = Earth sun distance

R_{sp} = sun planet distance

The respective planet distances from the sun are obtained from ephemeris data. In general the Earth-Mars distance varies from a low of 60 million km (usually a few months after departure) to a high of 400 million km (usually

occuring 6 to 8 months after encounter). For Venus these corresponding distances vary between a low of 40 million km and a high of 260 million km. These distances, as a function of time between 1968 and 1979, are presented in figures 58 through 60.

Communication problems arise because of solar noise which affects reception when the planet, Earth, and sun lie nearly in a straight line. Thus when the Earth and planet are on the same side of the sun, communication, though possible from the outer planet to the inner, is not possible from the inner to the outer. This situation corresponds to the minimum Earth-planet distance and is of academic interest only since this generally occurs during the middle of the transfer trajectory. However, when the Earth and planet are on opposite sides of the sun, corresponding to maximum Earth-planet distance, communication either way is impossible. The angle subtended at Earth by the Earth-sun line and the Earth-planet line α, and the angle subtended at the planet by the planet-Earth line and the planet-sun line β, are useful in examining this situation. The angles may be computed by

$$\alpha = \cos^{-1} \left[\frac{\vec{R}_{es} \cdot \vec{R}_{ep}}{|R_{es}| |R_{ep}|} \right]$$

and

$$\beta = \cos^{-1} \left[\frac{\vec{R}_{ep} \cdot \vec{R}_{ps}}{|R_{ep}| |R_{ps}|} \right] .$$

For Mars, these angles are presented in figures 61 through 63 for the period from 1968 to 1979. The angle subtended at Mars varies between 0 and 45 degrees, whereas, the Earth subtended angle varies between 0 and 180 degrees. The critical period occurs when the angles are simultaneously sufficiently close to zero. (These angles can never be identically zero unless, at the time of maximum communication, Mars is in the plane of the elliptic.) The above mentioned data indicate that there are periods of 50 to 100 days when two-way (command or reception) communication is not possible. This may place restrictions on transfer flight time and mission lifetime after encounter, especially when Type II transfers are employed. For example, in the 1975 Type II trajectories, with a time of flight approximately 400 days, transmission will be interrupted for 50 days beginning about 60 days after encounter.

For Venus, the relative magnitudes of α and β are interchanged with α varying between 0 and 45 degrees and β between 0 and 180 degrees. Since the relative rotation rate of Earth with respect to Venus is greater than that of Mars with respect to Earth, the periods of communication blackout for Venus are shorter. These data are presented in figures 64 through 66 for the years 1968 to 1979.

-142-

TABLE 28

VEHICLE PLANET DIRECTION COSINES -- MARS 1969 TYPE II

Time	XV'VP 1/15/69	XV'VP 1/30/69	XV'VP 2/14/69	XV'VP 2/24/69	YV'VP 1/15/67	YV'VP 1/30/69	YV'VP 2/14/69	YV'VP 2/24/69	ZV'VP 1/15/67	ZV'VP 1/30/67	ZV'VP 2/14/67	ZV'VP 2/24/69
0	-0.0654	-0.1284	-0.1823	-0.2098	-0.9666	-0.9838	-0.9832	-0.9725	0.2478	0.1246	-0.0076	-0.1008
2	-0.0739	-0.1356	-0.1872	-0.2126	-0.9708	-0.9853	-0.9818	-0.9693	0.2283	0.1037	-0.0302	-0.1236
5	-0.0864	-0.1458	-0.1935	-0.2156	-0.9764	-0.9867	-0.979	-0.9635	0.1981	0.0715	-0.0638	-0.1588
10	-0.1064	-0.1609	-0.2013	-0.2176	-0.9835	-0.9868	-0.972	-0.9514	0.1462	0.017	-0.1215	-0.218
20	-0.1412	-0.1824	-0.2056	-0.2091	-0.9893	-0.9785	-0.949	-0.9173	0.0364	-0.0963	-0.2388	-0.3388
40	-0.1779	-0.1819	-0.1646	-0.1408	-0.9643	-0.9264	-0.8644	-0.8048	-0.196	-0.3298	-0.0524	-0.5766
60	-0.1576	-0.1201	-0.0618	-0.0131	-0.8901	-0.8235	-0.7178	-0.6164	-0.4277	-0.5544	-0.6934	-0.7873
80	-0.0844	-0.009	0.0828	0.1462	-0.7649	-0.6609	-0.4916	-0.3313	-0.6386	-0.7504	-0.8669	-0.9321
100	0.0236	0.1278	0.2346	0.2897	-0.5825	-0.4261	-0.1764	0.0404	-0.8125	-0.8956	-0.956	-0.9562
120	0.1426	0.2586	0.3468	0.3659	-0.3357	-0.1183	0.1936	0.4183	-0.9311	-0.9587	-0.9177	-0.8313
140	0.2453	0.3476	0.3865	0.3643	-0.0313	0.227	0.5305	0.7033	-0.9689	-0.9098	-0.7545	-0.6105
160	0.3064	0.3738	0.3638	0.3191	0.2923	0.5379	0.7651	0.8697	-0.9059	-0.7556	-0.5313	-0.3765
180	0.3156	0.3489	0.3135	0.2648	0.5758	0.7605	0.8971	0.949	-0.7542	-0.5477	-0.3114	-0.171
200	0.2859	0.3009	0.2618	0.2188	0.7799	0.8922	0.9579	0.9758	-0.5568	-0.3368	-0.1181	0.0021
220	0.2395	0.2517	0.2211	0.1872	0.9041	0.957	0.974	0.9704	-0.354	-0.1438	0.0499	0.1525
240	0.1932	0.2126	0.1958	0.1719	0.9676	0.9766	0.9597	0.0411	-0.1628	0.032	0.2014	0.2913
260	0.156	0.1889	0.1871	0.1733	0.9876	0.0617	0.9193	0.8877	0.0182	0.1986	0.3461	0.4266
270	0.1625	0.1824	0.1886	0.1803	0.978	0.942	0.888	0.8507	0.1308	0.2816	0.4195	0.4938
280				0.1884				0.7906				0.5826

TABLE 29

VEHICLE - EARTH DIRECTION COSINES -- MARS 1969 TYPE II

Time	XV'VE				YV'YE				ZV'VP			
	1/15/69	1/30/69	2/14/69	2/24/69	1/15/69	1/30/69	2/14/69	2/24/69	1/15/69	1/30/69	2/14/69	2/24/69
0	-0.1108	-0.1613	0.1888	-0.7458	-0.9938	-0.9735	0.4576	-0.968	-0.0015	-0.1621	-0.8689	-0.5002
2	0.533	-0.6192	0.6266	0.7137	0.6088	0.5883	0.4935	0.6999	-0.5876	-0.5207	-0.6032	-0.0266
5	0.5297	0.6207	0.691	0.7198	9.5966	0.5752	0.6157	0.6693	-0.603	-0.5329	-0.3787	-0.1843
10	0.546	0.6483	0.7029	0.7277	0.6343	0.6342	0.6274	0.6719	-0.5472	-0.4214	-0.335	-0.138
20	0.5753	0.6796	0.731	0.739	0.6877	0.674	0.6682	0.6716	-0.4429	-0.2896	-0.1383	-0.0533
40	0.6237	0.6268	0.7383	0.7287	0.7600	0.5988	0.6575	0.636	-0.1827	-0.0829	0.1504	0.2539
60	0.6328	0.6341	0.6898	0.6562	0.7699	0.6124	0.5687	0.5044	0.0825	-0.4721	9.4482	0.5613
80	0.5966	0.6229	0.5738	0.5141	0.7171	0.5434	0.3636	0.2475	0.3602	0.5628	0.7338	0.8212
100	0.5052	0.4792	0.3974	0.336	0.5604	0.2826	0.0426	0.0852	0.6563	0.8309	0.9166	0.938
120	0.346	0.2898	0.2302	0.1983	0.244	-0.0758	-0.2743	-0.3628	0.9059	0.9541	0.9337	0.9105
140	0.1686	0.1434	0.1311	0.128	-0.1466	-0.3738	-0.4883	-0.5347	0.9747	0.9164	0.8628	0.8346
160	0.1034	0.0734	0.0919	0.1045	-0.3057	-0.5524	-0.6094	-0.6309	0.9465	0.8303	0.7875	0.7688
180	0.0218	0.0548	0.0862	0.1049	-0.5887	-0.6476	-0.6724	-0.6792	0.8081	0.7600	0.7352	0.7264
200	0.0237	0.0618	0.0959	0.1153	-0.6687	-0.6949	-0.7011	-0.6992	0.7431	0.7165	0.7066	0.7055
220	0.043	0.0794	0.111	0.1282	-0.7064	-0.7139	-0.7088	-0.7012	0.7065	0.6958	0.6966	0.7013
240	0.0685	0.1000	0.1262	0.1398	-0.7193	-0.7152	-0.7027	-0.6913	0.6913	0.6917	0.7002	0.7089
260	0.0942	0.1194	0.139	9.1482	-0.7167	-0.7051	-0.6873	-0.6732	0.691	0.699	0.713	0.7245
270	0.1061	0.1279	0.144	0.1509	-0.7113	-0.6969	-0.6773	-0.6617	0.6948	0.7057	0.7215	0.7344
280				0.1524				-0.6494				0.745

TABLE 30

VEHICLE CANOPUS DIRECTION COSINES -- MARS 1969 TYPE II

Time	XV'VC				YV'VC				ZV'VC			
	1/15/69	1/30/69	2/14/69	2/24/69	1/15/69	1/30/69	2/14/69	2/24/69	1/15/69	1/30/69	2/14/69	2/24/69
0	0.9704	0.9751	0.9824	0.9877	0	0	0	0	-0.2413	-0.2219	-0.187	-0.1563
2	0.9714	0.9765	0.9839	0.9891	0	0	0	0	-0.2375	-0.2157	-0.1788	-0.1471
5	0.9729	0.9786	0.9861	0.9911	0	0	0	0	-0.2312	-0.2058	-0.166	-0.1329
10	0.9757	0.9822	0.9897	0.9941	0	0	0	0	-0.219	-0.1876	-0.1434	-0.1082
20	0.9822	0.9893	0.9955	0.9984	0	0	0	0	-0.188	-0.1461	-0.0945	-0.0564
40	0.9944	0.9988	0.99995	0.9988	0	0	0	0	-0.1057	-0.4936	0.0097	0.0488
60	0.9999	0.99875	0.9942	0.9899	0	0	0	0	-0.1057	-0.0493	0.1072	0.1419
80	0.9968	0.9906	0.9826	0.9771	0	0	0	0	0.7981	0.1364	0.1855	0.2128
100	0.9881	0.9794	0.9708	0.966	0	0	0	0	0.1538	0.2018	0.2399	0.2587
120	0.9783	0.9696	0.9625	0.9595	0	0	0	0	0.2072	0.2447	0.2712	0.2818
140	0.9706	0.9636	0.9592	0.9582	0	0	0	0	0.1863	0.2672	0.2826	0.286
160	0.9666	0.9621	0.9605	0.9614	0	0	0	0	0.2564	0.2727	0.2781	0.2751
180	0.9662	0.9644	0.9654	0.9676	0	0	0	0	0.2578	0.2644	0.2609	0.2526
200	0.9689	0.9695	0.9723	0.9753	0	0	0	0	0.2475	0.245	0.2337	0.2209
220	0.9738	0.9763	0.9801	0.9833	0	0	0	0	0.2274	0.2166	0.1984	0.1821
240	0.98	3.9835	0.9876	0.9905	0	0	0	0	0.1992	0.1807	0.1566	0.1375
260	0.9864	0.9904	0.994	0.9961	0	0	0	0	0.164	0.1385	0.1095	0.08841
270	0.9896	0.9933	0.9964	0.998	0	0	0	0	0.1441	0.1154	0.0843	0.0624
280				0.9994				0				0.0357

TABLE 31

VEHICLE VEGA DIRECTION COSINES -- MARS 1963 TYPE II

Time	XV'VI				YV'VI				ZV'VI			
	1/15/69	1/30/69	2/14/69	2/24/69	1/15/69	1/30/69	2/14/69	2/24/69	1/15/69	1/30/69	2/14/69	2/24/69
0	-0.5889	-0.5461	-0.5242	-0.5243	0.7852	0.7443	0.6504	0.5628	0.1915	0.3844	0.5497	0.639
2	-0.5824	-0.5424	-0.5244	-0.5272	0.7828	0.734	0.6333	0.542	0.219	0.4087	0.5692	0.6544
5	-0.5732	-0.5379	-0.526	-0.5328	0.7771	0.7165	0.6059	0.5095	0.2597	0.4442	0.5968	0.6758
10	-0.5599	-0.5334	-0.5317	-0.5445	0.7616	0.6821	0.5563	0.4521	0.3263	0.5003	0.6386	0.7055
20	-0.5426	-0.5360	-0.5537	-0.5764	0.7086	0.5953	0.444	0.3278	0.4511	0.5986	0.7045	0.7485
40	-0.5526	-0.5827	-0.6252	-0.6552	0.527	0.3674	0.1865	0.5959	0.6457	0.7249	0.7579	0.753
60	-0.61	-0.6559	-0.6981	-0.7193	0.2813	0.1047	-0.8013	-0.2023	0.7408	0.7475	0.7115	0.6645
80	-0.6785	-0.7172	-0.7401	-0.7439	0.01803	-0.1531	-0.3224	-0.4282	0.7344	0.6798	0.5902	0.513
100	-0.7262	-0.7441	-0.7414	-0.7279	-0.2272	-0.3785	-0.5190	-0.6011	0.6487	0.5505	0.4253	0.33
120	-0.7402	-0.735	-0.7102	-0.6848	-0.4344	-0.5563	-0.6607	-0.7153	0.5133	0.3878	0.2429	0.1394
140	-0.7239	-0.7001	-0.6619	-0.6316	-0.5929	-0.6815	-0.7471	-0.774	0.3528	0.213	0.0607	-0.4364
160	-0.688	-0.6534	-0.611	-0.5822	-0.7019	-0.7559	-0.7838	-0.7852	0.1844	0.0399	-0.1111	-0.211
180	-0.6443	-0.6067	-0.5678	-0.5448	-0.7645	-0.7853	-0.7787	-0.758	0.1864	-0.1235	-0.2668	-0.3586
200	-0.6023	-0.5682	-0.5383	-0.5236	-0.7862	-0.7763	-0.7398	-0.7006	-0.1381	-0.2728	-0.4037	-0.4847
220	-0.5685	-0.5428	-0.525	-0.5193	-0.7728	-0.7356	-0.6737	-0.6198	-0.2822	-0.4053	-0.5201	-0.5884
240	-0.5468	-0.5327	-0.5279	-0.5308	-0.7293	-0.6683	-0.5856	-0.5202	-0.4112	-0.5192	-0.6161	-0.6691
260	-0.5392	-0.538	-0.5457	-0.5557	-0.6599	-0.5785	-0.4792	-0.4051	-0.5232	-0.613	-0.6874	-0.726
270	-0.541	-0.5462	-0.5595	-0.5724	-0.6165	-0.5261	-0.4199	-0.3425	-0.5721	-0.6518	-0.7146	-0.7451
280				-0.5911				-0.2766				-0.7577

TABLE 32

INTERPLANETARY DISTANCES MARS 1969 TYPE II

Time (days)	Vehicle-Earth (AU)				Vehicle-Planet (AU)				Vehicle-Sun (AU)			
	1/15/69	1/30/69	2/14/69	2/24/69	1/15/69	1/30/69	2/14/69	2/24/69	1/15/69	1/30/69	2/14/69	2/24/69
0	1.475×10^{-7}	2.766×10^{-7}	5.165×10^{-8}	6.852×10^{-7}	1.586	1.434	1.281	1.18	0.9837	0.9847	0.9868	0.9897
2	0.0042	0.0039	0.0039	0.0036	1.562	1.411	1.258	1.157	0.981	0.9829	0.9857	0.9890
5	0.0104	0.0098	0.0092	0.0088	1.528	1.376	1.224	1.123	0.9774	0.9806	0.9844	0.9884
10	0.0209	0.0195	0.0185	0.0177	1.469	1.318	1.166	1.066	0.9725	0.9777	0.9834	0.9884
20	0.04175	0.0387	0.0364	0.035	1.35	1.201	1.052	0.956	0.9666	0.976	0.9853	0.9924
40	0.08135	0.074	0.0689	0.0661	1.113	0.9724	0.8357	0.7494	0.9716	0.9887	1.004	1.015
60	0.113	0.101	0.0943	0.0912	0.8879	0.7631	0.6448	0.5735	0.9978	1.02	1.041	1.054
80	0.1322	0.1188	0.1157	0.1166	0.6878	0.5839	0.4898	0.4382	1.04	1.066	1.089	1.104
100	0.1418	0.1363	0.1457	0.1563	0.5211	0.4412	0.3762	0.3471	1.093	1.12	1.144	1.16
120	0.1564	0.1716	0.2006	0.2228	0.391	0.3366	0.3023	0.295	1.15	1.175	1.191	1.215
140	0.1982	0.2383	0.2858	0.3184	0.2958	0.2661	0.2583	0.267	1.207	1.229	1.252	1.267
160	0.2767	0.3364	0.3983	0.4397	0.2296	0.2196	0.2296	0.2462	1.258	1.278	1.298	1.313
180	0.3864	0.4595	0.5323	0.5809	0.1825	0.1848	0.2032	0.222	1.303	1.319	1.338	1.351
200	0.5183	0.6003	0.6813	0.736	0.1442	0.152	0.1722	0.1901	1.339	1.351	1.367	1.38
220	0.6645	0.7519	0.8391	0.8985	0.1071	0.116	0.1344	0.15	1.365	1.374	1.388	1.399
240	0.8176	0.908	0.9992	1.062	0.0677	0.0754	0.0908	0.1037	1.38	1.386	1.397	1.408
260	0.9711	1.062	1.155	1.22	0.0259	0.0294	0.0436	0.0538	1.384	1.387	1.397	1.406
270	1.046	1.136	1.23	1.295	0.0041	0.0091	0.0195	0.0282	1.382	1.384	1.392	1.402
280				1.366				0.0026				1.394

TABLE 33

APPROACH HYPERBOLA LOOK ANGLES, DEPARTURE DATE 30 JANUARY 1969

True Anomaly (degrees)	Mars		Earth		Canopus		Vega		Time (days)
	Cone Angle (degrees)	Clock Angle (degrees)	Cone Angle (degrees)	Clock Angle (degrees)	Cone Angle (degrees)	Clock Angle (degrees)	Cone Angle (degrees)	Clock Angle (degrees)	
250.835	73.2124	79.4932	45.0554	280.474	83.5154	0	130.944	223.573	0
250.854	73.1445	79.4730	45.0478	280.483	83.5326		130.977	223.529	0.12500
250.875	73.0760	79.4508	45.0402	280.493	83.5498		131.010	223.485	0.25000
250.898	73.0069	79.4264	45.0327	280.502	83.5669		131.043	223.440	0.375000
250.924	72.9371	79.3995	45.0252	280.512	83.5841		131.076	223.395	0.500000
250.952	72.8666	79.3696	45.0178	280.521	83.6012		131.109	223.351	0.62500
250.984	72.7951	79.3362	45.0105	280.530	83.6184		131.142	223.306	0.75000
251.020	72.7224	79.2986	45.0033	280.539	83.6355		131.174	223.261	0.87500
251.061	72.6483	79.2559	44.9961	280.549	83.6527		131.207	223.216	1.00000
251.109	72.5727	79.2072	44.9893	280.558	83.6698		131.239	223.172	1.12500
251.163	72.4948	79.1508	44.9825	280.567	83.6869		131.271	223.127	1.25000
251.227	72.4142	79.0849	44.9757	280.576	83.7040		131.303	223.082	1.37500
251.303	72.3299	79.0068	44.9688	280.585	83.7211		131.336	223.037	1.50000
251.395	72.2407	78.9126	44.9619	280.594	83.7383		131.368	222.991	1.62500
251.509	72.1451	78.7968	44.9547	280.603	83.7555		131.400	222.946	1.75000
251.562	72.1042	78.7420	44.9518	280.606	83.7625		131.413	222.927	1.80048
251.722	71.9949	78.5801	44.9444	280.616	83.7797		131.445	222.882	1.92548
251.933	71.8700	78.3659	44.9366	280.625	83.7970		131.477	222.836	2.05048
252.226	71.7208	78.0634	44.9282	280.634	83.8144		131.510	222.789	2.17548
252.661	71.5302	77.6277	44.9197	280.644	83.8318		131.542	222.743	2.30048
253.375	71.2596	76.9037	44.9110	280.653	83.8493		131.575	222.696	2.42548
254.769	70.7991	75.4872	44.9022	280.663	83.8668		131.607	222.649	2.55048
258.744	69.6632	71.4152	44.8934	280.673	83.8844		131.639	222.602	2.67548
273.235	66.5645	56.1358	44.8874	280.679	83.8964		131.661	222.570	2.76045
279.326	65.7219	49.5362	44.8867	280.680	83.8979		131.663	222.567	2.77045
289.842	64.9547	37.9909	44.8861	280.680	83.8993		131.666	222.563	2.78045
311.061	66.1360	14.6862	44.8854	280.681	83.9009		131.668	222.559	2.79045
355.560	78.5228	329.598	44.8848	280.681	83.9026		131.670	222.555	2.80045
360.000	80.2491	325.435	44.8848	280.681	83.9027		131.670	222.555	2.80048

TABLE 34

VARIATION IN MARTIAN APPROACH LOOK ANGLES--1969 TYPE II

| 15 January 1969			30 January 1969			14 February 1969			24 February 1969		
Time (days)	Cone Angle (degrees)	Clock Angle (degrees)	Time (days)	Cone Angle (degrees)	Clock Angle (degrees)	Time (days)	Cone Angle (degrees)	Clock Angle (degrees)	Time (days)	Cone Angle (degrees)	Clock Angle (degrees)
0	91.87	80.47	0	73.21	79.49	0	62.21	77.10	0	55.52	76.39
0.375	91.65	80.45	0.375	73.01	79.43	0.375	62.02	76.99	0.375	55.33	76.24
0.750	91.43	80.41	0.750	72.80	79.34	0.750	61.82	76.85	0.750	55.14	76.06
1.125	91.19	80.35	1.125	72.57	79.21	1.125	61.61	76.66	1.125	54.94	75.82
1.875	90.63	80.02	1.625	72.24	78.91	1.500	61.38	76.39	1.500	54.73	75.45
2.250	90.22	79.56	1.80048	72.10	78.74	1.875	61.12	75.89	1.875	54.47	74.74
2.625	89.39	78.20	2.05048	71.87	78.37	2.250	60.74	74.67	2.250	54.06	72.43
2.85809	87.41	74.11	2.17548	71.72	78.06	2.500	60.13	71.52	2.38916	53.71	68.85
2.88809	86.69	72.53	2.30048	71.53	77.63	2.59993	59.42	66.19	2.42916	53.56	66.26
2.90809	85.99	70.99	2.42548	71.26	76.90	2.61993	59.18	63.66	2.45916	53.45	62.75
2.92809	84.98	68.76	2.55048	70.80	75.49	2.63993	58.90	59.58	2.47916	53.45	58.64
2.94809	83.41	65.19	2.67548	69.66	71.42	2.64993	58.76	56.46	2.48916	43.56	55.49
2.96809	80.59	58.56	2.76045	66.56	56.14	2.65993	58.73	51.97	2.49916	53.85	51.00
2.97809	78.16	52.51	2.77045	65.72	49.54	2.66993	59.97	45.05	2.50916	54.64	44.11
2.98809	74.34	41.91	2.78045	64.95	37.99	2.67993	60.25	33.22	2.51916	56.92	32.48
2.99809	68.48	19.86	2.79045	66.14	14.69	2.68993	65.88	10.52	2.52916	64.71	10.66
3.00812	67.16	327.81	2.80048	80.25	325.44	2.69995	88.73	325.13	2.53918	92.75	327.44

TABLE 35

MARTIAN ORBITAL LOOK ANGLES, DEPARTURE DATE
30 JANUARY 1969 -- FIRST DAY

Time (hours)	True Anomaly (f)	Mars Cone Angle (degrees)	Mars Clock Angle (degrees)	Occultation Sun	Occultation Earth	Occultation Canopus	Occultation Vega
0	0	80.2492	325.435	no	no	yes	no
0.1	13.938	85.9493	312.617	no	no	no	no
0.2	27.388	91.6419	300.422	no	no	no	no
0.3	39.974	96.9066	288.953	no	no	no	no
0.4	51.483	101.482	278.251	no	no	no	no
0.6	71.137	108.275	259.147	no	no	no	no
0.8	86.843	112.292	242.946	no	no	no	yes
1.0	99.529	114.324	229.303	no	no	no	yes
1.2	110.007	115.066	217.794	no	no	no	yes
1.4	118.873	114.996	208.005	no	no	no	yes
1.7	130.040	114.003	195.775	no	no	no	no
2.0	139.439	112.425	185.688	no	no	no	no
2.3	147.648	110.544	177.096	no	no	no	no
2.7	157.367	107.786	167.224	no	no	no	no
3.3	170.417	103.344	154.475	no	no	no	no
3.7	178.637	100.212	146.706	no	no	no	no
4.2	188.881	96.0632	137.238	no	no	no	no
4.7	199.602	91.5473	127.485	no	no	no	no
5.2	211.485	86.4950	116.721	no	no	no	no
5.6	222.517	81.9122	106.628	no	no	no	no
5.9	232.248	78.0760	97.5427	no	no	no	no
6.2	243.917	73.8815	81.3165	no	no	no	no
6.5	258.566	69.5002	71.5780	no	no	no	no
6.7	270.828	66.8246	58.6792	no	no	no	no
6.9	285.959	65.0331	42.2113	no	no	no	no
7.1	304.888	65.3860	21.3429	no	no	yes	no
7.2	316.014	66.9257	9.2907	no	no	yes	no
7.3	328.251	69.6403	356.440	no	no	yes	no
7.4	341.444	73.5719	343.162	no	no	yes	no
7.5	359.389	80.1503	326.001	no	no	yes	no

TABLE 36

MARTIAN ORBITAL LOOK ANGLES, DEPARTURE DATE
30 JANUARY 1969 - 180th DAY IN ORBIT

Time (hours)	True Anomaly (degrees)	Mars		Occultation			
		Cone angle (degrees)	Clock Angle (degrees)	Sun	Earth	Canopus	Vega
0	207.152	24.5632	220.063	no	no	no	no
0.4	217.483	21.9361	245.599	no	yes	no	no
0.7	226.400	23.2162	268.732	no	yes	no	no
1.0	236.843	28.2639	289.982	no	yes	no	no
1.3	249.598	37.3746	306.642	no	no	no	no
1.5	259.999	45.9573	315.527	no	no	no	no
1.7	272.577	56.9944	323.279	no	no	no	no
1.9	288.141	71.1395	330.533	no	no	no	no
2.0	297.336	79.6206	334.210	no	no	no	no
2.1	307.616	89.1478	338.097	no	no	yes	no
2.2	319.032	99.7302	342.402	no	no	yes	no
2.3	331.531	111.247	347.453	no	no	yes	no
2.4	344.922	123.386	353.841	no	no	yes	no
2.5	358.838	135.536	2.684	no	no	yes	no
2.6	12.798	146.670	16.239	no	no	no	no
2.7	26.306	155.019	38.350	no	no	no	no
2.8	38.974	158.038	69.631	no	no	no	no
2.9	50.577	155.095	98.156	no	no	no	no
3.1	70.408	141.951	127.416	no	no	no	no
3.3	86.260	128.585	139.656	no	no	no	yes
3.6	104.569	112.112	148.992	no	no	no	yes
3.9	118.533	99.249	154.656	no	no	no	yes
4.3	133.070	85.772	160.131	no	no	no	no
4.7	144.796	74.924	164.663	no	no	no	no
5.1	154.844	65.706	168.923	no	no	no	no
5.5	163.873	57.538	173.310	no	no	no	no
6.0	174.380	48.272	179.547	no	no	no	no
6.5	184.589	39.697	187.569	no	no	no	no
7.0	195.040	31.742	199.263	no	no	no	no
7.5	207.046	24.702	220.076	no	no	no	no

TABLE 37

LOOK ANGLES TO EARTH DURING PLANETOCENTRIC ORBIT, DEPARTURE DATE 30 JANUARY 1969--MARS TYPE II

Days from Arrival	Cone Angle (degrees)	Clock Angle (degrees)
0	44.9	280.7
20	43.1	282.5
40	40.8	283.6
60	38.2	284.0
80	35.2	284.6
100	32.0	282.7
120	28.7	281.1
140	25.3	279.1
160	21.7	276.6
180	18.1	273.9
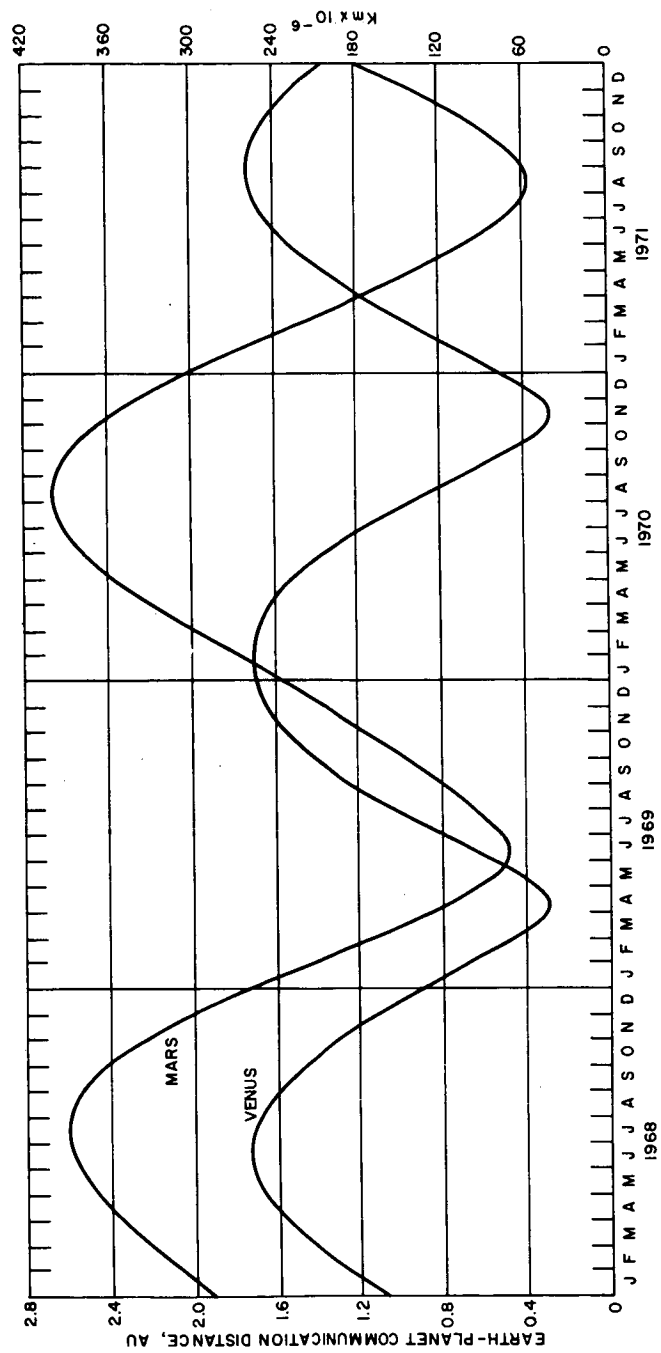
Figure 58 EARTH PLANET COMMUNICATION DISTANCE, 1968-1971

63-8750

-153-
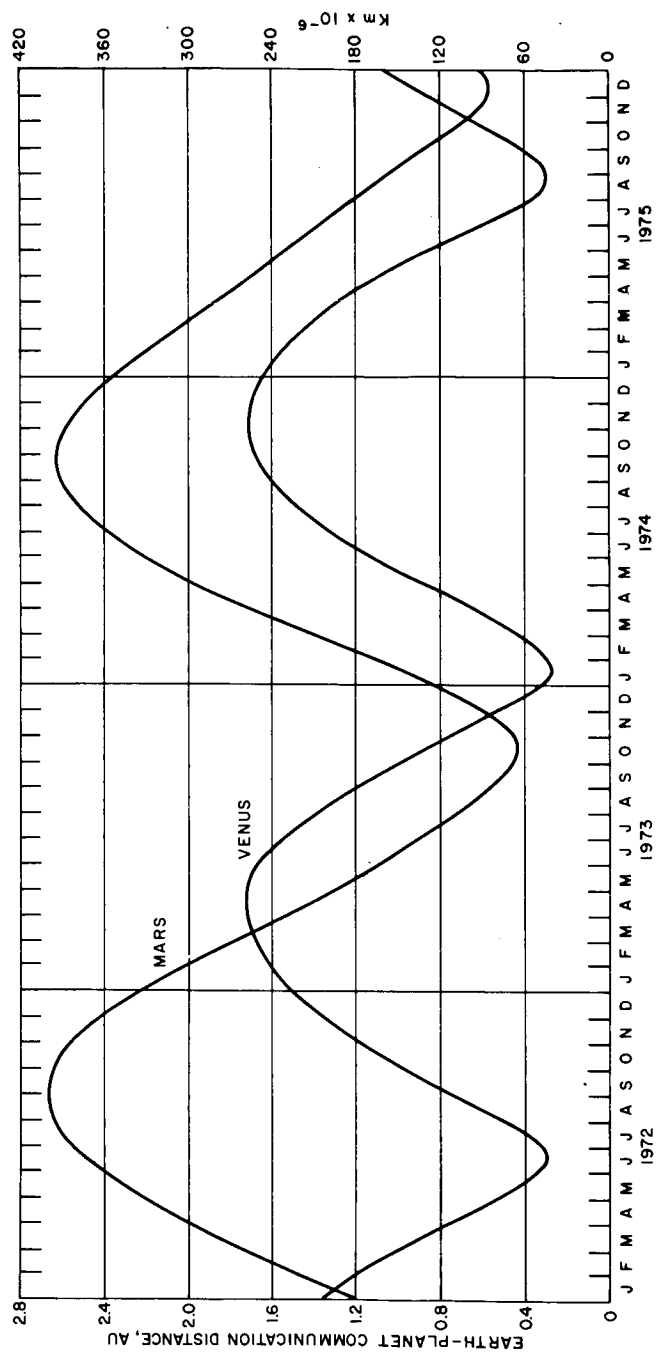
Figure 59 EARTH PLANET COMMUNICATION DISTANCE, 1972-1975

63-8751

-154-
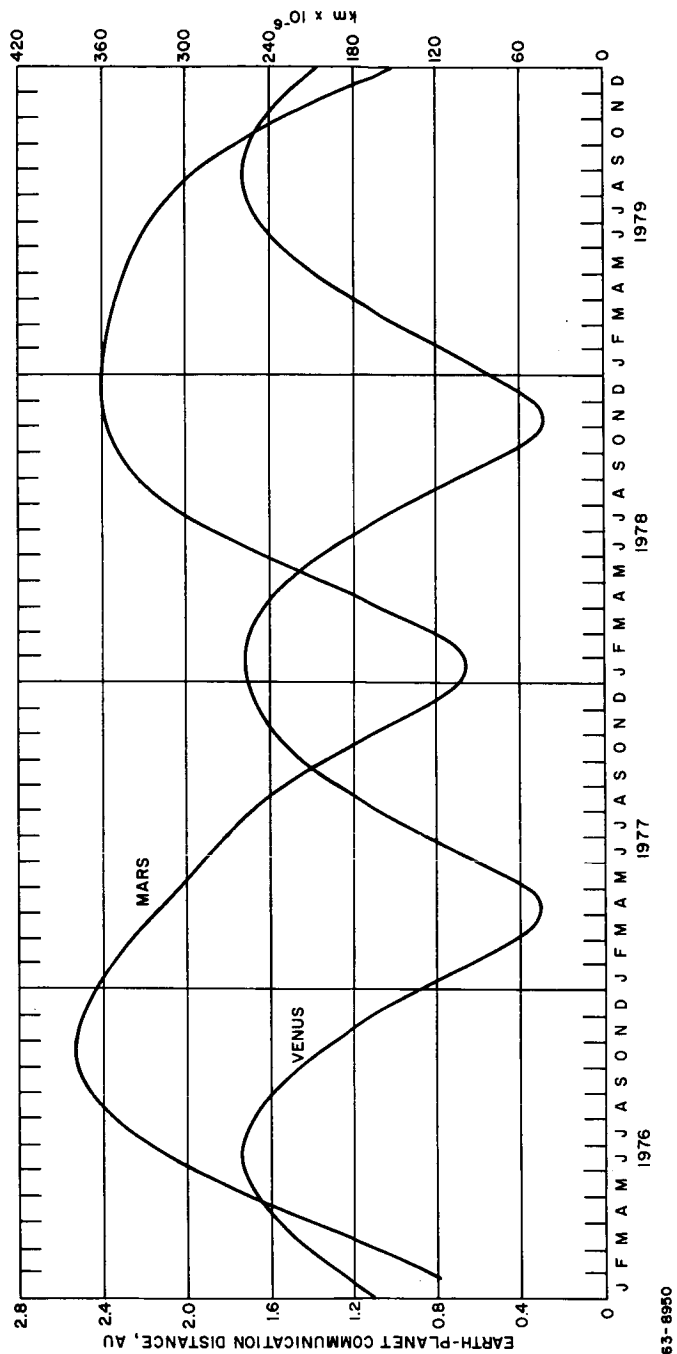
Figure 60   EARTH PLANET COMMUNICATION DISTANCE, 1976-1979

63-8950

-155-
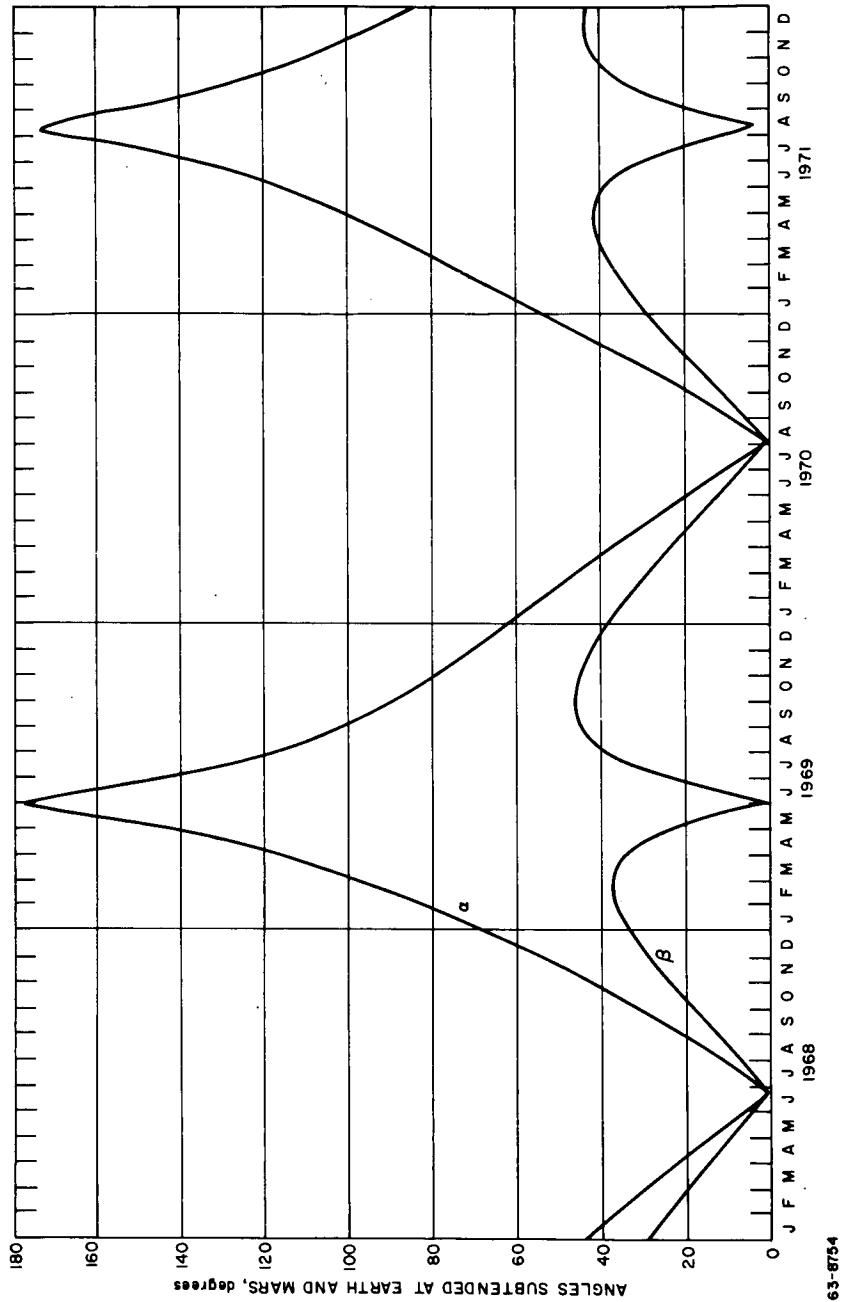
Figure 61 ANGLES SUBTENDED AT EARTH AND MARS, 1968-1971
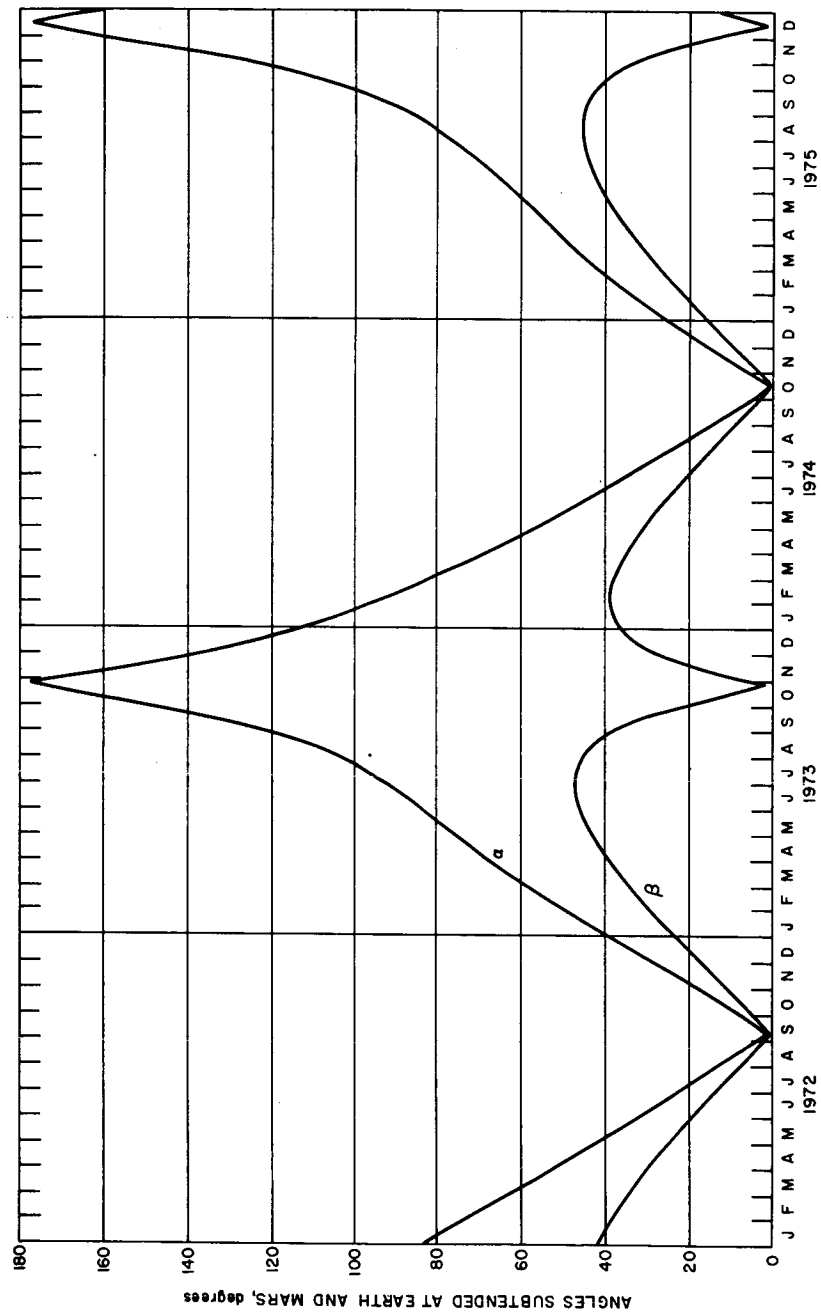
63-8754

Figure 62 ANGLES SUBTENDED AT EARTH AND MARS, 1972-1975

63-8755

-157-
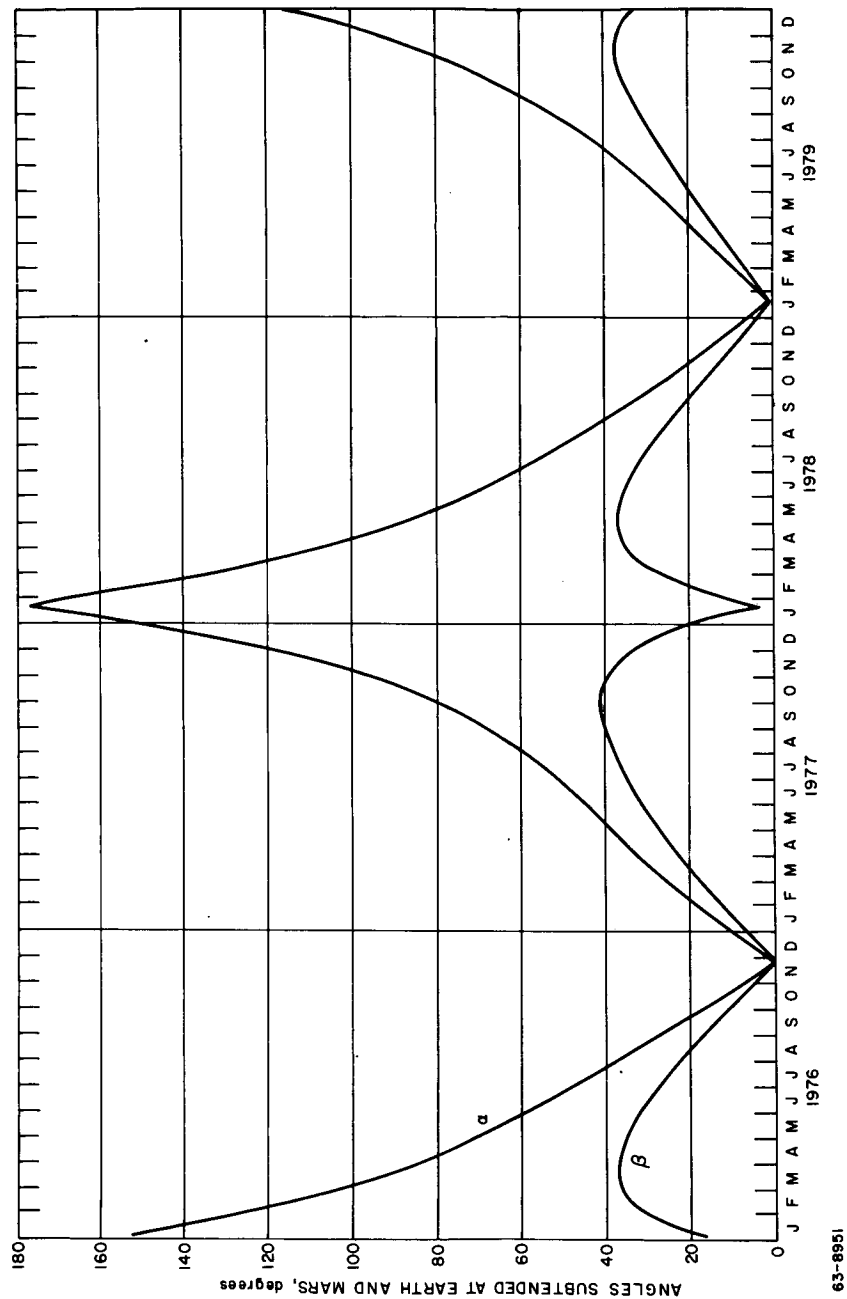
Figure 63 ANGLES SUBTENDED AT EARTH AND MARS, 1976-1979
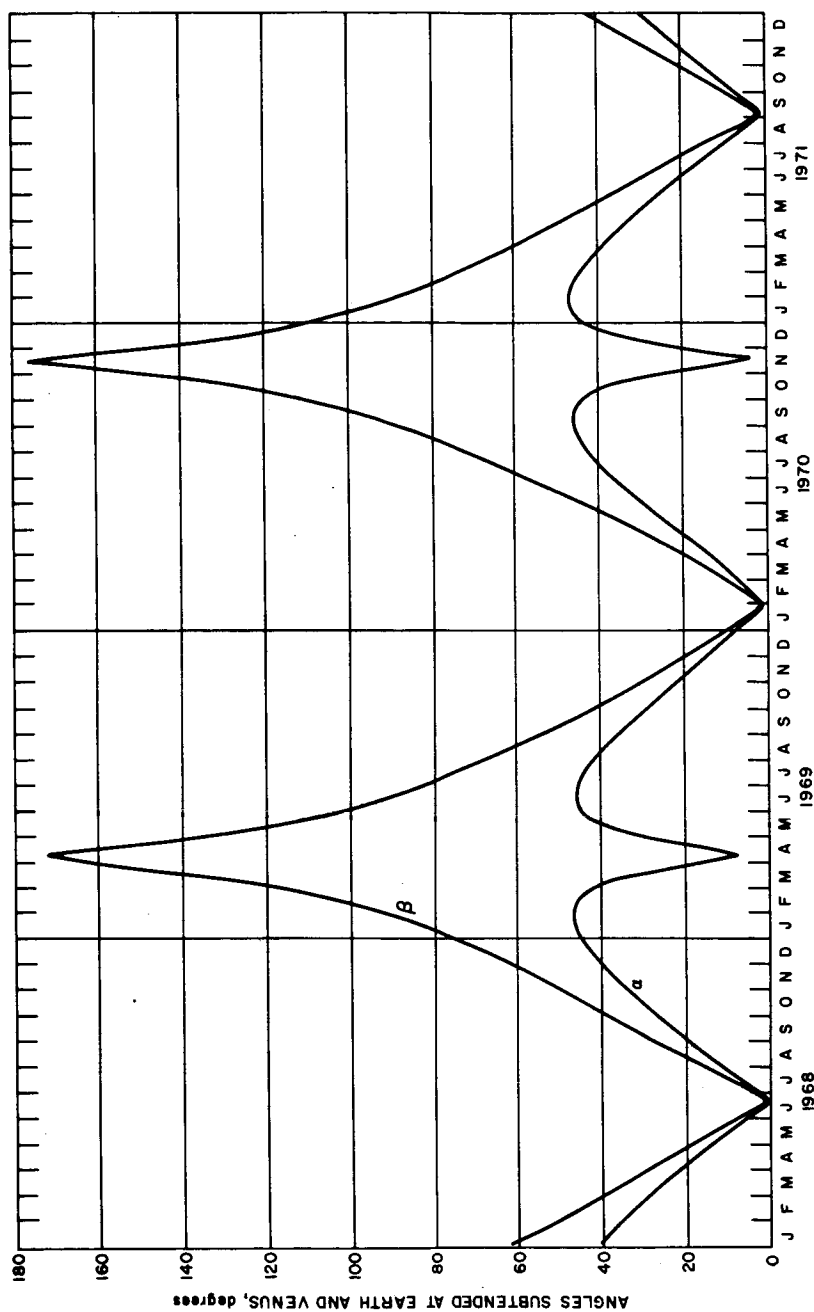
63-8951

Figure 64 ANGLES SUBTENDED AT EARTH AND VENUS, 1968-1971

ANGLES SUBTENDED AT EARTH AND VENUS, degrees

63-8752

-159-
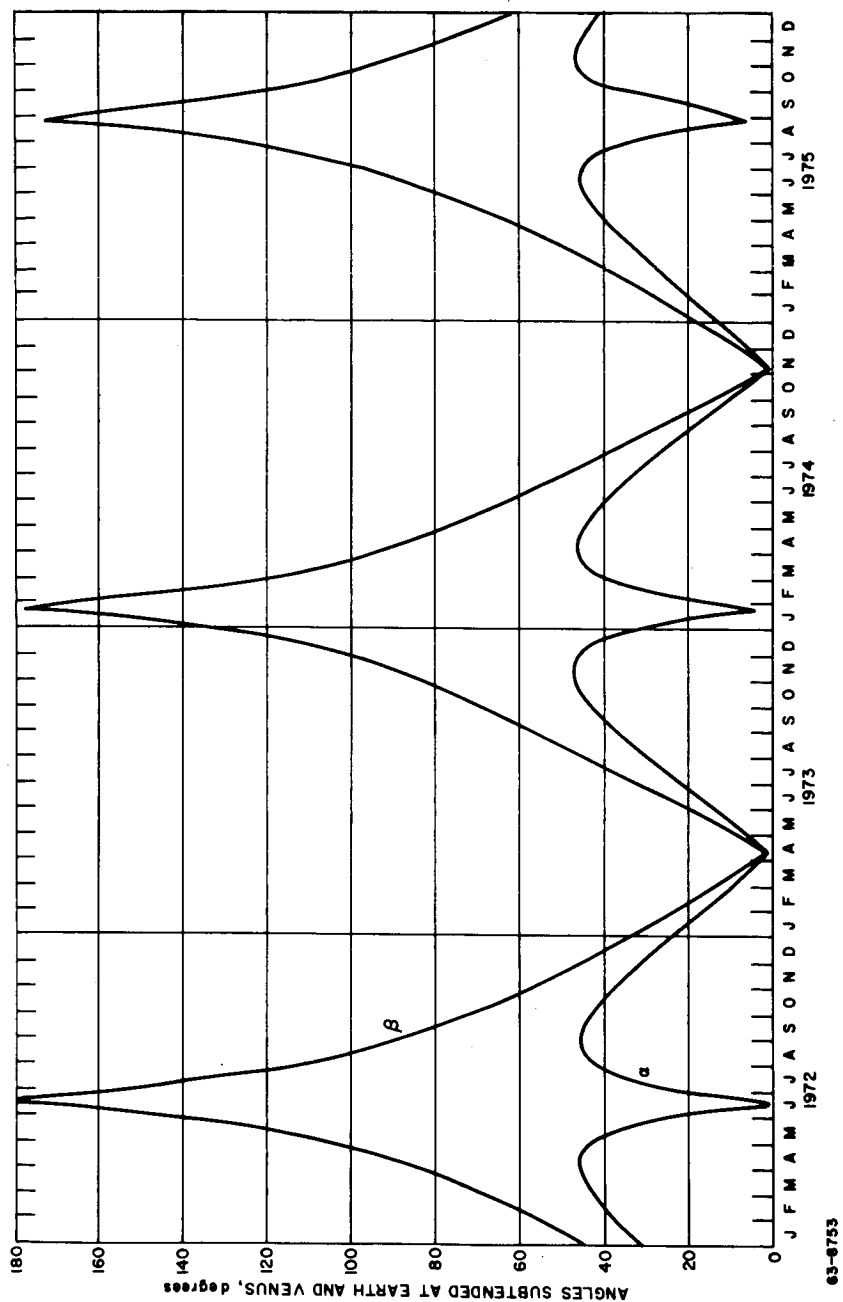
Figure 65 ANGLES SUBTENDED AT EARTH AND VENUS, 1972-1975

63-8753

-160-
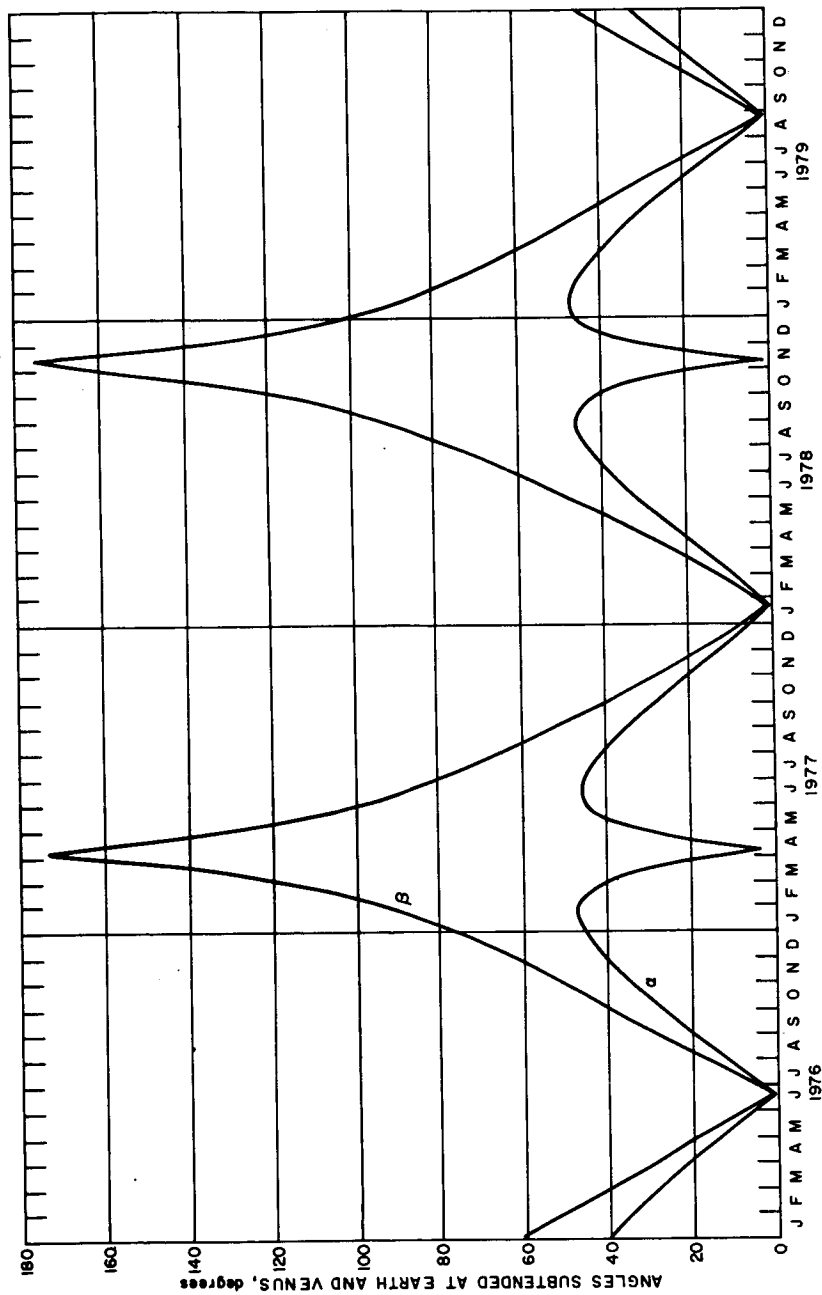
Figure 66 ANGLES SUBTENDED AT EARTH AND VENUS, 1976–1979

63-8952

-161-

2. <u>Direct Earth-lander communication link</u>. A direct Earth-lander communication link is a highly desirable feature since this removes the requirement for a relay orbiter for each mission. The communication time per day is a function of the lander latitude, the minimum elevation angle above the local horizon required for communication, and the elevation of the Earth line with respect to the Martian equator. In this analysis, it was assumed that the Earth must be at least 10 degrees above the lander local horizon for acceptable communications.

The Earth and Mars position vectors in a heliocentric equatorial coordinate system can be obtained from ephemeris data. The unit Earth-Mars vector may be obtained by

$$\underline{1}_{ME} = \frac{(E_x - M_x)\underline{i}_x + (E_y - M_y)\underline{i}_y + (E_z - M_z)\underline{i}_z}{\sqrt{(E_x - M_x)^2 + (E_y - M_y)^2 + (E_z - M_z)^2}} .$$

To determine the elevation of the Earth with respect to the Martian equator, the Martian North Pole vector must be determined. The Martian North Pole vector in the Martian orbital frame, defined by the positive x-axis in the direction of the ascending node, z-axis normal to the orbital plane, and the y-axis chosen in the orbital plane to form a right-handed system, is

$$\underline{1}_{M_{NP}} = 0.247\,\underline{i}_x - 0.343\,\underline{i}_y + 0.906\,\underline{i}_z .$$

This vector can be translated to the elliptic frame by

$$\begin{bmatrix} \underline{1}_{NP_{x'}} \\ \underline{1}_{NP_{y'}} \\ \underline{1}_{NP_{z'}} \end{bmatrix} = \begin{bmatrix} \cos\Omega & \cos i \sin\Omega & \sin i \sin\Omega \\ -\sin\Omega & \cos i \cos\Omega & \sin i \cos\Omega \\ 0 & -\sin i & \cos i \end{bmatrix} \begin{bmatrix} \underline{1}_{NP_x} \\ \underline{1}_{NP_y} \\ \underline{1}_{NP_z} \end{bmatrix}$$

where

i = inclination of Martian orbital plane (-1 deg. 51 min)

Ω = longitude of Martian ascending node (-49 deg. 13 min).

Finally, the North Pole vector can be obtained in the heliocentric equatorial system by a rotation of (-23 deg., 27 min) about the x axis and is defined by

$$\underline{1}_{NP} = 0.443\,\underline{i}_x - 0.407\,\underline{i}_y + 0.799\,\underline{i}_z .$$

-162-

The elevation angle of the Earth line with respect to the Martian equator is computed by

$$\eta = \sin^{-1} [\underline{1}_{NP} \cdot \underline{1}_{ME}].$$

This angle varies between ± 25 degrees and is presented for the time period between 1968 and 1979 in figures 67 through 69. The variation in this angle is extermely important in selecting lander locations where direct communication is possible. By definition, the angle between the Earth-line latitude and the lander latitude must be less than 80 degrees. Therefore, if the elevation of the Earth line is -25 degrees at encounter, the lander latitude must be constrained to be less than + 55 degrees for communication. From this consideration, the elevation of the Earth line must be employed as one constraint in selecting desirable lander locations.

The percent of communication time per day can be computed knowing the elevation of the Earth line η, the lander latitude L_L, and the communication cone half angle ζ, by

$$\bar{t} = \frac{1}{180} \sin^{-1} \left[\frac{\sqrt{\cos^2 L_L \sin^2 \zeta - (\sin \eta - \sin L_L \cos \zeta)}}{\cos L_L \cos \eta} \right]$$

provided there are no receiving restrictions with respect to Earth.

For lander latitudes of ± 80, ± 60, ± 30, and 0 degrees, the percent of communication time per day is presented in figures 70 through 75 for northern and southern latitude landers, respectively, from 1968 to 1979. These data indicate that on the average communication is possible 40 percent of the time for lander latitudes between ± 30 degrees. However, for lander latitudes near the polar caps, there are cyclic periods of several months duration where continuous communication is possible, and other periods of the same duration where no communication is possible.

In this analysis, no consideration was given to the possibility of communication blackout as determined by the angle subtended at Mars by the planet-Earth-line and planet-sun-line.

3. Orbiter-lander communication relay link. While an orbiter-lander communication relay link between the lander vehicle may not be desirable for all missions, there are several advantages associated with it. First it provides a redundant communication system in event the direct Earth-lander link fails to operate during atmospheric descent and, second, it allows for lander impact locations to be selected where direct Earth communication is not possible, as shown in the preceding section.
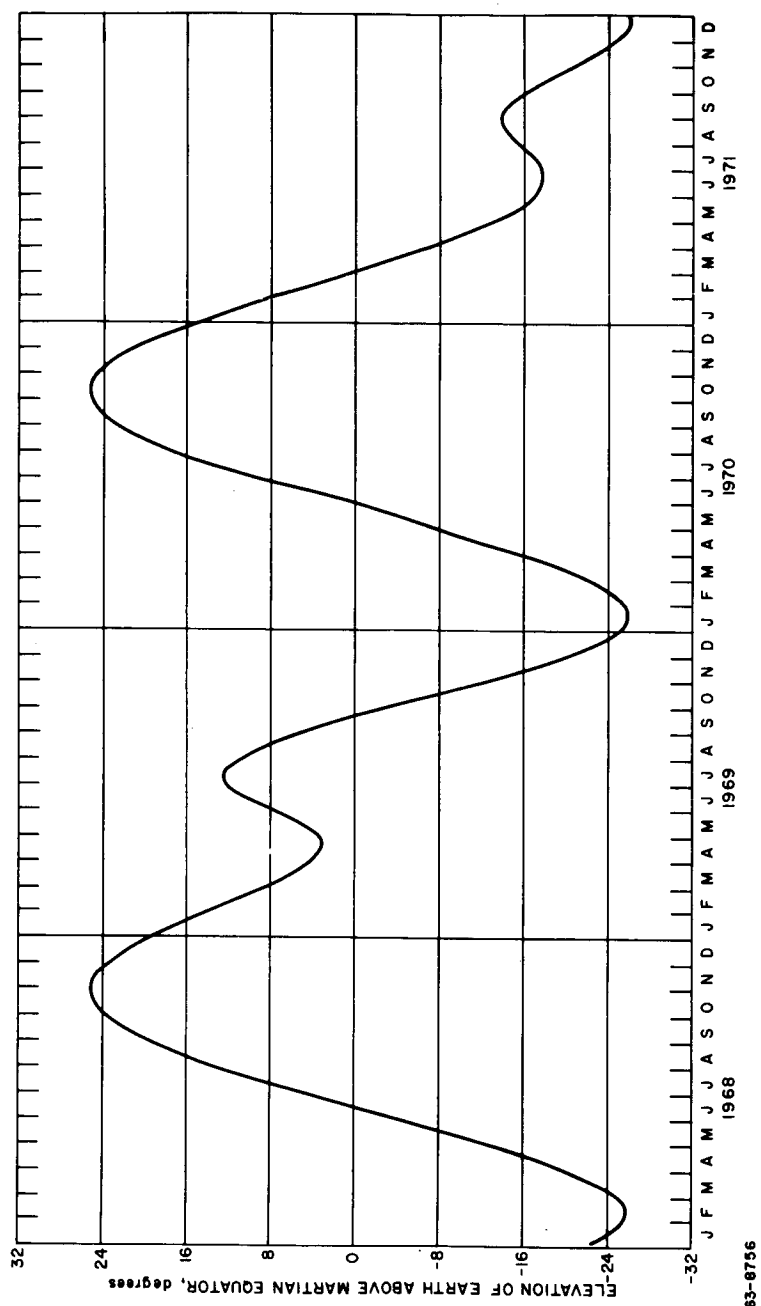
-163-

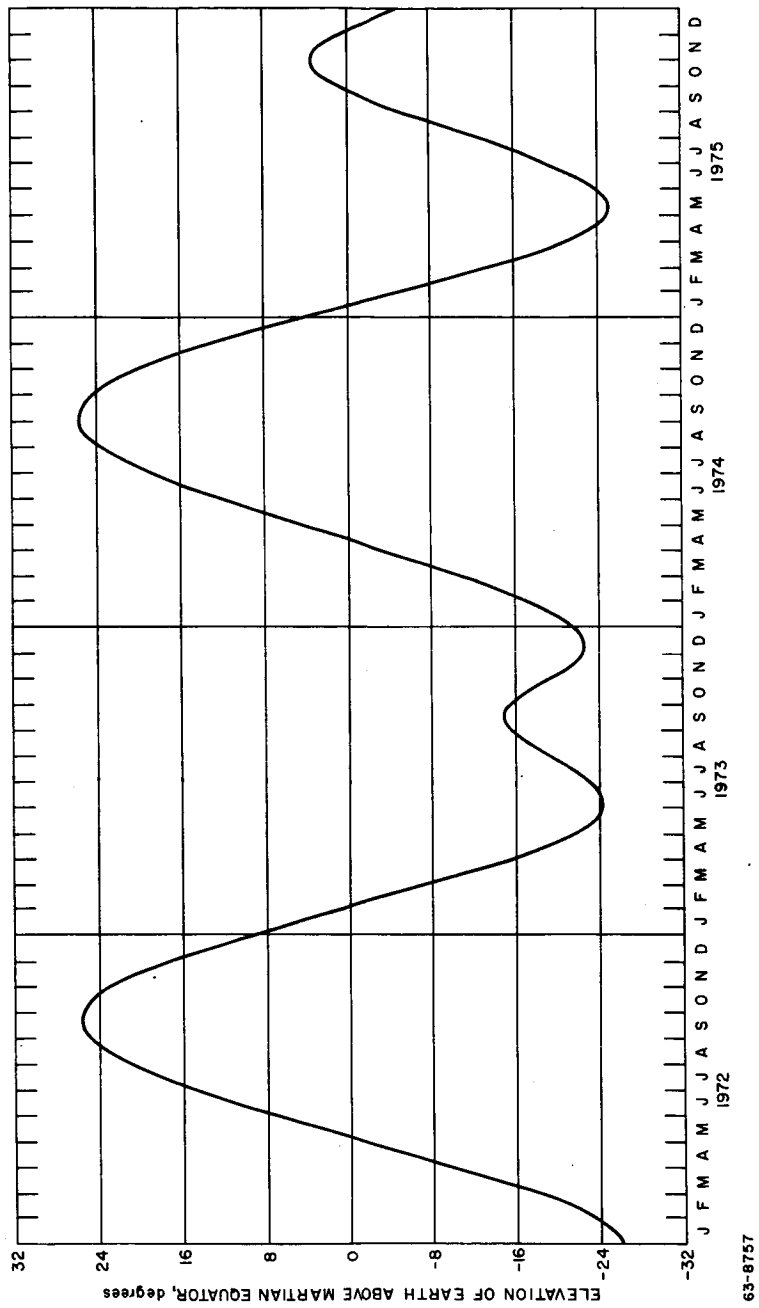Figure 67 ELEVATION OF EARTH ABOVE MARTIAN EQUATOR, 1968-1971

63-8756

-164-

Figure 68 ELEVATION OF EARTH ABOVE MARTIAN EQUATOR, 1972-1975

63-8757

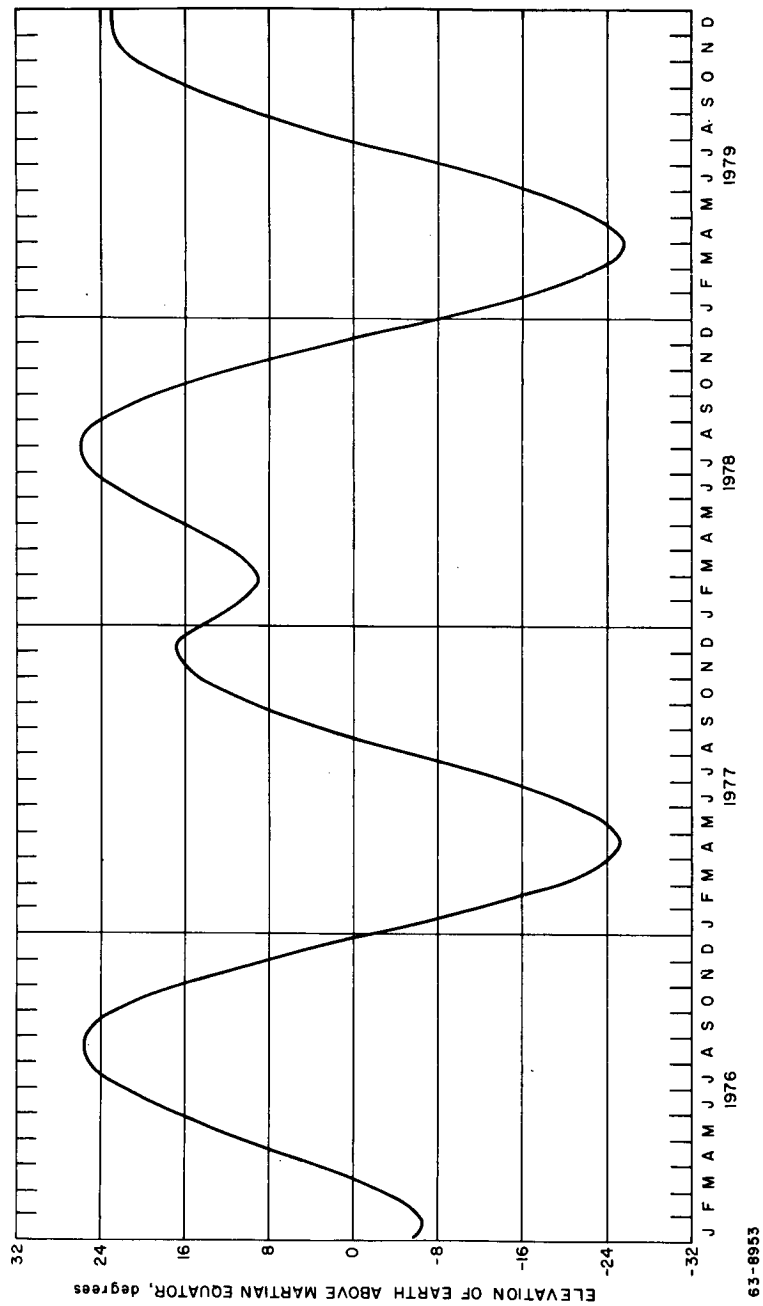ELEVATION OF EARTH ABOVE MARTIAN EQUATOR, degrees

-165-

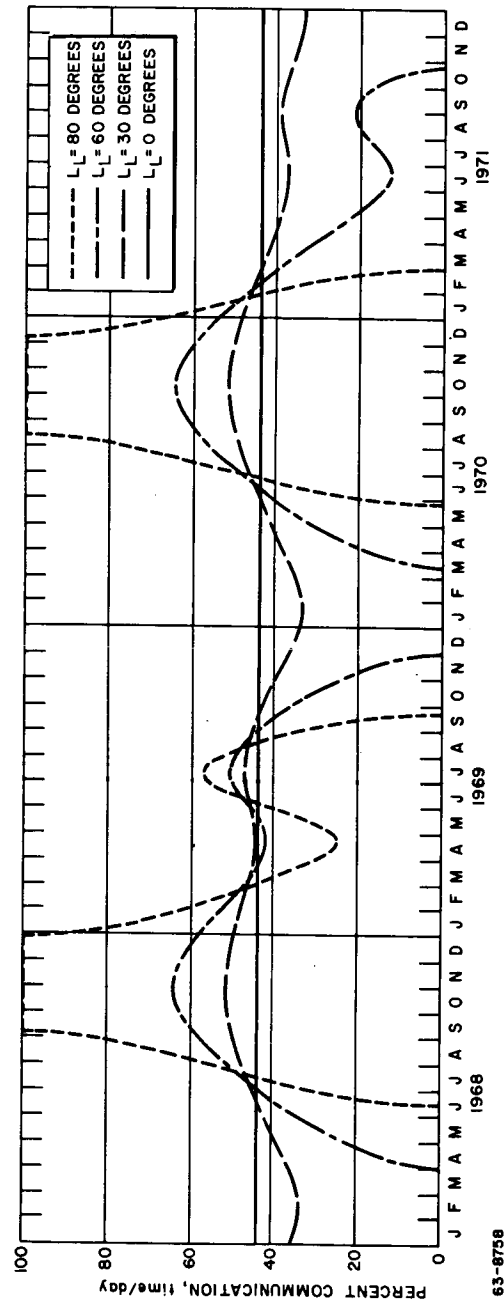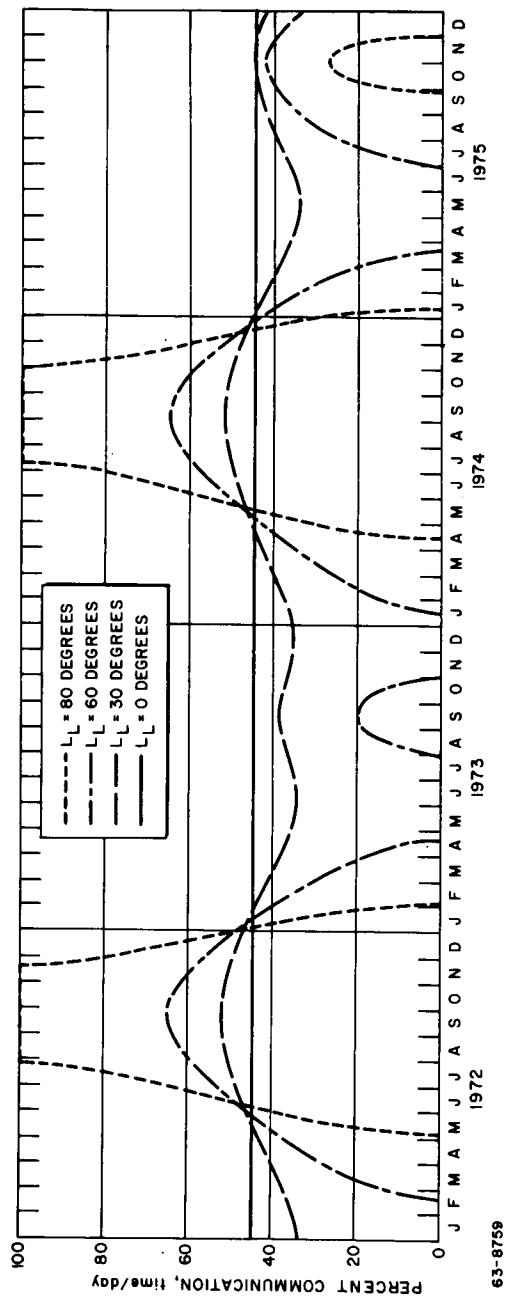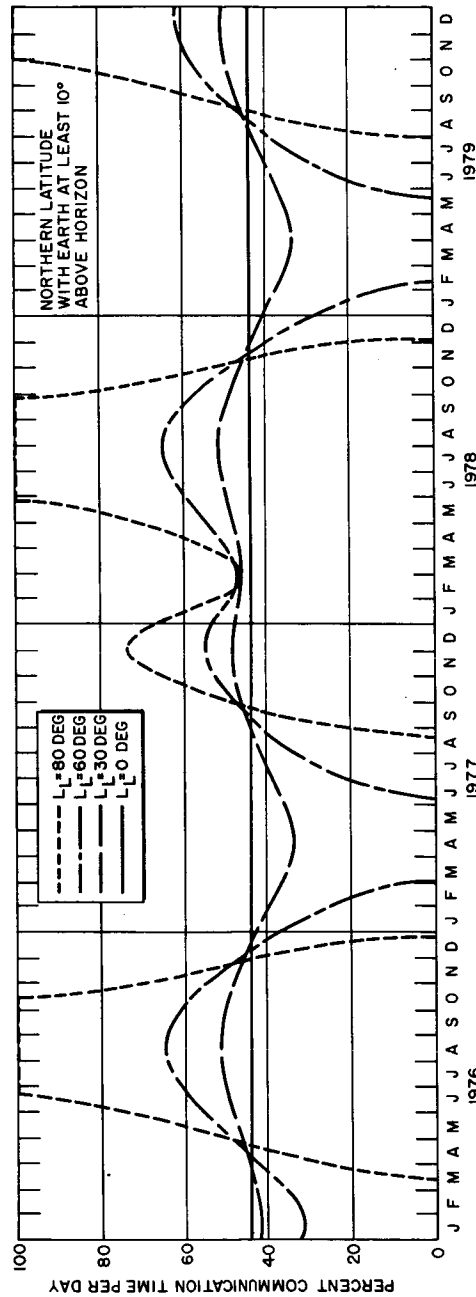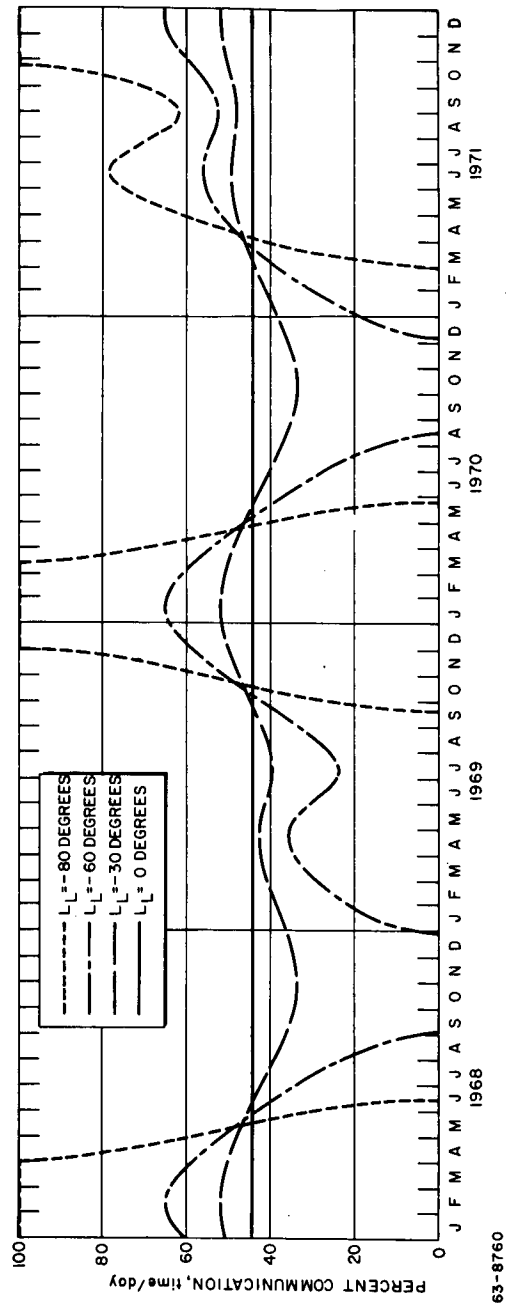Figure 69 ELEVATION OF EARTH ABOVE MARTIAN EQUATOR, 1976-1979

63-8953

-166-

Figure 70 EFFECT OF LOCATION OF MARTIAN LANDER ON COMMUNICATION
WITH EARTH 1968-1971

63-8758

-167-

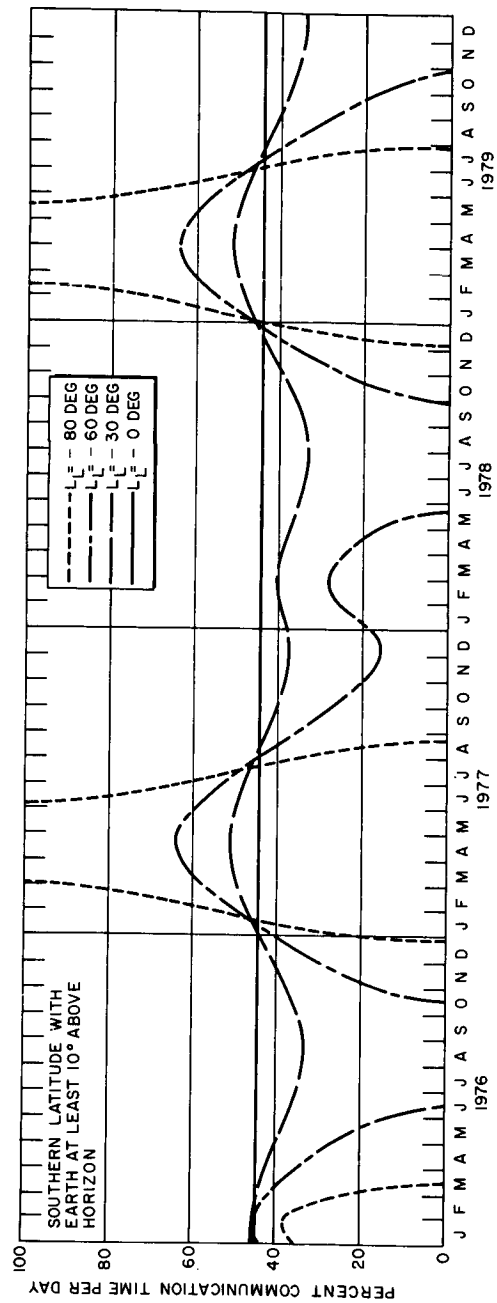Figure 71 EFFECT OF LOCATION OF MARTIAN LANDER ON COMMUNICATION
WITH EARTH 1972-1975

63-8759

Figure 72 EFFECT OF LOCATION OF MARTIAN LANDER ON COMMUNICATION
WITH EARTH 1976-1979

33-8954

-169-

Figure 73 EFFECT OF LOCATION OF MARTIAN LANDER ON COMMUNICATION
WITH EARTH 1968-1971

63-8760

-170-
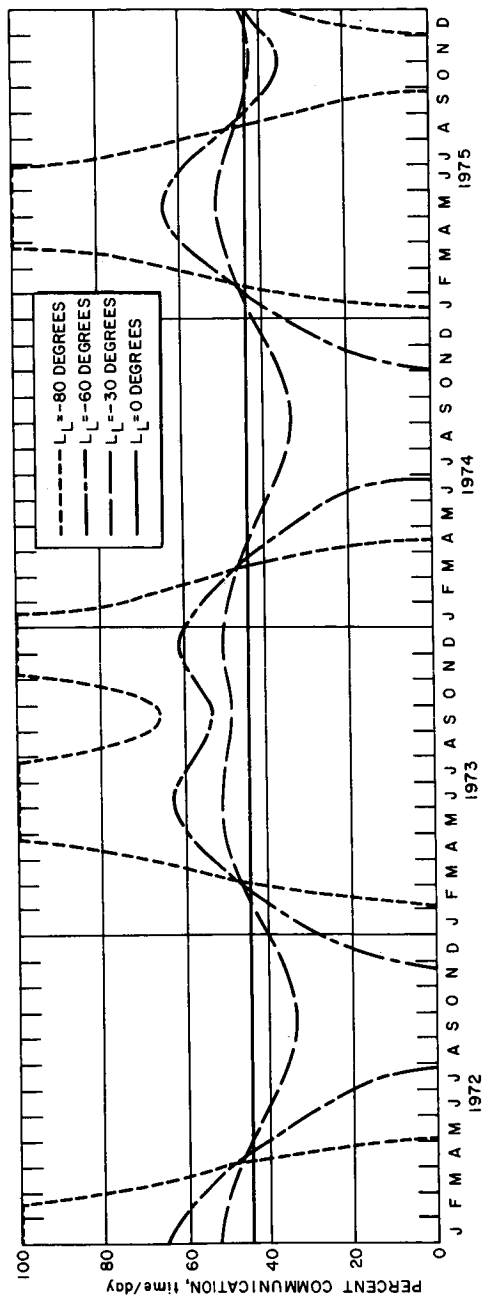
Figure 74 EFFECT OF LOCATION OF MARTIAN LANDER ON COMMUNICATION
WITH EARTH 1972-1975

63-8761

Figure 75 EFFECT OF LOCATION OF MARTIAN LANDER ON COMMUNICATION
WITH EARTH 1976-1979

63-8955

-172-

From the specification of the planetocentric orbit by the apogee and perigee radii, r_a and r_p, respectively, the size of the orbit is expressed in terms of the semimajor axis a, by

$$a = \frac{r_a + r_p}{2} ,$$

and the shape of the orbit is obtained from the orbital eccentricity e, by

$$e = \frac{r_a - r_p}{r_a + r_p} .$$

The semilatus rectum p, which is a function of a and e, is defined by

$$p = a (1 - e^2) .$$

The mean angular motion η and the orbital period P are functions of the semimajor axis only and may be expressed by

$$\eta = \sqrt{\frac{\mu}{a^3}}$$

and

$$P = \sqrt{\frac{2\pi}{\eta}}$$

where

μ = planetary gravitational constant.

The total time for which this analysis will be conducted can be expressed as a function of the total number of orbits n_t by

$$T_{stop} = n_t P .$$

In this analysis, the effect of orbital plane and apsidal line rotation due to planetary oblateness will be neglected.

A reference point defined by the intersection of the lander latitude plane and the ascending node of the orbit plane is selected as shown in figure 76. For this reference point to be defined, the inequality
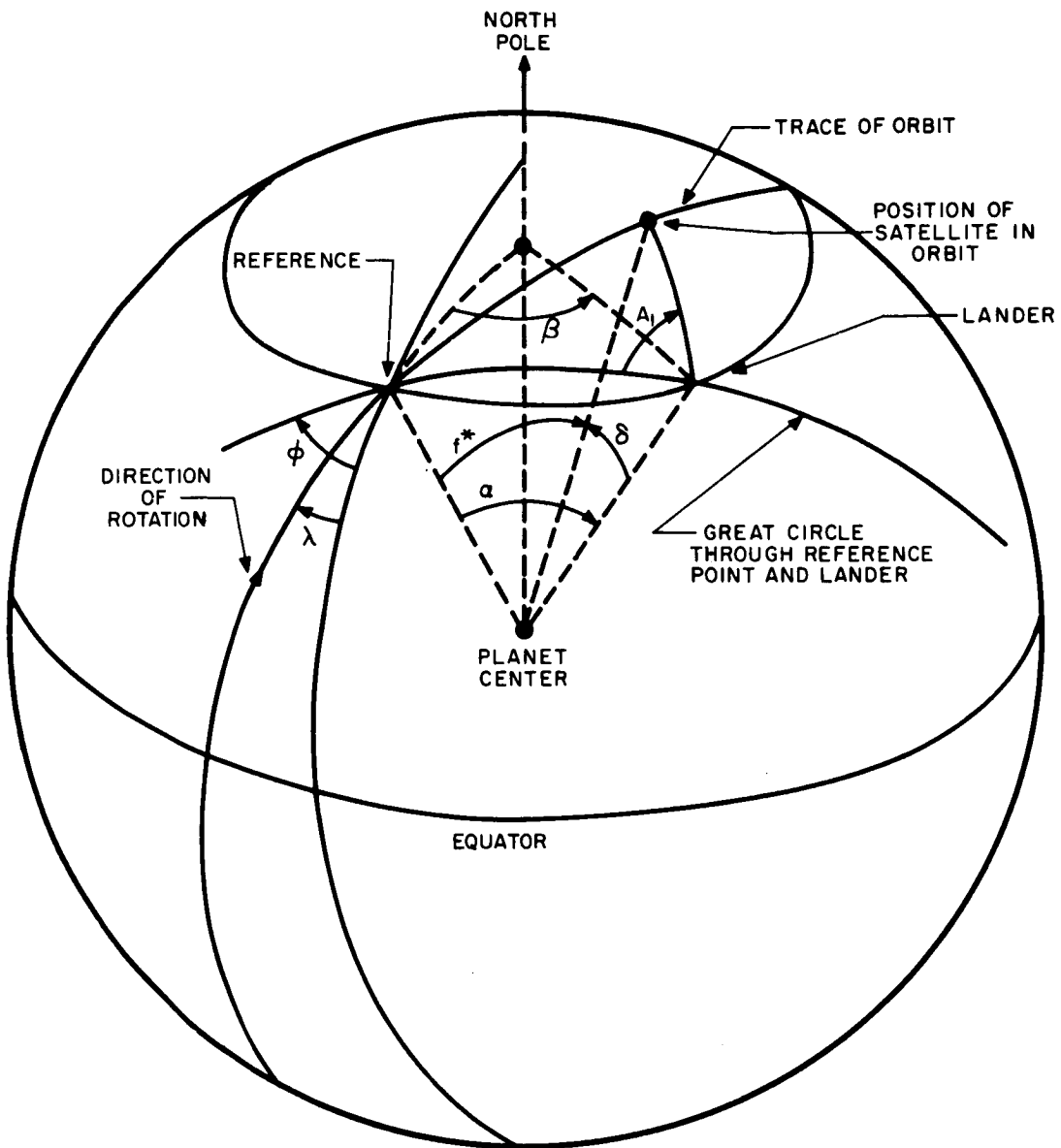
63-8945

Figure 76 ORBITER-LANDER COMMUNICATION GEOMETRY

$$i > L > 0$$

must be satisfied where:

    i = orbital inclination with respect to planetary equator

    L = lander latitude.

The angle between the reference point and the initial lander position is a function of time and is

$$\beta = \beta_o + \omega_p t$$

where

    β_o = initial separation.

The central angle between the reference point and the lander position a is

$$a = 2 \sin^{-1} \left(\cos L \; \sin \frac{\beta}{2} \right) \quad .$$

The difference between the two additional angles ϕ and λ, defined by

$$\phi = \tan^{-1} \left(\frac{\cot \beta/2}{\sin L} \right)$$

and

$$\lambda = \sin^{-1} \left(\frac{\cos i}{\cos L} \right) \quad ,$$

is the angle γ which is employed in conjunction with the central angle of the orbiter with respect to the reference point f^* and a to compute the central angle between the orbiter and lander δ by

$$\delta = 2 \sin^{-1} \left[1 \sin \frac{\gamma}{2} \right| \sqrt{ \sin^2 \left(\frac{f^* + a}{2} \right) + \cot^2 \frac{\gamma}{2} \; \sin^2 \left(\frac{f^* - a}{2} \right) } \; \right] \quad .$$

After having determined δ the range R and the elevation angle E of the satellite with respect to the lander can be obtained by

$$R = \sqrt{r^2 + r_o^2 - 2\,r\,r_o\,\cos\delta}$$

where

r_o = planet radius

r = radial distance of orbiter from planet center

$$E = \sin^{-1}\left(\frac{r\sin\delta - r_o}{R}\right).$$

The azimuth angle from the lander to the orbiter (due West defined as zero) is

$$A = 90 - \phi + A_1$$

where

$$A_1 = \tan^{-1}\left[\frac{2\cot\dfrac{\gamma}{2}\,\sin f^*}{\sin(f^* + \alpha) - \cot^2\dfrac{\gamma}{2}\,\sin(f^* - \alpha)}\right].$$

If E is greater than the minimum angle for communication E_1, the true anomaly is increment by Δf, the eccentricity anomaly and time from perigee computed. The time between the points where $E = E_1$ on the ascending and descending portions of the orbit with respect to the lander is the total communication time for that pass. The orbital plane remains fixed in inertial space as the orbiter proceeds by increments of Δf and the lander position changes due to planet rotation ω_p. The total time per pass is therefore computed and, if the orbiter proceeds through 360 degrees without $E \geq E_1$, no communication is possible on that pass. At the desired program stop, the time in communication per orbital pass, the number of passes where communication was not possible, and the total communication time are computed.

In this present analysis, it was assumed that an omnidirectional antenna would be employed on the lander; however, with the utilization of a directional antenna, the rate of change of the elevation angle $\dot{E}$, the rate of change of the azimuth angle $\dot{A}$, and the range rate $\dot{R}$ can be obtained by

$$\dot{E} = \cot E \left(\frac{\dot{R}}{R} - \frac{\dot{r}}{r} - \dot{\delta} \cot \delta \right)$$

$$\dot{A} = \dot{A}_1 - \dot{\phi}$$

$$\dot{R} = (r - r_0 \cos \delta) \frac{\dot{r}}{R} + \frac{r \, r_0 \, \dot{\delta} \sin \delta}{R}$$

where

r = radial distance of orbiter from center of planet

r_0 = planet radius

R = range from orbiter to lander.

The communication time is a function of the lander latitude, orbital inclination, size, and shape in addition to the location of periapsis.

In this analysis, lander locations of 2, 22, 42, 62, and 82 degrees were investigated where the periapsis latitude was varied between ± 90 degrees in 15-degree intervals. Due to symmetry, lander latitudes for the appropriate periapsis location, i. e., southern latitude lander with southern latitude periapsis locations are identical with northern latitude lander and periapsis locations, etc.

For a reference orbit with a periapsis altitude of 1500 km and an apoapsis altitude of 10,000 km, the number of orbital passes in which communication is possible, the total communication time per week, and the communication time per pass is a function of the lander and orbiter periapsis latitudes. In general, for lander latitudes in excess of 60 degrees, communication is possible each orbit regardless of the periapsis location. However, these lander locations do not maximize the total communication time when the corresponding periapsis locations are in the northern hemisphere. The total communication time for a fixed number of orbits (101 in this analysis) is essentially minimized when the lander and periapsis latitudes correspond and is maximized when these locations are separated by 180 degrees.   In part this is due to the variation in the rate of rotation of the orbiter radius vector in the vicinity of apogee and perigee and in part due to the increased altitude at apoapsis. For the nominal apoapsis and periapsis altitudes, the orbital period is such that the vehicle completes approximately 25 passes per week. This total communication time, and corresponding number of visible passes was separated into weekly intervals

and the results indicate that these parameters are nearly repetitive on a weekly basis. These results are summarized in table 38. For the first 30 orbits, the communication time per pass is presented in figures 77 through 81. In these graphs, only the points corresponding to an integral number of orbits are pertinent and the lines connecting the points are only intended to indicate the various lander latitudes.

The variation in total communication time and number of visible passes, as a function of apoapsis altitude, was analyzed for apoapsis altitudes between 5,000 and 15,000 km for a fixed orbiter periapsis latitude of 30 degrees.

The percentage of visible passes for a fixed number of orbital passes and the time in view per orbit increase as the apoapsis altitude is increased for a fixed lander and periapsis location. For an apoapsis altitude of 5000 km, the average time in view per orbit increased from 35 to 50 minutes as the lander latitude increased. The average time for a 10,000-km apoapsis altitude is essentially independent of lander latitude whereas the average time decreased from 150 minutes to 90 minutes as the lander latitude increased for a 15,000-km apoapsis altitude. This reversal in trend is related to the fact that the orbital period increases from 4.5 to 12 hours as the apoapsis altitude increases from 5000 to 15,000 km. These results are presented in figure 82.

An analysis was also conducted to determine the variation in communication time per orbit for other than polar orbits. Inclinations of 67.5 and 112.5 degrees were employed for lander latitudes between ± 62 degrees. As expected, the variation between these and polar orbits is quite negligible and the average communication time per orbit essentially decreases monotonically as the periapsis latitude increases from -62 to +62 degrees. The only exception to this is the near equatorial lander location. These results are presented in figures 83 through 85.
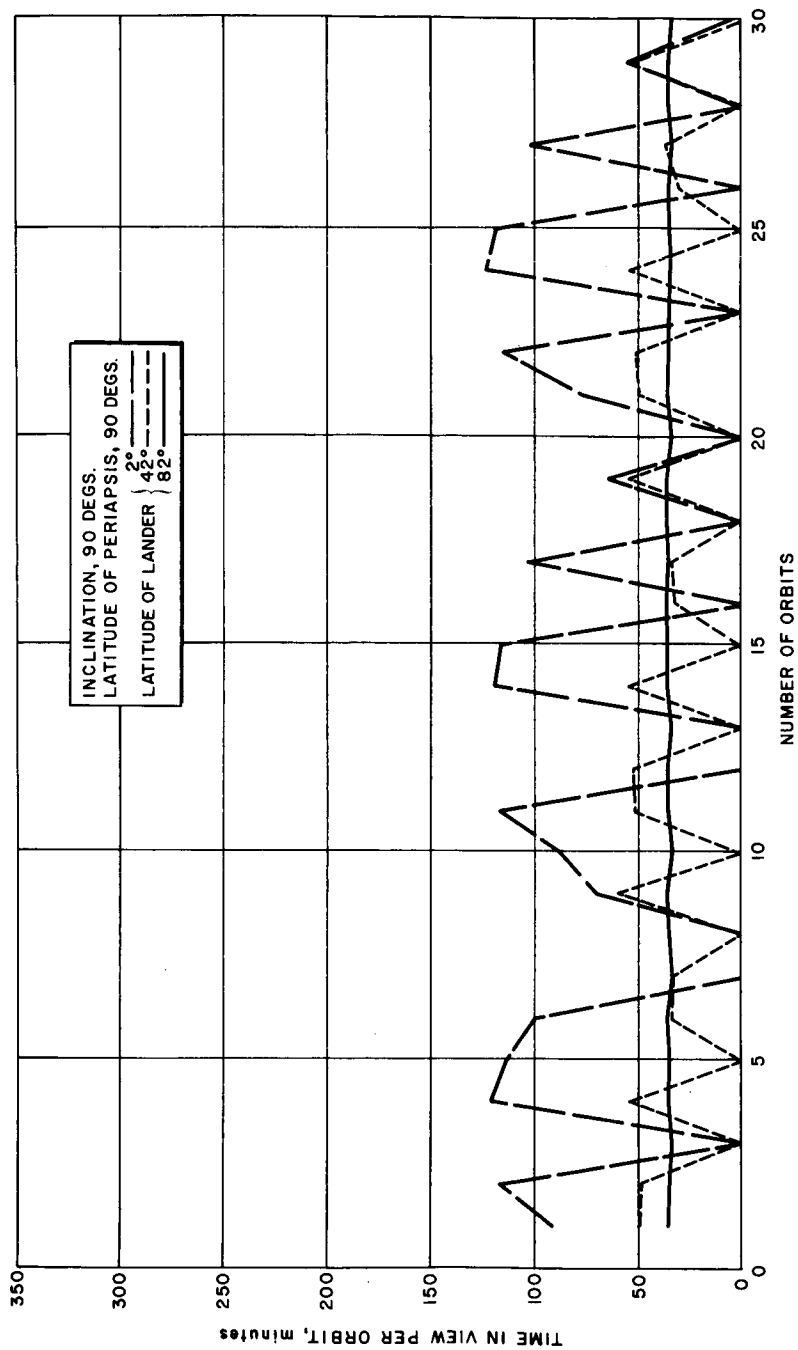
5.4 Mars Orbit Selection

1. Summary. The Voyager orbiter has the functional requirements of (a) providing an observation platform from which scientific information such as planet surface characteristics can be obtained, and (b) acting as a relay station to support data transmission from the planet surface to Earth.

Considering these requirements, in principle, it appears desirable to attempt to obtain a low-altitude circular orbit. In practice, there are considerations which limit our ability to achieve this goal. The dominant constraints being (a) To avoid the necessity of orbiter sterilization, the minimum orbital altitude must be such that the orbit decay time is in excess of 50 years.

TABLE 38

LANDER-ORBITER COMMUNICATION RELAY LINK

Latitude of Periapsis (degrees)	Latitude of Lander (degrees)	Number of Visible Passes	Total Communication Time (minutes)	First Week Visible Passes	Communication Time (minutes)	Second Week Visible Passes	Communication Time (minutes)	Third Week Visible Passes	Communication Time (minutes)	Fourth Week Visible Passes	Communication Time (minutes)
90	2	65	5925	16	1645	18	1350	16	1480	15	1450
	22	58	3665	15	982	14	884	15	951	14	848
	42	66	2764	15	697	15	657	17	713	18	669
	62	101	3316	25	822	25	820	25	824	25	815
	82	101	3480	25	863	25	859	25	863	25	860
45	2	68	7852	16	2062	16	1943	18	1955	17	1887
	22	56	5680	16	1603	13	1368	13	1307	13	1376
	42	77	4983	18	1305	18	1202	21	1269	19	1198
	62	101	5444	25	1361	25	1329	25	1353	25	1333
	82	101	5420	25	1342	25	1330	25	1354	25	1336
0	2	64	9409	16	2365	15	2268	15	2274	17	2384
	22	75	10001	18	2471	16	2383	21	2595	19	2480
	42	101	11926	25	2935	25	2831	25	2050	25	2927
	62	101	12797	25	3180	25	3123	25	3182	25	3140
	82	101	13004	25	3222	25	3200	25	3224	25	3213
-45	2	70	8515	18	2087	17	2032	18	2163	16	2104
	22	87	12256	25	3086	21	2872	21	3119	19	2995
	42	101	19494	25	4848	25	4822	25	4814	25	4699
	62	101	22478	25	5569	25	5532	25	5574	25	5517
	82	101	23730	25	5875	25	5852	25	5691	25	5860
-90	2	63	6791	18	1806	14	1506	16	1831	14	1564
	22	89	13418	24	3535	24	3275	20	3291	20	3156
	42	101	23346	25	5776	25	5726	25	5806	25	5719
	62	101	26726	25	6648	25	6328	25	6874	25	6569
	82	101	28013	25	6952	25	6924	25	6937	25	6912

Figure 77 ORBITER-LANDER COMMUNICATION INCLINATION 90 DEGREES, LATITUDE OF PERIAPSIS 90 DEGREES, LATITUDE OF LANDER 2, 42, AND 82 DEGREES
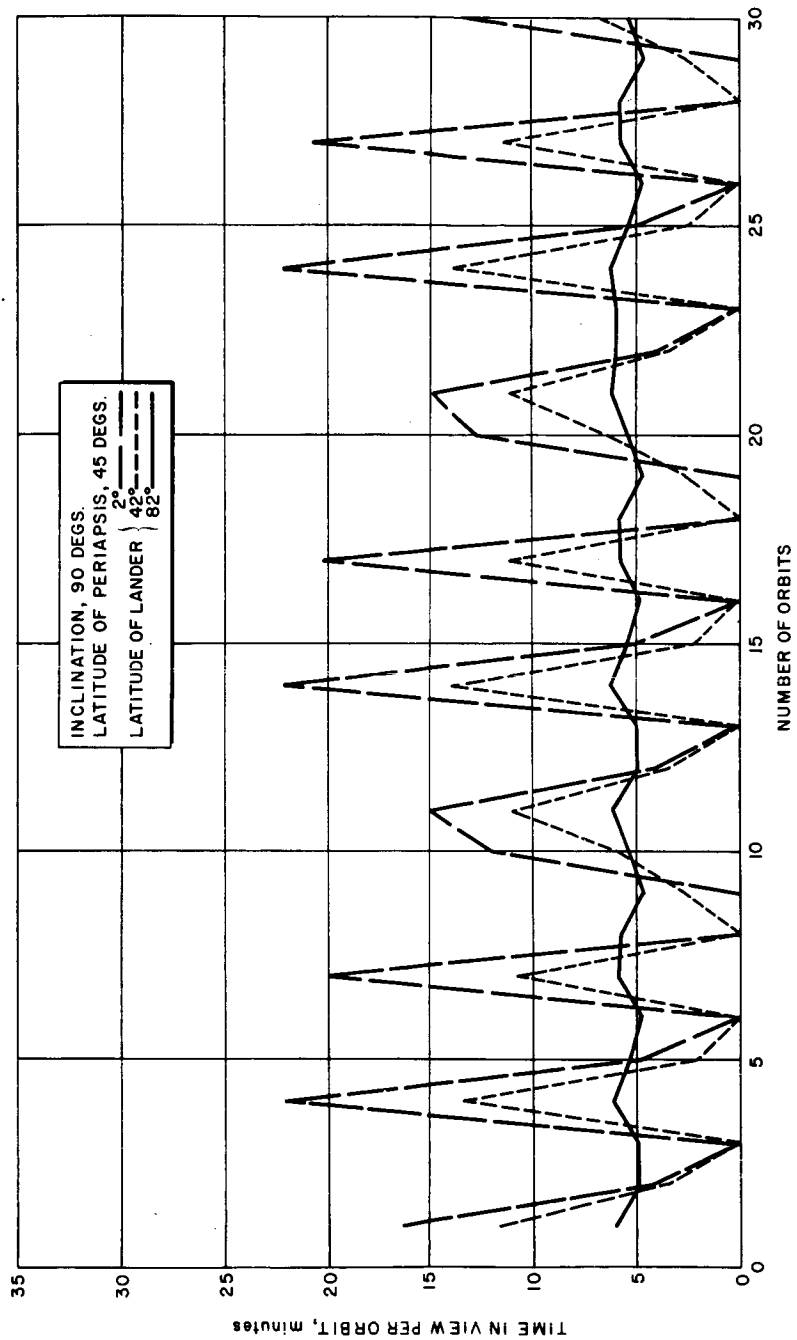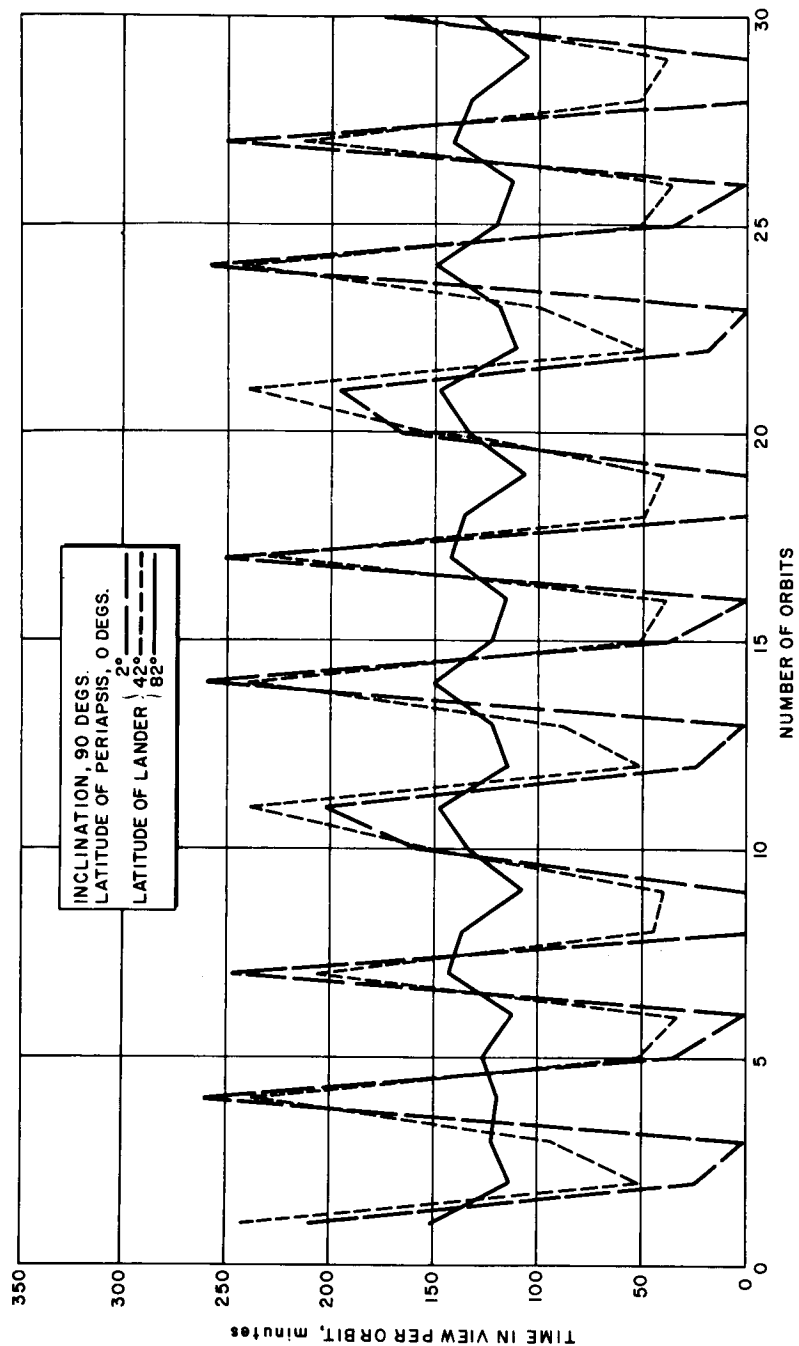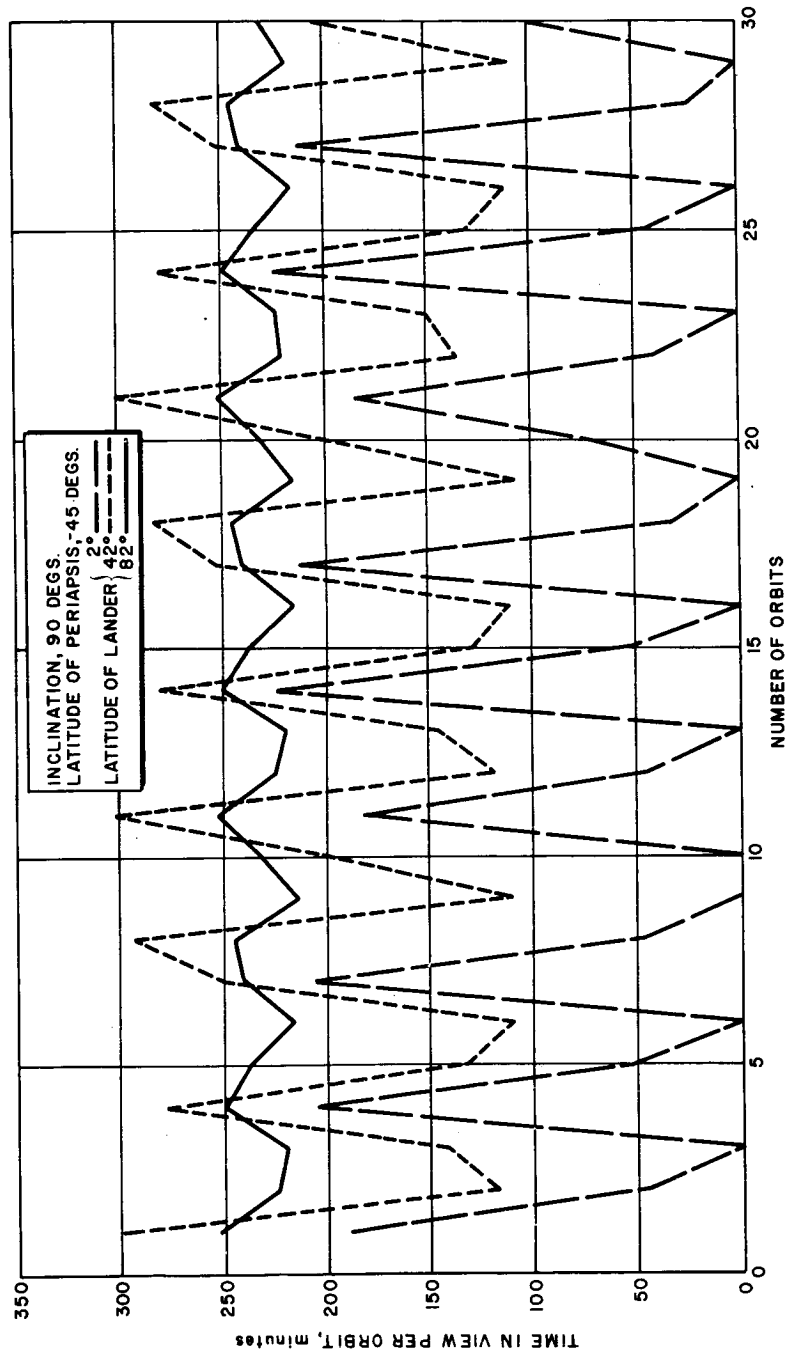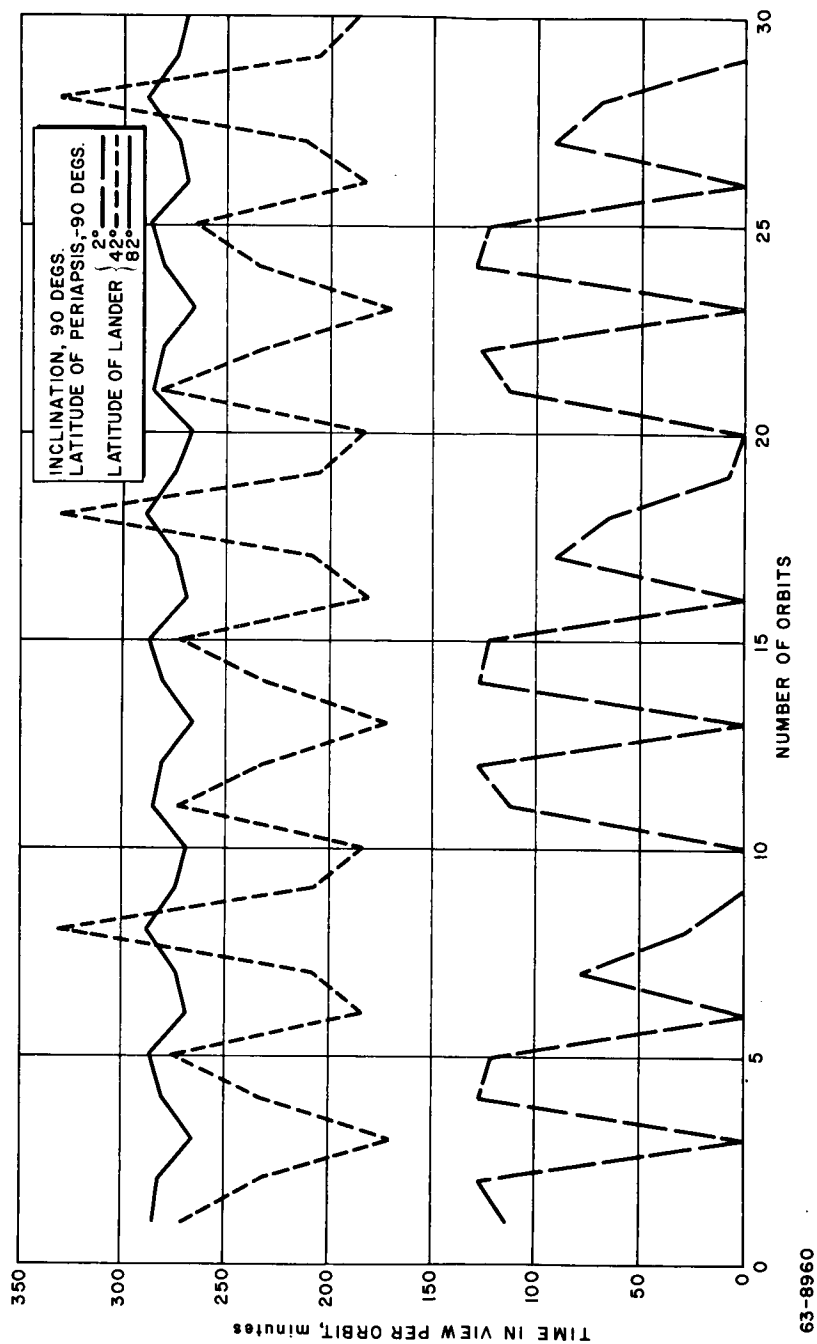
63-8956

-180-

Figure 78 ORBITER-LANDER COMMUNICATION INCLINATION 90 DEGREES,
LATITUDE OF PERIAPSIS 45 DEGREES, LATITUDE OF LANDER
2, 42, AND 82 DEGREES

63-8957

-181-

Figure 79 ORBITER-LANDER COMMUNICATION INCLINATION 90 DEGREES,
LATITUDE OF PERIAPSIS 0 DEGREES, LATITUDE OF LANDER
2, 42, AND 82 DEGREES

63-8958

Figure 80 ORBITER-LANDER COMMUNICATION INCLINATION 90 DEGREES,
LATITUDE OF PERIAPSIS –45 DEGREES, LATITUDE OF LANDER
2, 42, AND 82 DEGREES

63-8959

-183-

Figure 81 ORBITER-LANDER COMMUNICATION INCLINATION 90 DEGREES, LATITUDE OF PERIAPSIS -90 DEGREES, LATITUDE OF LANDER 2, 42, AND 82 DEGREES

63-8960

-184-
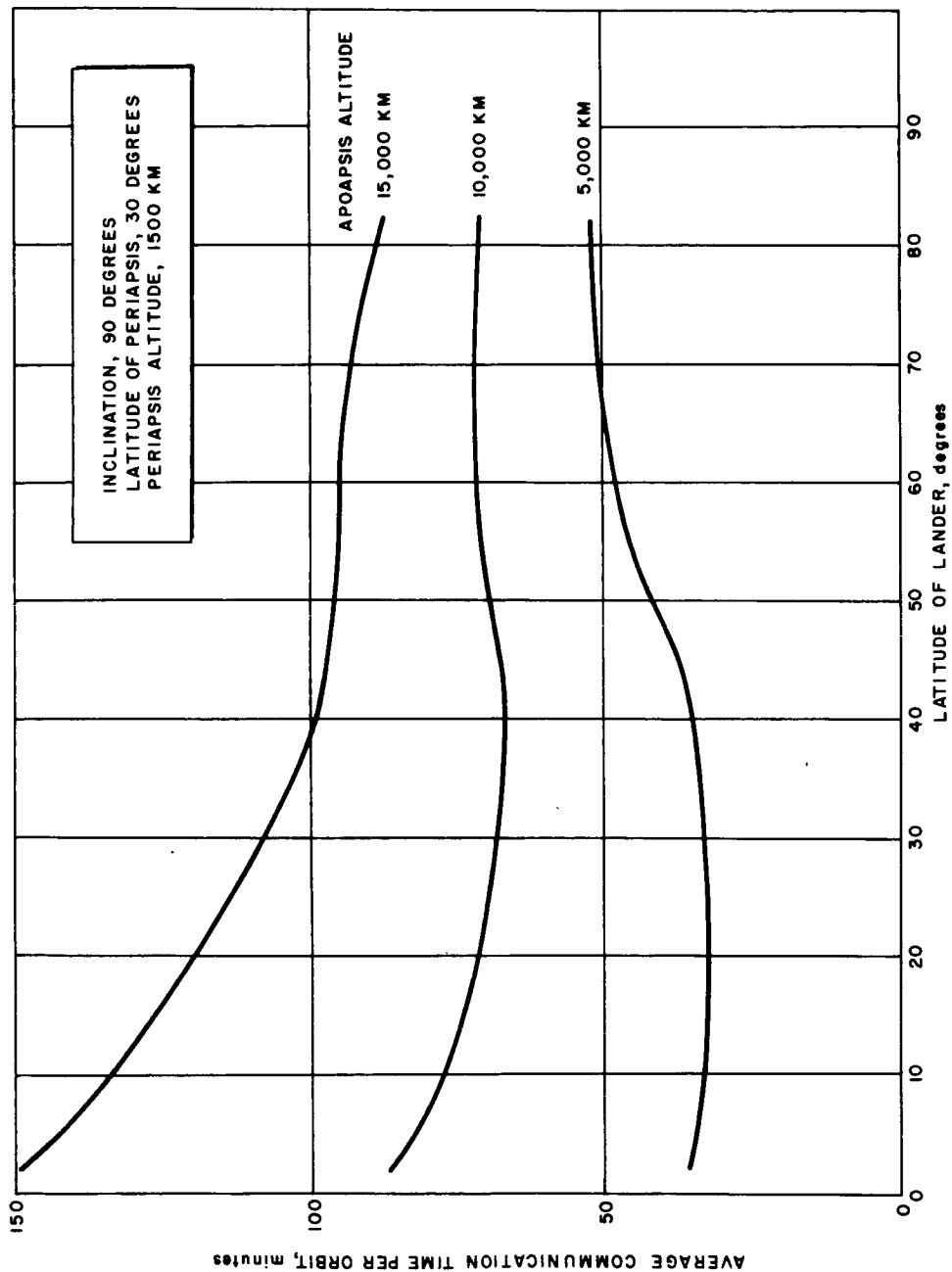
Figure 82 AVERAGE COMMUNICATION TIME PER ORBIT VERSUS LANDER LATITUDE
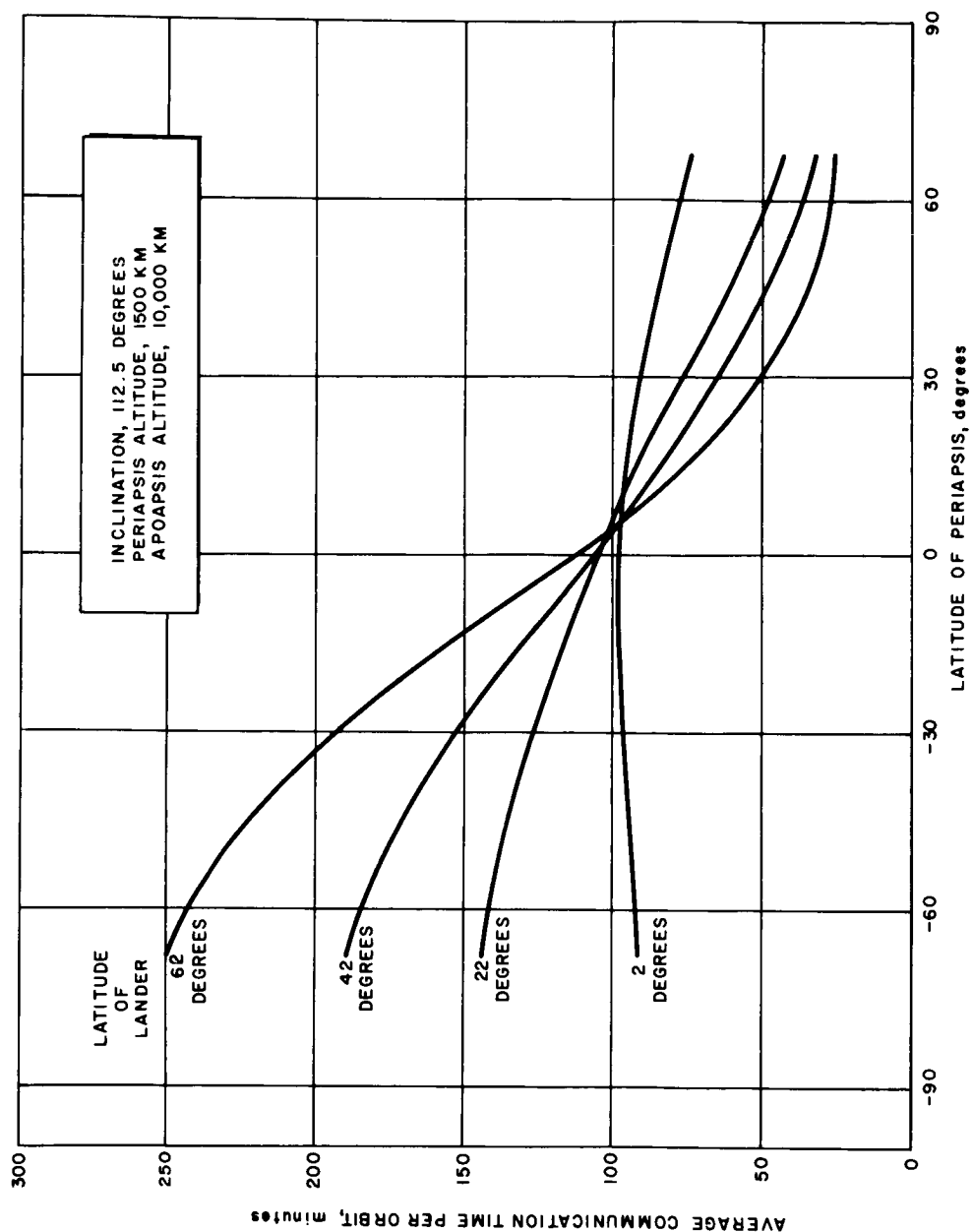
63-8946

-185-
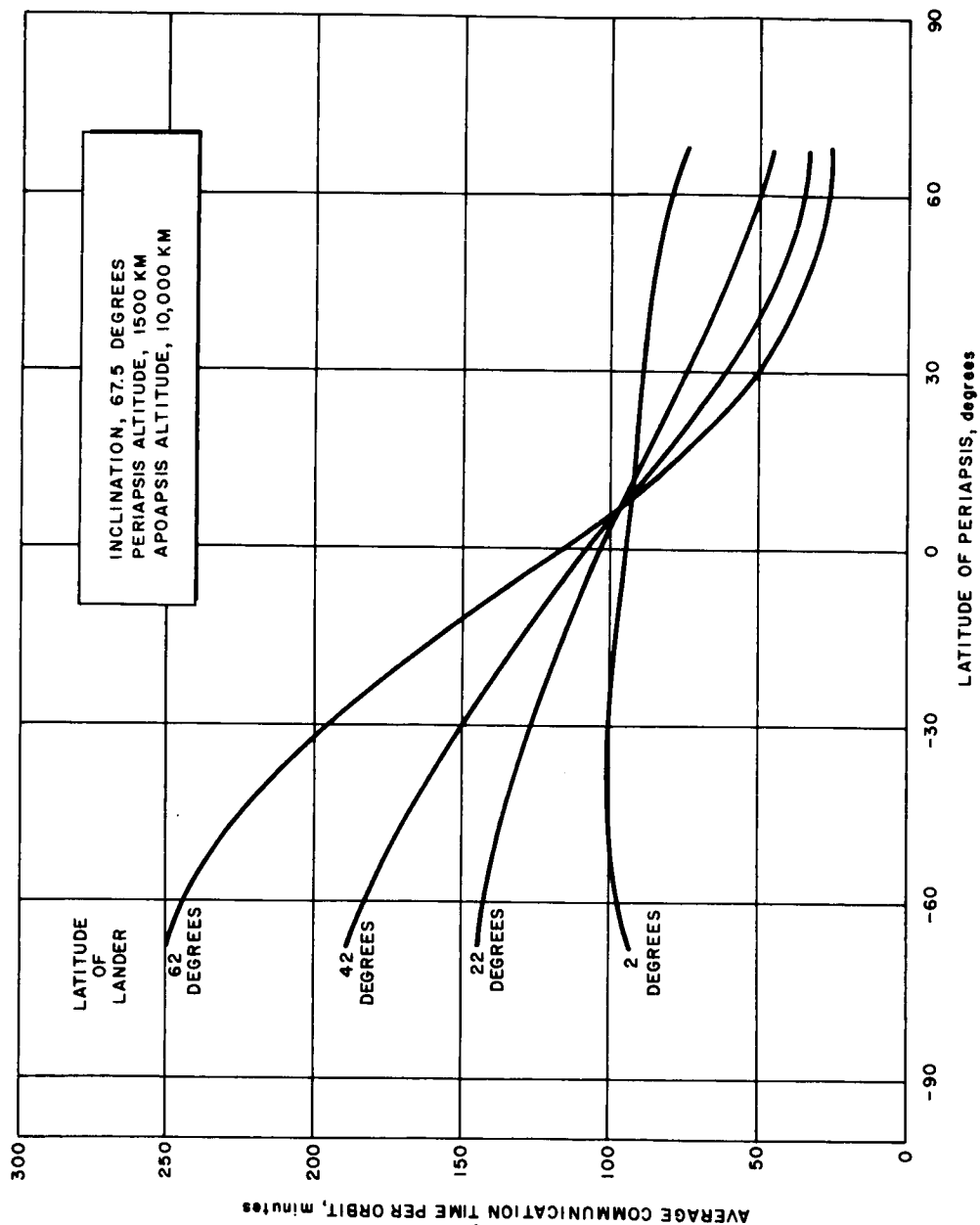
Figure 83 AVERAGE COMMUNICATION TIME PER ORBIT VERSUS PERIAPSIS
LOCATION, INCLINATION 67.5 DEGREES

63-8947

-186-
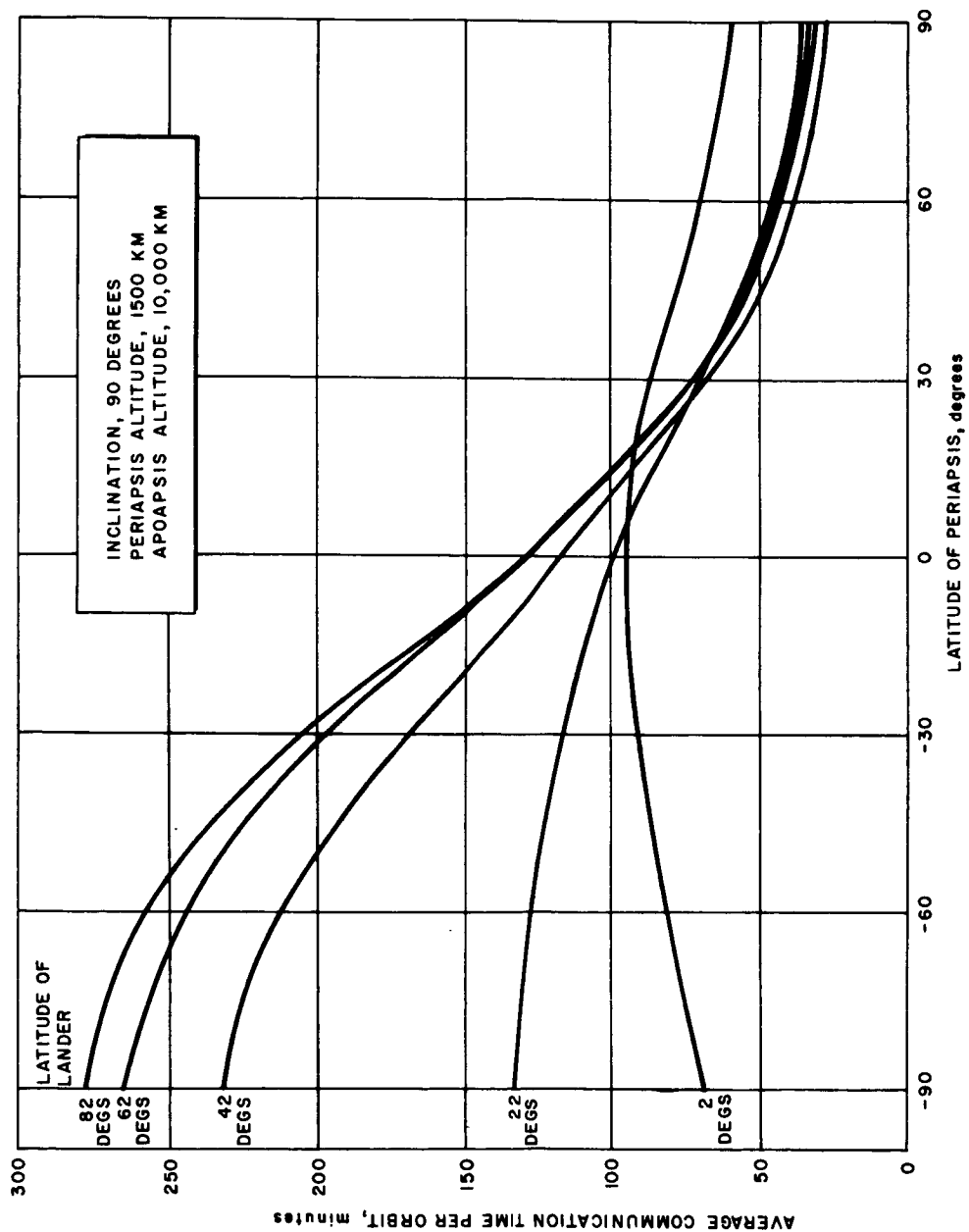
Figure 84 AVERAGE COMMUNICATION TIME PER ORBIT VERSUS PERIAPSIS LOCATION, INCLINATION 90 DEGREES

63-8948

-187-

Figure 85 AVERAGE COMMUNICATION TIME PER ORBIT VERSUS PERIAPSIS
LOCATION, INCLINATION 112.5 DEGREES

63-8949

-188-

This constraint leads to minimum altitudes of 1500 km for highly eccentric orbits and 1800 km for near circular orbits about Mars; and (b) The weight of propellant required for orbit injection is a strong function of the orbital eccentricity which makes circular orbits at any orbital altitude uneconomical with respect to weight.

The minimum altitude constraint is paramount in determining the best resolution that can be obtained from an orbital mapping system. Assuming that a mapping system characterized by an optical focal length of 2 meters with an imaging tube operated at a line density of 600 lines per inch represents a reasonable maximum in equipment capability, the highest resolution which could be obtained from an orbital altitude of 1500 km is approximately 40 meters. Although this represents an achievement 3 orders of magnitude better than the maximum capability from Earth while viewing at best planet oppositions, such a resolution would be inadequate for a low-risk manned landing. However, if the constraint of not sterilizing the orbiter is accepted, one orbital dimension (periapsis) is limited to the range between 1500 and 1800 km (neglecting injection inaccuracies).

The payload constraint affects the mapping task in two ways: (a) To obtain a reasonable map of the planet's surface, it is desirable to maintain a constant picture size along a longitudinal strip. For noncircular orbits, the picture size would vary linearly with altitude, and consequently variation of the optical system's characteristics as a function of altitude must be included, and (b) Regardless of the nature of the orbit with respect to viewing, it is necessary to transmit the data which are collected to Earth, and the weight penalty of achieving low eccentricity orbits would undoubtedly reduce the weight at which the collected data are transmitted.

In a weight versus scientific capability consideration for a spacecraft such as Voyager, there is, in general, a sharp break point below which data transmission and scientific capability is extremely small and above which a small percentage increase in weight makes a gross increase in scientific data collection capability. Due to the difficulties associated with highly accurate weight predictions in a conceptual design, it is extremely important that the conservative approach be taken. For this reason, an orbit with high eccentricity was selected for synthesizing the mapping and communications subsystems.

2. Factors influencing orbit selection.

a. Mapping resolution. For a nondiffraction-limited optical system, the surface resolution R is

$$R = \frac{h}{dF}$$

where

d = imaging tube line density

F = focal length

h = altitude.

Figure 86 is a plot of resolution versus altitude with focal length as a
parameter for a system using a line density of 600 lines per inch. One can
see that at the minimum altitude allowed for a nonsterilized orbiter and for
a focal length of 2 meters, the maximum resolution is 37.5 meters. If
preparation for a manned landing required an order of magnitude improve-
ment, clearly a much lower orbital altitude coupled with more cumbersome
optics would be required. Increasing line density may be considered to be
an alternative, but the amplitude response of present-day imaging systems
is marginal for line densities in excess of 600; and extending this limit would
result in "poor quality, high resolution" pictures of questionable value. The
sterilization constraints therefore tend to make the resolution consideration
an academic one. In this regard, we select the lowest altitude which is
allowed and design the mapping system to provide maximum capability.

b. Communications. Orbit selection has an effect on the data trans-
mission problem in two areas, the first resulting from the fact that the weight
available for communications diminishes with diminishing eccentricity, the
second being the effect of orbit parameters on the relay link performance.

Assuming that the weight saved in propulsion is used to increase data
transmission rates, figure 87 presents relative data transmission capability
as a function of apoapsis. This curve illustrates the acute sensitivity of
bit rate to estimates of orbiter weights. To ensure even modest communica-
tion capabilities, it is necessary in the conceptual design phase to select an
orbit which would not be critically affected by an increase in structural weight,
propulsion system specific impulse or mass fraction, and booster payload
capability.

In the selection of an orbit for relay communications, it is desirable to
have a high frequency of passes where communications can take place; and
further to have the duration of these intercepts as long as possible. Tables
39 and 40 represent the results of an analysis on the ability of a polar orbiter
to see the Mars lander for three representative orbits. Figure 88 presents
the average frequency of intercept versus apoapsis, and figure 89 presents
the time in hours to collect 10^8 bits from the lander as a function of apoapsis
altitude. The obvious result is, of course, that the low eccentricity orbits
require less time for lander data collection. If, however, the weight saved
in propulsion by accepting a high eccentricity were applied to the lander for

communications, the picture would change radically. If only 10 percent of the difference in orbiter weight for 1800 km circular and 1700 by 10,000 km orbits were used for lander communications, the time to playout would be less for the highly eccentric orbit.

c. Time to map. An important consideration in the mapping task is the total time required to map the planet. A computer program was written to obtain the total mapped area as a function of time for various orbits. It was found, however, when taking redundancy into account that the nonredundant mapping time was an extremely sensitive function of the orbital period and hence any attempts at producing a particular orbit within the precision of orbit injection will result in a large number of possible mapping life times for any set maximum tolerable redundancy. To illustrate this fact, figure 90 shows a plot of areas mapped versus time for various apoapsis altitudes with a constant 1500-km periapsis altitude. In the first 24 hours, all mapping is essentially nonredundant for all but equatorial orbits. Beyond this time, there is a finite probability that some mapping passes will overlap a large part of some previous mapping pass, thus introducing a great amount of re-dundancy. There is also a finite probability that the first overlapping pass may occur some large number of orbits later, and hence the nonredundant area mapped follows the extension of the pre-24-hour line for many days or weeks. On the average, the nonredundant area will certainly lie between the limits of the dotted extension line and the value of area mapped at 24 hours.

This phenomenon was thoroughly investigated by considering the sensi-tivity of the function $(n\theta)$ modulus 360 where θ is the angle between successive equator crossings for orbits of various size and inclination. The item of interest is the number "n" such the the nth mapping pass overlaps some fixed amount of the first pass.

Figure 91 shows how the number "n" varies as a function of the angle θ for a 1 degree nonoverlapping picture. The range of the angle θ in this figure roughly represents a range of orbital semimajor axes from 9076 to 9100 km.

Figure 92 is an expansion of the graph of figure 86 between $\theta = 107.18$ and 107.19. It can be seen from these figures that the number of nonredundant mapping passes varies in almost random fashion over the relatively small perturbation in orbit size and/or inclination.

Since the number of picture elements transmitted as a function of time is the important consideration rather than the area covered as a function of time and since the number of picture elements transmitted per unit time is determined by the average bit rate, the fact that circular orbits sweep out surface areas faster than elliptical orbits is of little consequence.

d. <u>Orbital periapsis location for successful mapping.</u> Having selected a 1700 by 10,000 km orbit, an evaluation of the possible orbital periapsis locations and precession was performed and is reported in appendix 6. The study showed that all desirable orbits (near polar) had initial periapsis locations over the planet's sunlit region. However, the periapsis point quickly precessed onto the dark side of the planet. This result favored a mapping system with two optical systems, one for mapping in the region of periapsis when it is in the sunlit region, and one for mapping in the region of apoapsis when it is elsewhere in the sunlit region. The reference mapping system design follows this technique and is described more fully in another volume.

e. <u>Conclusions.</u> The conclusion arrived at after considering the various factors involved in orbit selection is that the risk involved with basing subsystem designs, such as the mapping subsystem and the communications system, on the assumption that sufficient weight will be available to achieve a circular orbit is too great. Since the designs which result from assuming a highly eccentric orbit are more general, and consequently more flexible, in capability, modifying them to allow adaptation for circular orbits will result in a reduction of complexity. In addition, the performance of the mapping subsystem is dictated primarily by the lowest altitude achievable, rather than the eccentricity of the orbit; and the rate at which information can be collected is favored by highly eccentric orbits.
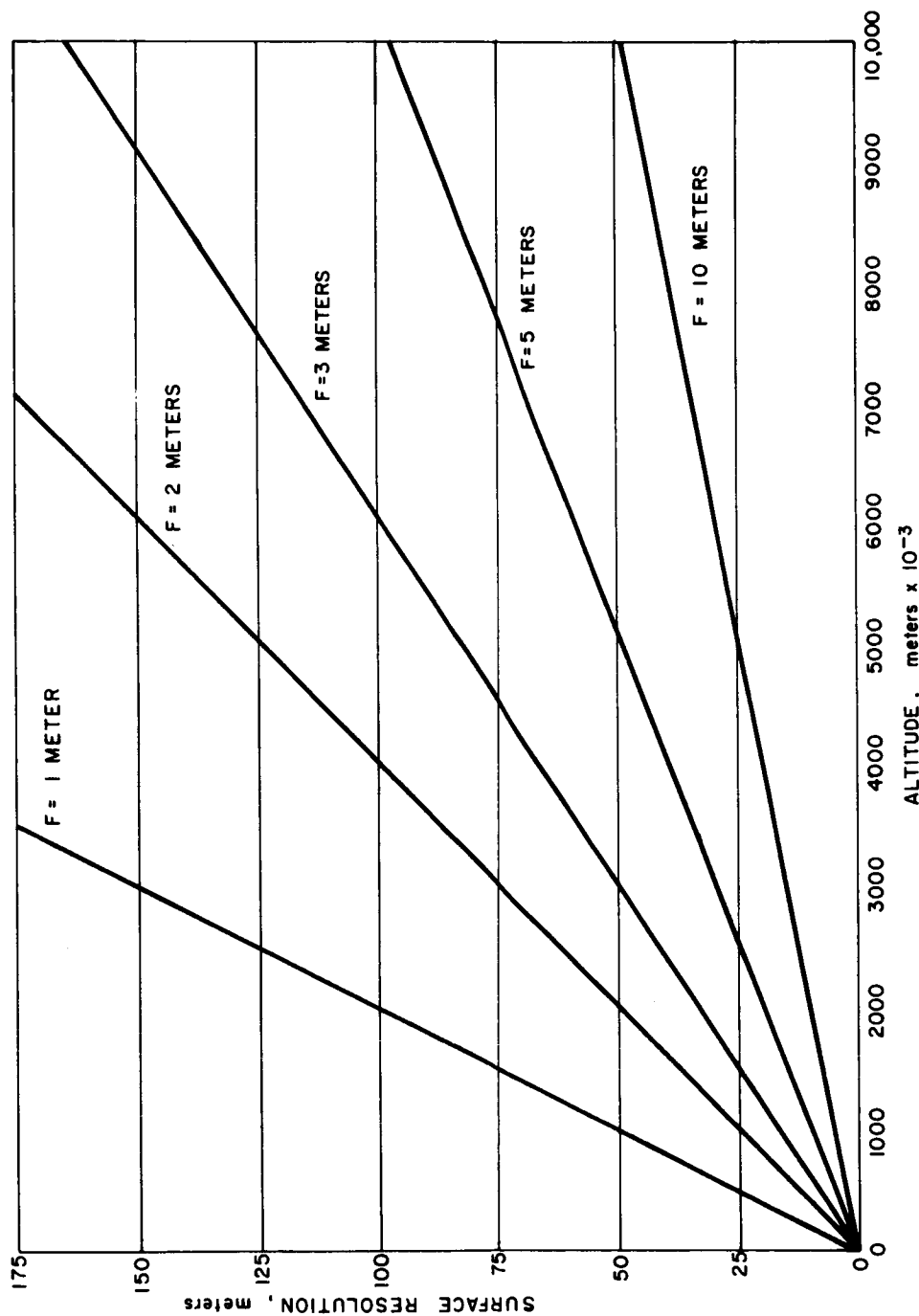
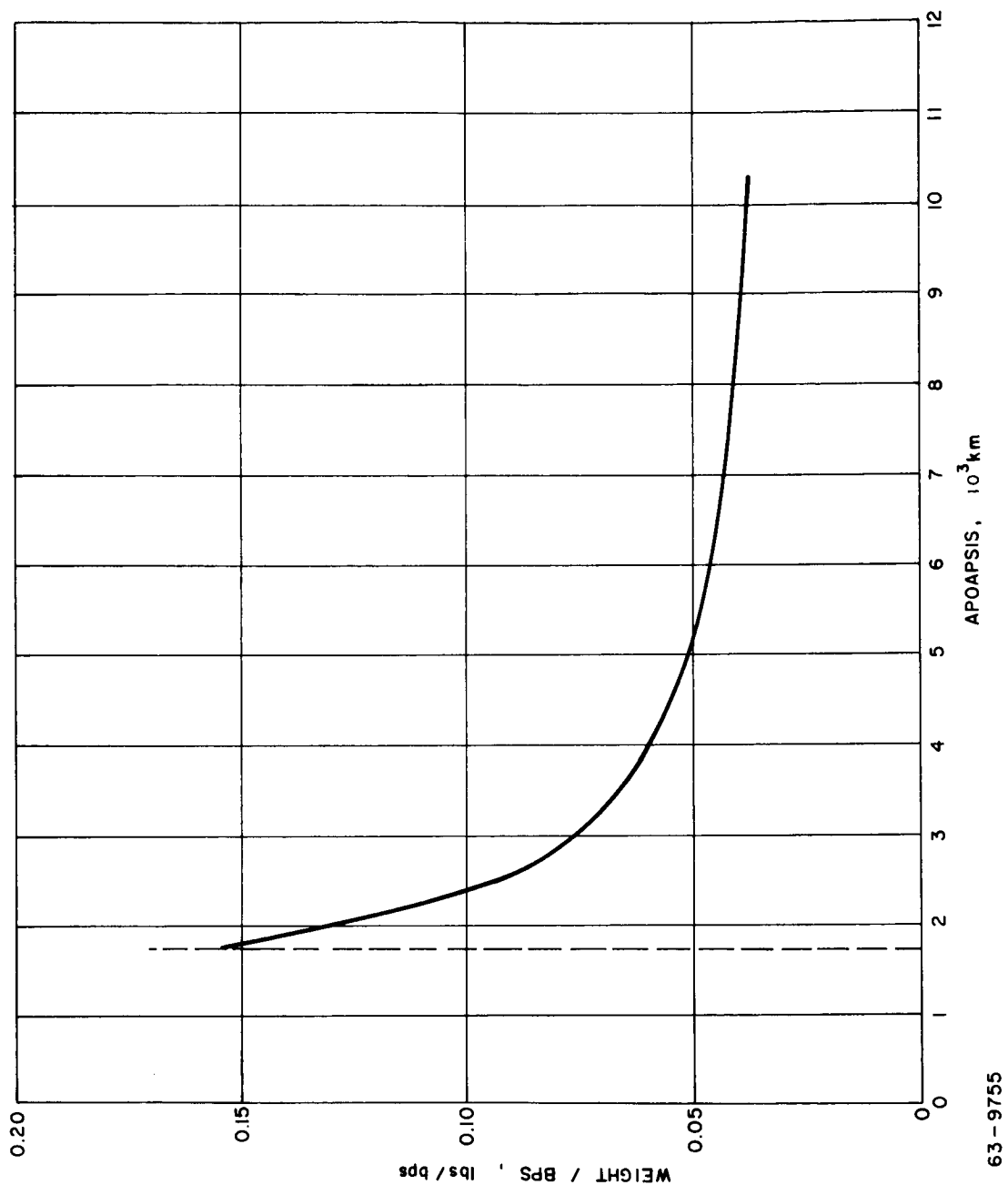Figure 86 SURFACE RESOLUTION VERSUS ALTITUDE, IMAGING TUBE LINE; DENSITY = 600 LINES/INCH

63-9754

-193-

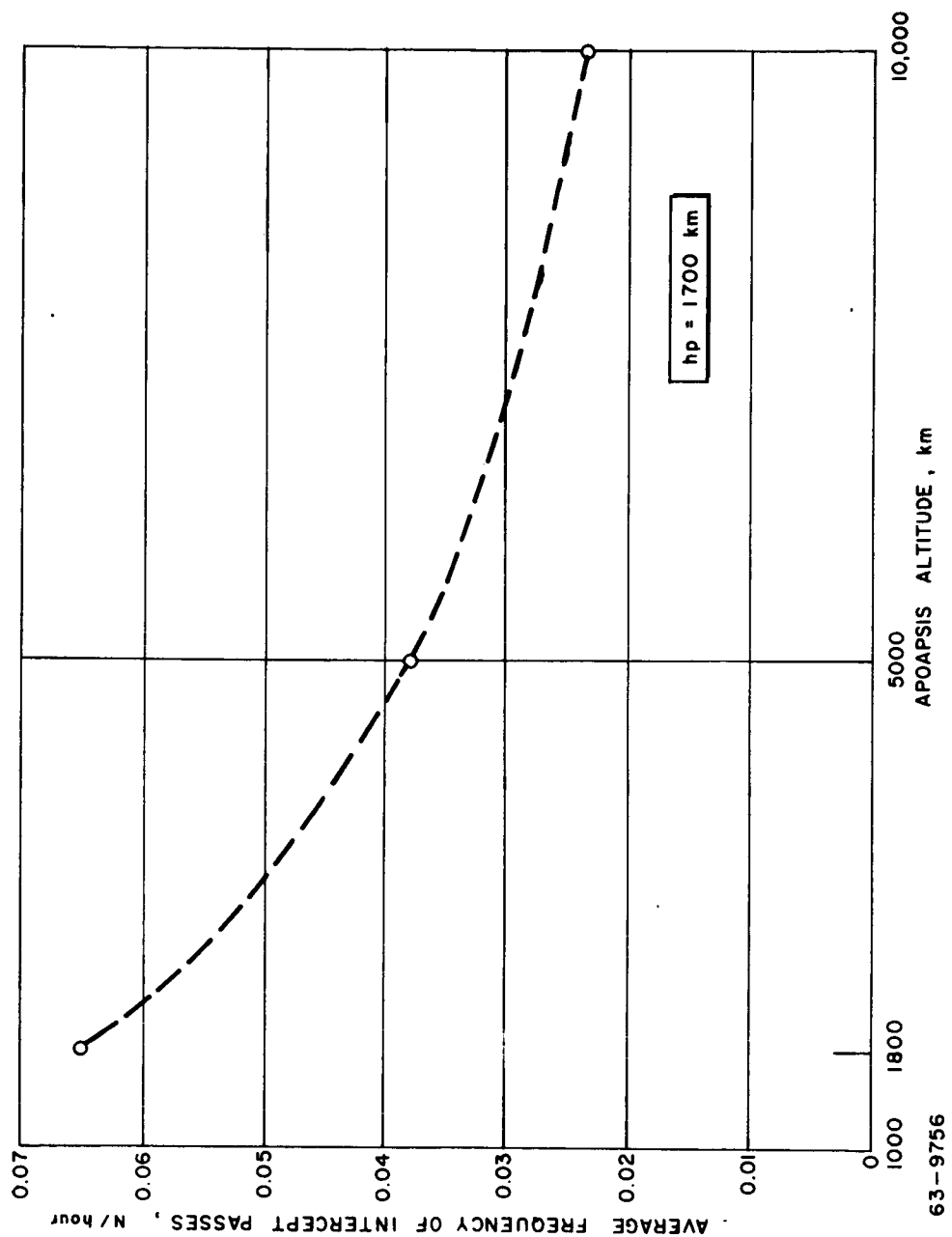Figure 87 ORBITER WEIGHT PER BPS VERSUS APOAPSIS FOR MARS 1969 II WITH 1800-POUND LANDER, $h_p = 1700$ KM

63-9755

-194-

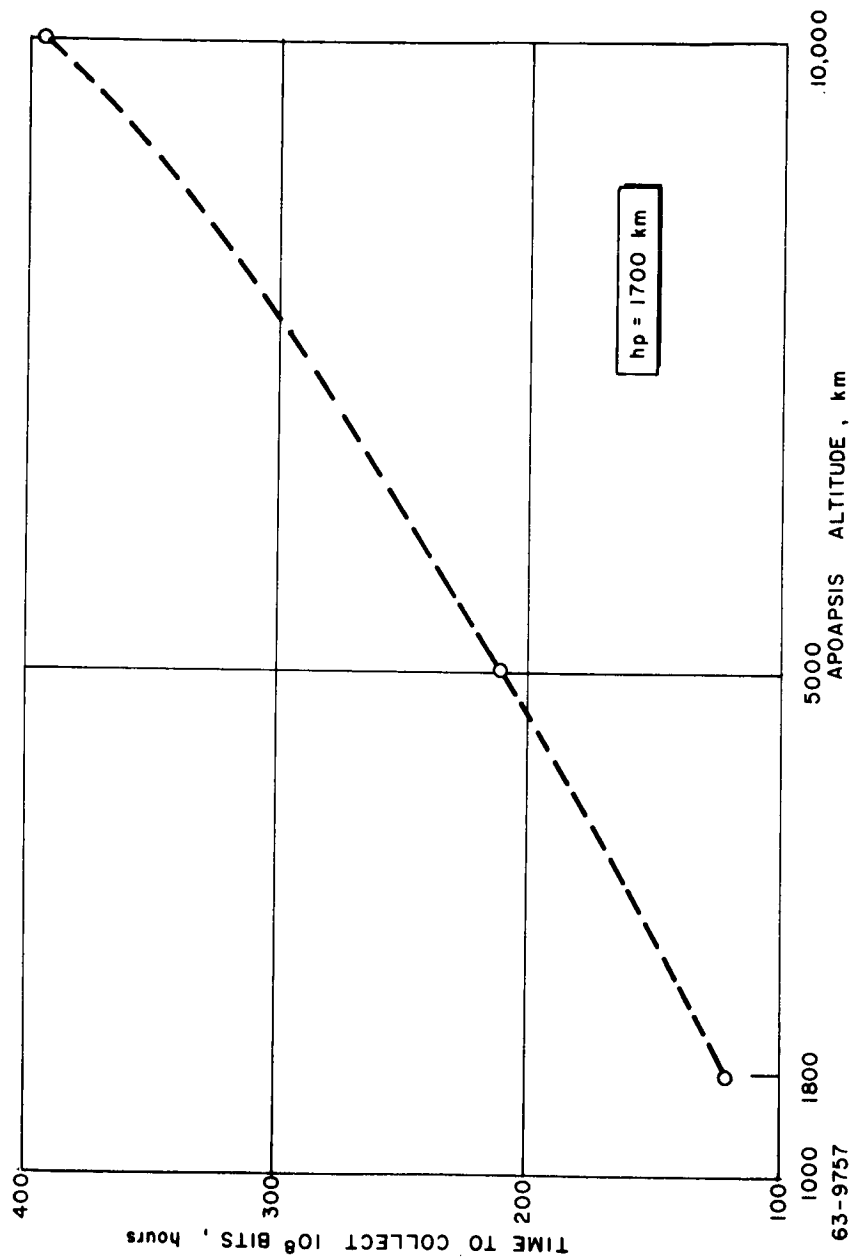Figure 88 AVERAGE FREQUENCY OF ORBITER-LANDER COMMUNICATIONS INTERCEPTS VERSUS APOAPSIS ALTITUDE $h_p = 1700$ KM

63-9756

Figure 89 TIME REQUIRED TO COLLECT 10^8 BITS OF INFORMATION FROM THE LANDER
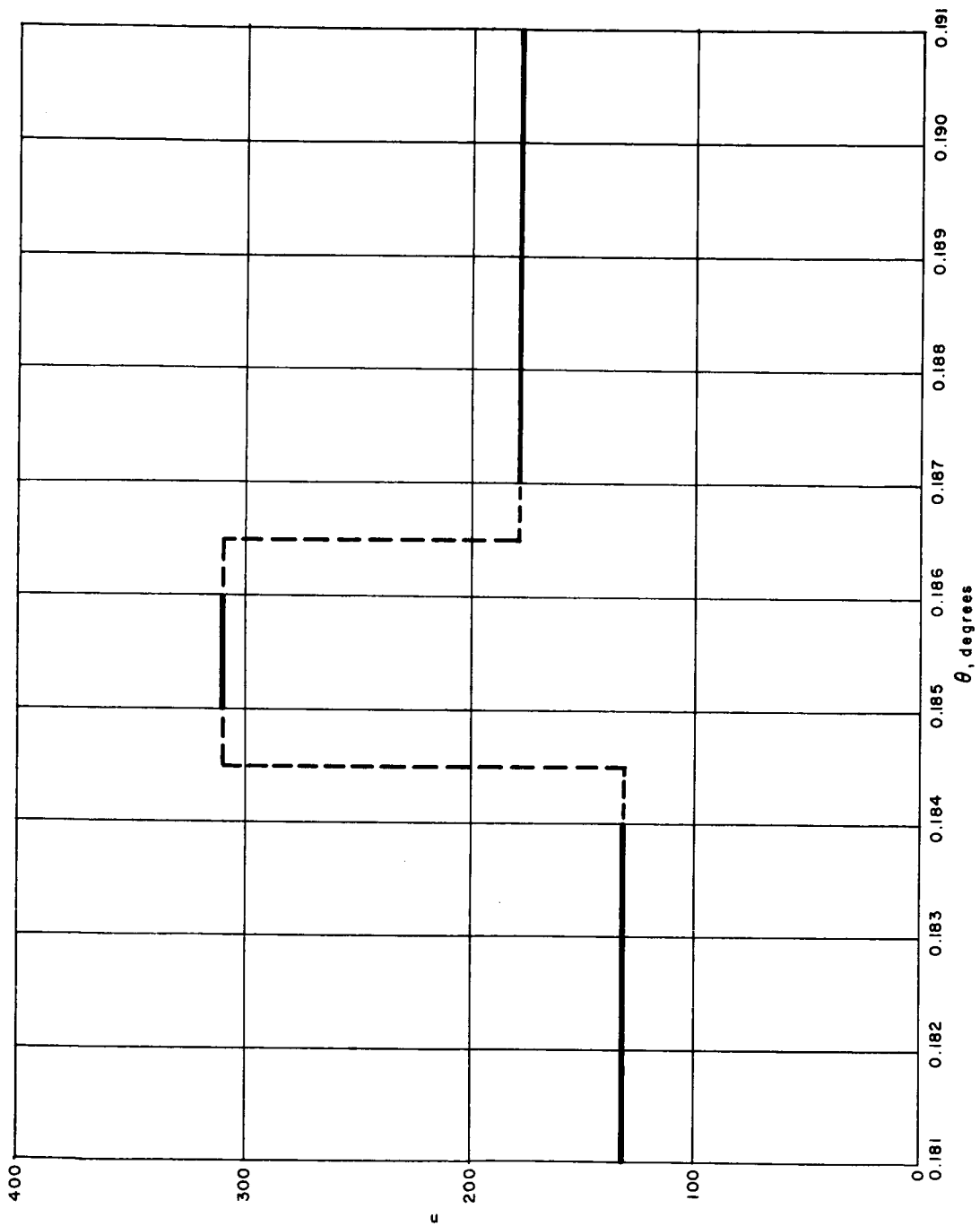VIA ORBITER RELAY VERSUS APOAPSIS ALTITUDE, $h_p = 1700$ KM

63-9757

-196-

Figure 90 MARS AREA MAPPED AS A FUNCTION OF TIME

63-9760

Figure 91 NUMBER OF NONREDUNDANT ORBITS (n) AS A FUNCTION OF THE ANGLE
BETWEEN SUCCESSIVE EQUATOR CROSSING ( ) FOR A 1 DEGREE
NONOVERLAPPING PICTURE

63-9758

-198-
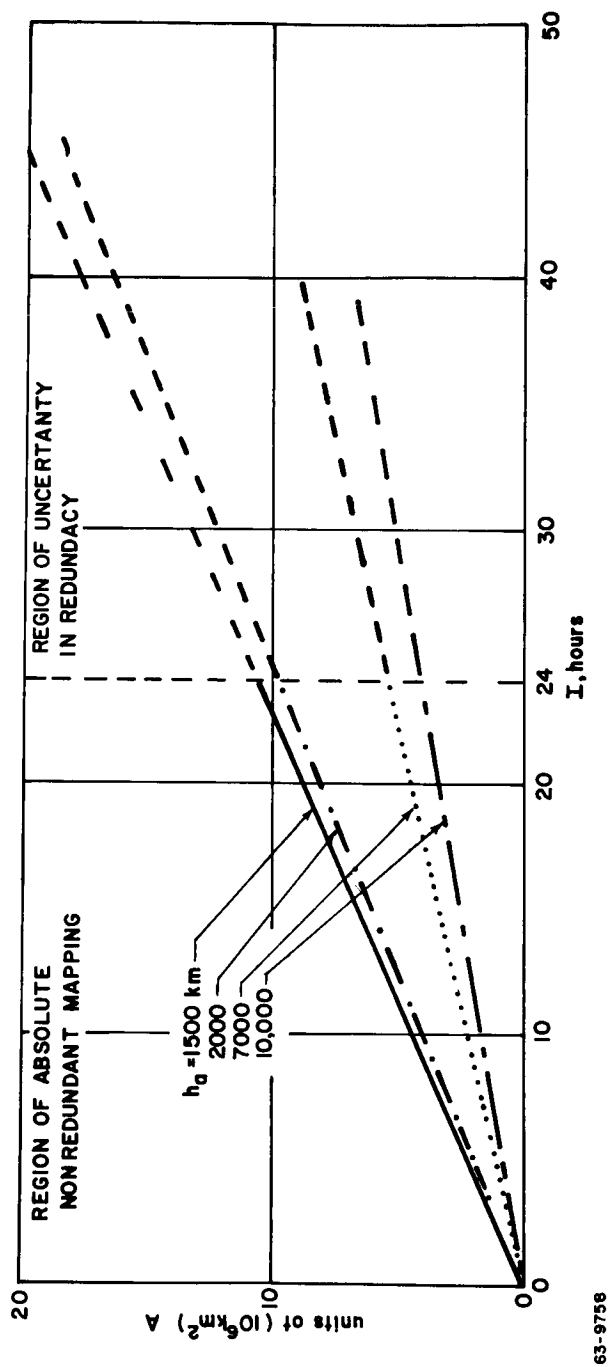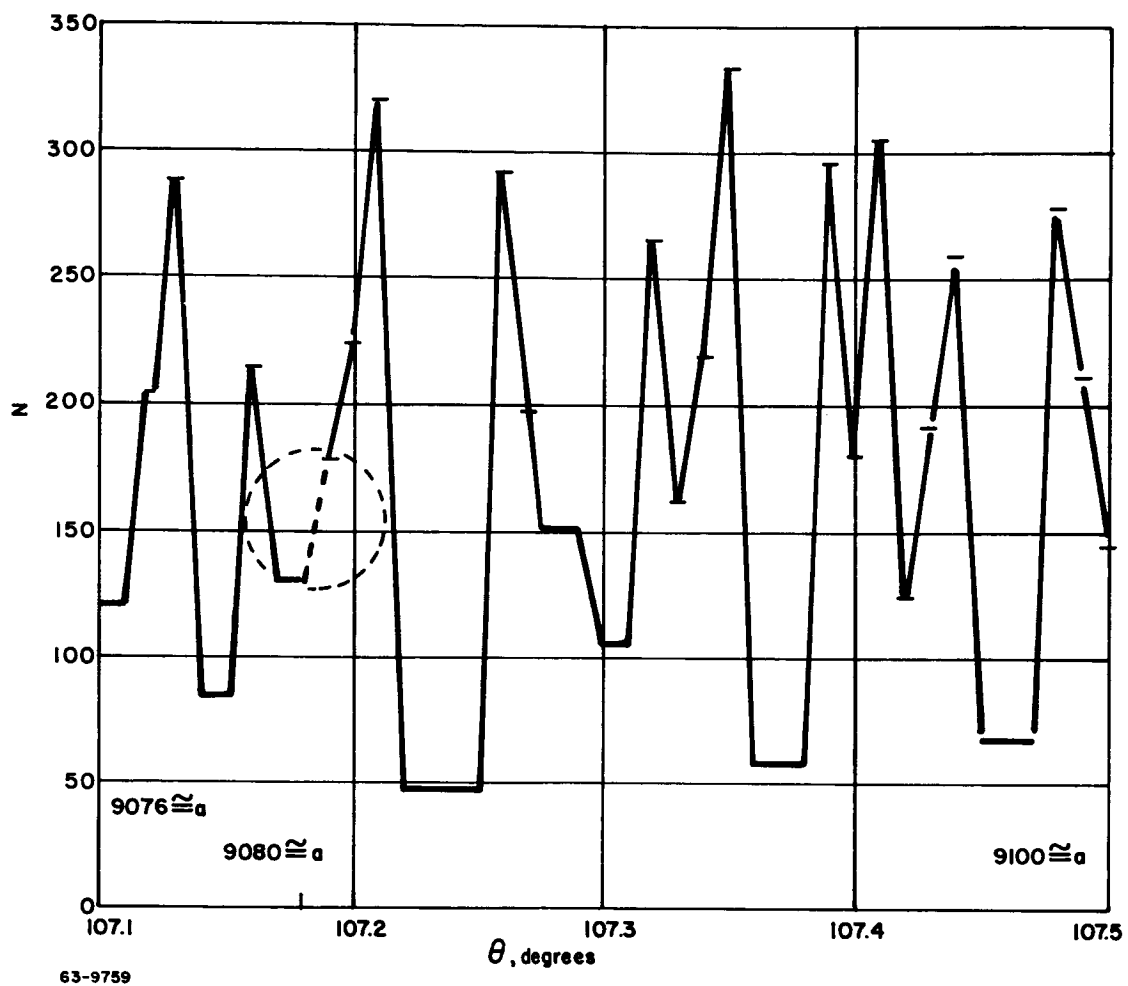
Figure 92 NUMBER OF NONREDUNDANT ORBITS (n) AS A FUNCTION OF THE ANGLE
BETWEEN SUCCESSIVE EQUATOR CROSSING ( ) FOR A 1 DEGREE
NONOVERLAPPING PICTURE OF A LIMITED RANGE

63-9759

TABLE 39

SAMPLE FREQUENCY OF ORBITER-LANDER
RELAY COMMUNICATIONS OPPORTUNITIES

Orbit	Communication Zone Planet Centered Angle (degrees)	Time In Orbit (hours)	Approximate Communication Time (minutes)
1,500 x 10,000 km orbit			
0	±30	0	22
10	±30	73	21
17	±30	125	15
20	±30	147	18
27	±30	198	20
30	±30	220	13
37	±30	271	22
47	±30	345	22
1,500 x 5,000 km orbit			
0	±30	0	25.4
6	±30	27.1	23
12	±30	54.2	19
23	±30	104	19.5
29	±30	131	24
35	±30	158	25
41	±30	185	23
1,800 km circular orbit			
0	±30	0	31
8	±30	25	30.5
16	±30	50	30
24	±30	75	27
31	±30	96	13
32	±30	100	25
39	±30	121	19.5
40	±30	124	21

TABLE 40

PROBABILITY P (N) OF COMMUNICATING WITHIN N ORBITS FOR THREE SAMPLE POLAR ORBITS

1,500 x 10,000 km orbit		
N	P(N)	Days After N = 0
0	0.14	1
1	0.31	1
2	0.47	1
3	0.56	1
4	0.67	2
5	0.78	2
6	0.92	2
7	0.94	3
8	0.97	3
9	1.0	3

1,500 x 5,000 km Orbit	
N	P(N)
0	0.17
1	0.34
2	0.51
3	0.68
4	0.86
5	1.0

1,800 km Circular Orbit	
N	P(N)
0	0.17
1	0.29
3	0.42
4	0.67
5	0.80
6	0.90
7	1.0

6. SYSTEMS ANALYSIS DURING PLANETARY ENCOUNTER

This section discusses the lander-to-orbiter communication relay requirements at planet encounter and the selection of separation and entry parameters for optimizing vehicle payloads and minimizing lander dispersion. System tradeoffs involving the effects of separation range, approach velocity, and entry angle on payloads, dispersion and transmitter characteristics are studied. The geometry of the lander-orbiter communication link during data transmission determines the requirements for lander lead time, lander transmitter range, antenna pattern, and orbiter-receiving-antenna look angle. The relay geometry also imposes constraints on the selection of landing sites. System studies also considered the tradeoffs between alternate methods of obtaining lander lead time. Unless otherwise noted, the analysis is based on a Mars mission.

6.1 Lander-Orbiter Communication Relay Geometry

1. Communication system requirements. Engineering and scientific measurements made by instruments on the lander during atmospheric entry and descent are recorded for later playback. These data are transmitted to the orbiter relay during a 10-minute period centered on planet impact. To obtain the necessary 10-minute communication time, the lander must reach the planet ahead of the orbiter, placing the orbiter within the lander antenna beam during the communication period. The zone of possible lander-to-orbiter communication must be large enough to encompass all trajectory uncertainties.

The major uncertainty is the lander descent time which taken over the large variety of postulated Martian atmospheres was found to vary by approximately 10 minutes including the uncertainty resulting from dispersion in the lander impact point. The error contribution due to uncertainty in orbiter position was found to be negligible. The orbiter must remain within the lander antenna pattern for at least 20 minutes to ensure sufficient communication time. To meet this condition, the orbiter position (point A in figure 93) at start of data transmission must be 20 minutes from the point at which the trailing edge of the lander antenna beam intersects the orbiter trajectory, assuming a minimum descent time. If the descent time is at its maximum value, data transmission will start when the orbiter is 10 minutes from the trailing edge of the beam (point B in figure 93). The orbiter position at start of transmission; the determines the required lander lead time. The required transmitter range is the distance from the farthest dispersion limit of the lander impact point (point D) to point A.

Figure 94 shows the geometry of the communication relay at the start of lander transmission for a typical case (approach velocity $V_\infty = 4$ km/sec). The lines emanating from each impact point represent the trailing edge of the

transmitter's 120-degree pattern. Except for the point related to γ_E = 45 degrees where the 3-sigma dispersion is included, nominal impact points are shown. The numbers along the orbiter approach trajectory represent time in minutes from periapsis. The effect of entry angle on impact point and consequent communication geometry is shown. The antenna pattern associated with large entry angles and related impact points is directed further backward along the orbiter trajectory than that for small angles. As a result, there is more communication time available at the steeper entry angles. However, the required transmitter range increases. At the shallower entry angles, a smaller section of the trajectory is subtended by the lander antenna pattern and the required antenna beamwidth increases, limited only by the horizon. Because of receiver noise problems, the beam should be elevated at least 10 degrees above the horizon, limiting the maximum beamwidth to about 160 degrees. Because of beamwidth limitation, there is insufficient communication time available for entry angles less than 25 degrees with approach velocities greater than 4 km/sec.

An additional constraint, most significant at the smaller entry angles, is the thrust phase for orbit injection occurring between 8 and 3 minutes before the periapsis of the approach trajectory. No communication from the orbiter to DSIF can be conducted during the thrust phase because the orbiter will be oriented for thrust application and the Earth-directed antenna will be stowed. Data can still be transmitted from the lander to orbiter and stored during the thrust phase. After thrust termination, the orbiter will be reoriented for relay to Earth.

Figures 95 and 96 show the requirements for transmitter beamwidth and range as functions of asymptotic approach velocities and lander entry angle for lander-orbiter separation ranges of 10^6 km and 0.5×10^6 km, respectively. The transmitter range requirements decrease somewhat as the separation range is reduced, since a smaller lander dispersion is experienced at 0.5×10^6 km separation range, based on the assumption that a terminal guidance system is employed. Without terminal guidance, there would be little or no difference between the two curves.

The results show that a lander transmission range of 15,000 km with a beamwidth of 120 degrees will provide adequate communication for landing sites corresponding to entry angles of from 45 to 90 degrees and for approach velocities ranging from 3 to 6 km/sec. For entry angles between 30 and 45 degrees, a beamwidth up to 150 degrees is required. Since the transmission range required is smaller at shallow entry angles, the lower gain portions of the antenna pattern should effectively provide communication up to a 160-degree beamwidth. Communication is marginal below entry angles of 30 degrees where there is insufficient communication time at approach velocities of 4, 5, or 6 km/sec.
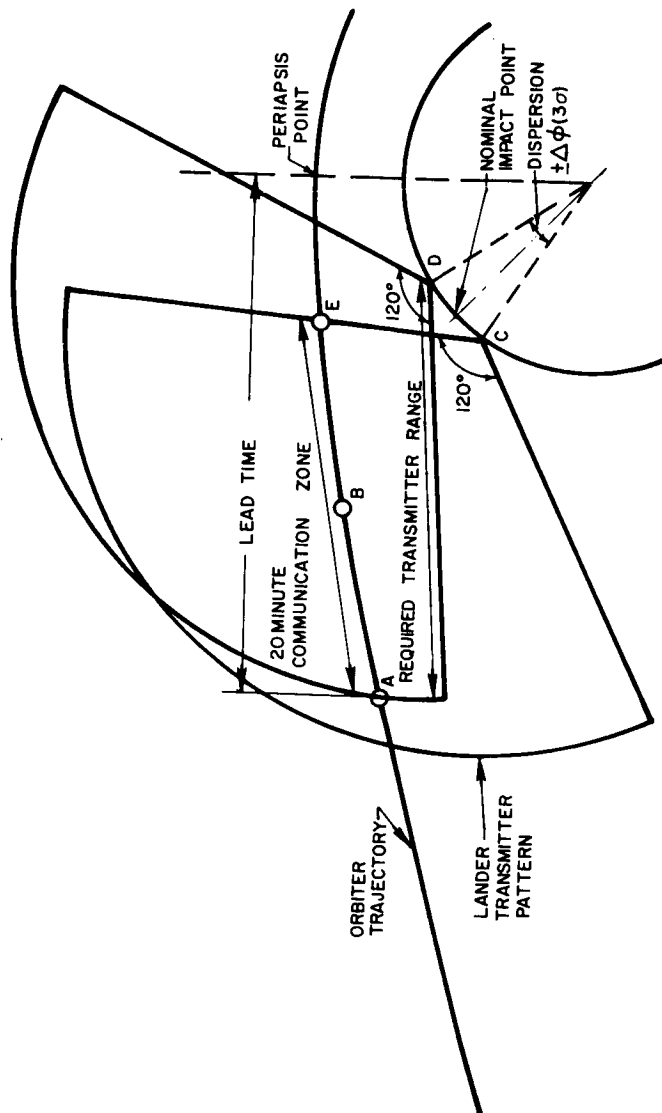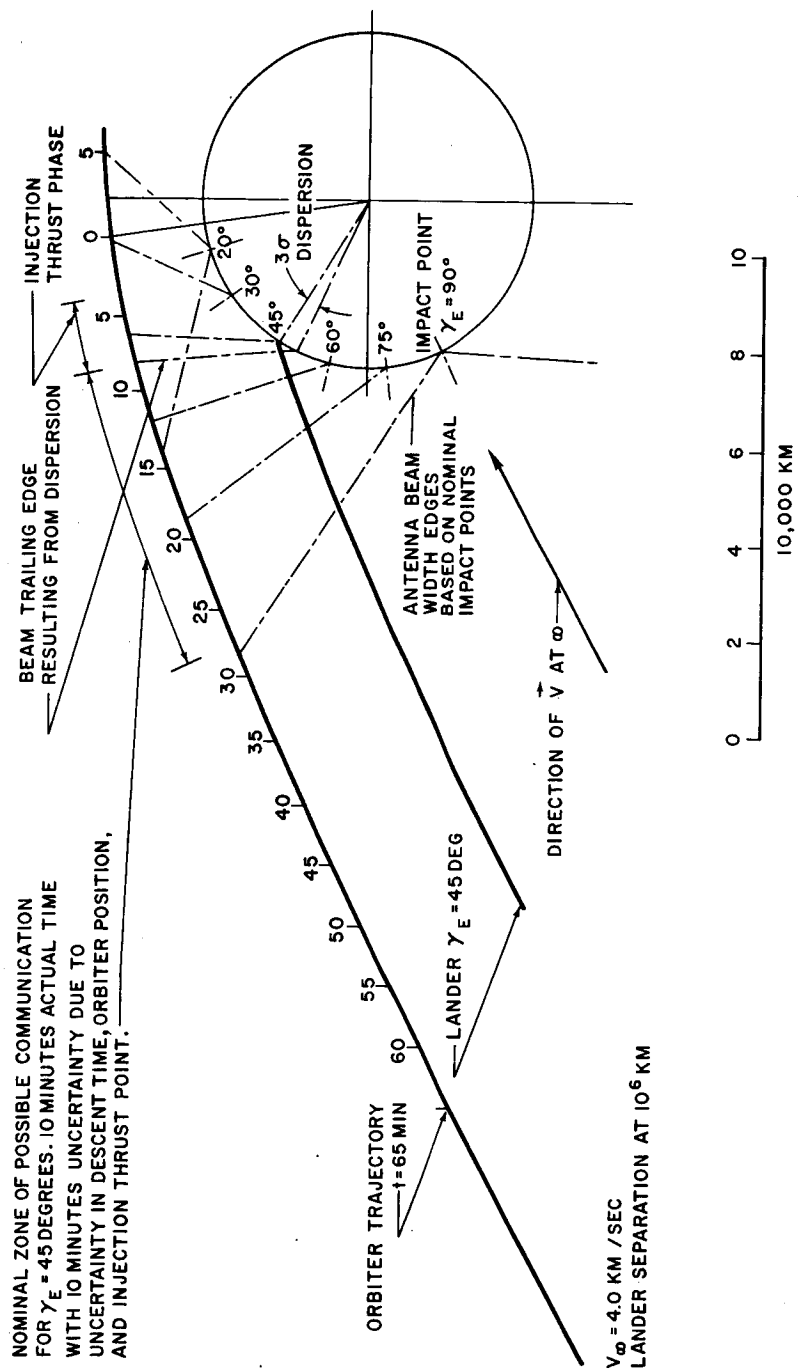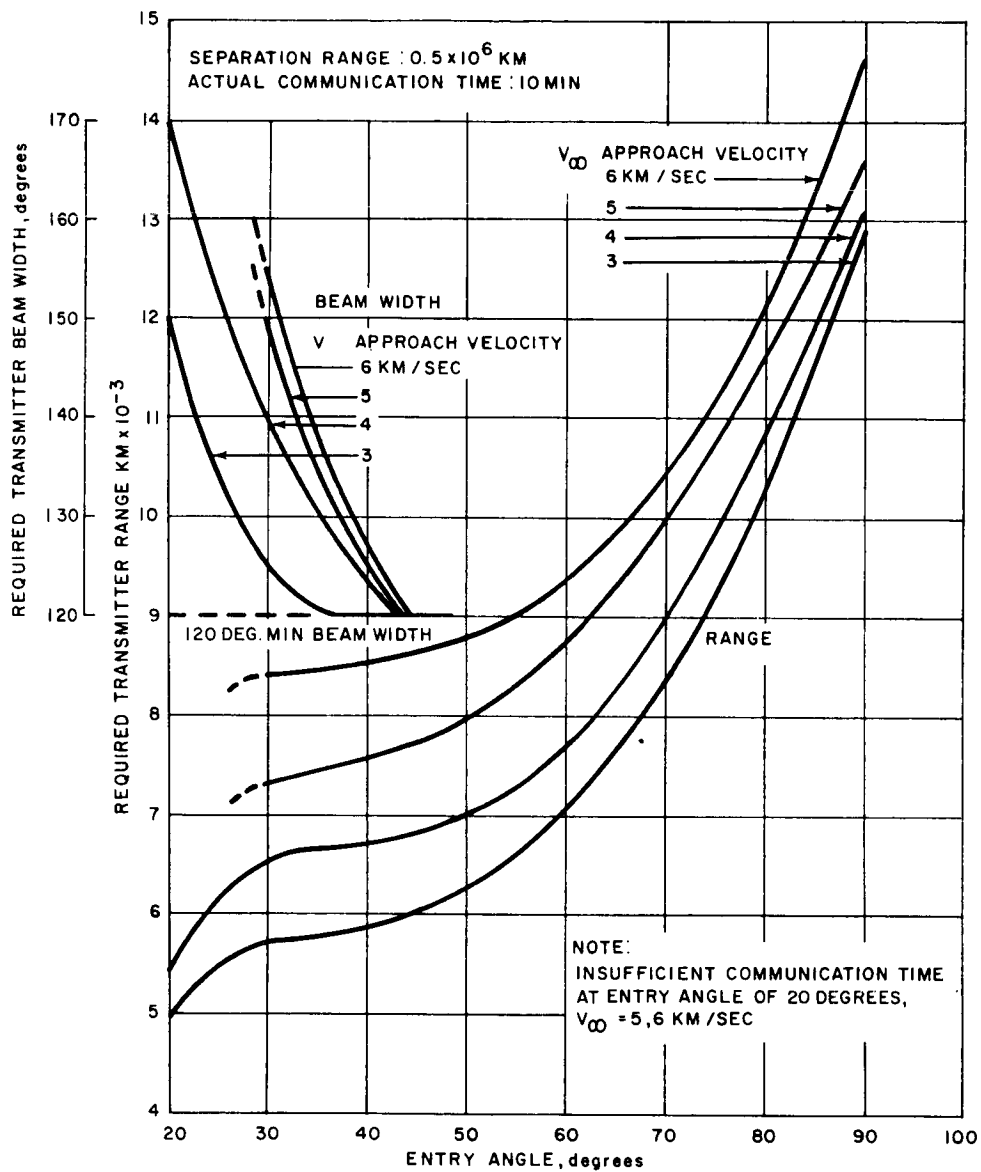
Figure 93 ORBITER-LANDER RELAY REQUIREMENTS

63-9146

NOMINAL ZONE OF POSSIBLE COMMUNICATION
FOR γ_E = 45 DEGREES. 10 MINUTES ACTUAL TIME
WITH 10 MINUTES UNCERTAINTY DUE TO
UNCERTAINTY IN DESCENT TIME, ORBITER POSITION,
AND INJECTION THRUST POINT.

BEAM TRAILING EDGE
RESULTING FROM DISPERSION

INJECTION
THRUST PHASE

DISPERSION

3σ

$20°$

$30°$

$45°$

$60°$

$75°$

IMPACT POINT
γ_E = 90°

ANTENNA BEAM
WIDTH EDGES
BASED ON NOMINAL
IMPACT POINTS

DIRECTION OF $\overrightarrow{V}$ AT ∞

ORBITER TRAJECTORY
t = 65 MIN

LANDER γ_E = 45 DEG

V_∞ = 4.0 KM /SEC
LANDER SEPARATION AT 10^6 KM

10,000 KM

Figure 94   ORBITER–LANDER RELAY GEOMETRY

63-9147

-205-

63-9148

Figure 95 LANDER TRANSMITTER REQUIREMENTS, SEPARATION
RANGE = 10^6 KM

-206-
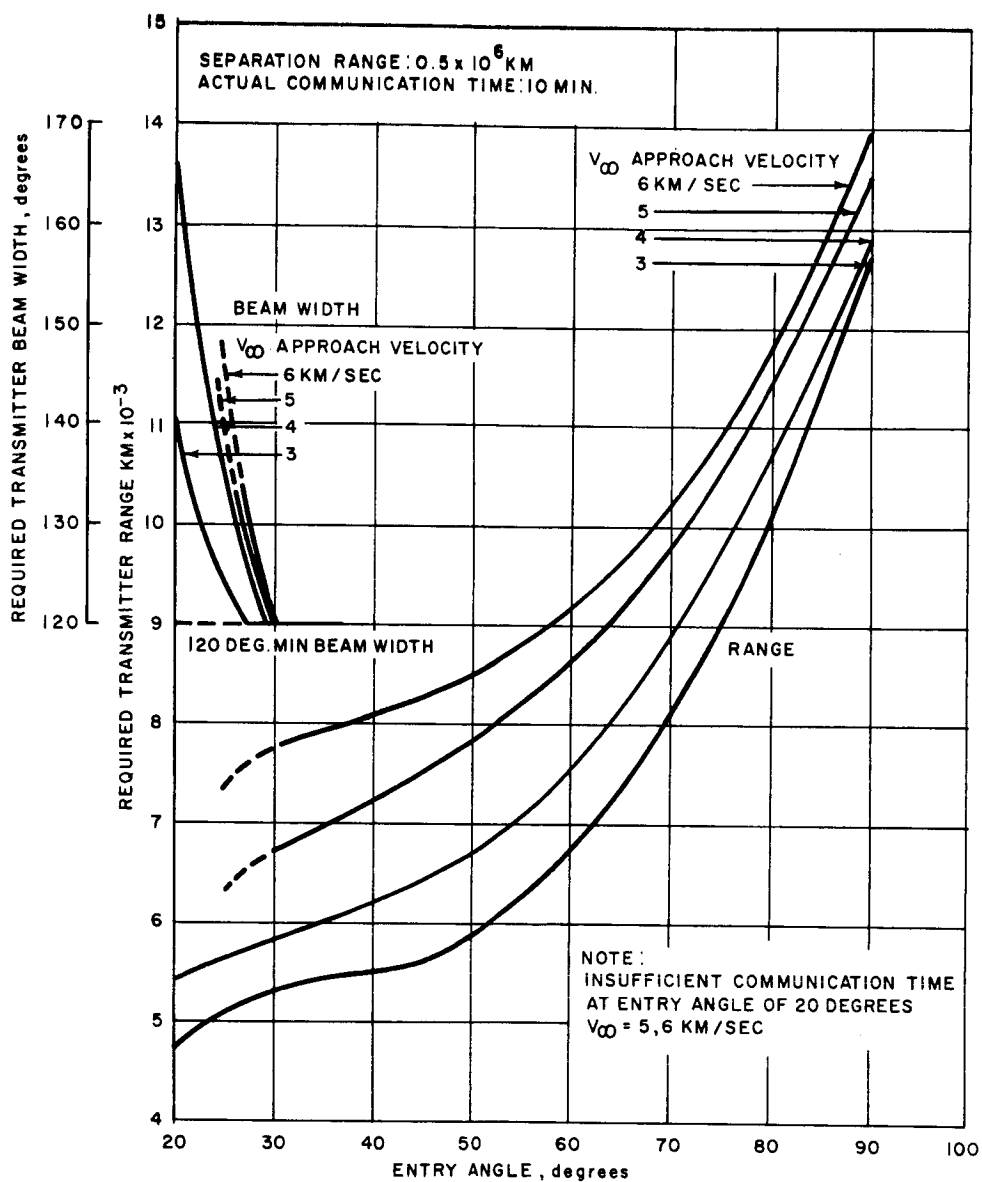
Figure 96 LANDER TRANSMITTER REQUIREMENTS, SEPARATION
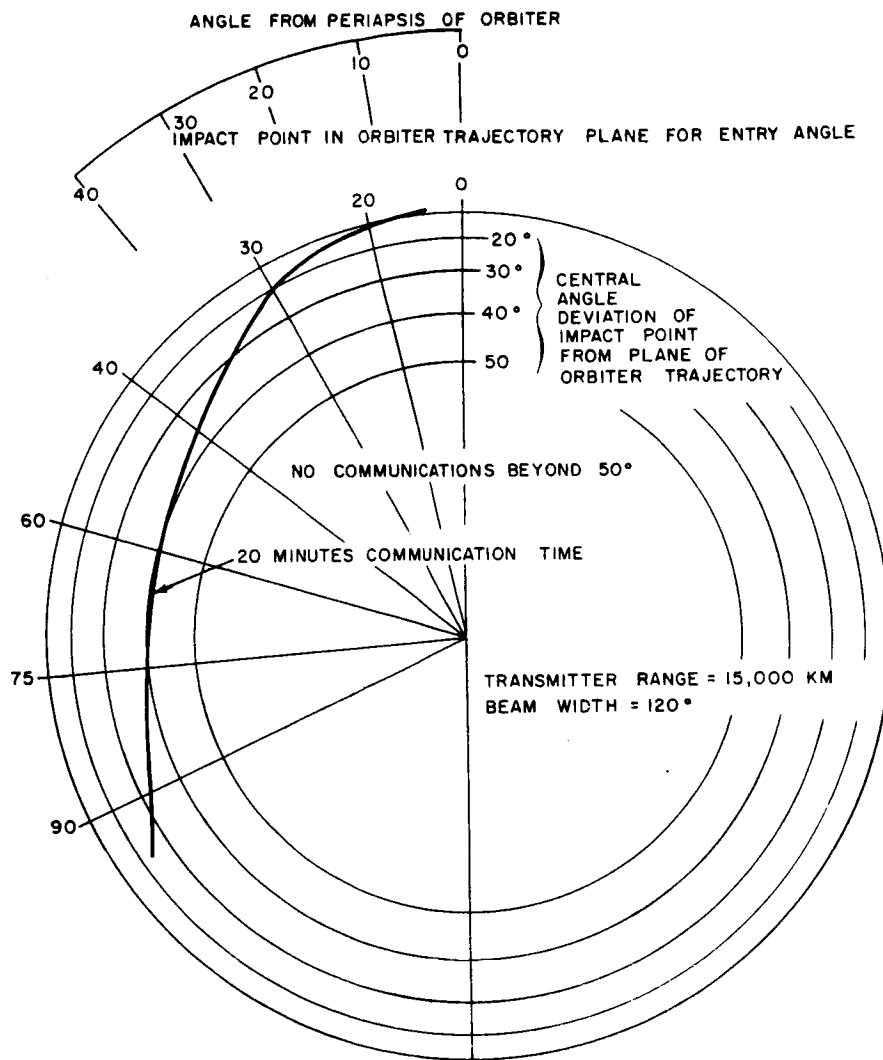RANGE = 0.5×10^6 KM

63-9149

2. Effect of landing site selection on relay communications. The main effect of the landing site selection on relay communications is to establish the orientation of the lander transmitter beam relative to the approaching orbiter. Figure 94 illustrates how the orientation of the beam trailing edge varies with lander impact point location. This variation causes the lander lead time required for the 20-minute communication zone to vary accordingly.

The communications relay geometry discussed throughout most of this study considers coplanar lander and orbiter trajectories. Evaluation of the relay geometry for out-of-plane lander trajectories was also accomplished. Figures 97 through 100 show the limit which the required 20-minute communication time places upon the planetocentric angle departure of the lander impact point from the plane of the orbiter. Also indicated are the surface impact points (corresponding to the coplanar lander trajectory) as related to the true anomaly angle of the orbiter. The impact points are identified by the corresponding entry angles. The assumed transmitter range is 15,000 km.

Figure 97 shows the central angle deviation of the 20-minute isochrone for the entry angle of 20 degrees to be zero. The maximum central angle deviation of approximately 40 degrees occurs for impact points associated with entry angles around 60 degrees (true anomaly angle of 70 degrees). The reason for this can be explained as follows: The antenna pattern of the lander is a 120-degree conical beam. The requirement for the duration of the orbiter passage through the lander antenna beam is 20 minutes or more. For the condition of $\gamma_E = 20$ degrees, the orbiter is close to the planet (near periapsis) when passing through the beam and, as a result, the duration of passage is limited. Central angle deviations other than zero do not accommodate the 20-minute communication time required. For entry angles greater than 60 degrees, the central angle deviation is limited by the 15,000-km transmitter range.
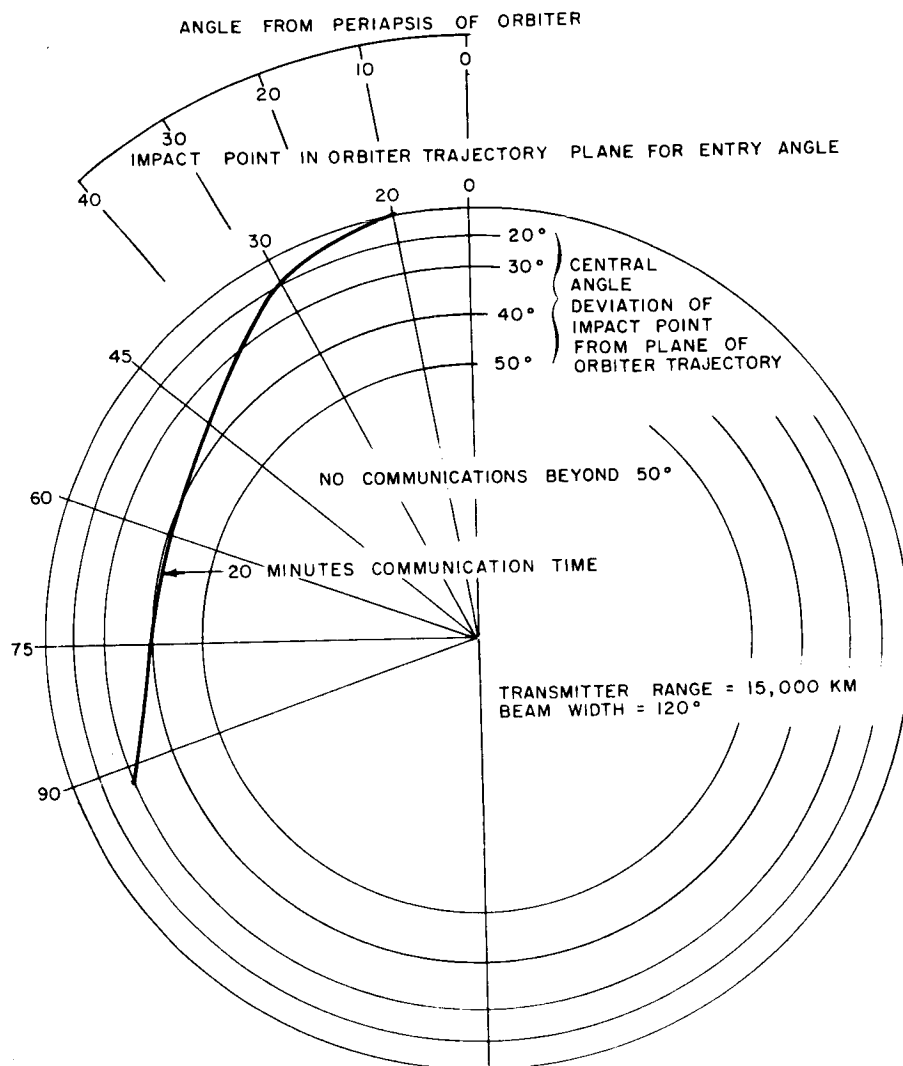
Variation of the approach velocity does not affect the maximum central angle deviation, but it does shift the isochrone line for the low entry angle condition.

3. Effect of orbit injection on communication relay. The thrust phase for the orbit injection maneuver considered in the relay geometry study considered a thrust of 2500-pound magnitude and a specific impulse of 315 seconds. The thrust direction and duration have been optimized to achieve the desired orbit. The orbit considered for Mars is elliptical with 1700 and 10,000 kilometers periapsis and apoapsis altitudes, respectively. The thrust phase is important relative to the relay geometry since in the shallow entry angle and high approach velocity case the thrust sequence affects the direct communication relay with Earth. The vehicle may not be oriented for orbit injection, lander-orbiter communication, and Earth-sighting, all at the same time.

ANGLE FROM PERIAPSIS OF ORBITER

IMPACT POINT IN ORBITER TRAJECTORY PLANE FOR ENTRY ANGLE

CENTRAL
ANGLE
DEVIATION OF
IMPACT POINT
FROM PLANE OF
ORBITER TRAJECTORY

NO COMMUNICATIONS BEYOND 50°

20 MINUTES COMMUNICATION TIME

TRANSMITTER RANGE = 15,000 KM
BEAM WIDTH = 120°

63—9151

Figure 97 PORTION OF MARTIAN SURFACE AVAILABLE FOR RELAY
COMMUNICATION $v_\infty = 3$ KM/SEC

-209-

ANGLE FROM PERIAPSIS OF ORBITER

IMPACT POINT IN ORBITER TRAJECTORY PLANE FOR ENTRY ANGLE

20°
30° } CENTRAL ANGLE
40° DEVIATION OF IMPACT POINT FROM PLANE OF
50° ORBITER TRAJECTORY

NO COMMUNICATIONS BEYOND 50°

20 MINUTES COMMUNICATION TIME

TRANSMITTER RANGE = 15,000 KM
BEAM WIDTH = 120°

63-9150

Figure 98 PORTION OF MARTIAN SURFACE AVAILABLE FOR RELAY
COMMUNICATION v_∞ = 3 KM/SEC

-210-

ANGLE FROM PERIAPSIS OF ORBITER

IMPACT POINT IN ORBITER TRAJECTORY PLANE FOR ENTRY ANGLE

CENTRAL ANGLE DEVIATION OF IMPACT POINT FROM PLANE OF ORBITER TRAJECTORY

NO COMMUNICATIONS BEYOND 50°

20 MINUTES COMMUNICATION TIME

TRANSMITTER RANGE = 15,000 KM
BEAM WIDTH = 120°
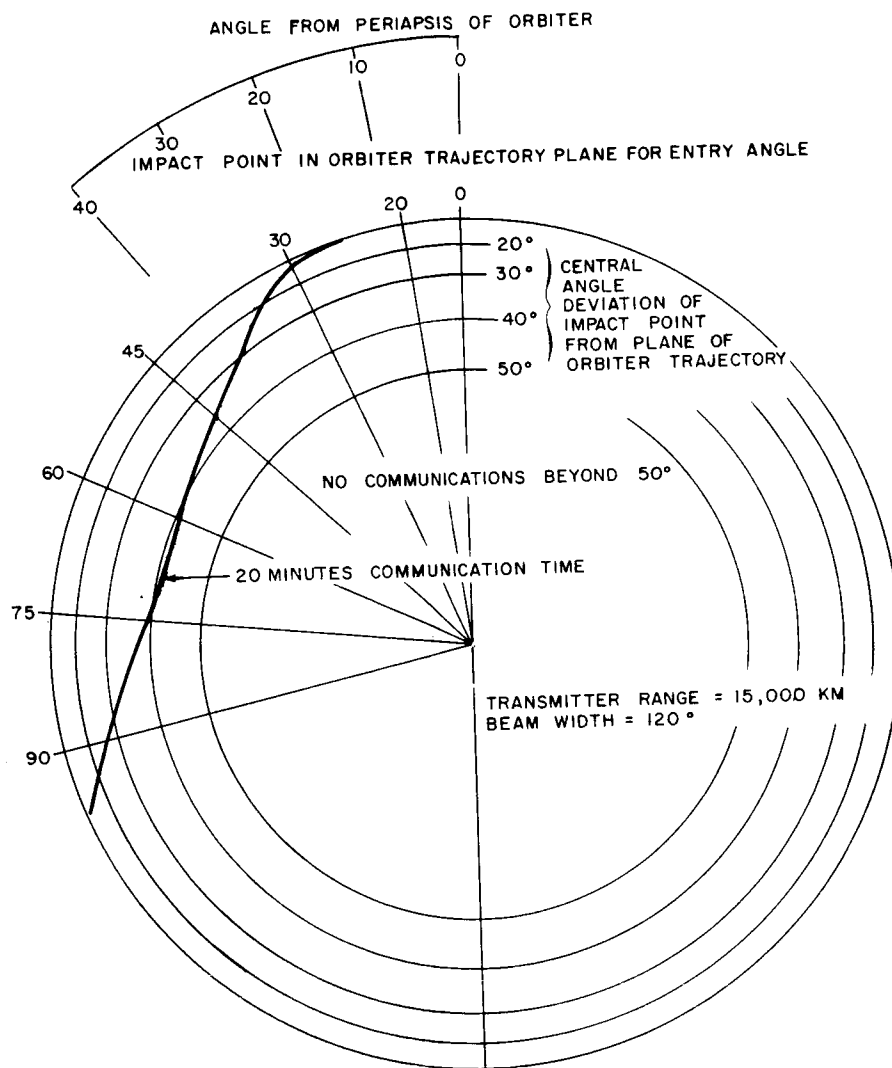
63-9152

Figure 99 PORTION OF MARTIAN SURFACE AVAILABLE FOR RELAY
COMMUNICATION $v_\infty = 5$ KM/SEC

ANGLE FROM PERIAPSIS OF ORBITER

IMPACT POINT IN ORBITER TRAJECTORY PLANE FOR ENTRY ANGLE

CENTRAL ANGLE DEVIATION OF IMPACT POINT FROM PLANE OF ORBITER TRAJECTORY

NO COMMUNICATIONS BEYOND 50°

20 MINUTES COMMUNICATION TIME

TRANSMITTER RANGE = 15,000 KM
BEAM WIDTH = 120°
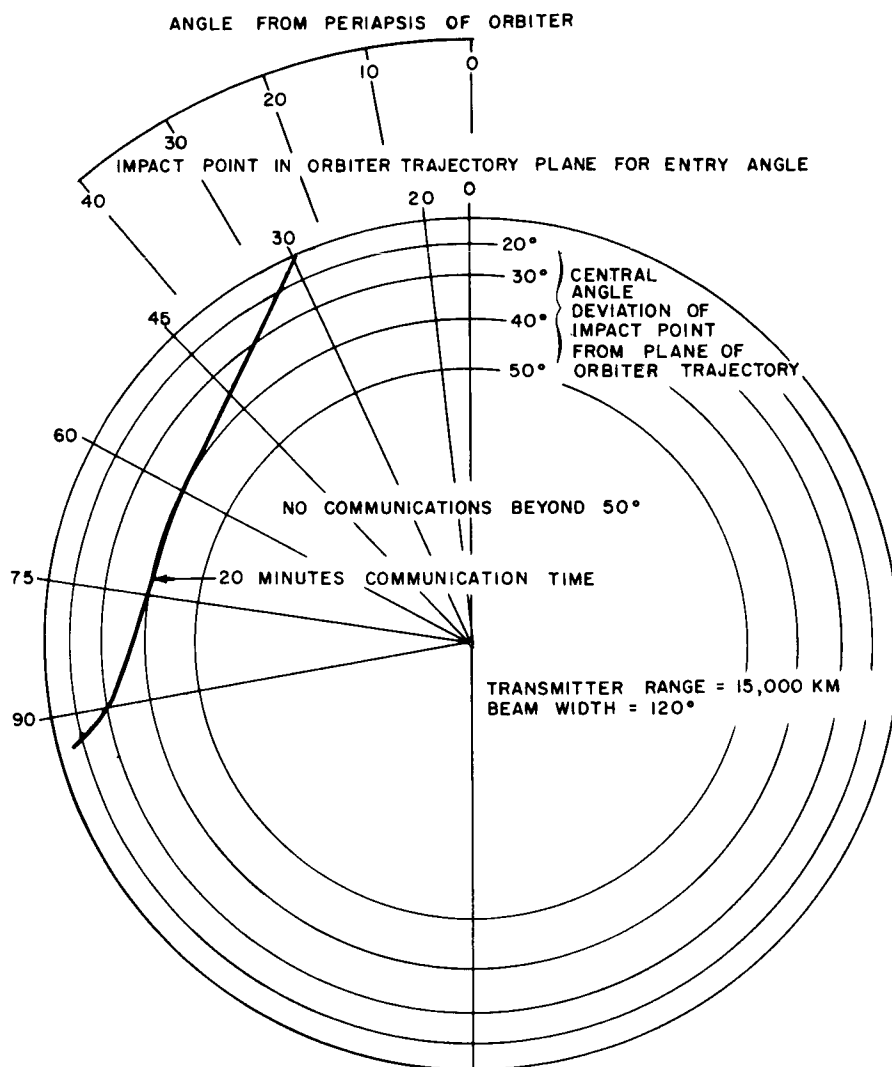
63-9153

Figure 100 PORTION OF MARTIAN SURFACE AVAILABLE FOR RELAY
COMMUNICATION $v_\infty = 6$ KM/SEC

The point of thrust initiation is a function of approach velocity, thrust magnitude, specific impulse, the desired final orbit, and the mass of the orbiter. The effect of an increase in approach velocity from 4 to 6 km/sec is to shift the thrust initiation point for a 4500-pound orbiter back from 26 to 29.5 degrees from the periapsis of the orbiter approach trajectory. The cutoff point for the above cases varies from 12 to 3 degrees before periapsis, respectively. During the orbit-injection thrust phase, data transmitted by the lander to orbiter must be stored in the orbiter for later retransmission to Earth.

4. <u>Look angles between orbiter and lander.</u> The antenna location and pattern for both the orbiter and lander are of utmost importance in the communication relay operation. Look angles were determined by relating the line of sight to a known body reference. Two basic angles were determined. One is lander-centered, the angle between the lander roll axis and the line of sight to the orbiter. The other is orbiter-centered, the angle between the orbiter longitudinal axis and the line of sight to the lander.

a. <u>Lander-centered angle.</u> During the approach phase, the lander will be transmitting to the orbiter. Figures 101 and 102 show typical examples of the lander-centered angle between the lander roll axis in the aft direction (along the centerline of the beam) and the line of sight to the orbiter. The angle is considered positive in the direction indicated in the figure.

During the relay transmission phase, after entry, the antenna beam is a 120-degree cone directed upward along the local vertical. Figure 103 shows the time history of lander-to-orbiter look angles during the relay phase for the typical asymptotic approach velocity of 4 km/sec. The orbiter passes overhead for entry angles of 60 degrees or less as indicated by the change in sign of the angle from positive to negative. The horizontal extremities of the lines define the available communication relay time. The time for the γ_E = 20 degrees case is limited to approximately 19 minutes. By comparing figures 103 and 104, the effect of a high approach velocity and low entry angle in increasing the look angle spread and reducing the available communication time can be noted.

b. <u>Orbiter-centered angles.</u> Placement of the relay antenna on the orbiter can best be determined by look angles between the orbiter roll axis and the line sight to the lander during the time the lander is transmitting. This transmission time occurs for a minimum of 10 minutes centered on lander impact. Figure 105 shows these look angles for an approach velocity of V_∞ = 4 km/sec. The look angles are plotted as a function of entry angle and time from periapsis of the orbiter approach trajectory. The roll axis of the orbiter is assumed to be oriented in the fixed direction for the thrust phase of orbit injection during the last hour of planetary approach. Assuming that the orbiter approaches the planet from left to right, the curves show that a field of view of from 25 to 145 degrees measured clockwise (downward and backward) from the forward end

of the orbiter roll axis will be necessary for complete coverage. The effect of increase in entry angle is to reduce the variation of look angle. The effect of an increase in approach velocity is to reduce the time from orbiter periapsis for the communication relay as shown in figure 106.

6.2 Lander-Orbiter Lead-Time Analysis

1. <u>Lander lead-time requirements.</u> The playback of entry and descent data will occur during a 5-minute period before planet impact, and transmission of real time status and scientific data will require 5 minutes after impact. If the lander and orbiter arrive at the planet at the same time, the orbiter relay will not be within the lander antenna beam or, in some cases, insufficient time is available for data playback before the orbiter leaves the antenna beam. Data playback could resume after the orbiter vehicle has successfully established a planetary orbit and comes into view again. However, if either the lander fails to survive impact or the orbiter fails to attain a planetary orbit, the data will be lost. By imparting, after lander-orbiter separation, a specified velocity increment in the direction of the flight path to either the lander or orbiter (retrovelocity in case of orbiter), the lander will precede the orbiter to the planet. More time will then be available for transmitting entry and descent data, before lander impact occurs. Lead time in this study is defined as the time for the orbiter to travel from its position at the instant the lander enters the planet's atmosphere to the periapsis of its approach trajectory.

The orbiter's position at the initiation of data transmission and the time history of the lander from entry to impact determine the required lander lead time. The lead time is a summation of the time the orbiter takes to go from its position at start of transmission to periapsis, plus the time the lander takes to go from entry to the point data playback begins. The lander-to-orbiter communication relay starts 5 minutes before impact. The orbiter position at this time is obtained from the geometric analysis (see figure 93) performed in the previous section.

Because of the variation in atmosphere, the time for descent can vary considerably. The difference between the minimum and maximum descent time is approximately 10 minutes for all entry angles between 20 and 90 degrees, resulting in a total required communication time of 20 minutes. The required lead time for a 20-minute allowable zone for communication (10 minutes actual communication time) is plotted as a function of entry angle and approach velocity in figures 107 and 108 for separation ranges of 10^6 and 0.5×10^6 km, respectively.

The lead-time requirement for an approach velocity of 3 km/sec varies from 27 to 69 minutes for entry angles between 20 and 90 degrees. The

requirement for the typical case of 4 km/sec and a lander entry angle of
45 degrees is 35 minutes. The curves for approach velocities greater than
3 km/sec terminate at the entry angle of 30 degrees since there is insufficient
communication time at smaller entry angles.

2. Methods of obtaining lander-orbiter lead time

a. Accuracy in achieving desired landing site. Attainment of the
desired or necessary lander-orbiter geometry/time relationship during the
spacecraft approach and orbit injection phases can be accomplished in two
ways. Both of these techniques were analyzed to a depth which permits
comparison and selection of the optimum approach from the standpoint of
system accuracy, payload weight, minimum complexity, and sterilization
requirements.

There are two basic techniques possible to achieve the desired spatial-
time relationships between the orbiter and lander. The first technique requires
acceleration of the lander to a relatively high velocity, with respect to the
orbiter shortly after the lander has been separated. Since separation occurs
at a substantial range from the planet (0.25×10^6 to 10^6 km) the additional
velocity increment possessed by the lander permits it to "lead" the orbiter to
the planet.

The second technique is a slight variation of the first and can be made to
yield the same basic results in terms of spatial-time relationships; however,
it possesses significantly different implementation requirements. This method
consists of applying a small "normal" velocity component to the lander
planetary approach velocity after the lander has been separated from the
orbiter. The orbiter is then decelerated to a suitable velocity which will yield
the desired spatial-time relationships between it and the lander. (The lander
planetary approach velocity vector is, as in the preceding case, identical to
that of the spacecraft until application of the "$\vec{\Delta V}$" to the lander.)

The objective of the analysis was the determination of the performance
characteristics of each technique, specifically the attainable lander impact
accuracy, as a function of spacecraft guidance and system errors. This was
accomplished with a planar error analysis program described in appendix E.
Considering first order terms and neglecting errors such as those resulting
from time-of-flight errors, then the uncertainty in desired lander impact
point $\Delta \phi_L$ as shown in appendix E is

$$\Delta \phi_L^2 = \left(\frac{\partial \phi}{\partial R_O} \Delta R_O^2 \right) + \left(\frac{\partial \phi}{\partial V_{OB}} \Delta V_{OB} \right)^2 + \left(\frac{\partial \phi}{\partial \gamma_{OB}} \Delta \gamma_{OB} \right)^2 + \left(\frac{\partial \phi}{\partial v_{OL}} \Delta v_{OL} \right)^2 + \left(\frac{\partial \phi}{\partial \theta_{OL}} \Delta \theta_{OL} \right)^2$$

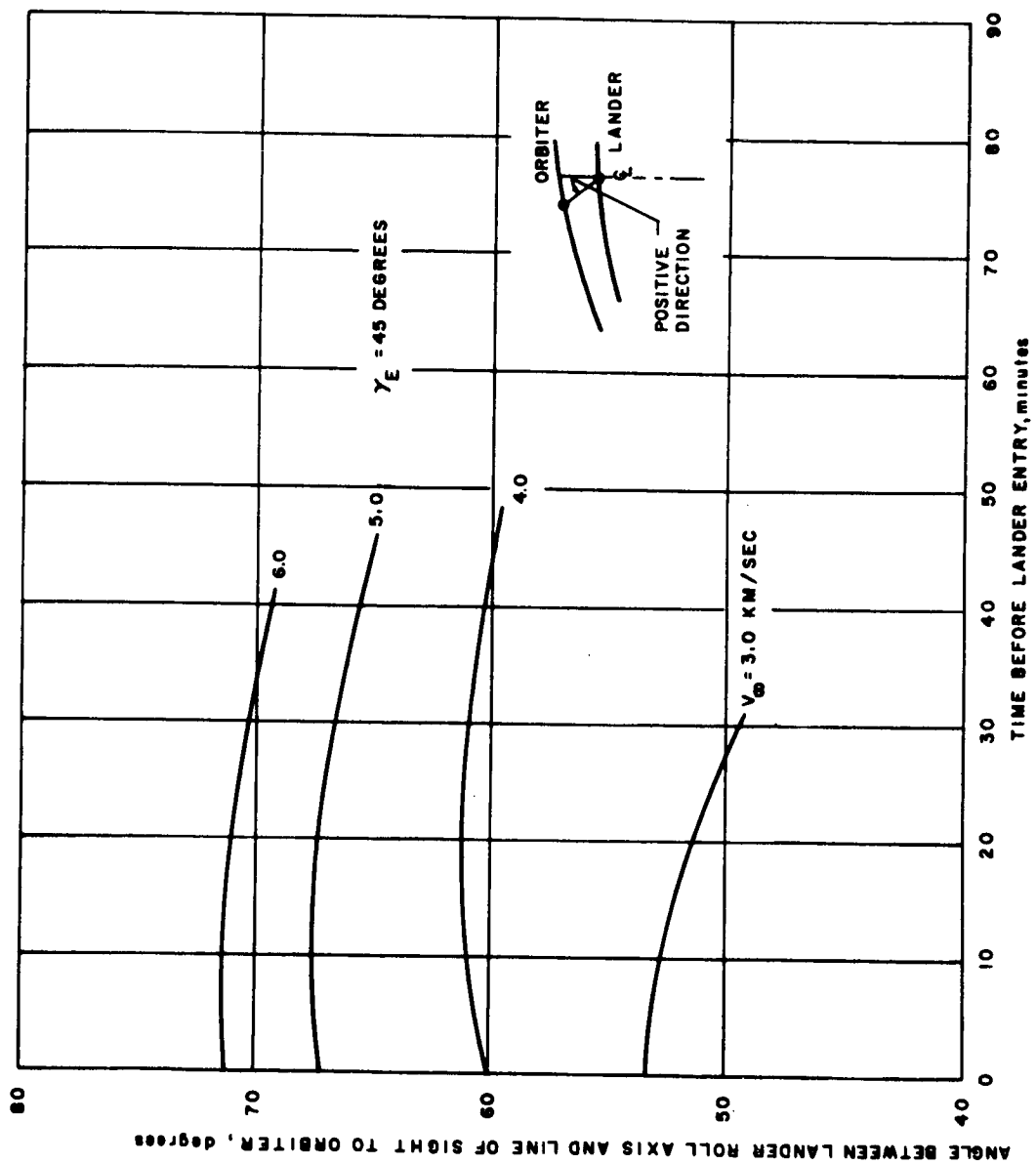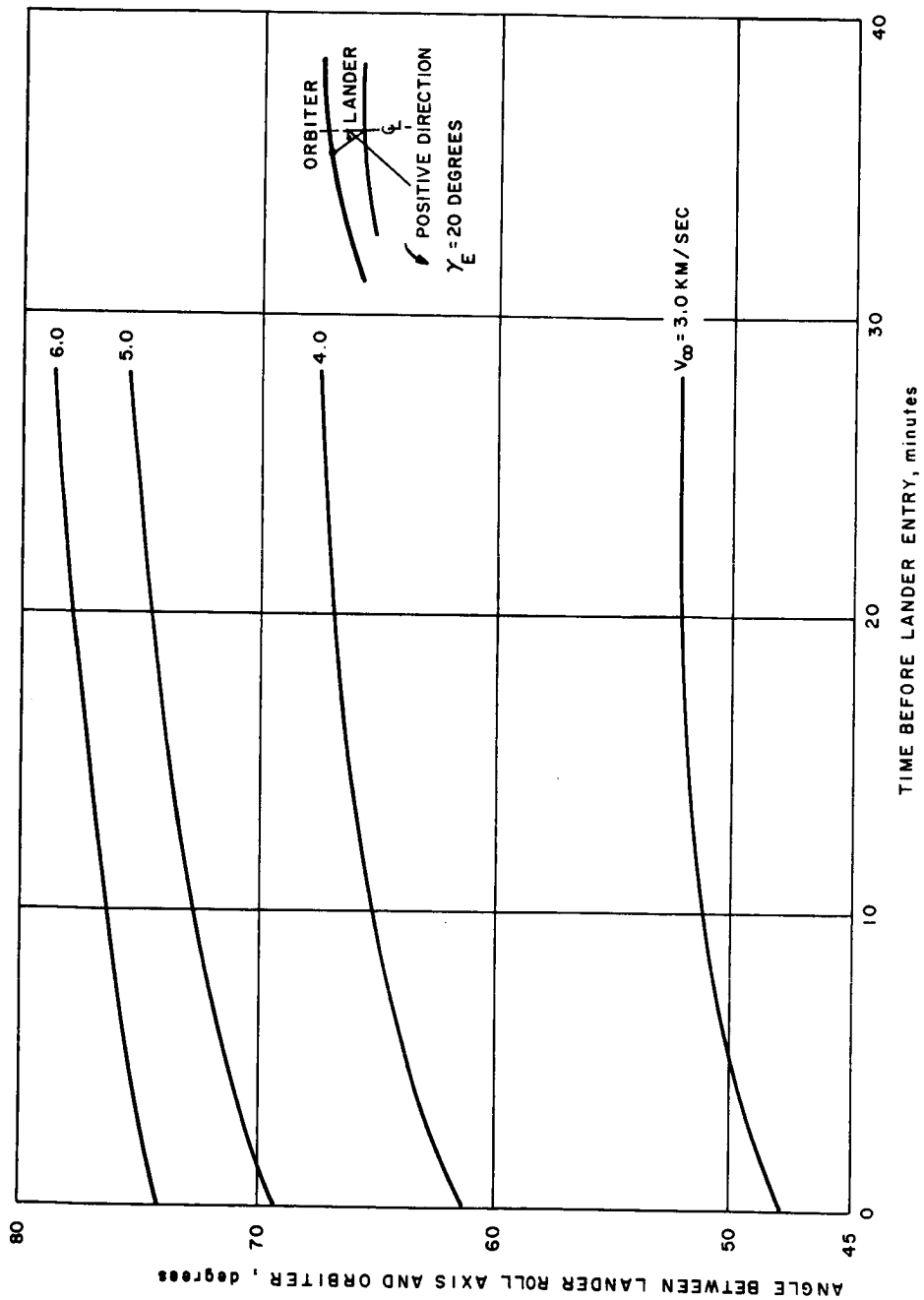$$(1) \qquad\qquad (2) \qquad\qquad (3) \qquad\qquad (4) \qquad\qquad (5)$$

Figure 101 LANDER TO ORBITER LOOK ANGLES PRIOR TO LANDER
ENTRY, γ_E = 45 DEGREES

63-9154

-216-

Figure 102 LANDER TO ORBITER LOOK ANGLES PRIOR TO LANDER ENTRY, γ_E = 20 DEGREES
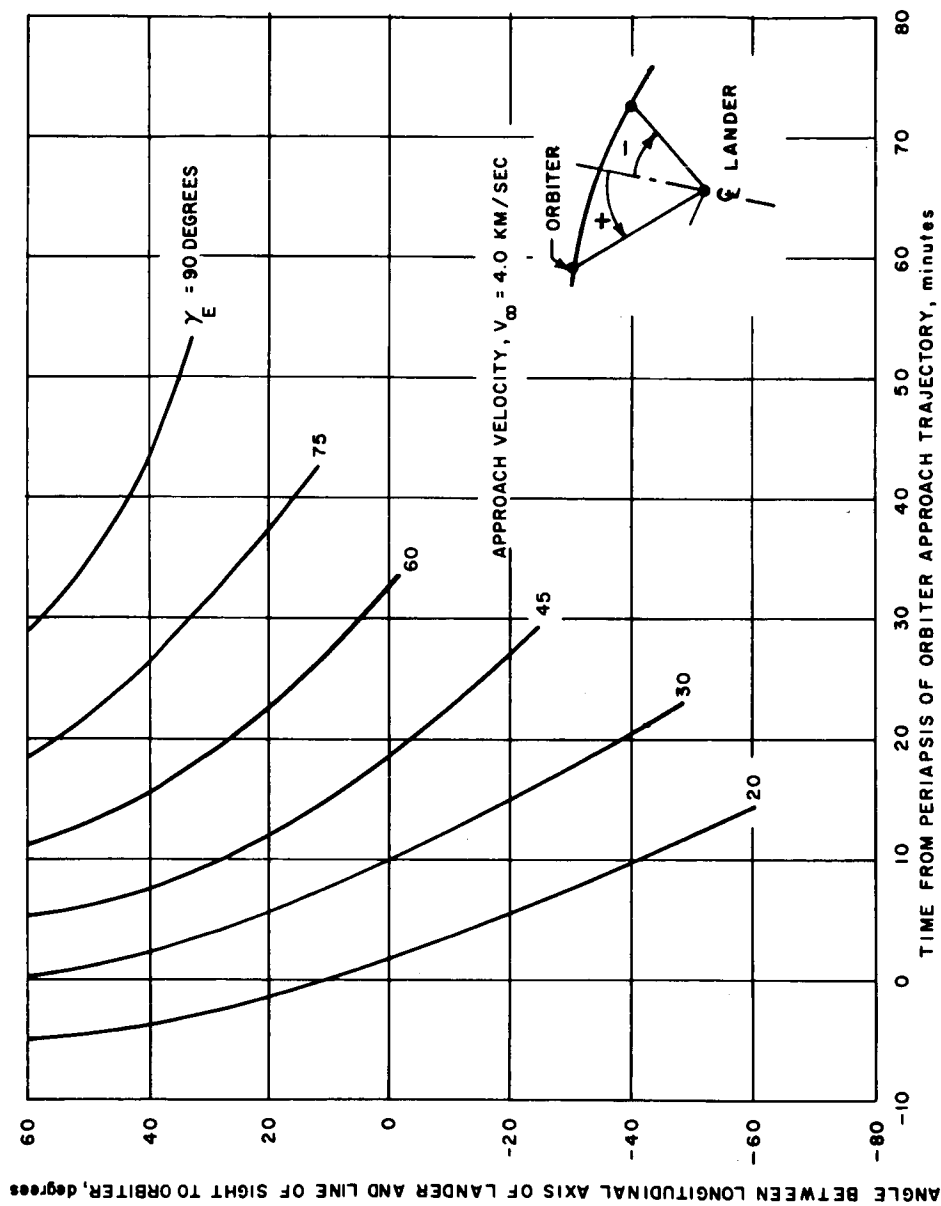
63-9155

-217-

Figure 103 LANDER TO ORBITER LOOK ANGLES DURING RELAY
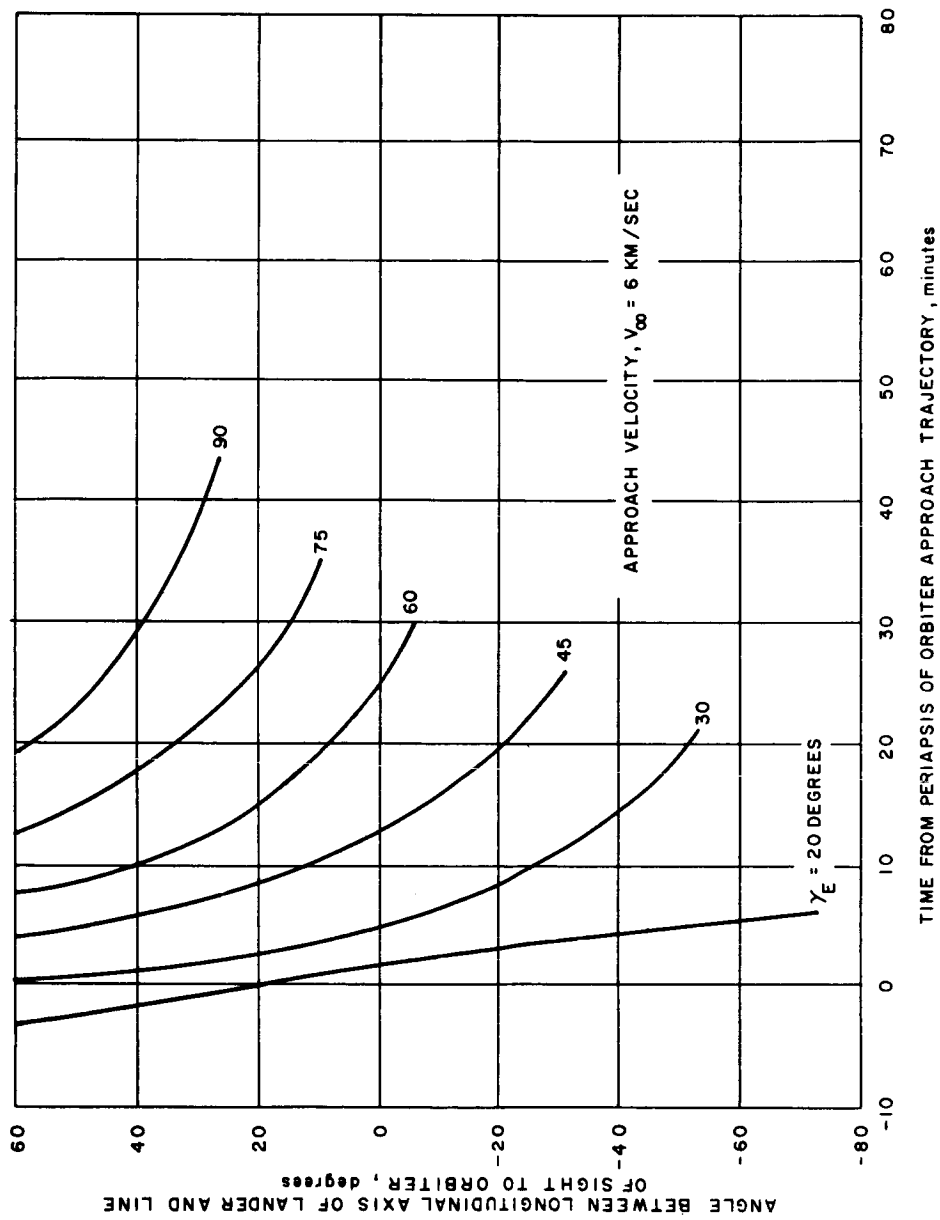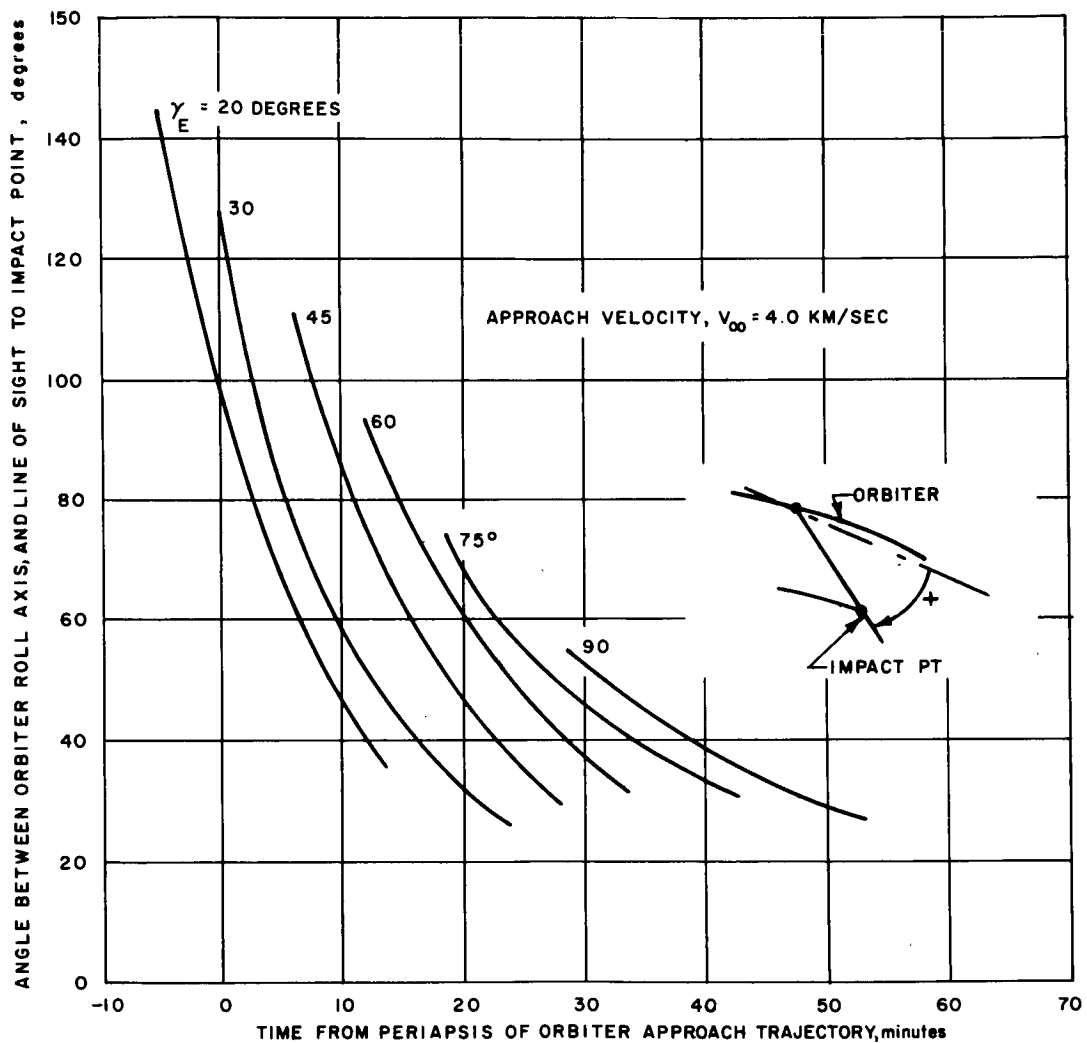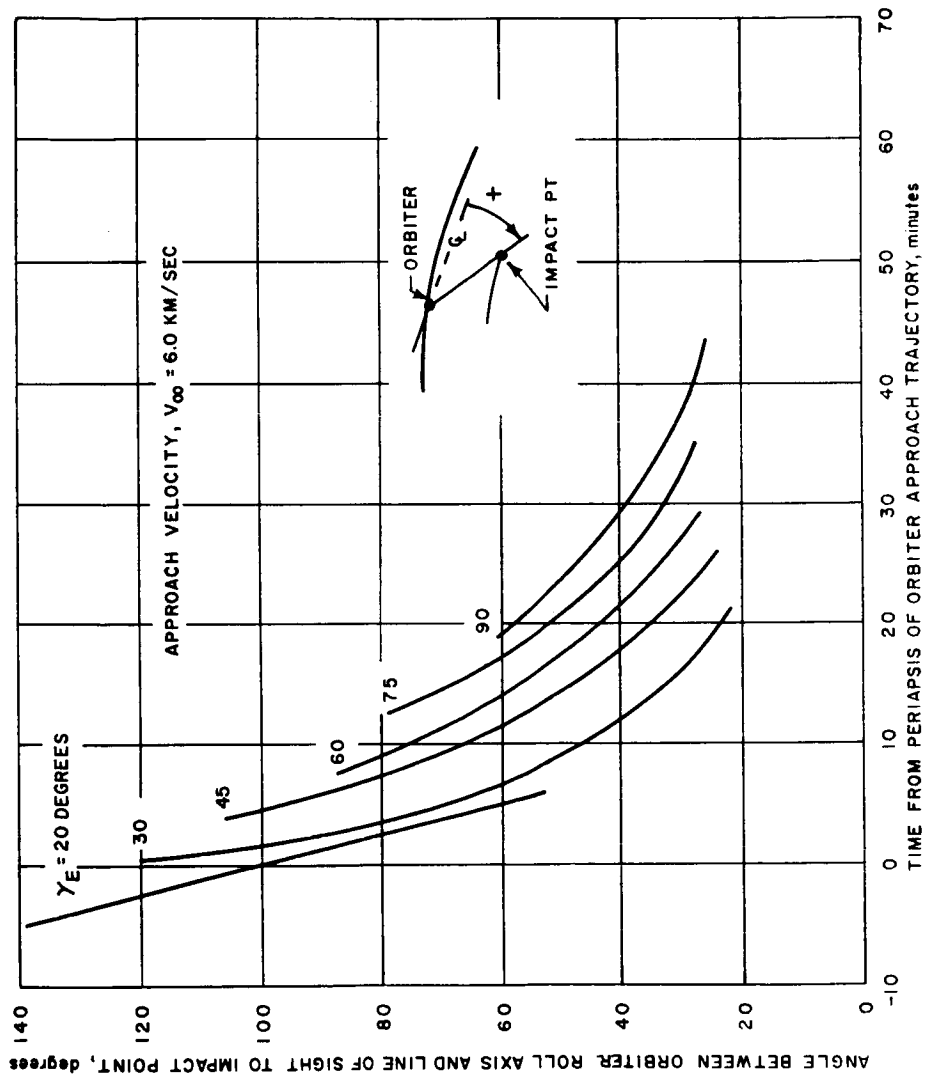COMMUNICATION, v_∞ = 4 KM/SEC

63-9156

-218-

Figure 104 LANDER TO ORBITER LOOK ANGLES DURING RELAY
COMMUNICATION, V_∞ = 6 KM/SEC
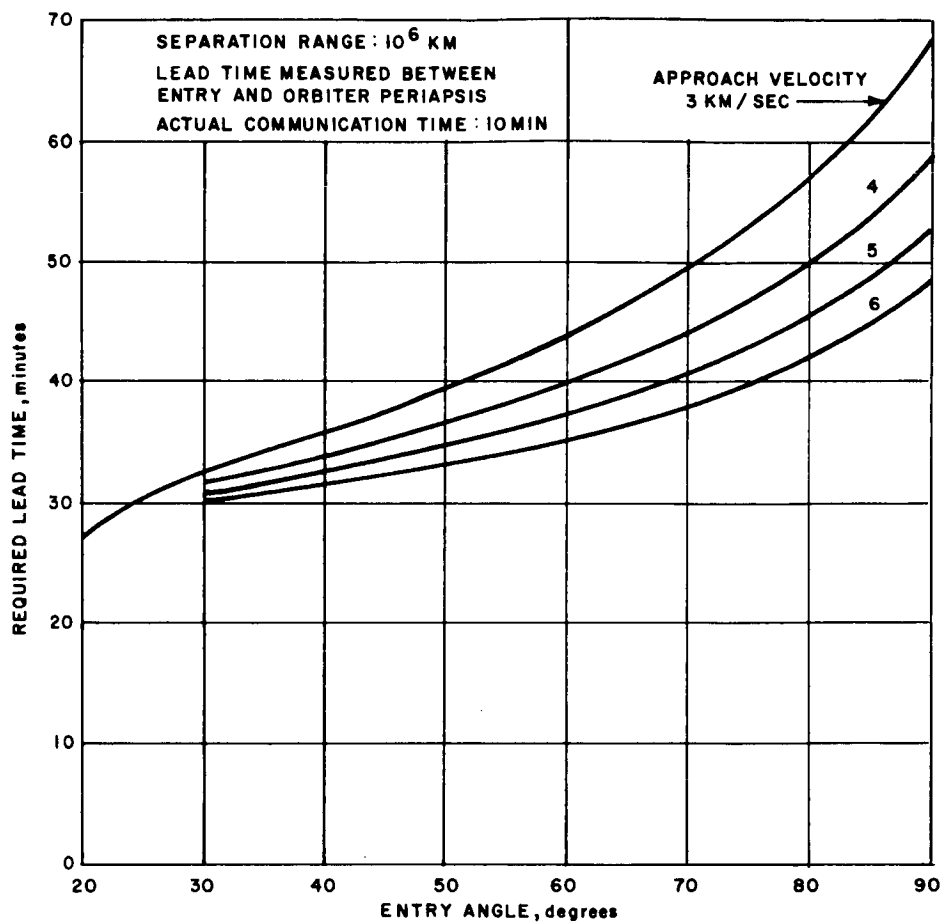
63-9158

Figure 105 ORBITER TO LANDER LOOK ANGLES DURING RELAY
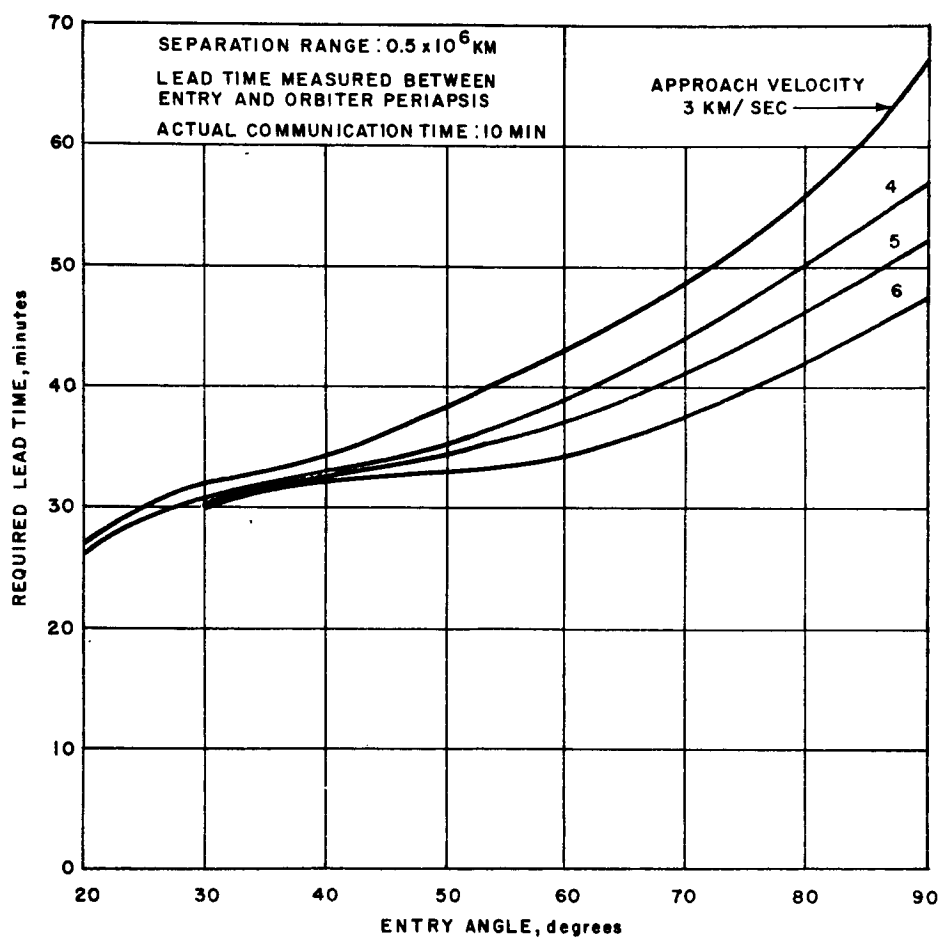COMMUNICATION, $V_\infty = 4$ KM/SEC

-220-

Figure 106 ORBITER TO LANDER LOOK ANGLES DURING RELAY
COMMUNICATION, v_∞ = 6 KM/SEC

63-9159

Figure 107 LANDER LEAD TIME REQUIREMENTS, SEPARATION RANGE = 10^6 KM

63-9160

Figure 108 LANDER LEAD TIME REQUIREMENTS, SEPARATION
RANGE = 0.5 x 10⁶ KM

63-9161

Terms (1), (2), and (3) are functions of the spacecraft guidance; they result from the uncertainty in knowledge of the state of the spacecraft relative to the destination planet at lander separation and are common to both techniques. For a valid comparison of both techniques, identical spacecraft guidance performance for both cases must be assumed.

Terms (4) and (5) result from the implementation of the desired $\vec{\Delta V}$. Term (4) represents the error resulting from uncertainty in the magnitude of an applied velocity increment, such as accelerometer error and thrust cutoff error. The velocity increment applied to the lander for the "lander speed-up" case is larger than that necessary in the "orbiter slow-down" case.

Term (5) represents the error resulting from the uncertainty in the angular orientation θ_{OL} of the applied velocity increment. This stems from spacecraft attitude control errors, separation tip-off rates, lander thrust axis misalignment, and lander principal axis offset. For "lander speed-up" θ_{OL} is small, usually less than 12 degrees; for "orbiter slow-down," θ_{OL} is 90 degrees.

Typical results are presented in figures 109 through 116 for the following flight conditions.

Separation range R_O from planet	0.5×10^6 and 10^6 km
Spacecraft planetary approach velocity V_∞	10,000 and 15,000 ft/sec
Periapsis of unperturbed spacecraft approach hyperbola R_{PB}	1,800 km
Applied velocity increment V_{OL} "Lander speed-up" "Orbiter slow-down"	500 ft/sec Variable
Error ΔV_{OL} in lander applied velocity increment V_{OL} "Lander speed-up" "Orbiter slow-down"	10 ft/sec 1 σ 0.5 ft/sec 1 σ
Application angle of V_{OL} "Lander speed-up" "Orbiter slow-down"	Variable 90 degrees
Angular orientation error θ in applying V_L. (Same for both "lander speed-up" and "orbiter slow-down" cases)	0.1 degree 1 σ
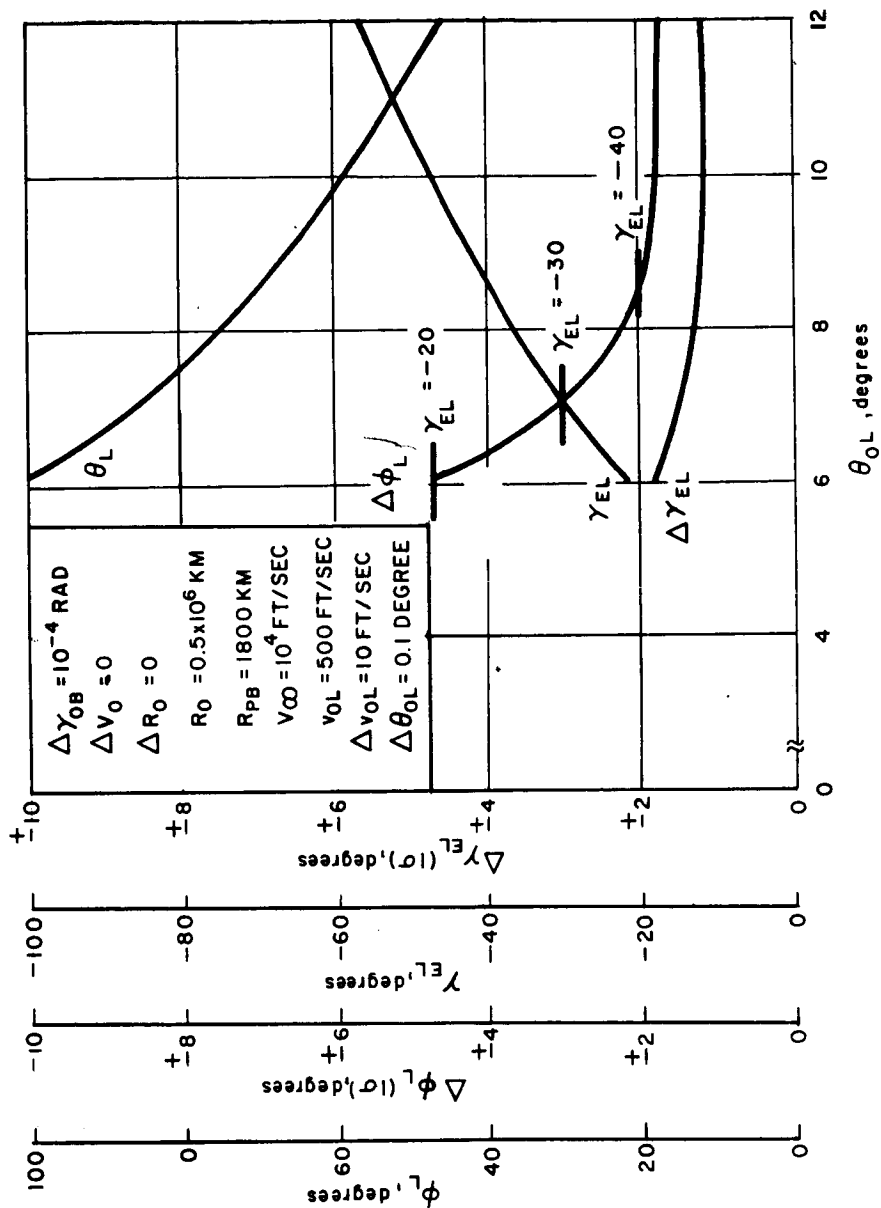
Figure 109 SYSTEM PERFORMANCE FOR LANDER SPEEDUP,
$V_\infty = 10^4$ FT/SEC, $R_o = 0.5 \times 10^6$ KM

63-9737

Figure 110 SYSTEM PERFORMANCE FOR ORBITER SLOWDOWN,
$V_\infty = 10^4$ FT/SEC, $R_o = 10^6$ KM

63-9738

-226-
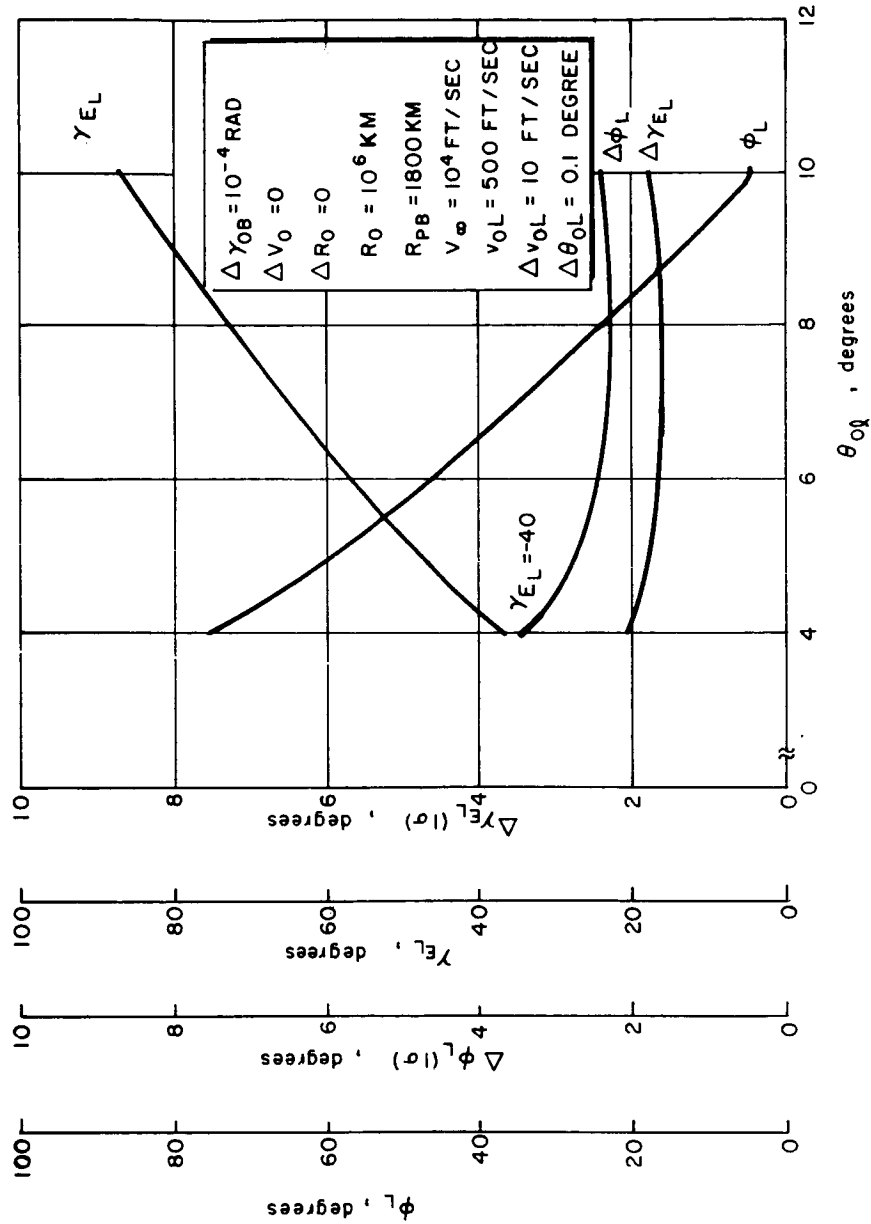
Figure 111 SYSTEM PERFORMANCE FOR LANDER SPEEDUP,
$V_\infty = 10^4$ FT/SEC, $R_o = 10^6$ KM

63-9739

-227-
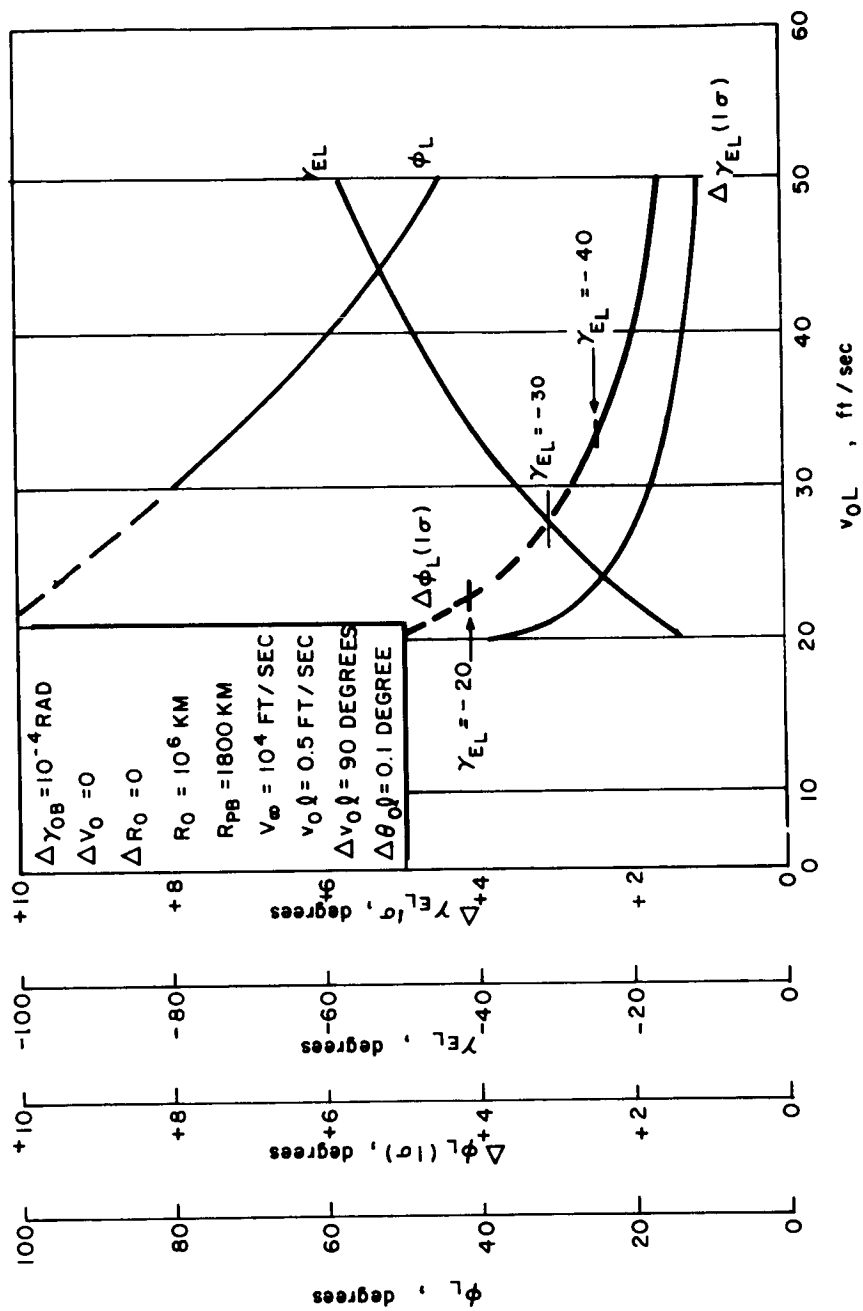
Figure 112 SYSTEM PERFORMANCE FOR ORBITER SLOWDOWN,
$V_\infty = 10^4$ FT/SEC, $R_Q = 10^6$ KM
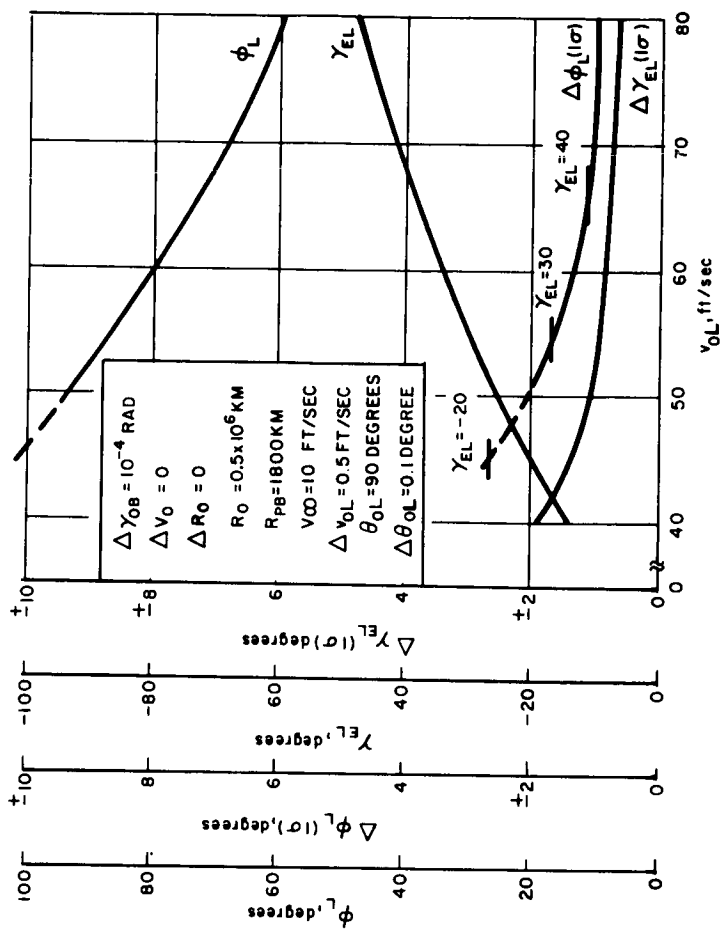
63-9740

-228-
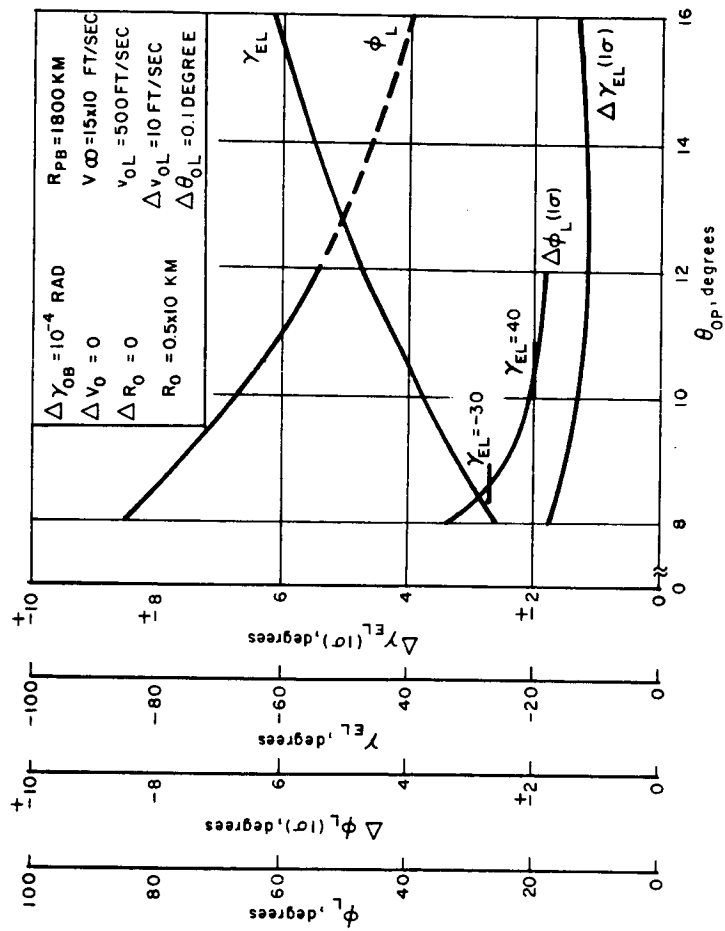
Figure 113 SYSTEM PERFORMANCE FOR LANDER SPEEDUP, $V_\infty = 15 \times 10^3$ FT/SEC, $R_o = 0.5 \times 10^6$ KM

63-9741

-229-
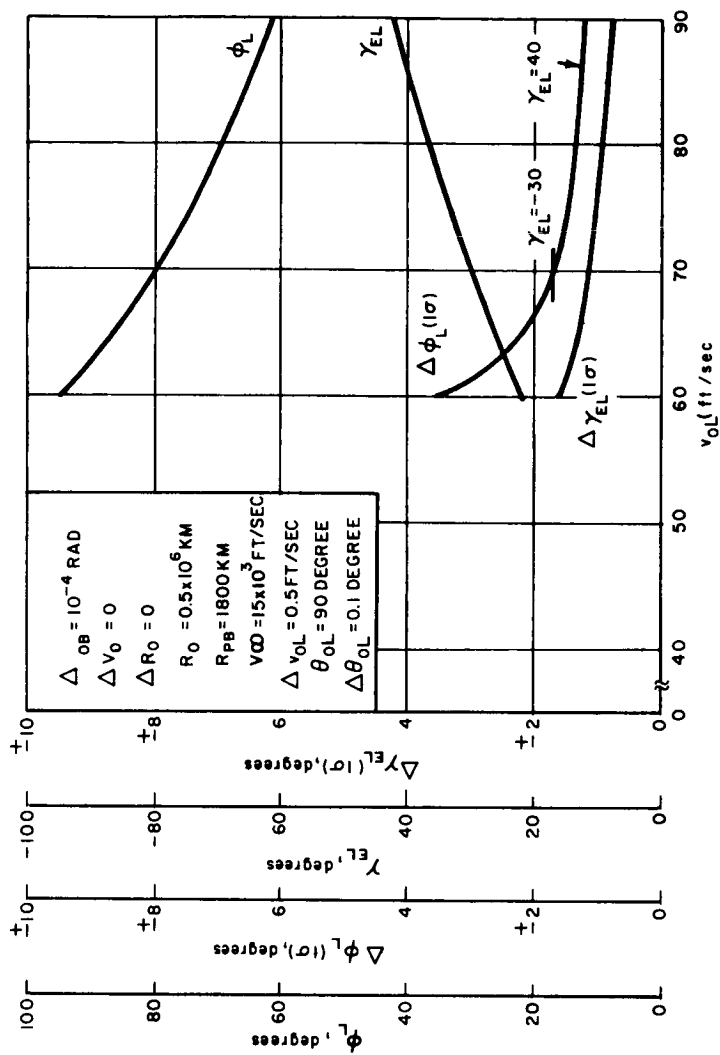
Figure 114 SYSTEM PERFORMANCE FOR ORBITER SLOWDOWN,
$V_\infty = 15 \times 10^3$ FT/SEC, $R_o = 0.5 \times 10^6$ KM

63-9742

Figure 115 SYSTEM PERFORMANCE FOR LANDER SPEEDUP,
$V_\infty = 15 \times 10^3$ FT/SEC, $R_o = 10^6$ KM

$\Delta \gamma_{0B} = 10^{-4}$ RAD
$\Delta v_0 = 0$
$\Delta R_0 = 0$
$R_0 = 10^6$ KM
$R_{PB} = 1800$ KM
$V_\infty = 15 \times 10^3$ FT/SEC
$v_{0L} = 500$ FT/SEC
$\Delta v_{0L} = 10$ FT/SEC
$\Delta \theta_{0L} = 0.1$ DEGREE

63-9743

Figure 116 SYSTEM PERFORMANCE FOR ORBITER SLOWDOWN,
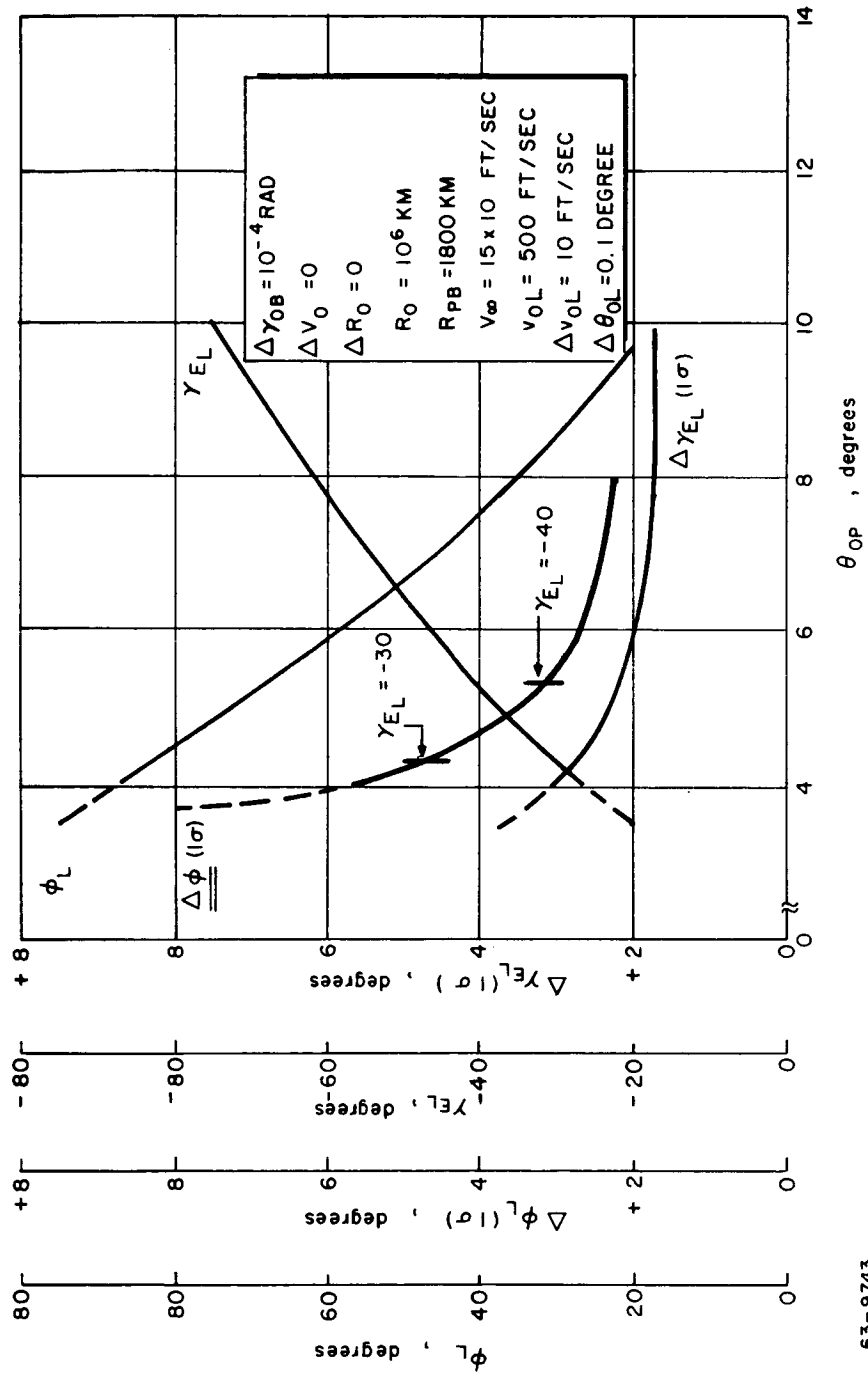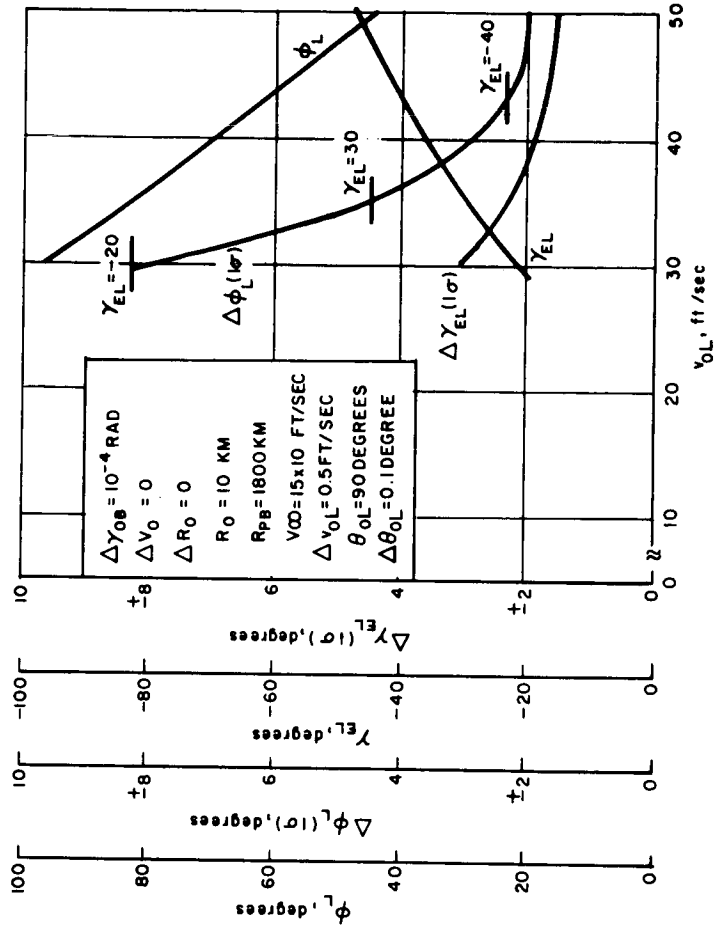$V_\infty = 15 \times 10^3$ FT/SEC, $R_D = 10^6$ KM

63-9744

-232-

Spacecraft guidance performance was identical in both cases and was assumed to be:

Range, R_O	ΔR_O km	ΔV_{OB}
10^6 km	100 km (1σ)	2 cm/sec (1σ)
0.5×10^6 km	50 km (1σ)	2 cm/sec (1σ)

These errors were transformed to a planetocentric polar coordinate system and interpreted in a manner which maximized the error in the direction of the spacecraft planetary approach velocity vector. The residual uncertainties in spacecraft initial range R_O speed V_{OB}, and anomaly ϕ_{OB} after this transformation were found to be negligible.

Expository discussion of these figures will be limited to figures 109 and 110 which present system performance for lander separation at a range of 0.5×10^6 km and approach velocity of 10^4 ft/sec for "lander speed-up" and "orbiter slow-down," respectively.

The ordinates of all of the figures are identical and represent:

1. Range angle ϕ_L traversed by the lander from separation to planetary impact (no atmosphere)

2. Uncertainty in range angle $\Delta \phi_L (1\sigma)$

3. Atmospheric entry flight path angle of lander γ_{EL} at a 800,000-foot altitude

4. Uncertainty in atmospheric entry flight path angle $\Delta \gamma_{EL}$

The abscissa of figure 109 ("lander-speed up") is the angle θ_{OL} with respect to the spacecraft planetary approach velocity to which the lander velocity increment v_{OL} is applied.

The abscissa of figure 110 (orbiter-slow-down) is the magnitude of the lander-applied velocity increment v_{OL}.

For the reader's convenience, some entry angles γ_{EL} in the range -20 to -40 degrees are noted on the $\Delta \phi_L$ curve, permitting easier comparison of performance. For example, at γ_{EL} = -30 degrees (figure 109, lander speed-up)

$$\phi_L \quad = 86 \text{ degrees}$$

$$\Delta\phi_L = 3 \text{ degrees}$$

$$\Delta\gamma_{EL} = 1.5 \text{ degrees}$$

and at $\gamma_{EL} = -30$ degrees (figure 110, orbiter slow-down)

$$\phi_L \quad = 86 \text{ degrees}$$

$$\Delta\phi_L = 1.6 \text{ degrees}$$

$$\Delta\gamma_{EL} = 0.9 \text{ degree.}$$

It should be noted that the range angle error $\Delta\phi_L$ will increase when atmospheric uncertainties are included.

Although the study was planar, the dispersion resulting from an angular orientation error normal to the trajectory plane is proportional to the applied velocity increment v_{OL}. Lateral dispersion performance of "lander speed-up" versus "orbiter slow-down" will vary with the ratio of the velocities applied to the lander. For the preceding case, $^*\gamma_{EL} = -30$ degrees, the lateral dispersion of the "lander speed-up case" will be a factor of 9 greater than that for "orbiter slow-down."

The analyses of figures 109 through 116 were performed on the assumption that the launch angle error was 0.1 degree, an unreasonably small estimate made such that the "orbiter slowdown" approach would not be unnecessarily penalized. Figure 117 shows the sensitivity of the $\Delta\phi_L$ and $\Delta\gamma_{EL}$ to the launch angle errors θ_{OP} for more reasonable values of $\Delta\theta_{OP}$.

To demonstrate the significance of the launch angle error if the lander speed-up method is employed, typical design parameters and an operational sequence are assumed. The design parameters are

Mass = 46.6 slugs

Transverse moment of inertia = 325 slug-ft^2

Roll moment of inertia = 190 slug-ft^2

Location of main rocket = on longitudinal axis 6 feet from c.g.

Location of spin rockets = 3.3 feet from longitudinal axis, directly over c.g.

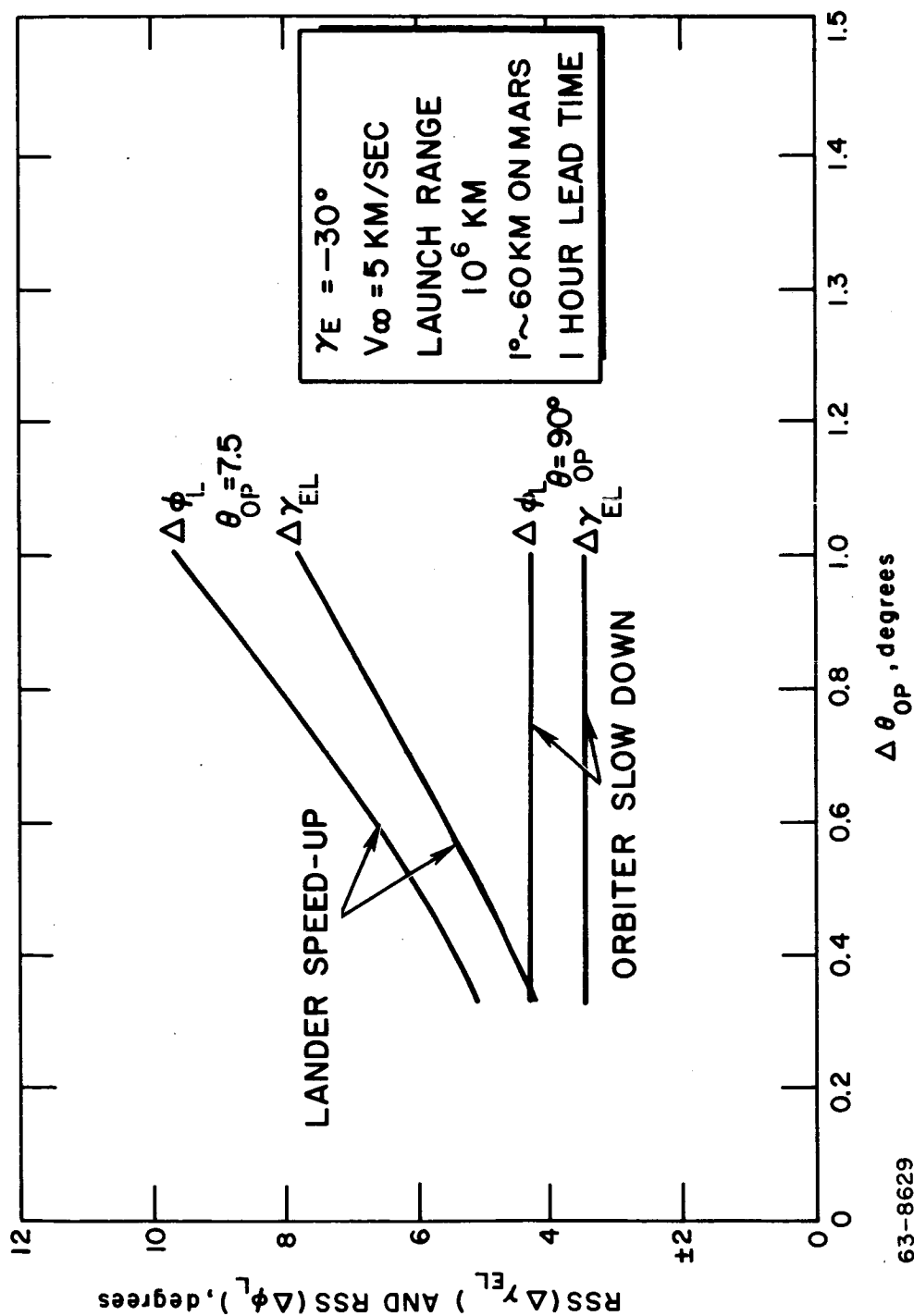Rocket location error = 0.01 foot (3 σ) in X, Y, Z, directions

-234-

Figure 117 PERFORMANCE COMPARISON OF LANDER SPEEDUP VERSUS ORBITER SLOWDOWN

63-8629

C.G. location error = 0.003 foot (3 σ) in X, Y, Z, directions

Angular misalignment of thrust axes = 0.2 degree (3 σ) in pitch and yaw.

The operational sequence is assumed as follows:

	Event	Time (sec)
1.	Separate orbiter and lander	0
2.	Eject lander by means of spring mechanism with 100 lb/sec impulse	0.1
3.	Initiate spin rockets	0.1
4.	Terminate spin-rocket thrust	2.1
5.	Initiate main rocket	5.0
	(5-second delay is necessary to prevent lander plume impingement on orbiter)	
6.	Terminate thrust	5.0 + T
	(Action time of rocket depends on thrust level and required velocity increment)	

The launch angle error was determined as a function of velocity increment, rocket action time, and spin rate for the above input conditions. The results are plotted in figures 118, 119, and 120.

Equation (1) was used to determine the dispersion resulting from a given launch angle error. A separation range R_L of 10^6 km and approach velocities of 3, 4, and 5 km/sec were assumed. From figures 107 and 108, the required lander lead time and from figures 121 through 124 the corresponding required velocity increments ΔV_T along the flight path were obtained as a function of entry angle. The normal velocity increment ΔV_N needed to shift the lander trajectory was obtained from figures 125 through 128 as a function of entry angle. The launch angle error corresponding to the total velocity increment ΔV_i is found from figure 118.

The results are plotted in figure 129 for two different spin rates: 1 rad/sec (9.6 rpm) and 2 rad/sec (19.2 rpm). For the case of a rocket action time of 10 seconds, a spin rate of 1 rad/sec, a separation range of 10^6 km, and an approach velocity of 4 km/sec, the 1-σ values for angular dispersion range from 3.8 to 8.2 degrees for entry angles between 30 and 90 degrees. Minimum

dispersion occurs at an entry angle of 48 degrees (on Mars, 1 degree of central angle equals 59.5 km).

To reduce the launch angle error to an acceptable level, the spin rate must be increased. The launch angle error could also be reduced by increasing rocket action time. However, the error approaches a limiting value which is unacceptably high.

b. <u>Accuracy of establishing terminal orbit.</u> If the lander is accelerated, the orbiter trajectory is unperturbed; however, retrothrust of the orbiter after separation increases the uncertainty in position and velocity of the orbiter. The orbiter error depends primarily on the accuracy with which the desired velocity change can be accomplished. It is here that the orbiter enjoys a distinct advantage. Since the orbiter is provided with a precise attitude control system, accelerometers, and restartable engine, it can eliminate the major contributions to error which make acceleration of the lander so difficult. If no trajectory corrections are made after separation (either by DSIF or terminal guidance), the orbiter velocity change could result in an error of 100 km in periapsis altitude in addition to that caused by position errors. It may be possible to make subsequent velocity corrections to reduce this error by means of either terminal or DSIF guidance. It appears that the error in establishing the orbit will be a stronger function of the injection accuracy itself than of errors introduced by slowing down the orbiter.

c. <u>Effect on weight of lander and orbiter.</u> If the lander is not accelerated along the trajectory, the equivalent savings in propulsion weight can be used to provide additional propulsion or payload on the orbiter. Since the orbiter must be decelerated anyway (at injection), this extra propulsion is a bonus. It is not so efficient to decelerate the orbiter at this range, but there is nevertheless a weight savings.

For example, the penalty in slowing down a 4500-pound orbiter (approaching at 5 km/sec) with a 500-fps tangential velocity increment at 10^6 km, rather than at the injection point, is about 42 pounds. At the same time the weight saving from not accelerating the lander is 97 pounds, resulting in a net weight saving of 55 pounds by decelerating the orbiter rather than accelerating the lander to obtain the required lander lead time.

d. <u>Effect on sterilization requirements.</u> Applying a velocity change to the orbiter may increase the probability of the unsterilized orbiter impacting on the planet. However, an unlikely sequence of events must occur to cause orbiter impact. The malfunction must be undetected prior to retrorocket firing. The velocity change due to the malfunction must be in the proper direction. The DSIF command to correct the trajectory error must fail to be carried out. If the probability of these events occurring is shown to be unacceptably high, the velocity change could be applied in smaller increments, allowing time between impulses to ensure by DSIF tracking that the retrothrust maneuver is being performed correctly.
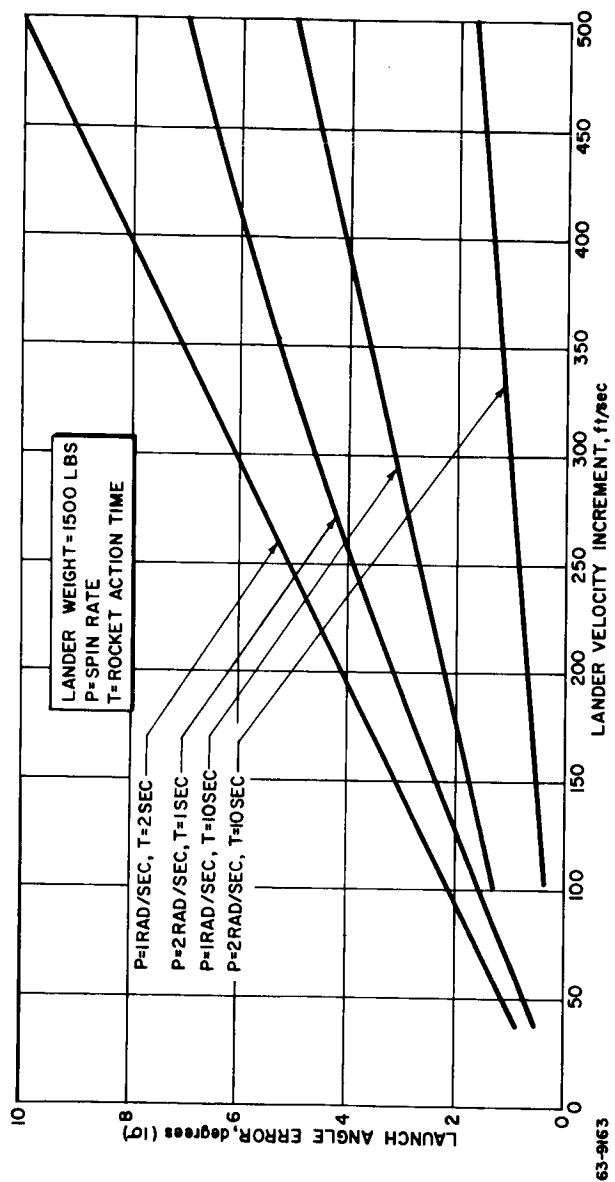
Figure 118 LAUNCH ANGLE VERSUS VELOCITY INCREMENT

63-9163

-238-
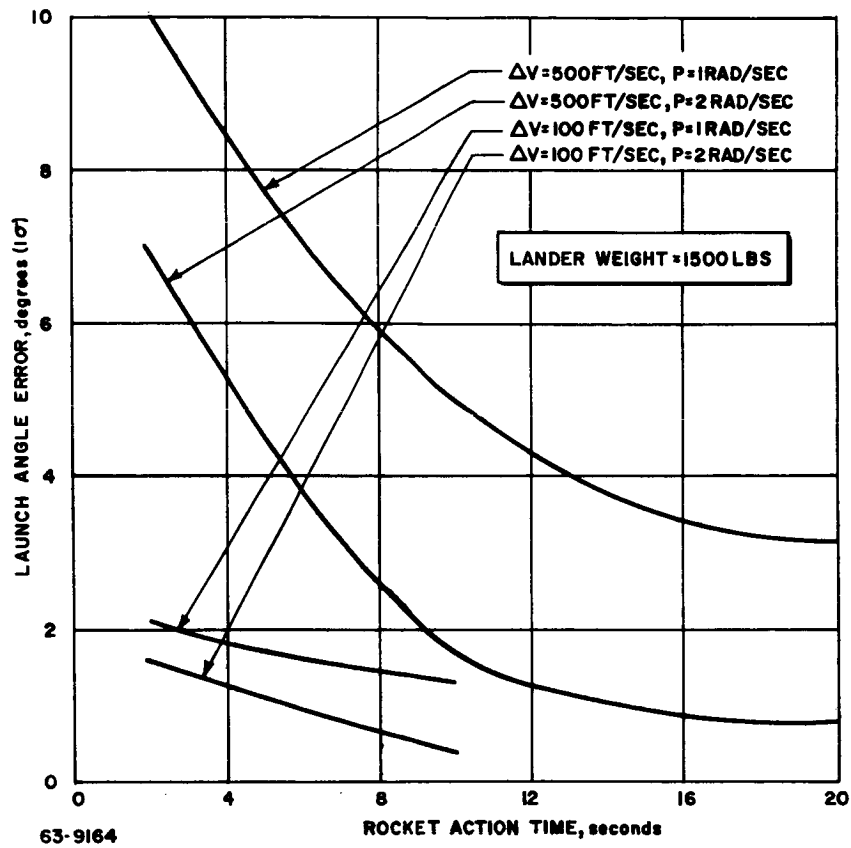
Figure 119 LAUNCH ANGLE ERROR VERSUS ROCKET ACTION TIME

63-9164
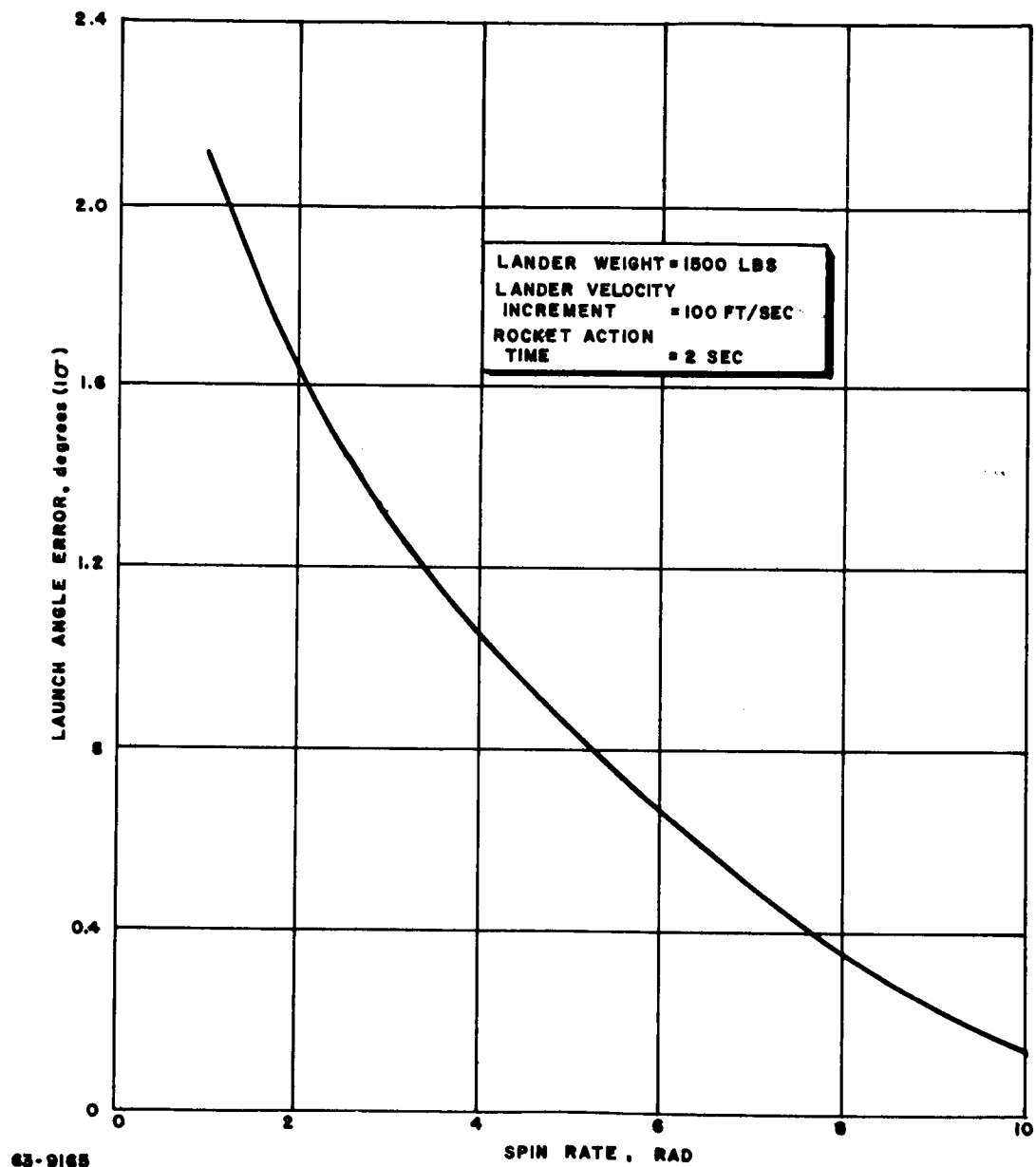
Figure 120 LAUNCH ANGLE ERROR VERSUS SPIN RATE

63-9165
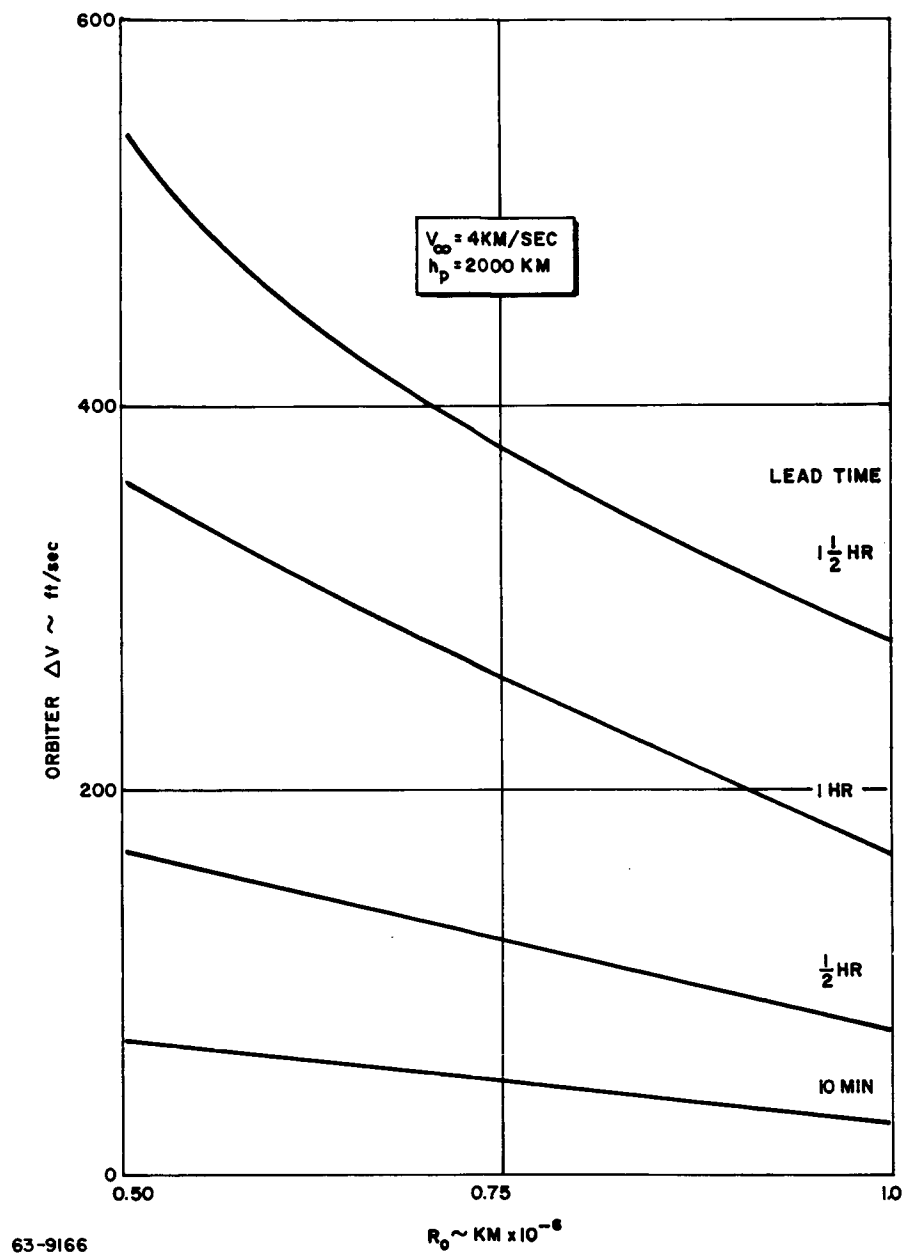
Figure 121 ORBITER RETRO VELOCITY VERSUS SEPARATION
DISTANCE, $V_\infty = 4$ KM/SEC

63-9166
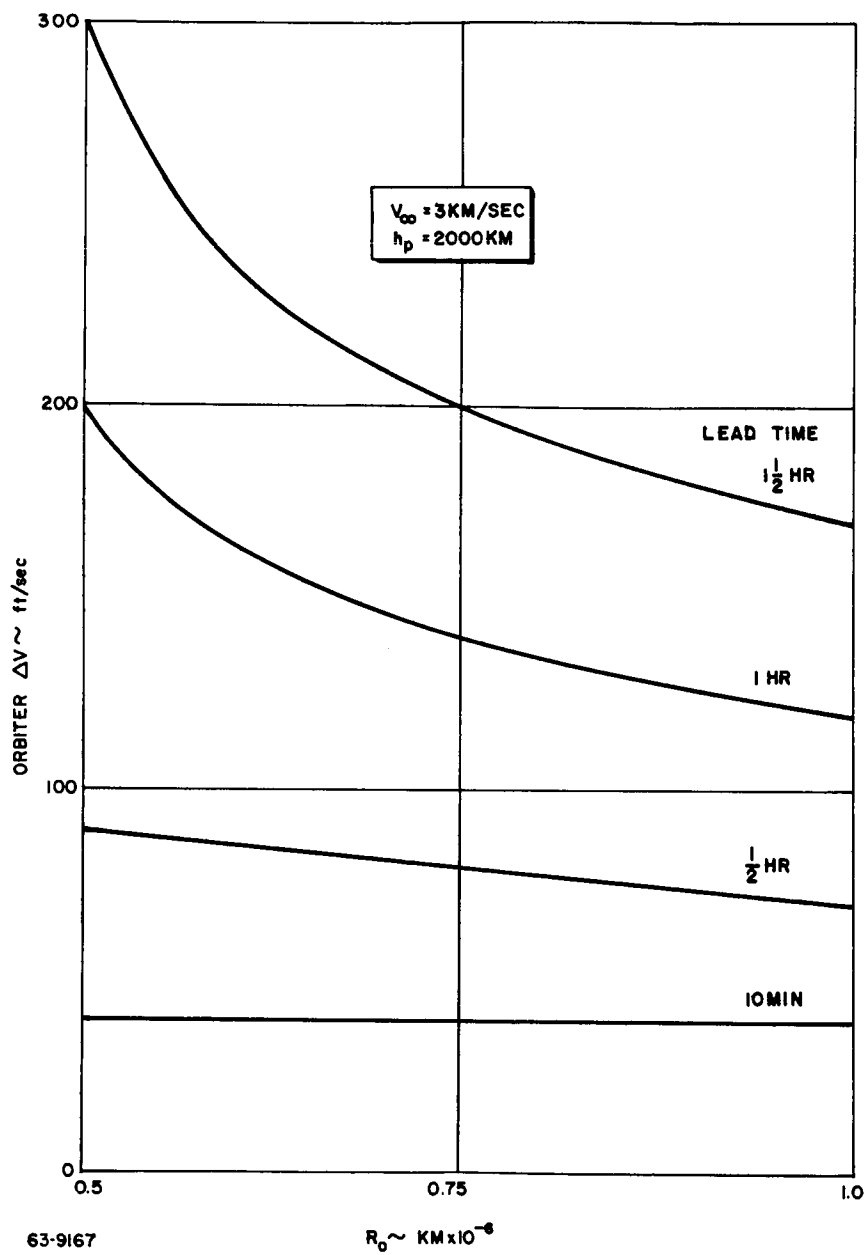
Figure 122 ORBITER RETRO VELOCITY VERSUS SEPARATION
DISTANCE, $V_\infty = 3$ KM/SEC
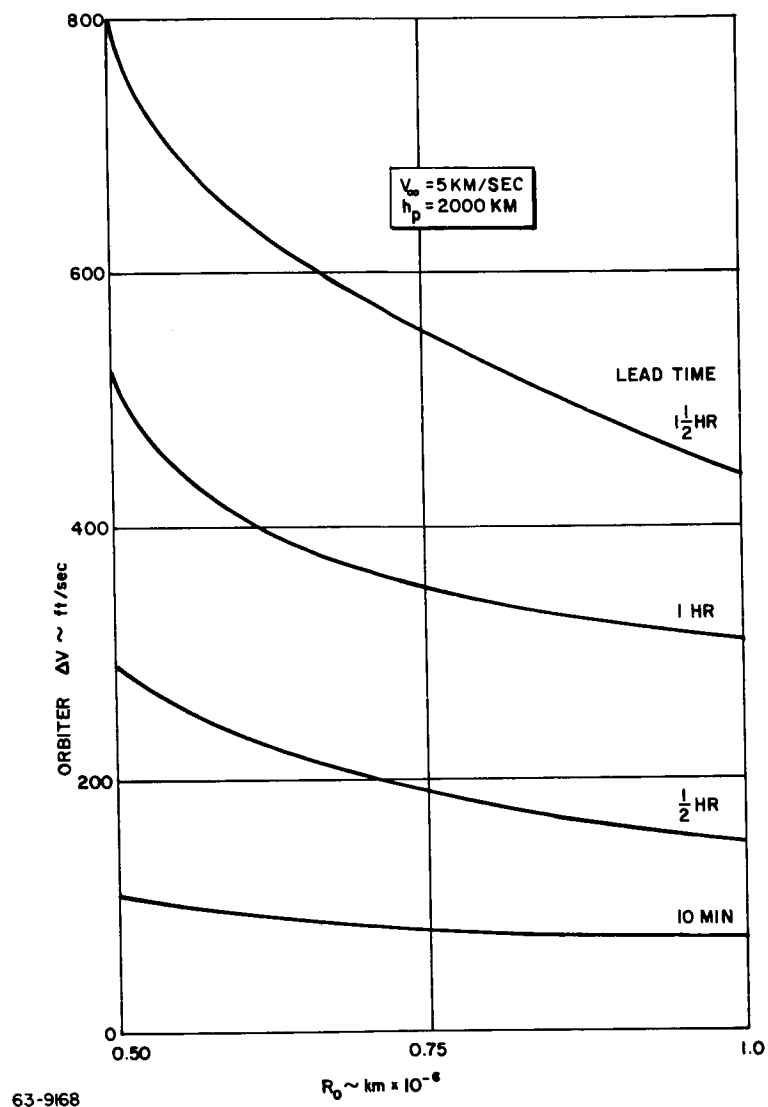
Figure 123 ORBITER RETRO VELOCITY VERSUS SEPARATION DISTANCE,
v_∞ = KM/SEC

63-9168
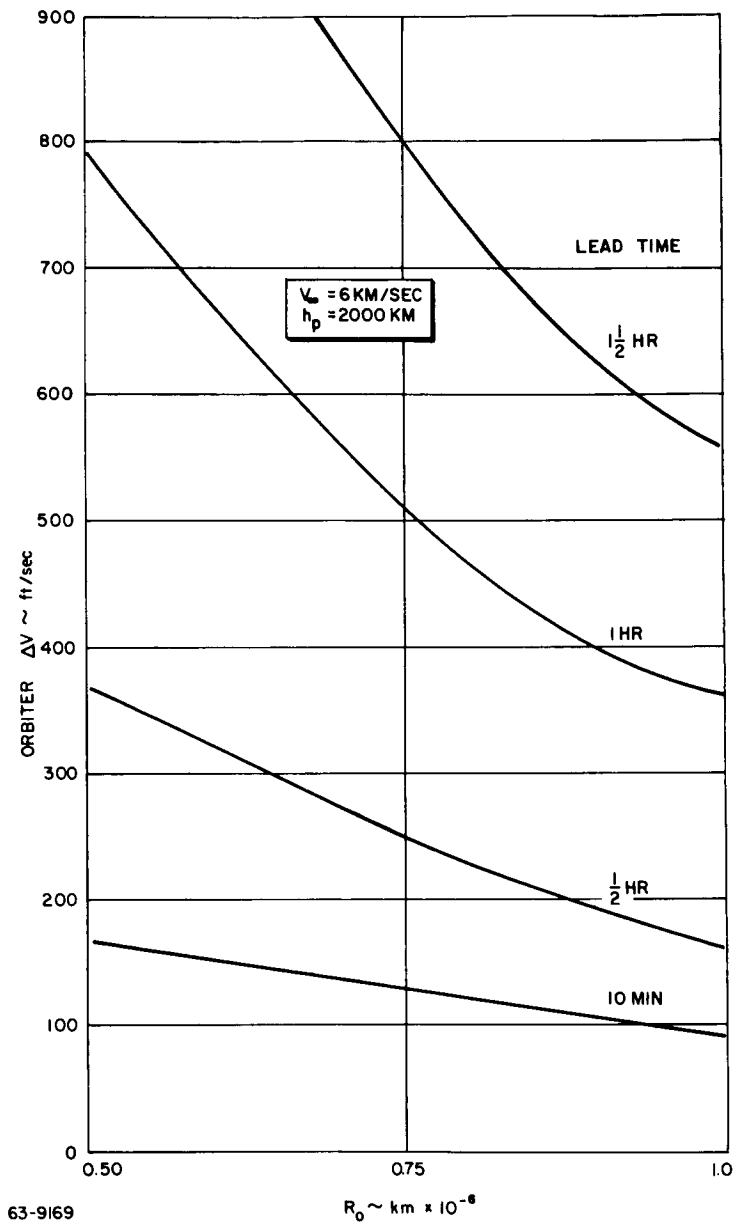
Figure 124 ORBITER RETRO VELOCITY VERSUS SEPARATION DISTANCE,
v_∞ = KM/SEC

63-9169

-244-
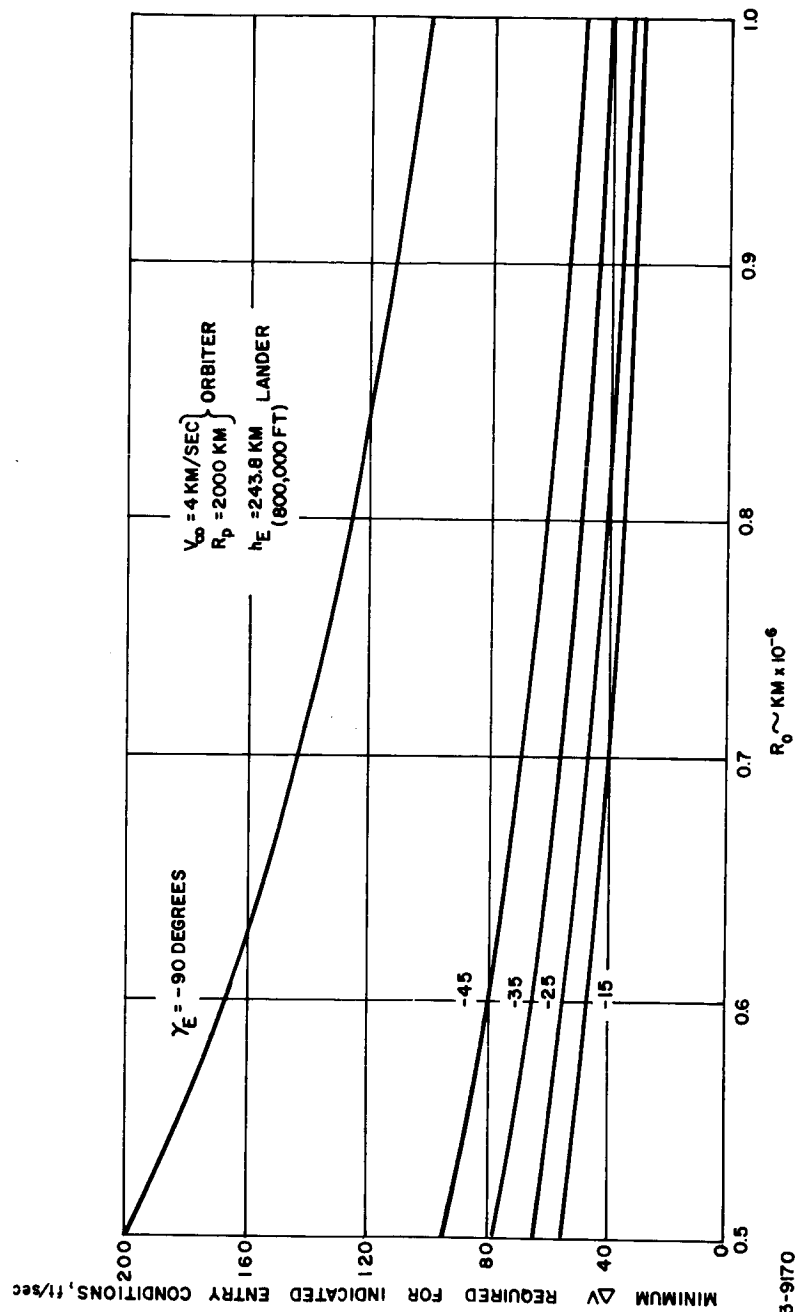
Figure 125 MARS LANDER MINIMUM Δv VERSUS SEPARATION
DISTANCE, $v_\infty = 4$ KM/SEC

63-9170

-245-
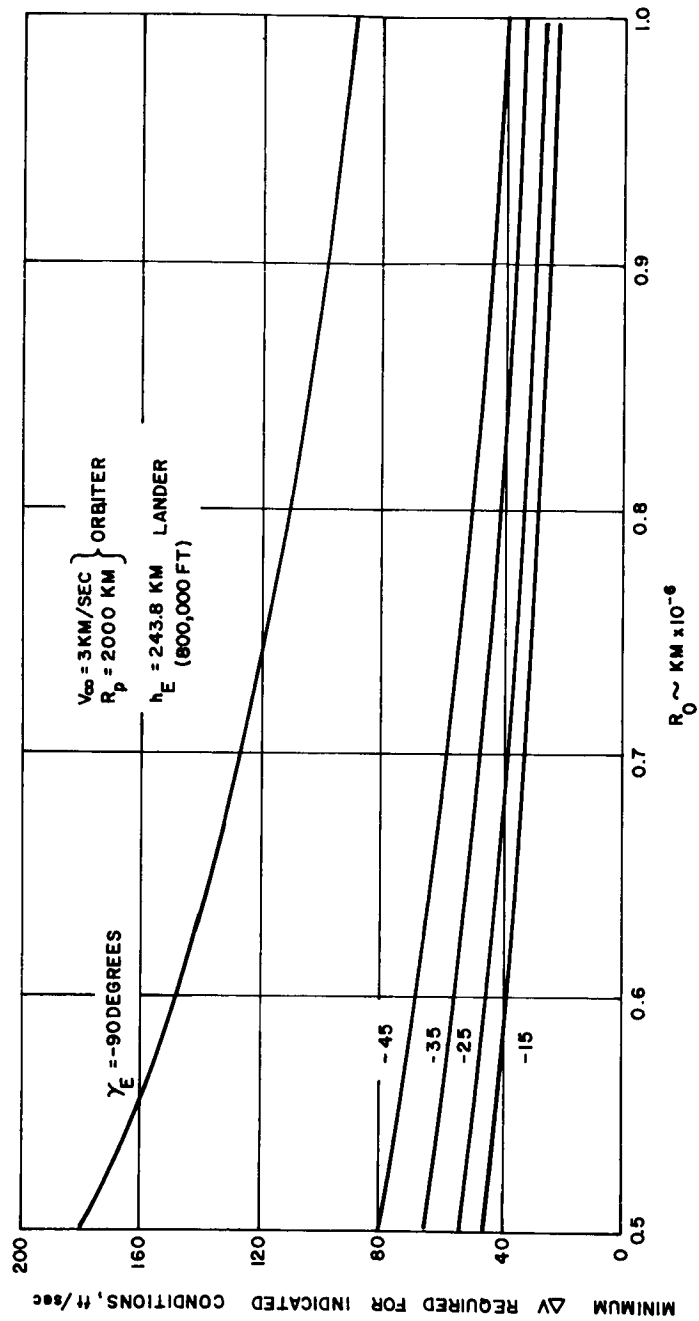
Figure 126 MARS LANDER MINIMUM ΔV VERSUS SEPARATION
DISTANCE, $V_\infty = 3$ KM/SEC

63-9171

-246-
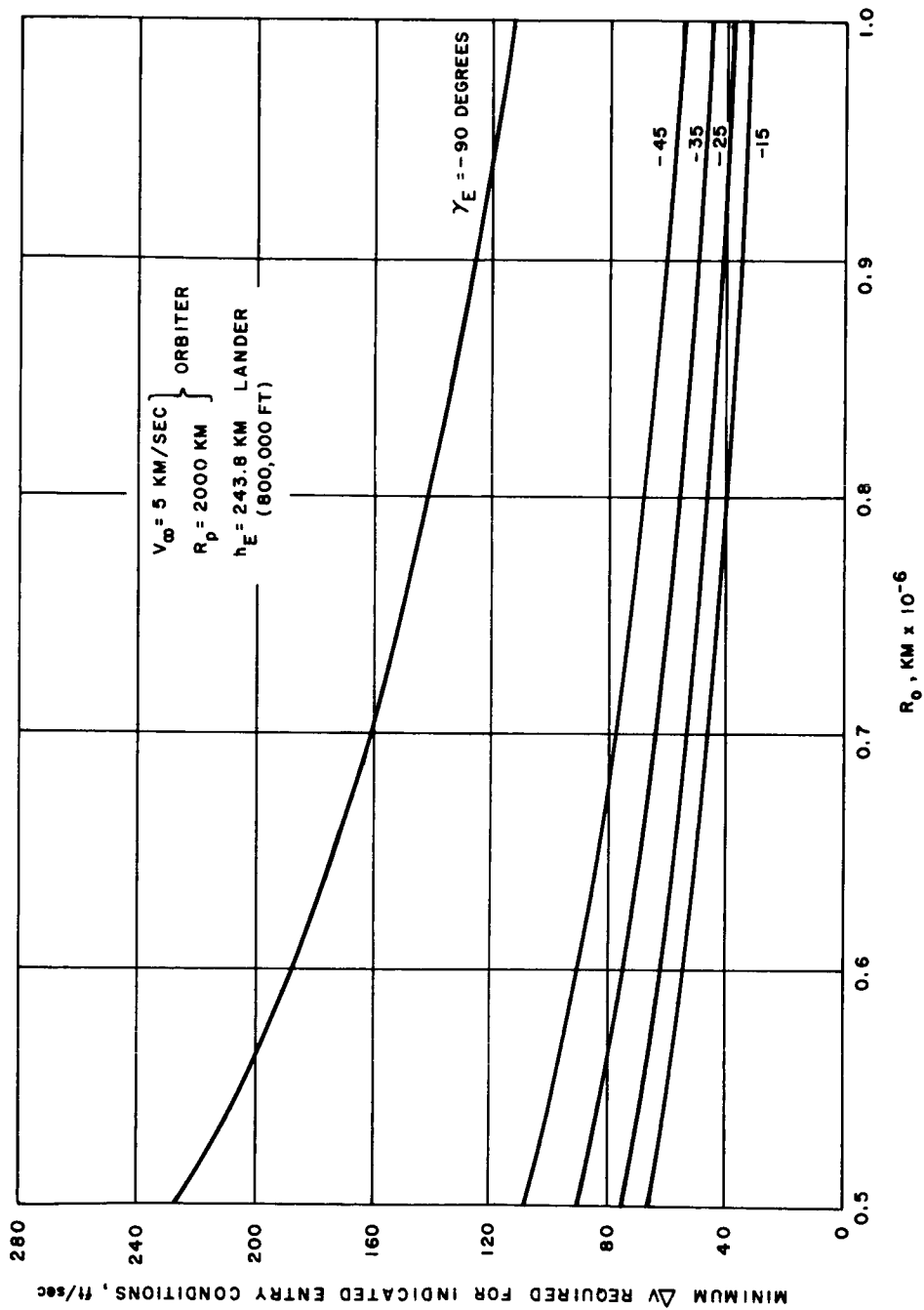
Figure 127 MARS LANDER MINIMUM ΔV VERSUS SEPARATION DISTANCE, $v_\infty = 5$ KM/SEC

63-9172

-247-
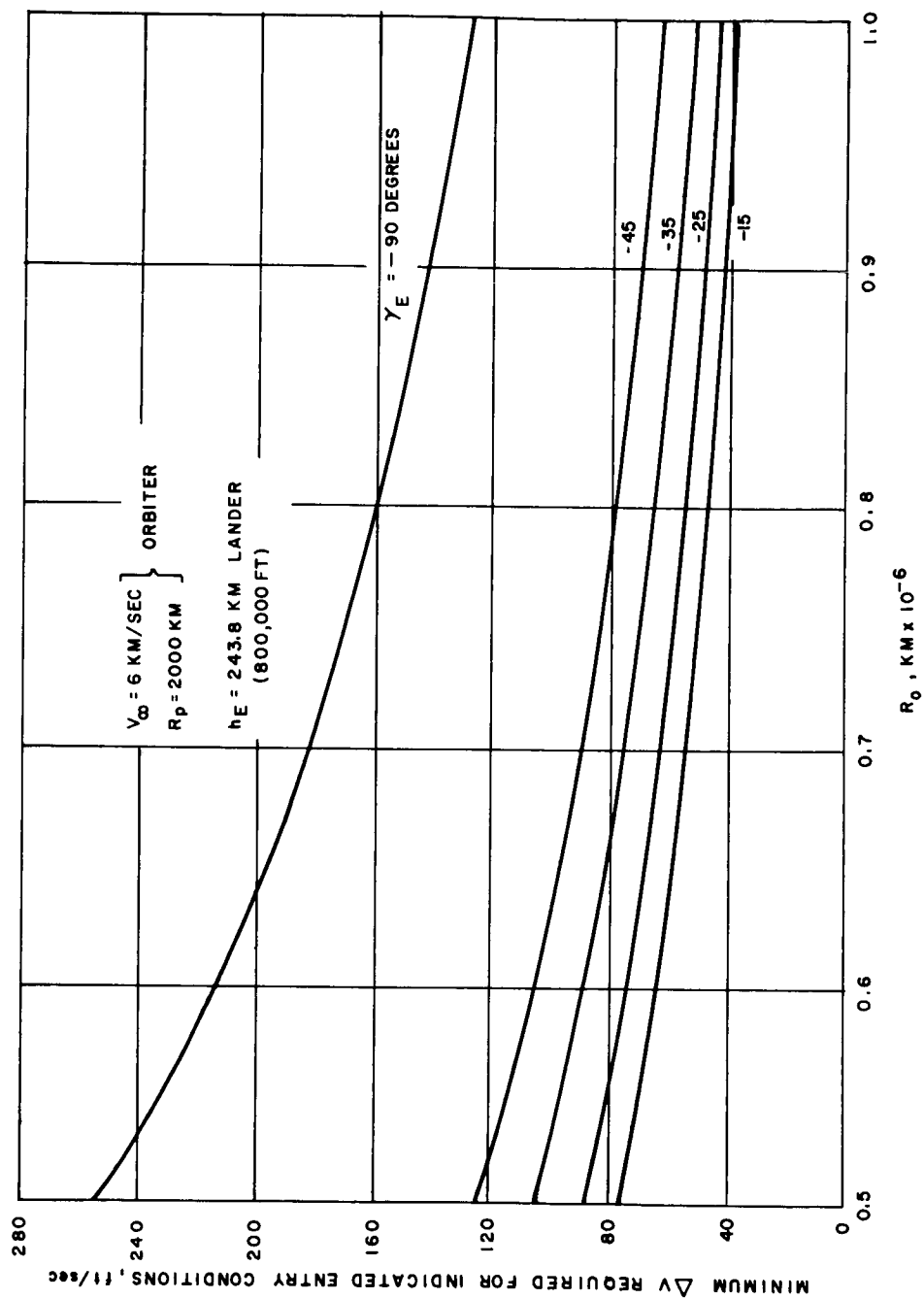
Figure 128 MARS LANDER MINIMUM Δv VERSUS SEPARATION DISTANCE, $V_\infty = 6$ KM/SEC

63-9173

-248-
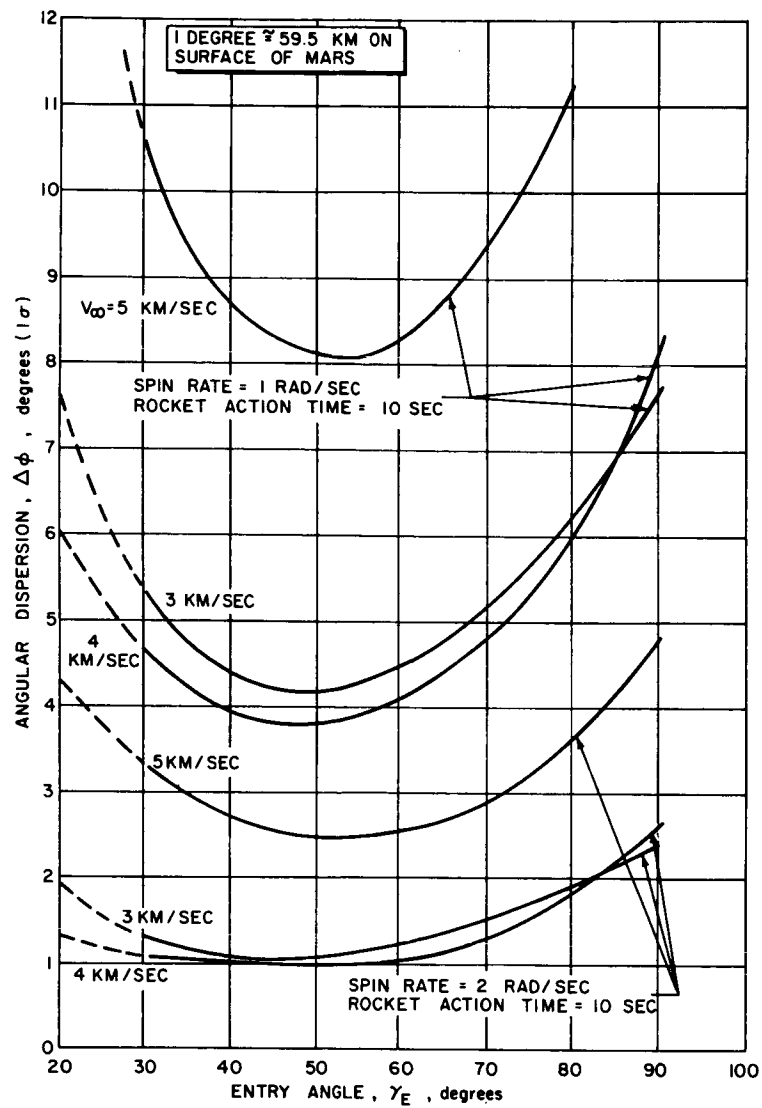
Figure 129 DISPERSION DUE TO LAUNCH ANGLE ERROR FOR
LANDER SPEEDUP

63-9174

e. Complexity of mechanization. Slow-down of the orbiter does not increase the complexity of the system, since it makes use of equipment already present. Furthermore it eases a number of difficult problems. If the lander is accelerated along the flight path, control of its attitude is critical. To avoid a closed loop attitude control system, spin stabilization is desirable; spin rates as high as 100 rpm may be required. Large spin rates impose severe structural and mechanical design problems; probably a despin device will be required prior to entry into the atmosphere.

3. Conclusion. The advantage of applying a retrograde velocity change to the orbiter is clear cut and constitutes the reference design. The orbiter will be slowed in its trajectory by a sufficient amount to provide the necessary lander lead time.

6.3 Lander-Orbiter Separation

1. Factors affecting separation range. At a precomputed time or distance from the arrival planet, the interplanetary vehicle will be oriented for lander separation, and the lander will be ejected, stabilized, and imparted a velocity increment for impacting at the desired site. The direction of velocity increment will be near normal to the orbiter approach velocity vector. After separation, the orbiter will be slowed down to allow the lander to lead the orbiter by the required amount for the communication relay operation.

Selection of the ideal separation range is largely a tradeoff between orbiter and lander payloads and the dispersion of the lander and orbiter, the dispersion being predominantly influenced by the launch-angle error and the type of guidance system employed. At present, two basic guidance systems have been considered. One technique relies entirely on the DSIF network which is theoretically able to compute the position of the vehicle approaching Mars to a constant $1-\sigma$ accuracy of ± 150 km. The 150 km error in position measured from an Earth coordinate frame translates into a flight path angle error in the planetocentric frame. The other guidance technique considered utilizes self-contained terminal guidance to supplement the DSIF network. This second system enables accuracy improvement in determining position and velocity as the vehicle approaches the planet.

2. Effect of separation range on payloads. The magnitudes of the velocity increments for establishing the desired lander and orbiter trajectories influence the payloads and are a function of the approach geometry, landing site, separation range, and desired lead time. In general, lander separation at the range between 300,000 to 1,000,000 km is considered feasible from the standpoint of dispersion, payloads, and communication relay.

The effect of separation range on payload is shown for the 4 km/sec approach velocity in figure 130. In this case, the combined vehicle weighs 6500 pounds and the lander weighs 2000 pounds. After separation, the lander is applied a velocity increment ΔV_N to rotate its velocity vector to provide the desired entry angle. The curves for γ_E = 45 degrees show that the effect of the decrease in range from 1,000,000 down to 500,000 km results in a 1 percent decrease in orbiter preinjection weight and lander weight. In the case of a higher approach velocity and steeper entry angle, the effect of decrease in range on the orbiter payload is more significant as shown in figures 130 through 133. In figure 133, we see that for V_∞ = 6 km/sec and γ_E = 90 degrees, the decrease in orbiter weight due to the decrease in separation range is 3 percent.

These results show that the effect of separation range on payload is of minor consequence for the ranges considered. The major factor, therefore, is that of landing site accuracy. In the cases where the two different types of guidance systems described are considered, the effects of low entry angle, high approach velocity, and short ranges are significant.

3. <u>Lander dispersion.</u> The dispersion of the lander at entry is a central-angle variation due primarily to the uncertainties in the approach velocity and initial position and in the imparting of a velocity vector change to the lander for landing site selection. As pointed out before, a major factor influencing the separation range is the resulting dispersion of the lander.

The effect of separation range on dispersion as a function of launch angle error is insignificant for the case of a constant entry angle and approach velocity. A decrease in the separation range is compensated for by the corresponding increase in the magnitude of the launch velocity increment.

4. <u>Effect of separation range on lander impact dispersion with DSIF guidance.</u> The error in achieving the desired landing point is primarily a result of the initial position and velocity errors of the orbiter prior to lander separation and the additional velocity error imparted to the lander during the separation sequence. The initial velocity error is negligible and the initial position error either remains a constant ± 150 km or decreases significantly with range, depending on whether or not the accuracy of the DSIF network is supplemented by application of a terminal guidance system on the orbiter. When no self-contained terminal guidance system is employed and the DSIF network is utilized alone, a constant value for dispersion ($\Delta\phi$) for each entry angle and approach velocity results. The dispersion $\Delta\phi$ refers to the variation in central angle measured at the planet's surface. For conversion from angular to linear units at the surface of Mars 1 degree equals 59.5 km. The 150-km error in position measured from an Earth-centered coordinate frame translates into a flight path angle error in the planetocentric frame. From figure 134 with V_∞ = 4 km/sec, the 1-sigma dispersion, $\Delta\phi$, for the entry angle γ_E of 45 degrees is 2.75 degrees. For the 90- and 30-degree entry angles, $\Delta\phi$ is

2.02 and 3.88 degrees, respectively. The figure also shows that an increase in approach velocity from 3 to 6 km/sec increases the dispersion from 2.43 to 3.02 degrees for the case of a 45-degree entry angle.

5. Effect of separation range on lander dispersion with terminal guidance.
When a self-contained terminal guidance system is used to supplement the Earth-based DSIF network, the accuracy in determining position and velocity of the vehicle as it approaches the planet is improved. Since terminal guidance is used, the errors in range and velocity reduce from that resulting from the DSIF system to zero as the range decreases to zero.

Figures 135 through 138 show the effect of range on dispersion as a function of approach velocity and entry angle. As shown in figure 135 where V_∞ = 4 km/sec, the 1-sigma dispersion for the case of an entry angle of 45 degrees is 2.1 and 1.1 degrees at the ranges of 10^6 and 0.5×10^6 km, respectively.

The effect of range on dispersion is especially significant in the case of low entry angles and high approach velocities. For example, figure 138, where V_∞ = 6 km/sec, shows that when γ_E = 30 degrees, the one-sigma (1σ) dispersion error $\Delta\phi$ is 5.8 degrees and 1.7 degrees for separation at 10^6 and 0.5×10^6 km, respectively.

A comparison of figure 134 and figures 135 through 138 shows that the accuracy of the terminally guided system for the shallow entry angle of 30 degrees is actually worse than that of the DSIF system until the vehicle has approached within a 0.75×10^6-km range. This result suggests using the DSIF system as long as possible for the shallow entry angle cases. For any separation range, the maximum propulsion requirements ΔV_N and ΔV_T exist for the steepest entry angle, 90 degrees. The lander dispersion at any range is the least for the 90-degree entry angle. Therefore, if the maximum allowable dispersion is known, the corresponding range for the 90-degree entry angle can be determined from figure 139. The amount of propulsion sized for that range will then be more than adequate for all shallower entry angles. For example, from figure 139 at the entry angle of 90 degrees, the range corresponding to a 1.2-degree (1σ) dispersion, $\Delta\phi$ is 10^6 km. The ΔV_N requirements for lander ejection and ΔV_T requirement for orbiter slow-down for this case are 90 and 133 fps, respectively. From the graph we see that for the same $\Delta\phi$ and a desired entry angle of 45 degrees, the separation range should be approximately 0.535×10^6 km. The corresponding propulsion requirements in terms of velocity increments are ΔV_N = 76 fps and ΔV_T = 104 fps, respectively, both less than required for the 10^6-km, γ_E = 90 degrees separation.

Figure 140 shows basically the same information in another form to better observe the relation between entry angle and range for constant dispersion and propulsion parameters. From it, we can see that for a 90-degree entry angle and a 3.6-degree (3σ) allowable dispersion, the separation range should be at

10^6 km, and for a 45-degree entry angle, the separation range should be at 0.535 x 10^6 km. The Δv_N and Δv_T requirements for the 90-degree and 45-degree entry angles are indicated.

6. Conclusions. In the case of a terminally guided vehicle, the ideal separation range depends on the desired landing site (entry angle) and corresponding allowable dispersion; for steep entry angles, separation should be at a long range (around 10^6 km), and for a shallow entry angles, separation should be closer to the planet (around 0.3 x 10^6 km). If more accuracy is required, then separation can be achieved at shorter ranges at the expense of a larger propellant penalty.

In the case of a vehicle relying entirely on the DSIF system for guidance, the ideal separation range, although not influenced by the variation in dispersion, is influenced by the propulsion requirements, and therefore, should be at a reasonably long range (around 10^6 km).

6.4 Characteristic Velocity Requirements for Special Maneuvers

1. Summary of ΔV requirements. Table 41 lists the individual velocity requirements and corresponding times for accomplishing the various maneuvers occurring from departure through terminal orbit injection.

2. Guidance aiming requirements to avoid a planetary atmosphere.

a. Introduction. Unless a spacecraft is sterilized, it is undesirable that it enter the atmosphere of another planet. Therefore the approach asymptote must be at such a distance from the planet that the periapsis altitude is above the top of the atmosphere. Guidance errors require that the spacecraft be aimed still further away to limit the probability of these errors resulting in a closer approach than desired. Therefore, an offset or "intentional miss" is required when guiding the spacecraft to a planet if it is necessary to miss the planetary atmosphere with a specified probability. Since this offset must be removed to achieve a subsequent planetary orbit, an additional velocity increment must be imparted to the vehicle.

b. Method of analysis. A statistical treatment of the problem may be considered in terms of the probability that a spacecraft aiming for a point located at a distance ρ from the center of the planet will pass within a circle of radius r around the planet and consequently be deflected to a periapsis of distance less than r.

For statistically independent gaussian random variables x and y with zero means and variances σ_x^2 and σ_y^2, the bivariate normal distribution function is

-253-

$$f(x, y) = \frac{1}{2\pi\sigma_x\sigma_y} e^{-\frac{1}{2}\left(\frac{x^2}{\sigma_x^2} + \frac{y^2}{\sigma_y^2}\right)} . \tag{2}$$

The probability of a point (x, y) falling within an area A is given by

$$P = \iint_A f(x, y) \, dx \, dy . \tag{3}$$

In principle, solving equation (3) will yield the value for ρ. However, in this case the rather rigorous method can be simplified by certain approximations. If ρ is much larger than r, then the assumption that $f(x, y)$ is constant over A is valid, then equation (3) becomes

$$P = \frac{r^2}{2\sigma_x\sigma_y} e^{-\frac{1}{2}\left(\frac{x^2}{\sigma_x^2} + \frac{y^2}{\sigma_y^2}\right)} \tag{4a}$$

$$= \frac{r^2}{2\sigma^2} e^{-\frac{\rho^2}{2\sigma^2}} \tag{4b}$$

when

$$\sigma_x = \sigma_y = \sigma \quad \text{and} \quad \rho^2 = x^2 + y^2 .$$

c. <u>First and second midcourse corrections for Mars</u>. For the case of a spacecraft approaching Mars at 20,000 ft/sec (6.1 km/sec), $r = 6220$ km for a periapsis altitude of 1800 km, the probability P of 1 in 10,000, and a guidance error σ of 20,000 km for the first midcourse correction, solving equation (4b) for the aiming distance results in $\rho_1 = 70,300$ km.

For the second midcourse correction, the guidance error 1-σ value is 2000 km, resulting in the aiming point distances ρ_2 of 9300 km from equation (4b). However, the assumption that $f(x, y)$ is constant over the area A is not valid when the offset is that small.

TABLE 41

MARS 1969 TYPE II — INCREMENTS REQUIRED

Event	Function	ΔV Required	Time
First Midcourse Correction	Correct injection errors	10 m/sec*	T + 5 days
Second Midcourse Correction	Vernier to previous correction	1 m/sec*	T + 10 days
Third Midcourse Correction	Correct effects of solar radiation pressure and time of arrival	30 m/sec*	E - 5 to 10 days
Separate Lander	Place lander on impact trajectory	9 to 78 m/sec	E - 2 to 5 days
Orbiter Slowdown	Provide lead time for lander	20 to 265 m/sec	E - 1 to 4 days
Terminal	Improve Accuracy of periapsis location	10 m/sec*	E - 0 to 2 days
Orbit Establishment	Inject orbiter into 1500 x 10,000 km orbit	2000 to 4000 m/sec	E

* - 1 Sigma Values
T - Time of Launch
E - Time of Orbit Injection
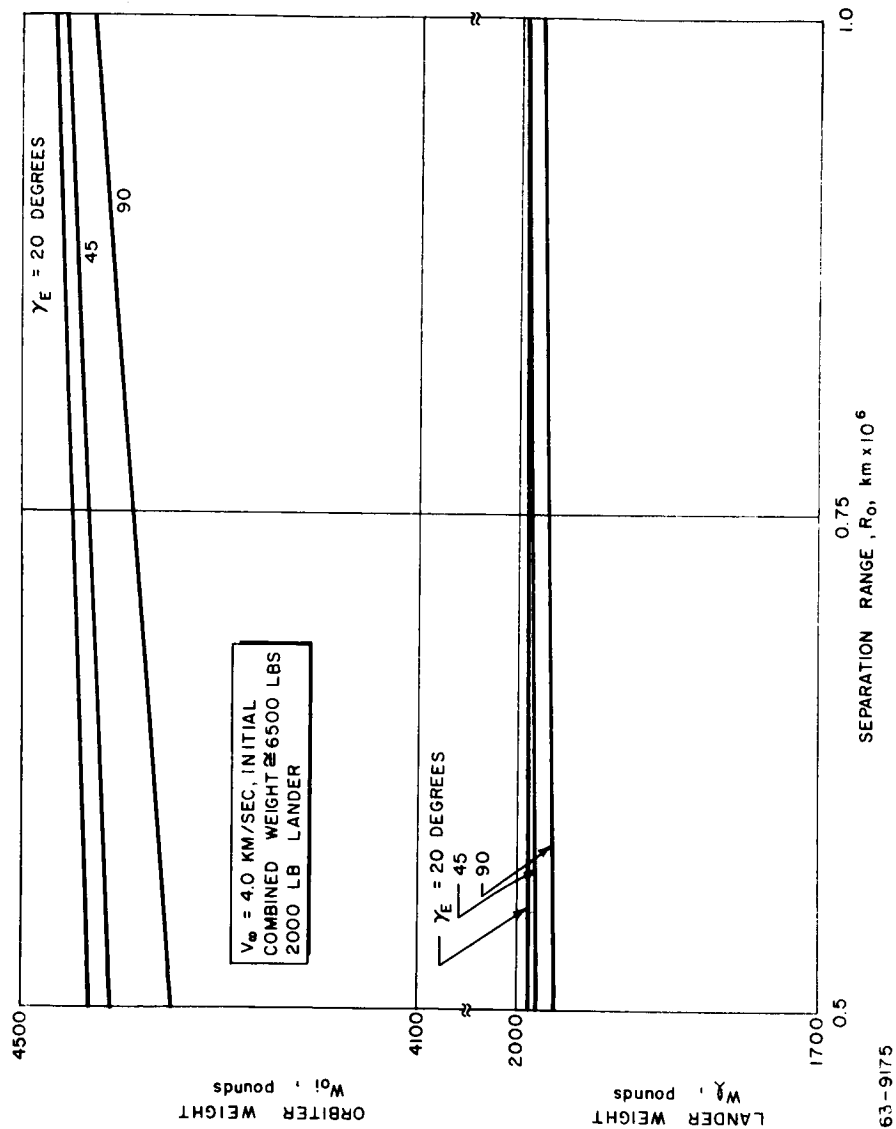
Figure 130 WEIGHT OF ORBITER AND LANDER AFTER ORBITER SLOWDOWN AND LANDER PATH CONTROL, V_∞ = KM/SEC

63-9175

-256-
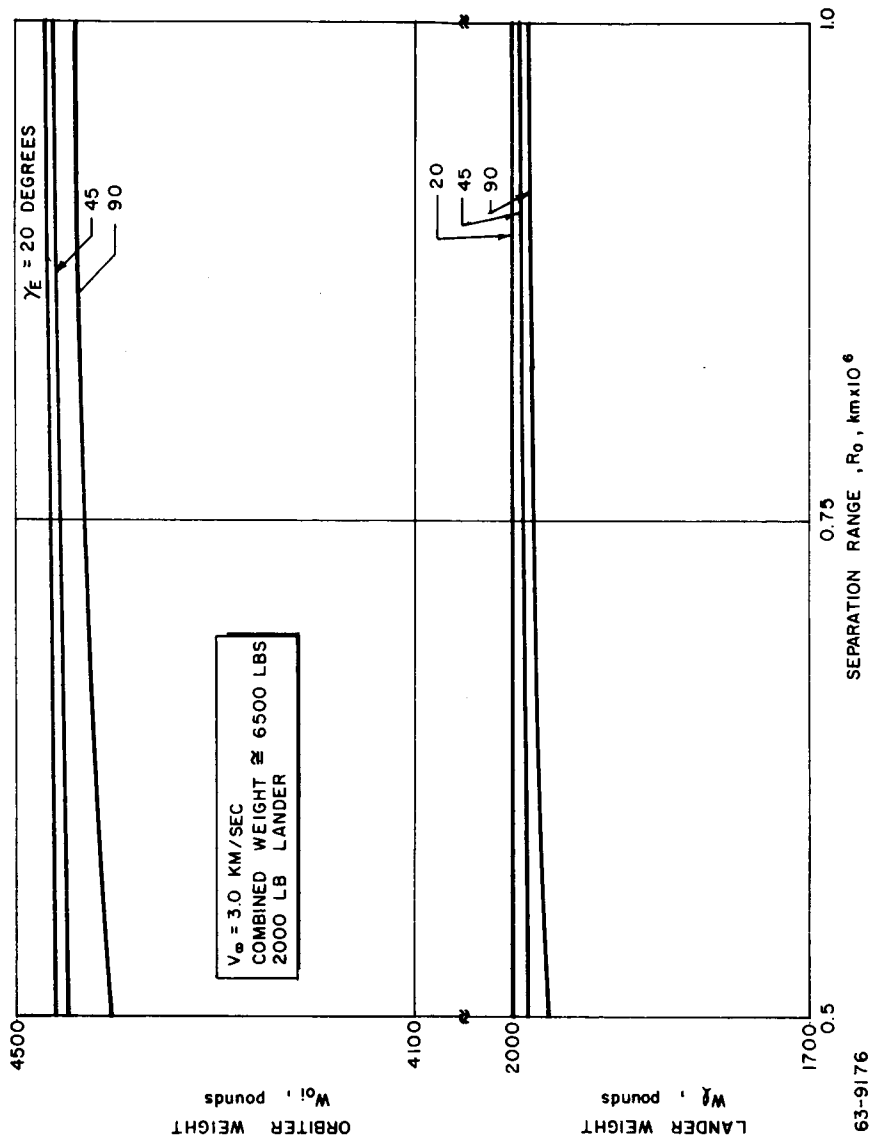
Figure 131 WEIGHT OF ORBITER AND LANDER AFTER ORBITER SLOWDOWN
AND LANDER PATH CONTROL, $v_\infty = 3$ KM/SEC

63-9176

-257-
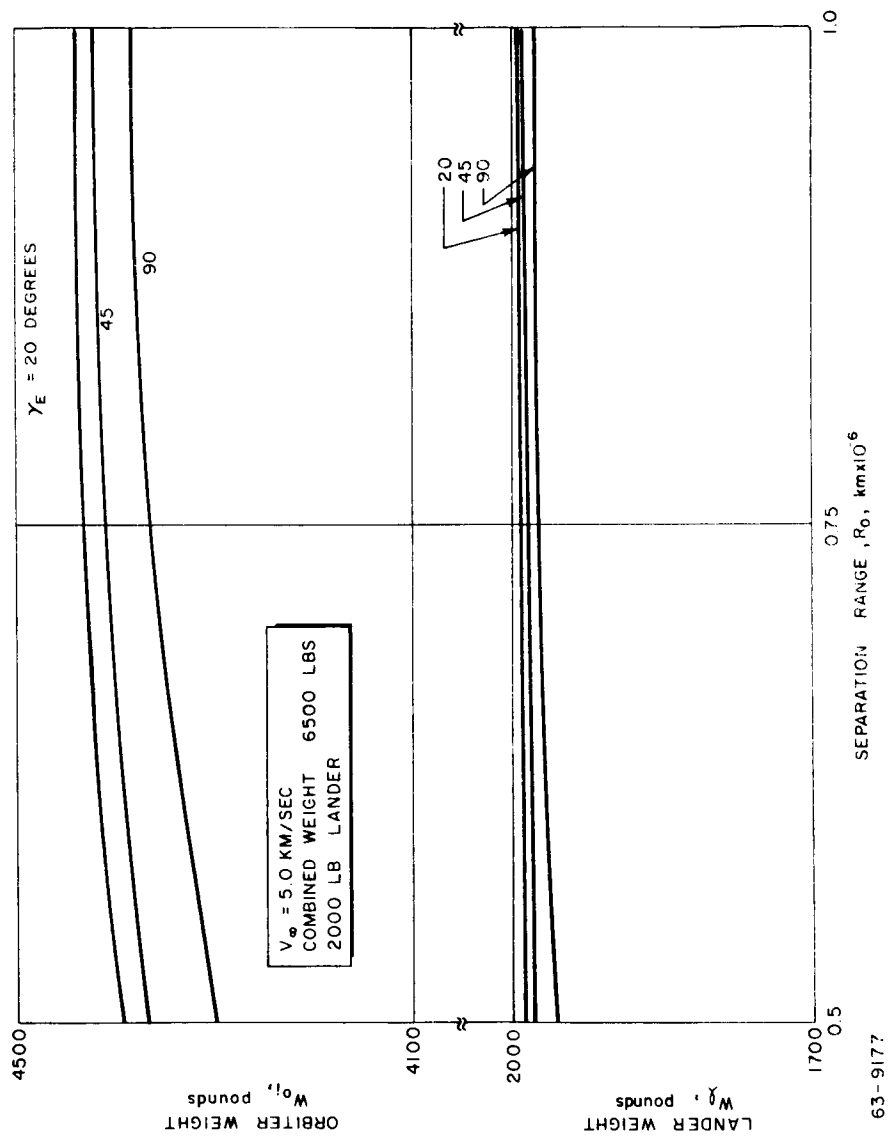
Figure 132. WEIGHT OF ORBITER AND LANDER AFTER ORBITER SLOWDOWN AND LANDER PATH CONTROL, $V_{\odot} = 5$ KM/SEC

63-9177

-258-
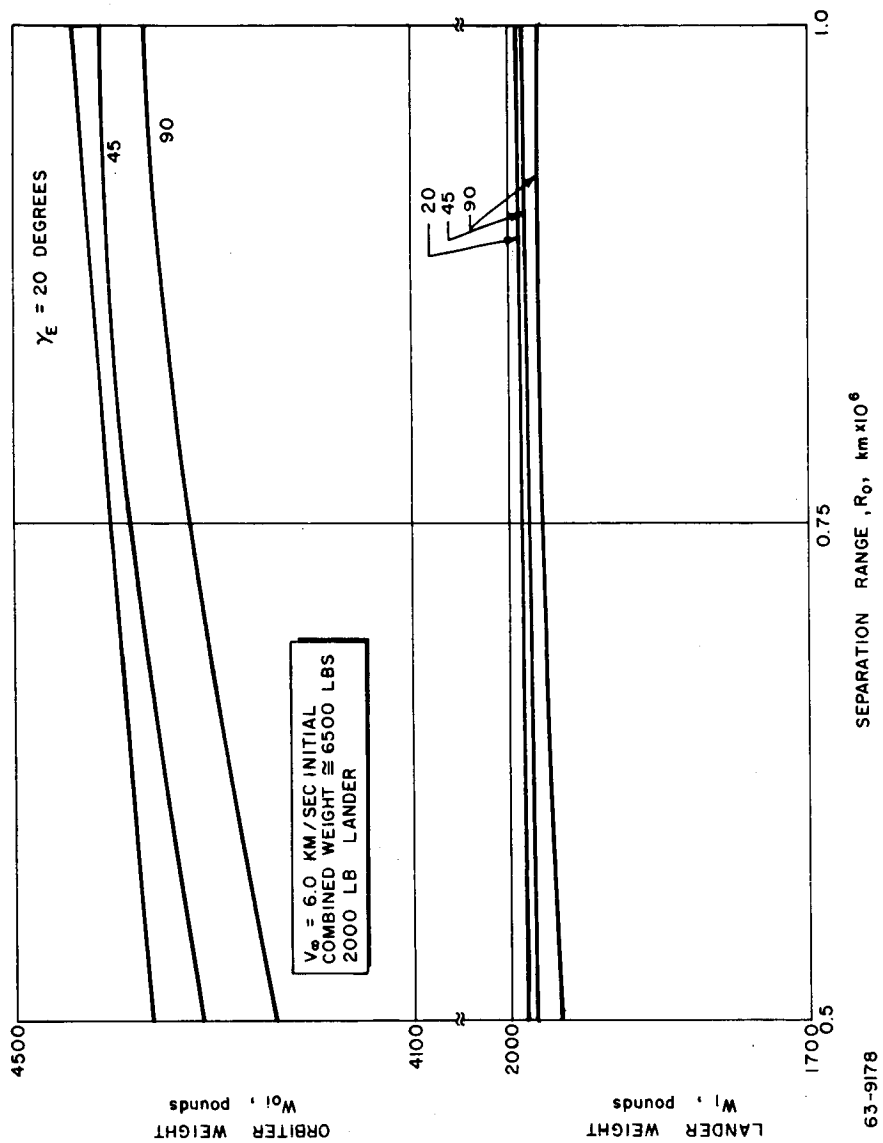
Figure 133 WEIGHT OF ORBITER AND LANDER AFTER ORBITER SLOWDOWN
AND LANDER PATH CONTROL, v_∞ = 6 KM/SEC
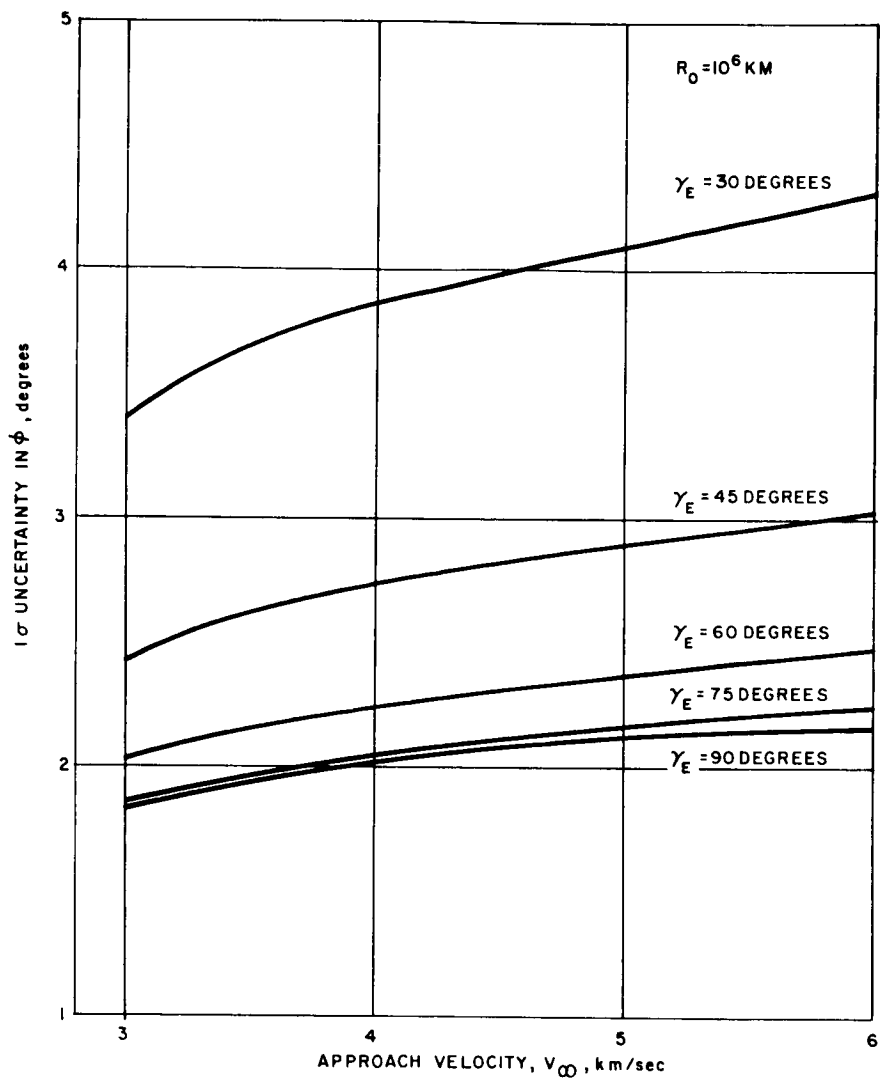
63-9736

Figure 134 LANDER DISPERSION WITH DSIF GUIDANCE
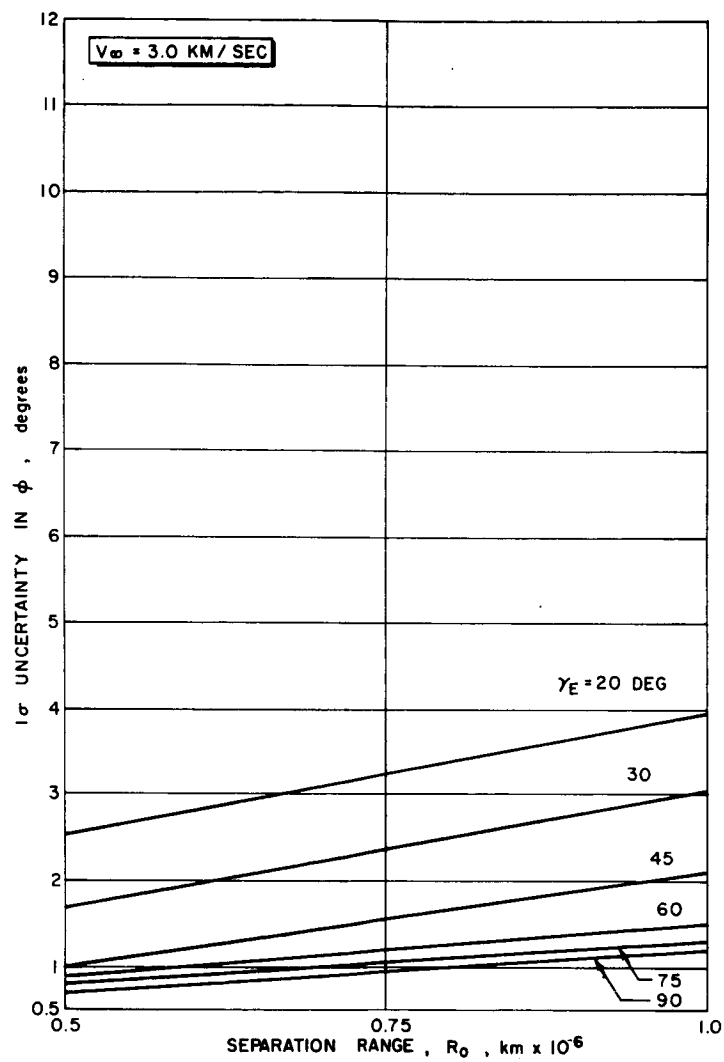
Figure 135 LANDER DISPERSION WITH TERMINAL GUIDANCE BEFORE
SEPARATION, V_∞ = 4 KM/SEC
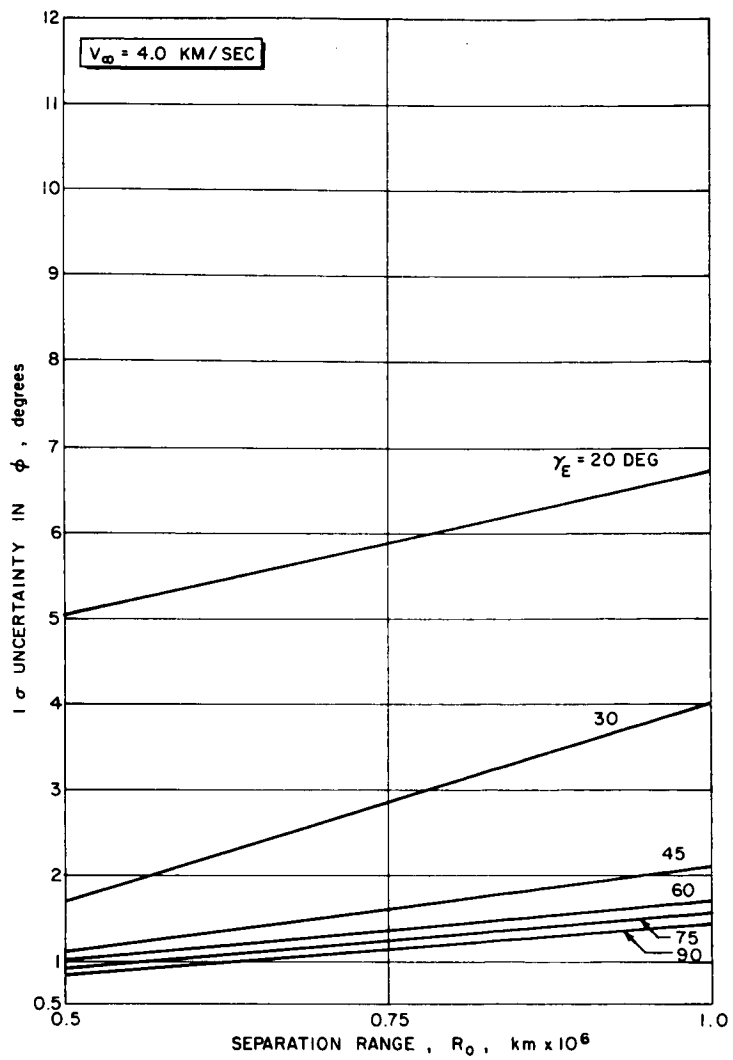
63-9184

63-9183

Figure 136 LANDER DISPERSION WITH TERMINAL GUIDANCE BEFORE
SEPARATION, $V_\sim$ = 3 KM/SEC
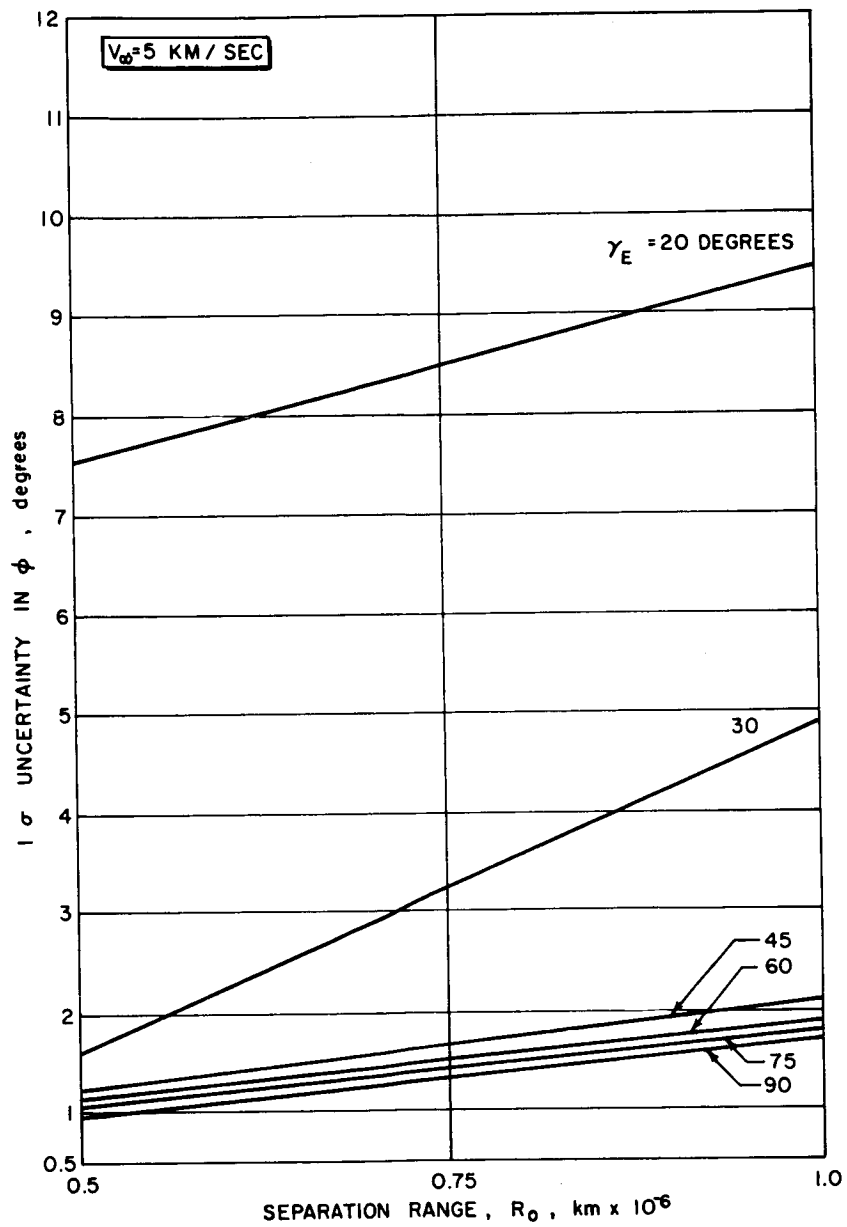
Figure 137 LANDER DISPERSION WITH TERMINAL GUIDANCE BEFORE
SEPARATION, v_∞ = 5 KM/SEC
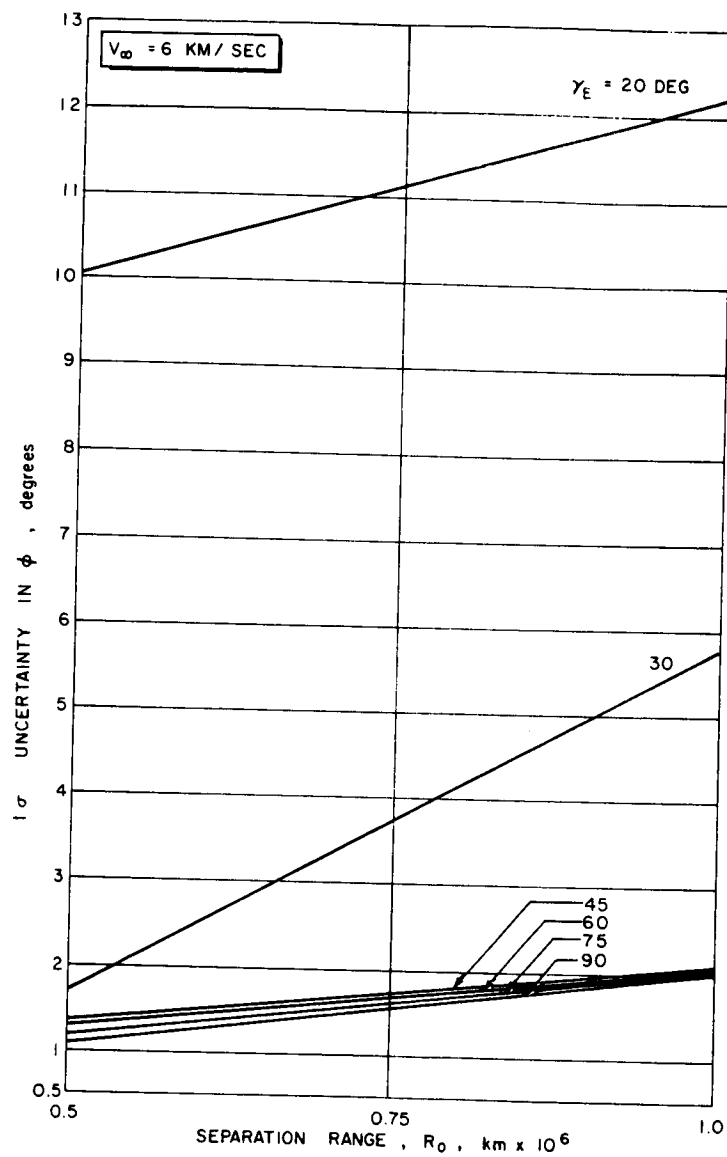
63-9185

Figure 138 LANDER DISPERSION WITH TERMINAL GUIDANCE BEFORE SEPARATION, V = 6 KM/SEC

63-9186

-264-
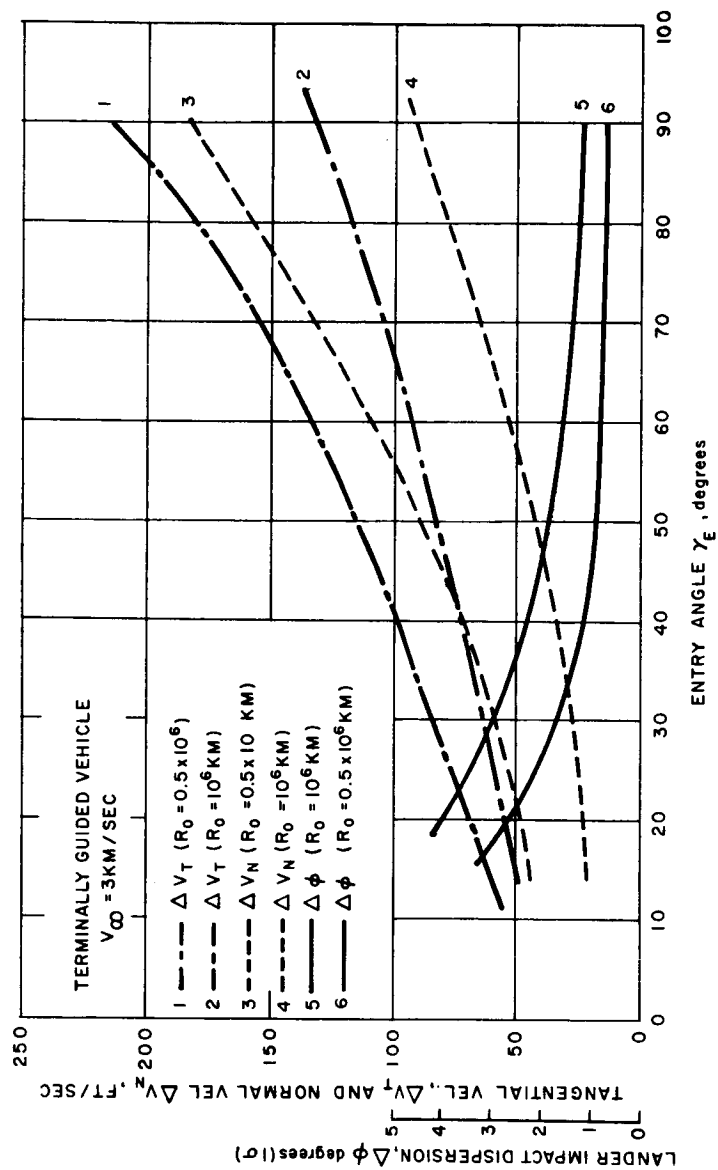
Figure 139 LANDER DISPERSION AND VELOCITY INCREMENT
TRADEOFFS, $v_\infty = 3$ KM/SEC

-265-
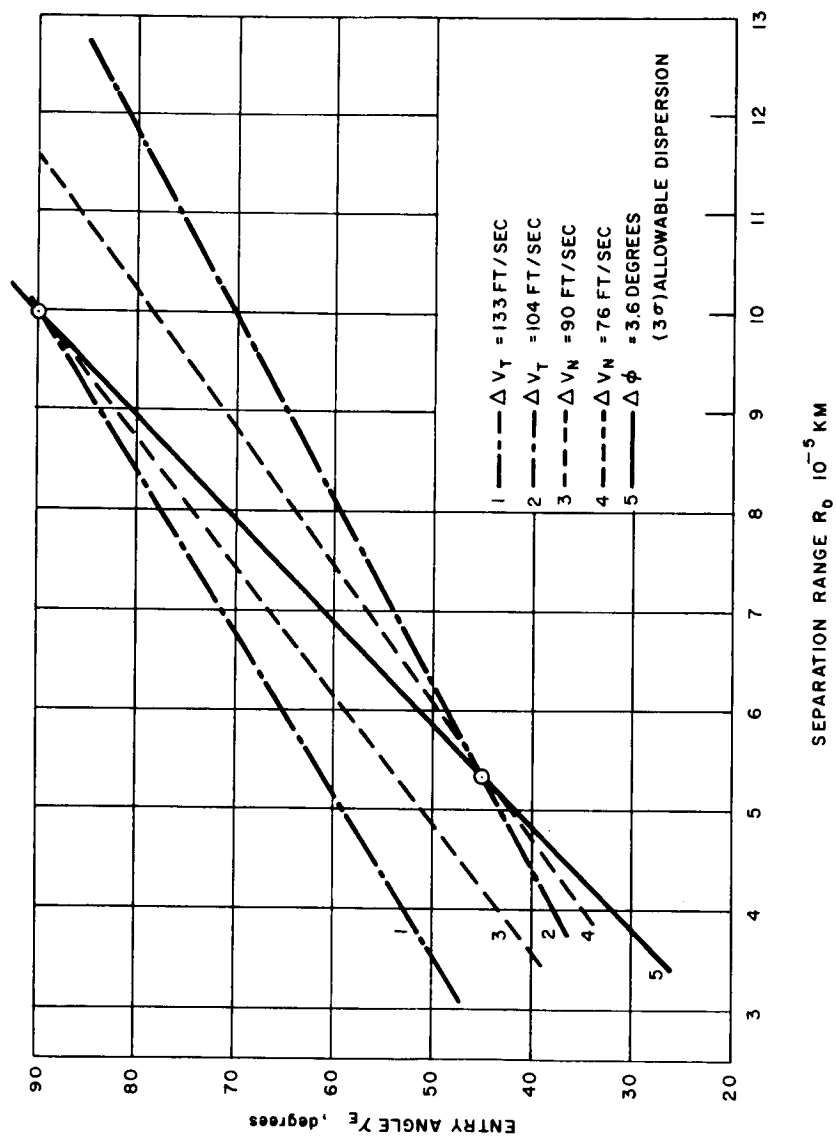
Figure 140 LANDER PROPULSION AND SEPARATION RANGE
REQUIREMENTS, $v_{\infty} = 3$ KM/SEC

63-9188

-266-

A more conservative approach is that the probability P' being outside of a circle of radius R centered at point $(0, 0)$ may be expressed as follows:

$$P' = 1 - \iint f(x, y) \, dx \, dy$$

$$= 1 - \int_0^R \frac{\rho}{\sigma^2} e^{-\frac{\rho^2}{2\sigma^2}} \, d\rho \qquad (5)$$

Integrating (5) yields

$$P' = e^{-R^2/2\sigma^2} \qquad . \qquad (6)$$

To ensure that the circle of radius r with its center at a distance ρ from the aiming point lies entirely outside the circle of radius R centered at the aiming point with probability P', then

$$\rho > R + r \qquad . \qquad (7)$$

If $R = \rho - r$ is substituted into equation (6), then

$$P' = e^{-\frac{(\rho - r)^2}{2\sigma^2}} \qquad (8)$$

and for $P' = 10^{-4}$ and $r = 6220$ km, solving equation (8) results in

$$\rho = 4.29\sigma + 6220 \qquad . \qquad (9)$$

Solving equation (9) for the aiming point ρ_2 for the second midcourse correction where $\sigma_2 = 2000$ km results in $\rho_2 = 14,800$ km instead of the 9300 km obtained from equation (4b). The true value which lies between these numbers can only be determined by integrating equation (3). For large values of ρ, equation (4b) is valid, and for the conservative case and small values of ρ equation (9) is valid.

d. <u>Third midcourse correction for Mars.</u> The final offset correction is made as the spacecraft enters the planetary field. It is made from 5 to 10 days before arrival and occurs at 1,000,000 to 3,000,000 km from the planet.

Using DSIF tracking, the guidance error σ_3 quoted for Mars distances is ±150 km. Since the calculated value of the offset ρ_3 will also be small, equation (9) is used, resulting in $\rho_3 = 6860$ km for avoiding the planetary atmosphere. If onboard tracking can reduce the guidance error, the bias can be reduced as well.

    e.   Required velocity changes for Mars.   To establish a given offset distance, it is necessary to correct for the difference or bias which exists at the time of correction. This correction maneuver requires a velocity change which imposes an additional propulsion penalty upon the spacecraft. In this example, the first correction is offset 70, 300 km, but the second is offset 14, 800 km. The difference of 55, 500 km ($\rho_1 - \rho_2$) represents the bias which must be removed at the time of second correction. The amount of velocity change to accomplish this would be less than 10 ft/sec for a typical Martian trajectory. The third correction must reduce the bias. The offset remaining is 14, 800 km from the planet center; the new aiming point is some 6800 km from the planet center. The bias to be removed is the difference $\rho_2 - \rho_3$ or 8000 km. If made 10 days prior to encounter, this will require an additional velocity change of about 25 ft/sec. Summing up the velocity increments for establishing the offsets results in 35 ft/sec (10.7 m/sec). It should be noted that these velocity corrections for establishing the offsets are independent of those listed in table 41 which covers other specified corrections.

    f.   Offset distances for a Venus mission.   Determining the offset requirements for avoiding the atmosphere of Venus can be done in the same manner as for Mars. The less stringent requirements require a probability of 1 in 100 that the spacecraft will encounter the atmosphere. For typical approach velocities, the amount of bias which must be removed at the time of the third correction is about 5000 km, compared to 8000 km for Mars. Similarly, the final bias at orbit injection can be smaller; three times the $1-\sigma$ guidance error rather than four times, as in the Mars case.

    3.   Changing the time of arrival.   As the vehicle approaches the planet, the approach direction is essentially fixed with respect to inertial space by the characteristics of the interplanetary transfer trajectory. At the nominal time of arrival, the desired landing site will be located so that it can be readily reached on the nominal landing trajectory. If midcourse guidance errors cause the time of arrival to differ from the nominal, the desired landing site will have rotated away from the desired inertial orientation. The fuel requirements to change the direction of the approach velocity vector sufficiently to compensate for this would be prohibitive, since the approach velocity is rather high. Changing the time of arrival so that the landing site will again be favorably located at the new arrival time is not so difficult, since a small change in velocity will make a significant change in time of arrival if it is applied early enough.

Figures 141 through 143 show the changes in arrival time versus incremental velocity requirements for various approach velocities and for ranges from the planet of 1×10^6, 2×10^6 and 3×10^6 km. The changes in arrival time appear to be entirely adequate, although it may be necessary to make the correction in the vicinity of 3×10^6 km for the higher approach velocities.

From figure 141 which corresponds to a range of 3×10^6 km, an incremental velocity change of 10 m/sec (33 fps) applied to the 4 km/sec approach velocity yields a change in arrival time of 0.5 hour. If the velocity change is applied when the spacecraft is at a range of 10^6 km, then the required increment for the 0.5 hour change in arrival is 96 fps.

The velocity increment for slowing down the orbiter to provide the lander with the necessary lead time for communication relay essentially changes the arrival time of the orbiter. This phase was described in the section on lead time requirements.

4.   <u>Velocity increment for lander path.</u> At somewhat closer ranges, it will be necessary to separate the lander from the orbiter and to modify the lander's trajectory so that it will enter the planet's atmosphere on a ballistic path to the desired landing site. The velocity correction is primarily intended to swing the approach velocity vector from a direction which would miss the planet to a direction which will cause impact. It is not intended to change the magnitude of the approach velocity and is therefore applied in a direction essentially normal to the existing vector and in the same trajectory plane. The incremental velocity requirements as a function of separation range and entry flight path angle are plotted in figures 125 through 128 for approach velocities of 3, 4, 5, and 6 km/sec. The magnitude ranges from 30 to 256 fps (9 to 78 km/sec), depending on the entry angle, approach velocity, and range. It was assumed that the unperturbed trajectory (the orbiter's) had a periapsis altitude of 2000 km. The application of the particular velocity increment has been described in the section on lander-orbiter separation.

If the orbital plane of the orbiter differs from the desired orbital plane of the lander, it will be necessary to make a plane rotation correction in addition to the lander separation correction. This consists of an out-of-plane incremental velocity correction. Figures 144 through 146 show the incremental velocity requirements as a function of the required plane rotation for various approach velocities and for separation ranges of 0.5×10^6, 0.75×10^6 km, and 1.0×10^6 km. It should be noted that since the lander separation increment and the plane rotation increment are both applied to the lander at approximately the same range, they can be vectorially combined (they are essentially normal to each other) to realize a slight reduction in the total incremental velocity requirement.

From figure 144, which pertains to a range of 10^6 km, the velocity increment for rotating the plane of a 4 km/sec trajectory 90 degrees is 136 fps. The effect of halving the range to 0.5×10^6 km is to double (approximately) the velocity increment to 276 fps.

The application of the velocity increment for plane rotation of the lander trajectory was covered in the section on lander-orbiter communication relay geometry. The discussion pointed out the limitation on lander trajectory plane rotation from the standpoint of sufficient relay communication time. Central angle deviations of the impact point from the orbiter trajectory plane beyond 40 degrees are not feasible. To satisfy such a requirement, the velocity increment for plane rotation at a 10^6 km separation distance is small (0.1 to 0.3 m/sec).

It will be noted that the periapsis altitude used for the change in arrival time and for the orbital plane rotation data differs from that used for the orbiter retrovelocity and (unless otherwise specified) lander separation data (1800 versus 2000 km). However, the dependence on periapsis altitude is not great and the incremental velocity requirements will remain essentially unchanged.

5. <u>Terminal velocity correction.</u> The terminal correction maneuver listed in table 41 is for improving the accuracy of the periapsis location of the approach trajectory. Therefore, the maneuver also affects the thrust program during orbit injection. In some cases the maneuver may actually be combined with the orbit injection or orbiter slowdown phase. The orientation of the thrust vector for this maneuver may be in any direction since both velocity and position uncertainties must be resolved. The 1-sigma velocity increment for the terminal correction is 10 meters/sec.

6. <u>Orbit establishment.</u> The magnitude of the velocity increment for the orbit injection maneuver is large enough (2000 to 4000 m/sec for a 4500-pound orbiter in an elliptical orbit around Mars) to make the other maneuvers insignificant in terms of propulsion requirements. Because of the magnitude of the increment required, the thrust direction and duration are programmed for optimum injection. The thrust initiation point is a function of the approach velocity, thrust magnitude, specific impulse, the desired final orbit, and the mass of the orbiter. The cutoff point which also varies in accordance with the above conditions occurs shortly before the periapsis of the approach trajectory.

63-9569

Figure 141   REQUIREMENTS FOR CHANGE IN ARRIVEL TIME, RANGE = 3 x 10^6 KM

-271-
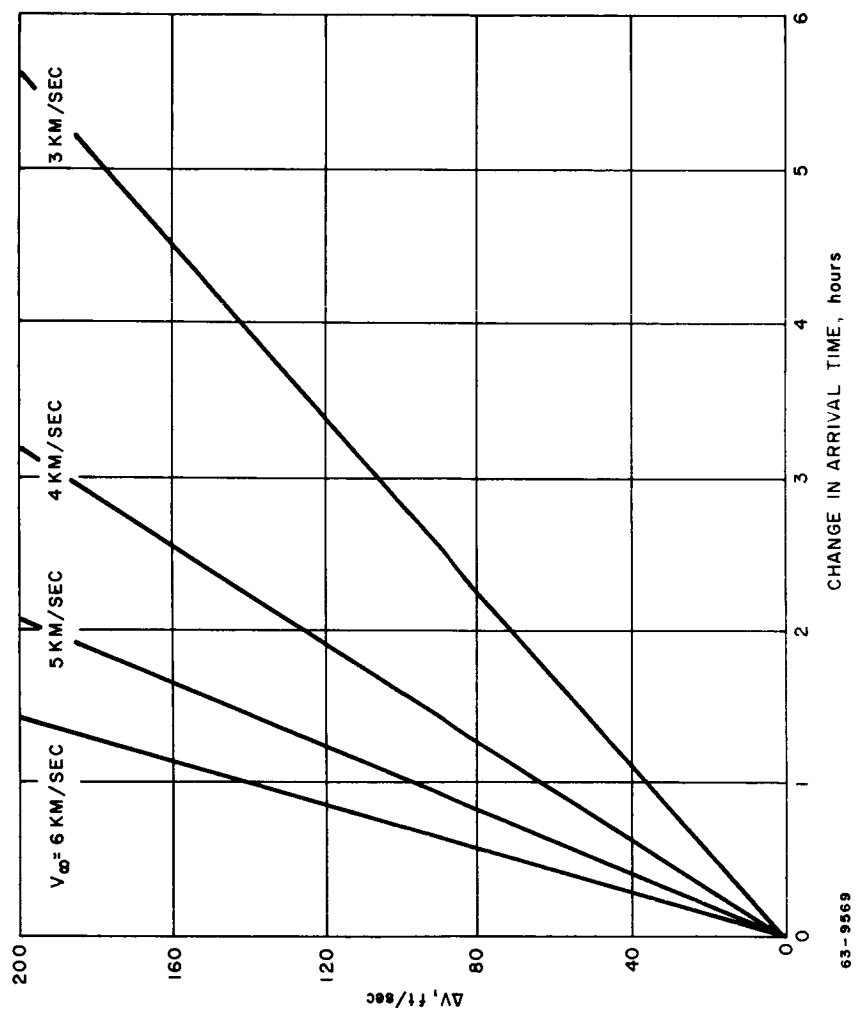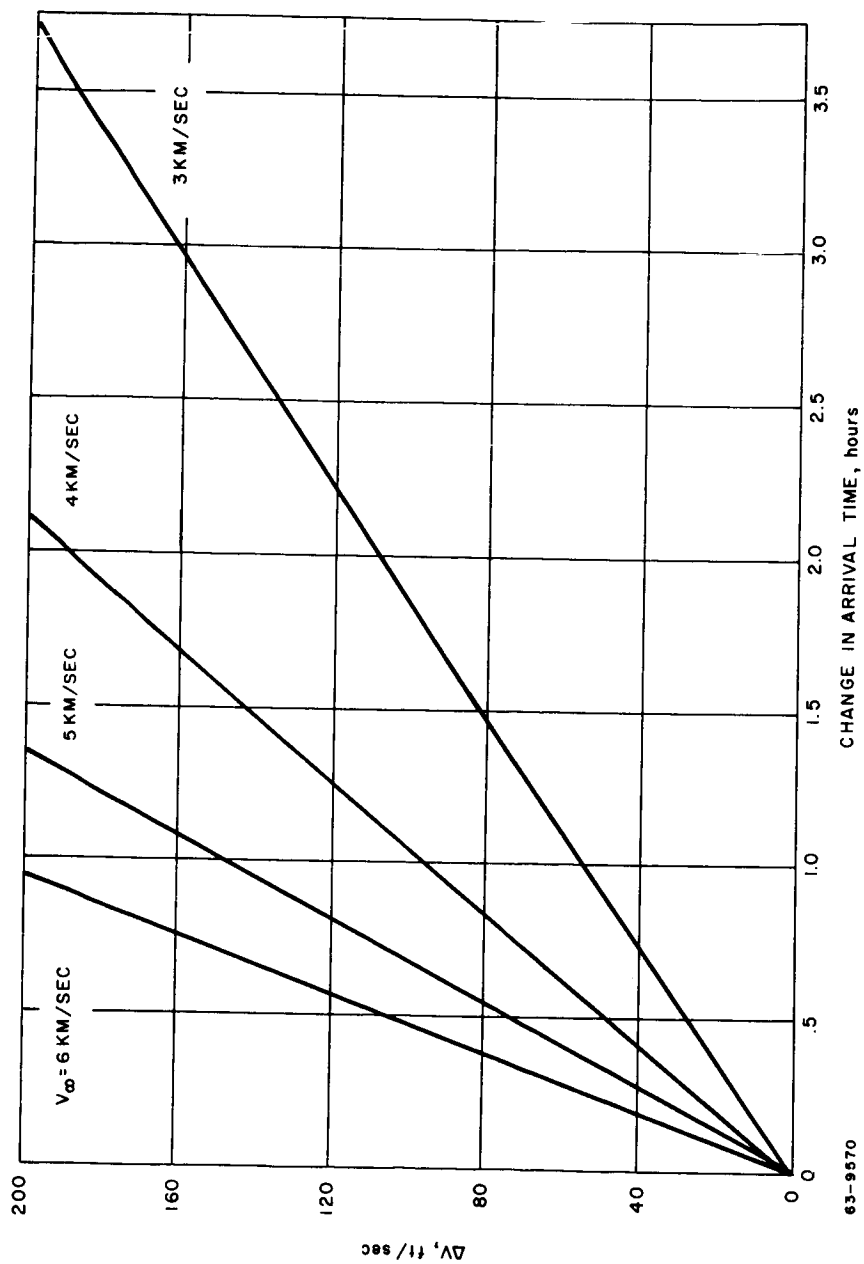
Figure 142   REQUIREMENTS FOR CHANGE IN ARRIVAL TIME, RANGE $= 2 \times 10^6$ KM

63-9570

-272-
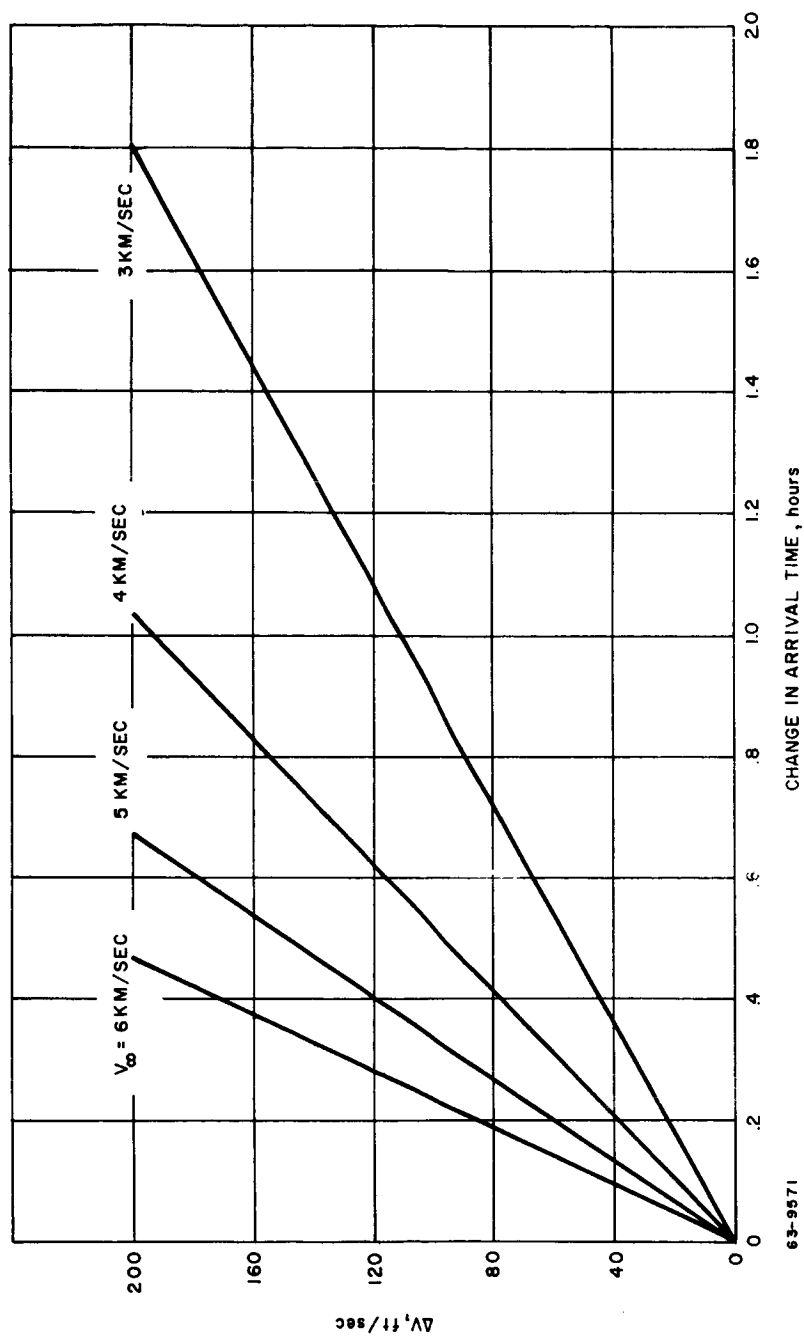
Figure 143 REQUIREMENTS FOR CHANGE IN ARRIVAL TIME, RANGE = 1×10^6 KM

63-9571

-273-
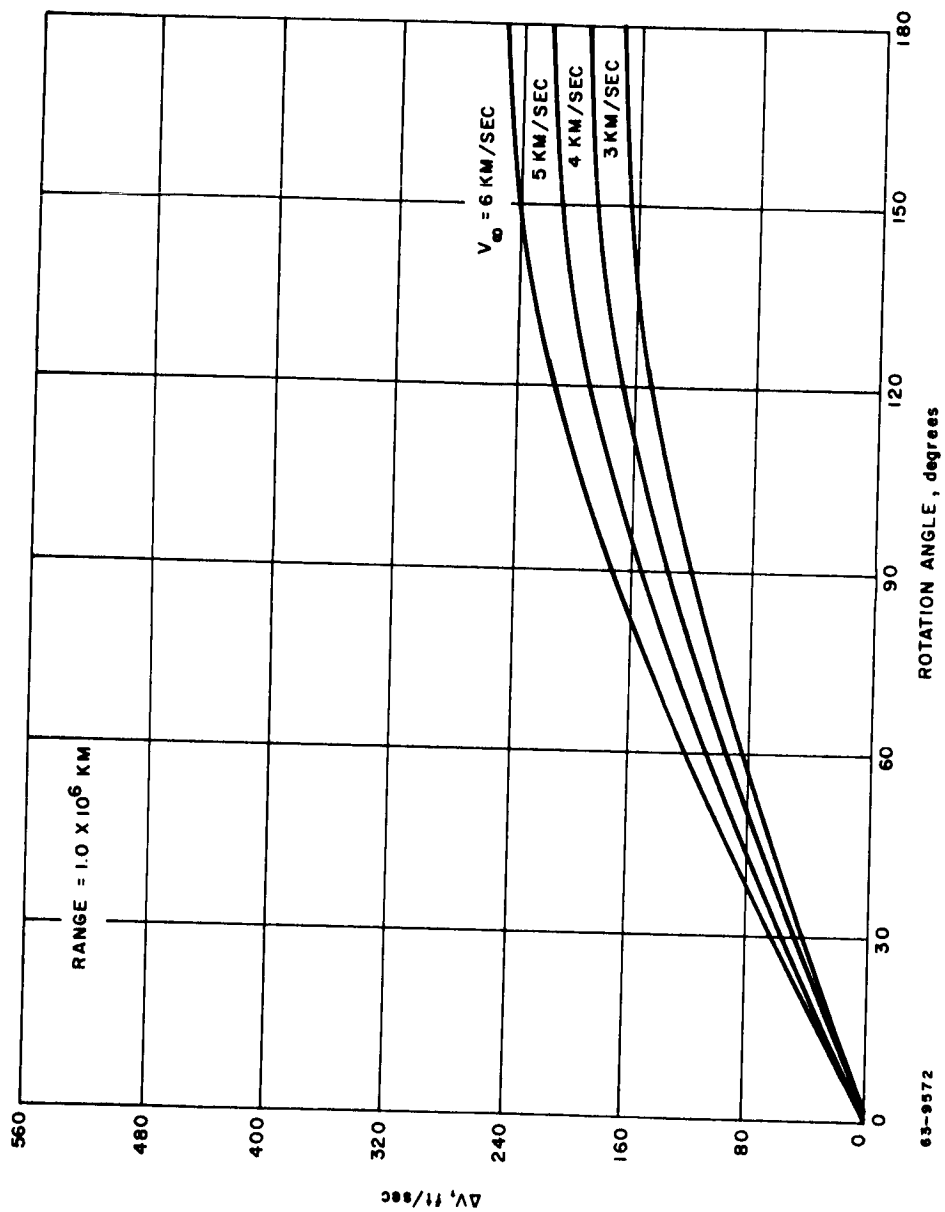
Figure 144   REQUIREMENTS TO ROTATE PLANE OF APPROACH TRAJECTORY,
RANGE = 10^6 KM

63-9572

-274-
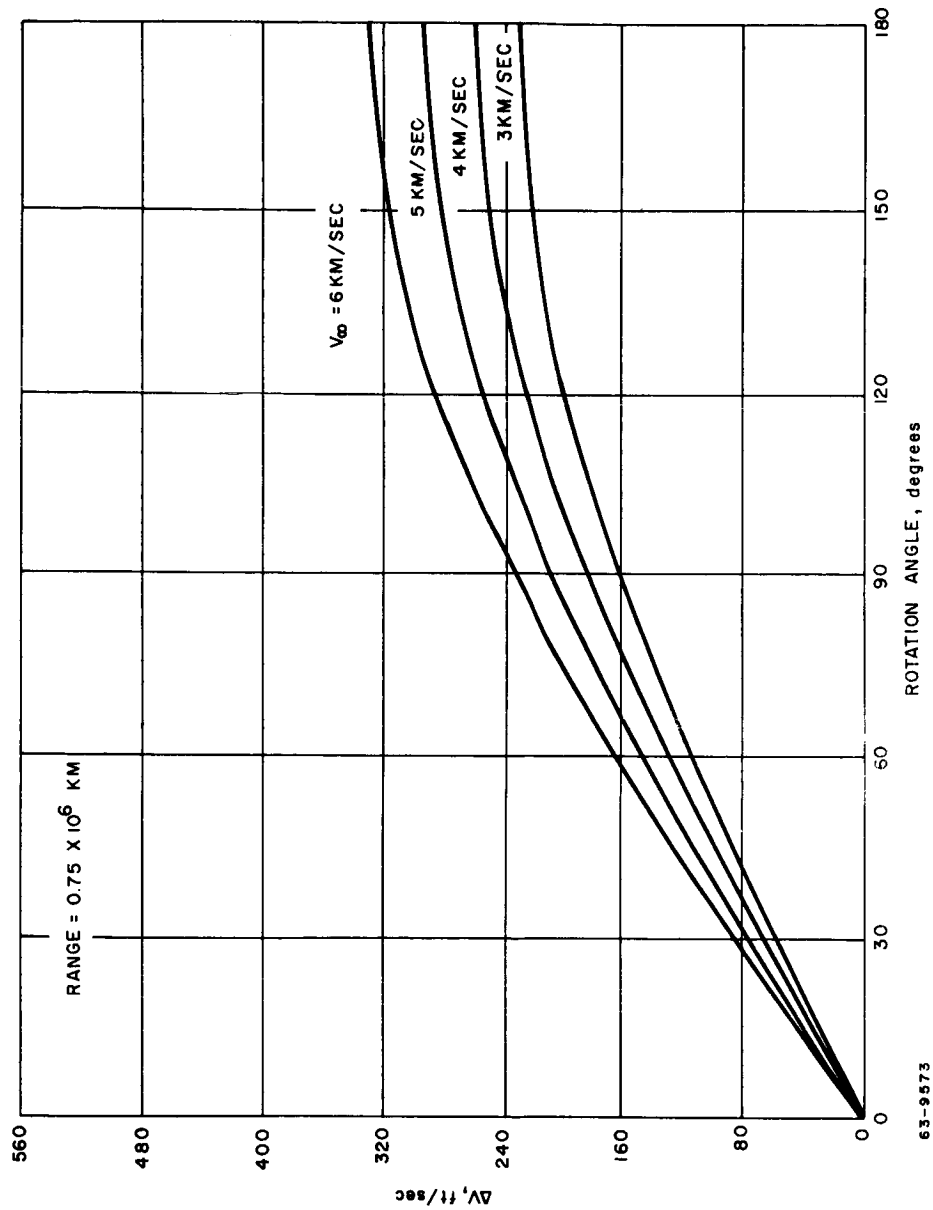
Figure 145   REQUIREMENTS TO ROTATE PLANE OF APPROACH TRAJECTORY,
RANGE = 0.75 x 10⁶ KM

63-9573
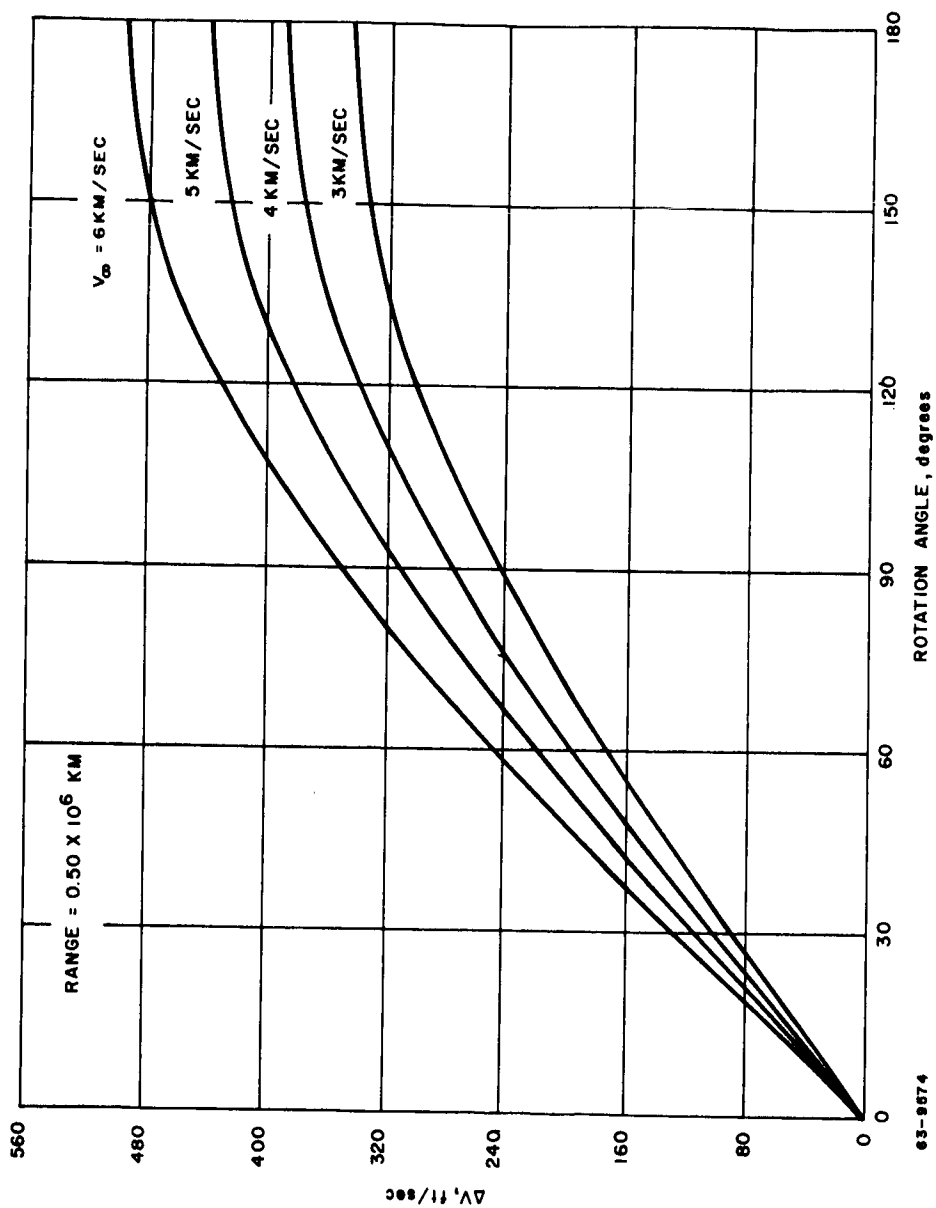
Figure 146   REQUIREMENTS TO ROTATE PLANE OF APPROACH TRAJECTORY, RANGE = 0.5×10^6 KM

63-9674

-276-

7. STERILIZATION

7.1 Introduction

The primary objective of spacecraft sterilization is to protect extraterrestrial bodies, such as Mars and Venus, from contamination by Earth organisms which might alter their ecology and might interfere with subsequent attempts at biological observation of these planets. (Refs. 3 through 7 and also 10.) The Voyager sterilization program would attempt to prevent launching of spacecraft which could possibly contaminate extraterrestrial bodies. However, such a degree of sterility must be demonstrated indirectly. Sterilization can only be discussed in terms of past experience with the methodology which is being employed through statistical analysis of the results previously attained through use of these techniques. Sterilization standards have been established based upon the probabilities of contaminating the planets between the present and 1980 assuming two launches per launch opportunity by both the United States and Soviet Russia to each of the target planets. It is argued that the risk of contaminating the planet should be maintained below the probability of obtaining no useful biological data for all other reasons. These arguments result in a sterilization requirement for each launch. The probability of contaminating Mars with viable terrestrial organisms must be less than 10^{-4}, and the risk of contaminating Venus with viable terrestrial organisms must be less than 10^{-2} (ref. 8).

The most direct means of avoiding contamination of a planet is to avoid any contact between the spacecraft and any portion of the planet or its atmosphere. This approach is quite acceptable for high altitude orbiters and fly-by vehicles as long as the probability of spacecraft-planet impact can be held to the required probability. This constraint has dictated a minimum orbital altitude of 1800 km for near circular orbits and 1500 km for highly eccentric orbits. These altitude restrictions prevent decay of the orbital trajectory to a dangerous degree for at least a 50-year period.

For entry capsules and landers, the situation is quite different. Direct sterilization of at least these portions of the spacecraft must be accomplished and maintained to the required probabilities. Sterilization by definition is the process of killing living microorganisms within or on the spacecraft. Hobby (ref. 9) has estimated that there may be a burden of 10^9 microorganisms in and on a spacecraft which is assembled under suitable clean room conditions; therefore, a reduction in the microorganism population by a factor of 10^{13} is required for Martian spacecraft and 10^{11} for Venusian spacecraft. There are several accepted procedures for sterilization of spacecraft which include the application of dry heat at 135°C for 24 hours, exposure to ethylene oxide (12 percent ethylene oxide mixed with 88 percent freon-12) for 18 hours at a temperature of 70 to 100°F and a relative humidity between 30 and 50 percent,

and exposure to a radiation dose of 1.2×10^{-7} rad (ref. 8). Other possible techniques which might be used to achieve sterilization include exposure to liquid sterilants, such as methanol or formalin, and various filtration techniques.

An objective of good design engineering is to produce a lander which can be completely sterilized by the application of dry heat. Certain components and subsystems of the lander, however, may be sensitive to the thermal environment necessary for dry heat sterilization. If this condition exists, a backup technique which allows removal of the thermolabile components and their subsequent sterile assembly should be utilized. The lander must be designed such that it can be heated to 135° C throughout without application of excessive temperatures to any particular portions. A great deal of attention must be placed on the maintenance of lander sterility once it is placed in its sterile container. Provisions must be made for handling and checkout of the lander while maintaining sterility.

As it is impossible to verify the complete sterility of all lander systems, sterilization certification must, of necessity, be accomplished by indirect statistical techniques. Models, mockups, and actual subsystems with known levels of contamination would be sterilized with the lander and monitored to determine the effectiveness of the sterilization processes. Only through extensive testing and experience with the sterilization facility and the particular spacecraft configuration can appropriate statistical verification of the sterility of the lander be achieved.

It is suggested that two sterilization facilities be constructed. A complete facility at the assembly site would be used for those portions of the sterilization processes which occur during lander assembly, checkout and acceptance testing. The second facility need only be a reproduction of the terminal portion of the sterilization facility to accommodate maintainance and modifications of the lander once it has been delivered to the launch site. Personnel trained in aseptic assembly, sterilization techniques, and microbiological procedures should be employed to operate the sterilization facility. A separate sterilization control group should be responsible for monitoring, control, certification, and maintenance of the sterilization facility.

7.2 Sterilization Facilities

An initial burden of approximately 10^9 viable organisms per lander vehicle is expected, assuming appropriate clean room assembly of all subsystems and components. Therefore, the sterilization process must be sufficient to meet the desired requirements for the Mars and Venus launches. Two general approaches can be used to achieve this reduction in population. The first assumes that the lander can be dry-heat sterilized. The second approach allows for a

-278-

limited number of components, materials, or subassemblies of the lander which are thermolabile; the major portion of the lander will still be dry-heat steriliz- ed. For a totally heat sterilizable lander, the only unique assembly facility requirement is the inclusion of a dry-heat oven capable of accepting the assem- bled lander. This facility is ultimately visualized as two buildings - one within the other. The exterior building for environmental protection consists of ap- proximately 16, 800 ft^2 and the internal building of approximately 12, 000 ft^2 having areas designated for the following functions:

1. Receiving and acceptance room (class II area) (see table 42) in which received goods are unpacked, grossly cleaned, and tested for compliance with specifications

2. Clean-up and packaging room (class II area) in which accepted hard- ware undergoes a more elaborate clean-up procedure and ultimate packaging into certified sterile polyethylene bags to be heat-sealed before storage. Articles will be bagged under hoods of class IV characteristics.

3. Storage room (class II area) for storage of components while awaiting receipt of all items necessary to complete subassemblies and final assemblies.

4. Major assembly room (class III area), a large area of approximately 3600 ft^2 in which multiple spacecraft will simultaneously be assembled.

5. Hardware monitor room devoted to equipment used for monitoring the cleanliness and biological status of assembly facility, efficiency of cleaning operations, and physical and biological results of all sterilization processes.

6. Personnel lockers and changing rooms adequately designed to permit efficient flow and suitable preparation of personnel while maintaining adequate safeguards to minimize contamination in the work areas.

7. Ground support equipment room to house all necessary electronic and test mechanical apparatus associated with spacecraft check-out and an isola- tion corridor protruding into the assembly area to permit test equipment access to any of several spacecraft being assembled. Sealed plug-in leads will permit attachment of test equipment to the craft without endangering cleanliness of the assembly area.

8. Dry-heat oven (20 by 20 by 20 feet), to heat the spacecraft to a tempera- ture of 135°C for 24 hours. The control timer will be initiated by a sensor in the chamber or attached to the surface or be placed within a thermometer well of the lander. If the chamber temperature is used as a guide, suitable heat lag data will be required to assure that the entire load has been at the proper temperature for the full 24 hours.

TABLE 42

STANDARD FUNCTIONAL CRITERIA
FOR
DESIGN AND OPERATION OF CLEAN ROOMS

	CLASS - I	CLASS - II	CLASS - III	CLASS - IV
DEFINITION	ELEMENTARY REQMTS. FOR PRECISION ELECTRONIC ASSY. AND CALIBRATION TYPE WORK. LESS CRITICAL INSTRUMENTS/MECHANICAL DEVICES AND COMPARABLE ITEMS.	BASIC RQMTS. OF DUST EXCLUSION AND ATMOSPHERIC CONTROLS SUITABLE FOR ASSY. AND CALIBRATION OF DELICATE INSTRUMENTS, ELECTRONIC & MECHANICAL DEVICES REQUIRING FINE TOLERANCES.	PROVIDES FOR PRECISION RQMTS. OF TEMPERATURE, HUMIDITY & DUST CONTROL AS REQUIRED FOR ASSEMBLY, CALIBRATION AND TEST OF THE MORE ADVANCED DELICATE INSTRUMENTS, ELECTRONIC/MECHANICAL DEVICES & NON-INERTIAL GUIDANCE COMPONENTS.	PROVIDES FOR PRECISION RQMTS. OF TEMPERATURE, HUMIDITY AND DUST CONTROL AS REQUIRED FOR THE ASSEMBLY, CALIBRATION & TEST FOR THE MORE SENSITIVE ULTRA-PRECISION COMPONENTS AND SYSTEMS KNOWN TO EXIST.
AIR CONDITIONING	TEMPERATURE LIMITS – COMMERCIAL AIR CONDITIONING DESIGNED FOR 70° FAHR. TEMPERATURE DIFFERENTIAL. HUMIDITY LIMITS – RELATIVE HUMIDITY 40% ± 10%.	TEMPERATURE LIMITS 72 ± 5° HUMIDITY LIMITS – RELATIVE HUMIDITY 40% ± 10%	TEMPERATURE LIMITS 72 ± 3° HUMIDITY LIMITS – RELATIVE HUMIDITY 40% ± 5%	TEMPERATURE LIMITS 72 ± 1° HUMIDITY LIMITS 40% ± 5%
PRESSURE DIFFERENTIAL	POSITIVE PRESSURE DIFFERENTIAL WITHIN THE CLEAN ROOM WILL BE MAINTAINED IN ORDER TO ELIMINATE INFILTRATION OF DUST LADEN OUTSIDE AIR.	POSITIVE PRESSURE DIFF. CLEAN ROOM TO HAVE HIGHEST PRESS. ANTE ROOM OR ENTRANCE – LOWEST PRESSURE AIR COND. OPERATE 24 HRS A DAY EVERY DAY OF THE YEAR & REHEAT CAPABILITY TO MAINTAIN TEMPERATURE.	SAME AS II	SAME AS II

AIR FILTRATION

	CLASS - I	CLASS - II	CLASS - III	CLASS - IV
FILTERING METHOD	TO BE DETERMINED BY DESIGN AGENCY TO MEET REQUIREMENTS BELOW.	SAME AS I	SAME AS I	CAMBRIDGE ABSOLUTE FILTERS OR EQUAL.
PARTICLE COUNT METHOD	DESIGN CRITERIA – NATIONAL BUREAU OF STANDARDS DISCOLORATION TEST. OPERATING CRITERIA – 10X MICROSCOPE, 100 DIAMETER MAGNIFICATION LIGHTFIELD TECHNIQUE.	DESIGN AND OPERATING CRITERIA – 10X MICROSCOPE, 100 DIAMETER MAGNIFICATION WITH LIGHTFIELD TECHNIQUE.	DESIGN AND OPERATING CRITERIA – 30X MICROSCOPE, 300 DIAMETER MAGNIFICATION WITH DARK FIELD TECHNIQUE.	DESIGN CRITERIA – ARMOUR CHEMICAL CORPS UNIFORM DISPERSION DIOCTYL-PHTHALATE (DOP) OPERATING CRITERIA – 30X MICROSCOPE, 300 DIAMETER MAGNIFICATION WITH DARK FIELD TECHNIQUE.
PARTICLE SIZE LIMIT		DESIGN CRITERIA – 10 MICRONS	DESIGN CRITERIA – 1 MICRON	DESIGN CRITERIA – .3 MICRON
PARTICLE COLLECTION METHOD	DESIGN AND OPERATING CRITERIA – GREENBERG-SMITH IMPINGER OR EQUIVALENT.	SAME AS I	SAME AS I	SAME AS I
PARTICLE COUNT TOLERANCE	1. DESIGN CRITERIA – 85% EFFICIENT 2. OPERATING CRITERIA 250,000 COUNTABLE PARTICLES PER CUBIC FOOT OF AIR LIGHT FIELD TECHNIQUE.	1. DESIGN CRITERIA – 50,000 PARTICLES PER CUBIC FOOT OF AIR. 2. OPERATING CRITERIA – A. MAXIMUM 85,000 PARTICLES PER CUBIC FOOT OF AIR BETWEEN .3 MICRONS AND 10 MICRONS. B. MAXIMUM OF 15,000 PARTICLES PER CUBIC FOOT GREATER THAN 10 MICRONS. LIGHT FIELD TECHNIQUE.	1. DESIGN CRITERIA – 20,000 PARTICLES PER CUBIC FOOT OF AIR. 2. OPERATING CRITERIA – MAXIMUM 35,000 PARTICLES PER CUBIC FOOT OF AIR BETWEEN .3 AND 10 MICRONS AND A MAXIMUM 6000 PARTICLES PER CUBIC FT. OF AIR GREATER THAN 1 MICRON. DARK FIELD TECHNIQUE.	OPERATING CRITERIA 1. MAXIMUM 10,000 PARTICLES PER CUBIC FOOT OF AIR BETWEEN .3 AND 10 MICRONS. 2. MAXIMUM 2000 PARTICLES PER CUBIC FT. OF AIR BETWEEN .3 AND 10 MICRONS. DARK FIELD TECHNIQUE.

FACILITY DESIGN

	CLASS - I	CLASS - II	CLASS - III	CLASS - IV
FACILITIES	HIGH STANDARD OF SHOP CLEANLINESS LOW DEGREE OF MAINTENANCE AND SERVICE COST.	MEET MORE ADVANCED REQMTS. OF AN ENVIRONMENTALLY CONTROLLED ATMOSPHERIC COND. THIS APPLIES TO ENTIRE AREA. CLEAN ROOM, CLEANING CHAMBERS AIR LOCKS, LOCKER AND WASH ROOMS.	MEET MORE ADVANCED REQUIREMENTS OF AN ENVIRONMENTALLY CONTROLLED ATMOSPHERE.	MEET ULTIMATE REQUIREMENTS OF A DUST FREE CONTROLLED ATMOSPHERE CLEAN ROOM.
FLOORS	FINISH WITH GREASE RESISTANT MATERIAL. NOTE PARTICULAR CARE TO INSURE STRONG PERMANENT BONDING OF THE FLOOR.	DUST RESISTANT VINYL MAT'L. MINIMUM OF CRACKS, SEALED JOINTS AND CRACKS STRONG PERMANENT BOND.	SAME AS II	SAME AS II
INTERIOR FINISH	WALLS, CEILINGS AND PAINTED FIXTURES TO BE PAINTED FOR TOUGH SMOOTH DUST RESISTANT SURFACE. RESISTANT TO CHIPPING, FLAKING OR POWDERING UNDER ABRASION.	SAME AS I SMOOTH PANEL CONSTRUCTION DOOR WINDOWS AND JOINTS TO BE SEALED.	SAME AS II DUST TIGHT SEAL AT ATTIC AND FOR ALL DUCTS AND UTILITY CONDUITS.	SAME AS III
UTILITIES AND FIXTURES	STANDARD UTILITIES AND FURNITURE FIXTURE. LIGHTING – 75 FOOT CANDLE SHADOWLESS ILLUMINATION THROUGHOUT.	FURN. & UTILITIES TO BE DUST-PROOF, MINIMUM USE OF PROTRUDING SERVICE LINES LIGHTING – 100 FOOT CANDLES. SHADOWLESS LIGHTING SYSTEM. HOT AIR DRIERS FOR FACE AND HANDS IN LIEU OF TOWELS.	SAME AS II ALL DOORS WILL HAVE BALL BEARING HINGES, INDIVIDUAL LOCKERS.	SAME AS III

SPECIAL CONSIDERATIONS

	CLASS - I	CLASS - II	CLASS - III	CLASS - IV
CLEANLINESS	LAYOUT WITH CONSIDERATION TO KEEP FLOORS, CORNERS, AISLES AND WORK BENCHES CLEAR TO FACILITATE EASY FREQUENT AND THOROUGH CLEANING.	SAME AS I FLEXIBLE LAYOUT, CENTRAL LOCATION FOR METERS, GAUGES AND CONTROLS. INSTALL IN THIS AREA DEVICE WHICH PROVIDES CONTINUOUS RECORD OF TEMPERATURE AND HUMIDITY CONDITIONS.	SAME AS II	SAME AS II
SHOES	PROVIDE ADEQUATE FACILITIES FOR SCRAPING, BRUSHING AND WIPING ALL DIRT OFF OF SHOES OF ALL PERSONNEL.	SHOE CLEANER WITH SOLE SIDE AND TOP BRUSHES INCORPORATED WITH A STRONG VACUUM AIR SUCTION.	SAME AS II	SAME AS II
CENTRAL VACUUM CLEANING SYSTEM	WET OR DRY PICK-UP FOR ENTIRE ROOM, INDUSTRIAL TYPE WITH PROVISIONS TO EMPTY DUST TANK WITHOUT CONTAMINATING ROOM OR INTAKE AIR. USE PLASTIC HOSE ONLY.	SAME AS I	SAME AS I	SAME AS I
SAFETY DEVICE FOR ELECTRONIC PRECIPITATOR		IN CASE OF POWER FAILURE FAN WILL NOT DRAW RELEASED DUST INTO CLEAN ROOM.		
VOLATILE VAPORS	IF PARTS CLEAN-UP AREA GENERATES VAPORS, PROVIDE FILTERED AIR WITH 100% EXHAUST TO OUTSIDE.			
AIRLOCK		INSTALLED AT ENTRANCE OF CLEAN ROOM AIR BLAST FOR DUSTING CLOTHING (HIGH VELOCITY 50 FEET PER SECOND) SEPARATE AIR LOCK FOR MOVEMENT OF MAT'L, TOOLS AND EQUIPMENT. GELATIN MATS AT ENTRANCE.	SAME AS II AIR LOCK BEFORE WASH ROOM. AN AIR LOCK BETWEEN WASH ROOMS AND CLEAN ROOM.	SAME AS III
STERILE HOODS	CAN BE INSTALLED WHEN APPLICABLE TO WORK REQUIREMENTS.	SAME AS I	SAME AS I	CONSIDER UTILIZATION OF EQUIPMENT TO PRECLUDE EXPENDITURE OF EXCESSIVE FUNDS. THIS IS DEEMED NECESSARY DUE TO THE IMPROBABILITY OF ACHIEVING DUST CONTROL TO THE REQUIRED DEGREE IN AREAS INHABITED BY OPERATING PERSONNEL. SAME AS I

AF-WP-O-SEP 61 136

It is probable however that the lander vehicle will <u>not</u> be completely dry-heat sterilizable. Several of the subsystems, particularly the scientific instruments, may be damaged by exposures to the dry-heat cycle. In this case, a second sterilization technique and associated facility is offered. This facility is comprised of two buildings, one within the other. The outer building will provide environmental protection and tempering of external influence upon the inner building, and will be approximately 20,000 ft^2. The interior building of this facility will be approximately 15,000 ft^2 and will include the following areas:

1. Receiving and acceptance room (class II area) in which received goods are unpacked, grossly cleaned and tested for compliance with specifications.

2. Clean-up and packaging room (class II area) in which accepted hardware undergoes a more elaborate clean-up procedure and ultimate packaging into certified sterile polyethylene bags to be heat-sealed before storage. Articles will be bagged under hoods of class IV characteristics.

3. Storage room (class II area) for storage of components while awaiting receipt of all items necessary to complete subassemblies and final assemblies.

4. A sterilization barrier area housing multiple sterilization equipment including radiation sterilization equipment.

5. A receiving and transfer corridor for sterile items.

6. Major assembly room (class III area), a large area of approximately 3600 ft^2 in which multiple spacecraft will be assembled simultaneously.

7. Ground support equipment room, to house all necessary electronic and mechanical apparatus associated with spacecraft check-out. An isolation corridor protruding into the assembly area will permit test equipment access to any of several spacecraft being assembled. Sealed plug-in leads will permit attachment of test equipment to the craft without endangering cleanliness of the assembly area.

8. Dry-heat, ethylene oxide sterilizer (20 feet by 20 feet by 20 feet).

9. A sterile assembly room (sterile area) for sterile reassembly of the lander vehicle after sterilization.

10. Hardware monitor room, devoted to equipment used for monitoring the cleanliness and biological status of the assembly facility, efficiency of cleaning operations, and physical and biological results of all sterilization processes.

11. Personnel lockers and changing rooms, adequately designed to permit efficient flow and suitable preparation of personnel while maintaining adequate

safeguards to minimize contamination in the work areas.

12. A suiting room with showers for preparing personnel entering the sterile room.

The specialized sterilization equipment includes:

1. A dry-heat ethylene oxide sterilizer, 20 feet wide by 20 feet deep by 20 feet high. The unit would be capable of accommodating 10 feet diameter landers through any of three doors. Doors will be 15 by 15 feet. Each door will have sight glass observation points. Vessel and doors will be capable of withstanding loads imposed during either dry-heat or ethylene oxide processing. The vessel interior will be nickel-copper alloy or types of stainless steel. Interior lighting will be provided by external sources through gas-tight sight glasses in ceiling and doors. High velocity fans will be placed on the interior of the vessel to force circulation of heated-air or ethylene oxide mixtures. Process controls and recording instruments will monitor sterilization cycles described below:

a. Dry heat, to attain temperature of 135°C, maintaining it for 24 hours. A control timer will be initiated by a sensor in the chamber space or attached to the surface or placed within the thermometer well of the lander. If chamber temperature is used as guide, suitable heat lag data will be required to assure that the entire load has been at temperature for 24 hours.

b. Ethylene oxide, the cycle will employ ethylene oxide mixed as 12 percent ethylene oxide and 88 percent freon-12 in an atmospheric pressure process to minimize stress on doors and walls of vessel. Several partial vacuums will be drawn to elute air; the process will not start timing until concentration of ethylene oxide exceeds 300 milligrams per liter as measured by an infrared analyzer calibrated with standardized gas which has been checked with a gas chromatograph. The temperature will be 110°F and the relative humidity will be 40 percent.

c. A double-door dry-heat sterilizer recessed on two walls with a sealing flange on the exit side, with mechanical convection incorporated, nickel clad interior, 2 feet wide by 3 feet high by 4 feet deep, either electrically or steam-heated will be used. The exposure timer will be adjustable from 1 to 48 hours and temperature control will be adjustable from 80 to 180°C.

d. A double-door steam autoclave recessed on two walls, with a sealing flange on the exit side (24 inches wide, 36 inches high, and 48 inches deep) will be used. The control system will employ an automatic, high-vacuum, hard-goods cycle and a high-speed liquid cycle. The interior of the vessel will be nickel clad. This facility will require steam at 60-lb pressure at a maximum rate of 360 lb/hr. Water at 70°F will be used at 5 gpm. Drain and vent services shall be provided as well as 115-volt AC, 15-amp , 60-cycle electrical

service.

e. A double-door, ethylene oxide sterilizer, recessed on two walls with a sealing flange on the exit side (24 inches wide by 36 inches high by 48 inches deep) will be required. This facility will be designed to use 12 percent ethylene oxide and 88 percent freon-12. The vessel will have a nickel clad interior. The facility requires the use of water at 70°F at 5 gpm, steam at 60-lb pressure at 5 lb/hr and 115-volt, AC, 15-amp, 60-cycle electrical service. An atmospheric vent is required.

f. A double-door formaldehyde methanol spray-wash unit with a sealing flange on the exit side, recessed on two walls (24 inches wide by 36 inches high by 48 inches deep) will be used. The facility will have a nickel clad interior and be designed to use formaldehyde vapors or methanol formaldehyde liquid under a controlled temperature. The facility requires use of water at 70°F at 10 gpm, and a formaldehyde methanol reservoir.

g. A special subsurface radiation facility will use a "hot" isotope as a radiation source to allow radiation sterilization of certain types of thermolabile components. By designing all sterilizers with identical dimensions, uniform interior equipment can be used. A considerable amount of special purpose assembly and support equipment will be necessary for moving, checking, and testing the landers being assembled. A schematic diagram of the proposed facility is shown in figure 147.

Equipment associated with monitoring and other functions is described in the Pilot Plant Section (7.7).

7.3 Procedures for Sterilization of a Lander Not Entirely Heat Sterilizable

1. Low burden of contamination (microorganisms and detritus) components and subassemblies are classified according to their abilities to undergo sterilization (see table 43 for the classification).

2. The components and subassemblies are cleaned, packaged, and stored. The microbiological load is checked.

3. The components and subassemblies are then sterilized by dry heat, steam, ethylene oxide, radiation, or chemicals (methanol-formalin, etc.), according to their sterilization classification. After sterilization, microbiological monitors are assayed for sterility.

LEGEND

CODE	MISSION FROM BOOSTER SEPARATION TO	SUCCESS PROBABILITY
A	LANDER SEPARATION	0.713
B	SUCCESSFUL LANDING	0.668
C	ORBIT ATTAINMENT	0.642
D	ORBITER 21 DAY MAPPING MISSION	0.631
E	ORBITER 70 DAY MAPPING MISSION	0.547
F	ORBITER 180 DAY MAPPING MISSION	0.397
G	24 HOUR BASIC LANDER MISSION (RELAY OPTION)	0.614
H	EXTENDED 30 DAY LANDER MISSION (RELAY OPTION)	0.593
I	EXTENDED 180 DAY LANDER MISSION (RELAY OPTION)	0.579
J	24 HOUR BASIC LANDER MISSION (DIRECT)	0.571
K	EXTENDED 30 DAY LANDER MISSION (DIRECT)	0.533
L	EXTENDED 180 DAY LANDER MISSION (DIRECT)	0.490

TRANSIT PERIOD ≈ 200 DAYS

63-8892

Figure 147 VOYAGER MISSION RELIABILITY PROFILE

-284-

TABLE 43

CLASSIFICATION SYSTEM BASED PRIMARILY UPON HEAT SENSITIVITY OF PARTS AND COMPONENTS

1. Non-heat sensitive
(can take more than three cycles at 135°C for 24 hours) with sterile or unsterile interior.
   1.1   Cleanable by ultrasonic (exterior)
   1.2   Cleanable by other technique.
   1.3   Cleaned at manufacturer.
2. Partially heat sensitive (can take two cycles at 135°C maximum for 24 hours) with sterile or unsterile interior.
   2.1   Exterior cleanable by ultrasonic.
   2.2   Exterior cleanable by other technique.
   2.3   Exterior cleaned at manufacturer.
3. Subject to heat ageing (cannot take more than one cycle at 135°C maximum for 24 hours)
   3.1.1   Sterile interior-exterior cleanable by ultrasonic.
   3.1.2   Sterile interior-exterior cleanable by other technique.
   3.1.3   Sterile interior-exterior cleaned at manufacturer

   3.2.1.1   Unsterile interior (can be penetrated by ETO) Exterior cleanable by ultrasonic.
   3.2.1.2   Unsterile interior (can be penetrated by ETO) Exterior cleanable by other technique.
   3.2.1.3   Unsterile interior (can be penetrated by ETO) Exterior cleaned at manufacturer.

   3.2.2.1   Unsterile interior (cannot be penetrated by ETO) Exterior cleanable by ultrasonic.
   3.2.2.2   Unsterile interior (cannot be penetrated by ETO) Exterior cleanable by other technique.
   3.2.2.3   Unsterile interior (cannot be penetrated by ETO) Exterior cleaned at manufacturer.
4. Heat sensitive (cannot take one cycle at 135°C maximum)
   4.1.1   Sterile interior-exterior cleanable by ultrasonic.
   4.1.2   Sterile interior-exterior cleanable by other technique.
   4.1.3   Sterile interior-exterior cleaned at manufacturer.

   4.2.1.1   Unsterile interior (can be penetrated by ETO) Exterior cleanable by ultrasonic
   4.2.2.2   Unsterile interior can be penetrated by ETO) Exterior cleanable by other technique.
   4.2.1.3   Unsterile interior (can be penetrated by ETO) Exterior cleaned at manufacturer.
   4.2.2.1   Unsterile interior (cannot be penetrated by ETO) Exterior cleanable by ultrasonic.
   4.2.2.2   Unsterile interior (cannot be penetrated by ETO) Exterior cleanable by other technique.
   4.2.2.3   Unsterile interior (cannot be penetrated by ETO) Exterior cleaned at manufacturer.

4. The components and sub-assemblies are then assembled, checked out, and monitors are assayed. The assembly area is white type where not more than 100 microorganisms/ft^2 will settle out from the air in 1 hour.

5. The assembled lander is then packaged (put in a protective can) and placed in a combination gas-dry-heat sterilizer (terminal sterilization). Components which are thermolabile will be removed before canning and sterilized by other techniques, e.g., ethylene oxide, radiation, or chemicals.

6. The canned lander is removed from the sterilizer directly into the sterile assembly area. The thermolabile components and subassemblies are then reassembled into the sterilized lander. The lander is "checked out" and monitors assayed. Individuals who work in these areas are to be completely enclosed in barrier suits and allowed access only through a sterile lock.

7. Terminal dry-heat sterilization times and temperatures currently recommended are

Mars: 24 hours at 135°C.

Venus: 21 hours at 135°C.

7.4 Personnel and Training

A workshop training program of 4 to 5 weeks duration will be designed to impart basic and applied information concerning required procedures in both clean room and sterile techniques. The course will be flexible and more extensive for those personnel selected to complete final assembly operations within barrier suits in sterile rooms. The course outline may be somewhat as follows:

1. Basic bacteriology -- course and workshop. A brief introductory program designed to acquaint members with identification, habits, size, growth characteristics, and transmission of microorganisms.

2. Basic clean room procedures. (Course and workshop designed to acquaint personnel with existing state-of-the-art developments starting with fundamentals of cleanliness based upon particle size. Workshop will demonstrate techniques for obtaining and measuring level of cleanliness.

3. Aseptic procedures - workshop. Designed primarily for final assembly technicians to assay their ability to work under the restrictions imposed by the high degree of cleanliness and/or sterility required in the final assembly facility. This will include work with open table tops, partial closures, and typical clean room benches.

4. Personal conduct and preparation for entry -- workshop. Designed to acquaint operating personnel with the proper techniques of decontamination and subsequent gowning and attendant procedures to introduce themselves into the working environment.

5. Sterile hood operation - workshop. Designed to familiarize personnel with sterile hood operation and to evaluate their ability to work within complete barrier systems of the type generally described as sterile hoods.

6. Sterile assembly within sterile room - course and workshop. This program will be made available only to previously qualified personnel and limited to those operators specifically designated for final assembly operations. This course and workshop will include the suit-up procedure and introduction of operators through sterilizing baths into sterile room and all attendant problems associated with prolonged work in this environment.

7. Monitor systems - course and demonstration. This course will be used to acquaint all personnel, and particularly supervisors, with the techniques used to monitor and clean sterile areas and all sterilizer operations.

Throughout the period of training, the evaluation of the ability of the operator to distinguish between "clean" and "sterile" operations, as well as his ability to work in a manner consistent with maintaining these conditions, will be assayed and scored.

The above training program can be conducted by qualified personnel either at the final assembly facility or in a mock-up pilot plant facility (see section 7.7). The latter approach has the advantage of concentrated effort which can possibly shorten the overall training period and produce effective personnel in less time than the half-day training sessions which may be conducted in the final assembly facility. All of the associated equipment necessary for training will be available for workshop use at a pilot facility, while the equipment will not be as readily available in the final assembly facility.

7.5 Monitoring Procedures Control, and Sterilization Certification

Of necessity, the demonstration of spacecraft sterility must be done in an indirect manner. This is accomplished through a pilot plant study of the entire sterilization process and monitoring of the components, subassemblies, and fully assembled vehicles, as they are processed in the final assembly and sterilization facility.

A Central Sterility Control (CSC) Group will be created and receive authority and responsibility for establishing systems of parts identification and control, including documentation. This is to include all flight hardware, tools, clothing and personnel. This group will monitor all incoming material,

sterilizer operations, work areas, and personnel as detailed below.

The statistical backup of the sterilization procedures will have to be verified from thermal and chemical death curves with adequate checks within the materials handling system to assure meeting the specified conditions. All sterilizer operations will be monitored with physical indicators and recorders as well as biological controls. All sterilized subassemblies will be quarantined 7 days to await the outcome of the biological assay. If unsatisfactory, the material will be reprocessed. The evidence used to support the various techniques will be an applied extension of classical kill curves, some of which are yet to be firmly established. A system of double check-offs would further minimize any chance of error in the process operations and recording.

Techniques to be employed for monitoring include the use of swabs, plate counts, air sampling, and spore controls designed to test for a large spectrum of microorganisms. The records obtained and logged by Central Sterility Control will become the evidence of performance and assurance of attainment of the facility objective.

It is expected that the sterilization pilot plant runs will yield information concerning the number of samples required to determine the level of sterility attained and the anticipated contamination ranges. This information will be used to establish statistics and procedures for the full-scale sterilization and assembly facility.

Checks on maintenance of sterility of items in sealed bags can be performed with detectable gases, or immersion with observation of bubbles. The leak rate can be correlated to pore size under the pressure differential established and an acceptable limit established to correspond with the size of a bacterium. Wetting agents in the solution will assist effectiveness. Helium, or argon, as the inert gas could be employed within the package. One recommended system for entry into the sterate assembly room requires the operator to don a complete barrier suit and enter through a liquid germicidal trap. The suit carries two hoses, one for air supply and the other for air exhaust. For communication, either a head set radio or wire communications through the lumen of the hose will suffice. The suit being positively sealed can be presented while the operator is in the germicidal bath. Any sign of leaks will require a suit change. A second observation will be conducted upon exit from the sterile assembly room and any leak manifested after performance of a task would require the day's assembly to be undone and the room and disassembled components gas-sterilized. All suits are leak tested at entry to the baffled germicidal liquid trap. Lintless towels, sterilized and sealed in polyethylene bags, are brought through with the operator. A sterile water shower in the sterile room prevents germicide from contacting the assembly. The towels will be used to dry off the suit after emergence within the sterile assembly room.

The "buddy system" shall be used on all entries and two operators, one from central sterilization control and the other from "traffic control", will

-288-

observe all entries and exits to certify tightness of suits as a safety measure.

7.6 Techniques and Procedures for the Maintenance of Sterility

Before the lander is placed in the large oven for terminal sterilization, it is completely enclosed in a sterilization can. The can will protect the lander from subsequent contamination and will also aid in its handling. If thermolabile parts have been removed and sterilized by other techniques, the sterilization can is removed and these items are replaced. This entire operation is completed within the sterile assembly area where the lander is checked out and monitored microbiologically before the sterilization can is replaced. A cartridge of compressed sterile gas is then released within the can, providing a positive outward pressure such that any leakage will not permit the entry of microorganisms. Ground support equipment will be designed to adequately sterile conditions within the can during transportation. All lifting and moving operations are to be performed with great care. A recorder will be attached to the sterile can to monitor changes in pressure that may occur as a result of environmental conditions, i.e., a cold night may contract the gas sufficiently to create a negative pressure.

Should an inward leak be recorded, a mobile ethylene oxide facility or a duplication of the large terminal sterilization facility is desirable insurance at the launch site.

Through the orbiter-lander interface, all electrical connections will be hermetically sealed, polarized connectors. Surface attachments to the lander "can" present no hazard. If the "can" is to be entered, it must be returned to the terminal sterilization facility for surface sterilization with ethylene oxide both before and after entry.

7.7 Sterilization Pilot Plant

It is strongly recommended that a pilot plant facility be erected, as soon as practicable, in which operating procedures may be developed and certified to meet the sterility objectives. This facility can be used to study the following:

1. Establishment of the sequence of operations

2. Development of monitoring procedures

3. Generation of statistics concerning (a) normal loads of microorganisms, and (b) effects of varying techniques of total processing (manufacturing,

handling, cleaning, etc.)

4. Establishment and initial operation of control and records procedures

5. Training and selection of personnel for assembly, control, monitoring, and supervision

6. Provision of data for purchase specifications of components and sub-assemblies

7. Acquisition of initial data on the costs of operating sterilization facilities

8. Destructive microbiological testing of representative components and subsystems to substantiate the recommended procedures

9. Refinement or improvement of the specifications for a full-scale sterilization facility.

Such a Pilot Plant will contain the following areas:

1. Entry and cleanup room -- an area used for receiving and personnel clothing change

2. An assembly room to be maintained under class II clean room conditions with work benches capable of maintaining class III or class IV cleanliness standards. Access will be permitted only to suitably garbed personnel.

3. A sterile room -- for sterile assembly operations. Entry of all equipment will be through sterilizers and all personnel will be in complete barrier systems.

4. Suit up room -- a special room for changing clothing for ultimate entrance into the sterile room.

5. Monitor room -- so situated that samples can be obtained from the assembly room and the sterile room without disturbing operations in either of these rooms.

Hardware to be used in conjunction with the above pilot plant facility should include the following items:

1. A Royco particle analyzer. This will be reusable in any final assembly facility.

2. Relative count particle analyzers, 3 units. Reusable.

3. Ultrasonic cleaner system with 12-by 22-inch chamber. Reusable.

4. Polyethylene bag sealer. Reusable.

5. Temperature-indicating recorders with six thermocouples. Two units. Reusable.

6. Bacteriologic monitoring apparatus such as incubators, plate counters, microscopes, millipore aerosol analyzer units and miscellaneous hardware necessary for monitoring sterility. Reusable.

7. Air compressor for complete barrier suits. Reusable.

8. Barrier suits, complete isolation type with lead-out hose assembly. Expendable.

9. Chromatograph for gas and vapor analysis. Reusable.

10. Class IV type work benches and/or hoods. Two units.

8. RELIABILITY ANALYSES

8.1 Introduction

In performing unique engineering and scientific tasks, Voyager spacecraft and their highly complex subsystems will be faced with a variety of potential reliability problems. Long term, frequently cycled operation and storage in hostile and poorly defined environments present problems which must be solved to assure a high probability of mission success. The reliability burden is further aggravated by the fact that only a few spacecraft will be built to be used during the limited number of favorable launch opportunities. Reliability studies in advance of the definitive design phase must show that acceptable levels of reliability can be attained.

Three major objectives have been established for introducing reliability efforts in this phase of the program. The first major objective was to ascertain that the program goals were economically feasible with the achievable reliability. In making this determination, it was necessary to (1) estimate in advance of the conceptual design the reliability feasible for the spacecraft; (2) establish the reliability goals necessary for the fulfillment of program objectives; (3) determine that the cost of launch configurations necessitated by the program goals, and the associated reliability levels, were reasonable.

The second major objective was to participate in the conceptual spacecraft design, recommending the most reliable approaches. In carrying out this objective, it was necessary to (1) apportion the spacecraft reliability goal among the various subsystems and components; (2) make reliability estimates of the subsystems to identify those weak links where the design reliability potentials would fall short of their goals; (3) perform engineering and redundancy improvement analyses on the identified weak links to recommend engineering guidelines for their reliability improvements; and (4) perform relative reliability analyses for the use of reliability as a criterion for choice among design alternatives.

The third major objective was to provide adequate planning for reliability efforts in subsequent program phases. In order to devise a comprehensive reliability plan, it was necessary to (1) establish a reliability philosophy for the Voyager Program; (2) convert this philosophy into a framework of workable controls throughout the program; (3) evaluate the role and scope of each reliability effort required throughout the program and to recommend an organization to implement the scale of reliability effort required for the Voyager Program; (4) evaluate a full-scale reliability program in terms of its cost effectiveness; and (5) work out a demonstration philosophy and plan to assure the Voyager Program will meet its reliability goals.

The results of this work are reported in the following pages. Further discussion of reliability considerations is found in an appendix, "Reliability versus Cost"; in Vol. II, Scientific Mission under mission evolution; in Vols. IV and V in design considerations of the various subsystems; and, finally, Vol. VI includes the reliability development plan.

8.2 Technical Aspects of Reliability

In this section, the technical reliability contributions made during the conceptual spacecraft design phase are comprehensively reviewed. The area of reliability estimation supplies a basic input needed to evaluate the fulfillment of program objectives and to analyze reliability versus cost. Reliability goals were allocated to the spacecraft subsystems to provide a basis for initiating reliability improvements. Preliminary reliability improvement guidelines have been established to achieve the specified levels of reliability. The reliability evaluation of alternate design concepts is briefly treated. The role of reliability as it affects the technical effort in the later phases of the Voyager Program is also described. The key elements of reliability control have been identified to assure the reliability efforts considered necessary to fulfill program requirements. A method of reliability demonstration and verification was devised to provide a means for satisfactorily proving that reliability goals are achieved. Finally, the critical reliability problem areas are indicated.

1. <u>Reliability estimation.</u> To determine the probabilities of fulfilling the Voyager Program objectives, the reliability capabilities of the spacecraft had to be evaluated. Based on conceptual design information, an analysis was performed to estimate the reliability of the Voyager spacecraft for several Mars/Venus mission types and mission segments. The study, which assumed that total mission success was required for the first launch, evaluated the failure contribution of the various spacecraft subsystems during their period of usage. The subsystem reliability predictions were factored into appropriate mathematical models to determine the probability of mission success.

Since the total mission success requirement was an unreasonable constraint to fulfilling the Voyager Program objectives, the spacecraft reliability estimates were reevaluated allowing for partial mission success. This aspect of the study evaluated the contribution of each mission segment to the success of the mission type considered and the related probability of mission completion. The latter reliability estimates included the projected effects of a reliability program designed to accomplish a sequential decrease in the spacecraft failure rate.

a. <u>Principal limitations.</u> At the time the spacecraft reliability analysis was performed, the principal limitations were as follows:

1)   The reliability analysis was performed concurrently with subsystem design. Frequently the estimates had to be made on the basis of conceptual designs, subject to change. However, these changes are expected to be compensating so that little difference will result in the spacecraft reliability estimate.

2)   The lack of a firm mission profile for the subsystems was another limitation of the study. Since reliability is a time-dependent, probabilistic expression, [1] any changes in the mission time of a subsystem would modify its reliability estimate. As in the previous case, this effect on the reliability prediction at the spacecraft level would be minimum.

3)   The availability of failure rate information for most components used in the space environment is quite limited. When available, these data often indicated wide variations in the failure rate experience of similar component types. To compensate for these deficiencies, a number of failure rate sources were examined to assure the selection of the most realistic failure rates available.

b.   Major assumptions. The following major assumptions were established prior to performing the reliability analysis:

1)   Except as noted, series operation was assumed for the spacecraft subsystems and their components. Therefore, successful operation of the spacecraft was assumed to be dependent upon nonfailure of any element in the spacecraft. [2]

2)   The components used in the reference subsystem designs were assumed to have the most realistic failure rates of current off-the-shelf missile and space components. Thus, these failure rates represent the present reliability of components used in the space environment. However, to attain even this level of component reliability will require a comprehensive reliability program.

3)   It is expected that further improvements in the current state of the art of these components will raise the level of their reliability by the time the Voyager Program goes into the hardware phase. These anticipated improvements were assumed to more than compensate for uncertainties in the selection of component failure rates, as well as to assure the attainment of a high level of reliability growth.

4)   It was assumed that a full-scale reliability program would be continued after the first Mars/Venus launches to maintain sequential reliability growth.

---

[1] Except in the case of one-shot items such as solid rockets.

[2] Successful operation of the spacecraft is defined as the satisfactory functioning of its various elements such that accuracy and performance requirements are achieved.

c. _Prediction techniques_. The following failure distributions were adjudged applicable to the general types of equipment used in the spacecraft:

1) For one-shot devices, e.g., solid rockets, the binomial failure distribution was applied.

2) For time-dependent equipment, e.g., electronic components, the exponential failure distribution was applied.

The exponential and binomial failure distributions incorporate both initial start-up and continuous operation survival probabilities during equipment use.

1) _Active element group (AEG) method_. An AEG consists of a transistor or electron tube with its passive network; an average AEG failure rate of 3.19×10^{-6} failure per hour has been observed in the space environment (ref. 11).

2) _Parts count method_. Failure rates were extracted from the appropriate failure rate data sources and assigned to the various parts/components used in the equipment.

3) _Structural reliability method_. The reliability of a structural element, such as a heat shield, was estimated by a failure mode and safety factor analysis of the structure.

4) _Test data method_. The evaluation of some devices was accomplished by the analysis of available test data; reliability values computed by this method were specified at various confidence levels.

d. _Bases for reliability estimations_. Since there were limitations in the design detail and failure rate availability, the subsystem reliability estimates were based on several types of reliability assessments. The bases for the reliability estimates are discussed below.

1) _Comparative subsystem reliability assessment_. The reliability estimates were based on the reliability appraisal of a comparable subsystem intended for use in another space program.

2) _Similar subsystem reliability assessment_. The estimate was based on a reliability analysis conducted for a similar subsystem.

3) _Reference design subsystem reliability assessment_. In this case, the assessment was made by appraising the reliability of a reference design which closely approximates the Voyager subsystem.

4) _Functional subsystem reliability assessment_. The prediction was based on a reliability analysis of the subsystem design as conceived by Avco at the time.

5) <u>Legislated subsystem reliability assessment</u>. The reliability estimate is legislated by the customer. A case in point is the orbiter and lander scientific payloads which were legislated a reliability of 1.0 by NASA.

Table 44 lists the various spacecraft subsystems, their reliability estimates, and the reliability assessment type employed. Where appropriate, the prediction technique utilized is also noted. As indicated in the table, one of the subsystem reliability estimates was based upon a combination of assessments.

e. <u>Mission reliability estimates</u>. The reliability of the Voyager spacecraft was predicted for several Mars/Venus mission types and mission segments. Total mission success, i.e., return of 100 percent of the engineering/scientific information sought, was used as a criterion for the first launch. The reliability estimates were determined using the techniques and bases described. The subsystem reliability estimates were factored into appropriate mathematical models to predict the reliability of the various mission segments and mission types. Table 45 presents these latter reliability estimates for the first Mars launch (excluding the booster reliability), together with the associated mathematical models. Table 46 gives similar reliability estimates for the first Venus launch and related mathematical models. The Voyager mission reliability profile for the first Mars launch is depicted graphically in figure 147.

A review of table 45 and table 46 indicates rather low levels of mission reliability, primarily attributable to the requirement for total mission success. [3] With these predicted reliability levels, the present Voyager Program objectives would not be fulfilled unless there were a substantial increase in the number of launch attempts and/or an unacceptable compromise in the program objectives. Therefore, the total mission success requirement was deemed unreasonable and the reliability capabilities of the spacecraft were reevaluated, allowing for partial mission success. In this aspect of the study, each mission segment was evaluated to determine its contribution to the total success of the mission type considered. The probability of successfully completing each mission segment was next estimated throughout the Voyager Program (table 47), assuming the projected effects of a reliability improvement program. [4] These factors were then combined using an expectation technique, to determine the probabilities of fulfilling the Voyager Program objectives. These results were used in selecting the combinations of orbiters and landers for each launch opportunity as part of the mission evolution discribed in Vol. II, Scientific Mission Analysis.

f. <u>Projected reliability growth</u>. The anticipated rate of reliability growth assumed for the Voyager Program was determined after evaluating the

---

[3] That is, 100 percent success is required or the mission is termed a failure.

[4] The mission reliability estimates for the first Mars/Venus launch were the same as those predicted under the total mission success ground rules.

projected growth rate of several missile and space reliability programs. The magnitude, scope, and objectives of these programs was examined in light of the reliability effort required for the Voyager Program. Of the various programs reviewed, one in particular -- the Apollo Program -- was felt to have a reasonably sufficient rate of reliability growth (ref. 12). Since the Apollo Program is a shorter mission life, manned space venture with opportunity for operator redundancy the growth rate was conservatively modified to compensate for the expected adverse conditions to be encountered by Voyager. All factors considered,[5] it was assumed that an average annual 25 percent reduction in the Voyager spacecraft failure rate could be achieved through the implementation of an effective reliability program, utilizing failure information from both tests and operational missions to produce sequential reliability growth. The details of the planned Voyager Reliability Program and presented in Vol. VI, Development Plan. The key elements of reliability control for this program are thoroughly discussed in section VII. D, Reliability Assurance Controls.

2. <u>Allocation of reliability goals.</u> Reliability apportionment may be defined as the allocation of numerical reliability goals to the various subsystems comprising the Voyager spacecraft, such that the overall spacecraft reliability requirement is fulfilled. Since the apportionment relates the reliability of the spacecraft to that of its subsystems, it is an invaluable tool to the designer. These allocated goals provide him with a numerical guide to the degree of subsystem reliability needed to fulfill the spacecraft requirement. The magnitude of the allocated values compared to estimated values indicates the feasibility of achieving the necessary subsystem reliability using existing designs for the intended missions. Furthermore, the comparison identifies those portions of the spacecraft which are potential weak links so that reliability improvements can be initiated.

a. <u>Spacecraft reliability goal.</u> In the absence of a contractual reliability requirement, a tentative spacecraft reliability goal of 0.833 was established. This goal was determined after an evaluation of the mission success criterion for the first Mars/Venus launch[6] and the level of reasonably attainable booster reliability. Based on preliminary Mars/Venus program objectives[7] of at least 4 successful Mars lander missions out of 8 launch attempts and at least 5 successful Venus orbiter missions out of 10 launch attempts, the success criterion for the first launch was concluded to be 0.50. A realistic assessment of booster reliability state of the art indicated that a reliability level of 0.60 could reasonably be assumed for the Saturn launch vehicle (ref. 13). The spacecraft reliability goal was then calculated using the following model:

---

[5]Consideration was given to such factors as component state-of-the-art improvement and development (including micromodules, integrated microcircuits, cryogenics), use of Minuteman (and later) high-reliable parts, and corrective action resulting from test/use failure analysis.

[6]The primary emphasis for the Mars missions was on the success of the lander, while that for the Venus missions was associated with orbiter success.

[7]These initial program objectives were later revised to those given in Vol. II, Scientific Mission Analysis.

TABLE 44

SPACECRAFT SUBSYSTEM RELIABILITY ESTIMATES
AND RELIABILITY ASSESSMENT TYPE EMPLOYED

Spacecraft Subsystem	Reliability Estimates[1]	Reliability Assessment Type Employed[2]
O-B Propulsion	0.901	Reference Design Assessment (Parts Count Method)
O-B Guidance	0.850	Reference Design and Similar Assessments (Parts Count Method)
O-B Attitude Control	0.966	Similar Assessment (Parts Count Method)
O-B Power Source	0.954	Comparative Assessment
O-B Communications	0.904	Functional Assessment (Active Element Group Method)
O-B Thermal Control	0.995	Comparative Assessment
O-B Structure	0.997	Comparative Assessment
O-B Separation (Booster)	> 0.999	Functional Assessment (Parts Count Method)
L-B Separation	> 0.999	Functional Assessment (Parts Count Method)
L Structure	0.997	Comparative Assessment
L Crushup	0.999	Functional Assessment
L Thermal Control	0.995	Comparative Assessment
L Erection	0.999	Functional Assessment (Parts Count Method)
L Power Source	0.924	Functional Assessment (Parts Count Method)
L Heat Shield	0.999	Reference Design Assessment (Structural Reliability Method)
L Communications (Direct)	0.920	Functional Assessment (Active Element Group Method)
L Propulsion	0.972	Functional Assessment (Test Data Method)
L Attitude Control	0.998	Comparative Assessment
L Spin Up	>0.999	Functional Assessment
L Descent Equipment	0.995	Functional Assessment (Parts Count Method)
L Sterilization	>0.999	Legislated Assessment
L Scientific Payload	1.0	Legislated Assessment
L Deployment Mechanism	0.991	Functional Assessment (Parts Count Method)
L Engineering Instrumentation	0.995	Functional Assessment (Parts Count Method)
O Scientific Payload	1.0	Legislated Assessment
O Engineering Instrumentation	0.995	Functional Assessment (Parts Count Method)
L-O Relay Communications	0.975	Reference Design Assessment (Active Element Group Method)

[1] These subsystem reliability estimates, which include the intransit reliability of the spacecraft, are associated with a 21-day orbiter mapping mission and a 24-hour lander experimentation mission.

[2] The various reliability assessment types are the bases for the subsystem reliability estimates. The associated prediction technique utilized is shown in parentheses, where appropriate.

L - Lander
O - Orbiter
B - Bus

TABLE 45

RELIABILITY ESTIMATES FOR FIRST MARS LAUNCH MISSIONS
(Excluding Booster Reliability)

Mission Type	Reliability Estimate								
	Lander			Orbiter			Joint		
	1 Day	30 Day	180 Day	21 Day	70 Day	180 Day	1 Day L 21 Day O	30 Day L 70 Day O	180 Day L and O
I. Lander (Direct)/Scientific Orbiter	-----	-----	------	-----	-----	-----	0.505	0.409	0.273
II. Lander (Direct or Relay Option)/ Scientific Orbiter (Relay Capability)	-----	-----	------	-----	-----	------	0.548	0.455	0.323
III. Scientific Orbiter	-----	------	------	0.631	0.547	0.397	-----	-----	-----
IV. Lander (Direct)	0.571	0.533	0.490	---	---	---	-----	-----	-----
V. Lander (Relay by Communication Orbiter)	0.547	0.487	0.402	----	----	----	-----	-----	-----
VI. Lander (Direct or Relay Option)	0.614	0.589	0.553	----	----	----	-----	-----	-----

TABLE 45 (Cont'd)

Mission Segment	Symbol	Reliability Estimate					
		Transit	1 Day	21 Day	30 Day	70 Day	180 Day
Transit (From Booster Separation to Lander Separation)	R_1	0.713	----	----	----	----	----
Scientific Orbiter Mapping (From Lander Separation)	R_2	---	----	0.885	----	0.768	0.557
Lander (From Separation Not Including Communications)	R_3	---	0.870	---	0.843	----	0.813
Lander Communications (Direct)	R_4	---	0.920	----	0.887	----	0.847
Lander-Orbiter Relay Link	R_5	---	0.975	----	0.911	----	0.853
Communications Orbiter	R_6	---	0.903	----	0.890	----	0.812
Lander (Scientific Orbiter, Relay or Direct Option)	$\left[1 - (1 - R_4)(1 - R_5)\right]$	---	0.998	----	0.989	----	0.975
Lander (Communication Orbiter, Relay or Direct Option)	$\left[1 - (1 - R_4)(1 - R_5 \cdot R_6)\right]$	---	0.990	----	0.979	----	0.953

TABLE 45 (Concl'd)

Mission Type	Mathematical Model
I. Lander (Direct)-Scientific Orbiter	$R_I = R_1 \cdot R_2 \cdot R_3 \cdot R_4$
II. Lander (Direct or Relay Option)-Scientific Orbiter (Relay Capability)	$R_{II} = R_1 \cdot R_2 \cdot R_3 \cdot \left[1 - (1 - R_4) \cdot (1 - R_5) \right]$
III. Scientific Orbiter	$R_{III} = R_1 \cdot R_2$
IV. Lander (Direct)	$R_{IV} = R_1 \cdot R_3 \cdot R_4$
V. Lander (Relay by Communication Orbiter)	$R_V = R_1 \cdot R_3 \cdot R_5 \cdot R_6$
VI. Lander (Direct or Relay Option)	$R_{VI} = R_1 \cdot R_3 \cdot \left[1 - (1 - R_4) \cdot (1 - R_5 \cdot R_6) \right]$

TABLE 46

RELIABILITY ESTIMATES FOR FIRST VENUS LAUNCH MISSIONS
(Excluding Booster Reliability)

Mission Type	Reliability Estimate						
	Lander	Orbiter			Joint		
		1 Day	21 Day	60 Day	Lander 1 Day O	Lander 21 Day O	Lander 60 Day O
I. Lander - Probe[1]	0.621	-----	-----	-----	-----	-----	-----
II. Scientific Orbiter	-----	0.644	0.631	0.576	-----	-----	-----
III. Lander (Probe) - Scientific Orbiter	-----	-----	-----	-----	0.623	0.610	0.558
IV. Lander - Direct Entry[2]	-----	-----	-----	-----	-----	-----	-----

[1] This is a small probe-type lander which is ejected from orbit and relays information through the orbiter.

[2] Because of the vagueness of the mission definition and uncertainty of the environmental hazard, there is no firm basis for reliability estimation.

TABLE 46 (Concl'd)

Mission Segment	Symbol	Reliability Estimate					
		Transit	Attaining Orbit	To Impact	1 Day	21 Day	60 Day
Transit (From Booster Separation to Lander Separation)	R_1	0.713	-----	-----	-----	-----	-----
Attaining Orbit	R_2	-----	~0.900	-----	-----	-----	-----
Lander--Probe	R_3	-----	-----	0.968	-----	-----	-----
Scientific Orbiter	R_4	-----	-----	-----	0.904	0.885	0.808

Mission Type	Mathematical Model
I. Lander--Probe	$R_I = R_1 \cdot R_2 \cdot R_3$
II. Scientific Orbiter	$R_{II} = R_1 \cdot R_4$
III. Lander (Probe--Scientific Orbiter)	$R_{III} = R_1 \cdot R_4 \cdot R_3$

TABLE 47

MARS-VENUS MISSION RELIABILITY GROWTH ESTIMATES
(Excluding Booster Reliability)

I. Mars Missions	Calendar Year			
1. Orbiter Mapping	1969	1971	1973	1975
a. 1 Day	0.644	0.803	0.896	0.946
b. 70 Days	0.596	0.772	0.878	0.937
c. 180 Days	0.472	0.685	0.828	0.910
2. Lander Experimentations	1969	1971	1973	1975
a. 1 Day	0.614	0.783	0.885	0.941
b. 30 Days	0.601	0.775	0.880	0.938
c. 180 Days	0.571	0.756	0.869	0.933
II. Venus Missions	Calendar Year			
1. Orbiter Mapping	1970	1972	1973	1975
a. 1 Day	0.644	0.803	0.848	0.921
b. 21 Days	0.638	0.799	0.845	0.920
c. 60 Days	0.604	0.777	0.828	0.909
2. Lander Experimentations	1970	1972	1973	1975
	0.621	0.788	1	1

[1] Since there is no firm basis for direct entry lander reliability esti-
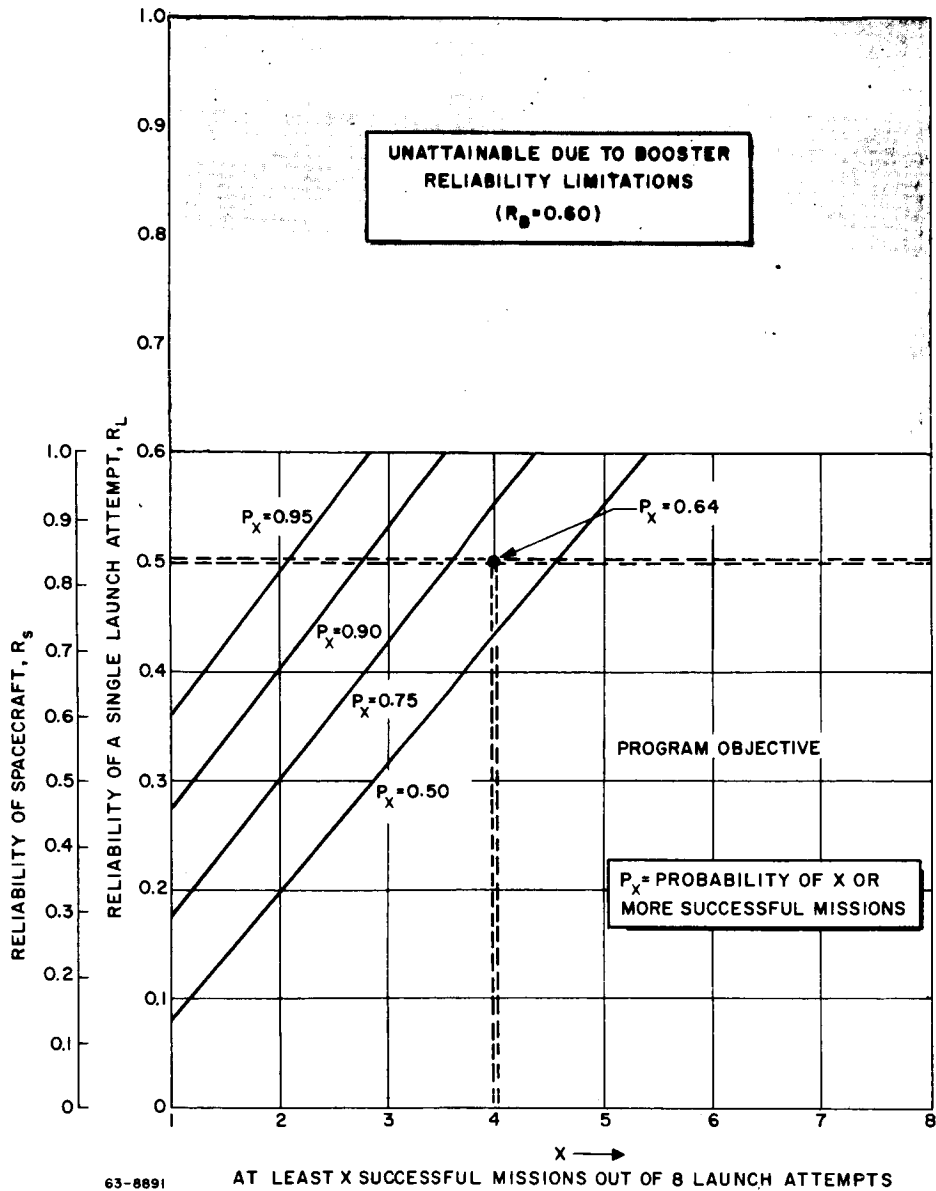mates, no growth figures are shown for these years.

Figure 148 MARS VOYAGER RELIABILITY ALTERNATIVES, LANDER EMPHASIS

63-8891

$$R_L = R_S \cdot R_B \ ,$$

then

$$R_S^o = \frac{R_L}{R_B}$$

where

R_S = the reliability of the spacecraft

R_S^o = the reliability goal for the spacecraft

R_L = the mission success criterion for the first Mars/Venus launch

R_B = the reliability of the Saturn booster.

From tables of the negative binomial distribution, the probability of 4 or more successful Mars landers out of 8 attempts and 5 or more successful Venus orbiters out of 10 attempts was determined to be 0.64 and 0.62, respectively. The probability of X or more successful missions for varying Mars/Venus program objectives and mission success criteria is shown in figure 148 for the lander and figure 149 for the orbiter. These figures also disclose the degree of spacecraft reliability needed to achieve these objectives and criteria for a fixed level of booster reliability equal to 0.60. It is interesting to note that even with a spacecraft reliability of 1.0, the reliability of a single Mars/Venus launch attempt (for the first launch) cannot exceed 0.60 because of the launch vehicle reliability limitations.

b. <u>Subsystem reliability goals</u>. Given a spacecraft reliability goal, the next step was to allocate reliability goals at the subsystem level. The apportionment of subsystem reliability goals was initially accomplished by a qualitative evaluation of such pertinent mission-design factors as relative complexity, mission time, relative importance (to the mission),[8] state of the art, and environmental hazard. The mathematical model for this allocation, based on qualitative factors, is as follows:

---

[8]The reliability apportionment considered the relative importance of the various subsystems for two Voyager missions, one in which the primary emphasis was on the Mars lander and the other in which the primary emphasis was on the Venus orbiter.
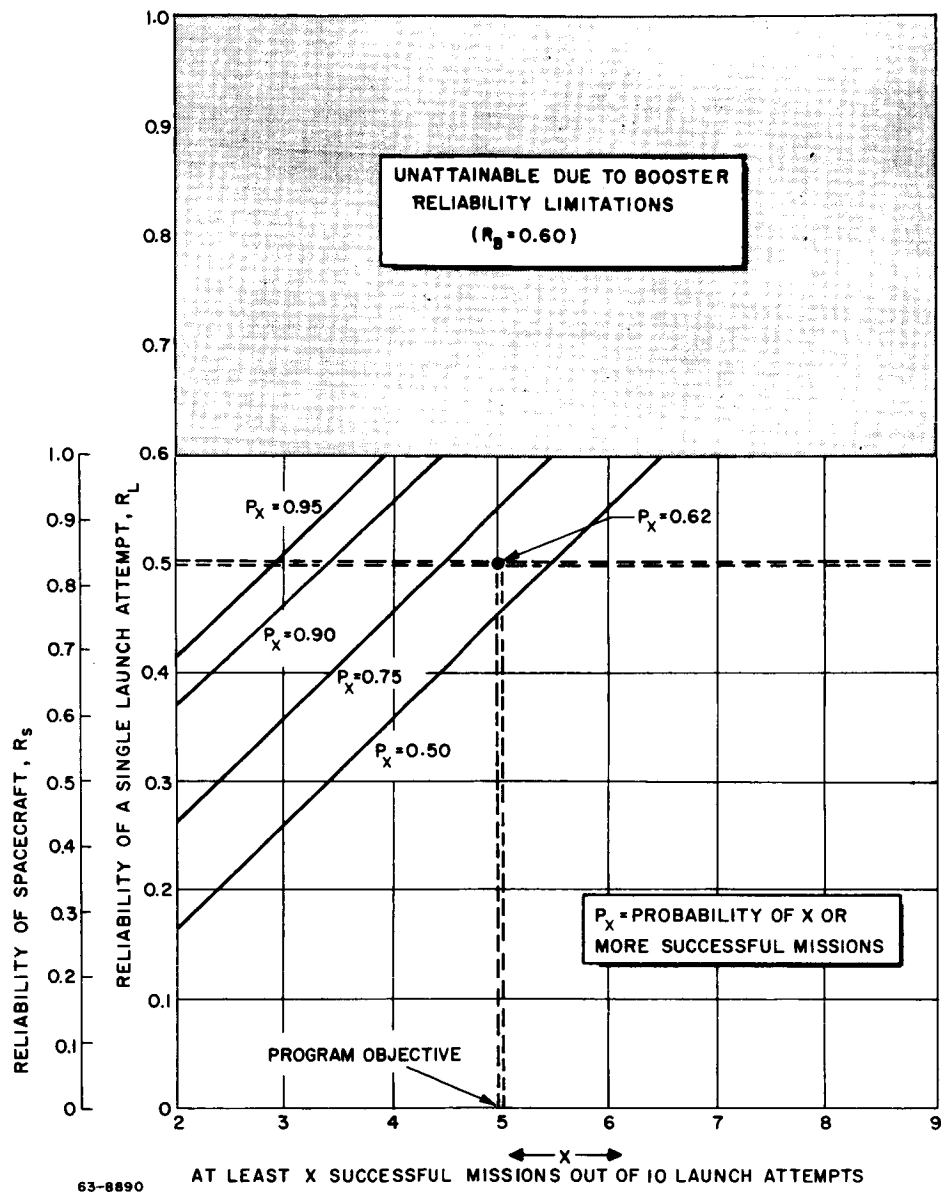
Figure 149 VENUS VOYAGER RELIABILITY ALTERNATIVES,
ORBITER EMPHASIS

63-8890
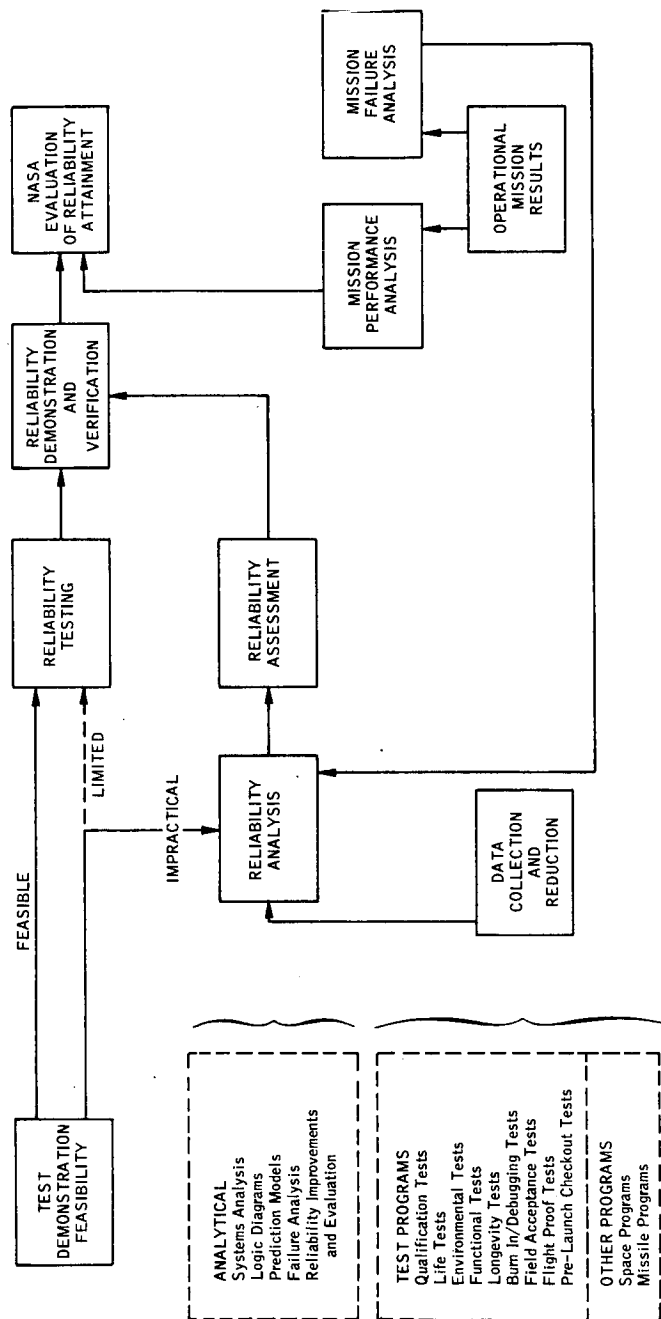
Figure 150 RELIABILITY DEMONSTRATION AND VERIFICATION PHILOSOPHY

63-8889

$$R_S^o = \prod_{i=1}^{n} \left[1 - \left\{ \left(\frac{\prod_{j=1}^{5} F_{ij}}{\sum_{i=1}^{n} \prod_{j=1}^{5} F_{ij}} \right) (1 - R_i^o) \right\} \right].$$

where

R_S^o = the reliability goal for the spacecraft

R_i^o = the reliability goal for the i"th" subsystem

F_{i1} = the relative importance of the i"th" subsystem

F_{i2} = the relative complexity of the i"th" subsystem

F_{i3} = the mission time of the i"th" subsystem

F_{i4} = the state of the art of the i"th" subsystem

F_{i5} = the environmental hazard of the i"th" subsystem.

The individual values assigned to the five factors pertaining to a particular subsystem were adjudged on an engineering review of each subsystem. These factors were then used in the above model to calculate the subsystem reliability goals. The results of this reliability allocation are presented in table 48. The range of allocated goals was intended to provide preliminary subsystem reliability guidelines for use during the early part of the conceptual design phase.

This reliability apportionment was later updated by a quantitative assessment of design reliability parameters associated with the failure contribution of each subsystem. The reliability capability of the subsystems was estimated using the techniques and ground rules described in Section VI. A. 3. The model for the subsequent allocation, based on quantitative factors, is given below.

$$R_S^o = \prod_{i=1}^{n} R_i^o = (R_S^*)^k = \left(\prod_{i=1}^{n} R_i^* \right)^k$$

TABLE 48

VOYAGER SPACECRAFT ALLOCATED SUBSYSTEM RELIABILITY GOALS[1]
(Overall Spacecraft Reliability Goal = 0.833)

Spacecraft Subsystem	Range of Allocated Reliability Goals	
	Lower Value	Upper Value
Orbiter-Bus Guidance	0.95713	0.96000*
Orbiter-Bus Structure	0.98125	0.98250*
Orbiter-Bus Propulsion	0.98147	0.98425*
Orbiter-Bus Communications	0.98285	0.98400*
Orbiter-Bus Thermal Control	0.98511	0.99444*
Orbiter-Bus Attitude Control	0.98541	0.98639*
Lander Scientific Payload	0.98694*	0.99753
Lander Thermal Control	0.98857*	0.99160
Orbiter Scientific Payload	0.99216	0.99756*
Orbiter-Bus Power Source	0.99334*	0.99643
Lander Deployment Mechanism	0.99357*	0.99622
Lander Erection	0.99524*	0.99527
Lander Structure	0.99550*	0.99669
Lander Crushup	0.99643*	0.99764
Lander Power Sources	0.99679*	0.99669
Lander Heat Shield	0.99857*	0.99874
Lander Attitude Control	0.99872*	0.99987
Lander Communications	0.99886*	0.99933
Orbiter Relay Communications	0.99905*	0.99924
Lander Engineering Instrumentation	0.99966*	0.99987
Orbiter Engineering Instrumentation	0.99971	0.99981*
Lander Spinup Mechanism	0.99993*	0.99997
Lander Propulsion	0.99995*	0.99996
Lander Sterilization	0.99997*	0.99999
Lander Separation Mechanism	0.99999*	0.99999
Bus Separation Mechanism	0.99999*	0.99999
Lander Descent Equipment	0.99999*	0.99999

NOTE: The asterisk refers to allocated reliability goals related to a Voyager mission whose primary emphasis is on a Mars Lander. Those without the asterisk pertain to a Voyager mission whose primary emphasis is on a Venus Orbiter.

[1] Based on Qualitative Factors

where

R_S^o = the reliability goal for the spacecraft

R_i^o = the reliability goal for the i"th" subsystem

R_S^* = the reliability estimate for the spacecraft

R_i^* = the reliability estimate for the i"th" subsystem

$$k = \frac{\log_e R_S^o}{\sum_{i=1}^{n} \log_e R_i^*} \quad .$$

The "k" factor in the above equation is the coefficient required to adjust the predicted (estimated) subsystem reliability values to the allocated goals. The resultant calculations yielded the subsystem reliability goals tabulated in table 49. For comparative purposes, predicted subsystem reliability estimates related to the first Mars mission are also given in this table.

3. Reliability improvement guidelines. An examination of table 49 reveals that reliability improvements will be necessary to achieve the subsystem allocations. The distribution of required improvement effort was determined from the relative failure contribution of each subsystem to the overall spacecraft. Mathematically, the relative improvement effort required for a particular subsystem was computed from the following equation:

$$E_i = \frac{\log_e R_i^*}{\sum_{i=1}^{n} \log_e R_i^*} \times 100$$

where

E_i = the relative percent of reliability improvement required for the i"th" subsystem

R_i^* = the reliability estimate for the i"th" subsystem.

Assuming an equal return for each dollar spent for reliability improvements, such percentages can serve as guidelines for the distribution of effort to be

TABLE 49

PREDICTED AND ALLOCATED SUBSYSTEM RELIABILITY VALUES
(Overall Spacecraft Reliability Goal = 0.833)

Spacecraft Subsystem	Predicted Reliability Estimates (Mars)	Allocated Reliability Goals[1]
Orbiter-Bus Propulsion	0.901	0.973
Orbiter-Bus Guidance	0.850	0.958
Orbiter-Bus Attitude Control	0.966	0.991
Orbiter-Bus Power Source	0.954	0.988
Orbiter-Bus Communications	0.904	0.974
Orbiter-Bus Thermal Control	0.995	0.999
Orbiter Bus Structure	0.997	> 0.999
Orbiter-Bus Separation (Booster)	> 0.999	> 0.999
Lander-Bus Separation	> 0.999	> 0.999
Lander Structure	0.997	> 0.999
Lander Crushup	0.999	> 0.999
Lander Thermal Control	0.995	0.999
Lander Erection	0.999	> 0.999
Lander Power Source	0.924	0.979
Lander Heat Shield	0.999	> 0.999
Lander Communications (Direct)	0.920	0.978
Lander Propulsion	0.972	0.992
Lander Attitude Control	0.998	0.999
Lander Spinup	> 0.999	> 0.999
Lander Descent Equipment	0.995	0.999
Lander Sterilization	> 0.999	> 0.999
Lander Scientific Payload	1.0	1.0
Lander Deployment Mechanism	0.991	0.998
Lander Engineering Instrumentation	0.995	0.999
Orbiter Scientific Payload	1.0	1.0
Orbiter Engineering Instrumentation	0.995	0.999
Lander-Orbiter Relay Communications	0.975	0.993
Joint Probability of Orbiter and Lander Success	~0.50	~0.83

[1] Based on Quantitative Factors

expended for such improvements. Specifically, preliminary guidelines were prepared for the types of effort required to realize the necessary reliability improvements. The type of effort recommended was dependent upon whether or not the incorporation of redundancy was feasible within a given subsystem. When feasible, the number of redundant elements needed to achieve the allocated subsystem reliability goal was determined. [9] For those subsystems which do not lend themselves to the use of redundancy, general guidelines were suggested for achieving the reliability goals. Table 50 presents the material pertinent to this discussion of reliability improvement guidelines, including the relative improvement effort allocated to each subsystem, the potential reliability weak link, and the recommended improvement.

More detailed discussion of design improvements aimed at increasing subsystem reliability are contained in the appropriate sections of the design volumes (Vols. IV and V).

4.   Reliability assurance controls. Reliability assurance controls embraces many facets of the reliability effort from adequate program planning to fastidious launch site preparation of operational equipment. However, certain key technical reliability controls, when successfully implemented, help to assure that a high degree of inherent reliability is designed into the spacecraft. These essential controls are treated, not necessarily in the order of importance, under the following subheadings:

   a.   Design guidelines

   b.   Subcontractor efforts

   c.   Reliability assessment

   d.   Design reviews

   e.   Test program

   f.   Failure analysis.

   a)   Design guidelines. By establishing a set of electronics/electromechanical design guidelines for the designer to follow, a spacecraft design can be evolved which utilizes preferred, highly reliable parts in standard, proven circuits. This will be accomplished by selecting, when possible, only parts which have a record of high performance and high reliability. These parts will then be derated as prescribed and applied in proven circuits. The adequacy of the part safety margins will be carefully evaluated by means of tolerance studies to determine the effects of drift conditions on successful circuit operation.

---

[9] Where possible, the additional weight and volume required for these redundant elements were determined, although not presented in this report.

TABLE 50

RELIABILITY IMPROVEMENT GUIDELINES

Spacecraft Subsystem (Relative Improvement Effort Allocated)	Potential Reliability "Weak Links"	Recommended Improvement
1. O-B Propulsion (15 percent)	1. a. Propellant tanks b. Pressure regulator c. Number of firings	1. a. Provide adequate puncture and leakage protection for propellant tanks. b. Provide backup pressure regulator for redundancy. c. Limit number of firings to 10.
2. O-B Guidance (24 percent)	2. a. Computer b. Gyros	2. a. Add standby computer for redundancy. b. Add three standby gyros for redundancy.
3. O-B Attitude Control (5 percent)	3. a. Fill valve b. Solenoid valves	3. a. Provide shutoff valve as backup for fill valve. b. Use fail-safe dual port solenoid valves and positive shutoff valves for leakage protection.
4. O-B Power Source (7 percent)	4. Solar Cell Modules	4. Allow 2 percent of solar cell modules to be redundant.
5. O-B Communications (15 percent)	5. Electronic part complexity in terms of AEG's*	5. Make 80 percent of AEG's redundant.
6. O-B Thermal Control (<1 percent)	6. Not identifiable	6. Select high durability paints.
7. O-B Structure (<1 percent)	7. Structure	7. Provide adequate design reliability - safety factors.
8. O-B Separation (<1 percent)	8. No significant weak links	8. None
9. L-B Separator (<1 percent)	9. No significant weak links	9. None
10. L Structure (<1 percent)	10. Structure	10. Provide adequate design reliability-safety factors.
11. L Crushup (<1 percent)	11. Crushup	11. Provide adequate design reliability-safety factors.
12. L Thermal Control (<1 percent)	12. Not identifiable	12. Provide increased thermal level safety margins.

TABLE 50 (Concl'd)

Spacecraft Subsystem (Relative Improvement Effort Allocated)	Potential Reliability "Weak Links"	Recommended Improvement
13. L Erection (<1 percent)	13. No significant weak links	13. None
14. L Heat Shield (<1 percent)	14. No significant weak links	14. None
15. L Power Source (12 percent)	15. Not identifiable	15. Noted as a critical development problem area.
16. L Communications Direct (12 percent)	16. Electronic part complexity in terms of AEG's*	16. Make 95 percent of AEG's redundant.
17. L Propulsion (4 percent)	17. Rocket	17. Select rocket with proven high reliability capability.
18. L Attitude Control (<1 percent)	18. No significant weak links	18. None
19. L Spinup (<1 percent)	19. No significant weak links	19. None
20. L Descent Equipment (<1 percent)	20. Not identifiable	20. Provide adequate design reliability-safety factors.
21. L Sterilization (<1 percent)	21. Not identifiable	21. None
22. L Scientific Payload (<1 percent)	22. Not identifiable	22. Monitor instrument design and production program.
23. L Deployment Mechanism (<1 percent)	23. Shaped charges	23. Make shaped charges 100 percent redundant.
24. L Engineering Instrumentation (<1 percent)	24. Quantity of transducers	24. Make 80 percent of transducers redundant or limit number of data monitoring points.
25. O Scientific Payload (<1 percent)	25. Not identifiable	25. Monitor instrument design and production program.
26. O Engineering Instrumentation (<1 percent)	26. Quantity of transducers	26. Make 80 percent of transducers redundant or limit number of data monitoring points.

*Active Element Group (AEG) - A transistor or electron tube with its passive network.

These studies will be supplemented by failure mode analyses to determine potential failure causes. In addition to the electronics and electromechanical guidelines, similar design assistance can be provided for mechanical and structural elements of the spacecraft. These guidelines will establish design criteria using safety factors determined from mode-of-failure reliability analyses.

b) Subcontractor efforts. To assure that the reliability of subcontracted equipment is not compromised, general and specific reliability requirements will be established for Voyager subcontractors. The reliability efforts of the various subcontractors will be closely monitored to assure that these requirements are met.

c) Reliability assessment. The reliability capability of the Voyager spacecraft will be continuously assessed, reflecting the receipt of more recent design/reliability information, to monitor the reliability growth progress. These repetitive assessments will mean modifying previous reliability estimates and allocations. Initial logic diagrams and mathematical models will be updated accordingly. The proposed incorporation of redundancy will be analyzed in tradeoff studies to determine the effect of redundant elements on spacecraft weight, volume, cost, accuracy, and performance. This iterative process will detect, through analytical means, potential reliability weak links, thus enabling the initiation at an early stage of the necessary followup action.

d) Design reviews. The reliability design review is considered to be a vital activity in assuring that a high degree of inherent reliability is designed into the overall spacecraft. A minimum of five design reviews are planned for the Voyager Program -- preliminary, first interim, second interim, final, and postrelease. The preliminary review will be held early in the program to consider the basic concepts and techniques, and their compatibility to be employed in the design. This will be followed by two interim reviews, the first being primarily a design standardization shakedown, and the second being an analysis of functional and environmental aspects of the design. The final review, which provides the last opportunity for evaluating the design prior to release of drawings to production, will involve a critical analysis of the hardware interface. After fabrication and assembly of the spacecraft has begun, a postrelease design review will be conducted to resolve any critical problem areas.

e) Test programs. Exhaustive testing is one of the essential principles upon which the Voyager Program reliability assurance philosophy is founded. The test programs will be planned to ensure that the objectives of each type of test are met. These test programs will include provisions for component life, engineering evaluation, environmental, longevity, flightproof, reliability, burn/debugging, functional, launch site, and prelaunch checkout tests. Specifications will be prepared which completely describe the test procedures, conditions, and requirements. The tests will be monitored to maintain effective reliability control and to assure the collection of meaningful data. The test results will become inputs to a dynamic corrective action loop.

f) <u>Failure analysis.</u> The analysis of failed parts is one of the keys to success of the corrective action activity. In the Voyager Program, failure analysis will be one means for initiating corrective action. All part failures occurring during tests will be removed from the units being tested and sent to a laboratory for a complete failure analysis. Efforts will be made to simulate the failure conditions and, where necessary, the part will be dissected and subjected to a microscopic analysis of its inner elements. The cause and mode of failure will be determined and the corrective action defined. This information will then be used to assign responsibility for the part failure. As a final step, the necessary engineering corrective action will be initiated with provisions for follow-up action.

g) <u>Related areas.</u> During the fabrication and assembly phase, it will be the role of Quality Assurance to maintain the high level of inherent reliability designed into the spacecraft. All purchased material will be subjected to incoming inspection, 100 percent, where feasible, or lot sampling where necessary. Any deviations in quality standards will be reviewed by a Material Review Board to ensure that quality (and reliability) is not compromised in an effort to meet production schedules. Tasks such as fabrication and assembly inspection, statistical quality control, vendor audits and surveillance, and final inspection will be implemented to minimize degradation of reliability during production. These tasks will be supplemented by in-process functional tests, burn-in/debugging tests, and functional acceptance tests. The shipping and handling of the spacecraft will be carefully controlled to eliminate any undue abuse which might induce operational failures.

5. <u>Reliability demonstration and verification</u>

a. <u>General.</u> "For complex equipment expected to perform satisfactorily in a space environment over long periods of time ... the optimum plans (providing both specified reliability for a given time and minimum amounts of testing to assure such reliability levels) ... require apparently an excessive amount of testing generally leading to prohibitive costs" (ref. 14).

The obvious limitations in demonstrating the achievement of specified reliability goals are the cost of the required number of test samples and the time required for testing. As an alternative to the classical, but economically unfeasible means of reliability demonstration, an approach is proposed which combines testing where practical and alternate means of verification where necessary.

In this plan, all items will receive some degree of reliability testing; many items will undergo extensive reliability testing. In general, subsystems and components which will require statistical demonstration of reliability are those

items (a) the role of which is extremely critical to the mission outcome (e.g., propulsion), (b) which have had little or no operational experience (e.g., RTG), and (c) which are of low cost and have short duty cycles, such that they are easily testable (e.g., separation mechanism).

For the others, limited (i.e., nonstatistical) reliability testing will be augmented by an analytic reliability verification based on extensive test and use data.

This two-pronged approach -- testing and analysis -- is combined through the use of a modified "equivalent systems technique"(ref. 15). Briefly, this technique entails the testing, under simulated operational conditions, of all components comprising a system. A sufficient quantity of these components is tested to collect data on enough "equivalent systems" that a statistical evaluation, at the system level, can be made to ensure that, at a specified confidence level, the required reliability levels are fulfilled. The modification consists of substituting conservative reliability analysis, supported by test and use data, where statistical testing is not feasible. Conservative measures can be built into the realiability analysis estimates by limiting the data sources to relevant and articulated programs and imposing the requirement that the reliability estimate exceed the required reliability by some prescribed safety margin. Preliminary estimates indicate a safety factor of 1.25 (i.e., 1.25 x predicted failure rate $\leq$ required failure rate) should be adequate.

The reliability demonstration and verification philosophy is depicted in figure 150. It is noted that the verification alternative to reliability demonstration requires the use of specific analytic tools, namely, systems analysis, logic diagrams, prediction models, failure analyses, and reliability improvement evaluation. Moreover, the data sources relevant as inputs to reliability verification are qualification tests, life tests, environmental tests, functional tests, longevity tests, burn-in/debugging tests, flightproof tests, field acceptance tests, prelaunch tests, and use data from earlier shots and other space and missile programs. On the basis of this approach, achievement of reliability is assured.

b. Test quantities. The number of samples to be tested using the equivalent system approach is a function of the confidence level desired, the number of allowable failures during the demonstration test, and specified reliability level for the system in question. The specified spacecraft reliability goal or level to be demonstrated is 0.833.[10] With this goal as a criterion, table 51 shows the number of complete spacecraft to be tested:

---

[10] This goal is associated with a booster reliability of 0.60 and a mission objective of 0.50 for the 1969 launch opportunity. With consideration for potential reliability growth, a reliability goal somewhat less than 0.833 could be selected for reliability demonstration in advance of 1969.

TABLE 51

SAMPLES TO BE TESTED
(Spacecraft Reliability = 0.833)

Number of Failures Allowed	Sample Size			
	50 Percent Confidence	75 Percent Confidence	80 Percent Confidence	90 Percent Confidence
0	~4	8	9	13
1	10	15	17	22
2	15	23	24	30
3	22	29	32	38

Based on the magnitude of test program costs and potential risk, a 75 percent confidence is expected to be the lowest acceptable level. The quantities and tests required to demonstrate a spacecraft reliability of 0.833 at the 0.75 confidence level are described in the subsequent pages. These quantities are associated with the testing (at the subsystem and lower levels) of eight complete spacecraft under simulated operational conditions. It is strongly emphasized that zero lethal failures are allowed with this minimum demonstration plan and that any other failures of a less serious nature (degradation type) must be rectified by prompt and effective corrective action. [11]

For those subsystems, the cost of testing of which is prohibitive, testing of lesser quantities will be tolerated provided that analytical verifications based on statistical/mathematical models, supported by test/operational data, are accomplished.

    a.   O-B Propulsion

       1)   Test A

           Option 1. Test 8 systems for one simulated mission of 11 cycled firings totalling 800 seconds.
           Option 2. Test 1 system for 8 simulated missions of 11 cycled firings totalling 800 seconds each. After each mission, inspect and repair as necessary to restore to a launch-ready status. For example, thrust chambers and fuel tanks may be replaced after each mission.

---

[11] Lethal failures are defined as destructive, nonrecoverable failures which result in a spacecraft mission abort. Degradation-type failures, for which corrective action is not acceptable, will also be classified as lethal failures.

2) **Test B**

Test 8 complete sets of propulsion system valves in a space simulated environment (i. e., vacuum and cold temperature) for anticipated mission duration. All valves must be exercised in accordance with their use during mission profile.

3) **Test C**

Test 1 complete system over a simulated operational mission to include cycling, duration, and environmental storage in their proper sequence.

b. **O-B Guidance**

1) **Test A -- digital computer unit**

Option 1. Test 8 digital computer units on a simulated mission to include anticipated operation for the time duration required (approximately 500 hours) and under specified environmental conditions.

Option 2. Determine a minimum cost reliability test program (evaluate hardware, test equipment, facilities, test labor, schedule) which will result in the accumulation of 4000 hours of computer test history.

2) **Test B -- inertial measuring unit**

a) **Gyros.** Test 24 gyros on a simulated mission, i. e., to include anticipated operation for the time duration required and under specified operational conditions.

b) **Accelerometers.** Test 24 accelerometers on a simulated mission.

c) **Sensors and trackers.** Test 8 complete sets of sensors and trackers for operation consistent with their missions.

c. **O-B Attitude Control**

1) **Test A**

Test 8 systems including electronics for one simulated mission, cycling each system in accordance with the mission profile.

2) **Test B**

Test 8 complete sets of valves in a space simulated environment for the anticipated mission duration. All valves must be exercised in accordance with their use during the mission profile.

d.   O-B Power Sources

1)   Test A -- batteries

Test 8 sets of batteries by charge-discharge cycling to the required discharge depths consistent with their mission profile.

2)   Test B -- solar panels

a)   Verify reliability through systems analysis supported by test and use data including mathematical models and success diagrams.

b)   Perform functional tests of one complete system for a simulated mission, monitoring performance parameters.

3)   Test C -- power conditioning equipment

Test 8 complete sets of equipment under simulated mission condition.

e.   O-B Communications

1)   Test A -- electronics

Test 8 complete systems for one simulated mission, cycling each portion of the system in accordance with the mission profile.

2)   Test B -- antennas

Test eight 4-foot and eight 8-foot antennas (16 total) over a simulated mission to include operational cycling and environmental conditions.

f.   O-B Thermal Control

1)   Test A

Environmental testing of paints to evaluate aging effects on absorption and emissivity.

2)   Test B

Test 8 fans for continuous operation during one simulated mission.

g.   L Structure   (integrated lander structure including descent equipment, crushup, erection, and deployment mechanism).

1)   Test A

Vibrate 8 structures to simulate peak and accumulated "g" loads expected to be encountered during the mission.

2)   Test B

Drop-test 8 structures (including dummy loads) from aircraft to simulate entry, descent, and impact conditions; follows vibration testing.

3)   Test C

Following drop test, perform functional tests of erection and deployment mechanisms consistent with mission profile.

h.   O-B and L-B Separation

1)   Test A

Vibrate 8 complete sets of each type of separation mechanisms under simulated mission conditions.

2)   Test B

Following vibration tests, perform functional tests on all 16 test systems to determine operational capability.

i.   L Thermal Control

Test 8 complete thermal control units under simulated environmental conditions to maintain desired ambient temperature.

j.   O-B Structure

Vibrate 8 structures to simulate peak and accumulated "g" loads expected to be encountered during the mission.

k.   L Heat Shield

1)   Test A

Perform stress testing of 8 heat shields to simulate entry loads and conditions.

2)   Test B

Perform small sample experiments, simulating conditions and atmospheric constituents expected during planetary entry. Verify reliability through systems analysis using test data and mathematical models.

1.   L Power Source

1)   Test A -- batteries

Submit 8 sets of batteries to vibration and drop testing, followed by functional charge-discharge cycling to the required discharge depth consistent with mission profile.

2)   Test B -- RTG

Perform mission life tests of 8 units; details not available at this time.

3)   Test C -- power conditioning equipment

Submit 8 sets of equipment to vibration and drop-testing, followed by functional tests under simulated mission conditions.

m.   L Communications (direct and relay link)

1)   Test A -- electronics

Submit 8 complete systems (of each type) to vibration and drop testing, followed by a simulated mission, cycling each portion of the system in accordance with the mission profile.

2)   Test B -- antennas and associated hardware

Submit 8 complete sets of antenna (of each type) complexes to vibration and drop testing, followed by a simulated mission to include operational cycling and environmental conditions.

n.   L Propulsion

After vibration testing, test 8 propulsion systems to simulate mission conditions.

o.   L Spinup

After vibration testing, test 8 spinup systems to simulate mission conditions.

6. <u>Critical reliability problem areas.</u> During the Voyager conceptual design study, several critical reliability problems not only limited the reliability of the spacecraft, but also impeded its reliability analysis. Because some of the problem areas were not completely resolved at the end of the study, they will necessitate further examination in the next phase of the Voyager Program. These problem areas are reviewed in this section to recognize their existence and point out the recommended corrective action.

The critical reliability problem areas were classified under three main headings -- developmental, environmental, and general. The problem areas and recommended action associated with each of these classifications are summarized in table 52.

Uncertainties concerning the reliability of the radioisotope thermionic generator (RTG) and the impact survivability of the lander and its related equipment are regarded as critical developmental problem areas. The RTG is still in the development stage, with very little data available to evaluate its reliability. To alleviate this problem, it is recommended that reliability testing be performed to demonstrate the RTG allocated reliability goal. In the case of the overall lander's ability to survive planetary impact, it is difficult to assess this aspect of the mission because little is known of the planetary terrain features. Simulation testing of lander structures, crushup, deployment mechanism, erection devices, etc., can be employed to obtain the necessary impact survival information.

The environmental problem areas result from the lack of knowledge concerning heat sterilization effects on component reliability and the limited information pertaining to space environment storages effects on spacecraft subsystem reliability. Exhibit I below is a typical example of the type of available information concerning the effects of heat sterilization on reliability, i.e., no significance between the occurrence of test failures and the thermal sterilization procedure. As a means of accumulating data in this area, it is recommended that proof testing, involving the life testing of heat sterilized samples and unsterilized samples be performed. The effects of environmental storage on reliability can be determined through carefully planned and space-simulated environmental tests. To supplement these data, it is suggested that results from prior space programs be analyzed.

EXHIBIT I

EFFECTS OF HEAT STERILIZATION ON RELIABILITY (ref. 16)

"One of the most serious technical problems concerns the effect of sterilizing heat cycles on the reliability of the spacecraft system. Although most of the spacecraft components now in use will survive heat cycles of 125°C for 24 hours, a number of critical items of

TABLE 52

SUMMARY STATEMENT OF CRITICAL RELIABILITY PROBLEM AREAS

Classification	Reliability Problem Areas	Recommendations
I. Developmental	1. Uncertainties concerning reliability of RTG.	1. Reliability demostration testing.
	2. Uncertainties concerning the ability of lander and associated equipment to survive planetary impact.	2. Simulation testing of structures, crushup, deployment mechanism, erection devices, etc.
II. Environmental	1. No knowledge of heat sterilization effects on component reliability.	1. Proof testing.
	2. Limited information of space environment storage effects on spacecraft subsystems reliability.	2. a. Environmental testing b. Analysis of prior space program results.
III. General	1. Limited availability of reliability data from the space environment for improving the accuracy of reliability estimates and identifying potential problem areas.	1. Establish reliability data files using JPL and NASA space program histories.
	2. Limited knowledge of the wearout characteristics of thrust chamber-nozzle, celestial and inertial sensors for long term, frequent use type mission.	2. Longevity testing to determine component operating life characteristic curves.

hardware are seriously affected. In addition, almost nothing is known about the effect of these cycles on component lifetime. Reliability testing of sufficiently large scale has never been done to obtain a statistical analysis of failure rates over long operating periods after exposure to thermal sterilization. It is therefore impossible at this time to make an intelligent analysis of the effect of heat sterilization on overall mission reliability. Most engineers are becoming increasingly concerned over these problems, and strong pressures are being exerted to waive the heated procedures for obtaining internal sterility of spacecraft in the lunar program. To date, no component failure can be traced directly to thermal sterilization. However, on Ranger 3 and 4 series spacecraft, three component failures occurred on the prototype model, which did not undergo heat sterilization, whereas on the flight models which were heat sterilized, nine component failures occurred during tests. In the Central Computer and Sequencer system, at least one failure occurred on each unit that was heated. Since the number of instruments tested was very small, it is not possible to establish the significance of these failures in relation to a thermal sterilization procedure. "

The general reliability problem areas concern the limited availability of reliability data from the space environment and the limited knowledge of the wearout characteristics of certain components used for long-term, frequent-use type missions. The former problem is particularly important, since appropriate reliability data are needed for improving the accuracy of reliability estimates and identifying potential reliability weak links. To overcome this problem, it is suggested that reliability data files be established using NASA/ JPL space program histories. Lastly, there is limited knowledge pertaining to the wearout characteristics of thrust chamber nozzle, and celestial and inertial sensors. Longevity testing of these components is recommended to reveal their operating life characteristic curves.

7. Special reliability studies

a. Evaluation of alternate design concepts. In addition to the major technical studies described above, special reliability studies were performed to evaluate alternate design concepts. These special reliability analyses are briefly discussed in this section.

The prediction techniques and failure distributions described in section on Reliability Estimation were also employed in the evaluation of the alternate design concepts. Since the object of these analyses was to measure the relative success probability of the design concepts under consideration, equipment common to all concepts, in both make-up and usage, were not included in the evaluation.

It was recognized that component failure rates possessed wide variations for similar component types. To combine the failure rate variance and yet show its effect in a meaningful way, a root mean square approach was used.[12] As a result, a range of likely failure rate values were computed at the subsystem level. These failure rates were then combined into pessimistic, nominal, and optimistic success probabilities. The results of the special studies were used in the conceptual design selection.

    1)   Relative reliability analysis of alternate orbit techniques. An analysis was made to evaluate the relative reliability of attaining an orbit (from a terminal point along the trajectory) about Mars or Venus, utilizing aerodynamic braking or retropropulsion techniques. The following alternatives were included in the study of each of these principles:

    a)   Aerodynamic braking

    1   With precursor vehicles (at least three out of five vehicles must operate successfully)

    2   Without precursor vehicles.

    b)   Retropropulsion -- liquid rocket system

    1   One engine configuration

    2   Three-engine configuration (any two of three engines must operate successfully).

Table 53 summarizes the results of the relative reliability analysis. A review of this table reveals that the differences in the success probabilities of the various orbit attainment techniques were relatively small (with the exception of the one-engine propulsion technique which possessed a much lower level of reliability). Therefore, it was concluded that exclusion of the different orbit attainment techniques could not be made on the basis of reliability alone. Consequently, it was recommended that the results of the relative reliability analysis be used as inputs to a more comprehensive selection process.

    2)   Relative reliability analysis of lander communications techniques. An analysis was made to evaluate the relative reliability of a lander communicating from Mars to Earth, either directly or through an orbiter relay link.

At the time the analysis was performed, the effects of entry and impact stresses on lander equipment had not been evaluated (a separate failure mode

---

[12]See Section 8.2,7 for a more detailed description of this approach.

analysis was later conducted in this area). Another factor which had not been evaluated, but later determined, was the probability of the orbiter attaining an orbit.

The results of the relative reliability analysis are shown in table 54. On the basis of the reliability estimates alone, it appeared as though the lander direct communications technique was the more reliable method because the relay link was extremely sensitive to the probability of the orbiter attaining an orbit. However, the latter technique offered certain operational advantages which assured that some information would be received, [13] whether or not an orbit was attained. Thus, it was concluded that the lander relay link was more desirable from a reliability standpoint.

3) <u>Relative reliability analysis of parachute actuation system.</u> An analysis was made to evaluate the relative reliability of two types of parachute actuation systems contemplated for use in the Mars lander-descent equipment. One system involved the use of an adjustable accelerometer which was preset before launch, but later readjusted to reflect the receipt of more accurate measurements occurring after separation of the lander from the orbiter. The alternate system would consist of an accelerometer, preset before launch and not changed thereafter. Since both systems were found to be highly reliable, i.e., probability of success > 0.99, it was recommended that the more accurate (from a performance standpoint) actuation system be selected.

4) <u>Passive versus active thermal control subsystem.</u> An analysis was made to evaluate the approximate increase in the in-transit reliability of the overall spacecraft, using two fans in the thermal control subsystem for cooling (circulating) purposes. The average ambient temperature with the passive subsystem (without fans) was 155°F, while the active subsystem (with fans) maintained an average temperature of 115°F. By use of the following relationship,

$$\lambda_2 = \lambda_1 \left[\frac{T_2}{T_1} \right]^n$$

where λ^2 = the failure rate at the higher temperature

λ_1 = the failure rate at the lower temperature

T_2 = the higher temperature ($^{\circ}$K)

T_1 = the low temperature ($^{\circ}$K)

n = a constant estimated to be 5 from studies of equipment failure rates as a function of temperature.

it was possible to approximate the change in spacecraft failure rate attributed to a passive thermal control subsystem. Converting these failure rates into probabilistic values, it was determined that the in-transit spacecraft reliability without

---

[13] The principal advantage was the possible use of the omnidirectional antenna for direct transmission of data to Earth. Even though such information would be transmitted at a reduced bit rate, there would be a backup mode of operation in the event the orbiter direct link experiences a malfunction.

TABLE 53

RELATIVE SUCCESS PROBABILITIES
FOR ALTERNATE ORBIT ATTAINMENT TECHNIQUES

Orbit Attainment Technique	Pessimistic Success Probability	Nominal Success Probability	Optimistic Success Probability
1. Aerodynamic Braking			
a. With Precursor Vehicles (At least three out of five)	0.952 P	0.961 P	0.970 P
b. Without Precursor Vehicles	0.968 P	0.974 P	0.978 P
2. Retropropulsion - Liquid Rocket System			
a. One-Engine Configuration	0.850 P	0.891 P	0.928 P
b. Three-Engine Configuration (Any two of three engines must operate successfully)	0.936 P	0.961 P	0.977 P

P = the reliability of all other common functions.

TABLE 54

SURVIVAL PROBABILITIES
FOR ALTERNATE LANDER COMMUNICATIONS TECHNIQUES
(For a 24-Hour Martian Day)

Communications Technique	Reliability Factor	Pessimistic Survival Probability	Nominal Survival Probability	Optimistic Survival Probability
A. Direct	1. High Gain Antenna	0.999616	0.999688	0.999744
	2. Lander Memory Unit	0.999226	0.999406	0.999568
	3. Error-Free Transactions	0.994000	0.999400	0.999940
Relative Reliability of Direct Communications Technique		$0.992842\ R_C$	$0.998494\ R_C$	$0.999162\ R_C$
B. Relay Link	1. Omnidirectional Antenna	0.999984	0.999991	0.999995
	2. Lander Power Source (Batteries)	0.999888	0.999936	0.999976
	3. Lander Memory Unit	0.999226	0.999406	0.999568
	4. Lander Relay Transmitter	0.995712	0.996272	0.996832
	5. Orbiter Relay Receiver	0.999624	0.999672	0.999720
	6. Orbiter Memory Unit	0.999226	0.999406	0.999568
	7. Error-Free Transactions	0.990000	0.999000	0.999900
Relative Reliability of Relay Link Communications Technique (Excluding Reliability of Orbiter)		$0.98379\ R_C$	$0.993683\ R_C$	$0.995559\ R_C$

NOTE: R_C = the reliability of common direct link equipment

fans was approximately 0.673 as compared to a 0.713 spacecraft reliability using an active thermal control subsystem. Since negligible weight and power are required by the addition of the two fans, their use was recommended as a means of improving the reliability of the overall spacecraft.

     5) <u>Dormant versus active spacecraft.</u> An analysis was made to evaluate the increase in reliability that would be attained by maintaining a dormant spacecraft, except for some reduced "housekeeping" tasks, during the in-transit portion of the mission. After evaluating the feasibility of shutting down each subsystem, it was estimated that the most substantial increases in reliability could be achieved in the guidance and attitude control subsystems (particularly the attitude control subsystem). These subsystem reliability increases in turn produced a factor of 1.06 gain in the in-transit reliability of the overall spacecraft, i.e., 0.757/0.713 where 0.757 = dormant spacecraft reliability and 0.713 = active spacecraft reliability. It would appear that such a small increase in reliability does not justify the compromise in mission usefulness which would result from a dormant spacecraft.

    b. <u>Prediction technique modifications</u>

     1) <u>Adaptation of the AEG prediction technique to space systems.</u> The AEG technique is a well accepted means of reliability estimation when detailed part information is not available (such as in advance of the conceptual design). The professional literature is replete with examples of this type prediction, but unfortunately its use in the analysis of space equipment has not been exploited. Therefore, some preliminary computer experimentation was carried out to facilitate the use of the AEG technique in the prediction of Voyager equipment reliability. Four sets of linear correlations were attempted on each of 11 satellite systems. Specifically, these correlations were between the AEG count (a complexity measure based on transistor/tube count) and the mean life of the equipment as determined by (a) parts failure rate method, (b) low stress AEG method, (c) medium stress AEG method, and (d) the observed (telemetered) experience. Although some degree of correlation was obtained between the change in AEG failure rate as the system complexity, only the average AEG failure rate, 3.19×10^{-6}/AEG as suggested by Willard (ref. 11) was used because of large standard errors of estimate.

     2) <u>Selection of failure rate values.</u> Bias in the choice of component failure rates can severely influence system reliability estimates. This is especially true when failure experience for similar component types indicates wide variation is possible. This is further deteriorated by the fact that, at best, precise application and environmental conditions are vaguely defined. To alleviate these difficulties, a means was devised to accommodate the failure rate variance without bias and yet show its effect in a meaningful way. Essentially, the approach was to treat the differences in failure rate as deviations (errors) from the average and to evaluate their combined effect, in much the same way as tolerances, through the use of the root-mean-square (rms) technique. When

-332-

this method was used, the system prediction based on the average values was considered to be the most likely value, while predictions based on the ± rms values were considered as the optimistic and pessimistic range through which the system estimate could vary.

8.3 Conclusions

The reliability studies have produced two major results:

1.   The quantitative evidence that there is a reasonable expectation that the program will be successful

2.   The development of a comprehensive reliability program plan which, when implemented, will enhance the expectation of program success.

Other significant contributions include

1.   The meaningful allocation of reliability goals

2.   The identification of potential weak reliability links

3.   The optimization of program costs on the basis of reliability effectiveness

4.   The recommendation of a method for reliability demonstration and verification

5.   The evaluation of alternate design concepts as inputs to the conceptual design selection.

REFERENCES

1. Clarke, V., Jr., W. E. Bollman, R. Y. Roth, W. J. Scholey: Design Parameters for Ballistic Interplanetary Trajectories.Part I, One-way Transfer to Mars and Venus. JPL Technical Report No. 32-77, 16 January 1963

2. Clarke, V. C., Jr.: A Summary of the Characteristics of Ballistic Interplanetary Trajectories, 1962-1977. JPL Technical Report No. 32-209, 15 January 1962.

3. Lederberg, J.: Science, vol. 132, 393, 1960.

4. Phillips, C. and R. Hoffman: Science, vol 132, 991, 1960.

5. Davies, R., and M. Communtzis: Proceedings of the 10th International Astronautical Congress, Springer-Verlag, Vienna, vol.1, 495, 1960.

6. CETEX, Science, vol. 128, 887, 1958.

7. CETEX, Nature, vol. 183, 925, 1959.

8. Jaffe, L.: JPL Technical Report No. 32-325, p. 6-7, Pasadena, 1963.

9. Hobby, G.: as cited in JPL Technical Report No. 32-325, p. 6, Pasadena, 1963.

10. For a recent survey of the state of the art, see Jaffe, L.: Astronautics and Aerospace Engineering, p. 22-29, August 1963.

11. Willard, C. F.: Final Report - Satellite Reliability Spectrum. ARINC Research Corporation, Washington, D. C., Publication No. 173-5-280, IDEP No. 347.40.00.00-A9-01, 30 January 1962.

12. Apollo Final Study Report,: vol. 5, Implementation Plan, Book 2 - Reliability, General Dynamics, Convair, 15 May 1961. Confidential

13. Moffat, W. H.: Analysis of Reliability Growth of Rocket Propulsion Stages Relative to Orbiting Bell Telephone Laboratories Communications Satellites, Aerojet-General, AZUSA, Report No. 2051, IDEP No. 347.40. 00.00-A7-09, July 1961.

REFERENCES (Concl'd)

14. Hock, C. D.: Some Remarks on Optimum Reliability Testing. NASA, 8th National Symposium on Reliability and Quality Control, Washington, D. C., 9-11 January 1962.

15. Kerins, D. J.: The Equivalent System Technique for Reliability Demonstration. 14th Convention of Southwestern IRE, Houston, Texas, April 1962.

16. Hobby, G. L.: A Review of Space Research. National Academy of Science, National Research Council, Review of the NASA/JPL Sterilization Program, Publication No. 1079, Appendix III, Ch. 9.

17. Neuner, G. E., and M. Lepow,: Figure of Merit Evaluation for Lunar Logistics, 23rd National Meeting of the Operations Research Society of America, Cleveland, Ohio, 28 May 1963.

APPENDIX A

OPTIMUM ALTITUDE FOR ESTABLISHMENT OF PLANETOCENTRIC CIRCULAR ORBITS

In the final mission payload analyses, a fixed orbit for Mars and a varying orbit for Venus resulted. It is apparent from these results that it is possible to establish circular orbits about these planets without a significant payload reduction in the basic orbiter bus. If in the future it should be desirous to establish such orbits, there is an optimum altitude to minimize the orbit establishment velocity decrement. The orbit establishment velocity decrement is:

$$\Delta V = \sqrt{V_\infty^2 + \frac{2\mu}{r_p}} - \sqrt{\frac{\mu}{r_p}} \qquad (A1)$$

where

μ = gravitational parameter of planet

r_p = periapsis radius

V_∞ = asymptotic approach velocity

By setting the partial derivative of ΔV with respect to r_p to zero, the optimum altitude, h_p, is obtained as

$$h_p = \frac{2\mu}{V_\infty^2} - r_E$$

where

r_E = planet radius.

During many launch opportunities the approach velocity associated with the minimum sum of the departure and arrival velocities is relatively constant. Since the optimum altitude is a function of the approach velocity, this in turn implies that a fairly constant optimum altitude can be obtained over the entire launch window.

The associated velocity decrement to establish this optimum orbit also is a function of the approach velocity and is

$$\Delta V_{min} = \frac{V_\infty}{\sqrt{2}} \qquad (A2)$$

For Mars and Venus, the optimum altitude and velocity decrement is presented in figures A1 and A2 as a function of the approach velocity. With an approach velocity of 4 km/sec, the optimum altitude for Mars is approximately 2000 km. However, to achieve the same altitude with respect to Venus, an approach velocity of approximately 8.85 km/sec is required. The burnout weight in orbit can be determined as a function of the weight along the approach hyperbola and approach velocity from figure A3.
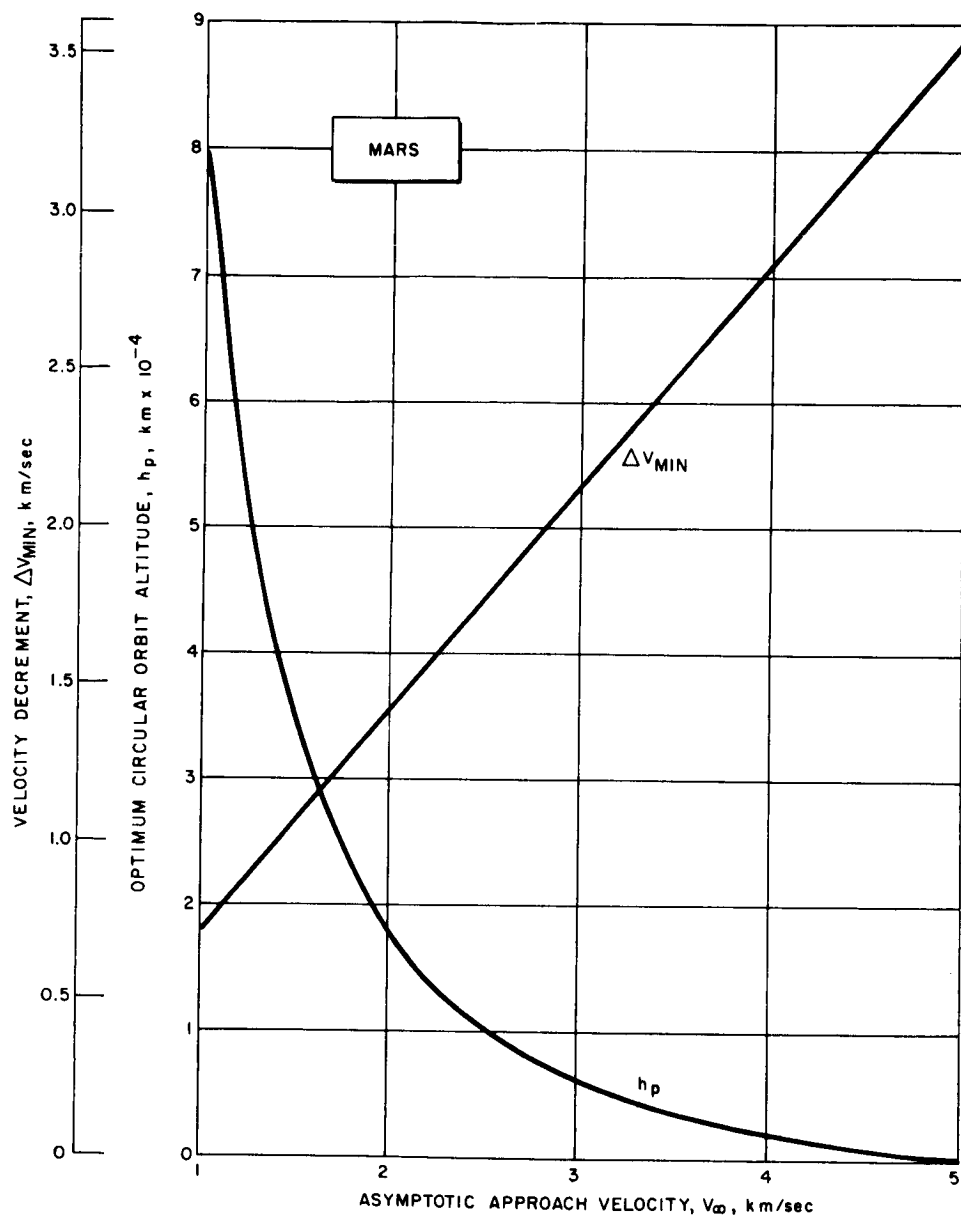
63-8928

Figure A1 OPTIMUM ORBIT ESTABLISHMENT PARAMETERS VERSUS
ASYMPTOTIC APPROACH VELOCITY (MARS)

-338-
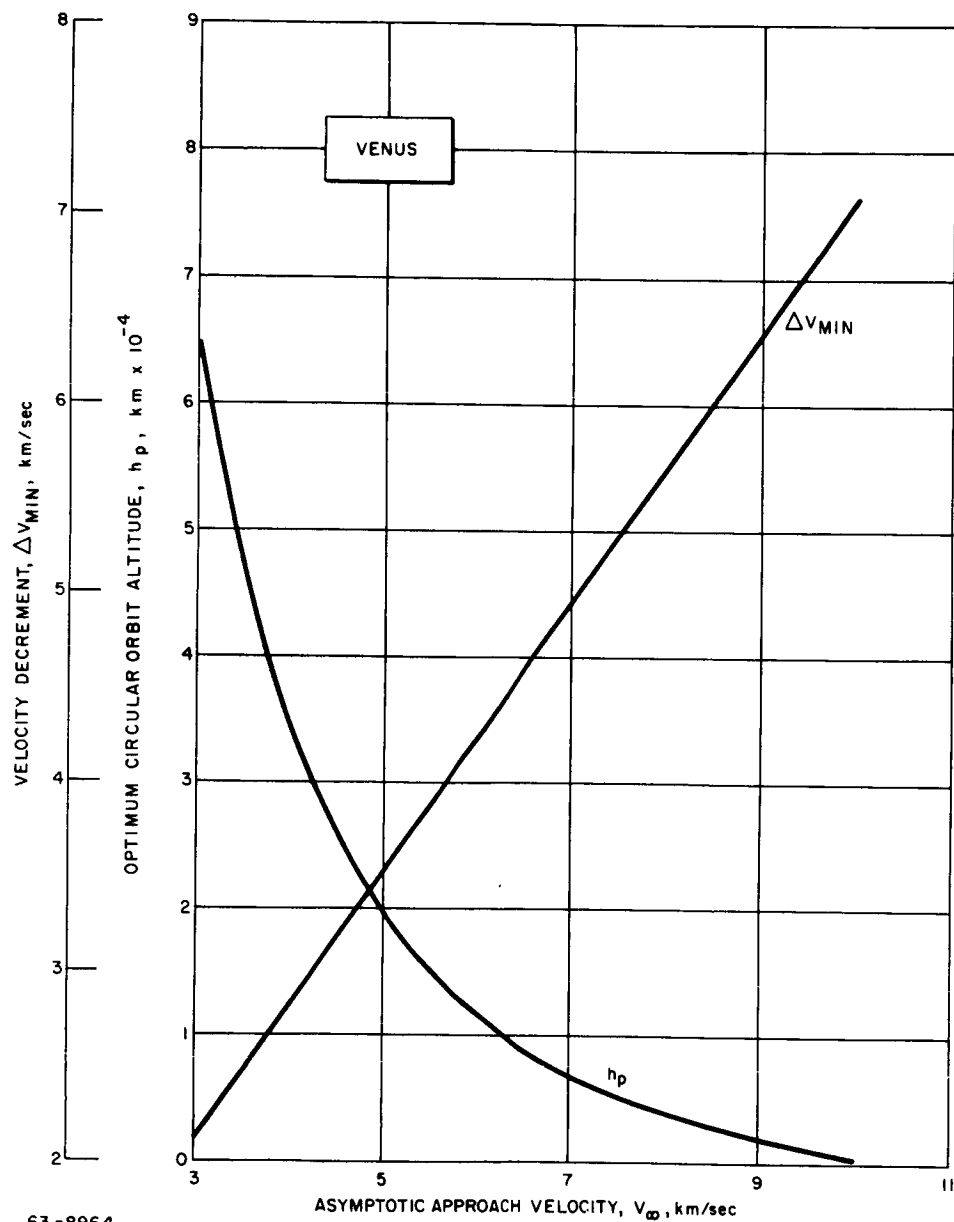
Figure A2 OPTIMUM ORBIT ESTABLISHMENT PARAMETERS VERSUS
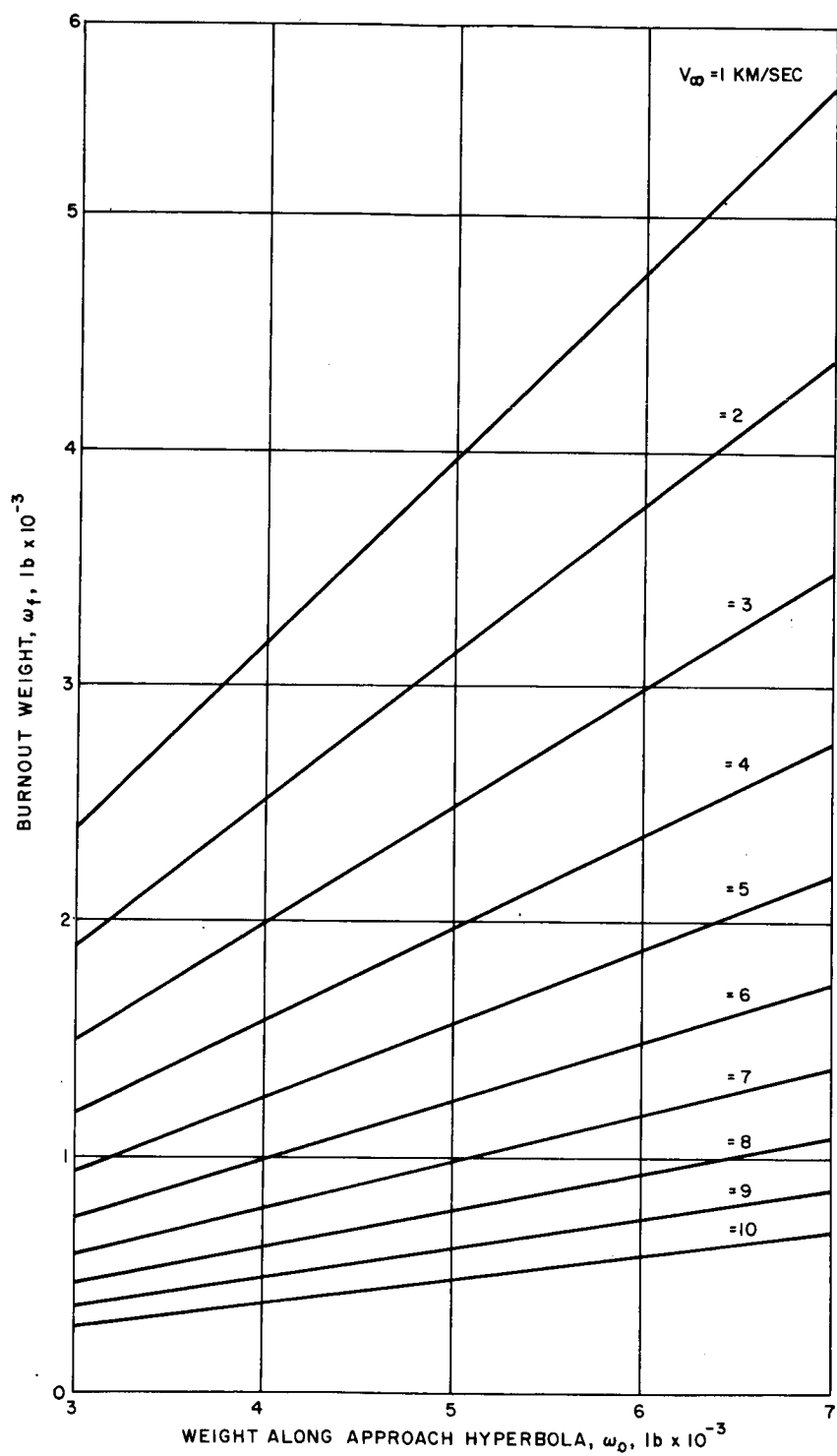ASYMPTOTIC APPROACH VELOCITY (VENUS)

63-8964

Figure A3 BURNOUT WEIGHT IN ORBIT VERSUS WEIGHT ALONG
THE WEIGHT HYPERBOLA

APPENDIX B

ANALYSIS TO DETERMINE REPEATABILITY OF TRAJECTORY AND MISSION PARAMETERS AT EXTREMES OF METONIC CYCLE

As pointed out in ref. 2 there is a cyclic recurrence of trajectory characteristics for launches to neighboring planets. In theory, there are four ballistic paths (over short intervals of time there may be six) per launch date for a given injection energy from Earth to the target planet for transfers of less than 360 degrees about the sun. However, with realistic departure velocities achievable with present boost vehicles, the launch window is restricted to several months duration when there is a favorable relation between the positions of Earth and the target planet. These favorable positions occur every synodic period (the time between two successive heliocentric conjunctions in celestial longitude). Thus, favorable launch opportunities to Venus occur every 19.2 months and to Mars every 25.6 months. The cyclic recurrence of trajectory characteristics reflect the same absolute space-fixed geometry of Earth and target planet. These cycles (metonic periods) are related to the synodic period and for Venus are very nearly 8 years or 5 synodic periods and for Mars about 15 years or 8 synodic periods.

The purpose of this analysis is to determine the variation in the trajectory parameters and mission payloads for 1962 and 1970 Venusian launch opportunities to determine the applicability of employing the 1962-1970 data for 8-year cycles thereafter. In order to assess the variation in the transfer orbit characteristics, the following parameters were investigated: (1) time of flight; (2) Earth-Venus communication distance; (3) asymptotic approach velocity vector; (4) heliocentric transfer angle; (5) angle between approach asymptote and Venusian orbital plane; (6) angle between approach asymptote and Sun-Venus vector; and (7) declination of geocentric asymptote.

These parameters, when plotted as a function of launch date, may be represented by a series of closed contours for constant departure energies. The vertical asymptotes of these contours represent the trajectory parameters associated with the daily minimum departure velocity.

In order to determine the variation between the 1962 and 1970 transfer orbit parameters, the extremes of a fixed energy contour (C_3 of 11 km^2/sec^2) were analyzed. This energy contour provided approximately a 45- and 28-day window for Type I and Type II transfer trajectories, respectively. The extremes of the contour were analyzed to determine if in addition to a variation in the trajectory parameters there also was a shift in the launch window. The existence of such a shift appears likely since there is a 3- to 4-day shift in date corresponding to the absolute minimum departure velocities for each opportunity. For Type I

and II transfers only minor variations in the trajectory parameters are evident. The entire contour shifts forward by 3 to 4 days in 1970 for the Type I transfer, while the window for a Type II transfer is shortened by 3 to 4 days, as only the latter portion of the window shifts forward. It is interesting to note that the absolute minimum departure velocity for Type I transfers is reduced by 0.033 km/sec in 1970, whereas for Type II transfers this velocity is increased by 0.019 km/sec. A summary of this analysis appears in tables B1 and B2 for Type I and II transfer trajectories, respectively.

While the variations between the trajectory parameters appear to be negligible, the effect of the minor velocity variations on the mission payload must be analyzed. For the all-orbiter and split-capsule orbiter/2000-pound lander mission, the maximum payload for Type I trajectories increases by approximately 12 pounds for the 1970 launch opportunity, and the maximum payloads are achieved approximately 5 to 7 days earlier. However, if this shift in the launch window is neglected, daily variations up to 50 pounds occur. The corresponding increase in the maximum mission payloads for Type II trajectories is indeterminable as the peak does not occur in the 120-day launch period investigated; however, the same trends noted in the Type I transfer are in evidence. Over most of the launch window, it appears that the 1970 launch window occurs 5 to 7 days earlier than the corresponding 1962 opportunity. Similarly, there is a 50-pound variation in payload if the shift is neglected. For these two missions, the variation in the payload for Type I and II transfer trajectories is presented in figures B1 and B2, respectively.

The results of this investigation indicate that for preliminary design purposes the trajectory and payload calculations for the 8-year (1962-1970) period can be applied to other 8-year cycles if allowance is made for a 5- to 7-day shift in the launch window.

ANALYSIS OF TRAJECTORY PARAMETER VARIATION FOR VENUSIAN 8-YEAR CYCLE -- TYPE I

| Trajectory Parameter	Units	Launch Date			Parameter Value		
		1962	1970	Variation	1962	1970	Variation
Time of flight	days	27 July 8 Sept.	23 July 5 Sept.	4 3	136 101	138 102	-2 -1
Earth-Venus communication distance	km x 10^6	27 July 8 Sept.	23 July 5 Sept.	4 3	53 62	53 60	0 2
Asymptotic approach speed	km/sec	27 July 8 Sept.	23 July 5 Sept.	4 3	5.8 5.25	5.78 5.31	0.02 -0.06
Heliocentric transfer angle	degrees	27 July 8 Sept.	23 July 5 Sept.	4 3	150 120	152 122	-2 -2
Angle between approach asymptote and planet's orbital plane	degrees	27 July 8 Sept.	23 July 5 Sept.	4 3	-35 -32	-34 -32	-1 0
Angle between approach asymptote and Venus-Sun line	degrees	27 July 8 Sept.	23 July 5 Sept.	4 3	43 43	43 44	0 -1
Declination of geocentric asymptote	degrees	27 July 8 Sept.	23 July 5 Sept.	4 3	-5 0	-5 0	0 0
Absolute minimum departure velocity	km/sec	23 Aug	19 Aug	4	2.952	2.919	0.033

TABLE B2

ANALYSIS OF TRAJECTORY PARAMETER VARIATION FOR VENUSIAN 8-YEAR CYCLE -- TYPE II

Trajectory Parameter	Units	Launch Date			Parameter Value		
		1962	1970	Variation	1962	1970	Variation
Time of flight	days	2 Sept. / 1 Oct.	2 Sept. / 27 Sept.	0.5 / 4.0	172 / 162	172 / 164	0 / -2
Earth-Venus communication distance	km x 106	2 Sept. / 1 Oct.	2 Sept. / 27 Sept.	0.5 / 4.0	133 / 154	136 / 154	-3 / 0
Asymptotic approach speed	km/sec	2 Sept. / 1 Oct.	2 Sept. / 27 Sept.	0.5 / 4.0	5.83 / 6.73	5.95 / 6.71	0.12 / 0.02
Heliocentric transfer angle	degrees	2 Sept. / 1 Oct.	2 Sept. / 27 Sept.	0.5 / 4.0	233 / 235	234 / 236	-1 / -1
Angle between approach asymptote planet's orbital plane	degrees	2 Sept. / 1 Oct.	8 Sept. / 27 Sept.	0.5 / 4.0	28 / 22	27 / 22.5	1 / -0.5
Angle between approach asymptote and Venus-Sun line	degrees	2 Sept. / 1 Oct.	2 Sept. / 27 Sept.	0.5 / 4.0	144 / 154	146 / 154	-2 / 0
Declination of geocentric asymptote	degrees	2 Sept. / 1 Oct.	2 Sept. / 1 Oct.	0.5 / 4.0	-47.5 / -31.0	-46 / -32.5	-1.5 / 1.5
Absolute minimum departure velocity	km/sec	19 Sept.	16 Sept.	3	3.230	3.249	-0.019
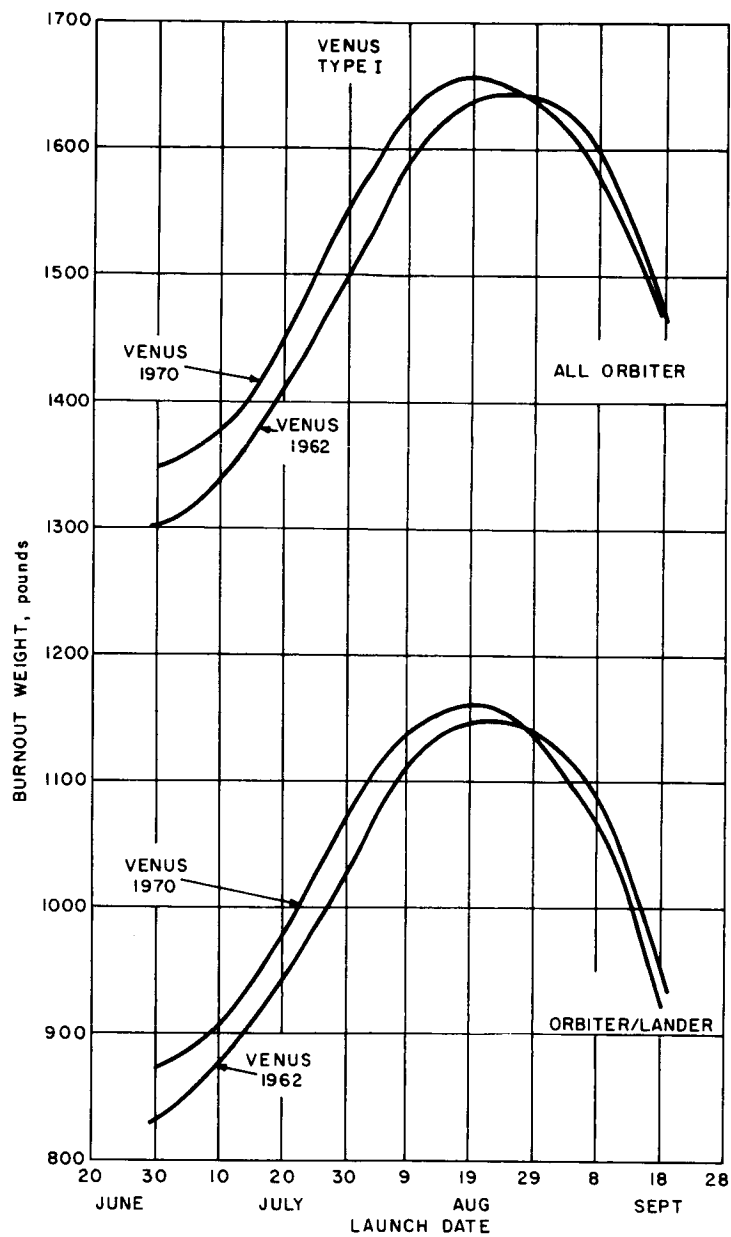
Figure B1 BURNOUT WEIGHT VERSUS LAUNCH DATE VENUS, TYPE I

63-8963
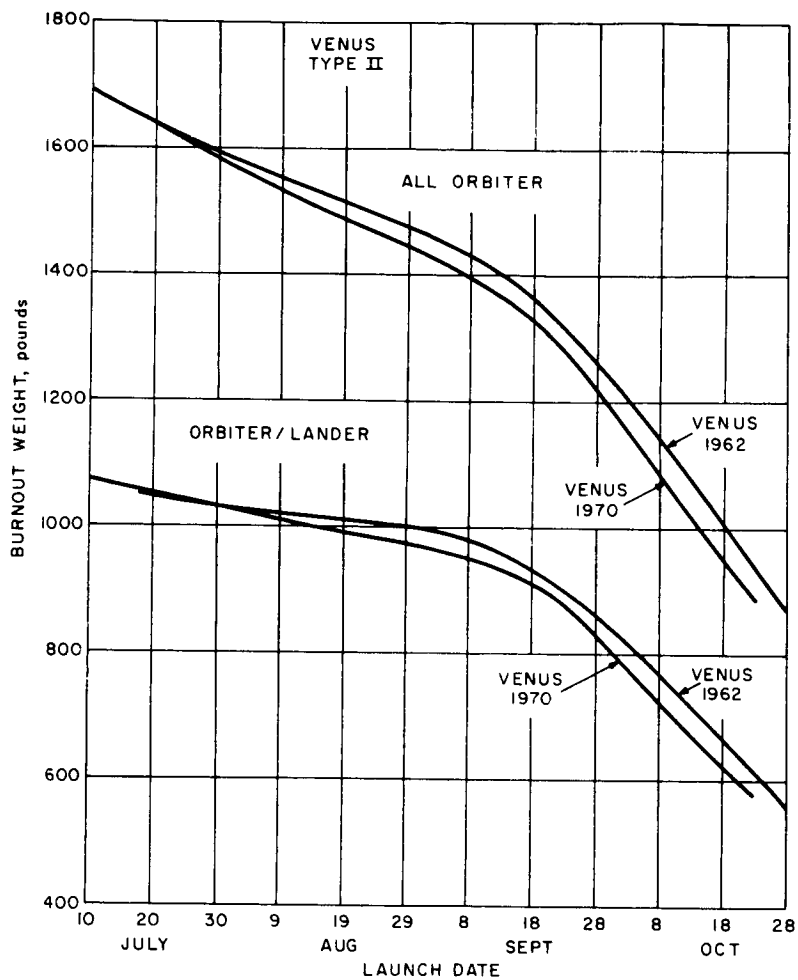
63-8924

Figure B2 BURNOUT WEIGHT VERSUS LAUNCH DATE VENUS, TYPE II

APPENDIX C

ORBIT TRIM REQUIREMENTS

Resulting from uncertainties due to the DSIF and on board guidance system, there will be an uncertainty in the periapsis altitude along the approach hyperbola, with a resultant velocity uncertainty prior to the establishment of the planetocentric orbit. This uncertainty may be expressed by

$$\delta(V_{Ph}) = -\frac{\mu_P r_{P_o}^2}{V_{Ph_o}} \delta r_P \quad , \tag{C1}$$

where:

V_{Ph_o} = nominal periapsis velocity

r_{P_o} = nominal periapsis radius.

The nominal orbit establishment velocity decrement is

$$\Delta V_N = V_{Ph_o} - V_{PE} \tag{C2}$$

when periapsis of the approach hyperbola and planetocentric orbit are coincident. Since the nominal orbit establishment velocity decrement will be employed, the periapsis velocity of the planetocentric orbit is, in the presence of an altitude error

$$V_{PE} = V_{Ph} - \frac{\mu r_{P_o}^2}{V_{Ph_o}} \delta r_P - \Delta V_N = \sqrt{\frac{r_a}{(r_P + \delta r_P)} \frac{2\mu}{(r_a + r_P + \delta r_P)}} \tag{C3}$$

the resultant apoapsis radius can then be computed and the variation from the nominal apoapsis radius

$$\delta r_{a_o} = r_{a_o} - r_a \tag{C4}$$

The two impulse orbital trim velocity requirement, to achieve the desired nominal orbit, is presented in figure C1.

If the orbital parameters result in a near synchronous orbit, the required perturbation in periapsis velocity to affect a change in the period is presented in figure C2.
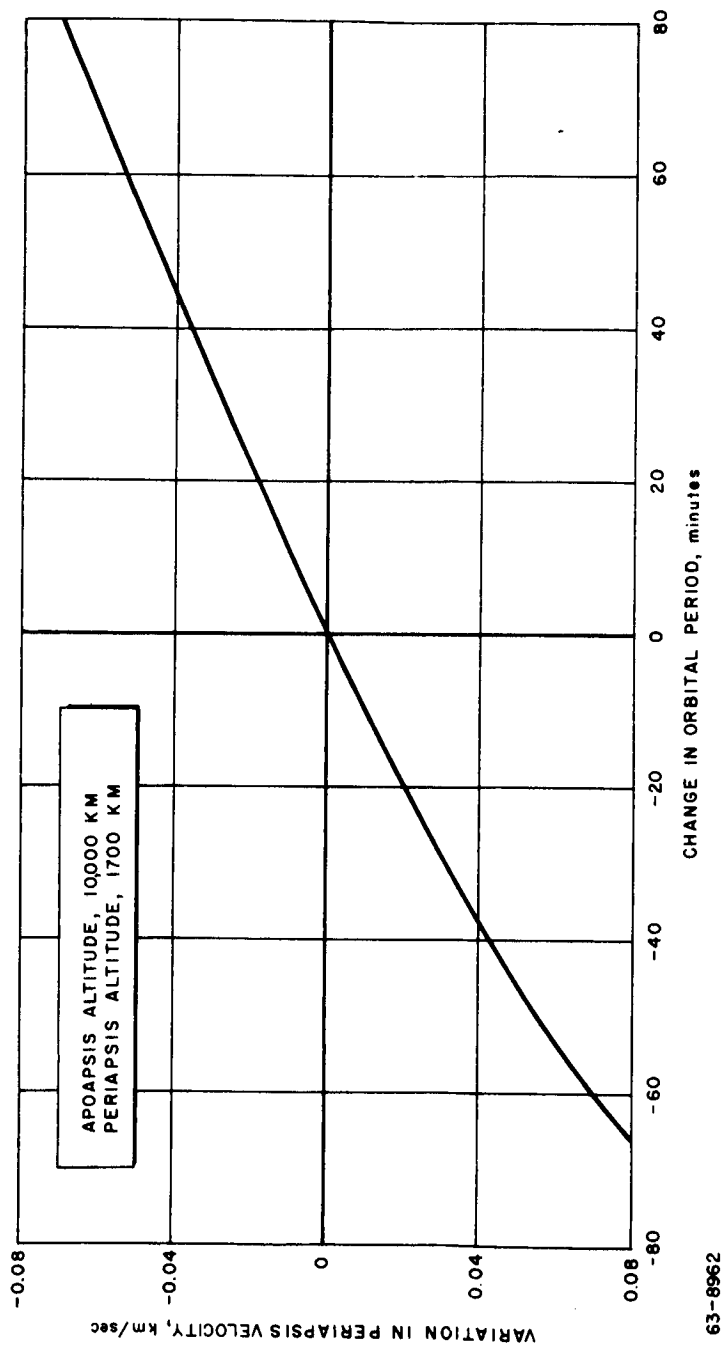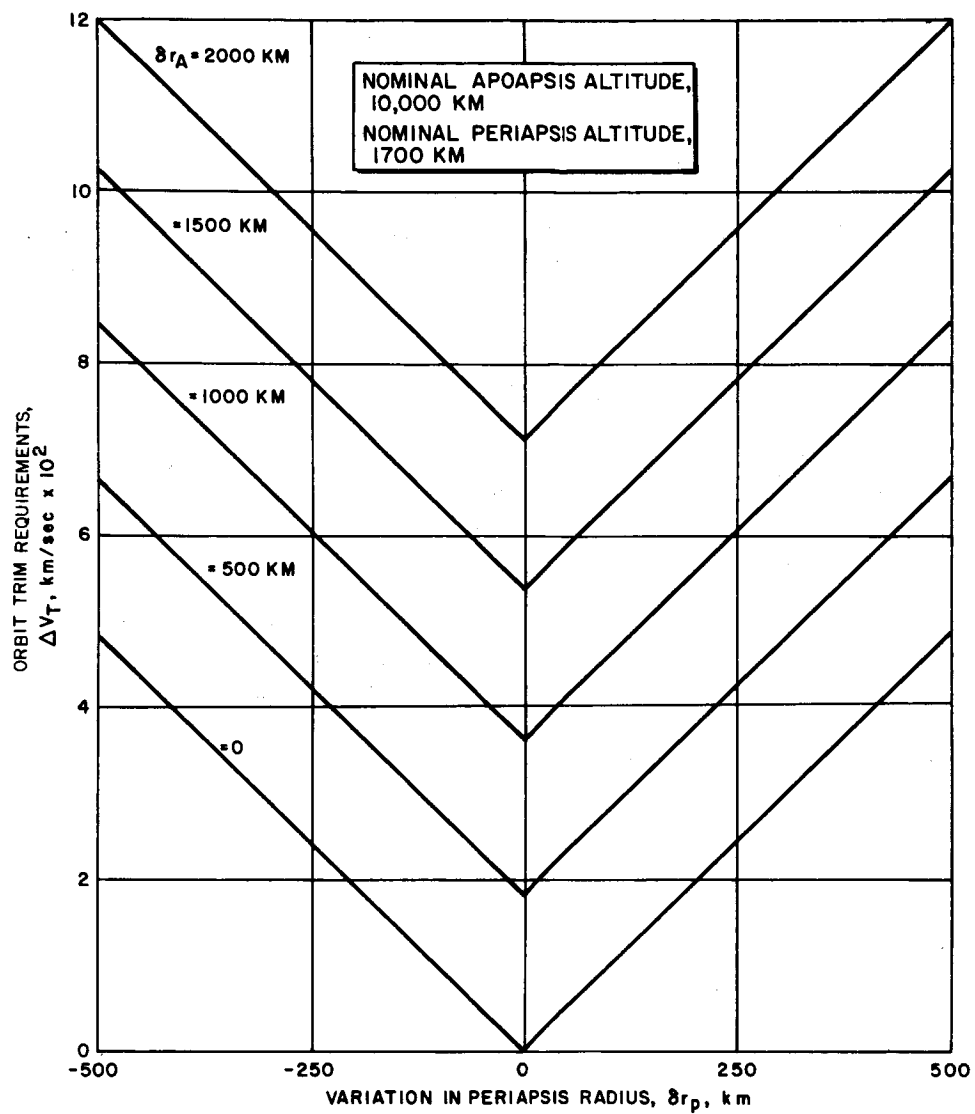
Figure C1 VARIATION IN ORBITAL PERIOD VERSUS CHANGE IN
PERIAPSIS VELOCITY

63-8962

-348-

63-8965

Figure C2 MARTIAN ORBITAL TRIM REQUIREMENTS VERSUS VARIATION
IN PERIAPSIS RADIANS

APPENDIX D

RELIABILITY VERSUS COST

The purpose of the following analysis is to determine the optimum level of reliability effort necessary to produce the highest expectation of fulfilling program objectives at the lowest total program cost. Briefly, the methods used are (1) to examine the relationship between reliability effort, (2) to project the effect of different levels of reliability growth on the fulfillment of program objectives, and (3) to determine the minimum cost reliability effort associated with the highest expectation of program success. Finally, the results are scrutinized for usefullness, sensitivity to assumptions, and consistency with other estimates of necessary reliability efforts.

1. <u>Reliability growth as a function of cost.</u> Reliability growth is discussed as the growth rate is affected by the relative size of the reliability effort. That is, the effect of change in the rate of reliability growth is expressed in terms of the percentage of funds allocated to the reliability effort.

It is well accepted that there is a time-phased impact of reliability effort upon program success. One can demonstrate that the earlier and larger the reliability effort, the greater the operational savings and thus lower net program costs. Let $R_o = e^{-\lambda_o \cdot t}$ be the reliability of an initial systems design. After n years this system will have a reliability of

$$R_n = e^{-\lambda_o (1 - i)^n \cdot t} \tag{D1}$$

where i is the annual fraction of failure rate removed and n is the number of years of constant reliability effort.[1]

Obviously, as the program matures (n increases) the failure rate improvement begins to compound; thus, a greater marginal return results. However, as i increases, the marginal yield of n has lesser effect. For midrange values of R, the value of i is fairly linear. As the reliability approaches 1 the value of i decreases slowly.

It is quite difficult to obtain accurate values of i and impossible to find exact values of i related to cost. Moreover, since the true costs of reliability efforts are often hidden in the design engineering costs, precise reliability costs from accounting records often are in error. Nevertheless, it is still possible

---

[1] $(1 - i)^n$ is a coefficient of λ_o, and is closely related to discount interest formulas.

to generate useful cost-improvement ratios for reliability efforts. The potential value of i which can be expected for a full-scale, dynamic reliability effort is estimated at 25 percent reduction in failure rate per year. So called full-scale reliability efforts have reliability funded in the range of 9 to 15 percent.[2] Thus, for an ambitious program a full-scale reliability effort might run 12 percent of program costs and yield a 25 percent annual failure rate reduction. While the scale is not constant, a 2 percent failure rate reduction per year for each 1 percent of program funds allocated for reliability efforts is a reasonable value and near linear for reliability efforts up to 20 percent of program costs.

Very small ($\leq$ 5 percent) or extremely large ($\geq$ 25 percent) reliability programs tend to be less efficient and maximum efficiency is in the range of 9 to 15 percent.

Proceeding on the basis that a 2-percent annual failure rate reduction per 1-percent program cost is feasible, one can evaluate sequential reliability growth for reliability efforts of several sizes as presented in figure D1.

Figure D1 illustrates the compounding effect of different rates of reliability growth for the same missions and levels of reliability effort.
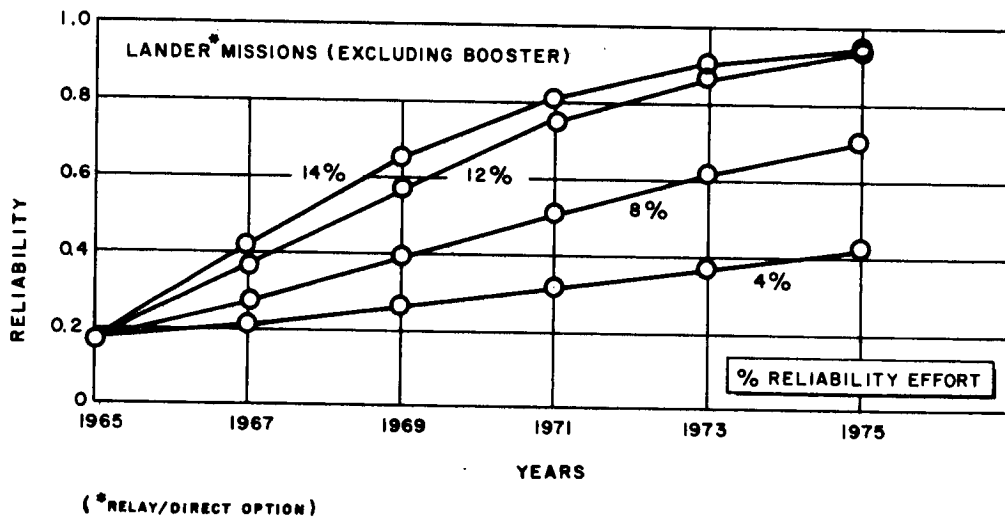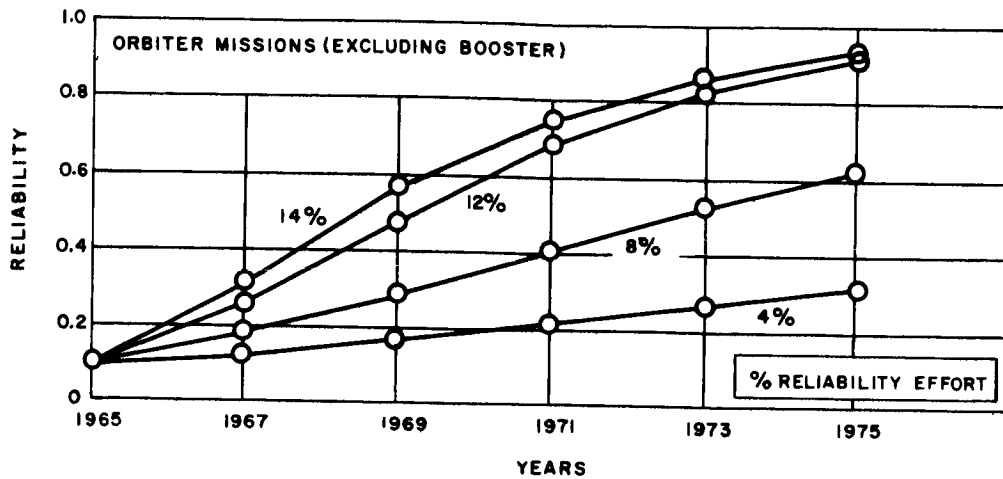
Later, these values are used to determine the optimum size of reliability effort which results in a program with lowest total program cost and highest expected probability of meeting its objectives.

2. Program expectation as a function of reliability growth. The expectation of program success for each of the reliability growth rates used above is examined next. Intuitively, the larger rates of reliability growth result in higher probabilities of success. The purpose of the following discussion is not to reinforce this point but to state the assumptions made and describe the model used to combine the reliability of various mission segments and the several missions into the program expectation.

The following assumptions were made:

    a. The relative program emphasis of Mars missions to Venus missions is 67 percent to 33 percent.

    b. The relative importance of Mars lander missions to orbiter missions is 60 percent to 40 percent.

    c. The relative importance of Venus orbiter missions to lander missions is 70 percent to 30 percent.

---

[2]Page 4, Reliability Special Report, Electronic Evaluation and Procurement, Volume 3 No. 7 (July 1963).

ORBITER MISSIONS (EXCLUDING BOOSTER)

14%
12%
8%
4%

% RELIABILITY EFFORT

RELIABILITY

YEARS

1965   1967   1969   1971   1973   1975

LANDER* MISSIONS (EXCLUDING BOOSTER)

14%
12%
8%
4%

% RELIABILITY EFFORT

RELIABILITY

YEARS

1965   1967   1969   1971   1973   1975

(*RELAY/DIRECT OPTION)

63-8893

Figure D1 RELIABILITY GROWTH FOR SEVERAL LEVELS OF RELIABILITY EFFORT

-352-

d. The fractional mission success for Mars orbiter missions is

Segment	Contribution
First 24 hours	= 0.25
1 day to 70 days	= (1-0.25) (69/180) = 0.29
71 days to 180 days	= (1-0.25) (110/180) = 0.46
Total	= 1.0

e. The fractional mission success for Mars lander missions is

Segment	Contribution
First 24 hours	= 0.75
1 day to 30 days	= 0.20
31 days to 180 days	= 0.05
Total	= 1.0

f. The fractional mission success for Venus orbiter missions is

Segment	Contribution
First 24 hours	= 0.25
1 day to 21 days	= $(1-0.25) (\frac{20}{60}) = 0.25$
22 days to 60 days	= $(1-0.25) (\frac{39}{60}) = 0.50$
Total	= 1.0

The technique to convert reliability growth to program expectation follows these steps:

1. For each growth rate, the expected success for each mission is calculated as the sum of the product of each mission segment contribution times the mission segment reliability (as determined from a mission reliability profile associated with that growth rate), summed over all mission segments.

2. Again for each growth rate, the expected fraction of a mission success for each mission type is weighted and summed over the program years in partial fulfillment of program objectives to give the expected total number of each type mission successes in the program.

3.   The expected total number of normalized mission successes for the program is the values in step 2 summed over all mission types in accordance with the assumed relative mission emphases, for each growth rate.

4.   The number of normalized program launches (trials) by mission types are summed over all missions in accordance with the assumed relative mission emphases.

5.   Then for each reliability growth rate, the ratio of step 3 to step 4 (normalized number of expected successes to normalized number of trials) gives a point estimate of the stochastic probability of fulfilling program objectives with that growth rate.

6.   The expectation of fulfilling program objectives is obtained as a binomial probability using as entering arguments - a normalized value for the assigned program launch configuration as the number of trials, a normalized value for the program objective (as the number of success required), and the stochastic normalized mission probability obtained in step 5 (above) as the outcome for each trial.

The mathematical models related to each step are as follows:

Step 1. $E_{ijkl.} = \sum_n (R_j') \cdot (R_{ijklm}) \cdot (P_m)$

Step 2. $E_{i.kl.} = \sum_j (E_{ijkl.})$

Step 3. $E_{i....} = \sum_k \sum_l (E_{i.kl.}) \cdot (P_k)(P_l)$

Step 4. $L.. = \sum_k \sum_l (L_{kl}) \cdot (P_k)(P_l)$

Step 5. $P'\{L..\}_i = \dfrac{E_{i....}}{L..}$

Step 6. $E\{0..\}_i = \sum_{0..}^{L..} \dfrac{(L..)!}{(0..)!\,(L..-0..)!} (P')^{L..} \cdot (1-P')^{L..-0..}$

where:

E   = expectation

R'   = booster reliability

R   = reliability of spacecraft type

0   = program objectives or success requirement

P   = fractional emphasis (weighting factor)

P'   = stochastic probability

L   = number of trials (launch attempts)

i   = reliability growth rate

j   = year of mission

k   = planet (Mars or Venus)

l   = spacecraft type (orbiter or lander)

m   = mission segments

The values obtained in carrying out steps 1 through 6 are shown in tables D1, D2, and D3, namely, expected number of mission successes, stochastic probabilities of program success, and binomial probabilities of fulfilling program objectives. When the values from table D3 are illustrated graphically, as in figure D1, it is apparent that reliability efforts in excess of 15 percent have diminishing returns and those below 5 percent are of dubious merit.

3.   Total program cost as a function of reliability effort.   The optimization of total program cost as a function of cost of the reliability efforts will be examined next.   The optimum level of reliability effort necessary to produce the highest expectation of fulfilling program objectives at the lowest total program cost will be determined.   In order to do this, the notion of equivalent operational costs (or the cost of equivalent operational success) is introduced.

Simply stated, equivalent operational costs are the cost of enough launch attempts to yield an equivalent of the required number of successes for efforts with different expectations.   For each level of reliability effort, the cost of equivalent operational success is the cost of the operational phase of the program divided by the program expectation.

TABLE D1

EXPECTED NUMBER OF MISSION SUCCESSES FOR SEVERAL RELIABILITY GROWTH RATES

Case	Planet	Orbiters	Landers
I 4-percent effort (i=0.07)	Mars Venus	1.35 1.66	3.22 1.70
II 8-percent effort (i=0.15)	Mars Venus	2.00 2.45	5.00 2.63
III 12-percent effort (i=0.25)	Mars Venus	2.83 3.47	6.79 3.58
IV 14-percent effort (i=0.30)	Mars Venus	3.01 3.69	7.17 3.78
Program trials	Mars Venus	6 6	12 6
Program success objectives	Mars Venus	2 2	5 2

TABLE D2

STOCHASTIC PROBABILITIES OF PROGRAM SUCCESS
FOR SEVERAL RELIABILITY GROWTH RATES

Case	Mars		Venus		Combined and Normalized Missions (P')
	Orbiter	Lander	Orbiter	Lander	
I 4-percent effort	0.225	0.268	0.277	0.284	0.264
II 8-percent effort	0.333	0.417	0.409	0.438	0.400
III 12-percent effort	0.472	0.566	0.580	0.596	0.557
IV 14-percent effort	0.502	0.597	0.615	0.630	0.588

Normalized Program Objective, $(O..)$

$$0.66 \; [2(0.4) + 5(0.6)] \; + 0.33 \; [2(0.7) + 2(0.3)] \; = 3.20$$

Normalized Program Launches, $(L..)$

$$0.66 \; [6(0.4) + 12(0.6)] \; + 0.33 \; [6(0.7) + 2(0.3)] \; = 8.4$$

TABLE D3

BINOMIAL PROBABILITIES OF FULFILLING PROGRAM OBJECTIVES
FOR SEVERAL GROWTH RATES

Case	Reliability Funds/Program Funds	Reliability Growth Rate	Program Expectation
I	4 percent	7 percent	0.39
II	8 percent	15 percent	0.662
III	12 percent	25 percent	0.900
IV	14 percent	30 percent	0.924

Estimates of program cost which were used for the purpose of reliability-versus-cost analysis do not represent actual cost estimates of the Voyager program. Since these estimates may be in error, a range of costs (minimum, probable, and maximum) were evaluated to test the sensitivity of the results to changes in cost. The results were found not sensitive to cost estimate changes so that final results are shown only for the probable costs. For each level of reliability effort, the sum of the scaled development cost and the cost of equivalent operational success is the equivalent total program cost. The program with the lowest equivalent total program cost would have the optimum size reliability effort. These results are presented in figure D2 to facilitate the determination of the optimum size reliability effort. The equivalent program cost for a 25-percent reliability effort was determined from scaled development and operational costs only, since there is virtual certainty that program objectives will be met (refer to figure D3).

In figure D2, note that the equivalent total program cost decreases rapidly as the reliability effort increases toward 10 percent. The cost continues to decline, but quite slowly, up to 14 percent effort, then gradually increases. Since there is virtually the same expected sucess from 11 percent effort and up, there is little yield by increasing the reliability effort. The optimum effort is then approximately 11 to 12 percent.

The relevant cost of the optimum reliability effort is 11 percent of the scaled development and operational costs less booster and launch site costs, or 0.11 $0.5 + 0.5 - 0.5 (1 - 0.6)$]. This figure includes the total cost of all reliability efforts of the system contractor, the subcontractors, and vendors.

As a final check for the sensitivity and reasonableness of results, we can evaluate the magnitude of change of the reliability task as the amount of funding for its changes. In figure D4, the ratio of effort spent on all other activities is compared to the effort spent on reliability activities. For reliability efforts of 5 percent and less, the task of covering other program dollars becomes so diluted that the reliability effectiveness becomes feeble. At the other extreme, reliability efforts of 20 percent and more, so much reliability money has been allocated that other efforts are dominated (ratio of $\leq 4:1$), and the funds are nonproductive. At 12 percent reliability effort, the span of coverage is 7:1, or about enough to provide adequate coverage over the areas of reliability concern.

4. Conclusion. An optimum reliability effort for the Voyager program is 11 to 12 percent of program funds for the system contractor, subcontractors, and vendors. Furthermore, these results are considered to be reasonable, valid, and not extremely sensitive to the assumptions made nor to the program cost estimates.
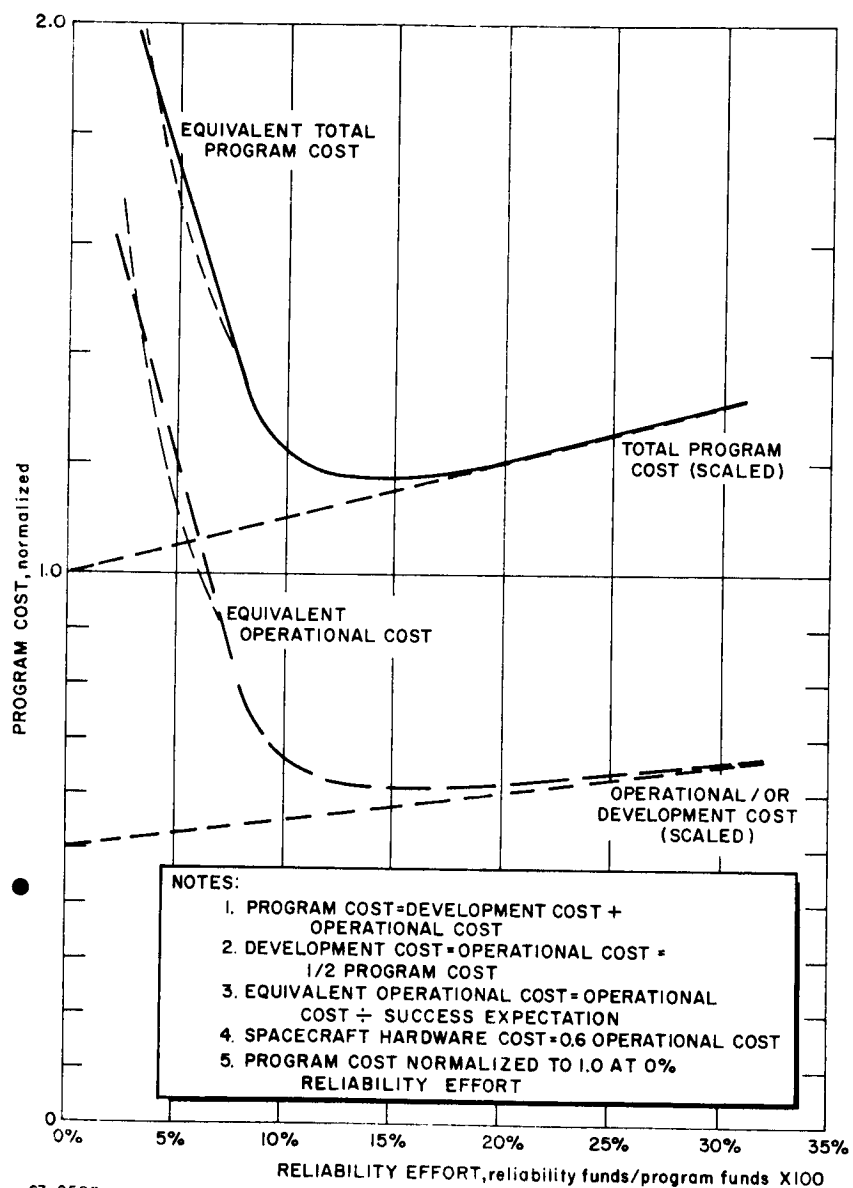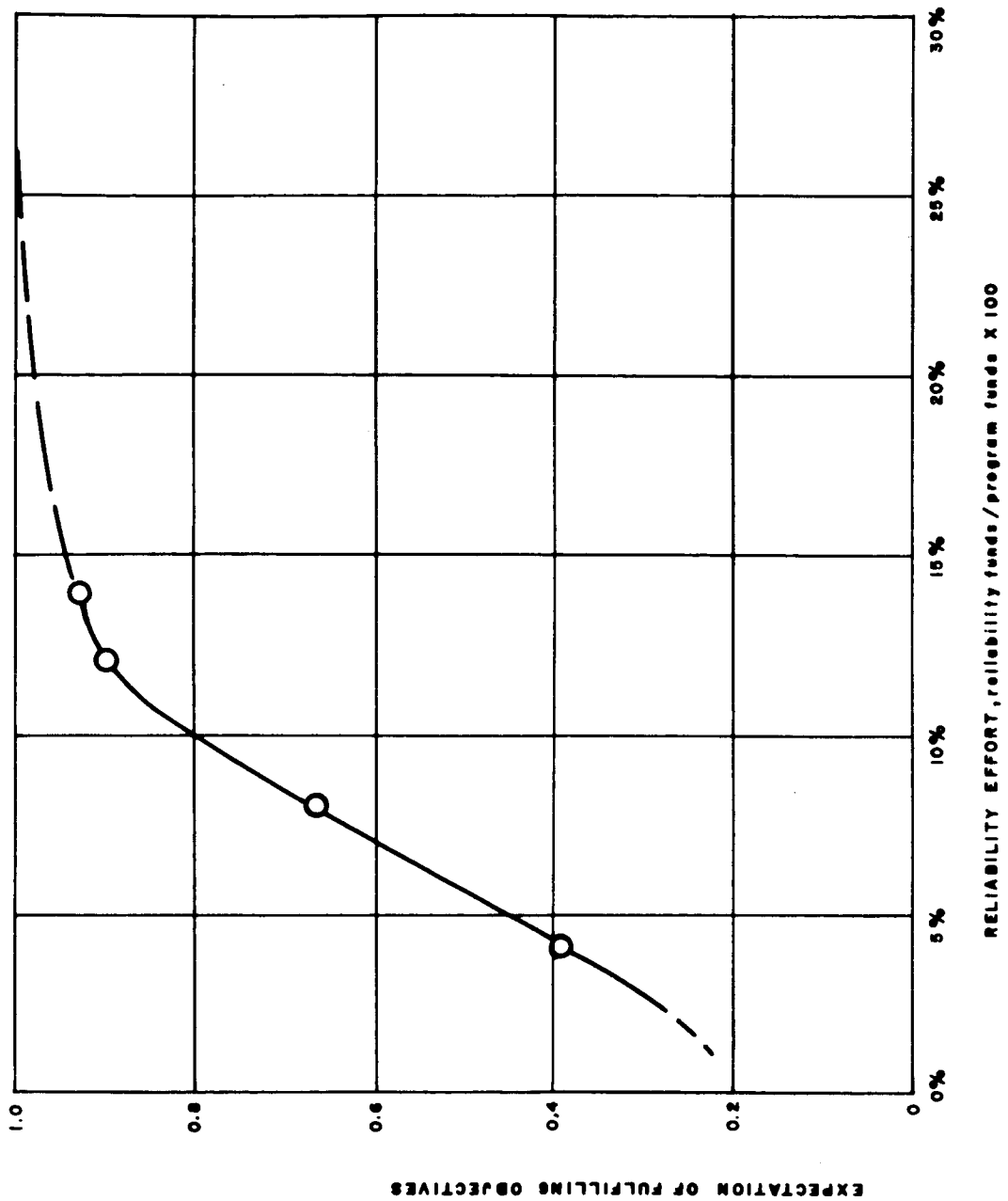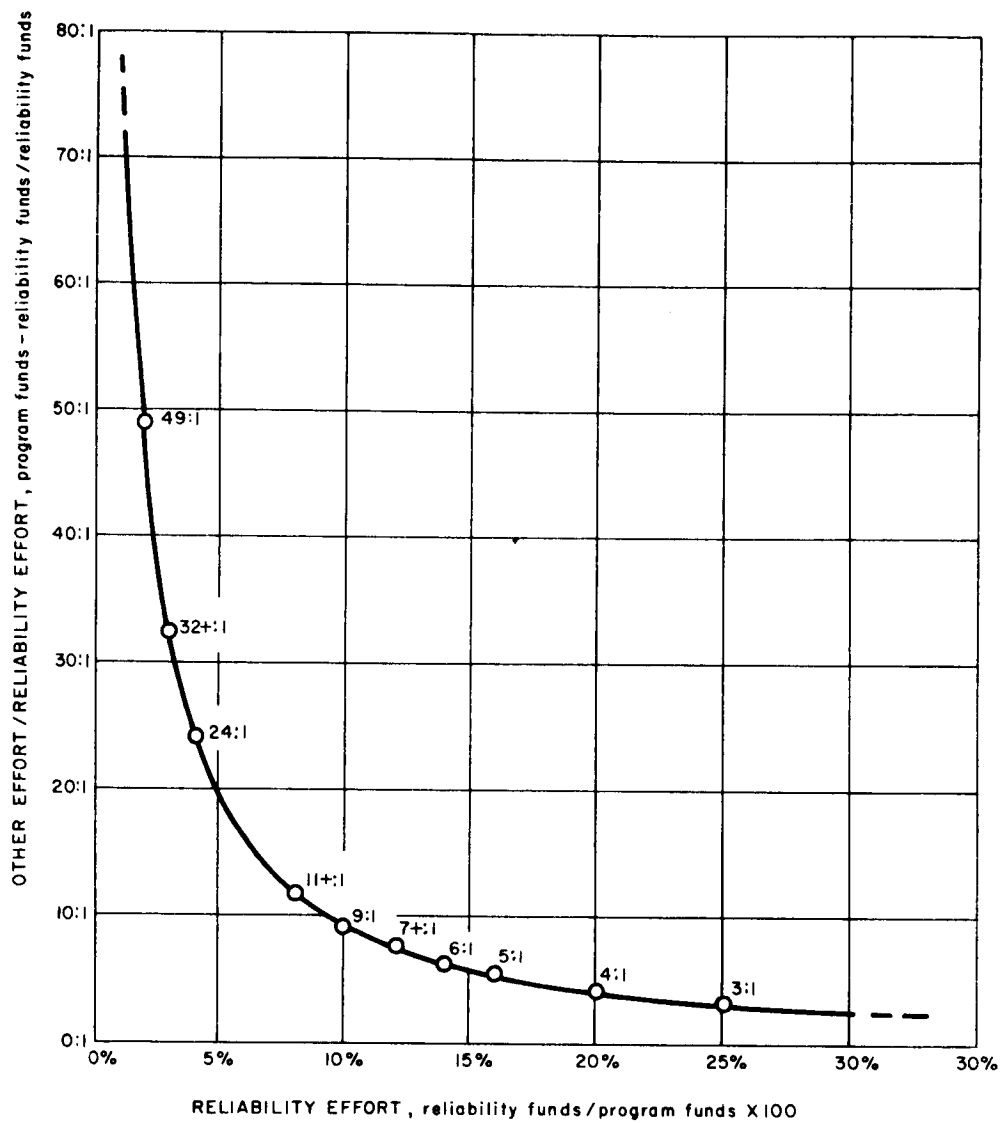
Figure D2 PROGRAM COST VERSUS RELIABILITY EFFORT

63-9582

-360-

Figure D3 EXPECTATION OF FULFILLING PROGRAM OBJECTIVES FOR
SEVERAL LEVELS OF RELIABILITY EFFORT

Figure D4 RELIABILITY EFFORT TO OTHER EFFORT FOR VARYING LEVELS
OF RELIABILITY EFFORT

63-8894

APPENDIX E

ERROR ANALYSIS

The errors in impact accuracy for a lander separated from the orbiter-spacecraft during planetary approach were evaluated using a digital computer simulation. A description of the sequence of events and computational procedure follows:

1. The spaceship approaches the planet (figure E1) on a hyperbolic trajectory. Range from the planet and velocity magnitude and direction with respect to the planet are known.

2. At a programmed range from the planet the lander is gently ejected from the spaceship. This range, R_O, is known along with the spaceship's velocity magnitude, V_{OB}, and flight path angle γ_{OB} relative to the planet. Uncertainties in the quantities R_O, V_{OL}, and γ_{OB}, also are known.

3. A velocity increment, v_{OL}, is applied to the lander (figure E2) at an angle θ_{OL} sufficient to place the lander on a planetary impact trajectory. v_{OL}, θ_{OL} relative to the spaceship velocity vector, and their associated uncertainties Δv_{OL} and $\Delta\theta_{OL}$ are known values.

4. The flight path angle, γ_{EL}, at the reference range, R_E, and a range angle, ϕ_L, at this same range are computed. At this point, partial derivatives of the quantities γ_{EL} and ϕ_L are taken with respect to the various initial conditions: R_O, V_{OB}, γ_{OB}, v_{OL}, θ_{OL}. The partials are then the influence coefficients relating the variation in the two angles (lander entry angle, γ_{EL} and the central angle, ϕ_L subtended at the planet by the portion of the lander trajectory from separation to entry - see figure E3 with variation in the basic quantities.

5. The virtual periapsis of the lander, R_{PL}, is computed. Partial derivatives are taken with respect to the initial conditions. These partials are the influence coefficients relating a change in virtual periapsis with a change in the basic quantities.

6. The uncertainties in γ_{EL}, ϕ_L, and R_{PL} are then computed as root-sum-square values,
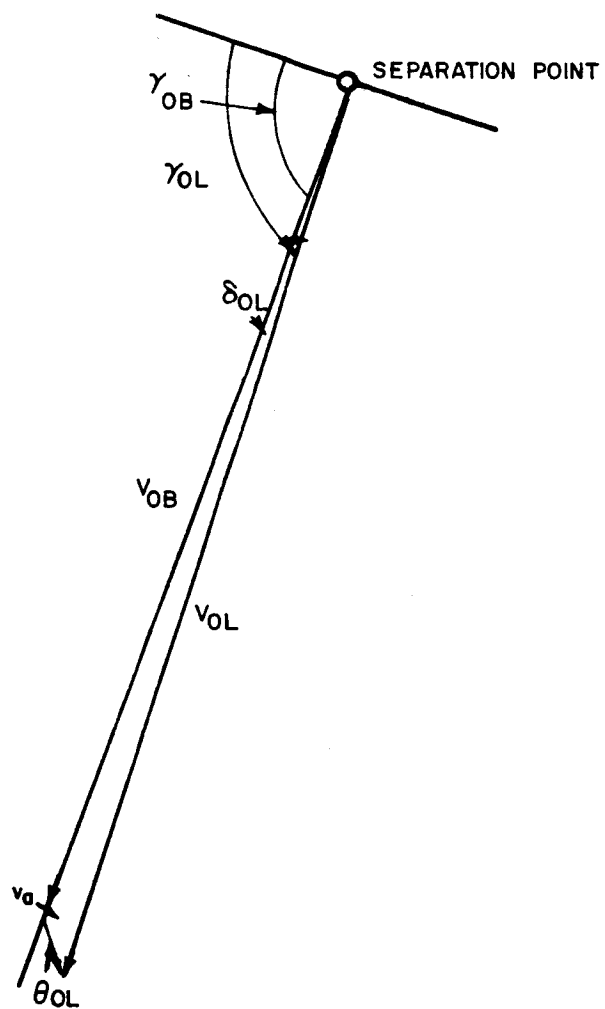
$$\text{RSS} (\Delta\gamma_{EL}) = \left[\sum_{i=1}^{5} \frac{\partial\gamma_{EL}}{\partial x_i} \Delta x_i \right]^{1/2} \text{, etc.} \tag{E1}$$

where the individual uncertainties, ΔR_O, ΔV_{OB}, $\Delta\gamma_{OB}$, Δv_{OL}, $\Delta\theta_{OL}$, are based on one-sigma values.
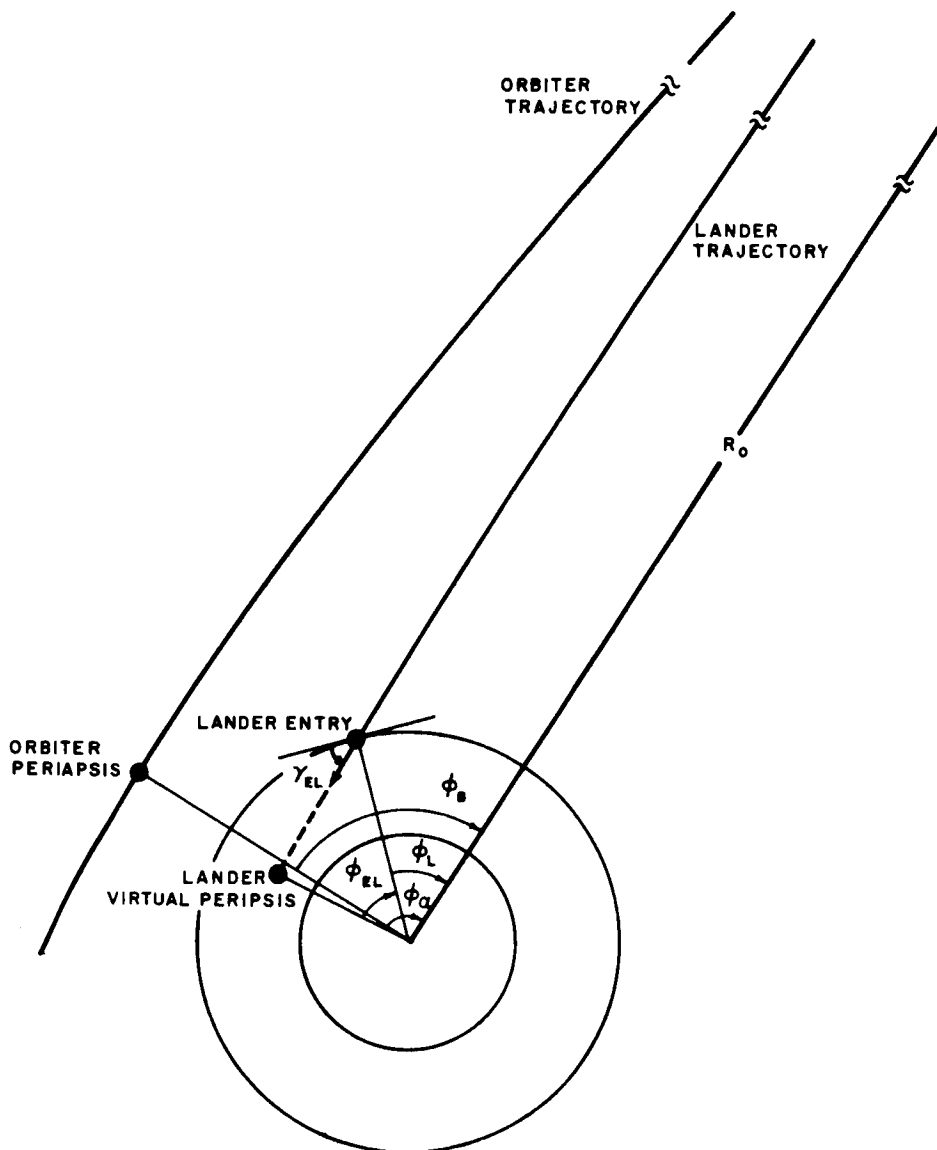
-363-
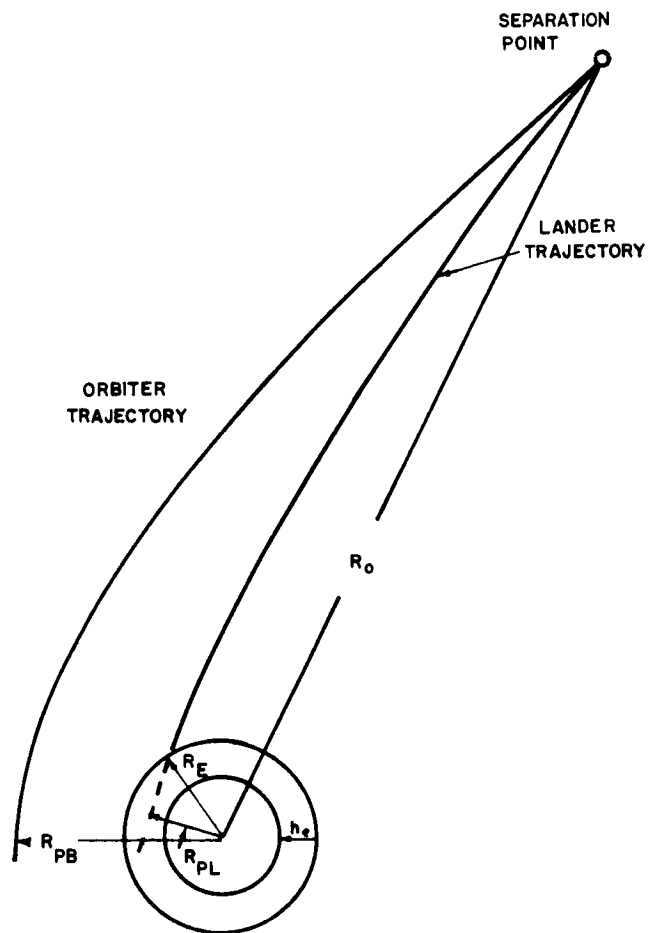
Figure E1 GEOMETRY

63-9751

- 364 -

63-9752

Figure E2 GEOMETRY AT SEPARATION

Figure E3 CENTRAL ANGLES

GLOSSARY OF SYMBOLS

a   semimajor axis of hyperbola

e   eccentricity of hyperbolic trajectory

h   altitude above the planet

R   radial distance from planet center

V   velocity of vehicle relative to target planet

v   velocity increment applied to lander

γ flight path angle; angle between velocity vector of the vehicle and local horizontal

δ difference between flight path angles of orbiter and lander at same range

Δ uncertainty

θ application angle of velocity increment, v, relative to spaceship velocity vector

ϕ central angle subtended by that portion of the trajectory from separation to entry (lander) or periapsis (orbiter)

μ planetary gravitational constant

Subscripts

first letter (point on trajectory):

    E   entry; reference range usually approximating the top of the sensible atmosphere

    O   separation range

    P   periapsis range

second letter (vehicle):

    B   orbiter

    L   lander

EQUATIONS

Equations programed are starred. Quantities printed out are double starred. Ranges and altitudes are given in feet. Velocity magnitudes are in feet per second. Angles are in radians.

  a. Orbiter (BUS) parameters at the time of lander launch. These quantities would be known approximately in actual flight.

* * $R_O = h_O + r$

* * $V_{OB} = \left[V_{\infty B}^2 + \dfrac{2\mu}{R_O} \right]^{1/2}$

* $R_{PB} = h_P + r$

* $V_{PB} = \left[V_{\infty B}^2 + \dfrac{2\mu}{R_{PB}} \right]^{1/2}$

* $\gamma_{OB} = \cos^{-1} \left[\dfrac{V_{PB}\, R_{PB}}{V_{OB}\, R_O} \right]$

  b. Orbiter parameters at planetary periapsis passage are:

$$R_{PB} = - \frac{\mu + \left[\mu^2 + (V_{\infty B}\, R_O\, V_{OB}\, \cos \gamma_{OB})^2 \right]^{1/2}}{V_{\infty B}^2}$$

$$\Delta R_{PB} = \frac{\partial R_{PB}}{\partial R_O}\, \Delta R_O + \frac{\partial R_{PB}}{\partial V_{OB}}\, \Delta V_{OB} + \frac{\partial R_{PB}}{\partial \gamma_{OB}}\, \Delta \gamma_{OB}$$

* * $\dfrac{\partial R_{PB}}{\partial R_O} = \dfrac{\partial R_{PB}}{\partial V_{\infty B}}\, \dfrac{\partial V_{\infty B}}{\partial R_O} + \left(\dfrac{\partial R_{PB}}{\partial R_O} \right)_1$

$$ ** \quad \frac{\partial R_{PB}}{\partial V_{OB}} = \frac{\partial R_{PB}}{\partial V_{\infty B}} \frac{\partial V_{\infty B}}{\partial V_{OB}} + \left(\frac{\partial R_{PB}}{\partial V_{OB}} \right)_1 $$

$$ ** \quad \frac{\partial R_{PB}}{\partial \gamma_{OB}} = \left(\frac{\partial R_{PB}}{\partial \gamma_{OB}} \right)_1 $$

$$ * \quad \frac{\partial V_{\infty B}}{\partial R_O} = \frac{\mu}{R_O^2 V_{\infty B}} $$

$$ * \quad \frac{\partial V_{\infty B}}{\partial V_{OB}} = \frac{V_{OB}}{V_{\infty B}} $$

$$ * \quad \left(\frac{\partial R_{PB}}{\partial R_O} \right)_1 = \frac{(R_O V_{OB} \cos \gamma_{OB})^2}{R_O \sqrt{\mu^2 + (V_{\infty B} R_O V_{OB} \cos \gamma_{OB})^2}} $$

$$ * \quad \left(\frac{\partial R_{PB}}{\partial V_{OB}} \right)_1 = \frac{(R_O V_{OB} \cos \gamma_{OB})^2}{V_{OB} \sqrt{\mu^2 + (V_{\infty B} R_O V_{OB} \cos \gamma_{OB})^2}} $$

$$ * \quad \left(\frac{\partial R_{PB}}{\partial \gamma_{OB}} \right)_1 = \frac{- (R_O V_{OB} \cos \gamma_{OB})^2 \sin \gamma_{OB}}{\cos \gamma_{OB} \sqrt{\mu^2 + (V_{\infty B} R_O V_{OB} \cos \gamma_{OB})^2}} $$

$$ * \quad \frac{\partial R_{PB}}{\partial V_{\infty B}} = \frac{(R_O V_{OB} \cos \gamma_{OB})^2}{V_{\infty B} \sqrt{\mu^2 + (V_{\infty B} R_O V_{OB} \cos \gamma_{OB})^2}} + \frac{2\mu - 2\sqrt{\mu^2 + (V_{\infty B} R_O V_{OB} \cos \gamma_{OB})^2}}{V_{\infty B}^3} $$

The uncertainty in the periapsis of the orbiter for its unperturbed path is:

$$\Delta R_{PB} = \left[\left(\frac{\partial R_{PB}}{\partial R_O} \Delta R_O \right)^2 + \left(\frac{\partial R_{PB}}{\partial V_{OB}} \Delta V_{OB} \right)^2 + \left(\frac{\partial R_{PB}}{\partial \gamma_{OB}} \Delta \gamma_{OB} \right)^2 \right]^{1/2}$$

where the individual uncertainties (ΔR_O, etc.) are one sigma values.

c. Lander parameters at separation. See figure E2

$$* V_{OL} = (V_{OB}^2 + v_{OL}^2 + 2 V_{OB} v_{OL} \cos \theta_{OL})^{1/2}$$

$$* \gamma_{OL} = \gamma_{OB} + \delta_{OL}$$

$$* \delta_{OL} = \sin \left(\frac{v_{OL} \sin \theta_{OL}}{V_{OL}} \right)$$

$$\Delta V_{OL} = \frac{\partial V_{OL}}{\partial R_O} \Delta R_O + \frac{\partial V_{OL}}{\partial V_{OB}} \Delta V_{OB} + \frac{\partial V_{OL}}{\partial \gamma_{OB}} \Delta \gamma_{OB} + \frac{\partial V_{OL}}{\partial v_{OL}} \Delta v_{OL} + \frac{\partial V_{OL}}{\partial \theta_{OL}} \Delta \theta_{OL}$$

$$* \frac{\partial V_{OL}}{\partial R_O} = \frac{\partial V_{OL}}{\partial V_{OB}} \frac{\partial V_{OB}}{\partial R_O} + \frac{\partial V_{OL}}{\partial \theta_{OL}} \frac{\partial \theta_{OL}}{\partial \gamma_{OB}} \frac{\partial \gamma_{OB}}{\partial R_O}$$

$$* \frac{\partial V_{OL}}{\partial V_{OB}} = \left(\frac{\partial V_{OL}}{\partial V_{OB}} \right)_1$$

$$* \left(\frac{\partial V_{OL}}{\partial \gamma_{OB}} \right) = \frac{\partial V_{OL}}{\partial \theta_{OL}} \frac{\partial \theta_{OL}}{\partial \gamma_{OB}}$$

$$* \left(\frac{\partial V_{OL}}{\partial V_{OB}} \right)_1 = \frac{V_{OB} + v_{OL} \cos \theta_{OL}}{V_{OL}}$$

-370-

$$\frac{\partial V_{OL}}{\partial v_{OL}} = \frac{v_{OL} + V_{OB} \cos \theta_{OL}}{V_{OL}}$$

$$* \quad \frac{\partial V_{OL}}{\partial \theta_{OL}} = - \frac{V_{OB} \, v_{OL} \sin \theta_{OL}}{V_{OL}}$$

$$* \quad \frac{\partial \theta_{OL}}{\partial \gamma_{OB}} = - 1$$

$$\Delta \delta_{OL} = \frac{\partial \delta_{OL}}{\partial R_O} \Delta R_O + \frac{\partial \delta_{OL}}{\partial V_{OB}} \Delta V_{OB} + \frac{\partial \delta_{OL}}{\partial \gamma_{OB}} \Delta \gamma_{OB} + \frac{\partial \delta_{OL}}{\partial v_{OL}} \Delta v_{OL} + \frac{\partial \delta_{OL}}{\partial \theta_{OL}} \Delta \theta_{OL}$$

$$* \quad \frac{\partial \delta_{OL}}{\partial R_O} = \frac{\partial \delta_{OL}}{\partial V_{OL}} \frac{\partial V_{OL}}{\partial R_O} + \frac{\partial \delta_{OL}}{\partial \theta_{OL}} \frac{\partial \theta_{OL}}{\partial \gamma_{OB}} \frac{\partial \gamma_{OB}}{\partial R_O}$$

$$* \quad \frac{\partial \delta_{OL}}{\partial V_{OB}} = \frac{\partial \delta_{OL}}{\partial V_{OL}} \frac{\partial V_{OL}}{\partial V_{OB}}$$

$$* \quad \frac{\partial \delta_{OL}}{\partial \gamma_{OB}} = \frac{\partial \delta_{OL}}{\partial V_{OL}} \frac{\partial V_{OL}}{\partial \gamma_{OB}} + \frac{\partial \delta_{OL}}{\partial \theta_{OL}} \frac{\partial \theta_{OL}}{\partial \gamma_{OB}}$$

$$* \quad \frac{\partial \delta_{OL}}{\partial v_{OL}} = \frac{\partial \delta_{OL}}{\partial V_{OL}} \frac{\partial V_{OL}}{\partial v_{OL}} + \left(\frac{\partial \delta_{OL}}{\partial v_{OL}} \right)_1$$

$$* \quad \frac{\partial \delta_{OL}}{\partial \theta_{OL}} = \frac{\partial \delta_{OL}}{\partial V_{OL}} \frac{\partial V_{OL}}{\partial \theta_{OL}} + \left(\frac{\partial \delta_{OL}}{\partial \theta_{OL}} \right)_1$$

$$* \quad N = \frac{v_{OL} \sin \theta_{OL}}{V_{OL}}$$

-371-

* $\left(\dfrac{\partial \delta_{OL}}{\partial v_{OL}}\right)_1 = \dfrac{N}{v_{OL}\,(1-N^2)^{1/2}}$

* $\left(\dfrac{\partial \delta_{OL}}{\partial \theta_{OL}}\right)_1 = \dfrac{v_{OL}\,\cos\theta_{OL}}{V_{OL}\,(1-N^2)^{1/2}}$

* $\dfrac{\partial \delta_{OL}}{\partial V_{OL}} = \dfrac{-N}{V_{OL}\,(1-N^2)^{1/2}}$

d.   Virtual periapsis of lander

** $V_{\infty L} = \left(v_{OL}^2 - \dfrac{2\mu}{R_O}\right)^{1/2}$

$= \left(V_{PL}^2 - \dfrac{2\mu}{R_{PL}}\right)^{1/2}$

$R_{PL}\,V_{PL} = R_O\,V_{OL}\,\cos\gamma_{OL}$

* $R_{PL} = \dfrac{-\mu + [\mu^2 + (V_{\infty L}\,R_O\,V_{OL}\,\cos\gamma_{OS})^2]^{1/2}}{V_{\infty L}^2}$

* $R_E = h_E + r$

e.   Lander parameters at reference range R_E

* $V_{EL} = \left(V_{\infty L}^2 + \dfrac{2\mu}{R_E}\right)^{1/2}$

$V_{\infty L} = \left(v_{OL}^2 - \dfrac{2\mu}{R_O}\right)^{1/2}$

$$\Delta V_{\infty L} = \frac{\partial V_{\infty L}}{\partial R_O} \; \Delta R_O + \frac{\partial V_{\infty L}}{\partial V_{OB}} \; \Delta V_{OB} + \frac{\partial V_{\infty L}}{\partial \gamma_{OB}} \; \Delta \gamma_{OB} + \frac{\partial V_{\infty L}}{\partial v_{OL}} \; \Delta v_{OL} + \frac{\partial V_{\infty L}}{\partial \theta_{OL}} \; \Delta \theta_{OL}$$

* $$\frac{\partial V_{\infty L}}{\partial R_O} = \frac{\partial V_{\infty L}}{\partial V_{OL}} \; \frac{\partial V_{OL}}{\partial R_O} + \left(\frac{\partial V_{\infty L}}{\partial R_O} \right)_1$$

* $$\frac{\partial V_{\infty L}}{\partial V_{OB}} = \frac{\partial V_{\infty L}}{\partial V_{OL}} \; \frac{\partial V_{OL}}{\partial V_{OB}}$$

* $$\frac{\partial V_{\infty L}}{\partial \gamma_{OB}} = \frac{\partial V_{\infty L}}{\partial V_{OL}} \; \frac{\partial V_{OL}}{\partial \gamma_{OB}}$$

* $$\frac{\partial V_{\infty L}}{\partial v_{OL}} = \frac{\partial V_{\infty L}}{\partial V_{OL}} \; \frac{\partial V_{OL}}{\partial v_{OL}}$$

* $$\frac{\partial V_{\infty L}}{\partial \theta_{OL}} = \frac{\partial V_{\infty L}}{\partial V_{OL}} \; \frac{\partial V_{OL}}{\partial \theta_{OL}}$$

* $$\left(\frac{\partial V_{\infty L}}{\partial R_O} \right)_1 = \frac{\mu}{R_O^2} \left(V_{OL}^2 - \frac{2\mu}{R_O} \right)^{-1/2}$$

* $$\frac{\partial V_{\infty L}}{\partial V_{OL}} = V_{OL} \left(V_{OL}^2 - \frac{2\mu}{R_O} \right)^{-1/2}$$

$$\Delta V_{EL} = \frac{\partial V_{EL}}{\partial R_O} \; \Delta R_O + \frac{\partial V_{EL}}{\partial V_{OB}} \; \Delta V_{OB} + \frac{\partial V_{EL}}{\partial \gamma_{OB}} \; \Delta \gamma_{OB} + \frac{\partial V_{EL}}{\partial v_{OL}} \; \Delta v_{OL} + \frac{\partial V_{EL}}{\partial \theta_{OL}} \; \Delta \theta_{OL}$$

* $\dfrac{\partial V_{EL}}{\partial R_O} = \dfrac{\partial V_{EL}}{\partial V_{\infty L}} \quad \dfrac{\partial V_{\infty L}}{\partial R_O}$

* $\dfrac{\partial V_{EL}}{\partial V_{OB}} = \dfrac{\partial V_{EL}}{\partial V_{\infty L}} \quad \dfrac{\partial V_{\infty L}}{\partial V_{OB}}$

* $\dfrac{\partial V_{EL}}{\partial \gamma_{OB}} = \dfrac{\partial V_{EL}}{\partial V_{\infty L}} \quad \dfrac{\partial V_{\infty L}}{\partial \gamma_{OB}}$

* $\dfrac{\partial V_{EL}}{\partial v_{OL}} \approx \dfrac{\partial V_{EL}}{\partial V_{\infty L}}$

* $\dfrac{\partial V_{EL}}{\partial \theta_{OL}} \approx \dfrac{\partial V_{EL}}{\partial V_{\infty L}} \quad \dfrac{\partial V_{\infty L}}{\partial \theta_{OL}}$

* $\dfrac{\partial V_{EL}}{\partial V_{\infty L}} = V_{\infty L} \left(V_{\infty L}^2 + \dfrac{2\mu}{R_E} \right)^{-1/2}$

** $\gamma_{EL} = \cos^{-1} \left(\dfrac{R_O \; V_{OL} \cos \gamma_{OL}}{R_E \; V_{EL}} \right)$

$\gamma_{OL} = \gamma_{OB} + \delta_{OL}$

$\Delta \gamma_{EL} = \dfrac{\partial \gamma_{EL}}{\partial R_O} \Delta R_O + \dfrac{\partial \gamma_{EL}}{\partial V_{OB}} \Delta V_{OB} + \dfrac{\partial \gamma_{EL}}{\partial \gamma_{OB}} \Delta \gamma_{OB} + \dfrac{\partial \gamma_{EL}}{\partial v_{OL}} \Delta v_{OL} + \dfrac{\partial \gamma_{EL}}{\partial \theta_{OL}} \Delta \theta_{OL}$

-374-

$$** \quad \frac{\partial \gamma_{EL}}{\partial R_O} = \frac{\partial \gamma_{EL}}{\partial \gamma_{OL}} \frac{\partial \gamma_{OL}}{\partial \delta_{OL}} \frac{\partial \delta_{OL}}{\partial R_O} + \frac{\partial \gamma_{EL}}{\partial V_{OL}} \frac{\partial V_{OL}}{\partial R_O} + \frac{\partial \gamma_{EL}}{\partial V_{EL}} \frac{\partial V_{EL}}{\partial R_O} + \left(\frac{\partial \gamma_{EL}}{\partial R_O} \right)_1$$

$$** \quad \frac{\partial \gamma_{EL}}{\partial V_{OB}} = \frac{\partial \gamma_{EL}}{\partial \gamma_{OL}} \frac{\partial \gamma_{OL}}{\partial \delta_{OL}} \frac{\partial \delta_{OL}}{\partial V_{OB}} + \frac{\partial \gamma_{EL}}{\partial V_{OL}} \frac{\partial V_{OL}}{\partial V_{OB}} + \frac{\partial \gamma_{EL}}{\partial V_{EL}} \frac{\partial V_{EL}}{\partial V_{OB}}$$

$$** \quad \frac{\partial \gamma_{EL}}{\partial \gamma_{OB}} = \frac{\partial \gamma_{EL}}{\partial \gamma_{OL}} \frac{\partial \gamma_{OL}}{\partial \delta_{OL}} \frac{\partial \delta_{OL}}{\partial \gamma_{OB}} + \frac{\partial \gamma_{EL}}{\partial V_{OL}} \frac{\partial V_{OL}}{\partial \gamma_{OB}} + \frac{\partial \gamma_{EL}}{\partial V_{EL}} \frac{\partial V_{EL}}{\partial \gamma_{OB}} + \frac{\partial \gamma_{EL}}{\partial \gamma_{OL}} \frac{\partial \gamma_{OL}}{\partial \gamma_{OB}}$$

$$** \quad \frac{\partial \gamma_{EL}}{\partial v_{OL}} = \frac{\partial \gamma_{EL}}{\partial \gamma_{OL}} \frac{\partial \gamma_{OL}}{\partial \delta_{OL}} \frac{\partial \delta_{OL}}{\partial v_{OL}} + \frac{\partial \gamma_{EL}}{\partial V_{OL}} \frac{\partial V_{OL}}{\partial v_{OL}} + \frac{\partial \gamma_{EL}}{\partial V_{EL}} \frac{\partial V_{EL}}{\partial v_{OL}}$$

$$** \quad \frac{\partial \gamma_{EL}}{\partial \theta_{OL}} = \frac{\partial \gamma_{EL}}{\partial \gamma_{OL}} \frac{\partial \gamma_{OL}}{\partial \delta_{OL}} \frac{\partial \delta_{OL}}{\partial \theta_{OL}} + \frac{\partial \gamma_{EL}}{\partial V_{OL}} \frac{\partial V_{OL}}{\partial \theta_{OL}} + \frac{\partial \gamma_{EL}}{\partial V_{EL}} \frac{\partial V_{EL}}{\partial \theta_{OL}}$$

$$** \quad Q = \frac{R_O V_{OL} \cos \gamma_{OL}}{R_E V_{EL}}$$

$$* \quad \frac{\partial \gamma_{EL}}{\partial \gamma_{OL}} = \frac{Q \tan \gamma_{OL}}{\sqrt{1 - Q^2}}$$

$$* \quad \frac{\partial \gamma_{EL}}{\partial R_O} = \frac{-Q}{R_O \sqrt{1 - Q^2}}$$

$$* \quad \frac{\partial \gamma_{EL}}{\partial V_{OL}} = \frac{-Q}{V_{OL} \sqrt{1 - Q^2}}$$

* $\dfrac{\partial \gamma_{EL}}{\partial v_{EL}}$ $\qquad$ $\dfrac{Q}{v_{EL} \sqrt{1 - Q^2}}$

* $\dfrac{\partial \gamma_{OL}}{\partial \gamma_{OB}}$ $= 1$

* $\dfrac{\partial \gamma_{OL}}{\partial \delta_{OL}}$ $= 1$

The uncertainty in lander atmospheric entry flight path angle is:

** $\Delta \gamma_{EL} = \left[\left(\dfrac{\partial \gamma_{EL}}{\partial R_O} \Delta R_O \right)^2 + \left(\dfrac{\partial \gamma_{EL}}{\partial V_{OB}} \Delta V_{OB} \right)^2 + \left(\dfrac{\partial \gamma_{EL}}{\partial \gamma_{OB}} \Delta \gamma_{OB} \right)^2 + \left(\dfrac{\partial \gamma_{EL}}{\partial v_{OL}} \Delta v_{OL} \right)^2 + \left(\dfrac{\partial \gamma_{EL}}{\partial \theta_{OL}} \Delta \theta_{OL} \right)^2 \right]^{1/2}$

where ΔR_O, ΔV_{OB}, etc., are input one sigma values.

f. Lander range angle as defined in figure E3

** $\phi_{OL} = \cos^{-1} \left[\dfrac{a (e^2 - 1) - R_O}{e R_O} \right]$

** $\phi_{EL} = \cos^{-1} \left[\dfrac{a (e^2 - 1) - R_E}{e R_E} \right]$

** $\phi_L = \phi_{OL} - \phi_{EL}$

where a and e are parameters of the lander hyperbola

$a = \dfrac{\mu}{v_{\infty L}^2} \qquad e = 1 + \dfrac{R_{PL}}{a}$

$\Delta \phi_L = \dfrac{\partial \phi_L}{\partial R_O} \Delta R_O + \dfrac{\partial \phi_L}{\partial V_{OB}} \Delta V_{OB} + \dfrac{\partial \phi_L}{\partial \gamma_{OB}} \Delta \gamma_{OB} + \dfrac{\partial \phi_L}{\partial v_{OL}} \Delta v_{OL} + \dfrac{\partial \phi_L}{\partial \theta_{OL}} \Delta \theta_{OL}$

$$** \quad \frac{\partial \phi_L}{\partial R_O} = \frac{\partial \phi_L}{\partial \phi_{OL}} \left[\frac{\partial \phi_{OL}}{\partial a} \frac{\partial a}{\partial R_O} + \frac{\partial \phi_{OL}}{\partial e} \frac{\partial e}{\partial R_O} + \frac{\partial \phi_{OL}}{\partial R_O} \right]$$

$$+ \frac{\partial \phi_L}{\partial \phi_{EL}} \left[\frac{\partial \phi_{EL}}{\partial a} \frac{\partial a}{\partial R_O} + \frac{\partial \phi_{EL}}{\partial e} \frac{\partial e}{\partial R_O} \right]$$

$$** \quad \frac{\partial \phi_L}{\partial V_{OB}} = \frac{\partial \phi_L}{\partial \phi_{OL}} \left[\frac{\partial \phi_{OL}}{\partial a} \frac{\partial a}{\partial V_{OB}} + \frac{\partial \phi_{OL}}{\partial e} \frac{\partial e}{\partial V_{OB}} \right]$$

$$+ \frac{\partial \phi_L}{\partial \phi_{EL}} \left[\frac{\partial \phi_{EL}}{\partial a} \frac{\partial a}{\partial V_{OB}} + \frac{\partial \phi_{EL}}{\partial e} \frac{\partial e}{\partial V_{OB}} \right]$$

$$** \quad \frac{\partial \phi_L}{\partial v_{OL}} = \frac{\partial \phi_L}{\partial \phi_{OL}} \left[\frac{\partial \phi_{OL}}{\partial a} \frac{\partial a}{\partial v_{OL}} + \frac{\partial \phi_{OL}}{\partial e} \frac{\partial e}{\partial v_{OL}} \right]$$

$$+ \frac{\partial \phi_L}{\partial \phi_{EL}} \left[\frac{\partial \phi_{EL}}{\partial a} \frac{\partial a}{\partial v_{OL}} + \frac{\partial \phi_{EL}}{\partial e} \frac{\partial e}{\partial v_{OL}} \right]$$

$$** \quad \frac{\partial \phi_L}{\partial \gamma_{OB}} = \frac{\partial \phi_L}{\partial \phi_{OL}} \left[\frac{\partial \phi_{OL}}{\partial e} \frac{\partial e}{\partial R_{PL}} \frac{\partial R_{PL}}{\partial \gamma_{OL}} \frac{\partial \gamma_{OL}}{\partial \gamma_{OB}} \right]$$

$$+ \frac{\partial \phi_L}{\partial \phi_{EL}} \left[\frac{\partial \phi_{EL}}{\partial e} \frac{\partial e}{\partial R_{PL}} \frac{\partial R_{PL}}{\partial \gamma_{OL}} \frac{\partial \gamma_{OL}}{\partial \gamma_{OB}} \right]$$

$$** \quad \frac{\partial \phi_L}{\partial \theta_{OL}} = \frac{\partial \phi_L}{\partial \phi_{OL}} \left[\frac{\partial \phi_{OL}}{\partial a} \frac{\partial a}{\partial \theta_{OL}} + \frac{\partial \phi_{OL}}{\partial e} \frac{\partial e}{\partial \theta_{OL}} \right]$$

$$+ \frac{\partial \phi_L}{\partial \phi_{EL}} \left[\frac{\partial \phi_{EL}}{\partial a} \frac{\partial a}{\partial \theta_{OL}} + \frac{\partial \phi_{EL}}{\partial e} \frac{\partial e}{\partial \theta_{OL}} \right]$$

$$* \quad \frac{\partial a}{\partial R_O} = \frac{\partial a}{\partial V_{\infty L}} \frac{\partial V_{\infty L}}{\partial R_O}$$

$$* \quad \frac{\partial e}{\partial R_O} = \frac{\partial e}{\partial a} \frac{\partial a}{\partial R_O} + \frac{\partial e}{\partial R_{PL}} \frac{\partial R_{PL}}{\partial R_O}$$

$$* \quad \frac{\partial a}{\partial V_{OB}} = \frac{\partial a}{\partial V_{\infty L}} \frac{\partial V_{\infty L}}{\partial V_{OL}} \frac{\partial V_{OL}}{\partial V_{OB}}$$

$$* \quad \frac{\partial e}{\partial V_{OB}} = \frac{\partial e}{\partial a} \frac{\partial a}{\partial V_{OB}} + \frac{\partial e}{\partial R_{PL}} \frac{\partial R_{PL}}{\partial V_{OB}}$$

$$* \quad \frac{\partial a}{\partial v_{OL}} = \frac{\partial a}{\partial V_{\infty L}} \frac{\partial V_{\infty L}}{\partial V_{OL}} \frac{\partial V_{OL}}{\partial v_{OL}}$$

$$* \quad \frac{\partial e}{\partial v_{OL}} = \frac{\partial e}{\partial a} \frac{\partial a}{\partial v_{OL}} + \frac{\partial e}{\partial R_{PL}} \frac{\partial R_{PL}}{\partial v_{OL}}$$

$$* \quad \frac{\partial a}{\partial \theta_{OL}} = \frac{\partial a}{\partial V_{\infty L}} \frac{\partial V_{\infty L}}{\partial V_{OL}} \frac{\partial V_{OL}}{\partial \theta_{OL}}$$

* $\dfrac{\partial \phi_{OL}}{\partial a} = \dfrac{1 - e^2}{e\, R_O\, \sqrt{1 - S^2}}$

* $\dfrac{\partial \phi_{OL}}{\partial e} = \dfrac{-\dfrac{a}{R_O}\,(e^2 + 1) - 1}{e^2\, \sqrt{1 - S^2}}$

*$T = \dfrac{a\,(e^2 - 1) - R_E}{e\, R_E}$

* $\dfrac{\partial \phi_{EL}}{\partial a} = \dfrac{1 - e^2}{e\, R_E\, \sqrt{1 - T^2}}$

* $\dfrac{\partial \phi_{EL}}{\partial e} = \dfrac{-\dfrac{a}{R_E}\,(e^2 + 1) - 1}{e^2\, \sqrt{1 - T^2}}$

* $\dfrac{\partial e}{\partial R_{PL}} = \dfrac{1}{a}$

* $\dfrac{\partial R_{PL}}{\partial V_{\infty L}} = \dfrac{(R_O\, V_{OL}\, \cos \gamma_{OL})^2}{V_{\infty L}\, \sqrt{\mu^2 + (V_{\infty L}\, R_O\, V_{OL}\, \cos \gamma_{OL})^2}} + \dfrac{2\mu - 2\,\sqrt{\mu^2 + (V_{\infty L}\, R_O\, V_{OL}\, \cos \gamma_{OL})^2}}{V_{\infty L}^3}$

* $\left(\dfrac{\partial R_{PL}}{\partial R_O}\right)_1 = \dfrac{(R_O\, V_{OL}\, \cos \gamma_{OL})^2}{R_O\, \sqrt{\mu^2 + (V_{\infty L}\, R_O\, V_{OL}\, \cos \gamma_{OL})^2}}$

* $\left(\dfrac{\partial R_{PL}}{\partial V_{OL}}\right)_1 = \dfrac{(R_O\, V_{OL}\, \cos \gamma_{OL})^2}{V_{OL}\, \sqrt{\mu^2 + (V_{\infty L}\, R_O\, V_{OL}\, \cos \gamma_{OL})^2}}$

$$* \quad \frac{\partial e}{\partial \theta_{OL}} = \frac{\partial e}{\partial a} \frac{\partial a}{\partial \theta_{OL}} + \frac{\partial e}{\partial R_{PL}} \frac{\partial R_{PL}}{\partial \theta_{OL}}$$

$$* \quad \frac{\partial a}{\partial V_{\infty L}} = \frac{-2\mu}{V_{\infty L}^3}$$

$$* \quad \frac{\partial e}{\partial a} = \frac{-R_{PL}}{a^2}$$

$$* \quad \frac{\partial V_{\infty L}}{\partial V_{OL}} = \frac{V_{OL}}{V_{\infty L}}$$

$$* \quad \frac{\partial V_{\infty L}}{\partial R_O} = \frac{\mu}{R_O^2 \, V_{\infty L}}$$

$$* \quad \frac{\partial \phi_L}{\partial \phi_O} = 1$$

$$* \quad \frac{\partial \phi_L}{\partial \phi_E} = -1$$

$$*S = \frac{a(e^2 - 1) - R_O}{e\, R_O}$$

$$* \quad \frac{\partial \phi_{OL}}{\partial R_O} = \left[\frac{a^2(e^2 - 1)}{R_O^2 \{(R_O + a)^2 - 2a^2(e^2 - 1)\}} \right]^{1/2}$$

-380-

$$* \quad \frac{\partial R_{PL}}{\partial \gamma_{OL}} = - \frac{(R_O V_{OL} \cos \gamma_{OL})^2 \tan \gamma_{OL}}{\sqrt{\mu^2 + (V_{\infty L} R_O V_{OL} \cos \gamma_{OL})^2}}$$

$$** \quad \frac{\partial R_{PL}}{\partial V_{OB}} = \frac{\partial R_{PL}}{\partial V_{\infty L}} \frac{\partial V_{\infty L}}{\partial V_{OL}} \frac{\partial V_{OL}}{\partial V_{OB}} + \frac{\partial R_{PL}}{\partial V_{OL}} \frac{\partial V_{OL}}{\partial V_{OB}} + \frac{\partial R_{PL}}{\partial \gamma_{OL}} \frac{\partial \gamma_{OL}}{\partial V_{OB}}$$

$$** \quad \frac{\partial R_{PL}}{\partial \gamma_{OB}} = \frac{\partial R_{PL}}{\partial \gamma_{OL}} \frac{\partial \gamma_{OL}}{\partial \gamma_{OB}}$$

$$** \quad \frac{\partial R_{PL}}{\partial R_O} = \frac{\partial R_{PL}}{\partial V_{\infty L}} \frac{\partial V_{\infty L}}{\partial R_O} + \left(\frac{\partial R_{PL}}{\partial R_O} \right)_1$$

$$** \quad \frac{\partial R_{PL}}{\partial v_{OL}} = \frac{\partial R_{PL}}{\partial V_{OL}} \frac{\partial V_{OL}}{\partial v_{OL}} + \frac{\partial R_{PL}}{\partial V_{\infty L}} \frac{\partial V_{\infty L}}{\partial v_{OL}} + \frac{\partial R_{PL}}{\partial \gamma_{OL}} \frac{\partial \gamma_{OL}}{\partial v_{OL}}$$

$$** \quad \frac{\partial R_{PL}}{\partial \theta_{OL}} = \frac{\partial R_{PL}}{\partial V_{OL}} \frac{\partial V_{OL}}{\partial \theta_{OL}} + \frac{\partial R_{PL}}{\partial V_{\infty L}} \frac{\partial V_{\infty L}}{\partial \theta_{OL}} + \frac{\partial R_{PL}}{\partial \gamma_{OL}} \frac{\partial \gamma_{OL}}{\partial \theta_{OL}}$$

$$* \quad \frac{\partial \gamma_{OL}}{\partial \gamma_{OB}} = 1$$

$$* \quad \frac{\partial \gamma_{OL}}{\partial \gamma_{OB}} = 1$$

$$* \quad \frac{\partial \gamma_{OL}}{\partial v_{OL}} = \frac{\partial \gamma_{OL}}{\partial \delta_{OL}} \left[\left(\frac{\partial \delta_{OL}}{\partial v_{OL}} \right)_1 + \frac{\partial \delta_{OL}}{\partial V_{OL}} \frac{\partial V_{OL}}{\partial v_{OL}} \right]$$

$$* \quad \frac{\partial \gamma_{OL}}{\partial \theta_{OL}} \quad = \quad \frac{\partial \gamma_{OL}}{\partial \delta_{OL}} \quad \left[\left(\frac{\partial \delta_{OL}}{\partial \theta_{OL}} \right)_1 \quad + \quad \frac{\partial \delta_{OL}}{\partial V_{OL}} \quad \frac{\partial V_{OL}}{\partial \theta_{OL}} \right]$$

$$* \quad \frac{\partial \gamma_{OL}}{\partial V_{OB}} \quad = \quad \frac{\partial \gamma_{OL}}{\partial \delta_{OL}} \quad \frac{\partial \delta_{OL}}{\partial V_{OL}} \quad \frac{\partial V_{OL}}{\partial V_{OB}} \quad .$$

The uncertainty in lander range angle is given then by:

$$\Delta \phi_L \quad = \quad \left[\left(\frac{\partial \phi_L}{\partial R_O} \Delta R_O \right)^2 + \left(\frac{\partial \phi_L}{\partial V_{OB}} \Delta V_{OB} \right)^2 + \left(\frac{\partial \phi_L}{\partial \gamma_{OB}} \Delta \gamma_{OB} \right)^2 + \left(\frac{\partial \phi_L}{\partial v_{OL}} \Delta v_{OL} \right)^2 + \left(\frac{\partial \phi_L}{\partial \theta_{OL}} \Delta \theta_{OL} \right)^2 \right]^{1/2}$$

where ΔR_O, ΔV_{OB}, etc., are, as previously, one-sigma values of uncertainties.

APPENDIX F

SATELLITE RECONNAISSANCE ORBITS

This study supplements work performed at JPL by C. E. Kohlhase entitled "Planetary Satellite Orbits." The JPL Study considered use of orbit plane rotation caused by planetary oblateness to keep the satellite plane within an acceptable sunlit region for reconnaissance. As an initial study the analysis utilized the simplifying assumption that the planetary equator and the plane of the planets motion about the sun be coincident. On this basis, optimum satellite orbits in the presence of system errors were determined. The optimum orbit found was defined as that which with errors present maximized the minimum expected stay time of the line of modes of the satellite orbit within the acceptable region.

As the purpose of the satellite mission is reconnaissance, it is probable that altitude bounds will exist between which the surveillance system must operate. An additional factor of importance is therefore the dwell time of the satellite periapsis point within the sunlit region. Furthermore, in actuality the Martian equator is inclined approximately 25 degrees to the plane of the planets motion about the sun; a factor not previously considered.

The present work studies both the periapsis dwell time in the sunlit region and the actual system geometry assuming no limitations on achievable orbits. In actuality, planetary approach conditions may force a restricted choice of orbits. For example, while it is desirable to have inclinations in the neighborhood of 90 degrees for large coverage of the planet certain approach conditions yield a periapsis motion directly out of the sunlit cone for these inclinations. The choice then would be between (1) lowering the inclination to less than approximately 64 degrees to achieve the correct periapsis motion or (2) utilizing an orbit whose altitude range doesn't fall outside the acceptable reconnaissance limits. The first choice restricts the surface of the planet which may be mapped while the second alternative may be costly in terms of fuel. This problem exists for both type I and II Martian trajectories for 1969 launch dates.

One further point should be stressed. If the entire sunlit face is available for reconnaissance then no reconnaissance dead zones exist. As one side of the orbit rotates out of the sunlit face the other portion rotates into it. With this in mind, all that remains to optimize is the amount of planetary coverage. This may be done by choosing a polar orbit as the coverage achieved is obviously a symmetric function of deviations from the 90-degree case. What has been accomplished in this manner is to maximize the minimum coverage possible.

Part A: Planetary Equator and Orbit Plane Coincident

The periapsis motion will first be studied retaining the simplified geometry of coincident planetary equator and orbit plane as shown on the celestial sphere in figure F1. The useful sunlit region is defined by a cone of central angle 180 degrees $-2a$ about the sun line. Defining

$$\left\{ \begin{array}{c} A_a \\ A_b \end{array} \right\} \qquad\qquad \left\{ \begin{array}{c} \text{above} \\ \text{below} \end{array} \right\} \quad \text{planetary orbit plane}$$

Satellite orbit arc in acceptable sunlit cone

It is thus necessary to determine A_a, A_b for the given satellite orbit inclination (i) as a function of γ, positive westward, the angle between the sun line and the line of intersection of the satellite plane and the planetary orbit plane. Once this has been done the portion of the satellite orbit within the sunlit region is known and the periapsis point may be chosen on the satellite orbit so as to maximize the time spent within the acceptable zone. The discussion has, so far, assumed that the satellite orbit parameters are selected on the basis of maximizing, in the presence of errors, the node line stay time within the acceptable cone. The only parameter left to be optimized is then the initial placement of the periapsis point on the satellite orbit.

The analysis shown that in some cases the periapsis point may leave the acceptable cone long before the node line crosses the boundary. In these cases, one may define a new optimum orbit by changing the satellite orbit parameters so that the minimum nodal dwell time is decreased while the periapsis dwell time is increased until the two are equal. The importance of this change depends, of course, on the reconnaissance system capability. If the system can tolerate an altitude variation of a factor of two or greater, this implies, for the orbits under consideration, surveillance capability for a central angle of approximately 90 degrees or greater on either side of the periapsis point. In this case the utility of obtaining the new optimum is doubtful.
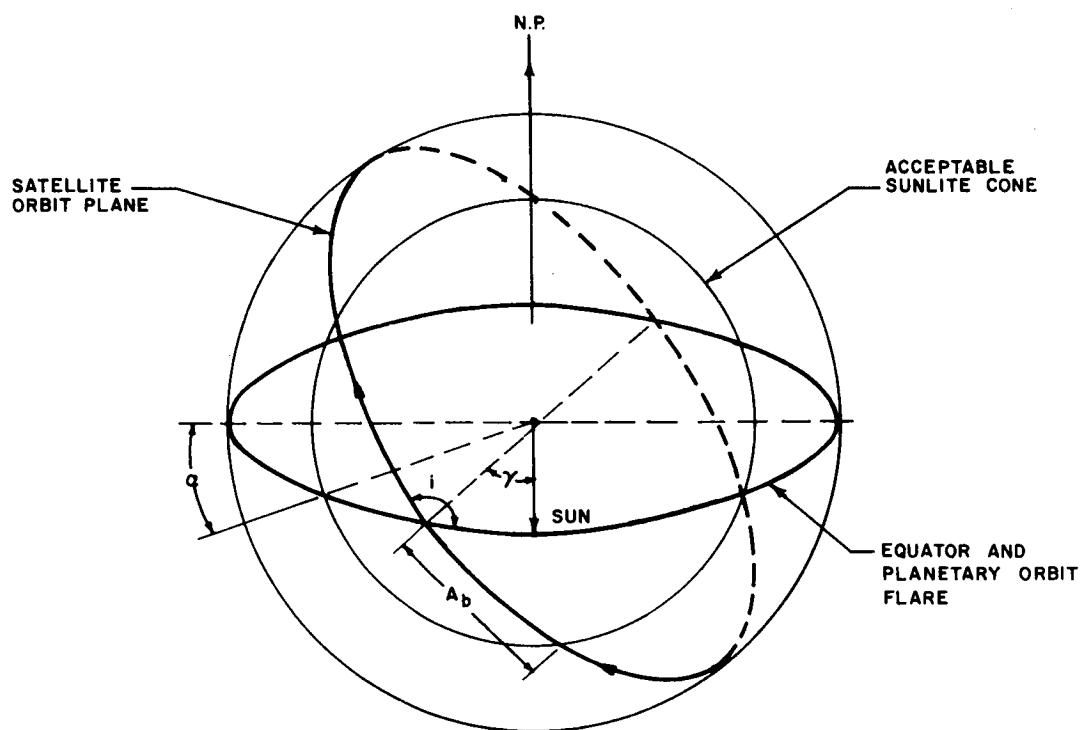
Defining

$$k = \frac{180 - 2a}{(90 - a) - \gamma_i} \quad ; \quad X = \frac{\dot{\theta}}{\dot{\psi}} \tag{F1}$$

where

$\dot{\theta}$ = rotation rate of satellite node line caused by planet oblateness

$\dot{\psi}$ = rotation rate of sun line caused by planetary motion about the sun

γ_i = initial value of γ

63-9745

Figure F1 SIMPLIFIED GEOMETRY

one has

$$\dot{\gamma} = \dot{\psi} - \dot{\theta} = \dot{\psi}\,(1 - X) \tag{F2}$$

Consider $X_1 = X' - \epsilon$ and $X_2 = X' + \epsilon$ where X' is the value of X such that for $X = X_1$ or X_2 the same life time is obtained. The value of $X = X'$ is thus optimum, that is, it assures the maximum of the possible minimum lifetimes. Therefore

$$(90 - a) = \gamma_i + \dot{\gamma_1} t = \gamma_i + \dot{\psi}\,(1 - X_1)\,t \tag{F3}$$

$$-(90 - a) = \gamma_i + \dot{\gamma_2} t = \gamma_i + \dot{\gamma}\,(1 - X_2)t \tag{F4}$$

Solving equations (F3) and (F4) for t and equating the two expressions, one finds

$$X' = 1 + \epsilon\,(1 - 2/k) \tag{F5}$$

With this value of X' substituted into either equations (F3) or (F4), the expected minimum lifetime T_{min} is found to be

$$T_{min} = \left(\frac{180 - 2a}{\dot{\psi}}\right)\,\frac{1}{2\epsilon} \tag{F6}$$

Returning now to the determination of the useful satellite arc within the cone one finds that

$$A_a = 2\tan^{-1}\left[\frac{\sin\dfrac{(i + \bar{B})}{2}}{\sin\dfrac{(i - \bar{B})}{2}}\ \tan\left(\dfrac{90 - (a + \gamma)}{2}\right)\right] \tag{F7}$$

$$A_b = 2\tan^{-1}\left[\frac{\cos\dfrac{(i - \bar{B})}{2}}{\cos\dfrac{(i + \bar{B})}{2}}\ \tan\left(\dfrac{90 - (a + \gamma)}{2}\right)\right] \tag{F8}$$

where

$$\bar{B} = \sin^{-1}\,[\sin\gamma\,\sin i/\cos a] \tag{F9}$$

The expressions are valid for both positive and negative values of γ.

Consider what occurs as the node line rotates eastward. When $\gamma = -(90-a)$ the node line is on the boundary of the sun lit cone and there is no useful arc below the planetary orbit plane ($A_b = 0$) for $i > 90$ degrees. There still exists, however, a useful arc above the plane given by

$$A_a = 2 \tan^{-1} [\cos (180 - i) \cot a] \qquad\qquad (F10)$$

The limit on γ for which A_a vanishes may be found by considering the equation for $\bar{B}$

$$\sin \bar{B} = \frac{\sin \gamma \sin i}{\cos a} \qquad\qquad (F11)$$

Since $|\sin \bar{B}|$ must be $\leq |$ then putting $\gamma = -(90-a)-\delta\gamma$

$$\frac{\sin (90 - a + \delta\gamma)}{\cos a} \leq 1$$

or

$$\cos (a - \delta\gamma) \leq \cos a / \sin i$$

from which, for given (a, i) one may compute the rotation of the node line beyond the sunlit cone ($\gamma\gamma$) after which the satellite orbit plane no longer intersects the cone.

As an example, the case where $a = 30$ degrees, $\gamma_i = 36$ degrees ($l_k = 5$), has been solved. In reference 1, one finds that for orbits with a fixed periapsis altitude of 1000 km the optimum orbit is one having an apoapsis altitude of 4000 km and an inclination of 106 degrees. The corresponding value of ϵ is 0.68 from which

$$T_{min} \quad - \quad 170 \text{ days}$$

where the value $\dot{\psi} = 0.524$ deg/day has been used.

The optimum X' is found from

$$X' = 1 + \epsilon \left(1 - \frac{2}{l_k}\right) = 1.408$$

hence

$$X_{max} = 2.088 \; ; \; X_{min} = 0.728$$

from which

$$\dot{\gamma}_{max} = 0.1425 \text{ deg/day} \quad ; \quad \dot{\gamma}_{min} = -0.57 \text{ deg/day}$$

The results of the computations for A_a and A_b are shown in figures F2 and F3 corresponding to X_{max} and X_{min} respectively. For the nominal orbit of $i = 106$ degrees, $h_p = 1000$ km, $h_a = 4000$ km and the apsidal line rotates at 0.8 deg/day in a direction opposite to the satellite motion. Assuming the periapsis point is initially on the boundary of the sunlit cone the motion of the point between A_a and A_b is shown. Shifting the line parallel to itself in the figures shows the effect of having the periapsis point at different initial positions. The maximum periapsis lifetime is soon to occur of the periapsis point initially on the boundary of the cone as shown.

In this case, in the presence of errors in initial periapsis location in the satellite plane, the initial periapsis point should be biased outside the sunlit cone. To illustrate suppose an error of 10-degree central angle might be expected. A comparison of periapsis lifetimes resulting from choosing different initial points and the 10-degree error about them shows that the aiming point should be biased approximately 10-degrees outside the cone. If this is done a minimum periapsis dwell time of 113 days is assured for either X_{max} or X_{min}

Part B: Planetary Equator and Orbit Plane Inclined to Each Other

The geometry associated with this case is shown on the celestial sphere in figure F4. The planetary equator and planetary orbit plane are inclined to one another with an angle ϕ and the satellite orbit has an inclination i to the planetary equator. The equatorial node line of the satellite orbit on the sunlit face makes an angle B with the line of intersection of the equatorial and planetary orbit planes. Finally, the line of intersection of the planetary and equatorial planes makes an angle γ with respect to the sun line. About the sun line, which lies in the planetary orbit plane, a cone of central angle 180 degrees -2α is drawn the interior of which defines the acceptable lightning conditions. The angle β is considered positive above the planetary orbit plane while γ is positive to the west of the sun line.

Defining, as before,

$$\left\{ \begin{array}{c} A_a \\ \\ A_b \end{array} \right\}$$
Satellite orbit are in acceptable sunlit cone

$\left\{ \begin{array}{c} \text{above} \\ \text{below} \end{array} \right\}$ Planetary orbit plane

one finds that

$$A_a = 2 \tan^{-1} \left[\frac{\sin \dfrac{(\delta + \bar{B})}{2}}{\sin \dfrac{(\delta - \bar{B})}{2}} \tan \left(\frac{90 - \alpha - \dfrac{(B_1 + \gamma)}{2}}{} \right) \right] \qquad (F12)$$

$$A_b = 2 \tan^{-1} \left[\frac{\cos \dfrac{(\delta - \bar{B})}{2}}{\cos \dfrac{(\delta + \bar{B})}{2}} \tan \left(\frac{90 - \alpha - (B_1 + \gamma)}{2} \right) \right] \qquad (F13)$$

where

$$\bar{B} = \sin^{-1} \left[\frac{\sin (B_1 + \gamma) \sin \delta}{\cos \alpha} \right] \qquad (F14)$$

and

$$B_1 = \tan^{-1} \left[\frac{\sin \dfrac{(i + \phi)}{2}}{\sin \dfrac{(i - \phi)}{2}} \tan B/2 \right] + \tan^{-1} \left[\frac{\cos \dfrac{(i + \phi)}{2}}{\cos \dfrac{(i - \phi)}{2}} \tan B/2 \right] \quad (F15)$$

$$A_1 + B_1 = 2 \tan^{-1} \left[\frac{\sin \dfrac{(i + \phi)}{2}}{\sin \dfrac{(i - \phi)}{2}} \tan B/2 \right] \qquad (F16)$$

$$\delta = 2 \sin^{-1} \left[\frac{\sin \dfrac{(i - \phi)}{2}}{\cos \dfrac{(A_1 + B_1)}{2}} \cos B/2 \right] \qquad (F17)$$

The expressions are valid for B, γ either positive or negative.

Denote by ω the control angle of the periapsis point of the satellite orbit above the ascending node. The latitude of the periapsis point above the planetary orbit plane is given by

$$L_d = \sin^{-1} [\sin \delta \sin (A_1 + \omega)] \tag{F18}$$

The longitude (L_n) of the peripsis point is measured in the planetary orbit plane westward from the sun line. It is determined from

$$L_n = \gamma + B_1 + \bar{B}_1 \tag{F19}$$

where γ and B_1 are as previously defined and

$$\bar{B}_1 = \cos^{-1} \left[\frac{\cos (A_1 + \omega)}{\cos (L_d)} \right] \tag{F20}$$

To test the validity of the simplified geometry previously considered the corresponding example is treated here. The initial conditions are taken to be $\gamma_i = 0$, $B_i = 36$ degrees. The planetary and equatorial orbits are inclined at 25 degrees for Mars ($\phi = 25$ degrees). Satellite orbit parameters are, as before, $h_p = 1000$ km, $h_s = 4000$ km, $i = 106$ degrees. If we define

$$X = \frac{\dot{\theta} \cos \phi}{\dot{\psi}}$$

and use the analysis of the simplified geometry ($\phi = 0$) to choose X' we have again for $\epsilon = 0.68$

$$X' = 1.408$$

and

$$X_{max} = 2.088 \quad ; \quad X_{min} = 0.728$$

now

$$\dot{\gamma} = \dot{\psi} = 0.524 \text{ deg/day}$$

and

$$\dot{B} = - \dot{\theta}$$

therefore

$$\dot{B}_{max} = -0.421 \text{ deg/day} \quad ; \quad \dot{B}_{min} = -1.207 \text{ deg/day}$$

In performing the calculations A_1, B_1 and δ are first found as functions of B then A_a, A_b determined as functions of time. The results are shown in figures F5 and F6 corresponding to X_{max} and X_{min} respectively. The line describing the periapsis motion corresponding to an initial periapsis location on the boundary of the cone and a 0.8 deg/day rotation of the apsidal line for the nominal orbit is shown on the figures.

It may be seen that the periapsis point remains within the sunlit cone for approximately the same time as for the simplified geometry. The lifetime of the node line, however, is appreciably different as shown below.

	Simplified Geometry	General Geometry
	Node line[1] in Sunlit Cone	Node line in Sunlit Cone
X_{max}	170 days	150 days
X_{min}	170 days	210 days

The difference in nodal life time corresponding to X_{max} and X_{min} in the general geometry case indicates that the optimal rotation rates have not been selected. One concludes that with respect to nodal lifetime the results obtained utilizing the simplified geometry are not directly applicable to the general case. The optimization problem for the general case has been formulated and can be carried out if restrictions on lighting conditions require it.

Reference: Kohlase, C. E. : Planetary Satellite Orbits. JPL Space Programs Summary 37-18.

---

[1] The node line referred to is the line of intersection of the satellite orbit and the planetary orbit plane.
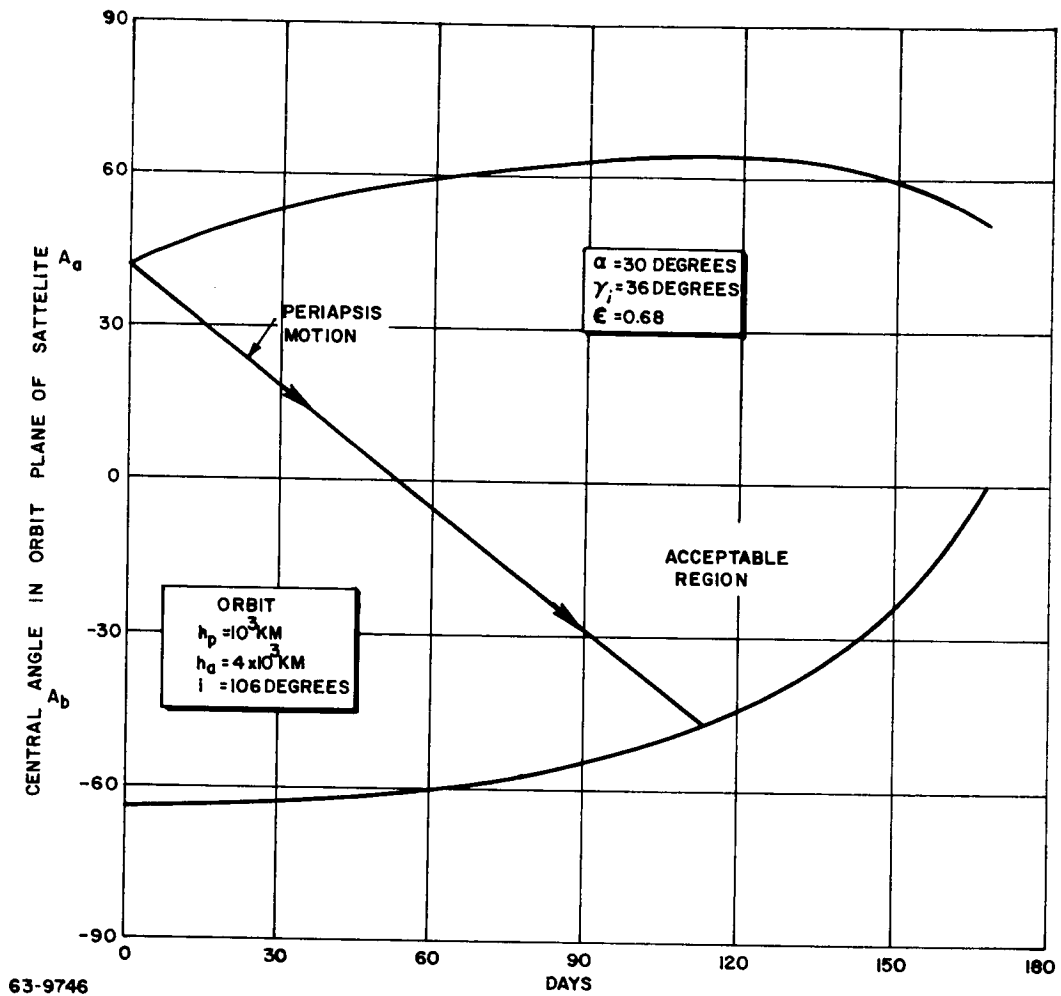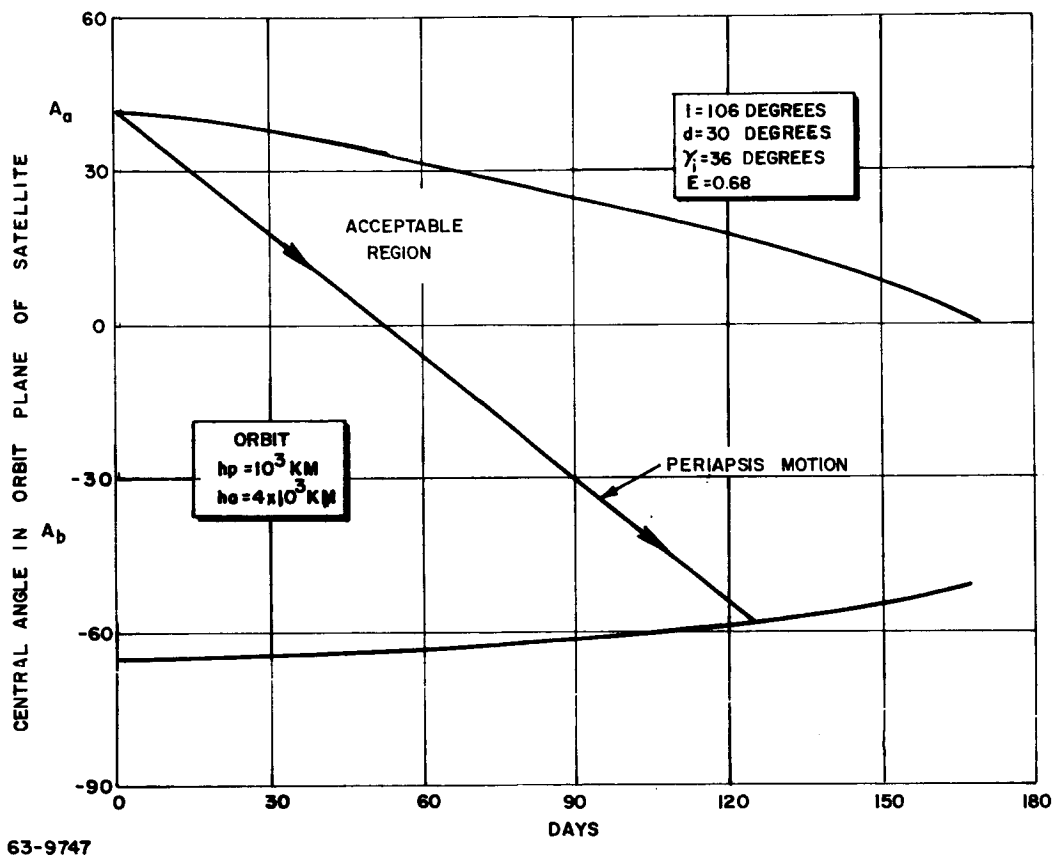
Figure F2 SIMPLIFIED GEOMETRY (X$_{mas}$)

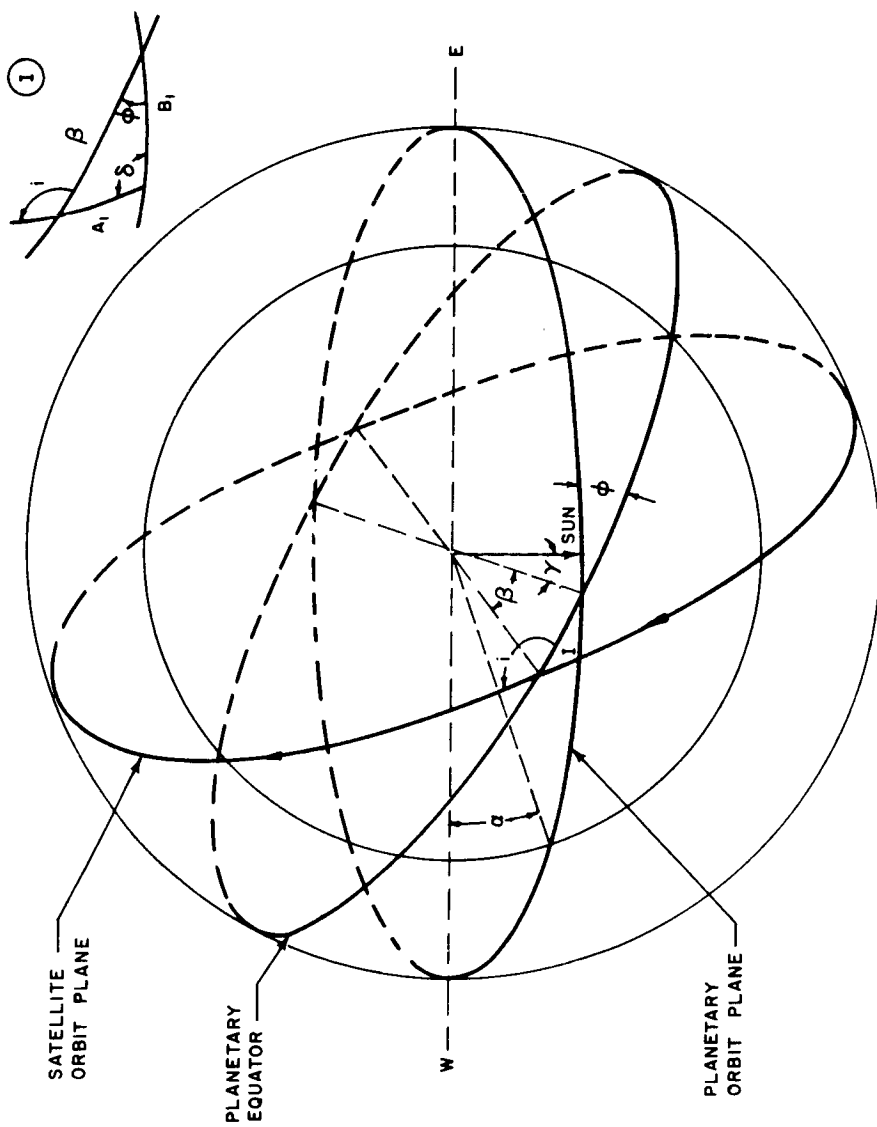63-9746

-392-

Figure F3 SIMPLIFIED GEOMETRY (X_{min})

63-9747

-393-

Figure F4 GENERAL GEOMETRY

63-9748

-394-

63-9749
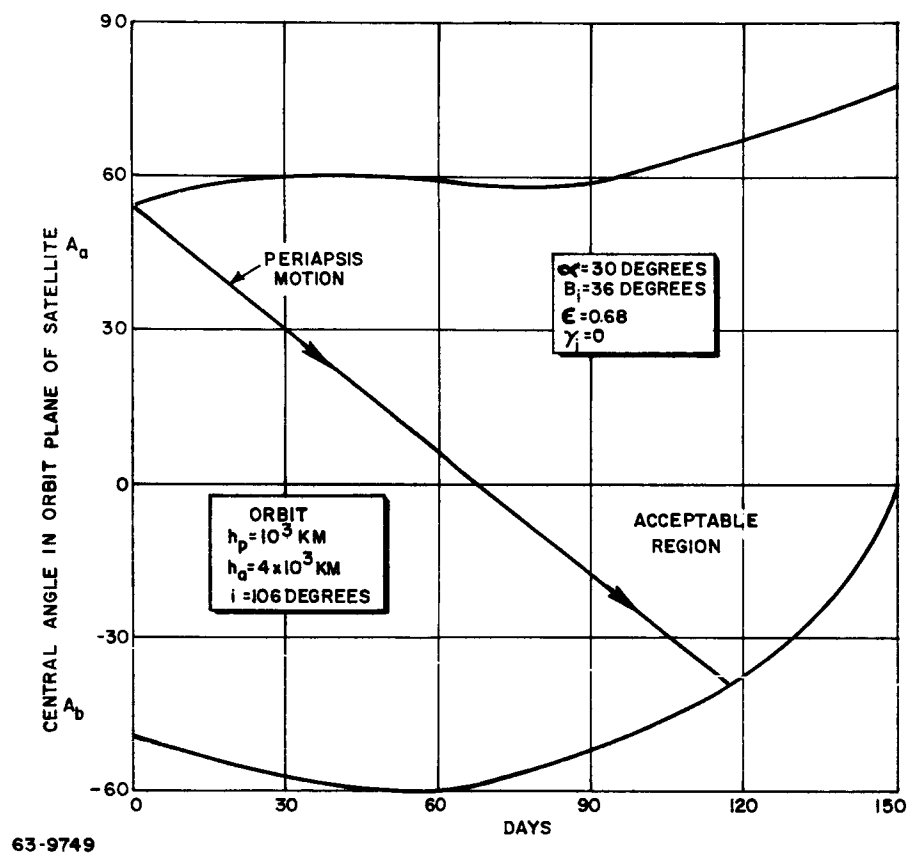
Figure F5 GENERAL GEOMETRY (X_{max})
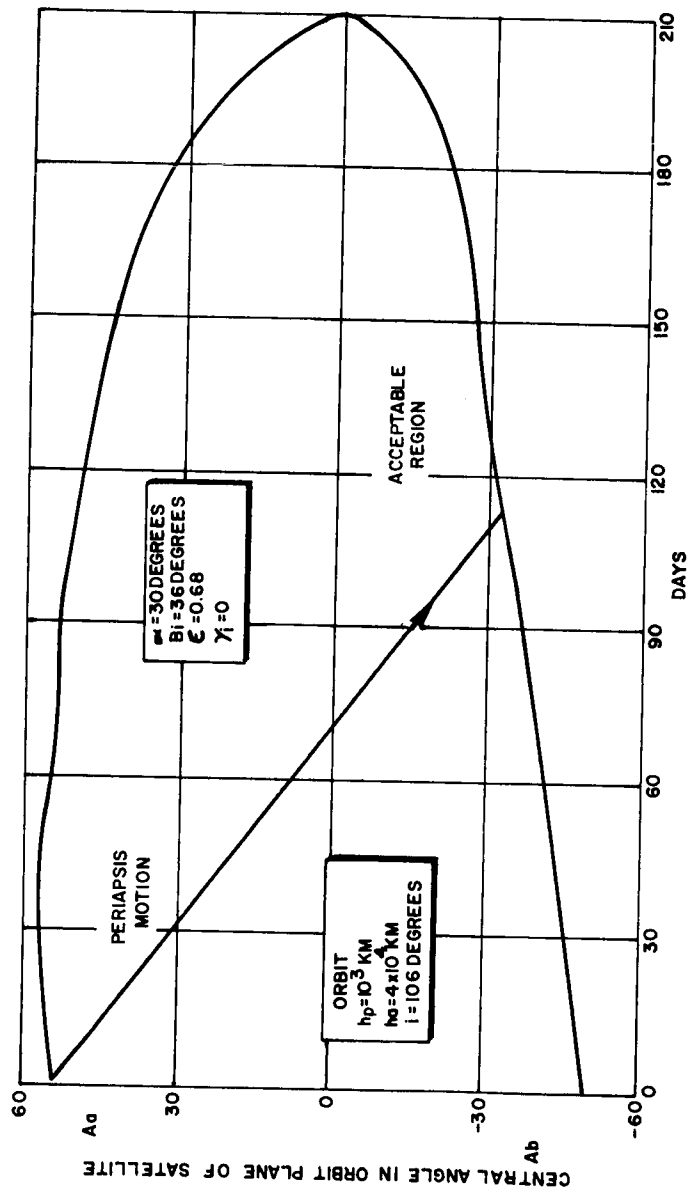
Figure F6 GENERAL GEOMETRY (X_{min})

63-9750

-396-

DISTRIBUTION

Addressee	No. of Copies
NASA	
Director, Lunar and Planetary Programs	10
400 Maryland Avenue SW	
Washington 25, D.C.	
Attn: D. P. Hearth, Code SL (+1 reproducible)	
Central Files	1
Document Control	5
Research Library	134